Alma Mater Studiorum - Università di Bologna

DOTTORATO DI RICERCA IN

CHIMICA

Ciclo 35

Settore Concorsuale: 03/C1 - CHIMICA ORGANICA

Settore Scientifico Disciplinare: CHIM/06 - CHIMICA ORGANICA

NEW CATALYTIC STRATEGIES FOR THE MANIPULATION OF ARENES

Presentata da: Lorenzo Lombardi

Coordinatore Dottorato

Luca Prodi

Supervisore

Marco Bandini

Co-supervisore

Paola Galletti

Esame finale anno 2023

ABSTRACT

The aim of this Doctoral Thesis is the development of new catalytic synthetic methodologies in the context of the modern organic chemistry setting, with special focus on the use of cheap, sustainable catalytic materials. Specifically, during the course my PhD, I focused my research on two main distinct catalytic strategies, namely: the use of carbonaceous materials as catalysts (carbocatalysis) and nickel catalysis, also investigating a synergistic combination of the two. These methodologies were explored as means for the manipulation of (hetero)aromatic cores, representing ubiquitous, easily accessible and privileged scaffolds in medicinal or natural products chemistry. Both polar and radical reaction manifolds were engaged as complementary reactivities, capitalizing on metal- as well as organo-based activation modes. Particular attention has been devoted to addressing modern synthetic challenges or highly sought-after methodologies. Specifically, protocols for direct substitution of alcohols, dearomatization of arene nuclei, formation of C-S bonds, carbon dioxide fixation, C-C bond activation and fluoroalkylation were successfully achieved under carbo- or nickel catalyzed conditions.

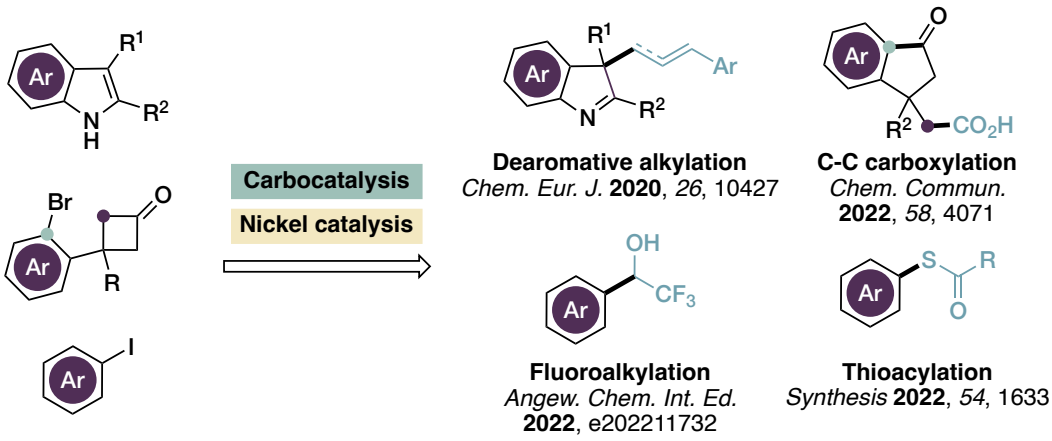

Significant effort has been devoted to the study and optimization of the reaction conditions and catalyst structure, in order to maximize the yield and selectivity of the processes as well as the breadth of substrate scope. Elements of conceptual novelty

emerged within the development of the titled methodologies, and close attention has been dedicated to unraveling the mechanistic aspects of the transformations via a synergistic combination of computational, analytical and experimental methods.

A dearomative allylation and allenylation of 2,3-disubstitued indoles with alcohols was realized under carbocatalytic regime in the presence of graphene oxide as carbocatalyst. The protocol features mild and environmentally friendly conditions and does not need any stoichiometric additive or metal, providing a valuable alternative to the state-of-the-art transition metal catalyzed protocols. Mechanistic investigations disclosed a covalent activation mode exerted by the oxygenated GO functionalities, with the material actually working as a regenerable coreagent rather than a catalyst.

A heterogeneous, reduced graphene oxide supported nickel catalyst (nickel nanoparticles) was described and successfully applied for the C-S cross coupling of readily available potassium thiocarboxylate salts and aryl iodides *en route* to valuable *S*-aryl thioesters. This transformation was, up to this report, unprecedented with nickel catalysis, and the protocol stands as a useful proof of concept for the realization of a challenging coupling reaction under heterogeneous conditions. The nanoparticles were thoroughly characterized with respect to morphology, structure and chemical speciation.

Homogeneous nickel catalysis was used in the cross electrophile coupling between the redox-active *N*-trifluoroethoxyphthalimide and iodoarenes for the synthesis of biologically relevant α-aryl-α-trifluoromethyl alcohols. The transformation proceeds via a radical pathway, with a pivotal solvent assisted 1,2-Hydrogen Atom Transfer (HAT) process that generates a nucleophilic α-hydroxy-α-trifluoromethyl C-centered radical intercepted by an aryl nickel complex. The protocol reproduces a formal arylation of trifluoroacetaldehyde under mild conditions in high yields and with large functional group tolerance.

A tandem C-C bond activation-carboxylation of cyclobutanones with CO_2 at atmospheric pressure under homogeneous nickel catalysis was realized, establishing a direct route to synthetically valuable, biologically relevant 3-indanone-1- acetic acids. A unique combination of aluminum trichloride and an axially chiral bipyridine ligand revealed key for achieving satisfactory yields.

Despite the conceptual diversity, the proposed protocols are connected by their potential contribution to the ever-evolving realm of modern sustainable catalysis and will hopefully represent useful advancements and inspiration for future research.

Table of contents

1. Introduction

"Scientific progress is measured by units of courage, not intelligence"
Paul Dirac

1.1 Organic synthesis: roots and evolution

K. C. Nicolaou has defined organic synthesis as "the art and science of constructing substances, natural or designed, whose primary element is carbon".[1] Although men have been performing transformations of organic matter since ancient times, and steadily refined their understanding of matter transitioning from alchemy to chemistry starting from the 18th century, the birth of this discipline in its modern sense can be traced back to 1828, when Wöhler accomplished the synthesis of urea from ammonium and cyanate salts. This was an achievement of paramount importance in that era, demonstrating for the first time that organic compounds, made by living organisms, could be replicated by men in the laboratory.[2]

Since this outstanding discovery, organic synthesis progressed enormously, along with analytical techniques that could provide structure elucidation, technologies and experimental methods, and theoretical concepts allowing better understanding of chemical bonds and their reactivity.

By the end of 19th century, chemists had already prepared a great number of molecules, including acetylsalicylic acid, indigo and glucose, and developed new reactions for their synthesis, particularly regarding aromatic compounds (Friedel-Crafts alkylation and acylation, 1877).[3] Notable chemists in this period were Emil Fischer and Adolf von Bayer, who were awarded, separately, with the Nobel prize in Chemistry in the first two years of its existence, for their work on "sugars and purins" and "organic dyes

[1] K. C. Nicolaou, *Proc. R. Soc. A.* **2014**, 470:20130690.
[2] F. Wöhler, *Ann. Phys.* **1828**, *88*, 253–256.
[3] C. Friedel, J.-M Crafts, *C. R. Acad. Sci. Paris* **1877**, *84*, 1392–1395.

and hydroaromatic compounds", respectively.[4] In the first part of the 20th century, venerable reactions still in use today such as the catalytic hydrogenation of multiple carbon-carbon bonds (Sabatier, 1897), the Grignard reaction (1900) and the Diels-Alder reaction (1928), had been discovered and applied, and their discovers awarded with the Nobel Prize in Chemistry (Sabatier and Grignard shared it in 1912, while Diels and Alder were awarded in 1950).[5] In the same years, the formulation of the quantum mechanics theory gifted the chemical world an absolute game-changer, that profoundly reshaped the way chemists thought about atomic interactions. In 1939 Linus Pauling collected his work on the application of quantum mechanics in the landmark textbook "The Nature of the Chemical Bond", providing chemists with the first formulation of Valence Bond Theory (VBT).[6] This book, that introduced key concepts such as resonance and orbital hybridization, has been dubbed "chemistry's most influential book of this century and its effective bible", and effectively marked the birth of modern chemical bond theories. For his contributions, Pauling was awarded the Nobel Prize in Chemistry in 1954. In the same years, also the Molecular Orbital Theory (MOT) was formulated, from seminal contributions by Hund, Mulliken, Hückel, Lennard-Jones and Slater.[7] Despite the many contributors, only Mulliken was awarded with the Nobel Prize in Chemistry, in 1966. This alternative approach resulted less successful than VBT in the first decades of 1900, being less intuitive and less suited to match Lewis' "shared electron pair" model of the chemical bond that was dominant in the beginning of the century, but became more and more popular, to the point of being perceived as the more complete model. Today, the two theories represent complementary models, each one with its own advantages and drawbacks depending on the phenomenon studied.[8]

---

[4] Nobelprize.org. *All Nobel Prizes in Chemistry.* See https://www.nobelprize.org/prizes/lists/all-nobel-prizes-in-chemistry/.

[5] a) P. Sabatier, *Ind. Eng. Chem.* **1926**, *18*, 1005–1008; b) V. Grignard, *Compt. rend. Hebd. Séances Acad. Sci.* **1900**, *130*, 1322; c) O. Diels, K. Alder, *Justus Liebigs Ann. Chem.* **1928**, *460*, 98–122.

[6] L. Pauling, *The nature of the chemical bond.* Cornell University Press: New York, NY, **1939**.

[7] R.S. Mulliken, *Spectroscopy, Molecular Orbitals, and Chemical Bonding* in *Nobel Lectures, Chemistry 1963–1970*, Elsevier: Amsterdam, **1972**, pp.131–160.

[8] J. M. Galbraith, S. Shaik, D. Danovich, B. Braïda, W. Wu, P. Hiberty, D. L. Cooper, P. B. Karadakov, T. H. Dunning, Jr, *J. Chem. Educ.* **2021**, *98*, 3617−3620.

With these new theorical tools in hand, the development of new instrumental techniques for structure elucidation, above all NMR and mass spectrometry, and the immense interest ignited by the success of penicillin towards the discovery and synthesis of new biologically active compounds, organic chemistry was set to make giant leaps forward from the 1950s on, especially in the field of total synthesis.

A major figure pioneering this revolution was American chemist Robert B. Woodward, who accomplished a great number of synthesis of natural compounds that went on to be milestones in the field, including strychnine, cephalosporine C and chlorophyll a.[9] His total synthesis in 1973 (in collaboration with Swiss chemist Albert Eschenmoser) of Vitamin B_{12}, the most complex compound assembled by men at that time, was a landmark within the chemical community, spreading the belief that no molecule was exceedingly complex to be prepared. He also encouraged the adoption of modern instruments and proposed new theories regarding chemical reactivity (Woodward-Hoffmann rules, 1965), and was awarded with the 1965 Nobel Prize in Chemistry for his immense contributions. Another notable practitioner in following years was legendary American chemist Elias J. Corey, who made further fundamental contributions that had a decisive impact on the field organic synthesis and were then recognized with the Nobel Prize in Chemistry in 1990. He accomplished the synthesis of a plethora of human secondary metabolites (hormones such as steroid, prostaglandins, leukotrienes), developed new reagents, protecting groups, catalysts and at least 300 new synthetic methods. Even more significantly, he introduced the theory of retrosynthetic analysis, formalizing a backwards, logical approach for the rational selection of the best synthetic route to a target molecule starting from available precursors, that he summarized in his renowned book "The logic of chemical synthesis" in 1989.[10]

The second half of the 20th century witnessed the introduction of several groundbreaking methodologies, whose impact elevated the art of synthesis allowing

[9] O. T. Benfey, P. J. T. Morris, *Robert Burns Woodward: architect and artist in the world of molecules.* Chemical Heritage Foundation: Philadelphia, PA, **2001**.

[10] E. J. Corey, X-M. Cheng, *The logic of chemical synthesis.* Wiley: New York, NY, **1989**.

more efficient, practical disconnections and access to new chemical space. H. G. Khorana (1986 Nobel Prize in Medicine) and R. B. Merrifield (1984 Nobel Prize in Chemistry) discovered, respectively, protocols for the formation of phosphate and amide bonds to synthetize nucleosides and peptides, greatly advancing the possibilities for studies on nucleic acids and proteins.[11] Other notable, now routinely used reactions developed in that time are the Wittig olefination and Brown's hydroboration, constituting efficient platforms for the preparation and functionalization of alkenes in a general, robust and stereoselective manner. In recognition of the utility of the reagents they developed, the two shared the 1979 Nobel Prize in Chemistry.[4]

Those years also saw the rise to prominence of transition metal catalysis (a theme that will be further discussed in the next chapter), that proved to be an extremely powerful tool to achieve unprecedented selectivity in stereocontrolled processes as well as brand new disconnections. Testament to the impact of the discoveries made in this field is the close sequence of three Nobel Prize in Chemistry awarded in the first years of the 21st century for methodology work. In 2001 K. B. Sharpless, R. Noyori and W. S. Knowles shared the prize for the development of enantioselective oxidation and reduction reactions. Sharpless worked on asymmetric oxidation, the most famous being the Ti catalyzed epoxidation of allylic alcohols, while Noyori and Knowles worked on enantioselective hydrogenation protocols employing chiral phosphine ligands with rhodium and ruthenium.[12] R. H. Grubbs, R. R. Schrock and Y. Chauvin won it in 2005 for the development of olefin metathesis, that allows unprecedented assembly of carbon-carbon double bonds via ruthenium or molybdenum catalysis.[13] In 2010, the prize was shared by R. Heck, A. Suzuki and E. Negishi for their studies on palladium catalyzed C-C cross couplings, making possible ipso-substitution of aryl (pseudo)halides.[14] Another high impact Pd-catalyzed reaction developed in the beginning of the century is the Buchwald-Hartwig amination, that permits C-N

[11] a) H. G. Khorana, *Science* **1979**, *203*, 614-625. b) R. A. Lerner, *Science* **2006**, *313*, 57.
[12] a) T. Katsuki, K. B. Sharpless, *J. Am. Chem. Soc.* **1980**, *102*, 5974−5976. b) W. S. Knowles, R. Noyori, *Acc. Chem. Res.* **2007**, *40*, 1238–1239.
[13] A. M. Rouhi, *Chem. Eng. News* **2002**, *80*, 29–38.
[14] A. Suzuki, *Angew. Chem. Int. Ed.* **2011**, *50*, 6722–6737 (Nobel Lecture).

coupling of aryl halides and amines and is heavily used in the pharmaceutical realm.[15] Last year, 2021, is also a memorable year for synthetic methodology; indeed, the Nobel Prize in Chemistry was awarded to David MacMillan and Benjamin List for their seminal work in the early 2000s on asymmetric organocatalysis, a new concept for the assembly of a great variety of chiral molecular architectures in a selective way (more discussion on this topic will follow in the next chapter).[16]

Any summary of such kind is inevitably incomplete and numerous notable scientists that greatly advanced the field have been left out. Hopefully though, this tentative historical sketch can give a blurred picture of how greatly the discipline of organic chemistry has advanced in less than 200 years.

By means of these synthetic and theoretical endeavors, fundamental principles and insights on reactivity and selectivity were embraced, that defined the frontiers of organic chemistry as it is in the modern times. As the science of matter, and in particular of the substances related to life, organic chemistry's path has always been tied hand in glove with the evolution of mankind and society. In the process of perfecting their art (even simply for the sake of the art itself without a clear understanding of the consequence of their discoveries), synthetic chemists provide solutions and innovations that address unmet needs of their time, contributing to the global wellness and progress; at the same time, the big goals they must strive for propel the evolution of the craft itself, establishing a productive symbiotic setting. It can confidently be stated that without organic chemistry, most of the things we take for granted in daily life – gasoline or plastics, dyes and clothing, medicines or cosmetics – would be either non-existent or suffer in quality.[17]

---

[15] R. Dorel, C. P. Grugel, A. M. Haydl, *Angew. Chem. Int. Ed.* **2019**, *58*, 17118.

[16] Nobelprize.org. *The Nobel Prize in Chemistry 2021.* a)https://www.nobelprize.org/prizes/chemistry/2021/macmillan/lecture/ b)https://www.nobelprize.org/prizes/chemistry/2021/list/lecture/.

[17] M. Beller, *Eur. J. Lipid Sci. Technol.* **2008**, *110*, 789–796.

1.2 Catalysis: an enabling phenomenon

The term “catalyzed” and “catalyst” have now become widespread even in the non-chemical community. In the common language, a catalyst is some agent that provokes or speeds up some subsequent event of action; indeed, this pictorial image is actually a fairly accurate translation of the chemical definition. The IUPAC defines as catalyst as “a substance that increases the rate of a reaction without modifying the overall standard Gibbs energy change in the reaction … The catalyst is both a reactant and product of the reaction.”[18] In other words, a catalyst is some compound that gives access, for a given chemical reaction, to an alternative potential energy surface featuring a lower activation energy, but does not perturb its thermodynamic equilibrium, given that it is neither consumed nor formed in the process (**Figure 1**, left). This translates to faster rates, so that the effect of the catalyst is to speed up the reaction it catalyzes, even to the point of making otherwise energetically inaccessible transformations possible.[19] The catalyst does so by participating in the chemical reaction via some kind of interaction with the substrates and/or intermediates, thus changing the operating mechanistic pathway (which equals to populating an alternative potential energy surface), but is left unchanged in the overall process: the sequence of mechanistic events leading to the product will eventually regenerate the catalyst, establishing what is called a catalytic cycle (**Figure 1**, right). It being capable of revolving in this cycle also implies that a catalyst can usually be used in substoichiometric quantity, which is one appealing feature of catalytic methods.[20]

---

[18] IUPAC. *Compendium of Chemical Terminology, 2nd ed. (the "Gold Book").* Compiled by A. D. McNaught and A. Wilkinson. Blackwell Scientific Publications: Oxford, **1997**. Online version (2019-) created by S. J. Chalk. *https://doi.org/10.1351/goldbook.*

[19] S. H. Bauer, *J. Chem. Educ.* **1999**, *76*, 440.

[20] E. Roduner, *Chem. Soc. Rev.* **2014**, *43*, 8226–8239.

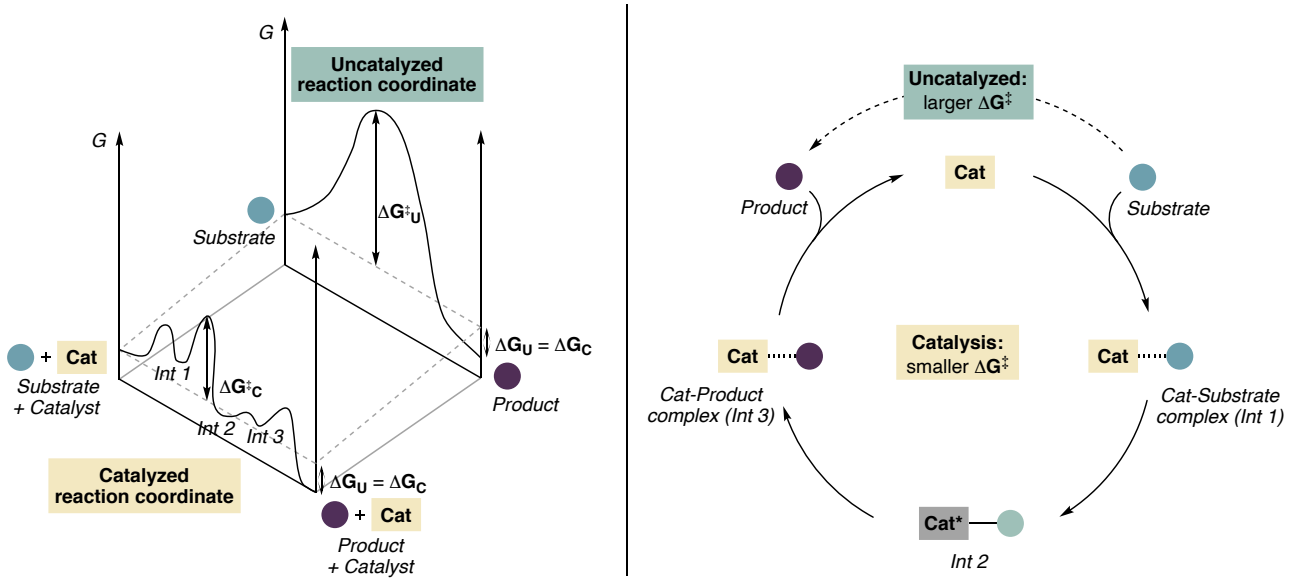

Figure 1. Left: representative comparison of the potential energy surface of an uncatalyzed *vs.* a catalyzed transformation. Note that catalysis does not change the overall Gibbs energy change, thus being irrelevant to the position of equilibrium. Right: representation of a model catalytic cycle.

Catalysis plays a central role in the existence of life itself, the biochemical reactions happening in our body being catalyzed by numerous enzymes, which are highly specific and efficient catalysts. The fermentation of sugars to produce alcohol, known since the beginning of human history, can be considered to be the first catalytic process (a biocatalytic one) utilized by men. In 1552 Valerius Cordus reported the first use of an inorganic catalyst, obtaining diethyl ether from ethanol in the presence of sulfuric acid, long before the concept of catalysis was enunciated or understood.[21] The term "catalysis" was coined in 1835 by Swedish chemist Jöns Jacob Berzelius, who systematically investigated recorded observations of the time and classified them as "catalysis", but the conceptual understanding of this phenomena dates back further.[22] In 1794, British chemist Elizabeth Fulhame demonstrated that the oxidation of carbon monoxide only proceeded in the presence of water, that it directly involved water and that water was regenerated at the end of the reaction, providing the first rigorous investigation of catalytic behavior.[23] In 1821 French Chemist Louis-Jacques Thenard

[21] J. Wisniak, *Educ. quím.* **2010**, *21*, 60–69.
[22] B. Lindström, L. J. Pettersson, *CATTECH* **2003**, *7*, 130–138.
[23] J. Mellor, *J. Phys. Chem.* **1903**, *7*, 557–610.

stated, with reference to his studies on the decomposition of hydrogen peroxide in the presence of finely divided metal powders, that "whichever it be the cause of the phenomena...is it not very probable that it is the same that produces so many other?". Indeed, several other examples of catalytic phenomena (like those classified from Berzelius) were known, and he recognized ahead of his time that this could very well be a general phenomenon.[21] Many years later, fundamental contributions came from Nobel Laurate Wilhelm Ostwald, who was awarded with the prize in 1909 "in recognition of his work on catalysis and for his investigations into the fundamental principles governing chemical equilibria and rates of reaction". He concluded that a catalyst was a "foreign" substance that when added to a combination of reactants could increase the rate of the transformation, but had no effect on the chemical equilibrium, basically enunciating the contemporary definition of catalyst. Even more, he refused the common belief that a catalyst could promote a reaction that would be impossible without it, asserting that those kind of reactions that were not observed in the absence of catalyst were simply too slow on our time scale to be recorded, but still had to be associated with a decrease in Gibbs' Free Energy and thus be attainable (spontaneous) in principle.[24] Ostwald's work gave a clear-cut difference between kinetic and thermodynamic aspects and founded the bases for the physical chemical understanding of catalytic behavior, but did not deal at all (as does not the definition of catalyst) with the molecular aspects of catalysis (*i.e.* how a catalyst actually operates, at the atomic level, the transformation it is involved in). The molecular view of a catalytic reaction as a cycle of elementary reaction steps was formulated by Sabatier, that proposed the principle of intermediate stability. He reasoned that the catalyst has to interact with the substrate to yield some intermediate that via subsequent transformation would evolve into the product, and that the intermediates in a catalytic cycle should be stable enough to be formed, but not so stable to be unreactive: when the two conditions are fulfilled, catalytic turnover can be operating.[25] In more recent times, the advent of modern analytical techniques that can provide information on the chemical structure of a

[24] G. Ertl, *Angew. Chem. Int. Ed.* **2009**, *48*, 6600–6606.
[25] G. Rothenberg, *Catalysis: Concepts and Green Applications*. 2nd Edition, Wiley-VCH: Weinheim, **2008**.

catalyst indeed allowed us to address the molecular aspects of a catalytic system, leading to greatly enhanced possibilities for rational design and optimization of catalysts with improved performance. The two approaches (molecular and physical chemical investigations) work synergistically: findings at the molecular level, such as detection or isolation of intermediates, isotope labeling studies or computational calculations are evaluated together with kinetics results, and vice versa, to propose what is the most likely mechanism based on the available data.[26]

Today, 90% of industrial scale chemical reactions use catalysis, and 35% of the global GDP (Gross Domestic Product) is based on catalysis. Catalysis has a prominent role in chemical industry, pharmaceuticals, agrochemicals, waste remediation technologies, diagnostics, energy harvesting technologies, and global manufacturing of goods. Its impact on society and human life is so profound, that two of the most important technologies that contributed to shape the modern world are based on catalysis. Without the Haber-Bosch process for ammonia synthesis, that uses an iron catalyst to react nitrogen and hydrogen gases, the world's population growth to 8 billion people would have been impossible. Indeed, ammonia is used for making fertilizers, and 50% of our body's nitrogen nowadays comes from synthetic ammonia produced with a catalytic reaction.[16a] Years later, Ziegler's and Natta's work on soluble titanium catalysts for the stereocontrolled polymerization of olefins was the sparkle that ignited the large scale production of polymers and plastics that revolutionized our daily life.[27]

These two milestone examples are instrumental to introduce an important difference in the types of catalysts. Heterogeneous catalysts, such as those use in the Haber-Bosh process, reside in a different phase (almost always a solid phase) than the starting materials and products. With homogeneous catalysts, like the one used in the Ziegler-Natta polymerization, all components reside in the same phase (almost always a liquid phase). Heterogeneous catalysts have the advantage of making catalyst separation from the product straightforward, and generally tend to be more stable even at high temperatures and retain their activity longer. These advantages, though, come with

[26] M. Beller, A. Renken, R. A.van Santen, *Catalysis: From Principles to Applications.* Wiley-VCH: Weinheim, **2012**.
[27] W. Kaminsky, *Polyolefins: 50 years after Ziegler and Natta I.* Springer Berlin: Heidelberg, **2013**.

some drawbacks. The reaction is only occurring at the interphase (*i.e.* the surface of the catalyst), so that mass transfer issues can make reaction kinetics potentially more sluggish. Furthermore, the study of the molecular aspects of the process is more difficult, requiring less "conventional" spectroscopic/imaging techniques, somewhat hampering rational design. Homogeneous catalysts, being molecularly defined compounds, can be studied relatively more easily by using conventional spectroscopic techniques, and offer the possibility to synthetize putative intermediates of the catalytic process to help the understanding of the mechanism. Also, as every component is within the same phase, the reaction can take place in any part of the solution, being each molecule of the catalyst readily accessible to the reactants. Homogeneous catalysis can often take place under much milder conditions than heterogeneous catalysts, making it more suitable for application to fine chemicals. These differences between the two technologies have made so that they are applied by different chemical communities: heterogeneous catalysis is the most used technology in large scale chemical industries, while homogenous catalysis dominates in organic synthesis, although there are several exceptions and significant efforts have been done to bridge this gap (and two conceptual examples will be provided in this thesis).[26]

The impact of catalysis in synthetic organic methodology is paramount. Indeed, most of the progress in synthetic methods in the last 40 years has been dealing with catalytic systems, as testified by the notable achievements and Nobel Prizes mentioned in the last part of the previous section. The simple concepts underlying catalysis put it in the position of serving an enabling role for synthetic organic chemistry in multiple ways. Catalysis can be used to speed up a recalcitrant transformation, and/or to realize it under milder, advantageous conditions; it can steer the selectivity of a given process; even more importantly, it can make possible otherwise unimaginable transformations, providing new synthetic handles and heightened retrosynthetic strategies; the understanding of a catalytic mechanism can give valuable, fundamental insight into new and established reactivity and deepen our knowledge of the chemical world; it can greatly reduce the amount of waste and coproducts with respect to stoichiometric

methods, providing cost-effective entry to valuable chemical structures with improved atom economy.

Starting from the first catalytic systems, mainly based on Brønsted and Lewis acids and bases (that still constitute valuable systems and solutions and are routinely used also in conjunction with other types of activation) and metal powders, catalysis has grown in sophistication and capabilities with the invention of new methods. A major breakthrough with concern to fine chemicals synthesis was Wilkinson's discovery of homogeneous hydrogenation with $RhCl(PPh_3)_3$.[28] His work crowned previous contributions in the field of metal coordination complexes, such those from Werner (Nobel Prize for coordination chemistry in 1923), Roelm (cobalt carbonyl catalyst for hydroformylation of olefins) and Wacker (Pd/Cu catalyzed oxidation of ethylene), and set the stage for the development of transition metal based catalysis, which dominated most part of the century. The ability of metal complexes to engage processes such as transmetalation, oxidative addition, reductive elimination, migratory insertion, and the possibility of tailoring the ligands around the metal center to tune the catalytic activity (including the use of chiral ligands for asymmetric induction) gave chemists great opportunities for developing new homogeneous catalytic reactions, ultimately culminated in the powerful methodologies for C-C and C-N bond formation routinely used today.[29]

Another "pillar" in catalytic methods is represented by biocatalysis, that identifies the use of enzymes as catalysts for synthetic applications. The birth of the discipline can be traced back to 1926, when James Sumner isolated urease and crystallized it, demonstrating that it was a protein.[30] Enzymes are highly complex architectures, with tertiary and often quaternary structure, that can be thought of as catalytically active centers (whose nature depends on the class of the enzyme) with a proteic backbone acting as a complex macro-ligand. These biological catalysts can promote transformations elusive to realize by purely chemical means, offering different

[28] J. A. Osborn, F. H. Jardine, J. F. Young, G. Wilkinson, *J. Chem. Soc. A*, **1966**, 1711–1732.
[29] C. C. C. Johansson Seechurn, M. O. Kitching, T. J. Colacot, V. Snieckus, *Angew. Chem. Int. Ed.* **2012**, *51*, 5062–5085.
[30] J. B. Sumner, *J. Biol. Chem.* **1926**, *69*, 435–441.

perspectives in synthetic strategies, are often highly chemo-, regio- and stereoselective (allowing access to highly sought-after optically pure compounds) and are associated with reduced environmental and safety concerns.[31] Their strengths come with the drawbacks of limited stability to non-aqueous solvents, pH and temperature (given the necessity to maintain their tertiary or quaternary structure in order to be active) and sometimes narrow scope given their sometimes very high specificity towards their natural substrate, although exceptions are known. Nowadays, many enzymes can be genetically engineered to tailor selectivity and substrate pool, and are recombinantly expressed in bacterial hosts. Use of purified enzymes, whole cells or extract of even immobilization on solid supports are employed.[26]

The early 2000s witnessed the introduction of a new system, dubbed "asymmetric organocatalysis".[32] Although small organic molecules have long been known to catalyzed various processes (Knoevenagel, esterifications, Stetter reaction to name a few), their power in inducing significant enantiocontrol was largely unforeseen, which also contributed to the great success of transition metal catalysis. Building on previous scarce reports,[33] MacMillan and List, among others, showed that the use of chiral, five membered cyclic secondary amines constitutes a general activation mode of carbonyl compounds that can be used in a great number of reactions to access enantioenriched structures in very high optical purity. Several other kind of catalysts and activation modes, based on either covalent or non-covalent interactions have been developed, such as the use of chiral phosphoric acids, stabilized carbenes, thioureas and quaternary ammonium salts.[34] The field advanced very rapidly, to the point that nowadays asymmetric organocatalysis effectively earned a place right next to bio- and metal catalysis as a mature catalytic technology.

The evolution of catalytic methodologies still retains immense interest, and numerous catalytic strategies are investigated in the contemporary era. Already in 1990, in his

---

[31] E. L. Bell, W. Finnigan, S. P. France, A. P. Green, M. A. Hayes, L. J. Hepworth, S. L. Lovelock, H. Niikura, S. Osuna, E. Romero, K. S. Ryan, N. J. Turner, S. L. Flitsch, *Nat. Rev. Methods Primers* **2021**, *1*, 46.
[32] D. W. C. MacMillan, *Nature* **2008**, *455*, 304–308.
[33] a) Z. G. Hajos, D. R. Parrish, *J. Org. Chem.* **1974**, *39*, 1615–1621; b) E. J. Corey, M. J. Grogan, *Org. Lett.* **1999**, *1*, 157–160.
[34] B. List, *Chem. Rev.* **2007**, *107*, 5413–5415.

famous paper “Organic Synthesis – Where now?”, Dieter Seebach stated that “the primary center of attention for all synthetic methods will continue to shift toward catalytic and enantioselective variants”.[35] Indeed, despite the increasing efforts made in recent time towards the development of new, stoichiometric reagent systems,[36] Seebach’s prediction was essential correct in foreseeing the central role of catalytic methodologies in the following years. Several contemporary catalytic methodologies will be highlighted in the next chapter.

[35] D. Seebach, *Angew. Chem. Int. Ed.* **1990**, *29*, 1320–1367.
[36] D. Y.-K. Chen, *Isr. J. Chem.* **2018**, *58*, 85–93.

1.3 Modern synthetic endeavors

The craft of synthesis grew so sophisticated and powerful that chemists can nowadays construct, with enough time and effort, nearly any conceivable structure. A striking example came in 2013 from Danishefsky, who achieved the total synthesis of a homogeneous, wild- type erythropoietin (EPO) with a relative molecular mass of 17868 Da, setting a new milestone in natural product synthesis.[37] These expanding boundaries, together with the evolution of the needs of society, require the chemical community to continuously reassess the paradigms of their time and provide inspiration to set new landmarks.[38]

The urgent issues of sustainability, environmental concerns, and resources exhaustion provoked a shift in focus in the community towards the development of methods that permit expedient access to high-value molecules in an economical, sustainable, and safe manner. In other words, today's organic chemist goal is to come up with general methodologies that can shape a great variety of diversified cores with their inherent selectivity in a rapid and efficient way, while fulfilling the requirements of atom-, step- and redox-economy, tolerance over the largest possible number of common functional groups, minimization of hazardous wastes and reagents and economical sustainability.[39] This new directions were already foreseen in 1975, when Hendrikson defined the "ideal synthesis" as one which: "…creates a complex molecule… in a sequence of only construction reactions involving no intermediary refunctionalizations, and leading directly to the target, not only its skeleton but also its correctly placed functionality".[40] In this context, Nature's efficiency and elegance in crafting her most complex architectures with spectacular selectivity represent for chemists an unmatched source of inspiration and insight into fundamental principles. Ultimately, practitioners should aspire to elevate their capabilities to the standards of

[37] P. Wang, S. Dong, J.-H. Shieh, E. Peguero, R. Hendrickson, M. A. S. Moore, S. J. Danishefsky, *Science* **2013**, 342, 1357–1360.
[38] G. M. Whitesides, *Angew. Chem. Int. Ed.* **2015**, *54*, 3196–3209.
[39] M. J. O'Neill, J. Cornella, *Chimia* **2018**, *72*, 601.
[40] J. B. Hendrickson, *J. Am. Chem. Soc.* **1975**, *97*, 5784.

Nature and possibly beyond that. To reach this ambitious goal, great effort must be dedicated towards basic research for investigation of new and elusive reactivity, with particular interest in permitting the utilization of native functionalities, thus avoiding prefunctionalization as much as possible.

These concepts and directions underpin the Key Green Chemistry Research Areas defined by the ACS Green Chemistry Institute® Pharmaceutical Roundtable in 2006 and updated in 2018.[41] The areas that made the top ten are:

1) Development of effective and versatile methodology utilizing cheap/sustainable metals.

2) General methods for catalytic/sustainable (direct) amide or peptide formation.

3) Aliphatic and aromatic C–H activation, using green oxidants and giving predictable site-selectivity.

4) Amide reductions avoiding $LiAlH_4$ and diborane.

5) Direct substitution of alcohols.

6) Catalyst immobilization without significant loss in kinetics.

7) Asymmetric hydrogenation of unfunctionalized olefins/enamines/imines.

8) Improved fluorination/trifluoromethoxylation.

9) Wittig chemistry without $Ph_3P{=}O$.

10) Alternatives for oxidations, C–O or C–N redox processes.

One can see that even a cornerstone transformation such as formation of the amide bond, that is the most widely used reaction in the pharmaceutical context, are far from being done improving. In fact, these heavily relied-on processes are the most sought-after to perfect, given the central place they occupy in synthesis.

A special mention must be made about medicinal chemistry. Indeed, medicinal chemists that prepare drug candidates for clinical testing represent the vast majority of practitioners of organic synthesis. The fast pace of drug development implies that after identification of a potential lead compound, a plethora of structural analogs must be supplied and evaluated in the shortest possible time. This in turn orients chemists

[41] M. C. Bryan, P. J. Dunn, D. Entwistle, F. Gallou, S. G. Koenig, J. D. Hayler, M. R. Hickey, S. Hughes, M. E. Kopach, G. Moine, P. Richardson, F. Roschangar, A. Steven, F. J. Weiberth, *Green Chem.* **2018**, *20*, 5082–5103.

towards the utilization of methodologies that are reliable, require easily accessible starting materials and are tolerant of the many functional groups exhibited by bioactive compounds.[42] Moreover, important concepts such as late-stage-functionalization amenability and scalability can play a significant role in evaluating a methodology.[43] The high throughput of analogues that is required can force chemists to *de novo* synthesis of the lead scaffold to accommodate the right substituents, a tedious process that is obviously detrimental to the cost- and time-efficiency of drug discovery and somewhat limits the diversity evaluated. Mild, selective methods that permit functionalization at a late stage of the synthesis without requiring the installation of a reactive functionality beforehand (LSF) provide an extremely valuable shortcut to the desired analogues; on the other hand, when the final compound is identified, it is then necessary to prepare it in large, industrial scales, which requires scalability of the synthesis. If this is not the case, then additional re-optimization and possibly re-design of the whole synthetic strategy must be done, with all the consequent drawbacks.[44]

It is also extremely important to note that biases in synthetic methods, *i.e.* the ease of access to certain motifs in expense to others, will inevitably result in biases in the molecular architectures evaluated for drug discovery, with the consequence of possibly missing out on better performing scaffolds, and uneven population of the chemical space. A real-life example of this bias can be found in the overpopulation of sp^2 hybridized carbons with respect to sp^3 ones in drug candidates, and especially in the much higher frequency of *para-para* disubstituted biaryls over other substitution patterns. This has been the natural consequence of the impact of transition metal (palladium above all) cross-coupling reactions, that permit fast, modular and reliable assembly of such aromatic structures and are therefore are highly used in medicinal chemistry synthesis.[45] In present years, significant effort has been devoted by the academic realm towards the development of new methodologies that fulfill the outlined

[42] D. G. Brown, J. Boström, *J. Med. Chem.* **2016**, *59*, 4443−4458.
[43] J. Börgel, T. Ritter, *Chem* **2020**, *6*, 1–11.
[44] T. Cernak, K. D. Dykstra, S. Tyagarajan, P. Vachalb, S. W. Krska, *Chem. Soc. Rev.* **2016**, *45*, 546.
[45] K. R. Campos, P. J. Coleman, J. C. Alvarez, S. D. Dreher, R. M. Garbaccio, N. K. Terrett, R. D. Tillyer, M. D. Truppo, E. R. Parmee, *Science* **2019**, *363*, 244.

general goals. As predicted by Seebach, the key role that catalysis has been playing in these endeavors cannot be overstated. Indeed, two of the aforementioned ten key areas directly use the term "catalyst" (2 and 6), and several other ones (1, 3, 5, 7 at least) are most likely to be tackled in a catalytic regime. An important general trend is represented by the renaissance of the utilization of radicals as reactive intermediates, largely fueled by new methods that permit access to such species under mild conditions. The idea of "radical retrosynthesis" is rapidly catching on, offering opportunities to complement established polar logic with "polarity agnostic" disconnections that feature different handles (including making use of innate reactivity), thus providing orthogonality to classical transformations and different selectivity patterns.[46] Among the most significant research topics evolving in recent years we find: development of cheap, non-precious transition metal catalysts as well as main group-based catalysts; chemo-, regio- and stereo-selective mild methods for C-H (and in minor extent C-C) functionalization; photochemical and electrochemical methods; asymmetric organocatalysis; biocatalysis; strategies for scaffold hopping and single atom editing logic.[47] Some selected examples with a brief outline of their underlying concepts will be presented in the following text.

The high costs, short or fluctuating supply, potential toxicity and significant environmental footprint associated with extraction and isolation are significant drawbacks of late transition metal catalysts commonly used in both medicinal chemistry and drug manufacturing settings. Earth abundant metals potentially offer not only solutions to these drawbacks (being generally cheaper, widely available and less toxic and therefore allowed in higher limits in APIs), but room for new reactivity and the activation of unconventional or challenging substrates. Nickel, copper and iron catalysts are particularly appealing;[48] however, challenges hindering the effective implementation of such systems are the usually higher catalysis loadings, less

[46] J. M. Smith, S. J. Harwood, P. S. Baran, *Acc. Chem. Res.* **2018**, *51*, 1807−1817.
[47] a) Y. Hu, D. Stumpfe, J. Bajorath, *J. Med. Chem.* **2017**, *60*, 1238−1246; b) J. Jurczyk, J.Woo, S. F. Kim, B. D. Dherange, R. Sarpong, M. Levin, *Nat. Synth.* **2022**, *1*, 352–364.
[48] F. Buono, T. Nguyen, B. Qu, H. Wu, N. Haddad, *Org. Process Res. Dev.* **2021**, *25*, 1471–1495.

predictable or erratic reactivity, narrower scope and non-trivial identification of general ligand structures for wide arrays of transformations.[41]

Starting from 2013, the Martin group has been showing the competence of nickel catalysis under reductive conditions for the fixation of carbon dioxide (CO_2) into various organic electrophiles. Direct utilization of CO_2 in carboxylation reactions is a highly valuable strategy for the utilization of this abundant, non-toxic greenhouse gas for the synthesis of ubiquitous carboxylic acids. In 2017, a striking protocol for the convergent carboxylation of regioisomeric mixtures of halogenated alkanes at a remote site was documented. By judicious choice of a phenanthroline ligand bearing bulky *ortho*-substituents, the authors were able to accelerate, after (net) oxidative addition at a secondary position, the often unwanted β-hydride elimination process, turning it into a desirable event to convergently access primary alkyl Ni(I) intermediates that are competent in CO_2 trapping (**Scheme 1**). Even more interestingly, a remarkable selectivity switch was reported by varying the temperature when an ester or amide moiety is present in the substrate. While at 10 °C the preferred product is the linear carboxylic acid, the branched product at the α position of the carbonyl group is formed with exquisite selectivity by simply raising the reaction temperature to 42 °C.[49]

[49] F. Juliá-Hernández, T. Moragas, J. Cornella, R. Martin, *Nature* **2017**, *545*, 84−88.

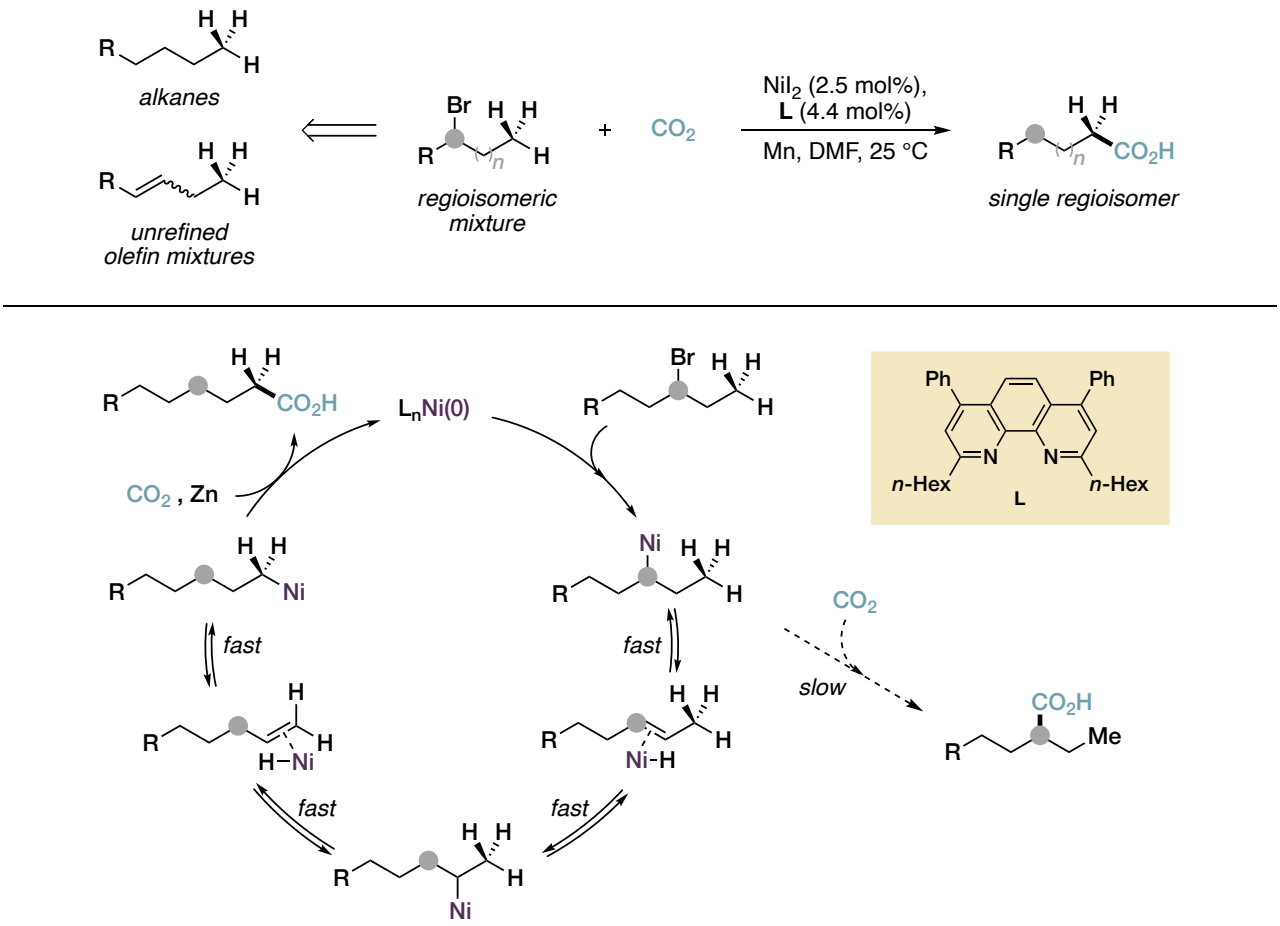

Scheme 1. Martin's regioconvergent remote carboxylation of alkyl bromides. Top: reaction conditions. Middle: proposed catalytic cycle for the chain-walking carboxylation event. Bottom: regiochemistry switch by varying the reaction temperature.

In 2016 the Baran group introduced the use of *N*-acyloxyphthalimides (dubbed "redox active esters", RAEs) as alkyl radical precursors upon reduction and subsequent decarboxylation, enabling the use of ubiquitous carboxylic acids as Csp^3 synthons in nickel catalyzed cross couplings. The ability of nickel to access open shell oxidation states makes possible to interface nickel catalysis with the generation of radical species, offering greatly enhanced possibilities for forging C-C bonds using unconventional retrosynthetic disconnections. An outstanding achievement of this kind of chemistry is

the Csp^3- Csp^3 cross coupling of RAEs with alkyl zinc reagents, enabling the formation of 1°-1°, 1°-2° and 1°-3° alkyl linkages, that would otherwise be extremely challenging to forge, with outstanding functional group tolerance (**Scheme 2**).[50] The authors demonstrated very interesting applications of this chemistry in the synthesis of pharmaceutical target analogues, and the tool of "decarboxylative cross coupling" is already showing an impact in medicinal chemistry strategies.[51]

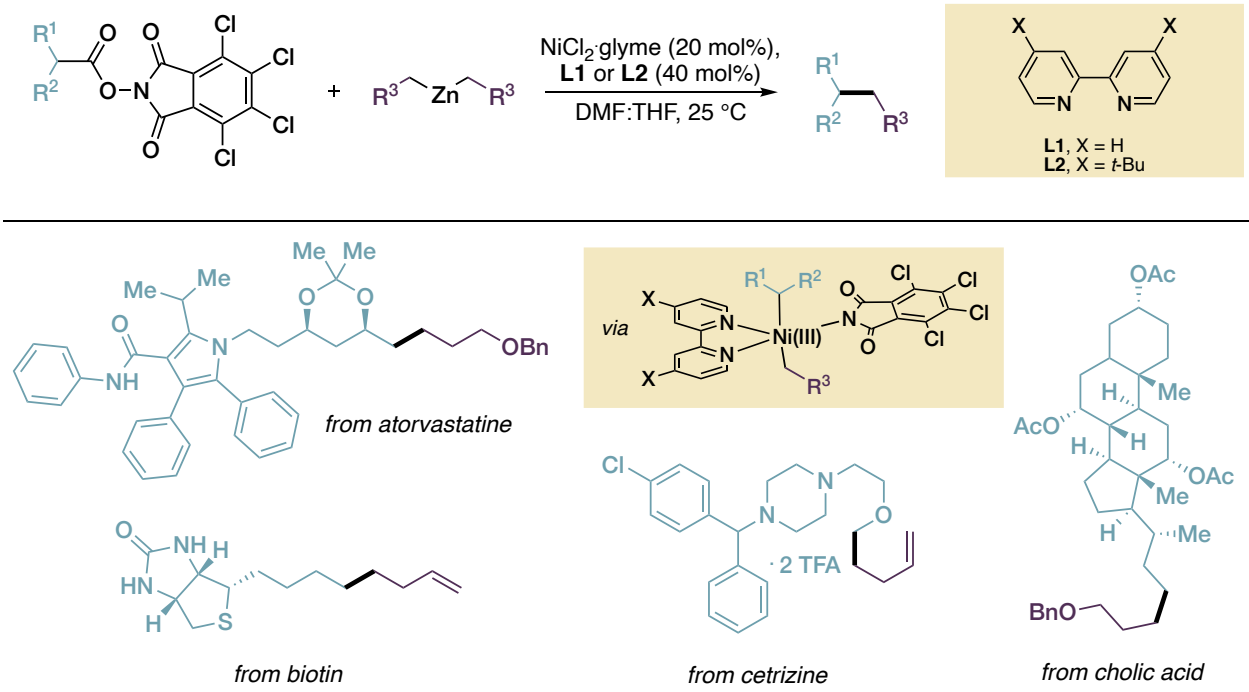

Scheme 2. Top: Baran's nickel catalyzed Csp^3-Csp^3 cross-coupling of unactivated alkyl fragments using RAEs and dialkylzinc reagents. Bottom: pharmaceutically relevant examples.

C-H functionalization offers the immense advantage of avoiding the necessity for prefunctionalized substrates, by using ubiquitous C-H bonds as synthetic handles. This approach poses the inherent challenge of achieving selectivity in such activation, given the plethora of different C-H bonds occurring in organic molecules. Radical generation via H atom abstraction, insertion of carbenes and nitrenes, or formation of

[50] T. Qin, J. Cornella, C. Li, L. R. Malins, J. T. Edwards, S. Kawamura, B. D. Maxwell, M. D. Eastgate, P. S. Baran, *Science* **2016**, *352*, 801–805.
[51] G. Laudadio, M. D. Palkowitz, T. E.-H. Ewing, P. S. Baran, *ACS Med. Chem. Lett.* **2022**, *13*, 1413–1420.

organometallic species by means of oxidative addition, deprotonation-metalation or σ-bond metathesis have all been shown viable approaches.[52] Metal catalyzed transformations that do not involve formation of organometallic species are also known, albeit rarer.[53] Further distinction can be done, in the realm of metal catalyzed C-H activation, between directed and non-directed approaches. Directed approaches use permanent or transient directing groups bound to the substrate to achieve selectivity in the metalation step, while non directed approaches capitalize on innate reactivity, such as steric and electronic biases, or in the use of templating ligands capable of interaction with the substrate.[54]

In 2014, a milestone achievement in the field was reported by Hartwig and coworkers. They developed a highly selective iridium catalyzed, non-directed C-H borylation of N-heteroarenes, proceeding under mild conditions with only 0.5 mol% catalyst loading. This methodology features general rules for selectivity predictions and has already been adopted within the pharmaceutical industry (**Scheme 3**).[55]

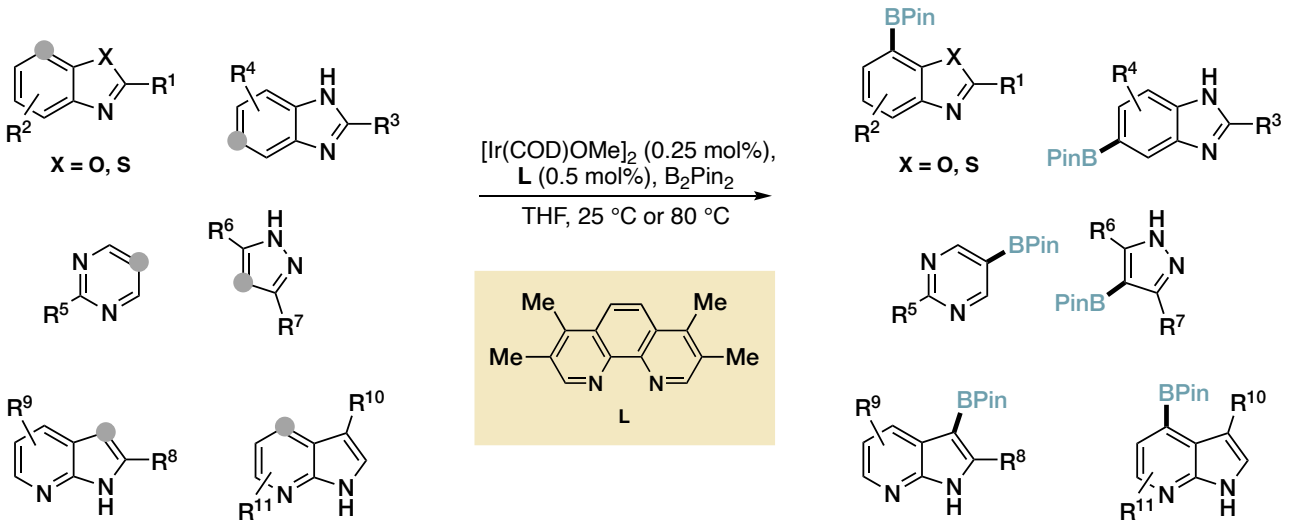

Scheme 3. Iridium catalyzed regioselective Csp^2-H borylation of azines.

[52] L. Guillemard, N. Kaplaneris, L. Ackermann, M. J. Johansson, *Nat. Rev. Chem.* **2021**, *5*, 522–545.
[53] K. Yamamoto, J. Li, J. A. O. Garber, J. D. Rolfes, G. B. Boursalian, J. C. Borghs, C. Genicot, J. Jacq, M. van Gastel, F. Neese, T. Ritter, *Nature* **2018**, *554*, 511–514.
[54] T. Dalton , T. Faber, F. Glorius, *ACS Cent. Sci.* **2021**, *7*, 245−261.
[55] M. A. Larsen, J. F. Hartwig, *J. Am. Chem. Soc.* **2014**, *136*, 4287.

Very recently, employing palladium catalysis, Yu has reported the *ortho* C-H hydroxylation of benzoic and phenylacetic acids using aqueous H_2O_2 as the oxidant. The transformation is made possible by the identification of a bidentate carboxylic acid-pyridone ligand, uses as low as 1% loading of the catalyst and does not need any exclusion of water or oxygen, featuring excellent scalability. Indeed, hydroxylation of ibuprofen was documented on a 200 gram scale (**Scheme 4**).[56]

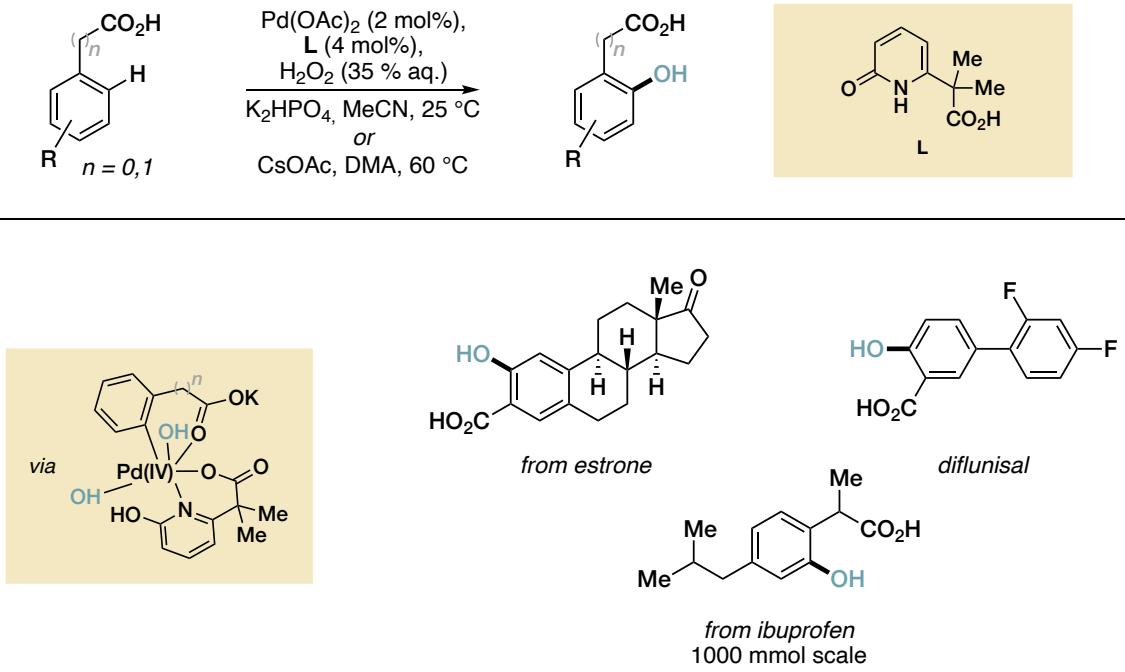

Scheme 4. Palladium catalyzed Csp^2-H hydroxylation of phenylacetic and benzoic acids using industrial grade hydrogen peroxide as oxidant.

In 2012, Baran reported on the facile synthesis of various zinc (fluoro)alkyl sulfinate salts from the corresponding sulfonyl chlorides and the use of such salts for the (fluoro)alkylation of a wide array of azines (**Scheme 5**). The reaction proceeds via a radical pathway under oxidative, Minisci-like conditions, and permits expedient access to a wide variety of analogues that would be arguably possible to make otherwise, albeit with sometimes only modest selectivity. Note that, in a LSF context, a poor

[56] Z. Li, H. S. Park, J. X. Qiao, K.-S. Yeung, J.-Q. Yu, *J. Am. Chem. Soc.* **2022**, DOI: 10.1021/jacs.2c08332.

selectivity can be not problematic: on the contrary, having simultaneous access to various isomers can turn out to be convenient in high throughput screening.[57]

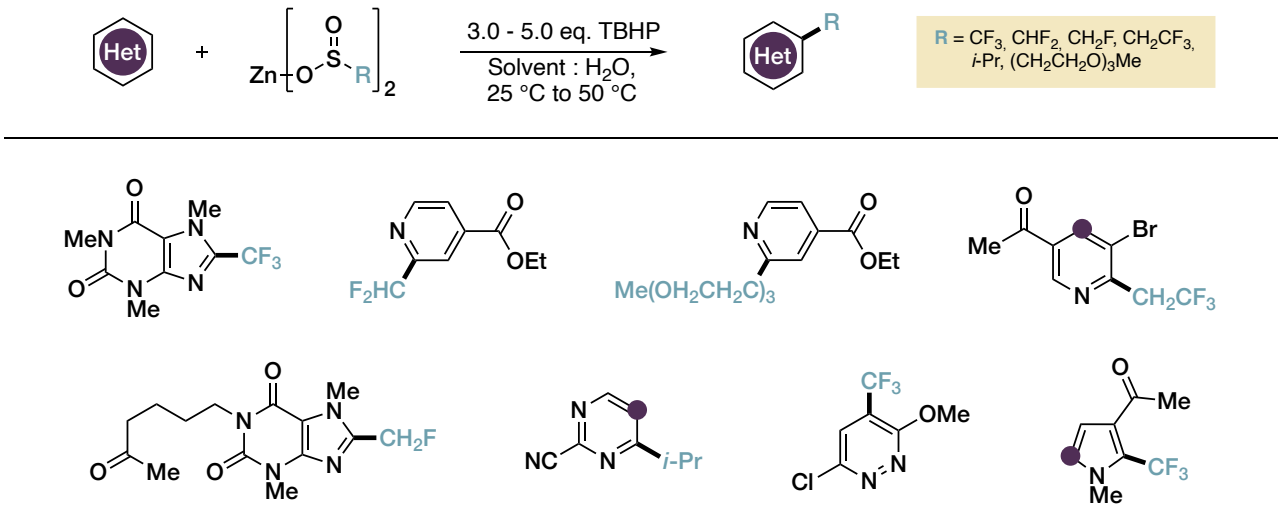

Scheme 5. Non-catalytic radical (fluoro)alkylation of various azines with zinc sulfinates developed by the Baran group. TBHP = *tert*-butyl hydroperoxide. The purple dot denotes the minor alkylation site.

In 2016 the Dong group reported an interesting rhodium catalyzed sequence of C-C and C-H activation for the conversion of β-aryl cyclopentanones to tetralones. This outstanding skeletal rearrangement requires an aminopyridine cocatalyst to allow the formation of a transient directing group and is thermodynamically driven by the formation of an aryl ketone from a less stable alkyl one, that permits to overcome the unfavorable equilibrium for the reversible C-C insertion (**Scheme 6**).[58]

[57] Y. Fujiwara, J. A. Dixon, F. O'Hara, E. D. Funder, D. D. Dixon, R. A. Rodriguez, R. D. Baxter, B. Herle´, N. Sach, M. R. Collins, Y. Ishihara, P. S. Baran, *Nature* **2012**, *492*, 95–99.
[58] Y. Xia, G. Lu, P. Liu, G. Dong, *Nature* **2016**, *539*, 546–550.

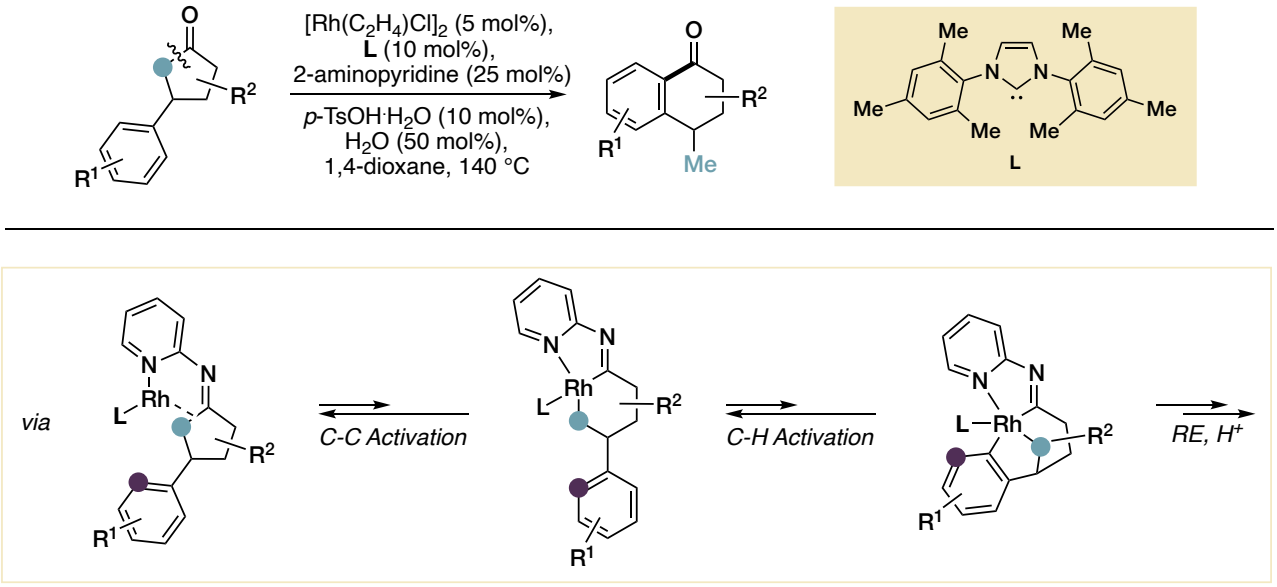

Scheme 6. Synthesis of tetralones from β-aryl cyclopentanones via a C-C and C-H bond activation sequence, using a transient directing group (2-aminopyridine) strategy under rhodium catalysis.

Photochemical methodologies using visible light have dramatically expanded in the latest years. Although photochemistry has been studied since decades, the use of high energy light sources often precluded application to functionalized substrates. The introduction of catalysts capable of absorbing light in the visible region to access an electronic excited state long-lived enough to interact with substrate molecules (*i.e.* photocatalysts) has prompted the blossoming of photocatalytic methodologies for synthetic purposes.[59] These electronically excited species engages energy or more often electron transfer with the reactant(s) yielding an intermediate (usually a radical-cation or -anion) that further evolves to the desired products, while the photocatalyst is regenerated by a subsequent electron transfer. These single electron transfer (SET) pathways often imply the intermediacy of radical species in this kind of methodologies. An interesting example of photochemically enabled reactivity was reported by the Melchiorre group in the context of direct substitution of allylic alcohols.[60] The employment of an iridium catalyst bearing a chiral phosphoramidite-olefin ligand was

[59] a) M. H. Shaw, J. Twilton, D. W. C. MacMillan, *J. Org. Chem.* **2016**, *81*, 6898−6926; b) D. Ravelli, M. Fagnoni, A. Albini, *Chem. Soc. Rev.* **2013**, *42*, 97–113.
[60] G. E. M. Crisenza, A. Faraone, E. Gandolfo, D. Mazzarella, P. Melchiorre, *Nat. Chem.* **2021**, 13, 575−580.

merged with visible light excitation to yield an excited Ir(III) allyl complex capable of performing SET oxidation of dihydropyridines (DHP), producing α-amino radicals then trapped at the metal center (**Scheme 7**). Enantioselective formation of a C-C bond at the allylic position via reductive elimination yields highly enantioenriched products (in very high branched:linear regioisomeric ratio) that would be challenging to make from the corresponding carbon pronucleophiles under a polar manifold.

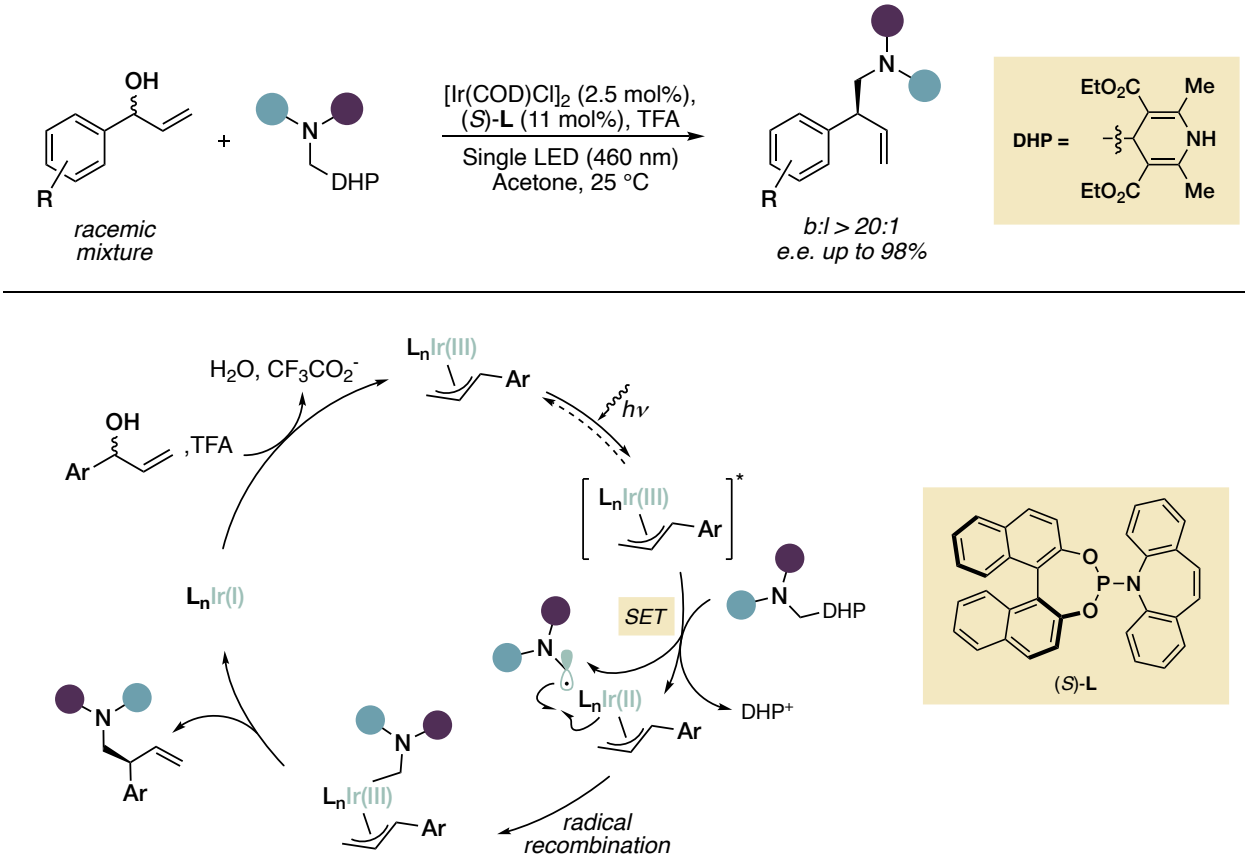

Scheme 7. Enantioselective, direct substitution of allylic alcohols with α-amino carbon nucleophiles promoted by iridium photoredox catalysis. The symbol * denotes an excited electronic state.

In 2020, the MacMillan and Hyster reported a remarkably elegant methodology for the kinetic dynamic resolution of racemic β-substituted cyclic ketones by merging organo-, photo- and biocatalysis (**Scheme 8**).[61]

[61] J. S. DeHovitz, Y. Y. Loh, J. A. Kautzky, K. Nagao, A. J. Meichan, M. Yamauchi, D. W. C. MacMillan, T. K. Hyster, *Science* **2020**, *369*, 1113−1118.

The protocol capitalizes on an organophotoredox cycle to induce a racemization equilibrium of the ketone starting material, proceeding by its condensation with one of the two organocatalysts (a racemic α-substituted pyrrolidine) and subsequent oxidation of the intermediate enamine by the excited state of the Ir(III) photocatalyst (**Scheme 8**). Deprotonation of the radical cation intermediate furnishes a pivotal radical species at the original β position with loss of stereochemistry, that after hydrogen atom transfer (HAT) from a thiol (the second organocatalyst) and liberation of the amine yields back the ketone. Reduction of the thiyl radical by reduced Ir(II) enables turnover of the two species. Kinetic resolution is operated biocatalytically using a ketoreductase yielding enantiopure γ-substituted cycloalkanols in very high diastereomeric ratio. The NADPH required as a cofactor for the enzymatic reduction can also be used catalytically by simply using an exogeneous reductant, in this case an excess of alcohol solvent. Both five and six membered ketones can be used, and extension to the use of aminotransferases for accessing enantioenriched amines in place of alcohols is viable. A striking feature of this work is the productive coexistence of four catalytic cycles working in synergy.

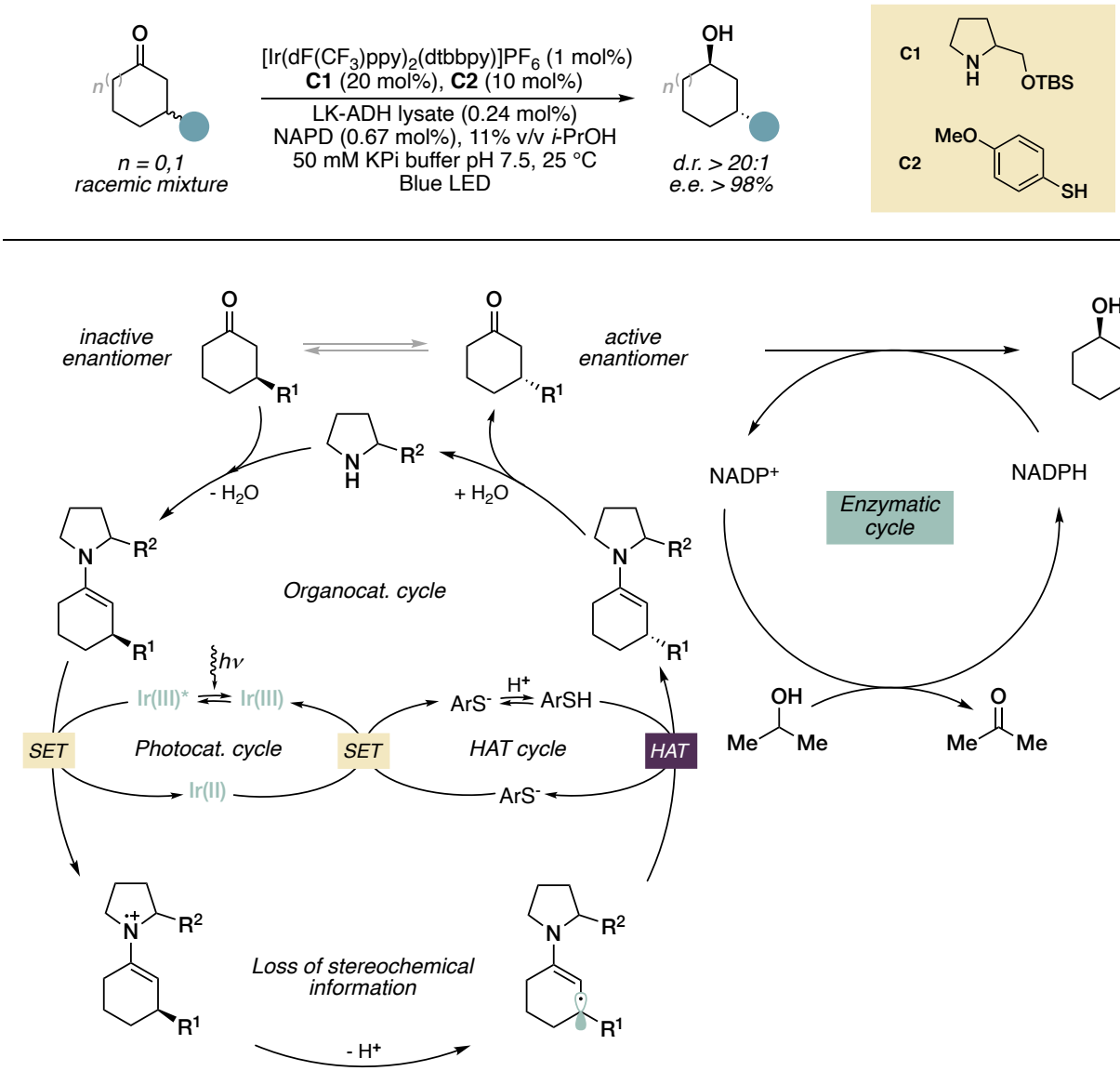

Scheme 8. Merging of photoredox-, organo- and biocatalysis for the kinetic dynamic resolution of racemic β-substituted cyclic ketones.

Electrochemical methods are now living a renaissance in synthetic organic chemistry. Investigations on electrochemistry date back way far, with the venerable Kolbe reaction that was in fact reported by Faraday already in 1834, and continued throughout the whole century with significant advancement.[62] Despite these results and the development of electrochemical processes on large scale in the industrial world, the wide adoption of this technology in academic settings or in fine chemicals synthesis is

[62] Y. Kawamata, P. S. Baran, *Joule* **2020**, *4*, 701–704.

a relatively recent trend. This has likely been due to the discouraging perception of electrochemistry as an "obscure" practice, involving heterogeneous processes, non-standardized apparatuses, and an additional number of variables to evaluate (nature of electrodes, current intensity, electrolytes etc.), making practitioners often choose more intuitive or "less cumbersome" pure chemical routes.[63] In fact, electrochemistry embodies a very simple and intimate activation concept, by directly providing or removing an electron from the substrate via application of an electric potential, without the need of any chemical reactant. This aspect makes electrochemical activation intrinsically atom-economical, and the possibility of careful tuning of the redox potential in a non-discrete manner gives room for unique selectivity profiles and reactivity.[64] A striking example of electrochemically enabled reactivity was reported very recently by the Baran group. The authors were able to achieve practical, scalable reductive electrochemical conditions for the partial reduction of arenes, in a Birch-like protocol that obviates the need for lithium metal and liquid ammonia.[65] Key to the success of the protocol are a Li-ion batteries chemistry inspired additive, namely tris(pyrrolidino)phosphoramide (TPPA), that is thought to inhibit the formation of a passivated layer at the cathode, and the use of dimethylurea (DMU) as proton donor (**Scheme 9**). Magnesium or aluminum can be used as sacrificial anodes. Mechanistic investigations ruled out the intermediacy of Li(0) or solvated electrons, suggesting a sequence of reduction of the arene substrate, protonation of the resulting radical anion, followed by further reduction and protonation. This method features good chemoselectivity, does not require exclusion of water or oxygen, was scaled up to 100 g scale and demonstrated competent for other reductive transformations such as debenzylation, epoxide and aziridine opening, McMurry coupling and ketone reduction.

---

[63] C. Kingston, M. D. Palkowitz, Y. Takahira, J. C. Vantourout, B. K. Peters, Y. Kawamata, P. S. Baran, *Acc. Chem. Res.* **2020**, *53*, 72−83.
[64] M.Yan, Y. Kawamata, P. S. Baran, *Chem. Rev.* **2017**, *117*, 13230−13319.
[65] B. K Peters, K. X Rodriguez, S. H Reisberg, S. B. Beil, D. P Hickey, Y. Kawamata, M. Collins, J. Starr, L. Chen, S. Udyavara, K. Klunder, T. J. Gorey, S. L Anderson, M. Neurock, S. D Minteer, P. S. Baran, *Science* **2019**, *363*, 838–845.

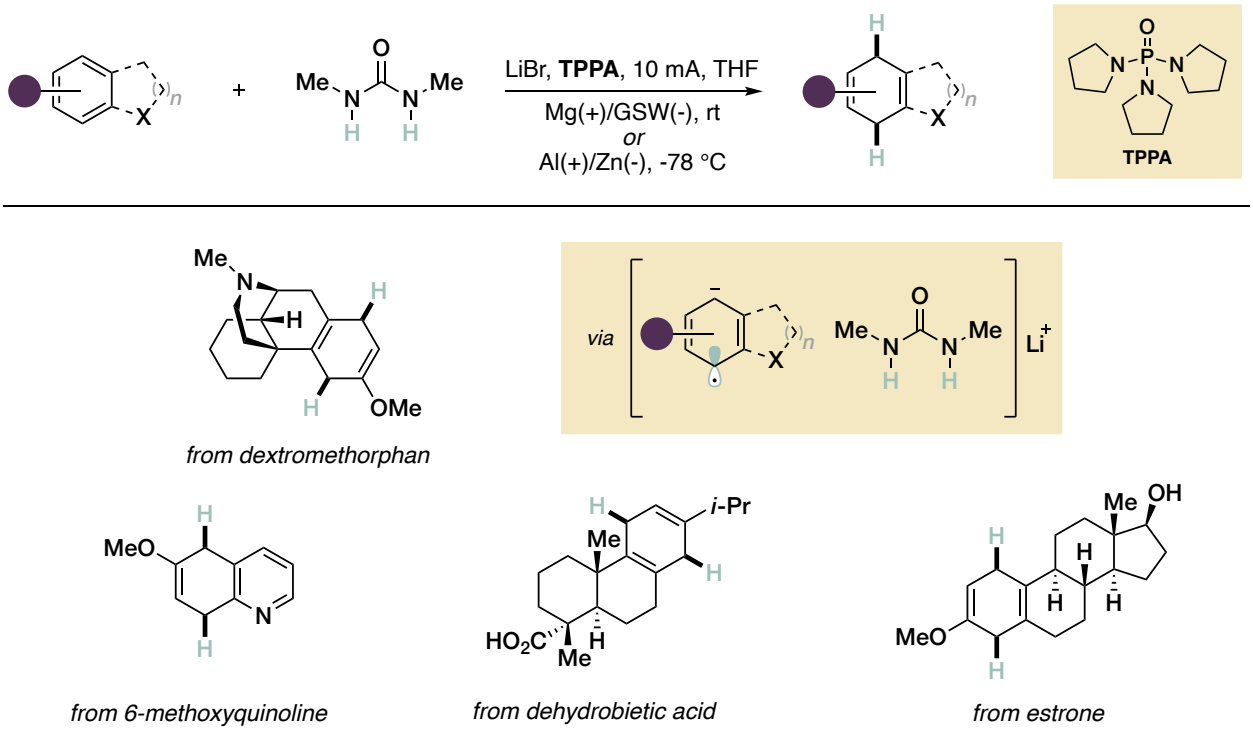

Scheme 9. Electrochemical, lithium metal- and ammonia-free Birch reduction of (hetero)arenes. Two different sets of electrodes can be used depending on the substrate, and a great functional group was demonstrated (protic groups that should be protected in a normal Birch protocol are well tolerated). Stabilization of the intermediate reduced arene radical anion by DMU as an ion pair with a lithium ion is thought to be important and precede protonation. X = NR, CH.

Another interesting example of the benefits of electrochemical conditions came in 2019 from Mei and coworkers, who developed an electrocatalytic methodology for the base-free cross coupling between aryl halides and aromatic thiols at room temperature.[66] Such C-S coupling usually requires elevated temperatures and strong bases such as KO*t*-Bu to quantitatively deprotonate the thiol and is non-trivial, given the propensity of thiolates to strongly bind to transition metals. With the use of an inexpensive Ni precatalyst and ligand, the transformation was electrochemically enabled without any added base using (hetero)aryl bromides and chlorides as coupling partners with vast functional group tolerance (**Scheme 10**). Formation of thiyl radicals was demonstrated, although the authors were unable to define a conclusive mechanism at this stage.

[66] D. Liu, H.-X. Ma, P. Fang, T.-S. Mei, *Angew. Chem. Int. Ed.* **2019**, *58*, 5033–5037.

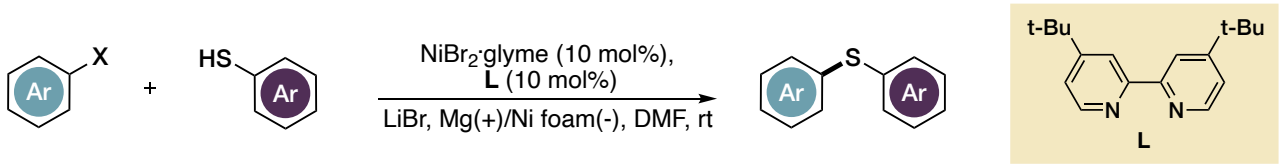

Scheme 10. Nickel-based electrocatalytic, base-free, C-S cross coupling developed by Mei and coworkers.

2. Aim of the Thesis

The aim of this Doctoral Thesis is the development of new catalytic synthetic methodologies in the context of the modern organic chemistry setting, with special focus on the use of cheap, sustainable catalytic materials. As a general trend, we tackled the manipulation of (hetero)aromatic cores as ubiquitous, easily accessible and highly relevant scaffolds, by employing two main distinct activation strategies. Namely, during the course of my PhD, I focused my research on the use of carbonaceous materials as catalysts (carbocatalysis) and nickel catalysis, also investigating a synergistic combination of the two. Both polar and radical reaction manifolds were engaged as complementary reactivities, capitalizing on metal- as well as organo-based activation strategies.

Particular attention has been devoted to addressing modern synthetic challenges or highly sought-after methodologies. Specifically, protocols for direct substitution of alcohols, dearomatization of arene nuclei, formation of C-S bonds, carbon dioxide fixation, C-C bond activation and fluoroalkylation were successfully achieved under carbo- or nickel catalyzed conditions.

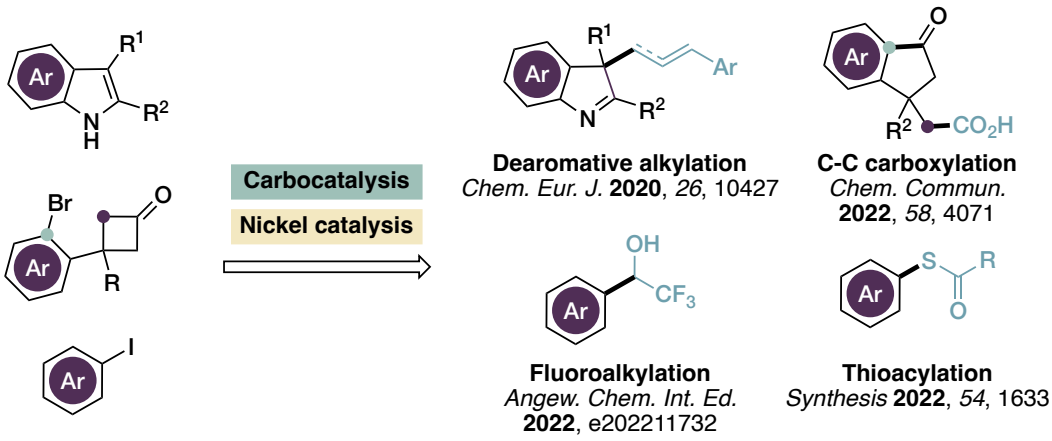

Significant effort has been dedicated to the study and optimization of the reaction conditions and catalyst structure, in order to maximize the yield and selectivity of the processes as well as the breadth of substrate scope. The presented methodologies

feature elements of conceptual novelty and the mechanistic aspects have been thoroughly investigated via experimental, computational and analytical methods of various kind including surface characterization techniques such as scanning electron microscopy (SEM), transmission electron microscopy (TEM) and X-ray photoelectron spectroscopy (XPS).

Despite the conceptual diversity, the proposed protocols are connected by their potential contribution to the ever-evolving realm of modern sustainable catalysis and will hopefully represent useful proof of concepts and inspiration for further advancements.

3. Allylic and Allenylic Dearomatization of Indoles Promoted by Graphene Oxide by Covalent Grafting Activation Mode

All the procedures and results here described can be found in:

- L. Lombardi, D. Bellini, A. Bottoni, M. Calvaresi, M. Monari, A. Kovtun, V. Palermo, M. Melucci, M. Bandini, "Allylic and Allenylic Dearomatization of Indoles Promoted by Graphene Oxide by Covalent Grafting Activation Mode". *Chem. Eur. J.* **2020**, *26*, 10427-10432.

ABSTRACT

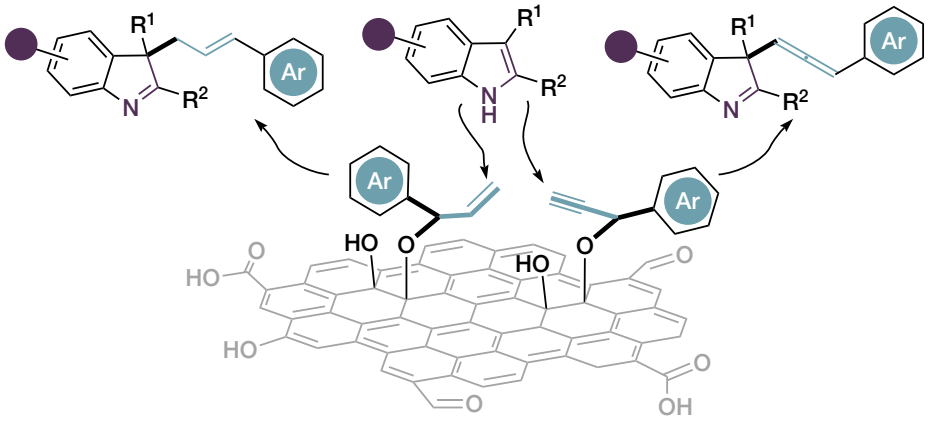

A dearomative allylation and allenylation of 2,3-disubstitued indoles with alcohols was realized under carbocatalytic regime in the presence of graphene oxide (GO, 10 wt%) as the promoter. Mild and environmentally friendly conditions (CH_3CN : H_2O, 55 °C) in the absence of any stoichiometric additive or transition metal provided excellent regio- and stereoselectivity for a broad substrate scope (33 examples, yield up to 92%). A covalent activation mode exerted by GO functionalities was corroborated by spectroscopic, experimental and computational methods. Recovery and regeneration of the GO promoter through simple acidic treatment was also documented.

3.1 Background

Being one of the most abundant elements on Earth, the utilization of carbon for catalytic applications is a very attractive scenario, that has been realized mainly by employing it as a solid support for heterogeneous metal catalysis. However, carbon can act as a catalyst itself, and the use of carbonaceous materials in catalytic reactions is named "carbocatalysis".[67] As early as 1925, Rideal and Wright showed that charcoal could catalyze the aerobic oxidation of oxalic acid;[68] in 1930 its competence in the oxidation of ferrocyanide to ferricyanide was demonstrated independently by Kutzelnigg and Kolthoff.[69] Later on, the interest of the new-born petrochemical industry in the dehydrogenation of hydrocarbons led to the discovery that carbon coke could catalyzed the oxidative dehydrogenation (ODH) of ethylbenzenes.[70] The production of phosgene from gaseous chlorine and carbon monoxide on a porous bed of activated carbon is a benchmark example of an industrial carbocatalytic process.[71] Despite such evidence, the low activity, limited stability and non-trivial study of these materials somewhat hampered further developments and the field, besides sparse reports, remained silent for a number of years.[67] The discovery of carbon nanomaterials with enhanced activity and stability, as well as more sophisticated imaging and characterization techniques, ignited renewed interest.[72] In 2008, Su and Schlögl demonstrated the ODH of light alkanes with surface modified carbon nanotubes,[73] and in 2010 Bielawski pioneered the use of carbocatalysis in the liquid phase by showing the competence of graphene oxide (*vide infra*) in the oxidation of alcohols and activated alkenes.[74] In virtue of their reduced dimensions in the nanoscale range, and the fact that for dispersible, single layer materials no restriction is present for diffusion at their

[67] D. S. Su, G. Wen, S. Wu, F. Peng, R. Schlögl, *Angew. Chem. Int. Ed.* **2017**, *56*, 936–964.
[68] K. Rideal, W. M. Wright, *J. Chem. Soc. Trans.* **1925**, *127*, 1347–1357.
[69] a) A. Kutzelnigg, *Ber. Dtsch. Chem. Ges. B* **1930**, *63*, 1753–1758; b) I. M. Kolthoff, *J. Am. Chem. Soc.* **1932**, *54*, 4473–4480.
[70] Y. Iwasawa, H. Nobe, S. Ogasawara, *J. Catal.* **1973**, *31*, 444–449.
[71] W. Schneider, W. Diller. *"Phosgene"* in *Ullmann's Encyclopedia of Industrial Chemistry.* Wiley-VCH: Weinheim, **2000**.
[72] P. Tang, G. Hu, M. Li, D. Ma, *ACS Catal.* **2016**, *6*, 6948−6958.
[73] J. Zhang, X. Liu, R. Blume, A. Zhang, R. Schlögl, D. S. Su, *Science* **2008**, *322*, 73–77.
[74] D. R. Dreyer, H.-P. Jia, C. W. Bielawski, *Angew. Chem. Int. Ed.* **2010**, *49*, 6813–6816.

surface, this kind of entities can be regarded as interesting bridge between heterogeneous and homogeneous catalysis.[75]

Depending on the structural arrangement, degree of sp^2 to sp^3 hybridization ratio and heteroatom (mainly oxygen) content, several kinds of nanocarbon materials can be distinguished, such as graphene-based materials, carbon nanotubes, fullerenes, and nanodiamonds and derivatives. Generally speaking, such defined carbocatalysts are made from active sites in which the steric and electronic properties of functional groups (heteroatoms) are tailored by a carbon structure that acts as a macroscopic ligand.[67] These materials embody great potential in sustainable processes, representing metal-free catalysts with the possibility of being derived from by biomass or naturally occurring feedstocks.[76] It is extremely important to note that since metals are involved in the production of many nanocarbons, enough care must be devoted in ascertaining the absence of metal contaminants and, when present, their non competence in the studied process in order to claim metal-free conditions.[77] Another controversial aspect deals with the very definition of "carbocatalyst". Indeed, in several transformations the material is not actually operating as a catalyst, being modified at the end of the reaction, and therefore does not comply to the IUPAC definition. For instance, it has been demonstrated in the case of Bielawski's seminal report that the graphene oxide used acts itself as the oxidant for the alcohol conversion and thus is more appropriately defined as a co-reagent.[78] Nonetheless, it is now widely accepted to "misuse" the term carbocatalysis to embrace processes promoted by carbonaceous materials, whether or not in a catalytic manner.

Among the various kind of materials, graphene oxide (GO) has been receiving a great deal of interest. This material was first prepared by Brodie in 1859 by oxidation of graphite with potassium chlorate and fuming nitric acid.[79] In 1958, Hummers introduced a different procedure involving sulfuric acid, sodium nitrate and potassium

---

[75] S. Navalon, A. Dhakshinamoorthy, M. Alvaro, H. Garcia, *Chem. Rev.* **2014**, *114*, 6179−6212.
[76] M.-M. Titirici, M. Antonietti, *Chem. Soc. Rev.* **2010**, *39*, 103–116.
[77] C. K. Chua, M. Pumera, *Chem. Eur. J.* **2015**, *21*, 12550–12562.
[78] S. Presolski, M. Pumera, *Angew. Chem. Int. Ed.* **2018**, *57*, 16713–16715.
[79] B. C. Brodie, *Philos. Trans. R. Soc.* **1859**, *149*, 249–259.

permanganate which is still used today, with some modifications.[80] The resulting material is composed by carbon, oxygen, hydrogen and minor amounts of sulfur and nitrogen. The introduction of oxygen functional groups disrupts the strong stacking of the graphene layers and permits exfoliation of the material into lamellar entities made up of a reduced number of quasi-bidimensional (presenting single atom thickness) layers. Strictly speaking, the material is distinguished in graphite oxide (GiO), when presenting more than five layers, and GO when mono- or few-layered. A high degree of oxidation is obtained, with a C:O ratio of roughly 2:1 (atomic basis). Several structural models have been proposed to address the elusive structure of this material, the most popular being the one proposed by Lerf and Klinowski.[81] According to this model, the GO sheet features two different randomly distributed domains: (a) pure graphene domains with sp^2-hybridized carbon atoms and (b) sp^3-hybridized and oxidized carbon domains. The oxidized domains are thought to bear epoxy and hydroxyl groups in the basal region, while carboxylic groups are present at the edges of the domain. Importantly, holes and defects and disruption of the ideal honeycomb graphene lattice are introduced as well. This model, despite being the most widely adopted, is far from being totally satisfactory, so that contributions from other models such as the Szabo-Dekany one,[82] proposing the presence of ketones, quinones and oxetane functionalities, are not to be disregarded (**Figure 1**).

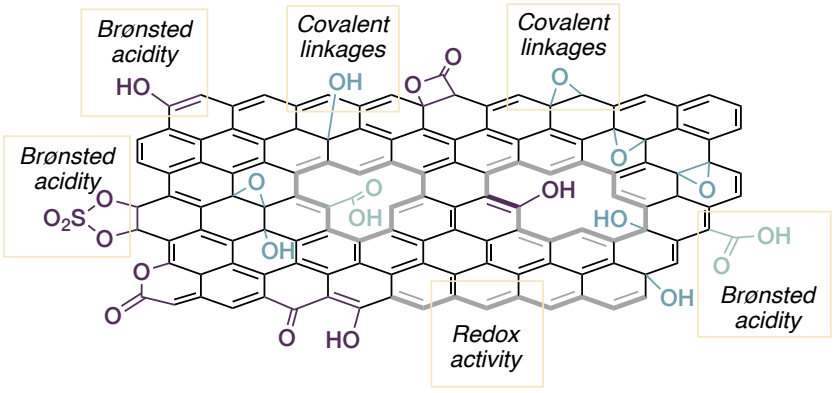

[80] W. S. Hummers, R. E. Offeman, *J. Am. Chem. Soc.* **1958**, *80*, 1339.
[81] A. Lerf, H. He, M. Forster, J. Klinowski, *J. Phys. Chem.* **1988**, *102*, 4477−4482.
[82] T. Szabo, O. Berkesi, P. Forgo, K. Josepovits, Y. Sanakis, D. Petridis, I. Dekany, *Chem. Mater.* **2006**, *18*, 2740−2749.

Figure 1. Pictorial representation of a GO sheet portion. Functional groups are shown accordingly to both the Lerf-Klinowski and Szabo-Dekany models. Hydroxy and epoxy groups are shown in teal; carboxylic acids in green; more oxidized functionalities proposed by Szabo and Dekany as well as Tour (*vide infra*) are shown in purple. Contributions of these groups to the catalytic activity of the material are noted.

A striking feature of GO is its considerable acidity: aqueous dispersions present pH values around 4-5, hardly rationalized by the presence of a limited number of carboxyl groups. Tour et al. performed a thorough investigation on the topic together with a critical review of the existing models by means UV−vis spectroscopy, FTIR, ^{13}C SSNMR (solid state NMR), thermogravimetric analysis (TGA), and scanning electron microscopy (SEM).[83] On the basis of these results, they proposed that the oxidizing conditions introduce covalent disulfates on the sheet surface as well as between the sheets, and that sp^2 domains are limited to five or six condensed rings. Hydrolysis during the washings cleaves the disulfates leading to 1,2-diols that further evolve via C-C cleavage to conjugated enols and ketone moieties, increasing the extension of sp^2 domains and C=O moieties, that could also be converted to hydrates and hemiacetalic forms. The conjugation of enolic OH to carboxylic moieties could explain the high acidity observed, although presence of sulfonic acids cannot be excluded either.

Regardless of its exact structure, the active sites for catalytic activity, besides the inherent acidity and high surface area, are thought to be: the large π domains capable of modulating the reactivity of unsaturated hydrocarbons; the combination of zig-zag sheets/vacancies edges, carrying unpaired electrons, holes and carboxylic acids that can promote SET events; alcoholic, epoxydic and sulfonate groups can trigger temporary covalent linkages with the reaction partners.[84]

Among the various kinds of transformations promoted by GO, reactions that permit direct substitution of alcohols for the formation of C-C bonds are of particular interest.[41]

[83] A. Dimiev, D. V. Kosynkin, L. B. Alemany, P. Chaguine, J. M. Tour, *J. Am. Chem. Soc.* **2012**, *134*, 2815−2822.
[84] L. Lombardi, M. Bandini, *Angew. Chem. Int. Ed.* **2020**, *59*, 20767–20778.

In 2015, He and Szostak documented on the use of GO in the Friedel–Crafts (FC) alkylation of electron-rich arenes with styrenes and primary/secondary benzylic alcohols as electrophiles.[85] The reaction required 200 wt% of GO and furnished the arylated products in moderate to excellent yields and high benzylic alkylation selectivity (**Scheme 1**, top).

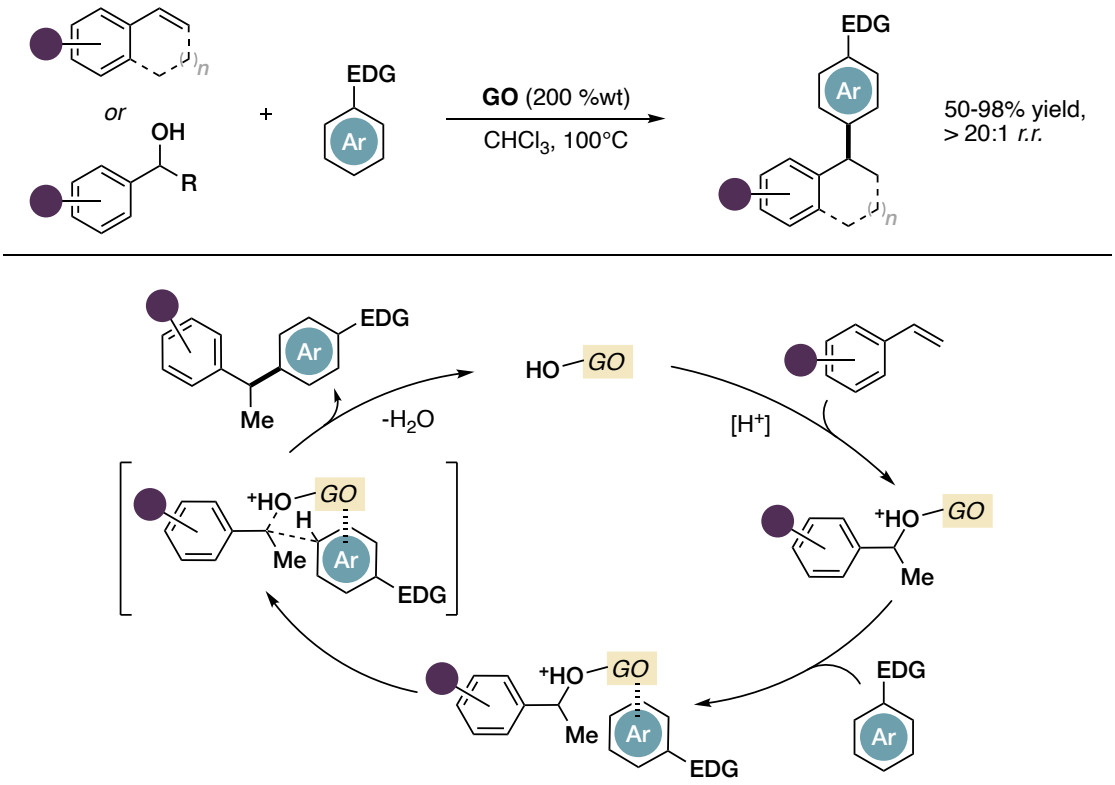

Scheme 1. Top: Szostak's GO promoted Friedel-Crafts alkylation of electron rich arenes with styrenes and alcohols. Bottom: proposed mechanism for a styrene substrate. Note that the OH group initially present is depleted as a water molecule in the final step.

Partial reduction of GO during the reaction course was ascertained (XPS and FT-IR), displaying a net decrease of C-O and C=O functional groups in the recovered GO. This evidence suggested their involvement in the process that was further corroborated by the inadequacy of reduced graphene oxide (rGO)[86] and graphite. Hammett studies

[85] F. Hu, M. Patel, F. Luo, C. Flach, R. Mendelsohn, E. Garfunkel, H. He, M. Szostak, *J. Am. Chem. Soc.* **2015**, *137*, 14473–14480.

[86] rGO is a graphene-based material obtained by chemical or thermal reduction of GO. This material features a much lower oxygen content, and significant restoration of sp^2 domains, although it maintains defects that render it competent in certain protocols. More discussion of this material will be found in the next chapter.

supported a transition state (TS) in which a positive charge is generated at the benzylic carbon of the electrophilic partner and competition experiments highlighted the higher reactivity of benzylic alcohols with respect to styrenes. Last but not least, contrarily to classic LA-assisted FC protocols, primary benzylic alcohol was found more reactive than that the bulkier phenylethanol and the corresponding acetate.

All at once, it was proposed a reaction mechanism occurring at the GO surface based on the initial carbinol activation by the GO oxygenated groups. The key mechanistic step involves the pre-coordination of the olefin by the π-matrix and subsequent hydration promoted by the oxygenated groups on the surface (**Scheme 1**, bottom). An *in situ* covalent activation mode is therefore realized. Upon pre-coordination of the nucleophile, a concerted C-C bond forming event yields the product with elimination of a water molecule, accounting for the observed reduction of GO after the process: this process is an example of non-catalytic behavior of this material.

In 2019, a similar approach was exploited by the same group in the alkylation of 1,3-dicarbonyl compounds with styrenes and benzylic alcohols. Conditions similar to their previous FC protocol enabled the benzylation of a range of structurally diverse β-diketones under base-free and relatively mild conditions (**Scheme 2**, top).[87] In contrast to the previous protocol, no reduction of GO was observed after the reaction, and also the acidity content was unchanged upon the catalytic transformation (pH 4.19 vs. 4.24 at 0.29 mg/mL concentration before and after reactions). The ketones seem to protect the GO from an over-reduction that was recorded their absence (C/O increased to 3.2 from 2.1 in the parent GO). This intriguing phenomenon was ascribed to the instauration of a network of H-bond interactions between the enolizable carbonyls and the oxygenated GO moieties. Mechanistically, the authors proposed a simplified pictorial sketch of the reaction profile that parallels in several parts the one of the arylation protocol. A double activation role of the GO was proposed even if no detailed explanations on the preservation of the GO structure and reutilization of the carbon-material were provided (**Scheme 2**, bottom).

---

[87] G. Meng, M. Patel, F. Luo, Q. Li, C. Flach, R. Mendelsohn, E. Garfunkel, H. He, M. Szostak, *Chem. Commun.* **2019**, *55*, 5379–5382.

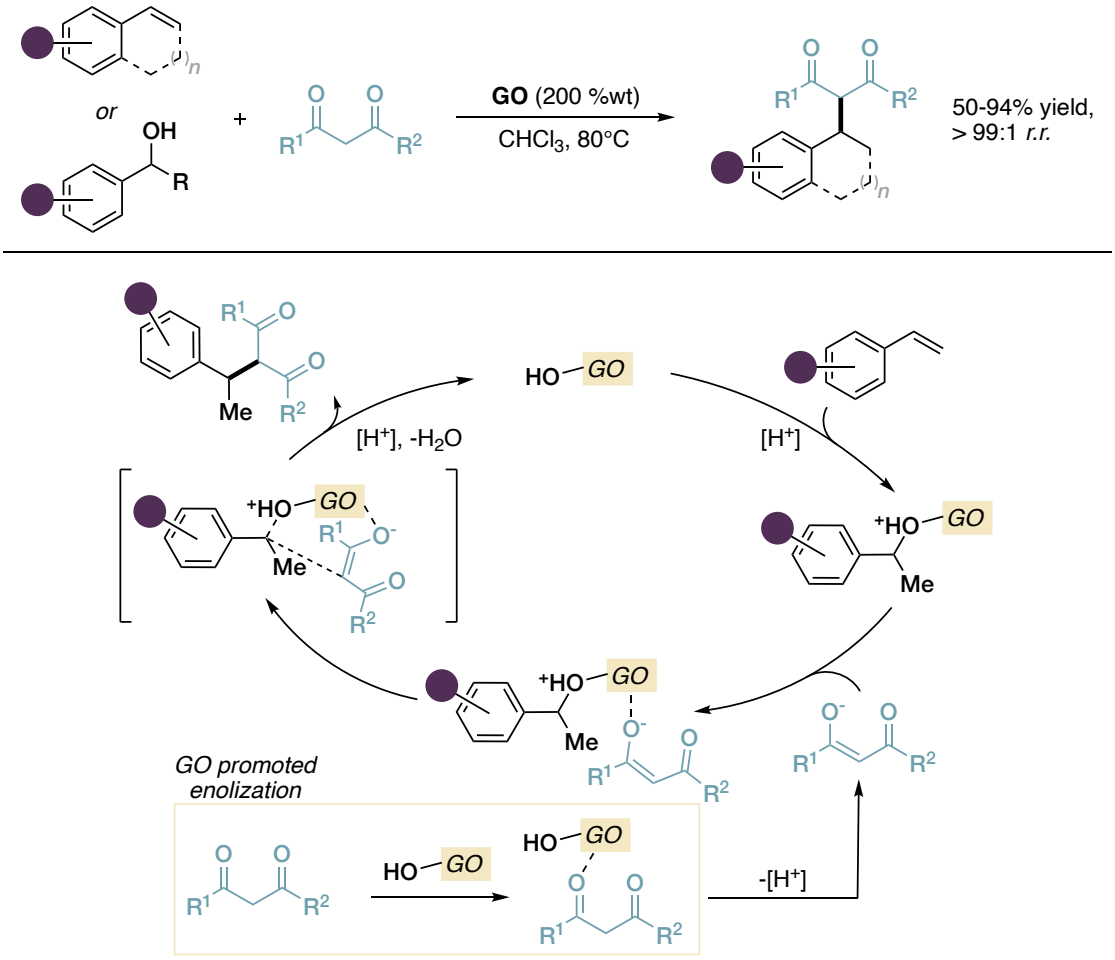

Scheme 2. Top: Szostak's GO promoted alkylation of β-diketones with styrenes and alcohols. Bottom: proposed mechanistic idea.

Our group (2018) contributed to the site-selective alkylation of arenes by exploiting the covalent activation mode exerted by GO. In particular, allylic alcohols were employed as alkylating agents for the FC allylation of thiophenes and bithiophenes.[88] Optimal conditions (1,4-dioxane, 90 °C) involved a remarkably low GO loading for C-C forming carbocatalytic protocols (25 wt%). The yields varied from modest to high (up to 90%) accompanied by a good α-regioselectivity and complete linear/branched as well as *E/Z* selectivity (**Scheme 3**, top).

[88] L. Favaretto, J. An, M. Sambo, A. De Nisi, C. Bettini, M. Melucci, A. Kovtun, A. Liscio, V. Palermo, A. Bottoni, F. Zerbetto, M. Calvaresi, M. Bandini, *Org. Lett.* **2018**, *20*, 3705–3709.

rGO and graphite proved inert as promoters, highlighting the importance of oxygenated functionalities. Control experiments using several organic acids under homogenous conditions excluded a simple acidic activation, while the combined use of benzoic acid and styrene oxide furnished the product in modest yield. These introductory findings suggested the synergic role of acidic functionalities and epoxide groups on the GO surface during the reaction course. C 1s XPS studies support this observation, showing a significant drop in epoxide content (from 40.3 to 27.4% atomic abundance) after the reaction. A detailed computational analysis complemented the experimental data, proposing the covalent binding of the alcohol to the GO surface by means of an acid promoted epoxide ring-opening event. Notably, the intrinsic Brønsted acidity of GO is known to promote ring-opening of strained epoxides of the surface, releasing α-carbocations stabilized by the π-conjugate motif of GO (**Scheme 3**, bottom).

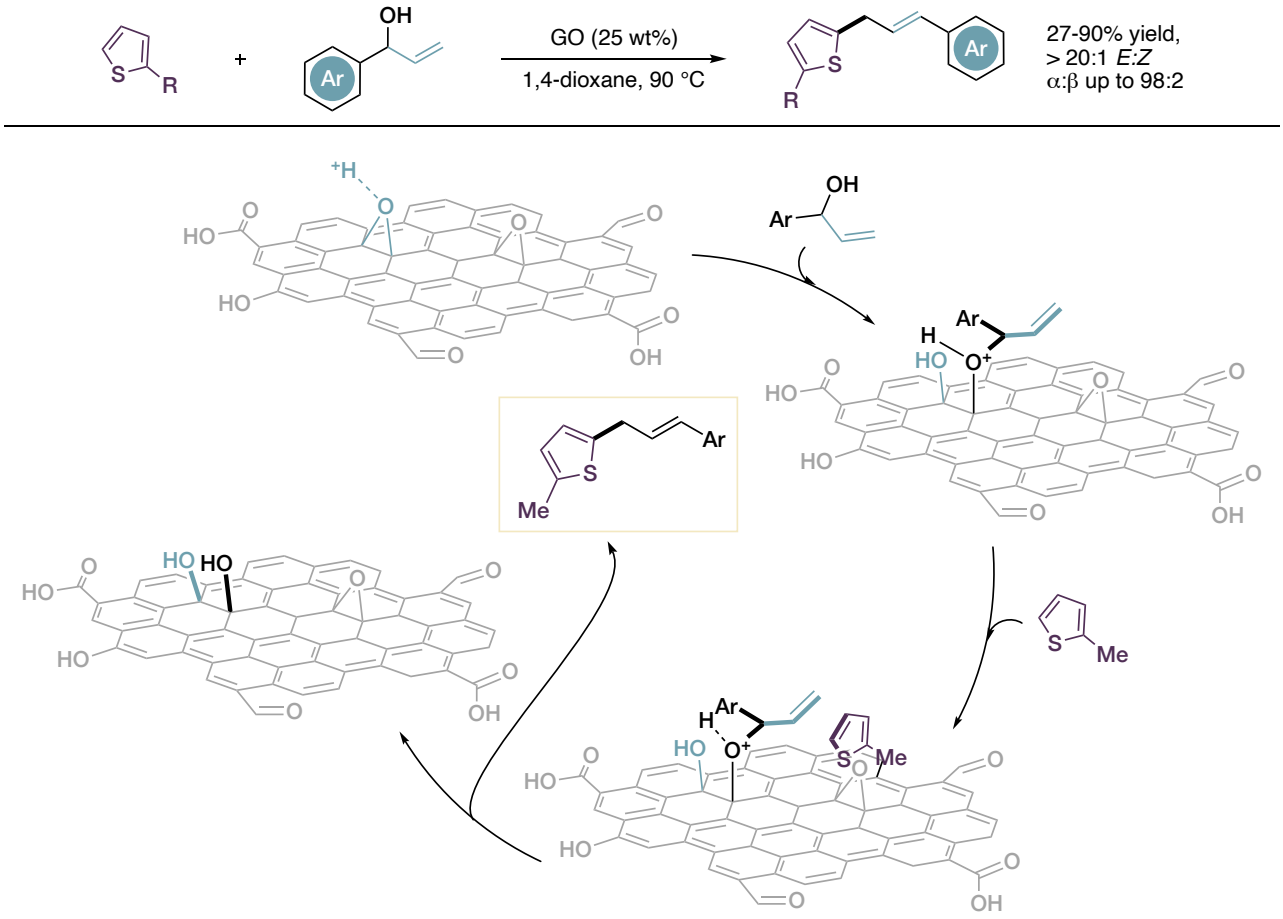

Scheme 3. Top: Bandini's GO promoted allylation of (bi)thiophenes with allylic alcohols. Bottom: proposed mechanism.

Overall, the formation of the product is accompanied by the net loss of one epoxide unit on the material surface, which is converted into a 1,2-diol moiety. Additionally, calculations provided a convincing rational for the observed regioselectivity with respect to the thiophene ring. Recovery and direct reuse of the GO revealed a progressive drop in catalytic performance (1st run: 88% Y, 4th run: 29%), supporting the afore-described mechanism and suggesting that in this specific process the GO is behaving more likely as a co-reagent than that a genuine catalyst.

In the context of aromatics manipulation, dearomatization reactions represent a powerful tool for convenient access to more structurally complex three-dimensional chemical space from largely available two-dimensional compounds. A common way to pursue such endeavor is by leveraging the innate nucleophilicity of electron-rich aromatics such as indoles, pyrroles, 2-naphthols and phenols, reacting them at an *ipso* position (which prevents re-aromatization from the Wheland intermediate) with suitable electrophiles.[89] Indole presents several favorable features that make it the most investigated scaffold in this kind of reactions, namely its enhanced nucleophilicity, strong electronic bias and reduced aromatic character with respect to carbocyclic counterparts, together with the possibility of disrupting the aromaticity of the five membered ring while preserving the benzene one, which results in reduced energy barriers.[90]

The utilization of allylic alcohols as electrophiles is particularly appealing: these commodity building blocks display the advantage of only producing water as byproduct and allow for further elaboration of the resulting products by using their π-system as synthetic handle; on the other hand, their implementation is challenging due

[89] a) S. P. Roche, J. A. Porco, *Angew. Chem. Int. Ed.* **2011**, *50*, 4068–4093; b) C.-X. Zhuo, W. Zhang, S.-L. You, *Angew. Chem. Int. Ed.* **2012**, *51*, 12662–12686.
[90] a) S. P. Roche, J.-J. Y. Tendoung, B. Tréguier, *Tetrahedron* **2015**, *71*, 3549–3591; b) Q. Ding, X. Zhoua, R. Fan, *Org. Biomol. Chem.* **2014**, *12*, 4807.

to the poor leaving group ability of the hydroxyl group in nucleophilic substitution reactions.[91] Dearomative allylation of indoles with allylic alcohols has been successfully realized by means of transition metal catalysis in conjuction with Brønsted or Lewis acid additives. Trost reported on the asymmetric Pd catalyzed allylative dearomatization of C3-substituted indoles, requiring a stoichiometric amount of 9-BBN-C_6H_{13} for activation of the alcohol (**Scheme 4**). Indolenines are obtained in moderate to good enantiomeric excess, and in the presence of a pending nucleophile cyclization at the 2 position was also documented.[92]

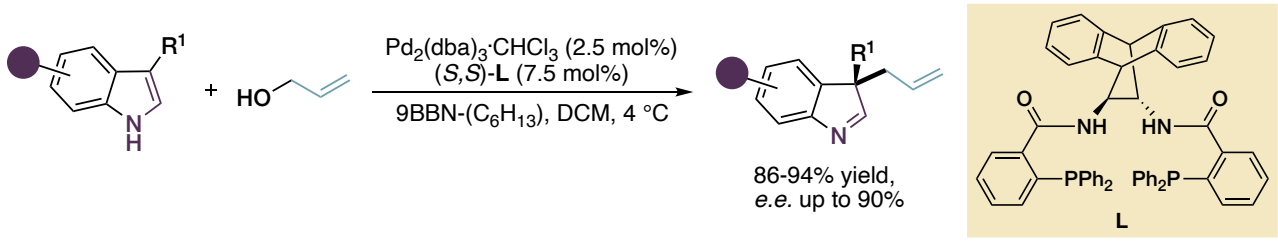

Scheme 4. Trost's palladium catalyzed protocol for the allylative dearomatization of 3-substituted indoles with allylic alcohols.

S.-L. You et al. demonstrated the competence of ruthenium catalysis in conjunction with substoichiometric amouns of *p*-TsOH (*p*-toluenesulfonic acid) in a racemic protocol. Indoles bearing C3 substituents with a pendant nucleophile were employed, yielding pyrrolo- and furoindoline with concomitant allylation at nitrogen (**Scheme 5**).[93]

[91] a) N. A. Butta, W. Zhang, *Chem. Soc. Rev.* **2015**, *44*, 7929; b) T. Sawano. R. Takeuchi, *Catal. Sci. Technol.* **2022**, *12*, 4100; c) A. Baeza, C. Nájera, *Synthesis* **2014**; *46*, 25–34.
[92] B. M. Trost, J. Quancard, *J. Am. Chem. Soc.* **2006**, *128*, 6314–6315.
[93] X. Zhang, Z.-P. Yang, C. Liu, S.-L. You, *Chem. Sci.* **2013**, *4*, 3239–3243.

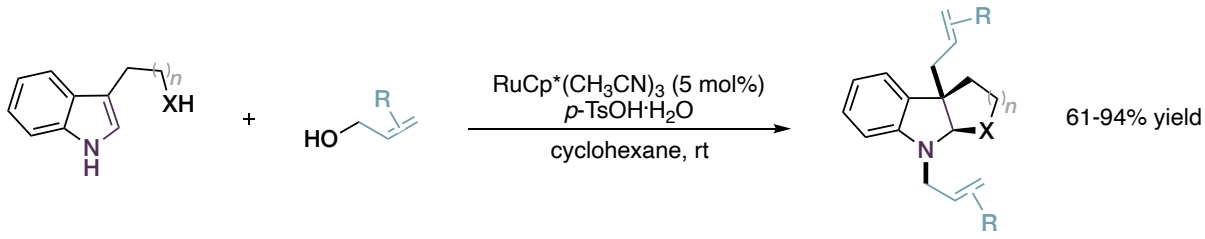

Scheme 5. Yu's ruthenium catalyzed protocol for the allylative dearomatization-cyclization of nucleophile tethered indoles with allylic alcohols. X = O, NH, CO_2, C(O)NBn, N(EWG).

A similar protocol was reported by the same group in 2014, employing an Ir(I) catalyst with a phosphoramidite-olefin ligand[94] for an asymmetric cinnamylation reaction of triptophols and triptamines. The same products were obtained in good to excellent enantioselectivities in the presence of a stoichiometric amount of $Fe(OTf)_2$.[95]

Despite the relevance of these and other[96] interesting reports, the use of late transition metals, stoiochiometric additives and the need for inert atmosphere represent major drawbacks, so that the realization of alternative, more sustainable and user-friendly protocols stands as a highly significant goal.

[94] M. Roggen, E. M. Carreira, *Angew. Chem., Int. Ed.* **2011**, *50*, 5568–5571.
[95] X. Zhang, L. Han, S.-L. You, *Chem. Sci.* **2014**, *5*, 1059–1063.
[96] a) H. Zhang, R.-B. Hu, N. Liu, S.-X. Li, S.-D. Yang, *Org. Lett.* **2016**, *18*, 28–31; b) S. Gao, Z. Wu, X. Fang, A. Lin, H. Yao, *Org. Lett.* **2016**, *18*, 3906–3909.

3.2 Aim of the project

Encouraged by the previous results on the allylation of thiophenes,[88] and in line with the group's research interest in the dearomatization of arenes,[97] we envisioned that a carbocatalytic strategy employing GO could be a viable alternative to the above-mentioned pitfalls in the realm of dearomative allylation of indoles with π-alcohols (**Scheme 6**). Specifically, we decided to focus our attention on allylic-benzylic alcohols, readily obtained from addition of vinyl Grignard reagents onto benzaldehydes, reasoning that they could be reactive enough to be activated under mild conditions by the synergistic action of the π-matrix, oxygenated functional groups and inherent acidity of GO.

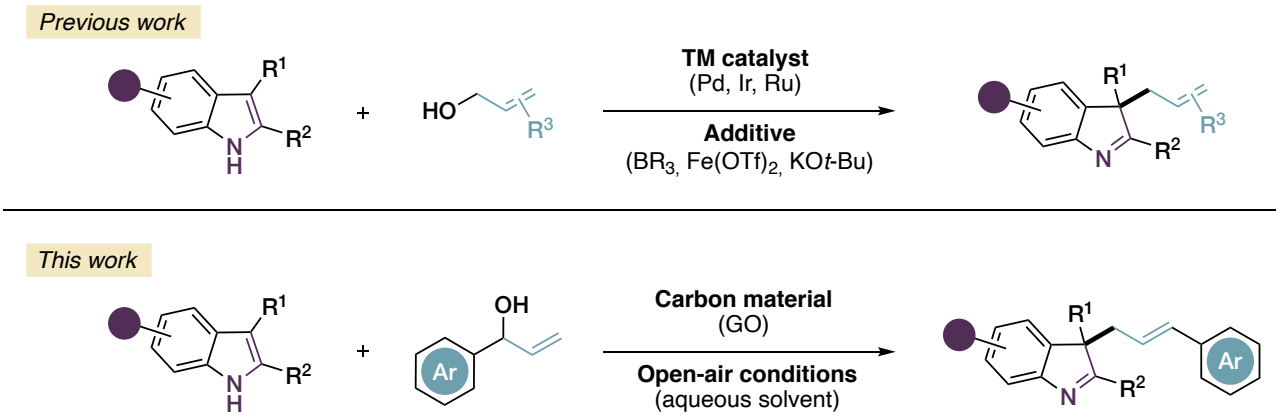

Scheme 6. Top: state of the art for the metal-catalyzed dearomative allylation of indoles with alcohols; Bottom: schematic representation of the desired metal-free carbocatalytic approach with GO.

This conceptually straightforward transformation potentially presents multiple challenges with respect to the control of the regiochemistry: in the presence of a C3 substituent, both *N*- and C2-alkylation (if unsubstituted) of the indole core can become

[97] a) J. An, L. Lombardi, S. Grilli, M. Bandini, *Org. Lett.* **2018**, *20*, 7380–7383; b) A. Cerveri, O. Nieto Faza, C. Silva López, S. Grilli, M. Monari, M. Bandini, *J. Org. Chem.* **2019**, *84*, 6347–6355; c) A. Cerveri, S. Pace, M. Monari, M. Lombardo, M. Bandini, *Chem. Eur. J.* **2019**, *25*, 15272; d) J. An, A. Parodi, M. Monari, M. C. Reis, C. S. Lopez, M. Bandini, *Chem. Eur. J.* **2017**, *23*, 17473; e) C. Romano, M. Jia, M. Monari, E. Manoni, M. Bandini, *Angew. Chem. Int. Ed.* **2014**, *53*, 13854-13857.

competitive, as well as reaction at the C5 position, although to a minor extent; moreover, regiochemical control over S_N2 and S_N2' pathways, leading to branched and linear alkylation products respectively, is to be controlled.

If successful, such strategy could also be extended to propargylic alcohols, presenting analogous regiochemical issues with both allenylated and propargylated products being attainable.

3.3 Discussion and results

At the outset of our investigation, we selected 2,3-dimethylindole **1a** and secondary racemic allylic alcohol **2a** as model substrates for the optimization. Upon an extensive survey of reaction conditions, the use of 10 wt% loading of GO enabled the selective formation of the desired C3-allylated dearomatized indolenine **3aa** in 70% yield under very mild conditions (CH_3CN : H_2O 4:1, 55 °C, 5 h, entry 1, **Table 1**).

Table 1. Summary optimization of reaction conditions.

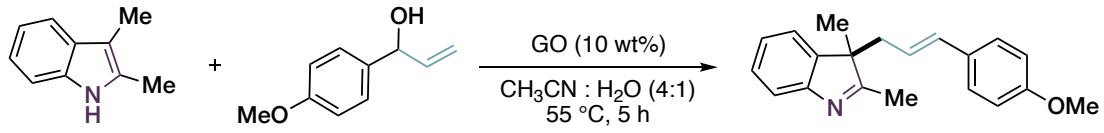

1a (+/-)-**2a** (+/-)-(*E*)-**3aa**

Entry[a]	Deviations from optimal	**3aa** Yield (%)[b]
1	none	70
2	No GO, 36 h	12
3	GO (5 wt%)	36
4	GO (25 wt%)	69
5[c]	Pre-sonication of GO	67
6	rGO (25 wt%) in place of GO	12
7	GO (25 wt%), 1,4-dioxane in place of CH_3CN	66
8	GO (25 wt%), THF in place of CH_3CN	30
9	Only CH_3CN as solvent, 24 h	25
10	GO (25 wt%), only H_2O as solvent	62
11	GO (25 wt%), only H_2O as solvent, rt, 16 h	47
12	GO (25 wt%), only H_2O as solvent, 80 °C, 16 h	62
13	AcOH in place of GO, pH = 4	44
14[d]	$Mn(OAc)_2{\cdot}4H_2O$ in place of GO	traces
15[e]	With EDTA as additive	68
16	Under N_2 atmosphere and degassed solvents	69
17[f]	Gram scale (5 mmol of **1a**)	78

[a]All reactions were carried out with reagent grade solvents, unless otherwise specified (**1a** : **2a**=1:2 on 0.15 mmol of 1a, 0.1M). [b]Determined after flash chromatography. [c]Sonication for 2 min, in probe sonicator. [d][Mn]: 1.8 mol%. [e]EDTA: 200 mL of 43 mM water solution. [f]GO (10 wt%), **3aa**: 1.13 g (16 h).

To our delight, the potentially competitive *N*- and C5-allylation products were observed only sporadically (traces), and indolenine (*E*)-**3aa** was recorded almost exclusively in a stereoselective manner (S_N2' pathway). A small extent of background reaction was recorded, although in much reduced yield (12% yield, 36 h, entry 2), and rGO and graphite proved ineffective, hinting to the key role of oxygenated functionalities. It is worth noting that high GO loading is one of the critical aspects usually encountered in GO-promoted transformation, with amounts commonly fluctuating around 100–200 wt%. In this methodology, we were pleased to verify that 10 wt% loading of GO turned out to be sufficient under optimal conditions.

Key to the observed reactivity was the determination of the best solvent system. In particular, the addition of water (ca. 20% v/v with CH_3CN) was found to be essential. This is a remarkable feature, not only because it is a testament to the mild conditions of the protocol, that obviously does not require any precaution in the exclusion of air or moisture (entry 16), but also because the use of water in allylation methodologies using alcohols is unprecedented, being water produced as a byproduct in the condensation.

Proofs of a genuine GO catalysis were gained via dedicated control experiments. First of all, the extent of a background Brønsted acid catalysis was assessed by running the model reaction in the presence of AcOH (entry 13, 44% Y) and *p*-TsOH (traces, see Supplementary Data, Chapter 3.5), that provided reduced yields. Potential roles played by metal contaminants of GO (*i.e.* Mn^{2+}) were ruled out via the use of $Mn(OAc)_2 \cdot 4H_2O$ (entry 14) and EDTA solution as metal ions scavenger (entry 15). Then, we investigated the scope of the reaction by subjecting several polysubstituted indoles (**1b-n**) to optimized conditions with **2a** (**Figure 2**, top).

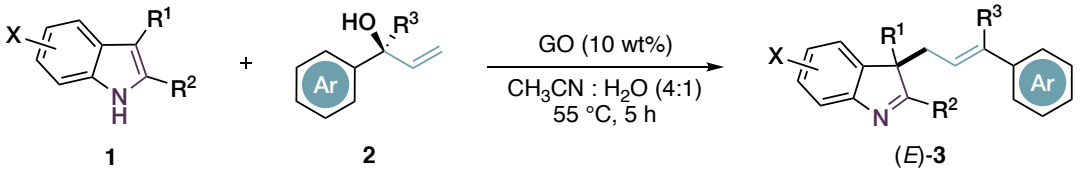

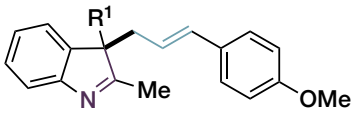

3ba, R^1 = Et, 68%
3ca, R^1 = *n*-Bu, 61%
3da, R^1 = Bn, 47%
3ea, R^1 = CH_2CO_2Et, 57%

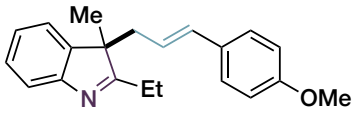

3fa, 68%

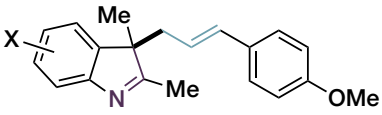

3ja, X = 5-F, 92%
3ka, X = 5-Cl, 77%
3la, X = 5-Br, 75%
3ma, X = 5-Me, 60%
3na, X = 6-Br, 60%

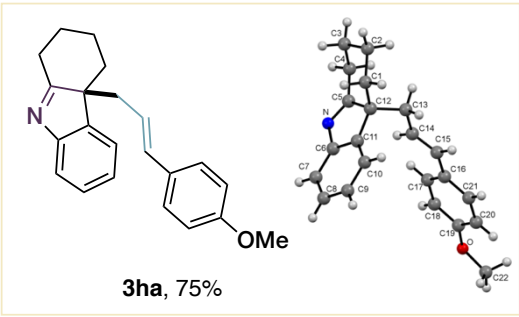

3ha, 75%

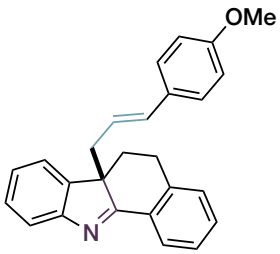

3ga, 35%

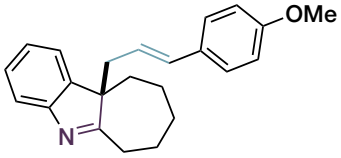

3ia, 58%

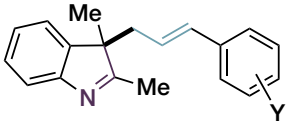

3ab, Y = 4-OBn, 65%
3ac, Y = 4-OTBS, 66%[a]
3ad, Y = 4-H, 0%[b]
3ae, Y = 4-SMe, 51%[c]
3af, Y = 4-O$(CH_2)_5N_3$, 76%
3ag, Y = 2-OMe, 40%
3ah, Y = 3,4-$(OMe)_2$, 76%
3ai, Y = 2,4,5-$(OMe)_3$, 81%[d]

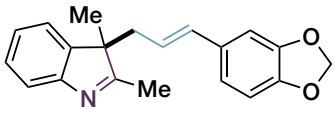

3aj, 66%

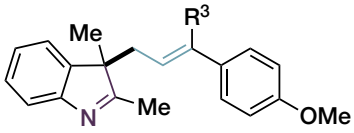

3an, R^3 = Me, 72%[e]
3ao, R^3 = *n*-Bu, 80%[e]

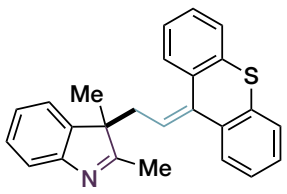

3ap, 84%[d]

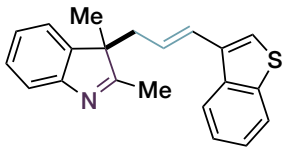

3al, 75%[a,c]

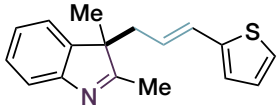

3ak, 63%[a]

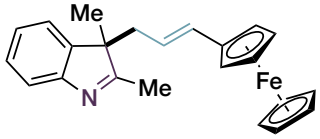

3am, 61%

Figure 2. Scope of the reaction for different indoles (top) and alcohols (bottom). All reactions were set up under optimal conditions (entry 1 in **Table 1**) except otherwise noted. All yields are given after flash chromatography. [a]10% of C3,C5-diallylated product was formed. [b]120 °C, isomerization of **2d** to the linear cinnamic isomer occurred. [c]70 °C. [d]RT. [e]The absolute configuration *E* of the double bond was determined by ^{1}H-NOE NMR experiments, see Supplementary Data, Chapter 3.5.

Different aliphatic as well as aromatic groups could be accommodated at C2 and C3 positions (Et, *n*-Bu, Bn, CH_2CO_2Et) leaving almost untouched the catalytic performance of the present methodology (yield up to 70%). Interestingly, tetrahydrocarbazole **1h** and seven-membered ring analog **3i** worked smoothly, delivering the corresponding indolenines **3ha** and **3ia** in 75% and 58% yield, respectively. Single crystal XRD analysis of product **3ha** unambiguously confirmed the exclusive *E* configuration. Tolerance of the protocol towards electronic perturbation of the benzene ring was assessed with indoles **1j-o**. Remarkably, good to excellent yields (up to 92%) were recorded regardless the electronic properties of the substituents (F, Cl, Br, Me) and their position. C2-unsubstituted indoles unfortunately proved unsuitable, with C2 alkylation being the major product.

We then moved on to assess the extendibility of the process to different allylic alcohols. A series of secondary (**2a-m**) and tertiary (**2n-p**) alcohols was treated with model substrate **1a**, providing in all cases, excellent regio- and stereoselectivity, delivering indolenines bearing an all-carbon quaternary C3 stereogenic center in up to 84% yield (**Figure 2**, bottom). A stringent limitation for the success of the protocol was the presence of electron-donating groups on the aromatic system, or electron-rich heteroarenes (*i.e.* ferrocene, thiophene, benzothiophene, thioxanthene). Unsubstituted arenes or benzenes carrying electron-withdrawing groups demonstrated unreactive even under forcing conditions (120 °C, 6 h, alcohol **2d**). In these cases, substantial isomerization of **2** to the linear cinnamyl isomer occurred exclusively (*vide infra* for mechanistic interpretation).

Intrigued by these results, we focused on elucidating the mechanism of the process by complementary studies with various surface characterization techniques as well as computational tools.

Significant structural modification of the GO surface functionality profile was observed by XPS analysis after reaction (**Figure 3**). While exposing GO to the reaction medium alone (**Figure 3**, top right) did not significantly affect the O:C ratio, treatment of GO with **1a** decreased slightly the O:C ratio (0.28:1, **Figure 3**, top right). More

importantly, marked O:C ratio variations were observed in the presence of **2a** (0.22:1, **Figure 3**, bottom left), as well as both reaction partners **1a** and **2a** (0.24:1, **Figure 3**, bottom right). After heating in the presence of **2a**, the epoxy content decreases from 38.3% to 17.9% and hydroxyl groups increase from 3.2% to 9.0% (see Supplementary Data, Chapter 3.5 for further details).

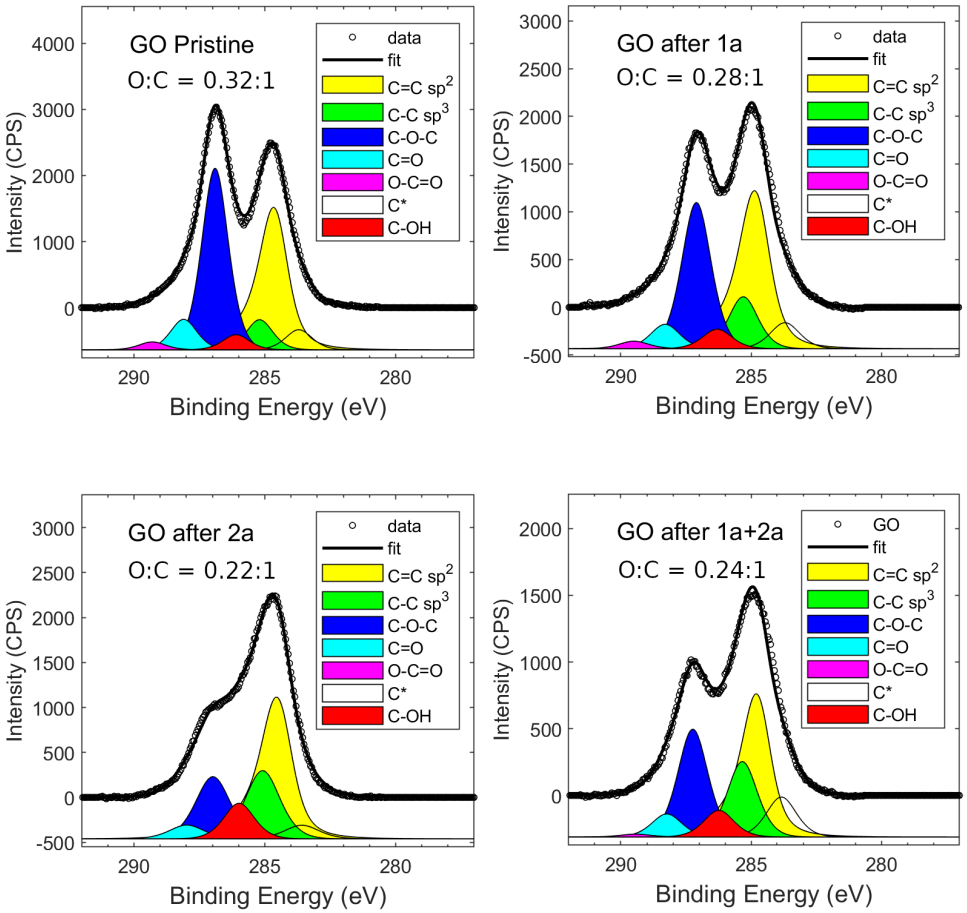

Figure 3. XPS C 1s signal of: pristine GO (Top left); GO treated with only **1a** under reaction conditions (Top right); GO treated with only **2a** under reaction conditions (Bottom left); GO after the actual reaction (Bottom right). For details on fit procedure and other spectra see SI.

This structure modification is compatible with a partial ring-opening of the epoxide units during the reaction course. A significant drop in carboxylic content of the GO surface upon treatment with **2a** or **1a** + **2a** (6 h, 55 °C) was observed as well (**Figure 3**, in pink). In particular, the carboxylic groups decrease from 1.6% to 0 and 0.6%,

respectively. This behavior can be ascribed to the esterification of the carboxylic group present and subsequent decomposition also through decarboxylative events.[85,87]

At this point, we combined all spectroscopic and experimental information with the QM/MM (quantum mechanics/molecular mechanics) study to elucidate in detail the reaction mechanism that results in a two-step process (**Figure 4**, top).

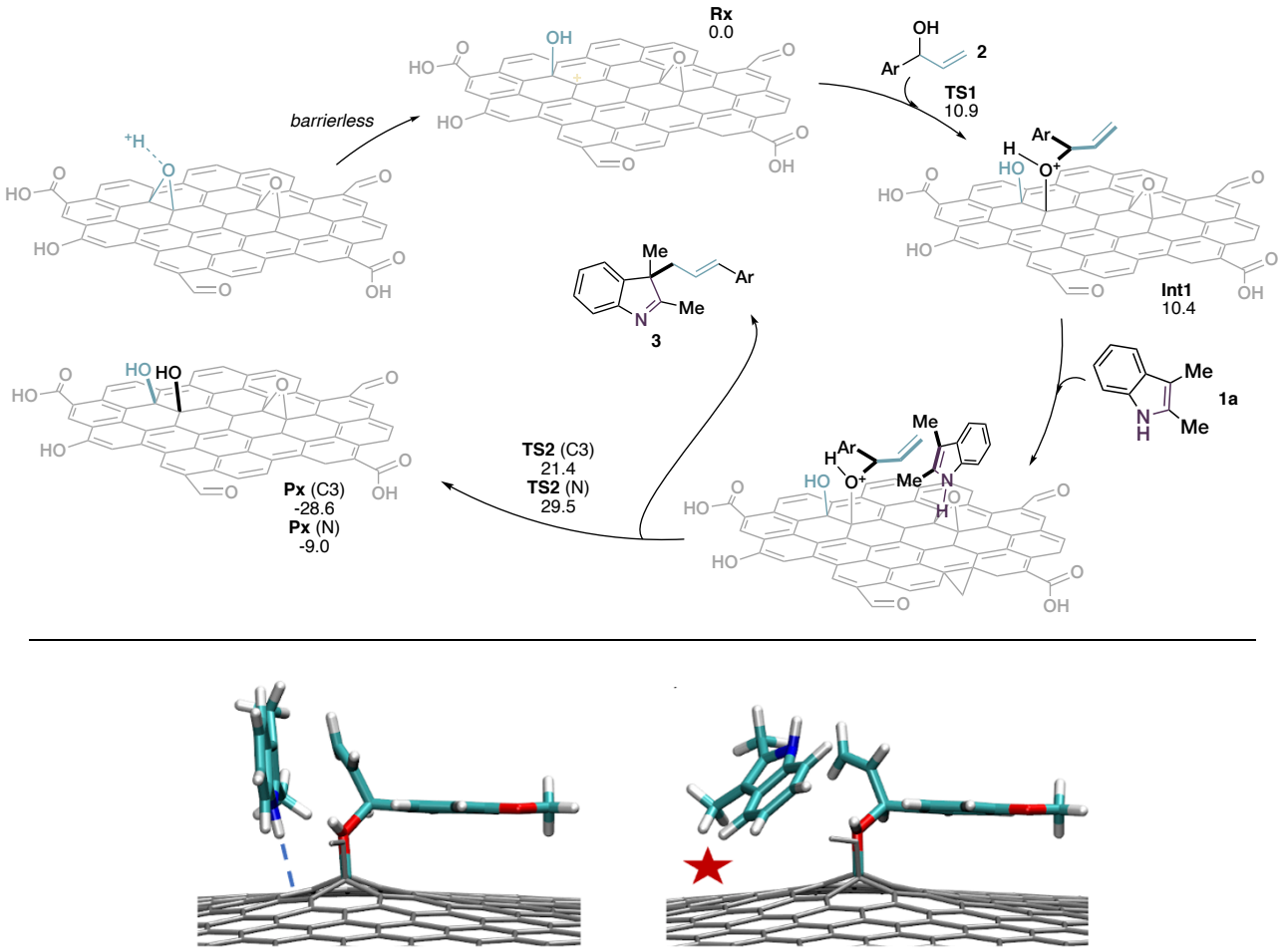

Figure 4. Top: schematic representation of the reaction mechanism. Energies of the identified critical points are reported (kcal/mol); Bottom: 3D representation of the identified transition states for C3-attack (left) and N-attack (right).

In step 1, an initial protonation of the epoxide ring on the GO surface leads to an unstable oxonium moiety that undergoes barrierless ring-opening.[98] This C-O cleavage

[98] R. Ramírez-Jiménez, M. Franco, E. Rodrigo, R. Sainz, R. Ferrito, A. M. Lam-sabhi, J. L. Aceña, M. Belén Cid, *J. Mater. Chem. A* **2018**, *6*, 12637–12646.

relieves ring strain and forms a highly stabilized α-carbocation (**Rx**), as already observed by Chen et al.[99] Then, the resulting α-carbocation undergoes a facile nucleophilic attack by the allylic alcohol (**TS1**), leading to the covalent grafting of **2a** onto the GO surface. The key role of electron-donating groups on the aromatic system is in agreement with the current mechanistic hypothesis. The comparison of the energetic reaction profiles for the GO grafting of different allylic alcohols showed that a significantly higher barrier is observed for **2d** (unsubstituted benzene) compared to **2a** (25.5 vs. 10.9 kcal/mol, Figure S12 in Supplementary data, Chapter 3.5). The presence of electron-donating groups on the aromatic system contributes to stabilize the positive charges delocalized on the GO surface through strong π–π interactions between GO and the aromatic moiety of the alcohol.

In step 2, the obtained protonated allyl ether undergoes a S_N2'-type attack by the indole nucleophile ultimately leading to the observed C3-allylated dearomatized compound. This nucleophilic attack follows a concerted mechanism where either C3 or the N atom can attack the allylic position (**TS2**), with an overall reorganization of the π-electrons, and the C3 selectivity emerges clearly from the calculated **TS2**(C3) and **TS2**(N) as a result of secondary interactions with the GO catalyst. In particular, the influence of GO on the regioselective attack by indole is determined by the following factors: i) in the dearomatization occurring at C3 a stabilizing interaction between the indole N-H group and the GO π-system is established (**Figure 4**, bottom left). On the contrary, the attack involving the N atom is accompanied by a destabilizing steric clash due between the C3 methyl group and the graphene sheet (**Figure 4**, bottom right);[100] ii) the above discussed interactions have also important effects on the orientation of the indole ring during the C-C bond forming event: when the reaction occurs at the C3 position, the indole ring can adopt an ideal spatial arrangement for a S_N2 attack, since its plane is orthogonal to the graphene sheet and parallel to the electrophilic site, maximizing orbital overlap. In contrast, for the attack to occur at N, a strong deviation from this optimal reaction geometry is necessary in order to minimize the steric repulsion

[99] V. D. Ebajo Jr., C. R. L. Santos, G. V. Alea, Y. A. Lin, C.-H. Chen, *Sci. Rep.* **2019**, *9*, 15579.
[100] As a partial support, when 1,2,3-trimethyl-indole was utilized in the process, the reaction was completely inhibited.

between the methyl group and the GO surface. As a consequence, **TS2**(C3) is significantly lower in energy than **TS2**(N) (8.1 kcal/mol), in perfect agreement with the experimentally observed outcome.

Interestingly, as in Step 1, also in Step 2 the presence of electron-donating groups on the aromatic system favors the reaction and a higher barrier is observed for the C3 allylic alkylation of **2d** compared to **2a** (28.0 vs. 21.4 kcal/mol, Figure S12 in Supplementary data, Chapter 3.5).

It is important to stress that, at the end of the reaction, the alcoholic OH group remains grafted on the GO surface, the carbomaterial thus acting as a promoter and co-reagent rather than displaying a strictly catalytic behavior. This is consistent with the overall increase of alcoholic moieties at expense of the oxirane ones spectroscopically observed by XPS analysis before and after the reaction.

To gain decisive evidence of this covalent grafting activation mode, we went on to try to isolate this grafted intermediate and characterize it by spectroscopic means. To this end, we synthetized allylic alcohol **2f** bearing an azide tag and subjected it to the optimized reaction conditions in the absence of the nucleophile, keeping in mind that XPS data showed that grafting is occurring under these conditions (epoxy- groups decrease accompanied by hydroy- groups increase). The recovered GO was then analyzed via FT-IR and compared to a control GO sample stirred with **2f** (CH_3CN : H_2O) at 0 °C for 30 min. This was done to account for surface adsorption phenomena, as under the latter conditions no grafting should be occurring, while the extent of adsorption is expected to be comparable in the two cases. In the former case, FT-IR displayed the diagnostic N_3 stretching at 2100 cm^{-1} (**Figure 5**, top). On the contrary, a significantly weaker signal was observed in the GO sample treated with **2f** at 0 °C (Figure S2 in Supplementary data, Chapter 3.5). The same results were recorded via XPS N 1s analysis that confirmed univocally the N_3 presence by the characteristic double peak of azides: 404.1 eV, N=N=N and 401.1 for N=N=N (**Figure 5**, bottom

right),[101] while both pristine GO and the control sample presented only residual amounts of amino groups in the region 402–399 eV (**Figure 5**, bottom left).

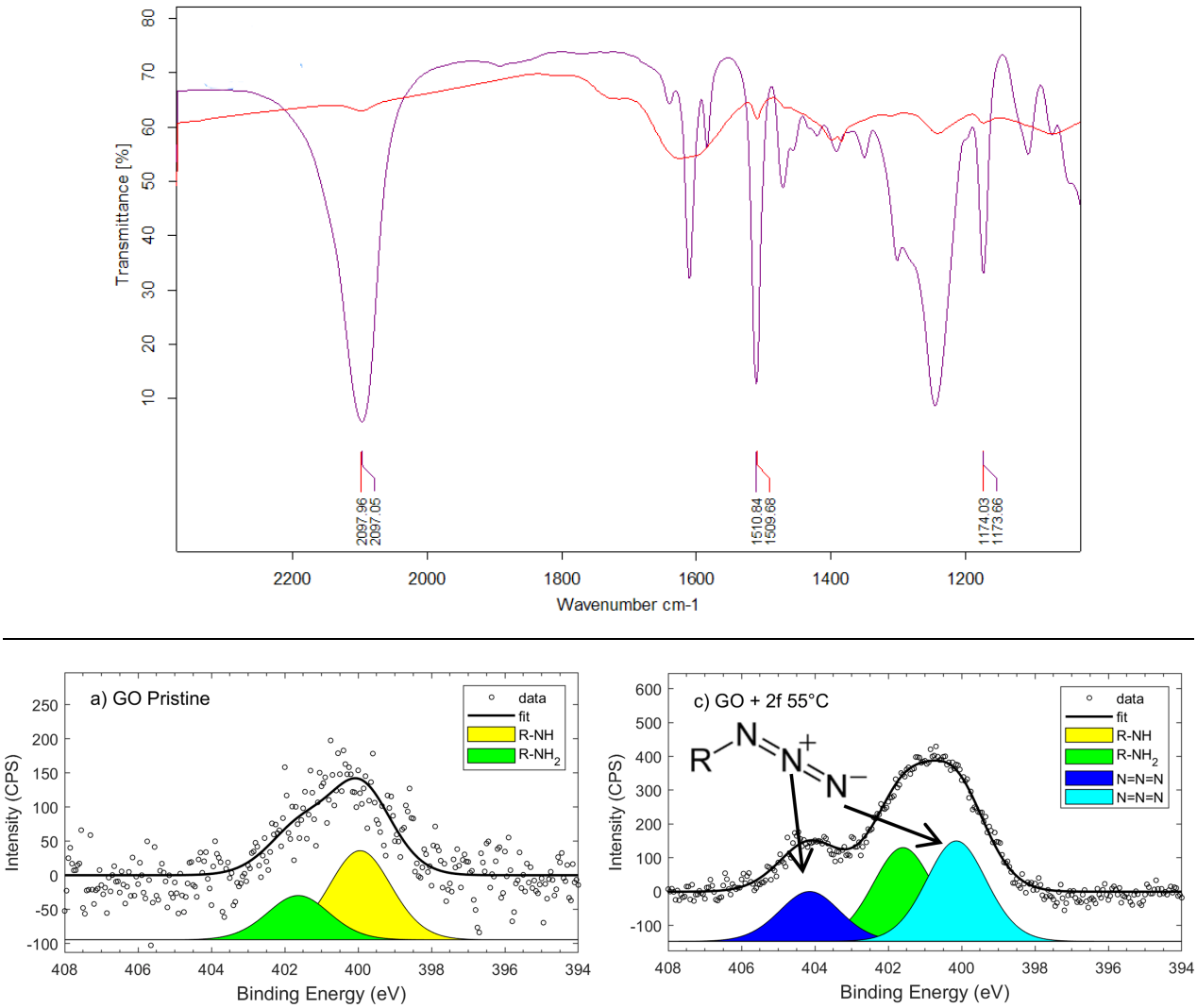

Figure 5. Top: FT-IR analysis of GO reacted with **2f**. Violet: alcohol **2f**; Red: GO+**2f** after 6 h in CH_3CN : H_2O (4:1) at 55°C. Bottom: XPS N 1s signal of: pristine GO (left); GO+**2f** after 6 h in CH_3CN : H_2O (4:1) at 55°C (right).

The obtained reactivity profile prompted us to investigate the possibility of extending the methodology to propargylic alcohols. Here, an interesting selectivity aspect emerges, in that depending on the regiochemistry of the nucleophilic attack, both

[101] a) M. Castelaín, G. Martínez, P. Merino, J. A. Martín-Gago, J. L. Segura, G. Ellis, H. J. Salavagione, *Chem. Eur. J.* **2011**, 18, 4965–46973; b) R. A. Zangmeister, T. A. Morris, M. J. Tarlov, *Langmuir* **2013**, *29*, 8619–8628.

propargylated and allenylated products can in principle be obtained. In particular, we were interested in verifying the hypothesis that the covalent binding of the carbynol unit on the GO should leave exposed to the approaching indole only the terminal acetylenic carbon, leading to the exclusive dearomative allenylation of indoles. This would be an unprecedented scenario, given that existing methods allow for S_N2-like, propargylic selectivity, and that installation of allenyl units in concomitance with indole dearomatization has yet to be realized.[102]

We were pleased to verify that the optimal reaction conditions adopted for the allylic alcohols proved also competent for secondary and tertiary propargylic ones **4a–e**. Both terminal and disubstituted propargylic alcohols demonstrated competent and reacted with exquisite selectivity delivering allenylic di-, tri- and tetrasubstituted indolenines **5** as exclusive products in good yields (40–94%) and modest diastereoisomeric ratio up to 4:1 (**Figure 6**).

[102] a) W. Shao, H. Li, C. Liu, C.-J. Liu, S.-L. You, *Angew. Chem. Int. Ed.* 2015, 54, 7684–7687; b) J. S. Yadav, B. V. Subba Reddy, K. V. Raghavendra Rao, G. G. K. S. Narayana Kumar, *Tetrahedron Lett.* **2007**, *48*, 5573–5576; c) H. Matsuzawa, K. Kanao, Y. Miyake, Y. Nishibayashi, *Org. Lett.* **2007**, *9*, 5561–5564; d) R. Sanz, D. Miguel, A. Martínez, M. Gohain, P. García-García, M. A. Fernández-Rodríguez, E. Álvarez, F. Rodríguez, *Eur. J. Org. Chem.* **2010**, 7027–7039; e) R. Roy, S. Saha, *RSC Adv.* **2018**, *8*, 31129–31193.

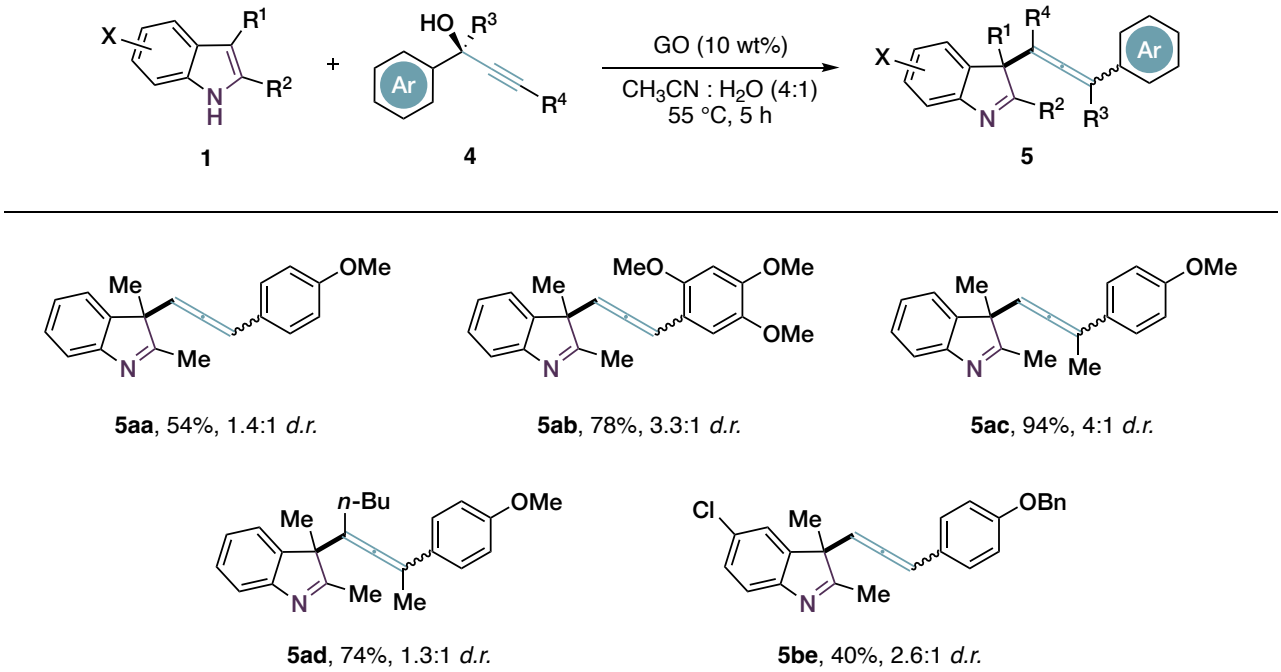

Figure 6. Scope of the GO-promoted dearomative allenylation of indoles. The diastereomeric ratio (*d.r.*) was determined on the reaction crude via ^{1}H NMR. For reaction times, see Supplementary Data, Chapter 3.5.

Interestingly, in this case the use of homogeneous Brønsted acids such as AcOH and *p*-TsOH was completely unsuccessful, the former only delivering trace amount of the desired product, while the latter led to complete decomposition of the propargylic alcohol.

As expected on the basis of the proposed mechanistic scenario, reusability experiments demonstrated a remarkable drop in catalytic performance of the recovered GO even after the first run (12% yield of **3aa** in 36 h, **Scheme 7**, bottom), in agreement with the lower content of epoxy- and carboxylic groups. Being direct recycling impossible, we directed efforts towards the implementation of a regeneration protocol. Inspired by a previous report,[99] we were pleased to observe that simple sonication of the recovered GO under acidic conditions (HCl 1M, 1 h, **Scheme 7**, top), could partially restore the carboxylic and the epoxydic content of the material. XPS analysis showed that the epoxy- and carboxylic groups increased from 24% to 30% and from 0.6% to 1.8%, respectively, upon this acid treatment, coming close to contents found in pristine GO (38% for epoxy-, 1.6% for carboxylic groups). Pleasingly, the regenerated GO gave

performances close to the pristine one when tested in the model reaction (**3aa**, 63 % yield, 36 h, **Scheme 7**, bottom).

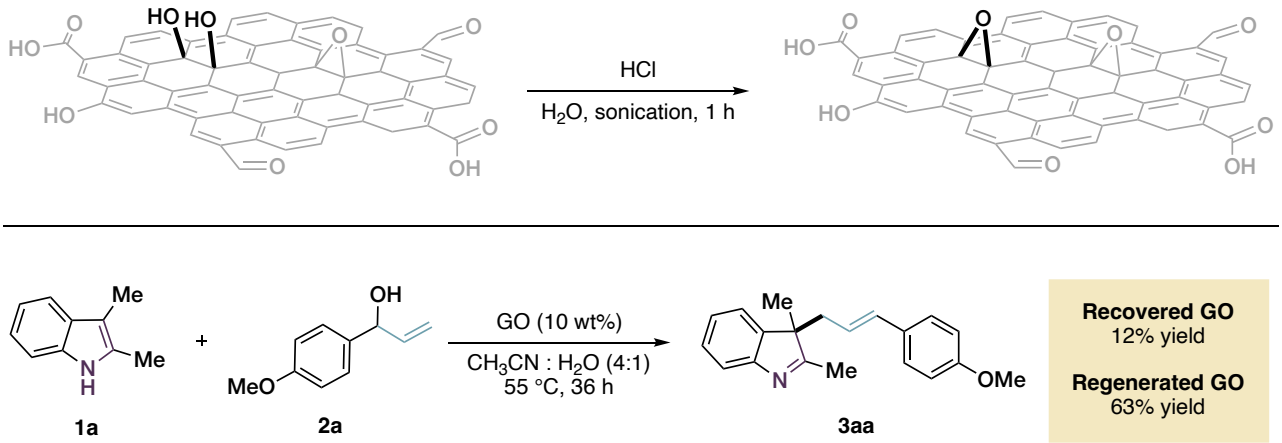

Scheme 7. Top: acidic regeneration of GO; Bottom: Comparing the effectiveness of recovered and regenerated GO in the model reaction.

3.4 Conclusion

In conclusion, an allylative and allenylative dearomatization of 2,3-disubstituted indoles with allylic and propargylic alcohols was realized under carbocatalytic conditions using graphene oxide as a promoter. The transformation proceeds under mild conditions with exquisite regioselectivity on both partners, and does not require late transition metal catalysis or stoichiometric additives, providing an operationally simple protocol towards indolenines bearing allyl or unprecedented allenyl substituted quaternary carbon centers at the C3 position. A synergistic action of the acidic and epoxydic functional groups decorating the graphene surface was highlighted, with multiple proofs of a covalent activation mode. Despite the non-catalytic behavior, an acid promoted regeneration of the activity of the material was also documented.

3.5 Supplementary data

General Methods.

^{1}H NMR spectra were recorded on Varian 400 (400 MHz) spectrometer. Chemical shifts are reported in ppm from TMS with the solvent resonance as the internal standard (deuterochloroform: 7.26 ppm). Data are reported as follows: chemical shift, multiplicity (s = singlet, d = doublet, t = triplet, q = quartet, sext = sextet, sept = septet, p = pseudo, b = broad, m = multiplet, dm = double multiplet), coupling constants (Hz). ^{13}C NMR spectra were recorded on a Varian 400 (100 MHz) spectrometer with complete proton decoupling. Chemical shifts are reported in ppm from TMS with the solvent as the internal standard (deuterochloroform: 77.0 ppm).

GC-MS spectra were taken by EI ionization at 70 eV on a Hewlett-Packard 5971 with GC injection. They are reported as: *m/z* (rel. intensity). LC-electrospray ionization mass spectra were obtained with an Agilent Technologies MSD1100 (nebulizer: 15.0 PSI, dry Gas: 5.0 L/min, dry temperature: 325 °C, capillary voltage positive scan: 4000 mA, capillary voltage negative scan: 3500 mA) single-quadrupole mass spectrometer. Chromatographic purification was done with 240-400 mesh silica gel. Anhydrous solvents were supplied by Sigma Aldrich in Sureseal® bottles and used without any further purification. Commercially available chemicals were purchased from Sigma Aldrich, Stream, TCI, Alfa Aeser and Fluorochem and used without any further purification. Melting points were determined with Bibby Stuart Scientific Melting Point Apparatus SMP 3 and are not corrected.

Indole **1a** was purchased from Merck-Aldrich and Fluorochem and used as received. Indoles **1h** and **1i** were purchased from Alfa Aeser and used as received.

Graphene oxide was purchased from Graphenea as powder and as water dispersion (4 mg/mL). The latter was dried before use.

FT-IR spectra were recorded on Brucker Alpha System spectrometer.

XPS spectra were acquired by using a Phoibos 100 hemispherical energy analyzer (Specs) using Mg K_{α} radiation ($\hbar\omega$ =1253.6 eV). The X-ray power was 125 W. The

spectra were recorded in the constant analyser energy (CAE) mode with analyser pass energies of 10 eV for the high-resolution spectra. Charging effects were corrected by energy calibration on C 1s at 285.0 eV. Overall resolution of 0.9 eV was determined on Ag $3d_{5/2}$. The base pressure in the analysis chamber during analysis was 1×10^{-9} mbar. High resolution XPS spectra of C 1s were analysed by CasaXPS (Casa software, Ltd), the curve fitting was carried out using Gaussian/Lorentzian curves shape (GL(30)) for C-O groups with a full width half-maximum of 1.4 eV and an asymmetric Voigt for the C-C sp^2. The C 1s peak revealed the relative amounts of functional groups:[103] aromatic carbon (C−C sp^2, 284.4 eV), aliphatic carbon (C−C sp^3, 285.0 eV), hydroxyl (C−OH, 285.7 eV), epoxy (C−O−C, 286.7 eV), carbonyl (C=O, 288.0 eV), carboxyl (O−C=O, 289.1 eV) and aromatic carbons near vacancies (C-C* sp^2, 283.5).[104] More detail on consistency of the fitting procedure are reported in our previous work on C 1s fit.[103] GO was measured as a dry powder in solid tablet form.

[103] A. Kovtun, D. Jones, S. Dell'Elce, A. Liscio, V. Palermo, *Carbon* **2019**, *143,* 268-275.
[104] R. Larciprete, P. Locovig, S. Gardonio, A. Baraldi, S. Lizzit, *J. Phys. Chem. C* **2012**, *116*, 9900-9908.

Additional optimizatiton data

Table S1. Optimization reaction conditions

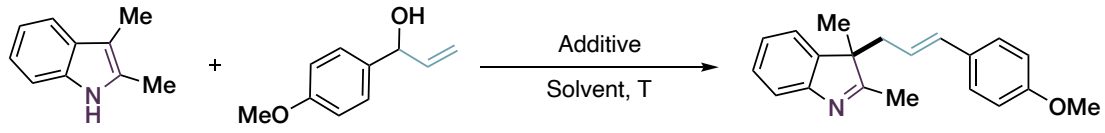

1a (+/-)-**2a** (+/-)-(*E*)-**3aa**

Run[a]	Additive	Solvent	T (°C)	Time (h)	Yield (%) **3aa**[b]
1[c]	GO (25 wt%, flakes)	CH_3Cl	105	5	37
2[c]	GO (50 wt%, flakes)	Toluene	105	8	traces
3[c d]	GO (50 wt%, flakes)	DMF	105	2	--
4[c,e]	GO (25 wt%, flakes)	EtOH	105	2	--
5[f]	GO (50 wt%, flakes)	Toluene : H_2O (7:3)	105	ON	traces
6[f]	GO (25 wt%, flakes)	CH_3Cl : H_2O (1:4)	55	5	67
7[f]	GO (25 wt%, flakes)	Dioxane : H_2O (4:1)	55	5	66
8[f]	GO (25 wt%, flakes)	THF : H_2O (4:1)	55	5	30
9	GO (10 wt%, powder)	CH_3CN : H_2O (4:1)	55	6	68
10[f]	Graphite (25 wt%)	CH_3CN : H_2O (4:1)	55	6	traces
11[f]	*p*-TsOH (pH = 4)	CH_3CN : H_2O (4:1)	55	6	traces
12[f]	Styrene oxide (1 eq)	CH_3CN : H_2O (4:1)	55	6	--
13	Styrene oxide (1 eq), AcOH (pH = 4)	CH_3CN : H_2O (4:1)	55	6	27
14	Used GO (10 wt%, powder)	CH_3CN : H_2O (4:1)	55	36	12
15	Regenerated GO (10 wt%, powder)	CH_3CN : H_2O (4:1)	55	36	63

[a] All the reactions were carried out with reagent grade solvents, unless otherwise specified (1a/2a = 1/2 on 0.15 mmol of 1a, 0.1 M). [b] Determined after flash chromatography. [c] **1a**/**2a** = 1:1.5. [d] Decomposition of indole 1a was observed. [e] Alcohol **2a** decomposed. [f] **1a**/**2a** = 1:3.

Synthesis and characterization of starting materials

Synthesis of allylic and propargylic acohols **2** and **4**

All alcohols were synthetized via addition of vinyl- or ethynylmagnesium bromide to the corresponding carbonyl compound according to literature procedures.[105a,e]

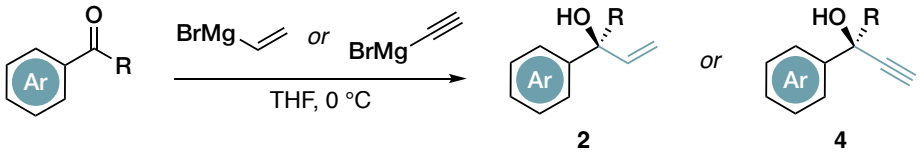

In a flame-dried three-necked round bottom flask, equipped with a dropping funnel, were added anhydrous THF (2.5 mL, 0.8 M) and carbonyl compound (2 mmol, 1 eq) under N_2 atmosphere and the mixture was cooled to 0 °C. Then vinylmagnesium bromide (1 M in THF, 2.4 mL, 2.4 mmol, 1.2 eq) or ethynylmagnesium bromide (0.5 M in THF, 4.8 mL, 2.4 mmol, 1.2 eq) was added dropwise. After the addition the ice bath was removed, and the mixture was allowed to warm at room temperature and stirred for 1-5 h. The reaction was quenched with a saturated aqueous NH_4Cl solution, extracted with EtOAc and the combined organic phases were washed with brine and then dried over Na_2SO_4. Solvent was removed by rotary evaporation and the crude was purified by column chromatography to give the desired product.

[105] a) L. Favaretto, J. An, M. Sambo, A. De Nisi, C. Bettini, M. Melucci, A. Kovtun, A. Liscio, V. Palermo, A. Bottoni, F. Zerbetto, M. Calvaresi, M. Bandini, *Org. Lett.* **2018**, *20*, 3705–3709; b) M. Agirre, S. Henrion, I. Rivilla, J. I. Miranda, F. P. Cossío, B. Carboni, J. M. Villalgordo, F., Carreaux, *J. Org. Chem.* **2018**, *83*, 14861–14881; c) S. F. Musolino, O. S. Ojo, N. J. Westwood, J. E. Taylor, A. D. Smith, *Chem. Eur. J.* **2016**, *22*, 18916–18922; d) S. Prvost, N. Dupr, M. Leutzsch, Q. Wang, V. Wakchaure, B. List, *Angew. Chem. Int. Ed.* **2014**, *53*, 8770–8773; e) Y. Horino, M. Murakami, M. Ishibashi, J. H. Lee, A. Watanabe, R. Matsumoto, H. Abe, *Org. Lett.* **2019**, *21*, 9564-9568; f) M. Isomura, D. A. Petrone, E. M. Carreira, *J. Am. Chem. Soc.* **2019**, *141*, 4738-4748.

Characterization of allylic and propargylic acohols **2** and **4**

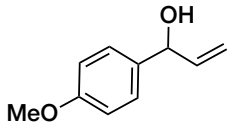

2a. Pale yellow oil; yield = 88% (289 mg, *c*Hex:EtOAc 3:1). Spectral data match those reported in the literature.[105a]

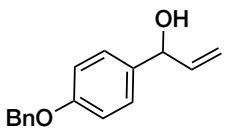

2b. White solid; yield = 67% (322 mg, *c*Hex:EtOAc 4:1). Spectral data match those reported in the literature.[105b]

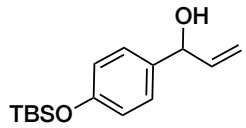

2c. Yellow oil; yield = 50% (264 mg, *c*Hex:EtOAc 8:1). **^{1}H NMR** (400 MHz, $CDCl_3$) δ 7.23 – 7.18 (m, 2H), 6.82 – 6.77 (m, 2H), 6.03 (ddd, *J* = 17.1, 10.3, 5.7 Hz, 1H), 5.31 (d, *J* = 17.1 Hz, 1H), 5.17 (d, *J* = 10.3 Hz, 1H), 5.13 (d, *J* = 5.7 Hz, 1H), 1.92 (brs, 1H), 0.97 (s, 9H), 0.18 (s, 6H). **^{13}C NMR** (100 MHz, $CDCl_3$) δ 155.27, 140.34, 135.35, 127.57, 120.06, 114.71, 74.89, 25.65 (9C), 18.17 -4.45 (6C). **LC-MS** (m/z): $[M\text{-}OH]^+$ = 247.0. Anal. Calc**.** for ($C_{15}H_{24}O_2Si$: 264.44): C, 68.13; H, 9.15; found: C, 68.31; H, 9.26.

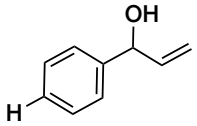

2d. Colourless oil; yield = 80% (215 mg, *c*Hex:AcOEt = 4:1). Spectral data match those reported in the literature.[105c]

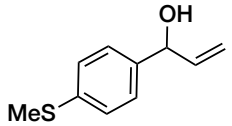

2e. Pale yellow solid; yield = 83% (314 mg, *c*Hex:EtOAc = 4:1). **^{1}H NMR** (400 MHz, $CDCl_3$) δ 7.26 (d, *J* = 8.4 Hz, 2H), 7.22 (d, *J* = 8.4 Hz, 2H), 6.00 (ddd, *J* = 17.1, 10.3, 5.9 Hz, 1H), 5.31 (d, *J* = 17.1 Hz, 1H), 5.17 (d, *J* = 10.3 Hz, 1H), 5.13 (d, *J* = 5.9 Hz, 1H), 2.46 (s, 3H), 2.14 (brs, 1H). **^{13}C NMR** (100 MHz, $CDCl_3$) δ 140.07, 139.48, 137.83, 126.86, 126.73, 115.17, 74.88, 15.89 (3C). **LC-MS** (m/z): $[M\text{-}OH]^+$ = 163.0; $[M+OH]^+$ = 197.0; $[M+K]^+$ = 219.0. Anal. Calc. for ($C_{10}H_{12}OS$: 180.27): C, 66.63; H, 6.71; found: C, 66.55; H, 6.81.

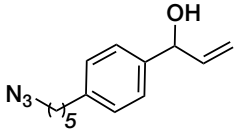

2f. Pale yellow oil; yield = 65% (349 mg, *c*Hex:EtOAc = 4:1). Spectral data match those reported in the literature.[105a]

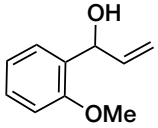

2g. Colourless oil; yield = 68% (223 mg, *c*Hex:EtOAc = 4:1). Spectral data match those reported in the literature.[105b]

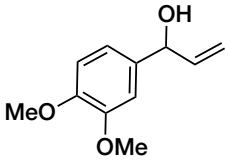

2h. White solid; yield = 69% (268 mg, *c*Hex:EtOAc = 2.5:1). Spectral data match those reported in the literature.[105b]

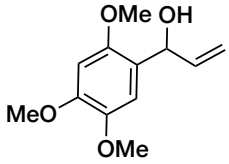

2i. Pale yellow solid; yield = 80% (359 mg, *c*Hex:EtOAc = 1.5:1). **^{1}H NMR** (400 MHz, $CDCl_3$) δ 6.85 (s, 1H), 6.51 (s, 1H), 6.07 (ddd, *J* = 17.1, 10.4, 5.4 Hz, 1H), 5.38 (dddd, *J* = 17.2, 5.5 Hz, 1.5 Hz, 1,5 Hz, 1H), 5.29 (ddd, *J* = 17.2, 1.5 Hz, 1,5 Hz, 1H), 5.14 (ddd, *J* = 10.4, 1.5 Hz, 1.5 Hz, 1H), 3.86 (s, 3H), 3.82 (s, 6H), 2.58 (d, *J* = 5.5 Hz, 1H).**^{13}C NMR** (100 MHz, $CDCl_3$) δ 150.80, 148.92, 143.13, 139.72, 122.47, 114.10, 111.28, 97.68, 70.27, 56.48 (3C), 56.31 (3C), 56.12 (3C). **LC-MS** (m/z): 207.0 $[M\text{-}OH]^+$, 247.0 $[M+Na]^+$, 471.0 $[2M+Na]^+$. Anal. Calc. for ($C_{12}H_{16}O_4$: 224.26): C, 64.27; H, 7.19; found: C, 64.16; H, 7.25.

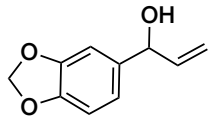

2j. Yellow oil; yield = 70% (250 mg, *n*Hex:EtOAc 4:1). Spectral data match those reported in the literature.[105b]

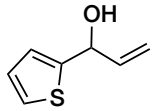

2k. Yellow oil; yield = 51 % (143 mg, *c*Hex:EtOAc = 6:1). Spectral data match those reported in the literature.[105c]

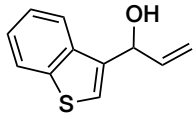

2l. Yellow oil; yield = 65% (247 mg, *c*Hex:EtOAc = 4:1). **^{1}H NMR** (400 MHz, $CDCl_3$)) δ 7.92 – 7.87 (m, 1H), 7.87 – 7.82 (m, 1H), 7.47 – 7.30 (m, 3H), 6.18 (ddd, *J* = 17.2, 10.3, 5.7 Hz, 1H), 5.53 (d, *J* = 5.7 Hz, 1H), 5.45 (d, *J* = 17.2 Hz, 1H), 5.28 (d, *J* = 10.3 Hz, 1H), 2.30 (s, 1H). **^{13}C NMR** (100 MHz, $CDCl_3$) δ 138.38, 136.07, 134.88, 134.63, 121.91, 121.49, 120.68, 120.29, 120.00, 113.53, 68.10.

LC-MS (m/z): $[M\text{-}OH]^+$ = 173.0. Anal. Calc. for ($C_{11}H_{10}OS$: 190.26): C, 69.44; H, 5.30; found: C, 69.21; H, 5.18.

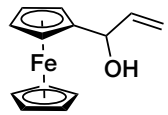

2m. Red oil; yield = 60% (291 mg, *n*Hex:EtOAc = 6:1). **^{1}H NMR** (400 MHz, $CDCl_3$) δ 6.07 (ddd, *J* = 17.1, 10.4, 5.9 Hz, 1H), 5.31 (d, *J* = 17.1 Hz, 1H), 5.16 (d, *J* = 10.4 Hz, 1H), 4.84 (dd, *J* = 5.9 Hz, 5.1 Hz, 1H), 4.21 – 4.14 (m, 9H), 1.91 (d, *J* = 5.1 Hz, 1H).**^{13}C NMR** (100 MHz, $CDCl_3$) δ 139.59, 114.99, 91.80, 70.65, 68.41 (5C), 68.19, 68.15, 66.69, 66.47. **LC-MS** (m/z): $[M]^+$ = 242.0. Anal. Calc. for ($C_{13}H_{14}FeO$: 242.10): C, 64.50; H, 5.83; found: C, 64.31; H, 5.58.

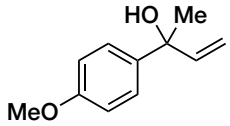

2n. Pale yellow oil; yield = 88% (314 mg, *c*Hex:EtOAc = 25:1). Spectral data match those reported in the literature.[105d]

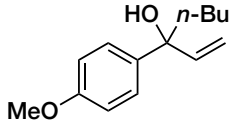

2o. Colourless oil; yield = 60% (264 mg, *c*Hex:EtOAc = 20:1). **^{1}H NMR** (400 MHz, $CDCl_3$) δ 7.34 (d, *J* = 8.9 Hz, 1H), 6.86 (d, *J* = 8.9 Hz, 1H), 6.16 (dd, *J* = 17.2, 10.7 Hz, 1H), 5.26 (dd, *J* = 17.2, 1.0 Hz, 1H), 5.12 (dd, *J* = 10.7, 1.0 Hz, 1H), 3.78 (s, 3H), 1.94 – 1.80 (m, 2H), 1.78 (s, 1H), 1.33 – 1.03 (m, 4H), 0.85 (t, *J* = 7.1 Hz, 3H). **^{13}C NMR** (100 MHz, $CDCl_3$) δ 158.33, 144.47, 137.87, 126.57, 113.44, 112.17, 55.20, 41.81, 25.78, 22.99, 14.00. **LC-MS** (m/z): $[M\text{-}OH]^+$ = 203.0. Anal. Calc. for ($C_{14}H_{20}O_2$: 220.31): C, 76.33; H, 9.15; found: C, 76.18; H, 9.01.

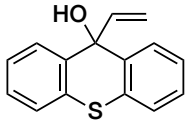

2p. Pale yellow solid; yield = 70% (336 mg, cHex:EtOAc = 6:1). **^{1}H NMR** (400 MHz, $CDCl_3$) δ 7.85 (dd, J = 7.8, 1.2 Hz, 2H), 7.39 (dd, J = 7.6, 1.1 Hz, 2H), 7.31 (ddd, J = 7.6, 7.6, 1.4 Hz, 2H), 7.24 (ddd, J = 7.5, 7.5,1.5 Hz, 2H), 5.91 (dd, J = 17.1, 10.2 Hz, 1H), 5.03 (dd, J = 10.2, 0.8 Hz, 1H), 4.79 (dd, J = 17.1, 0.8 Hz, 1H), 2.73 (brs, 1H). **^{13}C NMR** (100 MHz, $CDCl_3$) δ 138.53, 138.24, 130.64, 127.49, 126.65, 126.18, 125.74, 114.45, 75.42. **LC-MS** (m/z): 223.0 $[M\text{-}OH]^+$. **Anal. Calc.** for ($C_{15}H_{12}OS$: 240.32): C, 74.97; H, 5.03; found: C, 74.79; H, 5.21.

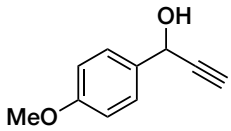

4a. Pale yellow oil which solidifies on standing; yield = 90% (291 mg, *c*Hex:EtOAc = 3.4:1). Spectral data match those reported in the literature.[105e]

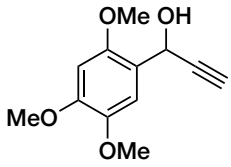

4b. White solid; yield = 75% (333 mg, cHex:EtOAc = 1.5:1). **^{1}H NMR** (400 MHz, $CDCl_3$) δ 7.13 (s, 1H), 6.52 (s, 1H), 5.67 (dd, J = 5.9, 2.2 Hz, 1H), 3.88 (s, 3H), 3.86 (s, 3H), 3.85 (s, 3H), 2.81 (d, J = 5.9 Hz, 1H), 2.60 (d, J = 2.3 Hz, 1H). **^{13}C NMR** (100 MHz, $CDCl_3$) δ 151.05, 149.92, 143.09, 119.87, 111.77, 97.59, 83.37, 73.92, 60.32, 56.54, 56.44, 56.19. **GC-MS** (m/z): 222 (100) $[M]^+$, 205 (58) $[M\text{-}OH]^+$, 191 (31) $[M\text{-}OMe]^+$. **Anal. Calc.** for ($C_{12}H_{14}O_4$: 222.24): C, 64.85; H, 6.35; found: C, 64.71; H, 6.20.

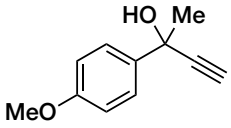

4c. Pale yellow solid; yield = 36% (127 mg, *c*Hex:EtOAc = 4:1). Spectral data match those reported in the literature.[105f]

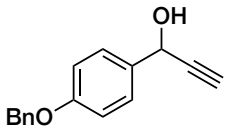

4e. White solid; yield = 68% (324 mg, cHex:EtOAc = 5:1). **^{1}H NMR** (400 MHz, $CDCl_3$) δ 7.49 – 7.44 (m, 2H), 7.44 – 7.35 (m, 4H), 7.35 – 7.29 (m, 1H), 7.01 – 6.93 (m, 2H), 5.40 (dd, J = 5.7, 1.9 Hz, 1H), 5.07 (s, 2H), 2.65 (d, J = 2.2 Hz, 1H), 2.21 (d, J = 5.9 Hz, 1H).**^{13}C NMR** (100 MHz, $CDCl_3$) δ 158.97, 136.79, 132.60, 128.58 (2C), 128.07 (2C), 127.99, 127.40 (2C), 114.96 (2C), 83.64, 74.64, 70.05, 64.01.**GC-MS** (m/z): 238 (6) $[M]^+$, 91 (100), 65 (13). **Anal. Calc.** for ($C_{16}H_{14}O_2$: 238.29): C, 80.65; H, 5.92; found: C, 80.33; H, 5.68.

Synthesis of aldehyde precursors and propagylic alcohol **4d**

Alcohol **2b**: This compound was synthetized from 4-hydroxybenzaldehyde according to literature procedure.[106a]

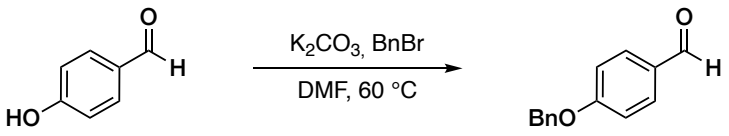

Alcohol **2f**: This compound was synthetized from 4-hydroxybenzaldehyde according to know literature procedures.[105a]

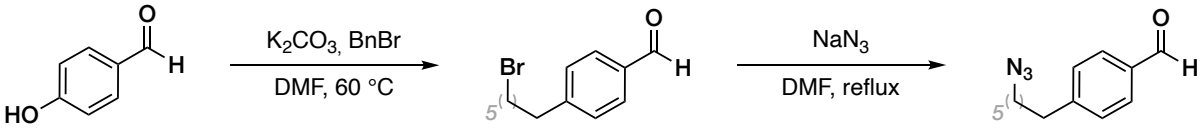

Alcohol **2f**: This compound was synthetized by oxidation of piperonol using IBX.

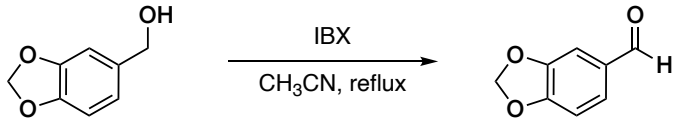

In a flame-dried two-necked round bottom flask were added anhydrous CH_3CN (7.5 mL, 0.4 M), piperonol (475 mg, 3 mmol, 1 eq) and IBX (1.68 g, 6mmol, 2 eq) under N_2 atmosphere. The mixture was refluxed overnight. The reaction mixture was filtered on a pad of Celite and the solvent was removed under vacuum. The crude was then dissolved in CH_2Cl_2 and washed with a saturated $NaHCO_3$ aqueous solution, then with a $Na_2S_2O_3$ aqueous solution (1 M) and dried over Na_2SO_4. Solvent was removed by rotary evaporation and the crude was purified by column chromatography.

---

[106] a) W. Kurosawa, T. Kan, T. Fukuyama, *J. Am. Chem. Soc.* **2003**, *125*, 8112–8113; b) K. Natte, A. Dumrath, H. Neumann, M. Beller, *Angew. Chem. Int. Ed.* **2014**, 53, 10090–10094; c) , J. K. Park, W. K. Shin, D. K. An, *Tetrahedron Lett.* **2013**, *54*, 3199–3203; d) D. Lebœuf, A. Simonneau, C. Aubert, M. Malacria, V. Gandon, L. Fensterbank, *Angew. Chem. Int. Ed.* **2011**, *50*, 6868-6871.

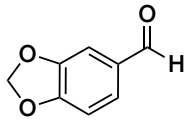

Yellow oil; yield = 86% (387 mg, *n*Hex:EtOAc = 6:1). Spectral data match those reported in the literature.[106b]

Alcohol **2o**: This compound was synthetized from 4-methoxybenzoyl chloride according to know literature procedures.[106c]

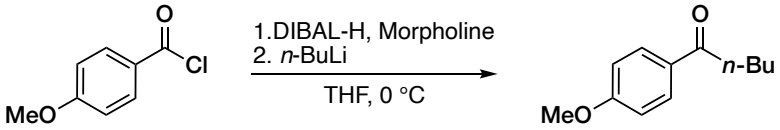

Alcohol **4d**: This compound was synthetized from 4-methoxyacetophenone and hex-1-yne according to a general known procedure.[106d]

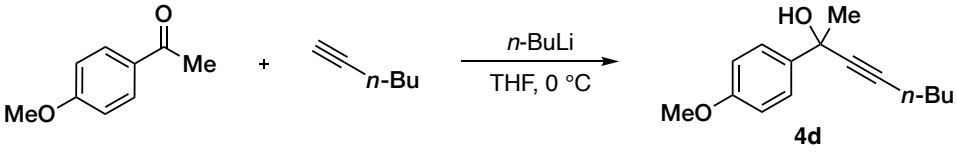

In a flame-dried three-necked round bottom flask were added anhydrous THF (4 mL) and hex-1-yne (0.49 mL, 4.4 mmol, 2.2 eq). *n*-BuLi (2.5 M in Hex, 1.6 mL, 4 mmol, 2 eq) was added dropwise at -78°C and the mixture was stirred at -78°C for 1 hour. Then a solution of 4-methoxyacetophenone (300 mg, 2 mmol, 1 eq) in THF (2.5 mL) was added dropwise at -78°C. After the addition the mixture was allowed to warm to room temperature and stirred overnight. The reaction was quenched with a saturated aqueous NH_4Cl solution, extracted with EtOAc and the combined organic phases were washed with brine and then dried over Na_2SO_4. Solvent was removed by rotary evaporation and the crude was purified by column chromatography to give the desired product.

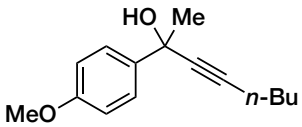

4d. Pale yellow oil; yield = 51% (238 mg, *n*Hex:EtOAc = 6:1). **^{1}H NMR** (400 MHz, $CDCl_3$) δ 7.56 (d, *J* = 8.6 Hz, 2H), 6.86 (d,

J = 8.6 Hz, 2H), 3.79 (s, 3H), 2.26 (t, *J* = 7.0 Hz, 2H), 2.22 (s, 1H), 1.72 (s, 3H), 1.57 – 1.38 (m, 4H), 0.91 (t, *J* = 7.2 Hz, 3H). **^{13}C NMR** (100 MHz, $CDCl_3$) δ 158.94, 138.45, 126.22, 113.42, 85.48, 83.85, 69.66, 55.27, 33.41, 30.72, 21.96, 18.39, 13.56. **GC-MS** (m/z): 214 (100) $[M\text{-}H_2O]^+$, 172 (36), 128 (56). Anal. Calc. for ($C_{15}H_{20}O_2$: 232.32): C, 77.55; H, 8.68; found: C, 77.21; H, 8.57.

Synthesis and characterization of 2,3-disubstituted indoles **1b-c**, **1e-g**, **1j-o**.

Indoles were synthetized from aryl hydrazines and ketones using Fischer's indole synthesis and are known compounds. All commercially available carbonyl compounds were used without further purification.

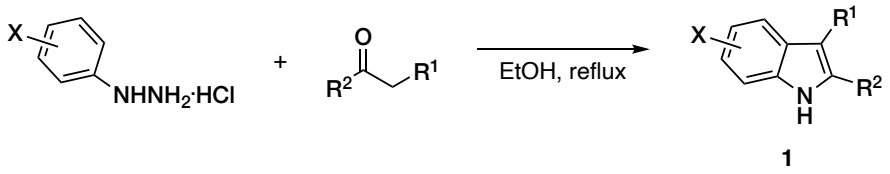

1

A Schenk tube was charged with aryl hydrazine hydrochloride (3 mmol, 1.5 eq), ketone (2mmol, 1 eq) and reagent grade ethanol (4 mL, 0.5 M). The reaction mixture was stirred at refluxed until complete consumption of the ketone.

After cooling, the solvent was removed under vacuum, the crude was dissolved in ethyl acetate and washed with 2M aqueous HCl, saturated aqueous $NaHCO_3$, deionized water, brine and dried over Na_2SO_4. Solvent was removed by rotary evaporation and (when necessary) the crude was purified by column chromatography to give the desired indole.

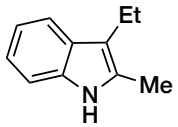

1b. Pale brown solid, yield = 46% (147 mg, *n*Hex:Acetone = 16:1). Spectral data match those reported in the literature.[107a]

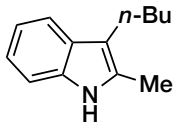

1c. Yellow oil, yield = 49% (184 mg, *n*Hex:Acetone = 10:1). Spectral data match those reported in the literature.[107b]

[107] a) H.-D. Xia, Y.-D. Zhang, Y.-H. Wang, C. Zhang, *Org. Lett.* **2018**, *20*, 4052–4056; b) C. A. Simoneau, B. Ganem, *Tetrahedron* **2005**, *61*, 11374–11379; c) D. A. Vargas, A. Tinoco, V. Tyagi, R. Fasan, *Angew. Chem. Int. Ed.* **2018**, *57*, 9911–9915; d) H. Long, K. Xu, S. Chen, J. Lin, D. Wu, B. Wu, X. Tian, L. Ackermann, *Org. Lett.* **2019**, *21*, 3053-3056; e) N. Douglas, C. J. Neef, R. A. Rogers, J. A. Stanley, J. Armitage, B. Martin, T. W. Hudnall, W. J., *J. Phys. Org. Chem.* **2013**, *26*, 688–695; f) Y. Li, T. Yan, K. Junge, M. Beller, *Chem. Int. Ed.* **2014**, *53*, 10476–10480.

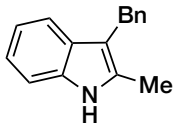

1d. Pale orange solid, yield = 50% (221 mg, *c*Hex:AcOEt = 4:1). Spectral data match those reported in the literature.[107a]

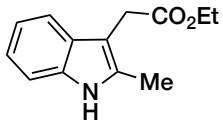

1e. Yellow oil, yield = 48% (209 mg, *n*Hex:Acetone = 3.5:1). Spectral data match those reported in the literature.[107c]

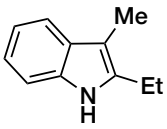

1f. Yellow oil, yield = 52% (166 mg, *n*Hex:Acetone = 16:1). Spectral data match those reported in the literature.[107a]

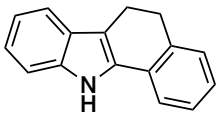

1g. Pale brown solid, yield = 64% (281 mg, *n*Hex:Acetone = 10:1). Spectral data match those reported in the literature.[107d]

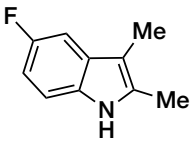

1j. Pale brown solid, yield = 59% (193 mg, *c*Hex:AcOEt = 12:1). Spectral data match those reported in the literature.[107e]

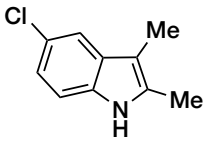

1k. White solid, yield = 54% (194 mg, *c*Hex:AcOEt = 8:1). Spectral data match those reported in the literature.[107f]

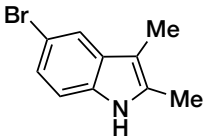

1i. Orange solid, yield = 67% (300 mg, No purification). Spectral data match those reported in the literature.[107f]

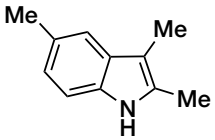

1m. Brown solid, yield = 93% (296 mg, No purification). Spectral data match those reported in the literature.[107f]

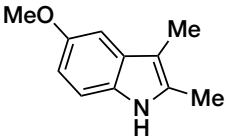

1n. Pale brown solid, yield = 44% (154 mg, *n*Hex:Acetone = 8:1). Spectral data match those reported in the literature.[107f]

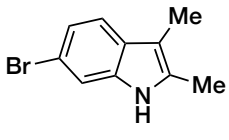

1o. Pale brown solid, yield = 30% (135 mg, *n*Hex:AcOEt = 10:1). Spectral data match those reported in the literature.[107f]

Synthesis of aryl hydrazines

Aryl hydrazines were synthetized the from corresponding commercially available anilines that were used without further purification.[108]

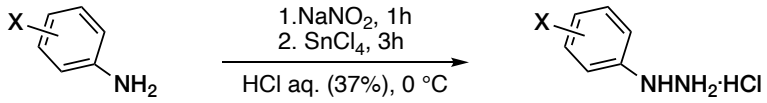

A one neck round-bottom flask is charged with aniline (1 eq) then HCl (37%) is added dropwise at 0 °C (for hydrazine **4f** at -15 °C). An aqueous solution of $NaNO_2$ (1.5 eq, 2 M) is added dropwise and the solution is stirred for 1 h at 0°C (for hydrazine **4f** at -15 °C). Then a solution of $SnCl_4$ (3 eq, 1 M) in aqueous conc. HCl (37%) is added in one portion and the mixture is stirred for another 3 hours at 0 °C. The solution is then filtered and the solid is washed with a small amount of deionized water (0 °C) and then Et_2O to yield the hydrochloride salt of the desired aryl hydrazine. The obtained hydrochloride salts were employed in the synthesis of the indoles without further purifications.

[108] S. V. Kumar, D. Ma, *Chin. J. Chem.* **2018**, *36*, 1003－1006.

General procedure for the allylic dearomatization of indoles

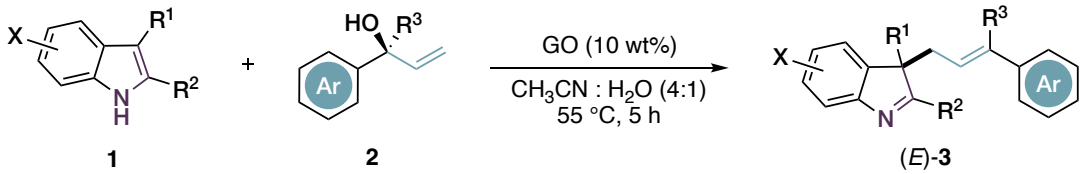

A screw-capped vial is charged with CH_3CN (1.2 mL), allylic alcohol **2** (0.3 mmol, 2 eq), indole **1** (0.15 mmol, 1 eq), GO dried flakes (10 wt% with respect to indole) and deionized water (0.3 mL). The reaction mixture was stirred at 55 °C (unless otherwise noted) until complete consumption of indole (*vide infra* for reaction times). The mixture was then filtered on a Gooch funnel and the GO washed with EtOAc. The collected organic layers were dried over Na_2SO_4 and evaporated to dryness under vacuum. The crude was purified by column chromatography to give the desired product **3**.

Characterization data of products 3

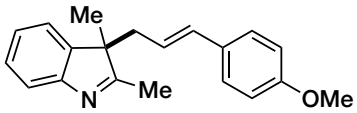

3aa. Yellow oil, yield = 70% (31 mg, 6 h, *n*Hex:Et_2O = 1:1.8). **^{1}H NMR** (400 MHz, $CDCl_3$) δ 7.52 (d, *J* = 7.6 Hz, 1H), 7.33 – 7.25 (m, 2H), 7.18 (t, *J* = 7.4 Hz, 1H), 7.07 (d, *J* = 8.6 Hz, 2H), 6.75 (d, *J* = 8.6 Hz, 2H), 6.25 (d, *J* = 15.7 Hz, 1H), 5.47 (ddd, *J* = 15.7, 8.0, 6.7 Hz, 1H), 3.74 (s, 3H), 2.72 (dd, *J* = 13.9, 6.7 Hz, 1H), 2.48 (dd, *J* = 13.9, 8.0 Hz, 1H), 2.28 (s, 3H), 1.33 (s, 3H).**^{13}C NMR** (100 MHz, $CDCl_3$) δ 186.67, 158.95, 154.09, 143.47, 132.53, 129.78, 127.72, 127.23, 124.99, 121.91, 121.87, 119.85, 113.81, 57.74, 55.22, 40.34, 21.61, 16.00. **LC-MS** (m/z): 147.2 $[C_{10}H_{11}O]^+$, 314.2 $[M+Na]^+$. Anal. Calc. for ($C_{20}H_{21}NO$: 291.39): C, 82.44; H, 7.26; found: C, 82.31; H, 7.31.

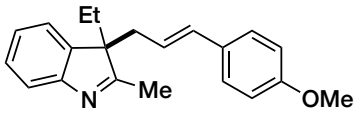

3ba. Pale yellow oil, yield = 68% (31 mg, 16 h, *n*Hex:Et_2O = 1:2). **^{1}H NMR** (400 MHz, $CDCl_3$) δ 7.50 (d, *J* = 7.6 Hz, 1H), 7.29 (dt, *J* = 7.6, 1.4 Hz, 1H), 7.25-7.21 (m, 1H), 7.18 (dt, *J* = 7.5, 0.8 Hz, 1H), 7.09 – 7.00 (m, 2H), 6.77 – 6.68 (m, 2H), 6.23 (d, *J* = 15.6 Hz, 1H), 5.41 (ddd, *J* = 15.6, 8.0, 6.6 Hz, 1H), 3.73 (s, 3H), 2.75 (ddd, *J* = 13.9, 6.6, 1.4 Hz, 1H), 2.49 (ddd, *J* = 13.9, 8.0, 0.8 Hz, 1H), 2.24 (s, 3H), 2.01 (dq, *J* = 15.0, 7.4 Hz, 1H), 1.84 (dq, *J* = 15.0, 7.4 Hz, 1H), 0.37 (t, *J* = 7.4 Hz, 3H). **^{13}C NMR** (100 MHz, $CDCl_3$) δ 185.54, 158.89, 155.24, 141.38, 132.29, 129.84, 127.68, 127.19, 124.88, 122.01, 121.87, 119.71, 113.77, 62.99, 55.21, 40.01, 28.85, 16.30, 8.12. **LC-MS** (m/z): 147.2 $[C_{10}H_{11}O]^+$, 328.2 $[M+Na]^+$. Anal. Calc. for ($C_{21}H_{23}NO$: 305.42): C, 82.58; H, 7.59; found: C, 82.36; H, 7.69.

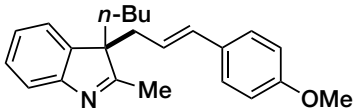

3ca. Yellow oil, yield = 61% (31 mg, overnight, Hex:Et_2O = 1:1). **^{1}H NMR** (400 MHz, $CDCl_3$) δ 7.50 (d, *J* = 7.6 Hz, 1H), 7.29 (t, *J* = 7.5 Hz, 1H), 7.24 (d, *J* = 7.3Hz, 1H), 7.18 (t, *J* = 7.3 Hz, 1H), 7.05 (d, *J* = 8.5 Hz, 2H), 6.73 (d, *J* = 8.6 Hz, 2H), 6.22 (d, *J* = 15.7 Hz, 1H), 5.40 (ddd, *J* = 15.7, 8.1, 6.6 Hz, 1H), 3.73 (s, 3H), 2.74 (dd, *J* = 13.9, 6.6 Hz, 1H), 2.48 (dd, *J* = 13.9, 8.1

Hz, 1H), 1.95 (td, *J* = 12.9, 4.6 Hz, 1H), 1.78 (td, *J* = 12.8, 4.6 Hz, 1H), 1.21 – 1.06 (m, 2H), 0.80 – 0-63 (m, 4H), 0.63 – 0.49 (m, 1H). **^{13}C NMR** (100 MHz, $CDCl_3$) δ 185.80, 158.89, 155.04, 141.81, 132.31, 129.84, 127.64, 127.20, 124.87, 121.98, 121.81, 119.71, 113.77, 62.42, 55.21, 40.29, 35.70, 25.80, 22.81, 16.35, 13.73. **LC-MS** (m/z): 147.0 $[C_{10}H_{11}O]^+$, 356.2 $[M+Na]^+$. Anal. Calc. for ($C_{23}H_{27}NO$: 333.48): C, 82.84; H, 8.16; found: C, 82.65; H, 8.02.

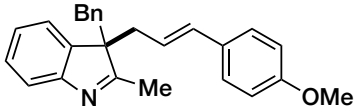

3da. Pale yellow oil, yield = 47% (26 mg, 7h, *n*Hex:Et_2O = 1:1.1, then *n*Hex:Acetone 4:1). **^{1}H NMR** (400 MHz, $CDCl_3$) δ 7.38 (d, *J* = 7.6 Hz, 1H), 7.25 (ddd, 8.4, 7.7, 3.7 Hz, 1H), 7.19 – 7.12 (m, 2H), 7.10 – 6.99 (m, 5H), 6.79 – 6.68 (m, 4H), 6.27 (d, *J* = 15.7 Hz, 1H), 5.34 (ddd, *J* = 15.7, 8.1, 6.5 Hz, 1H), 3.73 (s, 3H), 3.28 (d, *J* = 13.6 Hz, 1H), 2.95 (d, *J* = 13.6 Hz, 1H), 2.89 (dd, *J* = 14.0, 6.5 Hz, 1H), 2.68 (dd, *J* = 14.0, 8.1 Hz, 1H), 2.34 (s, 3H). **^{13}C NMR** (100 MHz, $CDCl_3$) δ 184.60, 158.94, 154.97, 140.90, 135.79, 132.57, 129.73, 129.30, 127.85, 127.75, 127.23, 126.65, 124.61, 122.92, 121.51, 119.82, 113.77, 63.03, 55.22, 42.01, 39.70, 16.96. **LC-MS** (m/z): 147.0 $[C_{10}H_{11}O]^+$, 390.0 $[M+Na]^+$. Anal. Calc**.** for ($C_{26}H_{25}NO$: 367.49): C, 84.98; H, 6.86; found: C, 84.71; H, 6.71.

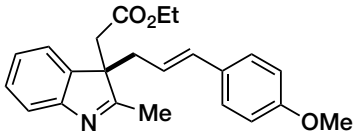

3ea. Yellow oil, yield = 57% (31 mg, *n*Hex:Et_2O = 1:3). **^{1}H NMR** (400 MHz, $CDCl_3$) δ 7.49 (d, *J* = 7.6 Hz, 1H), 7.30 (m, 2H), 7.17 (t, *J* = 7.4 Hz, 1H), 7.07 (d, *J* = 8.6 Hz, 2H), 6.75 (d, *J* = 8.6 Hz, 2H), 6.25 (d, *J* = 15.7 Hz, 1H), 5.45 (ddd, *J* = 15.7, 7.7, 6.7 Hz, 1H), 3.81 (q, *J* = 7.1 Hz, 2H), 3.74 (s, 3H), 2.95 (d, *J* = 14.5 Hz, 1H), 2.81-2.72 (m, 2H), 2.46 (dd, *J* = 13.8, 7.7 Hz, 1H), 2.34 (s, 3H), 0.88 (t, *J* = 7.1 Hz, 3H). **^{13}C NMR** (100 MHz, $CDCl_3$) δ 184.30, 169.22, 159.06, 154.78, 140.15, 133.37, 129.55, 128.24, 127.30, 124.94, 122.50, 120.66, 119.98, 113.83, 60.46, 59.39, 55.23, 39.83, 39.82, 16.42, 13.66. **LC-MS** (m/z): 147.0 $[C_{10}H_{11}O]^+$, 386.0 $[M+Na]^+$, 749.2 $[2M+Na]^+$. Anal. Calc. for ($C_{23}H_{25}NO_3$: 363.46): C, 76.01; H, 6.93; found: C, 75.85; H, 6.81.

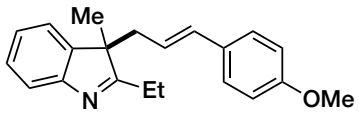

3fa. Pale yellow oil, yield = 68% (31 mg, 16 h, *n*Hex:Acetone = 3.5:1). **^{1}H NMR** (400 MHz, $CDCl_3$) δ 7.50 (d, *J* = 7.7 Hz, 1H), 7.29 (dt, *J* = 7.5, 1.4 Hz, 1H), 7.26 – 7.21 (m, 1H), 7.18 (ddd, *J* = 7.5, 7.5, 0.9 Hz, 1H), 7.05 (d, *J* = 8.7 Hz, 2H), 6.73 (d, *J* = 8.7 Hz, 2H), 6.23 (d, *J* = 15.7 Hz, 1H), 5.41 (ddd, *J* = 15.6, 8.0, 6.7 Hz, 1H), 2.75 (ddd, *J* = 13.9, 6.6, 1.3 Hz, 1H), 2.49 (ddd, *J* = 14.0, 8.1, 0.9 Hz, 1H), 2.24 (s, 3H), 2.00 (dq, *J* = 14.9, 7.5 Hz, 1H), 1.84 (dq, *J* = 14.5, 7.3 Hz, 1H), 0.37 (t, *J* = 7.4 Hz, 3H). **^{13}C NMR** (100 MHz, $CDCl_3$) δ 185.54, 158.90, 155.21, 141.37, 132.30, 129.84, 127.67, 127.19, 124.88, 122.01, 121.87, 119.71, 113.78, 62.99, 55.21, 40.00, 28.84, 16.28, 8.11. **LC-MS** (m/z): 147.0 $[C_{10}H_{11}O]^+$, 328.2 $[M+Na]^+$. Anal. Calc**.** for ($C_{21}H_{23}NO$: 305.42): C, 82.58; H, 7.59; found: C, 82.31; H, 7.71.

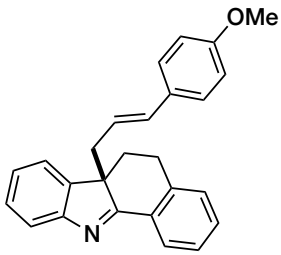

3ga. White solid, yield = 35% (19 mg, nHex:Acetone = 6.5:1). **MP** = 51.2-53.5 °C. **^{1}H NMR** (400 MHz, $CDCl_3$) δ 8.15 (d, J = 7.6 Hz, 1H), 7.69 (d, *J* = 7.7 Hz, 1H), 7.21 (t, *J* = 7.4 Hz, 1H), 7.46 – 7.28 (m, 5H), 7.14 (d, *J* = 8.6 Hz, 2H), 6.79 (d, *J* = 8.6 Hz, 2H), 6.18 (d, *J* = 15.7 Hz, 1H), 5.81 (ddd, *J* = 15.7, 7.6, 7.3 Hz, 1H), 3.35 (ddd, *J* = 18.0, 12.5, 5.7 Hz, 1H), 3.00 (dd, *J* = 17.9, 5.9 Hz, 1H), 2.73 (dd, *J* = 13.7, 7.6 Hz, 1H), 2.58 (dd, *J* = 13.5, 5.3 Hz, 1H), 2.24 (dd, *J* = 13.7, 7.3 Hz, 1H), 1.75 (ddd, *J* = 13.2, 12.5, 6.1 Hz, 1H). **^{13}C NMR** (100 MHz, $CDCl_3$) δ 180.31, 156.39, 153.20, 140.81, 137.16, 130.43, 128.51, 127.46, 127.39, 126.41, 125.55, 124.67, 124.28, 123.55, 122.33, 119.92, 119.24, 118.28, 111.30, 53.11, 52.69, 33.55, 27.05, 23.17. **LC-M*S*** (m/z): 147.0 $[C_{10}H_{11}O]^+$, 218 $[C_{16}H_{11}N]^+$,388.0 $[M+Na]^+$, 404.3 $[M+K]^+$. Anal. Calc. for ($C_{26}H_{23}NO$: 365.48): C, 85.45; H, 6.34; found: C, 85.21; H, 6.23.

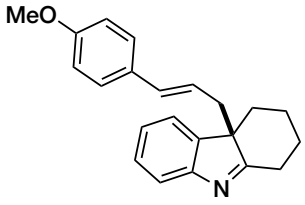

3ha. White solid, yield = 75% (36 mg, 6 h, *n*Hex:Et_2O = 1:1.5). **MP** = 124.5-125.3 °C. **^{1}H NMR** (400 MHz, $CDCl_3$) δ 7.58 (d, *J* = 8.1 Hz, 1H), 7.34 – 7.26 (m, 2H), 7.17 (dt, *J* = 7.1, 0.5 Hz 1H), 7.08 (d, *J* = 8.7 Hz, 2H), 6.75 (d, *J* = 8.7 Hz, 2H), 6.25 (d, *J* =

15.7 Hz, 1H), 5.49 (ddd, 15.6, 7.4, 6.5 Hz, 1H), 3.74 (s, 3H), 2.88 (brs d, J = 8.7 Hz, 1H), 2.77 (ddd, J = 13.6, 6.5, 0.8 Hz, 1H), 2.66 – 2.50 (m, 2H), 2.41 (dd, J = 13.3, 1.8 Hz, 1H), 2.20 (brs d, J = 13.1 Hz, 1H), 1.86 (tq, 13.6, 3.6 Hz 1H), 1.69 (brs, 1H), 1.43 (tq, 13.6, 3.6 Hz 1H), 1.16 (td, J = 13.5, 4.0 Hz, 1H). **^{13}C NMR** (100 MHz, $CDCl_3$)) δ 188.85, 158.91, 154.84, 144.70, 132.48, 129.87, 127.61, 127.21, 124.60, 122.00, 121.61, 120.18, 113.80, 57.88, 55.22, 36.62, 36.57, 30.17, 28.80, 21.08. **LC-MS** (m/z): 147.0 $[C_{10}H_{11}O]^+$, 340.2 $[M+Na]^+$. **Anal. Calc**. for ($C_{22}H_{23}NO$: 317.43): C, 83.24; H, 7.30; found: C, 83.03; H, 7.41.

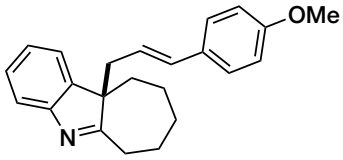

3ia. Pale yellow oil, yield = 58% (29 mg, overnight, *n*Hex:Acetone = 4.5:1). **^{1}H NMR** (400 MHz, $CDCl_3$) δ 7.49 (d, J = 7.6 Hz, 1H), 7.28 (t, J = 7.5 Hz, 1H), 7.23 (d, J = 7.1 Hz, 1H), 7.16 (t, J = 7.3 Hz, 1H), 7.08 (d, J = 8.5 Hz, 2H), 6.75 (d, J = 8.5 Hz, 2H), 6.21 (d, J = 15.7 Hz, 1H), 5.54 (ddd, 15.7, 7.9, 6.9 Hz, 1H), 3.75 (s, 3H), 2.93 (ddd, J = 13.2, 5.7, 4.1 Hz, 1H), 2.72 (dd, J = 13.6, 6.9 Hz, 1H), 2.63 (ddd, 14.0, 10.8, 3.6 Hz, 1H), 2.47 (dd, J = 13.6, 7.9 Hz, 1H), 2.18 – 1.97 (m, 2H), 1.91 – 1.78 (m, 2H), 1.79 – 1.69 (m, 1H), 1.68 – 1.53 (m, 1H), 1.52 – 1.40 (m, 1H), 0.73 (dt, J = 14.5, 10.7 Hz, 1H). **^{13}C NMR** (100 MHz, $CDCl_3$) δ 190.71, 158.89, 154.89, 143.80, 132.49, 129.93, 127.68, 127.21, 124.81, 121.92, 121.89, 119.74, 113.80, 62.40, 55.22, 40.74, 34.74, 31.59, 30.49, 28.64, 24.63. **LC-MS** (m/z): 147.0 $[C_{10}H_{11}O]^+$, 354.2 $[M+Na]^+$. **Anal. Calc**. for ($C_{23}H_{25}NO$: 331.46): C, 83.34; H, 7.60; found: C, 83.55; H, 7.51.

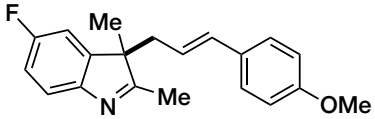

3ja. Pale yellow oil, yield = 92% (43 mg, 7 h, *n*Hex:Et_2O = 1:2.3). **^{1}H NMR** (400 MHz, $CDCl_3$) δ 7.42 (dd, $J_{H\text{-}F}$ = 9.1, $J_{H\text{-}H}$ 4.6 Hz, 1H), 7.07 (d, J = 8.7 Hz, 2H), 7.02 – 6.91 (m, 2H), 6.75 (d, J = 8.7 Hz, 2H), 6.25 (d, J = 15.7 Hz, 1H), 5.42 (ddd, J = 15.5, 7.8, 6.9 Hz, 1H), 3.74 (s, 3H), 2.68 (ddd, J = 14.1, 6.9, 1.2 Hz, 1H), 2.49 (dd, J = 14.0, 7.9 Hz, 1H), 1.32 (s, 3H).**^{13}C NMR** (100 MHz, $CDCl_3$) δ 186.31 (d, $J_{C\text{-}F}$ = 3.7 Hz, 1C), 161.02 (d, $J_{C\text{-}F}$ = 243.5 Hz, 1C), 159.03, 150.18, 145.52 (d, $J_{C\text{-}F}$ = 8.5 Hz, 1C), 132.85, 129.61, 127.25, 121.25, 120.43

(d, $J_{C\text{-}F}$ = 8.9 Hz, 1C), 114.26 (d, $J_{C\text{-}F}$ = 23.6 Hz, 1C), 113.83, 109.59(d, $J_{C\text{-}F}$ = 24.4 Hz, 1C), 58.34, 55.21, 40.26, 21.58, 15.98. **^{19}F NMR** (377 MHz, $CDCl_3$) -117.62 (td, $J_{F\text{-}H}$ = 9.2, 5.2 Hz). **LC-MS** (m/z): 147.0 $[C_{10}H_{11}O]^+$, 332.2 $[M+Na]^+$. **Anal. Calc.** for ($C_{20}H_{20}FNO$: 309.38): C, 77.64; H, 6.52; found: C, 77.42; H, 6.71.

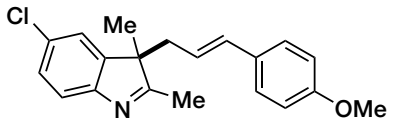

3ka. Pale yellow oil, yield = 77% (38 mg, 4 h, *n*Hex:Et_2O = 1:1.8). **^{1}H NMR** (400 MHz, $CDCl_3$) δ 7.41 (d, *J* = 8.0 Hz, 1H), 7.29 – 7.20 (m, 2H), 7.07 (d, *J* = 8.7 Hz, 2H), 6.75 (d, *J* = 8.7 Hz, 2H), 6.25 (d, *J* = 15.7 Hz, 1H), 5.39 (ddd, *J* = 15.6, 7.9, 6.8 Hz, 1H), 3.74 (s, 3H), 2.70 (ddd, *J* = 14.0, 6.7, 1.3 Hz, 1H), 2.50 (ddd, *J* = 14.1, 8.0, 0.9 Hz, 1H), 2.26 (s, 3H), 1.32 (s, 3H). **^{13}C NMR** (100 MHz, $CDCl_3$) δ 187.06, 159.04, 152.79, 145.37, 132.91, 130.81, 129.57, 127.90, 127.27, 122.39, 121.18, 120.71, 113.84, 58.30, 55.22, 40.25, 21.59, 16.04 **LC-MS** (m/z): 147.0 $[C_{10}H_{11}O]^+$. **Anal. Calc**. for ($C_{20}H_{20}ClNO$: 325.84): C, 73.72; H, 6.19; found: C, 73.51; H, 6.01.

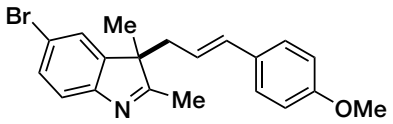

3la. Yellow oil, yield = 75% (42 mg, 4 h, *n*Hex:Et_2O = 1:1.8). **^{1}H NMR** (400 MHz, $CDCl_3$) δ 7.41 (m, 2H), 7.36 (d, *J* = 8.0 Hz, 1H), 7.07 (d, *J* = 8.7 Hz, 2H), 6.75 (d, *J* = 8.8 Hz, 2H), 6.25 (d, *J* = 15.7 Hz, 1H), 5.39 (ddd, *J* = 15.5, 8.0, 6.7 Hz, 1H), 3.74 (s, 3H), 2.70 (ddd, *J* = 14.0, 6.7, 1.4 Hz, 1H), 2.50 (ddd, *J* = 14.1, 8.0, 1.0 Hz, 1H), 2.25 (s, 3H), 1.32 (s, 3H). **^{13}C NMR** (100 MHz, $CDCl_3$) δ 187.07, 159.05, 153.27, 145.78, 132.92, 130.81, 129.57, 127.28, 125.26, 121.23, 121.17, 118.75, 113.84, 58.36, 55.23, 40.25, 21.59, 16.06. **LC-MS** (m/z): 147.0 $[C_{10}H_{11}O]^+$, 392.0/394.0 $[M+Na]^+$. Anal. Calc. for ($C_{20}H_{20}BrNO$: 370.29): C, 64.87; H, 5.44; found: C, 64.71; H, 5.31.

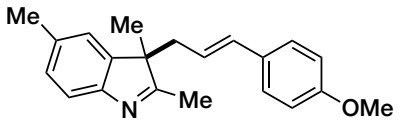

3ma. Yellow oil, yield = 60% (28 mg, 7 h, *n*Hex:Et_2O = 1:1.1). **^{1}H NMR** (400 MHz, $CDCl_3$) δ 7.39 (d, *J* = 7.6 Hz, 1H), 7.14 – 7.04 (m, 4H), 6.75 (d, *J* = 8.6 Hz, 2H), 6.26 (d, *J* = 15.7 Hz, 1H), 5.44 (ddd, *J* = 15.7, 8.1, 6.3 Hz, 1H), 3.74 (s, 3H), 2.70 (dd, *J* = 14.0, 6.3 Hz, 1H), 2.48 (dd, *J* =

14.0, 8.1 Hz, 1H), 2.38 (s, 3H), 2.24 (s, 3H), 1.31 (s, 3H). **^{13}C NMR** (100 MHz, $CDCl_3$) δ 185.54, 158.91, 152.08, 143.67, 134.62, 132.32, 129.86, 128.28, 127.22, 122.65, 122.15, 119.37, 113.79, 57.53, 55.22, 40.41, 21.81, 21.48, 15.98. **LC-MS** (m/z): 147.0 $[C_{10}H_{11}O]^+$, 328.0 $[M+Na]^+$. Anal. Calc. for ($C_{21}H_{23}NO$: 305.42): C, 82.58; H, 7.59; found: C, 82.31; H, 7.41.

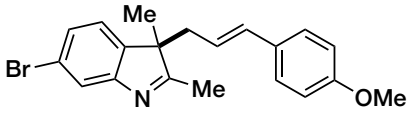

3na. Pale yellow oil, yield = 70% (39 mg, 4h, *n*Hex:Et_2O = 1:1.3, then Hex:Acetone 4:1). **^{1}H NMR** (400 MHz, $CDCl_3$) δ 7.64 (d, *J* = 1.5 Hz, 1H), 7.31 (dd, *J* = 7.9, 1.6 Hz, 1H), 7.13 (d, *J* = 7.9 Hz, 1H), 7.08 (d, *J* = 8.7 Hz, 2H), 6.76 (d, *J* = 8.7 Hz, 2H), 6.24 (d, *J* = 15.7 Hz, 1H), 5.43 (ddd, *J* = 15.7, 8.0, 6.6 Hz, 1H), 3.75 (s, 3H), 2.70 (ddd, *J* = 13.9, 6.6, 0.9 Hz, 1H), 2.46 (dd, *J* = 13.9, 8.0 Hz, 1H), 2.27 (s, 3H), 1.31 (s, 3H). **^{13}C NMR** (100 MHz, $CDCl_3$) δ 188.45, 159.06, 155.73, 142.46, 132.88, 129.55, 127.78, 127.27, 123.29, 123.08, 121.25, 121.06, 113.86, 57.79, 55.24, 40.17, 21.48, 16.11. **LC-MS** (m/z): 147.0 $[C_{10}H_{11}O]^+$, 392.0/394.0 $[M+Na]^+$. Anal. Calc. for ($C_{20}H_{20}BrNO$: 370.29): C, 64.87; H, 5.44; found: C, 64.88; H, 5.37.

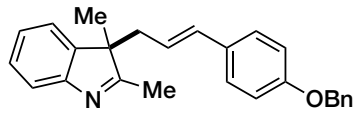

3ab. Pale yellow oil, yield = 65% (36 mg, 16 h, *n*Hex:Et_2O = 1:1.8). **^{1}H NMR** (400 MHz, $CDCl_3$) δ 7.53 (d, *J* = 7.6 Hz, 1H), 7.43 – 7.25 (m, 7H), 7.19 (t, *J* = 7.4 Hz, 1H), 7.08 (d, *J* = 8.7 Hz, 2H), 6.83 (d, *J* = 8.7 Hz, 2H), 6.24 (d, *J* = 15.8 Hz, 1H), 5.48 (ddd, *J* = 15.8, 8.1, 6.7 Hz, 1H), 5.01 (s, 2H), 2.73 (ddd, *J* = 13.9, 6.7, 1.1 Hz, 1H), 2.48 (dd, *J* = 14.1, 8.1 Hz, 1H), 2.28 (s, 3H), 1.34 (s, 3H). **^{13}C NMR** (100 MHz, $CDCl_3$) δ 186.57, 158.15, 154.27, 143.52, 136.91, 132.48, 130.06, 128.54, 127.91, 127.72, 127.38, 127.25, 124.95, 122.08, 121.90, 119.89, 114.79, 69.97, 57.74, 40.35, 21.64, 16.04. **LC-MS** (m/z): 91.0 $[Bn]^+$, 145.0 $[C_{10}H_{11}N]^+$, 223.2 $[C_{16}H_{15}O]^+$, 390.2 $[M+Na]^+$, 406.0 $[2M+Na]^+$. Anal. Calc. for ($C_{26}H_{25}NO$: 367.49): C, 84.98; H, 6.86; found: C, 84.71; H, 6.71.

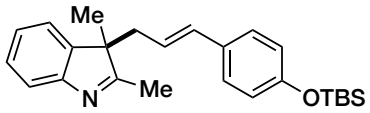

3ac. Yellow oil, yield = 66% (39 mg, 36h, *n*Hex:Et_2O = 1.2:1). **^{1}H NMR** (400 MHz, $CDCl_3$) δ 7.52 (d, *J* = 7.6 Hz, 1H), 7.32 – 7.26 (m, 2H), 7.18 (t, *J* = 7.4 Hz, 1H), 7.01 (d, *J* = 8.5 Hz, 1H), 6.68 (d, *J* = 8.5 Hz, 1H), 6.25 (d, *J* = 15.7 Hz, 1H), 5.45 (ddd, *J* = 15.7, 8.1, 6.6 Hz, 1H), 2.72 (ddd, *J* = 14.0, 6.6, 1.3 Hz, 1H), 2.47 (ddd, *J* = 14.0, 8.1, 0.7 Hz, 1H), 2.27 (s, 1H), 1.33 (s, 1H), 0.95 (s, 9H), 0.15 (s, 6H). **^{13}C NMR** (100 MHz, $CDCl_3$) δ 186.62, 155.06, 154.24, 143.52, 132.60, 130.32, 127.70, 127.17, 124.96, 122.02, 121.88, 119.98, 119.87, 77.32, 77.00, 76.69, 57.73, 40.35, 25.64, 21.66, 18.17, 16.03, -4.46. **LC-MS** (m/z): 247.0 $[C_{15}H_{23}Si]^+$, 414.0 $[M+Na]^+$. Anal. Calc. for ($C_{25}H_{33}NOSi$: 391.63): C, 76.67; H, 8.49; found: C, 76.65; H, 8.41.

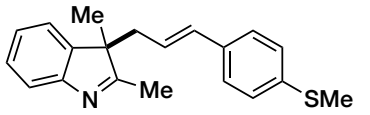

3ae. Yellow oil, yield = 51% (24 mg, 70°C, 36h, *n*Hex:Et_2O = 1:1.8). **^{1}H NMR** (400 MHz, $CDCl_3$) δ 7.51 (d, *J* = 7.6 Hz, 1H), 7.32 – 7.23 (m, 2H), 7.21 – 7.14 (m, 1H), 7.10 (d, *J* = 8.5 Hz, 2H), 7.05 (d, *J* = 8.4 Hz, 2H), 6.24 (d, *J* = 15.7 Hz, 1H), 5.55 (ddd, *J* = 15.7, 8.2, 6.8 Hz, 1H), 2.73 (dd, *J* = 14.0, 6.8 Hz, 1H), 2.49 (dd, *J* = 14.2, 8.2 Hz, 1H), 2.42 (s, 3H), 2.27 (s, 3H), 1.33 (s, 3H). **^{13}C NMR** (100 MHz, $CDCl_3$) δ 186.43, 154.22, 143.38, 137.34, 133.96, 132.46, 127.76, 126.63, 126.50, 125.00, 123.65, 121.87, 119.91, 57.69, 40.33, 21.65, 16.00, 15.89. **LC-MS** (m/z): 163.0 $[C_{10}H_{11}S]^+$, 330.0 $[M+Na]^+$, 346.0 $[M+K]^+$. Anal. Calc. for ($C_{20}H_{21}NS$: 307.46): C, 78.13; H, 6.88; found: C, 78.01; H, 6.93.

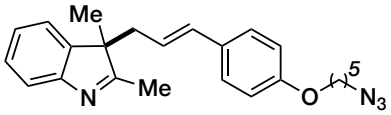

3af. Orange oil which solidifies on standing, yield = 76% (44 mg, 4 h, *n*Hex:Et_2O = 1:1.8). **^{1}H NMR** (400 MHz, $CDCl_3$) δ 7.51 (d, *J* = 7.6 Hz, 1H), 7.33 – 7.22 (m, 2H), 7.18 (dt, *J* = 7.4, 0.8 Hz, 1H), 7.06 (d, *J* = 8.7 Hz, 2H), 6.73 (d, *J* = 8.7 Hz, 2H), 6.24 (d, *J* = 15.7 Hz, 1H), 5.46 (ddd, *J* = 15.7, 8.0, 6.7 Hz, 1H), 3.90 (t, *J* = 6.3 Hz, 2H), 3.27 (t, *J* = 6.8 Hz, 2H), 2.72 (ddd, *J* = 13.9, 6.7, 1.3 Hz, 1H), 2.47 (ddd, *J* = 14.0, 8.0, 0.9 Hz, 1H), 2.27 (s, 3H), 1.81 – 1.71 (m, 2H), 1.68 – 1.59 (m, 2H), 1.57 – 1.46 (m, 2H), 1.33 (s, 3H). **^{13}C NMR** (100 MHz, $CDCl_3$ δ 186.60, 158.33, 154.24, 143.51, 132.50, 129.75, 127.69, 127.23,

124.94, 121.90, 121.87, 119.86, 114.37, 67.53, 57.74, 51.30, 40.35, 28.74, 28.60, 23.33, 21.64, 16.03. **LC-MS** (m/z): 244.0 $[C_{14}H_{18}N_3O]^+$, 411.0 $[M+Na]^+$. Anal. Calc. for ($C_{24}H_{28}N_4O$: 388.52): C, 74.20; H, 7.26; found: C, 74.11; H, 7.39.

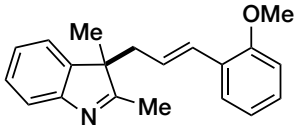

3ag. Yellow oil, yield = 40% 17.5 mg, *n*Hex:Et_2O = 1:1.4). **MP** = 132.5-135.5 °C. **^{1}H NMR** (400 MHz, $CDCl_3$) δ 7.52 (d, J = 7.8 Hz, 1H), 7.29 (t, J = 6.9 Hz, 2H), 7.22 – 7.07 (m, 3H), 6.84 – 6.74 (m, 2H), 6.63 (d, J = 15.9 Hz, 1H), 5.58 (ddd, J = 15.9, 8.0, 6.7 Hz, 1H), 3.76 (s, 3H), 2.76 (dd, *J* = 13.9, 6.7 Hz, 1H), 2.52 (dd, *J* = 13.9, 8.0 Hz, 1H), 2.28 (s, 3H), 1.34 (s, 3H). **^{13}C NMR** (100 MHz, $CDCl_3$) δ 184.13, 153.76, 151.68, 141.00, 125.69, 125.41, 125.08, 124.16, 123.63, 122.36, 122.35, 119.37, 117.98, 117.25, 108.17, 55.19, 52.84, 38.14, 19.05, 13.48. **LC-MS** (m/z): 147.0 $[C_{10}H_{11}O]^+$, 292.2 $[M+H]^+$. Anal. Calc. for ($C_{20}H_{21}NO$: 291.39): C, 82.44; H, 7.26; found: C, 82.24; H, 7.51.

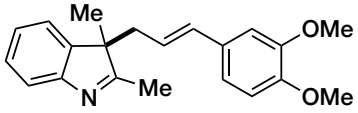

3ah. Pale yellow oil, yield = 76% (37 mg, overnight, *n*Hex:Et_2O = 1:6). **^{1}H NMR** (400 MHz, $CDCl_3$) δ 7.50 (d, *J* = 7.6 Hz, 1H), 7.32 – 7.22 (m, 1H), 7.17 (t, *J* = 7.4 Hz, 1H), 6.74 – 6.65 (m, 2H), 6.64 (s, 1H), 6.23 (d, *J* = 15.7 Hz, 1H), 5.44 (ddd, *J* = 15.7, 7.9, 6.7 Hz, 1H), 3.80 (s, 3H), 3.79 (s, 3H), 2.72 (ddd, *J* = 13.9, 6.7, 1.0 Hz, 1H), 2.48 (ddd, *J* = 13.9, 7.9, 0.6 Hz, 1H), 2.27 (s, 3H), 1.33 (s, 3H). **^{13}C NMR** (100 MHz, $CDCl_3$) δ 186.52, 154.24, 148.85, 148.56, 143.47, 132.77, 130.15, 127.70, 124.96, 122.24, 121.90, 119.84, 118.98, 111.06, 108.95, 57.74, 55.87, 55.77, 40.30, 21.63, 16.02. **LC-MS** (m/z): 177.0 $[C_{11}H_{13}O_2]^+$, 344.0 $[M+Na]^+$, 665.2 $[2M+Na]^+$. Anal. Calc. for ($C_{21}H_{15}NO_2$: 321.42): C, 78.47; H, 7.21; found: C, 78.62; H, 7.33.

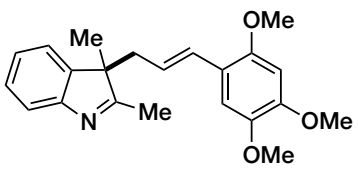

3ai. White oil, yield = 81% (43 mg, 2 h, 25 °C, *n*Hex:AcOEt = 1:2). **^{1}H NMR** (400 MHz, $CDCl_3$) δ 7.50 (d, *J* = 7.6 Hz, 1H), 7.31 – 7.25 (m, 2H), 7.17 (t, *J* = 7.4 Hz, 1H), 6.57 (s, 1H), 6.53 (d, *J* = 15.8 Hz, 1H), 6.40 (s, 1H), 5.41 (ddd, *J* = 15.8, 8.0, 6.7 Hz, 1H), 3.82

(s, 3H), 3.73 (s, 3H), 3.70 (s, 3H), 2.73 (dd, *J* = 13.8, 6.7 Hz, 1H), 2.51 (dd, *J* = 13.8, 8.0 Hz, 1H), 2.27 (s, 3H), 1.33 (s, 3H).**^{13}C NMR** (100 MHz, $CDCl_3$) δ 186.75, 154.22, 151.02, 149.21, 143.60, 143.28, 127.61, 127.47, 124.95, 122.82, 121.96, 119.70, 118.26, 110.32, 98.02, 57.89, 56.75, 56.51, 56.05, 40.71, 21.58, 16.02. **LC-MS** (m/z): 207.2 $[C_{12}H_{15}O_3]^+$, 374.4 $[M+Na]^+$. Anal. Calc. for ($C_{22}H_{25}NO_3$: 351.45): C, 75.19; H, 7.17; found: C, 75.08; H, 7.31.

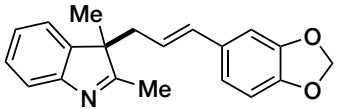

3aj. Yellow oil, yield = 66% (30 mg, 16 h, *n*Hex:Et_2O = 1:2.4). **^{1}H NMR** (400 MHz, $CDCl_3$) δ 7.51 (d, *J* = 7.6 Hz, 1H), 7.34 – 7.23 (m, 2H), 7.18 (td, *J* = 7.4, 0.7 Hz, 1H), 6.65 (d, *J* = 8.0 Hz, 1H), 6.65 (d, *J* = 1.5 Hz, 1H), 6.58 (dd, *J* = 8.0, 1.5 Hz, 1H), 6.21 (d, *J* = 15.7 Hz, 1H), 5.88 (s, 2H), 5.42 (ddd, *J* = 15.7, 8.1, 6.7 Hz, 1H), 2.71 (ddd, *J* = 13.9, 6.7, 1.3 Hz, 1H), 2.46 (ddd, *J* = 13.9, 8.1, 0.9 Hz, 1H), 2.27 (s, 3H), 1.33 (s, 3H). **^{13}C NMR** (100 MHz, $CDCl_3$) δ 186.47, 154.23, 147.80, 146.90, 143.41, 132.63, 131.45, 127.75, 124.97, 122.37, 121.85, 120.57, 119.90, 108.09, 105.49, 100.92, 57.71, 40.24, 21.62, 16.01. **LC-MS** (m/z): 144.2 $[C_{10}H_{10}N]^+$, 161.0 $[C_{10}H_{19}O_2]^+$, 328.0 $[M+Na]^+$. Anal. Calc. for ($C_{20}H_9NO_2$: 305.38): C, 78.66; H, 6.27; found: C, 78.41; H, 6.42.

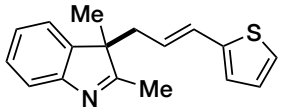

3ak. Pale yellow oil, yield = 63% (25 mg, 36h, *n*Hex:Et_2O = 1:1.7). **^{1}H NMR** (400 MHz, $CDCl_3$) δ 7.52 (d, *J* = 7.6 Hz, 1H), 7.28 (m, 2H), 7.18 (t, *J* = 7.4 Hz, 1H), 7.04 (d, *J* = 4.7 Hz, 1H), 6.85 (dd, *J* = 4.7, 3.3 Hz, 1H), 6.77 (d, *J* = 3.3 Hz, 1H), 6.42 (d, *J* = 15.5 Hz, 1H), 5.52 (ddd, *J* = 15.5, 8.1, 6.9 Hz, 1H), 2.69 (dd, *J* = 13.9, 6.9 Hz, 1H), 2.43 (dd, *J* = 13.9, 8.1 Hz, 1H), 2.27 (s, 3H), 1.33 (s, 3H). **^{13}C NMR** (100 MHz, $CDCl_3$) δ 186.31, 154.19, 143.28, 141.93, 127.79, 127.16, 126.23, 125.01, 124.92, 123.95, 123.76, 121.94, 119.95, 57.57, 40.13, 21.47, 16.00. **LC-MS** (m/z): 123.0 $[C_7H_7S]^+$, 268.0 $[M+H]^+$. Anal. Calc. for ($C_{17}H_{17}NS$: 267.39): C, 76.36; H, 6.41; found: C, 76.24; H, 6.19.

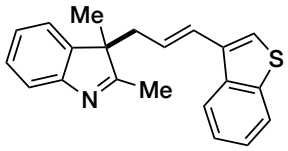

3al. Yellow oil, yield = 53% (25 mg, 70 °C, 36 h, *n*Hex:Et_2O = 1:1.6). **^{1}H NMR** (400 MHz, $CDCl_3$) δ 7.78 (m, 1H), 7.59 – 7.51 (m, 2H), 7.36 – 7.26 (m, 4H), 7.20 (t, *J* = 7.1 Hz, 1H), 7.12 (s, 1H), 6.51 (d, *J* = 15.8 Hz, 1H), 5.61 (ddd, *J* = 15.8, 8.0, 6.7 Hz, 1H), 2.82 (ddd, *J* = 13.9, 6.7, 1.2 Hz, 1H), 2.59 (ddd, *J* = 13.9, 8.0, 0.8 Hz, 1H), 2.32 (s, 3H), 1.38 (s, 3H). **^{13}C NMR** (100 MHz, $CDCl_3$) δ 186.36, 154.29, 143.34, 140.23, 137.52, 133.70, 127.84, 126.32, 125.42, 125.09, 124.29, 124.10, 122.74, 121.90, 121.82, 121.59, 119.96, 57.80, 40.63, 21.68, 16.03. **LC-MS** (m/z): 173.0 $[C_{11}H_9S]^+$, 318.0 $[M+H]^+$, 340.2 $[M+Na]^+$. Anal. Calc. for ($C_{21}H_{19}NS$: 317.45): C, 73.46 H, 6.03; found: C, 73.61; H, 5.89.

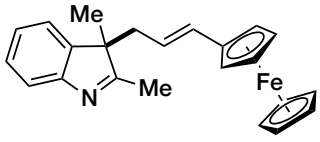

3am. Red oil which solidifies on standing, yield = 61% (34 mg, 1 h, 25 °C, *n*Hex:Et_2O = 1.2:1, then *n*Hex:Acetone 5:1). **^{1}H NMR** (400 MHz, $CDCl_3$) δ 7.54 (d, *J* = 8.0 Hz, 1H), 7.33 – 7.27 (m, 2H), 7.21 (t, *J* = 7.3 Hz, 1H), 5.96 (d, *J* = 15.5 Hz, 1H), 5.15 (ddd, *J* = 15.5, 7.6, 7.2 Hz, 1H), 4.12 – 4.01 (m, 4H), 3.88 (s, 5H), 2.61 (dd, *J* = 13.9, 7.6 Hz, 1H), 2.44 (dd, *J* = 13.8, 7.2 Hz, 1H), 2.31 (s, 3H), 1.32 (s, 3H). **^{13}C NMR** (100 MHz, $CDCl_3$) δ 186.36, 154.39, 143.66, 130.30, 127.77, 124.94, 121.80, 121.01, 119.88, 82.78, 69.02 (5C), 68.35, 68.25, 66.73, 65.96, 57.89, 40.50, 21.95, 16.02. **LC-MS** (m/z): 225.0 $[C_{13}H_{13}Fe]^+$, 369.0 $[M]^+$. Anal. Calc. for ($C_{23}H_{23}FeN$: 369.29): 74.81; H, 6.28; found: C, 74.66; H, 6.15.

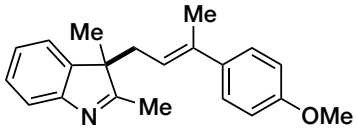

3an. Pale yellow oil, yield = 72% (33 mg, 6 h, *n*Hex:Et_2O = 1:1.5). **^{1}H NMR** (400 MHz, $CDCl_3$) δ 7.54 (d, *J* = 7.6 Hz, 1H), 7.28 (m, 2H), 7.16 (t, *J* = 7.4 Hz, 1H), 7.04 (d, *J* = 8.8 Hz, 2H), 6.74 (d, *J* = 8.8 Hz, 2H), 5.01 (ddd, *J* = 7.6, 7.0, 1.1 Hz, 1H), 3.74 (s, 3H), 2.74 (dd, *J* = 14.7, 7.0 Hz, 1H), 2.54 (dd, *J* = 14.7, 7.6 Hz, 1H), 2.29 (s, 3H), 1.88 (s, 3H), 1.36 (s, 3H). **^{13}C NMR** (100 MHz, $CDCl_3$) δ 186.90, 158.61, 154.06, 143.64, 136.92, 135.96, 127.72, 126.72, 125.04, 121.80, 120.19, 119.74, 113.45, 57.77, 55.21,

35.80, 21.68, 16.31, 15.82. **LC-MS** (m/z): 161.2 $[C_1H_{13}O]^+$, 344.2 $[M+K]^+$. Anal. Calc. for ($C_{21}H_{23}NO$: 305.42): C, 82.58; H, 7.59; found: C, 82.37; H, 7.71.

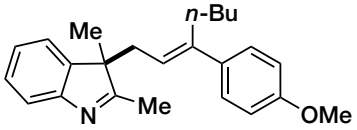

3ao. Yellow solid, yield = 80% (42 mg, 5 h, *c*Hex:AcOEt = 3:1). **MP** = 162.7-163.6 °C. **^{1}H NMR** (400 MHz, $CDCl_3$) δ 7.52 (d, J = 7.6 Hz, 1H), 7.27 (m, 2H), 7.15 (t, *J* = 7.4 Hz, 1H), 6.99 (d, *J* = 8.8 Hz, 2H), 6.73 (d, *J* = 8.8 Hz, 2H), 4.85 (t, *J* = 7.1 Hz, 1H), 3.74 (s, 2H), 2.73 (dd, *J* = 14.9, 7.0 Hz, 1H), 2.53 (dd, *J* = 14.9, 7.3 Hz, 1H), 2.36 – 2.28 (m, 2H), 2.27 (s, 3H), 1.35 (s, 3H), 1.29 – 1.18 (m, 2H), 1.18 – 1.07 (m, 2H), 0.82 (t, *J* = 7.2 Hz, 3H). **^{13}C NMR** (100 MHz, $CDCl_3$) δ 186.72, 158.49, 154.36, 143.70, 142.41, 135.25, 127.67, 127.31, 124.96, 121.81, 120.57, 119.79, 113.43, 57.66, 55.17, 35.48, 30.64, 29.85, 22.76, 21.79, 15.92, 13.93. **LC-MS** (m/z): 203.2 $[C_{14}H_{19}O]^+$, 370.2 $[M+Na]^+$. Anal. Calc. for ($C_{24}H_{29}NO$: 347.50): C, 82.95; H, 8.41; found: C, 82.76; H, 8.21.

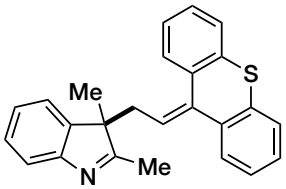

3ap. White solid, yield = 84% (46 mg, 5 h, 25 °C, *n*Hex:AcOEt = 2:1). **MP** = 61.8-62.6 °C. **^{1}H NMR** (400 MHz, $CDCl_3$) δ 7.47 (d, *J* = 7.6 Hz, 1H), 7.45 – 7.40 (m, 1H), 7.29 (m, 3H), 7.26 – 7.20 (m, 3H), 7.18 (dd, *J* = 7.3, 0.8 Hz, 1H), 7.16 – 7.08 (m, 3H), 5.07 (dd, *J* = 8.6, 5.9 Hz, 1H), 3.02 (dd, *J* = 15.2, 5.9 Hz, 1H), 2.86 (dd, *J* = 15.2, 8.6 Hz, 1H), 2.05 (s, 3H), 1.28 (s, 3H). **^{13}C NMR** (100 MHz, $CDCl_3$) δ 186.46, 154.44, 143.18, 138.19, 138.17, 134.17, 133.40, 131.74, 128.52, 127.87, 127.14, 126.89, 126.82, 126.74, 125.77, 125.73, 125.37, 125.25, 125.14, 121.63, 119.93, 77.33, 77.02, 76.70, 57.86, 36.15, 22.22, 15.70. **LC-MS** (m/z): 223.0 $[C_{15}H_{11}S]^+$, 390.0 $[M+Na]^+$, 757.2 $[2M+Na]^+$. Anal. Calc. for ($C_{25}H_{21}NS$: 367.51): C, 81.71; H, 5.76; found: C, 81.91; H, 5.65.

General procedure for the allenylic dearomatization of indoles

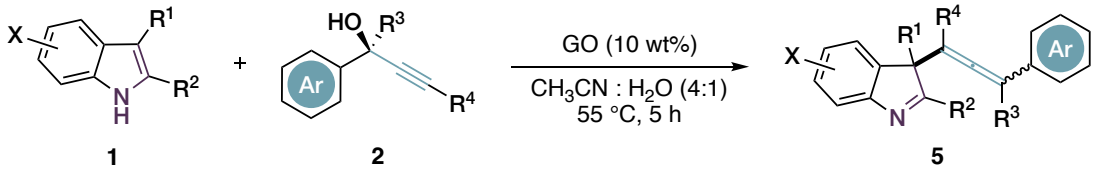

A screw-capped vial is charged with CH_3CN (0.8 mL), propargylic alcohol **4** (0.3 mmol, 3 eq), indole **1** (0.10 mmol, 1 eq), GO dried flakes (10 wt% with respect to indole) and deionized water (0.2 mL). The reaction mixture was stirred at 55 °C (unless otherwise noted) until complete consumption of indole (*vide infra* for reaction times). The mixture was then filtered on a Gooch funnel and the GO washed with EtOAc. The collected organic layers were dried over Na_2SO_4 and evaporated to dryness under vacuum. The crude was purified by column chromatography to give the desired product as a mixture of two diastereomers **5'** and **5''**.

Characterization data of products 5

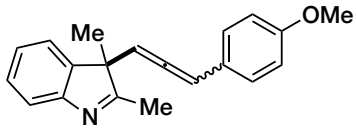

5aa'+5aa''. Yellow oil, yield = 54% (15.6 mg, 48 h, *n*Hex:Acetone = 6:1), *d.r.* = 58:42. **^{1}H NMR** (400 MHz, $CDCl_3$) δ 7.57 – 7.50 (m, 1H), 7.39 – 7.27 (m, 2H), 7.27 – 7.14 (m, 3H), 6.93 – 6.82 (m, 2H), 6.41 – 6.33 (m, 1H), 5.35 – 5.29 (m, 1H), 3.84 – 3.76 (m, 3H), 2.38 – 2.28 (m, 3H), 1.42 – 1.38 (m, 3H). **^{13}C NMR** (100 MHz, $CDCl_3$) δ 204.99, 204.87, 185.73, 185.50, 159.11, 159.08, 154.12, 154.08, 144.07, 143.91, 128.09, 128.05, 127.85, 127.82, 125.98, 125.94, 125.45, 125.38, 122.42, 122.24, 120.01, 119.96, 114.29, 97.97, 97.01, 96.79, 58.02, 55.30, 20.51, 20.22, 15.97, 15.89. **GC-MS** (m/z): 289 (28) $[M]^+$, 274. (4) $[M\text{-}Me]^+$, 145 (100) $[M\text{-}C_{10}H_{10}N]^+$. Anal. Calc. for ($C_{20}H_{19}NO$: 289.38): C, 83.01; H, 6.62; found: C, 82.82; H, 6.46.

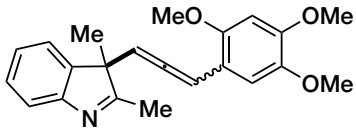

5ab'+5ab''. Orange oil, yield = 78% (27.8 mg, 3 h, *n*Hex:AcOEt = 1:1). *d.r.* = 77:23. **^{1}H NMR** (400 MHz, $CDCl_3$) δ 7.55 – 7.49 (m, 1H), 7.34 – 7.27 (m, 2H), 7.21 – 7.15 (m, 1H), 6.81 – 6.73 (m, 2H), 6.50 – 6.48 (m, 1H), 5.40 – 5.32 (m, 1H), 3.89 – 3.86 (m, 3H), 3.84 – 3.79 (m, 3H), 3.72 (s, 3H), 2.38 – 2.30 (m, 3H), 1.41 (s, 3H). **^{13}C NMR** (100 MHz, $CDCl_3$) δ 205.09, 185.51, 154.03, 150.68, 149.32, 144.33, 143.53, 128.06, 127.97, 125.40, 125.31, 122.26, 122.18, 120.02, 119.97, 113.54, 110.15, 97.97, 96.52, 92.36, 58.03, 57.93, 56.78, 56.14, 56.12, 20.54, 20.37, 15.96. **GC-MS** (m/z): 349 (22) $[M]^+$, 205 (100) $[M\text{-}C_{10}H_{10}N]^+$, 144 (94) $[C_{10}H_{10}N]^+$. Anal. Calc. for ($C_{22}H_{23}NO_3$: 349.43): C, 75.62; H, 6.63; found: C, 75.46; H, 6.29.

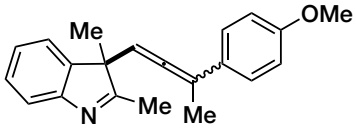

5ac'+5ac''. Orange oil, yield = 94% (28.4 mg, 12 h, *n*Hex:AcOEt = 2.8:1), *d.r.* = 80:20 **^{1}H NMR** (400 MHz, $CDCl_3$) δ 7.56 – 7.50 (m, 1H), 7.36 – 7.25 (m, 4H), 7.23 – 7.16 (m, 1H), 6.92 – 6.84 (m, 2H), 5.22 – 5.16 (m, 1H), 3.82 – 3.79 (m, 3H), 2.35 – 2.30 (m, 3H), 2.18 – 2.11 (m, 3H), 1.39 – 1.36 (m, 3H). **^{13}C NMR** (100 MHz, $CDCl_3$)

δ 204.11, 204.10, 185.95, 158.81, 158.79, 154.11, 154.05, 144.29, 144.22, 128.67, 128.62, 127.99, 127.93, 126.79, 126.73, 125.36, 125.33, 122.28, 119.93, 119.90, 113.90, 104.37, 104.30, 94.85, 94.67, 58.49, 58.41, 55.29, 20.43, 20.22, 17.67, 17.52, 16.02, 15.78. **GC-MS** (m/z): 303 (15) $[M]^+$, 288 (8) $[M\text{-}Me]^+$, 159 (100) $[M\text{-}C_{10}H_{10}N]^+$. Anal. Calc. for ($C_{21}H_{21}NO$: 303.41): C, 83.13; H, 6.98; found: C, 83.01; H, 6.75.

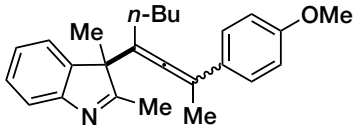

5ad'+5ad''. Orange oil, yield = 74% (26.6 mg, 6 h, *n*Hex:AcOEt = 4:1), *d.r.* = 56:44. **^{1}H NMR** (400 MHz, $CDCl_3$) δ 7.60 – 7.51 (m, 1H), 7.47 – 7.36 (m, 2H), 7.36 – 7.16 (m, 3H), 6.97 – 6.85 (m, 2H), 3.86 – 3.77 (m, 3H), 2.34 – 2.24 (m, 3H), 2.25 – 2.19 (m, 3H), 1.46 – 1.38 (m, 1H), 1.32 – 1.23 (m, 4H), 1.23 – 1.13 (m, 2H), 1.13 – 0.99 (m, 2H), 0.71 – 0.63 (m, 3H). **^{13}C NMR** (100 MHz, $CDCl_3$) δ 202.20, 202.12, 186.62, 158.64, 158.60, 154.80, 154.74, 144.01, 143.90, 129.78, 129.70, 127.90, 127.88, 126.57, 126.51, 125.38, 125.35, 122.10, 122.03, 119.94, 119.88, 113.94, 113.90, 107.85, 107.65, 104.95, 104.85, 61.91, 61.82, 55.33, 55.31, 29.78, 27.77, 27.70, 22.28, 22.19, 20.73, 20.68, 18.20, 17.75, 16.16, 15.71, 13.82, 13.79. **GC-MS** (m/z): 359 (10) $[M]^+$, 344 (2) $[M\text{-}Me]^+$, 215 (100) $[M\text{-}C_{10}H_{10}N]^+$. Anal. Calc. for ($C_{25}H_{29}NO$: 359.22): C, 83.52; H, 8.13; found: C, 83.31; H, 8.01.

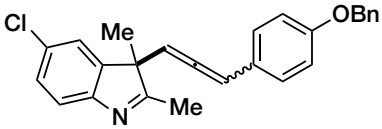

5be'+5be''. Pale yellow oil, yield = 40% (16.1 mg, 4 days, *n*Hex:Et_2O = 1:1.8), *d.r.* = 72:28. **^{1}H NMR** (400 MHz, $CDCl_3$) δ 7.47 – 7.35 (m, 5H), 7.35 – 7.25 (m, 3H), 7.25 – 7.19 (m, 2H), 6.99 – 6.92 (m, 2H), 6.39 (d, *J* = 6.3 Hz, 1H), 5.33 – 5.27 (m, 1H), 5.09 – 5.05 (m, 2H), 2.37 – 2.27 (m, 3H), 1.39 (s, 3H). **^{13}C NMR** (100 MHz, $CDCl_3$) δ 205.14, 204.94, 186.24, 186.08, 158.42, 158.37, 152.65, 152.60, 145.83, 145.74, 136.80, 131.23, 128.58, 128.26, 128.22, 127.98, 127.91, 127.89, 127.41, 127.39, 125.94, 125.87, 123.00, 122.85, 120.86, 120.80, 115.32, 115.30, 98.35, 98.26, 96.37, 96.21, 70.07, 58.37, 20.26, 20.22, 15.99, 15.89. **LC-MS** (m/z): 221.2 $[C_{16}H_{13}O]^+$,

400.2/402.2 $[M+H]^+$. Anal. Calc. for ($C_{26}H_{22}ClNO$: 399.92): C, 78.09; H, 5.55; found: C, 77.35; H, 5.42.

Gram scale reaction and recycling of GO (entry 17, Table 1)

In a Schlenk tube are added in a sequence reagent grade CH_3CN (28 mL), allylic alcohol **2a** (1.64 g, 10 mmol), indole **1a** (725 mg, 5 mmol), GO (72.5 mg, 10 % wt, powder) and deionized water (7 mL). The reaction mixture was stirred at 55 °C overnight. The mixture was then filtered on a Gooch funnel and the GO washed with EtOAc. The filtrate was concentrated by rotary evaporation to remove CH_3CN and then extracted with EtOAC. The collected organic layers were dried over Na_2SO_4 and evaporated to dryness under vacuum. The crude was purified by column chromatography to give the desired product **3aa** in 78% yield (1.135 g). The graphene recovered from the mixture by filtration was then washed with water, acetone, methanol and DCM. Then, GO was suspended in DCM and stirred for 2 hours at room temperature. The mixture was filtered on a Gooch funnel, and the GO washed with some fresh DCM. This process was repeated 3 times; after that the GO was dried under vacuum for 4 hours.

The so obtained GO was used in place of pristine GO in the model reaction which was set up according to the general procedure. The product **3aa** was isolated in 12% yield (36 h).

GO regeneration

The used GO was sonicated in 1 M HCl, following the procedure described by C.-H. Chen *et al.* for the regeneration of epoxides.[99]

The so obtained GO was used in place of pristine GO in the model reaction. The product **3aa** was isolated in 63% yield (36 h).

Grafting experiment

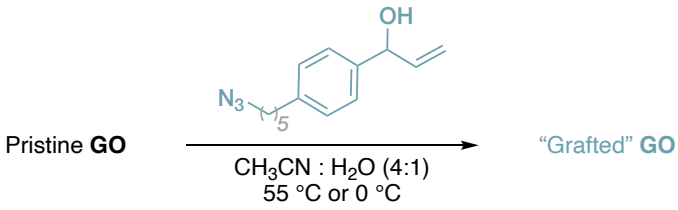

In a screw-capped vial are added in a sequence: CH_3CN (3 mL), allylic alcohol **2f** (76 mg, 0.75 mmol), GO (5.4 mg) and deionized water (0.75 mL). The reaction mixture was stirred at 55 °C for 4 hours. The mixture was then filtered, and the recovered GO was washed with water, acetone, methanol and DCM. The GO was then suspended in DCM and the suspension was stirred for 2 hours at room temperature. The solvent was removed by pipette, and the graphene was washed again with some fresh DCM. This process was repeated 3 times; after that the GO was dried under vacuum for 4 hours. The reaction was also performed at 0° C following the same procedure with a reduced time reaction of 30 minutes.

FT-IR analysis

FT-IR spectra of various samples were acquired using transmission mode. The samples were prepared grinding GO (*ca.* 0.5 mg) with KBr and then pressing them into disks.

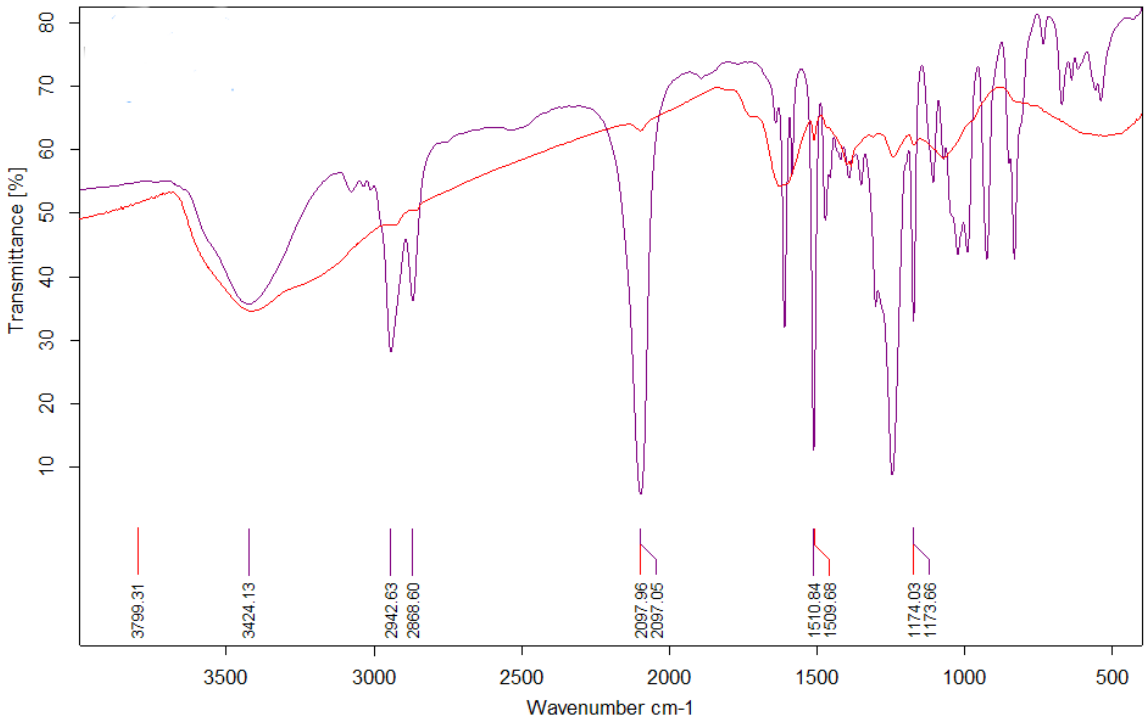

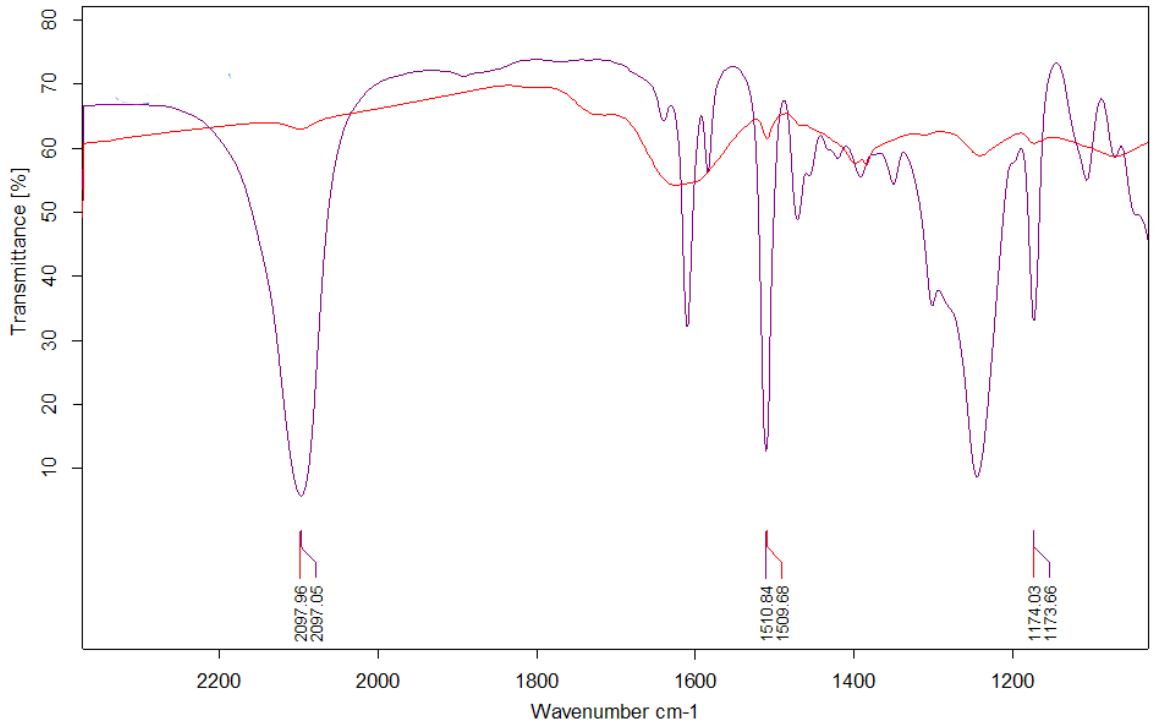

Figure S1. Top: Violet: alcohol **2f**. Red: GO + **2f** after 6 h in CH_3CN:H_2O 4:1 at 55 °C. b) Zoomed region showing characteristic peaks of alcohol **2f** matching with the "grafted" GO peaks.

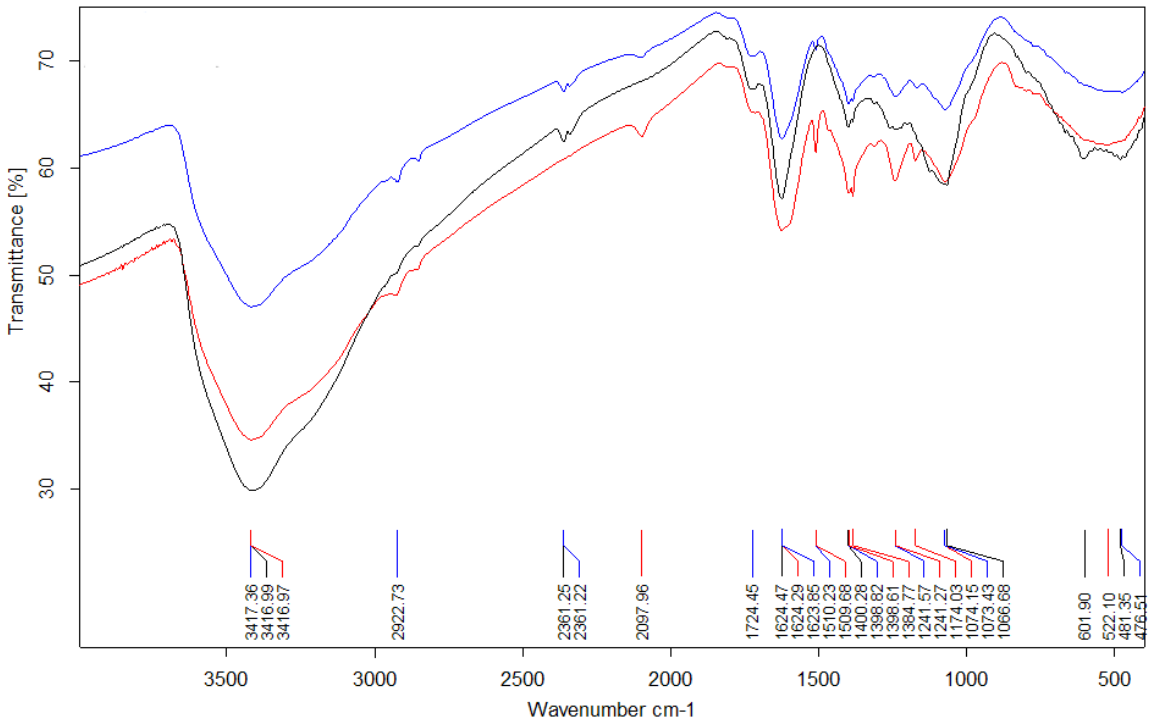

Figure S2. Black: pristine GO. Blue: GO + **2f** after 6 h in CH_3CN:H_2O 4:1 at 0 °C. Red: GO + **2f** after 6 h in CH_3CN:H_2O 4:1 at 55 °C. The peaks associated with alcohol **2f** (2098, 1510, 1174 cm^{-1}) are completely absent in pristine GO.

XPS-analysis

The O:C ratio was obtained from the fit of C 1s peak, the general trends of all functional groups are reported in Table S2 and Figures S3/S4.

XPS N 1s of azide is reported to be a double peak with 4 eV relative shift, the high energy peak corresponding to the central nitrogen (N=N=N) is between 405-403 eV, while the two-external nitrogen (N=N=N) are in the 401-399 eV region. The pristine GO presents a residual amount (<0.7% at.) of indole and amino groups in the region 402-399 eV (Figure S5).[109]

The C 1s peak in Figure S6 support the grafting of **2f**, the decrease of epoxy group confirms the epoxy ring open, as already observed in Figure 2 for GO after **2a**. Moreover, no increase of hydroxyl group was observed.

The epoxidation of GO was confirmed by the increase of epoxy group after the HCl treatment (Figure S7) from 24% of reacted GO (GO after **1a**+**2a**) up to 30%.

[109] R. A. Zangmeister, T. A. Morris, M. J. Tarlov, *Langmuir*, **2013**, *29*, 8619-8628.

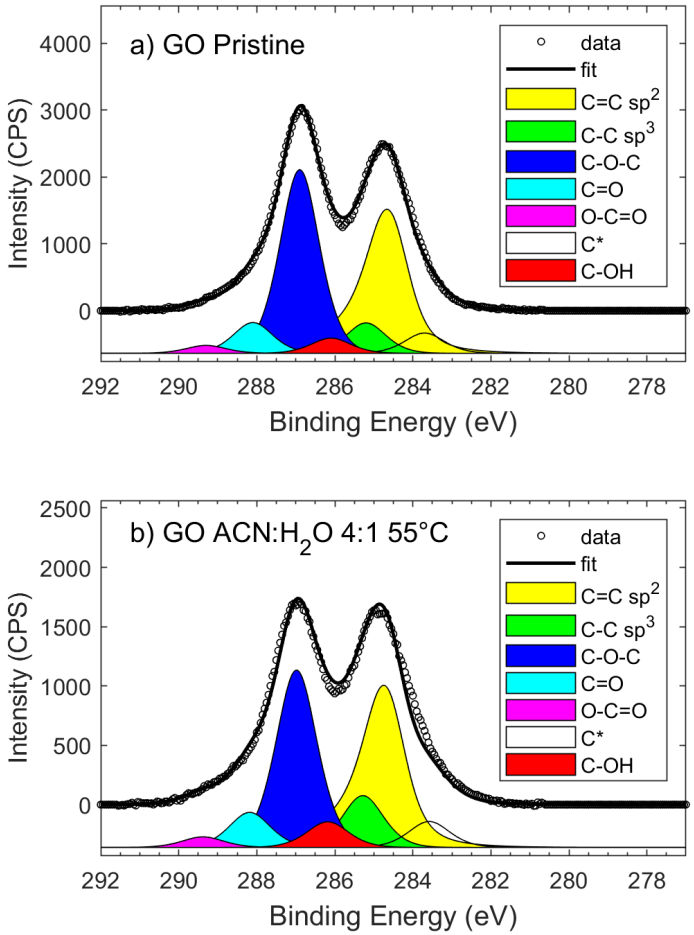

Figure S3. C 1s spectrum of GO: a) as given and b) after 5 h in ACN:H_2O 4:1 at 55 °C.

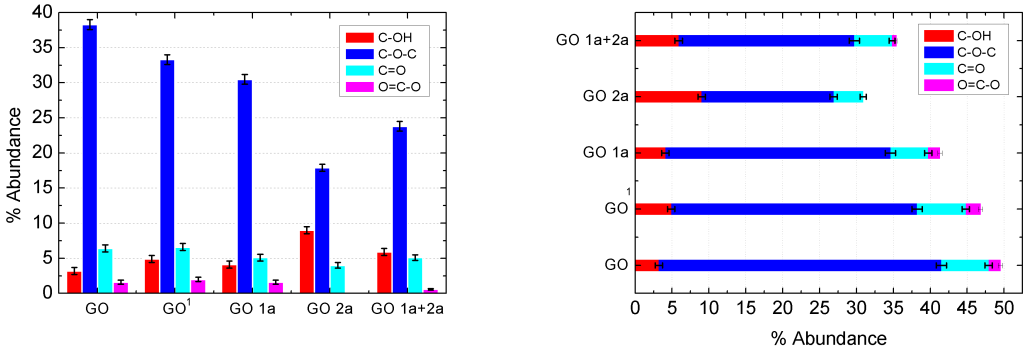

Figure S4. XPS fit of C 1s of GO after different experimental conditions. Only C-O groups are reported.

Table S2. XPS fit of C 1s of GO after different experimental conditions. The components used in fit are: aromatic carbon (C−C sp^2, 284.4 eV), aliphatic carbon (C−C sp^3, 285.0 eV), hydroxyl (C−OH, 285.7 eV), epoxy (C−O−C, 286.7 eV), carbonyl (C=O, 288.0 eV), carboxyl (O−C=O, 289.1 eV) and aromatic carbons near vacancies (C-C* sp^2, 283.5).

Sample	C-C sp^2	C-C sp^3	C=C*	C-OH	C-O-C	C=O	O=C-O	O/C_{fit}
GO	39.9±0.8	10.5±0.5	4.2±0.3	3.2±0.3	38.3±0.8	6.4±0.4	1.6±0.2	0.32±0.02
GO (solvent)	38.7±0.8	14.6±0.5	4.9±0.3	4.9±0.3	33.3±0.8	6.6±0.4	2.0±0.2	0.32±0.02
GO after **1a**	42.5±0.8	16.3±0.5	5.4±0.4	4.1±0.3	30.5±0.8	5.1±0.4	1.6±0.2	0.28±0.02
GO after **2a**	45.5±0.8	23.6±0.6	3.9±0.3	9.0±0.5	17.9±0.6	4.0±0.3	0.0±0.2	0.22±0.01
GO after **1a**+**2a**	39.1±0.8	25.5±0.6	8.8±0.5	5.9±0.4	23.8±0.7	5.1±0.4	0.6±0.2	0.24±0.02
Regenerated GO	37.4±0.8	12.2±0.5	9.5±0.5	3.4±0.3	30.2±0.8	5.5±0.3	1.8±0.2	0.28±0.02
GO + **2f** 0°C	28.7±0.7	14.4±0.5	5.2±0.4	10.1±0.5	33.2±0.8	5.6±0.4	2.7±0.3	0.38±0.02
GO + **2f** 55 °C	39.1±0.8	16.8±0.5	0.4±0.2	5.7±0.4	30.8±0.8	3.1±0.3	2.4±0.2	0.29±0.02

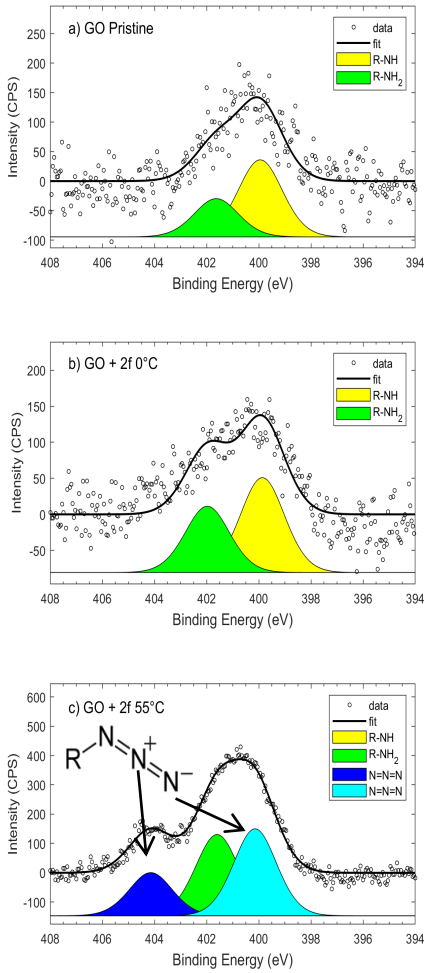

Figure S5. XPS N 1s signal of a) pristine GO, b) GO + **2f** after 6 h in CH_3CN:H_2O 4:1 at 0 °C and c) GO + **2f** after 6 h in CH_3CN:H_2O 4:1 at 55 °C.

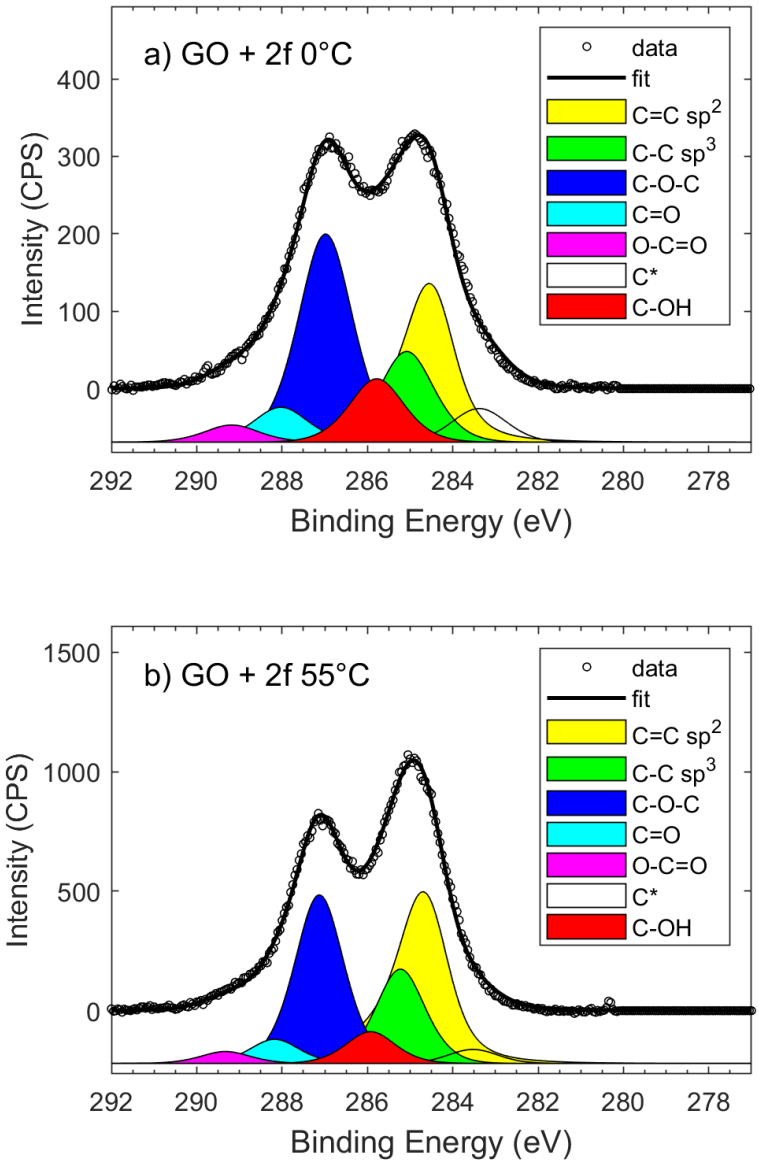

Figure S6. XPS C 1s signal of a) GO + **2f** after 6 h in CH_3CN:H_2O 4:1 at 0 °C and b) GO + **2f** after 6 h in CH_3CN:H_2O 4:1 at 55 °C.

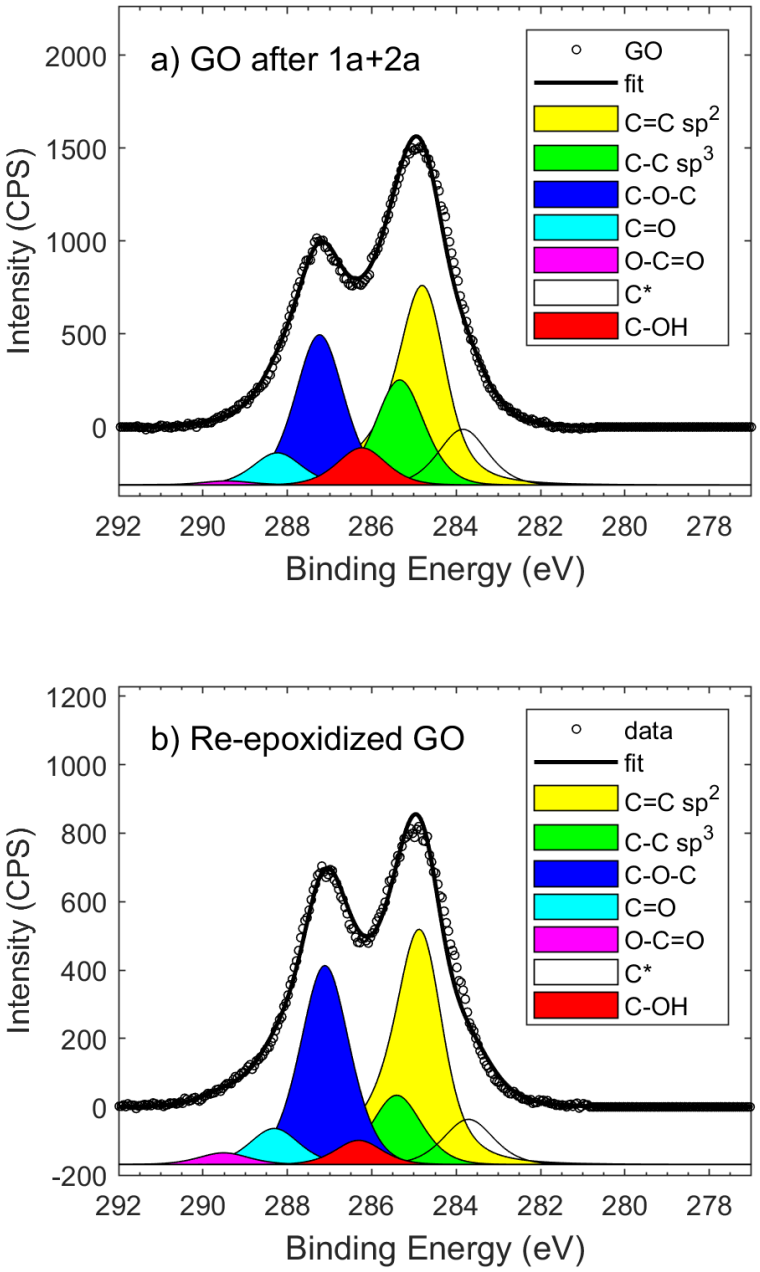

Figure S7. XPS C 1s signal of a) GO after **1a**+**2a** and b) Re-epoxidized GO.

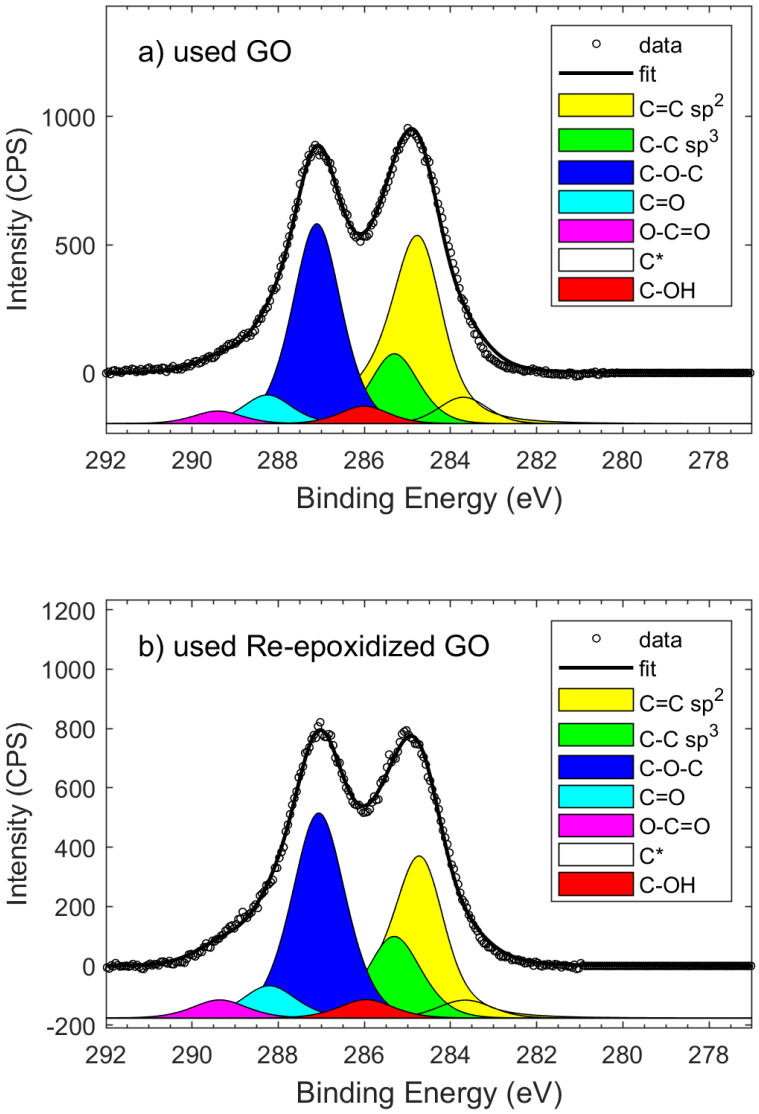

Figure S8. XPS C 1s signal of a) used GO and b) used Re-epoxidized GO.

Computational details

All calculations were carried out using the combined quantum mechanical and molecular mechanical (QM/MM) method in the ONIOM formalism, as implemented within the Gaussian 16 program suite.[110] The coupled QM/MM method adopted here is a two-layer ONIOM scheme, where the reactive region is treated at DFT level using the density functional M06-2X (a functional able to account for π-π interactions) and 6-1G*basis set.[111] The remaining region is treated using the UFF force field.[112] The global potential can be referred as M06-2X/6-31G*:UFF potential. ONIOM calculations were performed considering mechanical and electrostatic embedding. In the MM calculations partial atomic (point) charges were used to compute the electrostatic interactions. These charges were calculated using the QEq formalism.[113] Frequency calculations were carried out at the same level of theory to check the nature of critical points. The presence of the solvent (water) is taken in account employing the polarizable continuum model (PCM) using the integral equation formalism variant (IEFPCM).[114]

---

[110] Gaussian 09, Revision A.02, M. J. Frisch, G. W. Trucks, H. B. Schlegel, G. E. Scuseria, M. A. Robb, J. R. Cheeseman, G. Scalmani, V. Barone, G. A. Petersson, H. Nakatsuji, X. Li, M. Caricato, A. Marenich, J. Bloino, B. G. Janesko, R. Gomperts, B. Mennucci, H. P. Hratchian, J. V. Ortiz, A. F. Izmaylov, J. L. Sonnenberg, D. Williams-Young, F. Ding, F. Lipparini, F. Egidi, J. Goings, B. Peng, A. Petrone, T. Henderson, D. Ranasinghe, V. G. Zakrzewski, J. Gao, N. Rega, G. Zheng, W. Liang, M. Hada, M. Ehara, K. Toyota, R. Fukuda, J. Hasegawa, M. Ishida, T. Nakajima, Y. Honda, O. Kitao, H. Nakai, T. Vreven, K. Throssell, J. A. Montgomery, J. E. Peralta, F. Ogliaro, M. Bearpark, J. J. Heyd, E. Brothers, K. N. Kudin, V. N. Staroverov, T. Keith, R. Kobayashi, J. Normand, K. Raghavachari, A. Rendell, J. C. Burant, S. S. Iyengar, J. Tomasi, M. Cossi, J. M. Millam, M. Klene, C. Adamo, R. Cammi, J. W. Ochterski, R. L. Martin, K. Morokuma, O. Farkas, J. B. Foresman, D. J. Fox, Gaussian, Inc., Wallingford CT.

[111] R. Ditchfield, W. J. Hehre, J. A. Pople, *J. Chem. Phys.* **1971**, *54*, 724.

[112] A. K. Rappé, C. J. Casewit, K. S. Colwell, W. A. III Goddard, W. M. Skiff, *J. Am. Chem. Soc.*,**1992**, *114*, 10024-10035.

[113] A. K. Rappé, L. M. Bormann-Rochotte, D. C. Wiser, J. R. Hart, M. A. Pietsch, C. J. Casewit, W. M. Skiff, *Mol. Phys.* **2007**, *105*, 301-324.

[114] M. Cossi, V. Barone, R. Cammi, J. Tomasi, *Chem. Phys. Lett.* **1996**, *255*, 327-335.

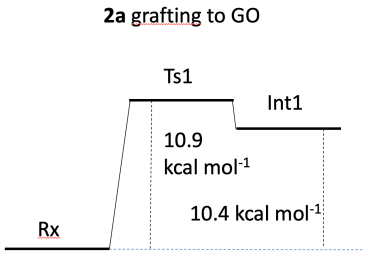

Figure S9. Energy profile for the covalent grafting of **2a** to the GO surface.

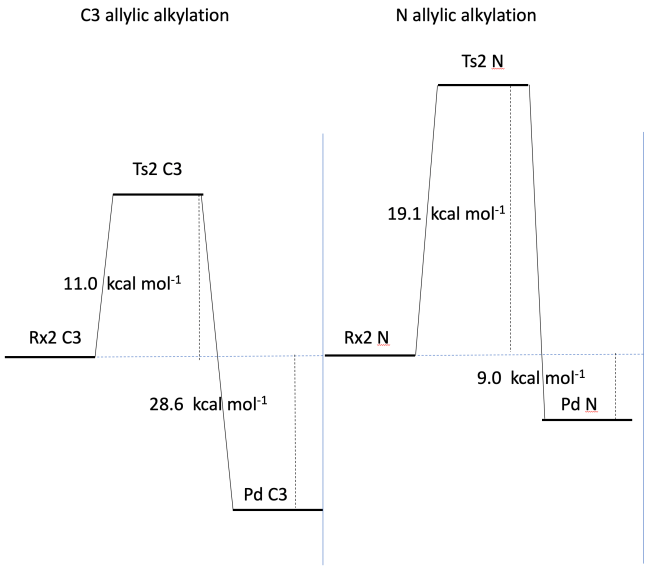

Figure S10. Energy profiles for the C3/N allylic alkylation of **1a**.

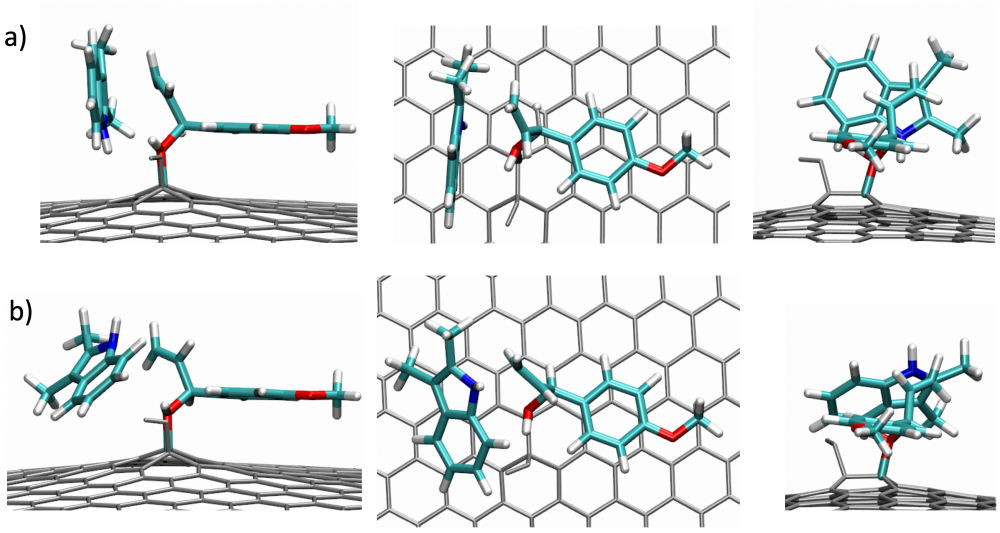

Figure S11. Side view (left), top view (center) and front view (right) of the identified transition states for the C(3) (a, Ts2 C3) and (N) (b, Ts2 N) allylic alkylation of **1a**.

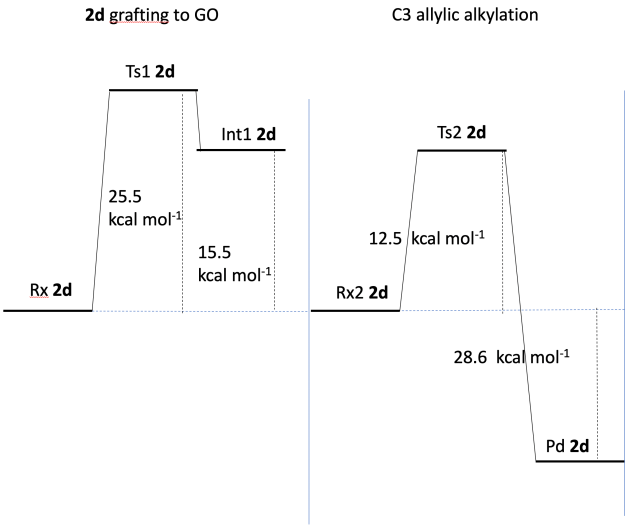

Figure S12. Energy profiles for the a) covalent grafting of **2d** to the GO surface and b) C3 allylic alkylation of **1a.**

Crystallographic data collection and structure determination for 3ha

The X-ray intensity data were measured on a Bruker Apex II CCD diffractometer using MoKα radiation. Cell dimensions and the orientation matrix were initially determined from a least-squares refinement on reflections measured in three sets of 20 exposures, collected in three different regions, and eventually refined against all data. A full sphere of reciprocal space was scanned by 0.3steps. The software SMART[115] was used for collecting frames of data, indexing reflections and determination of lattice parameters. The collected frames were then processed for integration by the SAINT program[115] and an empirical absorption correction was applied using SADABS.[116] The structures were solved by direct methods (SIR 2014)[117] and subsequent Fourier syntheses and refined by full-matrix least-squares on F^2 (SHELXTL)[118] using anisotropic thermal parameters for all non-hydrogen atoms. The hydrogen atoms were placed in calculated positions, refined with isotropic thermal parameters U(H)= 1.2 Ueq(C) or U(H)= 1.5 Ueq(methyl) and allowed to ride on their carrier carbons. Crystal data and details of data collections for compound **3ha** are reported in Table S1. Molecular drawings were generated using Mercury.[119] Crystallographic data have been deposited with the Cambridge Crystallographic Data Centre (CCDC) as supplementary publication number CCDC 1964157. Copies of the data can be obtained free of charge upon request (www.ccdc.cam.ac.uk/).

---

[115] *SMART & SAINT Software Reference Manuals*, version 5.051 (Windows NT Version), Bruker Analytical X-ray Instruments Inc.: Madison, Wi, **1998.**

[116] G. M. Sheldrick, *SADABS-2008/1-Bruker AXS Area Detector Scaling and Absorption Correction*, Bruker AXS: Madison, Wisconsin, USA, **2008**.

[117] M. C. Burla, R. Caliandro, B. Carrozzini, G. L. Cascarano, C. Cuocci, C. Giacovazzo, M. Mallamo, A. Mazzone, G. Polidori, *J. Appl. Cryst.* **2015**, *48*, 306-309.

[118] G. M. Sheldrick, *Acta Cryst C71* **2015**, 3-8.

[119] C. F. Macrae, I. J. Bruno, J. A. Chisholm, P. R. Edgington, P. McCabe, E. Pidcock, L. Rodriguez-Monge, R. Taylor, J. van de Streek, P. A. Wood, *J. Appl. Cryst.* **2008**, *41*, 466-470.

Table S3. Crystal data and structure refinement for compound **3ha**.

Compound	**3ha**
Formula	$C_{22}H_{23}NO$
Fw	317.41
T, K	296
λ, Å	0.71073
Crystal symmetry	Monoclinic
Space group	*P2₁/c*
a, Å	9.577(2)
b, Å	10.592(2)
c, Å	16.415(3)
α	90
β	91.56(3)
γ	90
Cell volume, $Å^3$	1664.5(6)
Z	4
D_c, Mg m^{-3}	1.267
μ(Mo-$K_α$), mm^{-1}	0.077
F(000)	680
Crystal size/ mm	0.30 x 0.10 x 0.05
θ limits, °	2.127 - 24.495
Reflections collected	14923
Unique obs. Reflections [F_o >	2453 [R(int) =
Goodness-of-fit-on F^2	1.375
R_1 $(F)^a$, wR_2 $(F^2)^b$ [I > 2σ(I)]	0.1073, 0.2281
Largest diff. peak and hole, e. $Å^{-3}$	0.224 and -0.247

[a] $R_1 = \Sigma||F_o|-|F_c||/\Sigma|F_o|$. [b] $wR_2 = [\Sigma w(F_o^2-F_c^2)^2/\Sigma w(F_o^2)^2]^{1/2}$ where $w = 1/[\sigma^2(F_o^2) + (aP)^2 + bP]$ where $P = (F_o^2 + F_c^2)/3$.

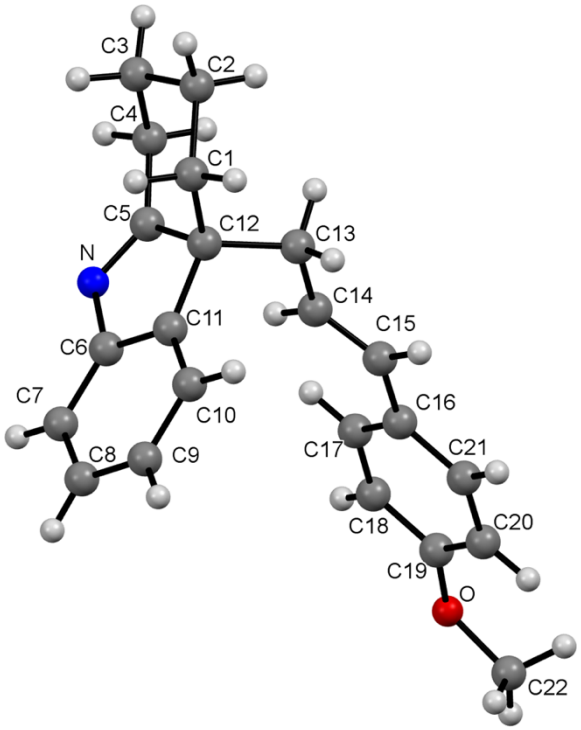

Figure S13. Crystal structure of **3ha.**

4. NiNP@rGO Nanocomposites as Heterogeneous Catalysts for Thiocarboxylation Cross-Coupling Reactions

All the procedures and results here described can be found in:

- L. Lombardi, R. Mazzaro, M. Gazzano, A. Kovtun, V. Morandi, G. Bertuzzi, M. Bandini, "NiNP@rGO Nanocomposites as Heterogeneous Catalysts for Thiocarboxylation Cross-Coupling Reactions". *Synthesis* **2022**, *54*, 1633-1642.

ABSTRACT

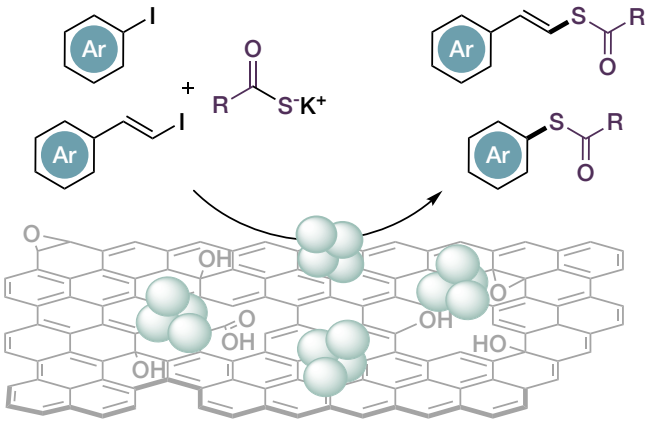

A new type of ligand-free Ni-nanoparticles supported on rGO (size distribution average d = 9 ± 3 nm) was prepared and fully characterized via morphological (FE-SEM), structural (P-XRD, HR-TEM), and spectroscopic (ICP-EOS, XPS) analysis. The composite material was successfully tested in the unprecedented heterogeneously Ni-catalyzed cross-coupling reaction of aryl/vinyl iodides and thiocarboxylate salts. A range of *S*-aryl as well as *S*-vinyl thioesters (15 examples) were prepared in high yields (up to 82%), under mild reaction conditions and good functional group tolerance, with an operationally simple protocol.

4.1 Background

The name "nickel" has roots in German mythology and bears a mischievous connotation: it derives from "Kupfernickel", which means "Devil's Copper". 15th century miners who were searching for copper, but could not extract it from such ores, blamed some evil sprite named "Nickel" (similar to "Old Nick", a nickname for Satan in Christian traditions) for tricking them. Nickel was first isolated and classified as an element in 1751 by Swedish mineralogist Axel Fredrik Cronstedt, who also initially mistook the ore for a copper mineral, in the cobalt mines of Los, Hälsingland, Sweden.[120]

Mystical aspects aside, the name revealed somewhat appropriate to describe the capricious nature of this element, and Sabatier himself, in reviewing the state of the art and properties of nickel catalysts, stated that "it can be compared to a spirited horse, delicate, difficult to control, and incapable of sustainable work".[121] Since those times, enormous progress has been made in dealing with this element, especially since the birth of homogeneous nickel catalysis that can be traced back to the work of Reppe and Wilke, among other notable scientist, in the field of poly- and oligomerization of alkenes.[122]

Nickel has been demonstrated to be an extremely powerful and versatile catalyst for a plethora or reaction types, including: reductive cyclizations and reductive couplings of unsaturated systems, carbonylations, carboxylations, C-C and C-X (X denotes heteroatoms) bond forming cross couplings, hydrogenations, C-H and C-C activation processes. In particular, its capability of activating challenging and "unconventional" electrophiles (for example C-O or C-F bonds), its suitability for the accommodation of Csp^3 fragments, and relatively facile access to odd oxidation numbers with open-shell

[120] Y. Tamaru, *Modern Organonickel Chemistry.* Wiley-VHC: Weinheim, **2005**.
[121] P. Sabatier, *Catalysis in Organic Chemistry*. D. Van Nostrand Company: New York, **1922**.
[122] a) L. Mond, C. Langer, F. Quincke, *J. Chem. Soc., Trans.* **1890**, *57*, 749–753; b) G. Wilke, *Angew. Chem. Int. Ed.* **1988**, *27*, 185–206; c) W. Keim, *Angew. Chem. Int. Ed.* **1990**, *29*, 235–244.

configuration stand as powerful features to capitalize on.[123,120] In the direction of developing versatile, powerful and more sustainable methodologies with cheap and widely available metals, nickel catalysis holds a paramount place, as testified by the ever-expanding number of publications in the field in the last ten years.

As observed from the early investigations above-mentioned, the difficulty in "taming" the reactive nature of this metal still remains and accompanies its remarkable potential. A large number of nickel catalyzed transformations require highly reactive, nucleophilic Ni(0) species to be accessed, and their usually extreme instability and air-sensitivity can hamper practicality. One approach is the use of Ni(II) precatalysts for the formation of active species *in situ*. Despite the success and wide adoption of this method, and the existence of Ni(II) precatalysts that permit modular accommodation of the desired ligands[124], ligand exchange/transmetallation/reduction sequences are necessary to achieve the desired catalytic complex, resulting in undefined metal–ligand ratios and possible undesired reactivity from the ancillary ligands. On the other hand, direct utilization of Ni(0) precatalysts is made challenging by the extreme reactivity of such species, making mandatory the adoption of rigorous Schlenk techniques or working in a glovebox setting, thus limiting the practicality of this approach. Furthermore, since its first preparation by Wilke[125], highly unstable and expensive bis(1-5-cyclooctadiene)nickel(0), *i.e.* $Ni(COD)_2$, still is the most widely, if not the only, Ni(0) precatalyst used for synthetic purposes thanks to the high lability of the olefin ligands.[126] This quest towards the adoption of more stable and practical Ni(0) entities has been greatly stimulating research for a long time[127], and culminated in very

---

[123] a) S. Ogoshi, *Nickel Catalysis in Organic Synthesis.* Wiley-VHC: Weinheim, **2020**; b) S. Z. Tasker, E. A. Standley, T. F. Jamison, *Nature* **2014**, *509*, 299–309; c) J. B. Dicciani, T. Diao, *Trends in Chemistry* **2019**, *1*, 830–844; d) V. P. Ananikov, *ACS Catal.* **2015**, *5*, 1964−1971.

[124] a) For a general review on Pd and Ni precatalysts see: N. Hazari, P. R. Melvin, M. M. Beromi, *Nat. Rev. Chem.* **2017**, *1*, 0025; b) E. A Standley, T. F. Jamison, *J. Am. Chem. Soc.* **2013**, *135*, 1585−1592; c) J. D. Shields, E. E. Gray, A. G. Doyle, *Org. Lett.* **2015**, *17*, 2166−2169; d) N. H. Park, G. Teverovskiy, S. L. Buchwald, *Org. Lett.* **2014**, *16*, 220−223; e) S. Ge, J. F. Hartwig, *Angew. Chem. Int. Ed.* **2012**, *51*, 12837–12841.

[125] G. Wilke, *Angew. Chem.* **1960**, *72*, 581−58.

[126] L. Nattmann, R. Saeb, N. Nöthling, J. Cornella, *Nat. Catal.* **2020**, *3*, 6–13.

[127] a) A. J. Nett, S. Cañellas, Y. Higuchi, M. T. Robo, J. M. Kochkodan, M. T. Haynes, J. W. Kampf, J. Montgomery, *ACS Catal.* **2018**, *8*, 6606−6611; b) S. S. Kampmann, A. N. Sobolev, G. A. Koutsantonis, S. G. Stewart, *Adv. Synth. Catal.* **2014**, *356*, 1967–1973.

recent reports of general air stable Ni(0) precatalysts bearing stilbene or olefin-quinone ligands by the groups of Cornella[126,128] and Engle[129], respectively (**Figure 1**).

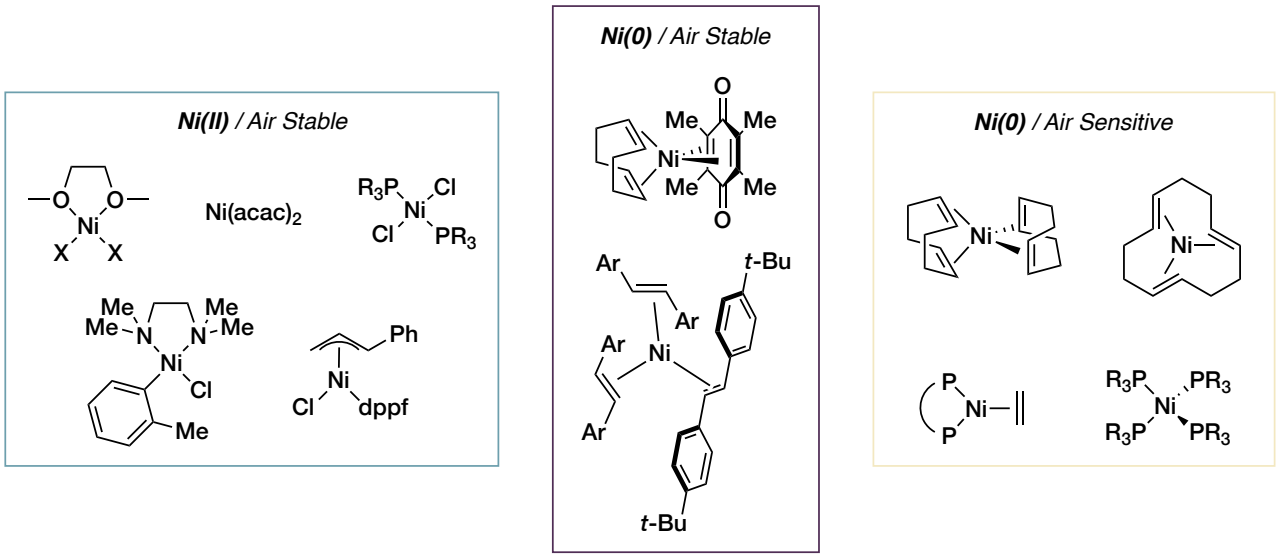

Figure 1. Overview of some common Ni(II) and Ni(0) precatalysts, classified by their stability to air.

A parallel strategy that can provide a solution to access easy-to-handle low valent Ni entities is represented by the use nickel nanoparticles (NPs).

Metal NP catalysts constitute a topic of great interest in both academia and industry, due to their large surface areas conferring them high catalytic activity, and also for their nano-size effect that imparts unique selectivity and different behavior from their bulk metal counterparts.[130] Such species are excellent candidates for cheap, robust heterogeneous catalysts conjugating high stability and activity with ease of separation and reusability, and offering much reduced contamination of the products, a parameter of paramount importance in the context of active pharmaceutical ingredients (APIs) preparation. In light of these features, NPs retain great potential for the development of heterogeneous catalysis for fine chemical synthesis, an area that has traditionally

[128] L. Nattmann, J. Cornella, *Organometallics* **2020**, *39*, 3295−3300.
[129] V. T. Tran, Z.-Q. Li, O. Apolinar, J. Derosa, M. V. Joannou, S. R. Wisniewski, M. D. Eastgate, K. M. Engle, *Angew. Chem. Int. Ed.* **2020**, *59*, 7409–7413.
[130] M. J. Ndolomingo, N. Bingwa, R. Meijboom, *J. Mater. Sci* **2020**, *55*, 6195–6241.

lagged behind compared to bulk chemical processes.[131] The very small dimensions attainable with these materials (an accepted definition to classify as NP is having at least two dimensions below 100 nm, but metal clusters with dimensions down to 1 nm are known) offer an interesting conceptual bridge between homogeneous and heterogeneous systems.[132] As similarly noted earlier about nanocarbons, it can be argued that in modern times the boundary between the two extremes has been getting more and more blurred. Due to their surface area, NPs are metastable materials, and therefore a suitable stabilizing agent is necessary for their synthesis. Stabilization can be achieved with electrostatic or steric effects or by means of ligands, supports or interaction with the reaction medium.[133] For reusability purposes, deposition on solid supports can often be preferred. The use of a support is intended to maximize the production of highly dispersed NPs with a narrow size distribution, leading to better catalytic performance. Besides preventing aggregation and sintering (that would lead to bigger entities with lowered surface area and reduced catalytic activity), and reducing the spontaneous overgrowth of NPs, the support can fulfill the role of a macroscopic ligand to the metal sites, providing additional stabilization and modulating the catalytic activity, concurring in a synergic manner to the catalytic performance.[134] Graphene based materials combine several useful features in this direction: being high surface area 2D materials of single atom thickness, every particle can be accessible to the substrates, providing high atom efficiency and no diffusion restrictions; their defective π-matrix can interact strongly with NPs and substrates, facilitating adsorption, enhancing NPs stabilization, reducing leaching and modulating the electron density on the metal, substrates and intermediates, possibly aiding in elementary steps; the presence of defects, holes and edges can expose metal atoms with lower coordination number and enhanced catalytic activity; the presence of oxygenated functional groups can result in strong specific interactions with NPs or substrates,

[131] S. Kobayashi, *Nanoparticles in Catalysis.* Springer Nature Switzerland: Cham, **2020**.
[132] a) L. Liu, A. Corma, *Chem. Rev.* **2018**, *118*, 4981−5079; b) A. Cid, J. Simal-Gandara, *J. Inorg. Organomet. Polym.* **2020**, *30*, 1011–1032.
[133] D. Astruc, F. Lu, J. R. Aranzaes, *Angew. Chem. Int. Ed.* **2005**, *44*, 7852–7872
[134] A. Ghatak, M. Das, *ChemistrySelect* **2021**, *6*, 3656–3682.

overall tuning the performances and provides additional, distinct catalytic sites; for first row transition metals, such as Cu and Ni, their atomic radius corresponds to the dimensions of hexagonal rings on the surface, resulting in a templating effect of the support for the growth of such NPs.[135] The strong affinity of Ni for unsaturated carbon systems perfectly matches this cooperative scenario, providing high stabilization for Ni(0) entities. Ni NPs supported on graphene materials have emerged as promising catalysts in a number of hydrogenation, transfer hydrogenation, C-C and C-X cross coupling reactions.[136]

De and coworkers reported the use of rGO supported Ni NPs for the Kumada-Corriu cross coupling reaction of Grignard reagents and aryl halides.[137] The catalytic material was prepared starting from cheap GO and $NiCl{\cdot}6H_2O$ in a three-step procedure. In the first step, an hydrothermal reaction in the presence of HMT (hexamethylenetetramine) as a stabilizing agent yielded a [GO-Ni(OH_2)] composite, that was heated in air in the second step to obtain NiO NPs embedded rGO sheets. Further reduction of NiO NPs under H_2 gas flow yields the desired NiNPs@rGO (A) (@ denotes deposition) material that was determined to contain a high Ni content (40 wt%). Characterization revealed a high surface area (125 m^2/g) and the presence of highly monodispersed NiNPs with an average size of 11 nm (**Scheme 1**). The material resulted a highly competent catalyst in the Kumada-Corriu cross coupling of aryl iodides, bromides, chlorides and even fluorides proving biaryl products in high yield (72-91%) at room temperature, using a Ni loading of 10 mol%.

---

[135] S. Navalon, A. Dhakshinamoorthy, M. Alvaro, H. Garcia, *Coord. Chem. Rev.* **2016**, *312*, 99–148.

[136] a) N.-D. Jaji, H. L. Lee, M. H. Hussin, H. M. Akil, M. R. Zakaria, M. B. H. Othman, *Nanotechnology Reviews* **2020**, *9*, 1456–1480; b) M. Nasrollahzadeh, Z. Issaabadi, M. Mostafa Tohidi, S. M. Sajadi, *Chem. Rec.* **2018**, *18*, 165–229; c) W. Gao, J. E. Mueller, J. Anton, Q. Jiang, T. Jacob, *Angew. Chem. Int. Ed.* **2013**, *52*, 14237–14241; d) F. Alonso, P. Riente, M. Yus *Acc. Chem. Res.* **2011**, *44*, 379–391.

[137] K. Bhowmik, D. Sengupta, B. Basu, G. De, *RSC Adv.* **2014**, *4*, 35442–35448.

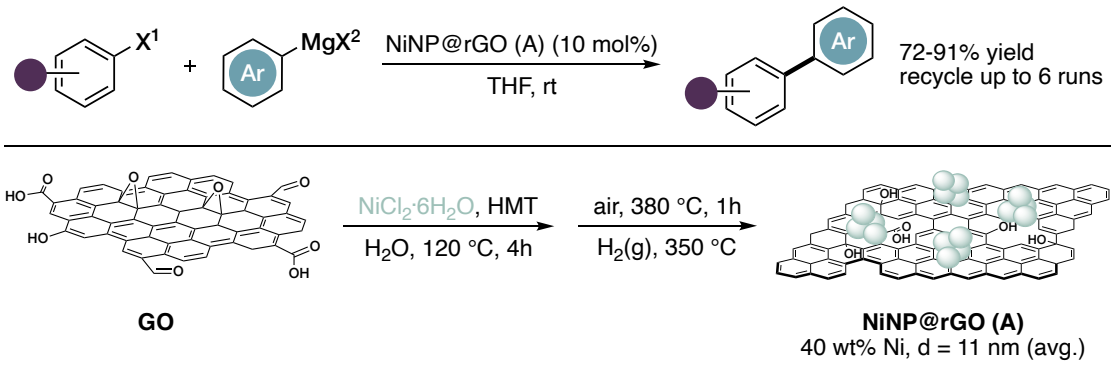

Scheme 1. Top: De's NiNP@rGO-catalyzed Kumada-Corriu cross coupling. X^1 = Br, I, Cl, F; X^2 = Br, Cl. Bottom: Synthesis of the metal nanocomposite catalyst. Avg. = average.

The catalyst could be separated from the products and recovered by simple aqueous work up followed by evaporation and was shown to be reusable up to six runs with only slight detriment in yields. Interestingly, P-XRD (Powder X-Ray diffraction) analysis of the material after the reaction showed no oxidation of the Ni centers, and incorporation of a significant amount of Mg oxides and hydroxides despite thorough washing; this phenomenon did not affect the catalytic performance.

The same authors later employed this catalyst for the C-S cross coupling or aryl thiols and aryl halides.[138] A 15 mol% loading of Ni was found to be sufficient to obtain aryl-aryl thioethers in high yields (84-93%) from aryl iodides; bromides were also found to be suitable coupling partners but necessitated the addition of a stoichiometric amount of Zn dust (**Scheme 2**). Very interestingly, the reaction could proceed in the absence of base (albeit with longer reaction time), and aliphatic thiols were also demonstrated competent. Cl, F and NO_2 were all tolerated, and the catalyst recycling up to six runs showed no decrease in performance.

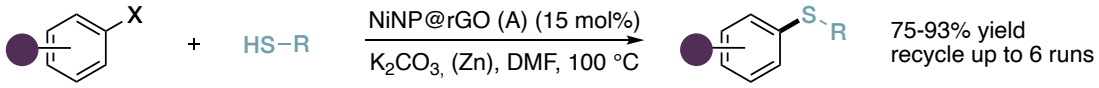

[138] D. Sengupta, K. Bhowmik, G. De, B. Basu, *Beilstein J. Org. Chem.* **2017**, *13*, 1796–1806.

Scheme 2. De's NiNP@rGO-catalyzed C-S cross coupling between aryl halides and thiols. When X = Br, 1 equivalent of Zn dust is needed.

Thorough characterization of the material after the reaction was carried out and highlighted some interesting aspects. P-XRD analysis revealed a crystallite size of 12 nm for Ni(0) NPs, demonstrating that no agglomeration was occurring under reaction conditions. Signals of $Ni(OH)_2$ were also observed both in P-XRD and XPS analyses, and deconvolution allowed to determine that the recovered catalyst contained 17% Ni(0) and 83% Ni(II) species. Consistent results were obtained by TEM imaging. The untouched catalytic performance of the recovered material points to the fact that Ni(II) NPs are also competent in the reaction, and this was proved by preparing and employing a $Ni(OH)_2$@rGO composite that showed only slightly worse results than the original material. The authors propose that $Ni(OH)_2$ is formed during aqueous work up, and that thiolate anions could reduce Ni(II) species to catalytically active Ni(I) species, so that the reaction could be occurring both in a Ni(0)/Ni(II) and Ni(I)/Ni(III) manifolds depending on the nature of the metal site, as reported in previous investigations.[139]

A very interesting report came for Das and coworkers in 2015.[140] By the combination of GO, $NiCl_2$ as nickel source and hydrazine hydrate as a reductant, they were able to prepare ferromagnetic NiNPs deposited on rGO surface in pure aqueous medium. Careful characterization by means of P-XRD, FT-IR, TGA (thermogravimetric analysis), TEM, SEM-EDS (scanning electron microscopy-energy dispersive X-ray spectroscopy) and VSM (vibrating sample magnetometer) techniques highlighted the formation of very small, narrowly distributed ferromagnetic NiNPs with 2.7 nm average size. Complete reduction of GO to rGO and absence of Ni(II) species was observed. The combination of CuI (8 mol%), K_2CO_3 and nanomaterial (NiNPs@rGO (B)) with an overall Ni loading of 15 mol% in NMP as solvent at 120 °C proved successful for the Sonogashira coupling of (hetero)aryl iodides, bromides and chlorides

[139] G. T. Venkanna, H. D. Arman, Z. J. Tonzetich, *ACS Catal.* **2014**, *4*, 2941–2950.
[140] N. Hussain, P. Gogoi, P. Khared, M. R. Das, *RSC Adv.* **2015**, *5*, 103105–103115.

with phenylacetylene, providing internal alkynes in above 90% yield in most cases (**Scheme 3**).

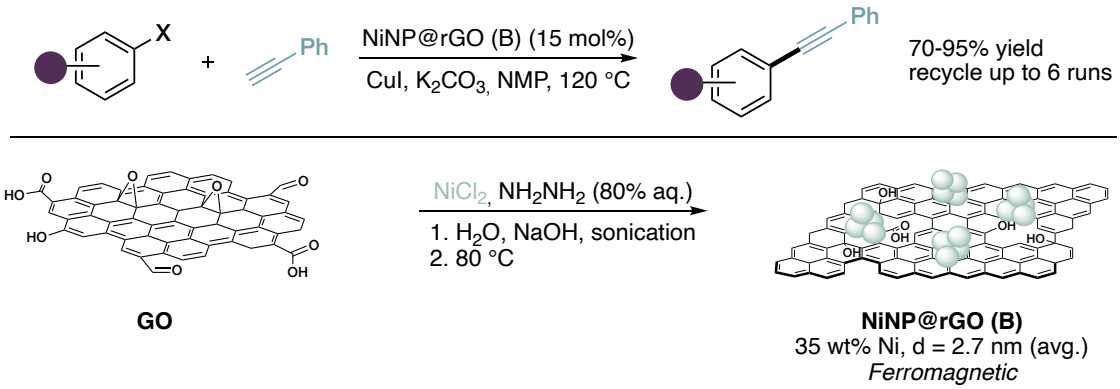

Scheme 3. Sonogashira cross coupling catalyzed by NiNP@rGO (B), obtained by simoultaneous hydrazine reduction of a Ni(II) salt and GO.

The catalyst could be very easily recovered by physical means exploiting its ferromagnetic nature and demonstrated active up to six runs with only minor detriment in activity. Characterization after the reaction showed no significant modification in Ni content, size and morphology; a hot filtration test was also performed, ruling out leaching of NPs in the course of the reaction.

In 2020, Ghaedi *et al.* described a different kind of approach by using a chemically modified graphene oxide as a support. By using amide coupling chemistry with EDC (1-Ethyl-3-(3-dimethylaminopropyl)carbodiimide) and NHS (*N*-hydroxysuccinimide) as coupling reagents they were able to attach metformin units onto the carboxylic groups of GO, and used them as anchoring sites for NiNPs obtained by reduction of $NiCl_2$ with hydrazine hydrate (**Scheme 4**, bottom).[141] Multiple analyses of the material including SEM, TEM, EDS, FT-IR, P-XRD, TGA, and ICP-OES (inductively coupled plasma optical emission spectroscopy) were used for characterization. In this case the GO sheet resulted not to be reduced to rGO, and NiNPs were observed bound both to the metformin units and carbon matrix. Interestingly, a difference in size was noted in

[141] F. Raoufi, M. Monajjemi, H. Aghaei, K. Zare, M.Ghaedi, *ChemistrySelect* **2020**, *5*, 211–217.

the two cases, with NPs bound to the organic ligand having an average size of 10 nm, while NPs deposited on GO showed average of size of 30 nm. The Ni content was assessed to be around 5 wt%.

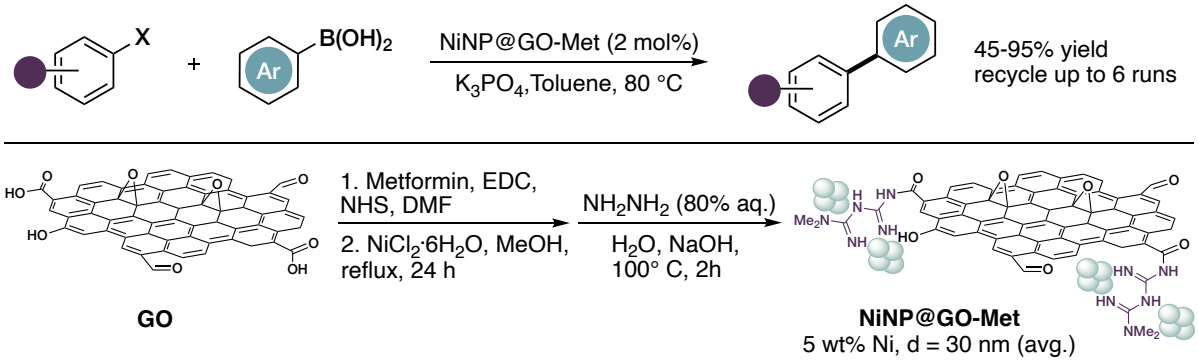

Scheme 4. Top: Suzuki cross coupling using NiNPs deposited on a covalently modified GO. Bottom: Preparation on the NiNP@GO-Met catalyst.

This material was successfully tested in the Suzuki coupling of an array of aryl iodides, bromides and chlorides with phenylboronic acid (**Scheme 4**, top). The use of K_3PO_4 and NiNPs catalyst in only 2 mol% metal loading in toluene emerged as optimal conditions. The catalyst could be separated by simple centrifugation, washing and drying steps and reusability was demonstrated up to six runs with no loss in catalytic activity.

Suresh reported the use of environmental friendly ascorbic acid for the preparation of a NiNPs@rGO (C) composite material by simultaneous reduction of GO and $NiCl{\cdot}6H_2O$ in water, in the absence of any stabilizer.[142] Characterization highlighted the uniform dispersion of magnetic NiNPs of 10 nm average size, with an overall 20 wt% Ni content, and assessed complete reduction of GO to rGO. The material was used as catalyst for the reduction of nitro arenes with $NaBH_4$ as a reducing agent (**Scheme 5**). A 6.8 mol% metal loading and a high excess of reductant in a 1:1 methanol-water mixture at room temperature allowed quantitative formation of aniline products with

[142] M. Karthik, P. Suresh, *ChemistrySelect* **2017**, *2*, 6916–6928.

exquisite selectivity. Nitrile, ketone, halide and pyridine functionalities were all tolerated, and two examples of nitroalkanes were also documented. The catalyst could be mechanically recovered with a magnet, and showed no decrease in activity after five runs, and no noticeable modifications were observed by P-XRD and FT-IR techniques; hot filtration test and ICP-OES analysis ruled out any nickel leaching. Mechanistically, the authors propose that hydride ions arising from ionization of the reductant are adsorbed onto the NiNPs to form nickel hydride species and then delivered to the strongly adsorbed nitro arenes.

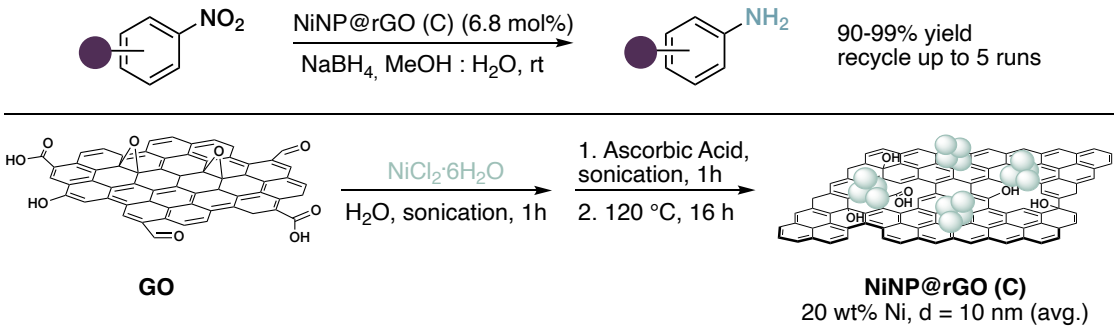

Scheme 5. Top: NiNPs@rGO-catalyzed reduction of nitroarenes with sodium borohydride. Bottom: Preparation on the NiNP@rGO (C) catalyst by simultaneous reduction of a Ni(II) salt and GO matrix by ascorbic acid.

Thioesters (IUPAC name *S*-alkyl (*S*-aryl) carbothioates) are sulfur analogues of carboxylic esters in which the alcoholic O is replaced by a S atom. A sometimes overlooked functional group, this moiety presents in fact multiple interesting structural features, synthetic utilizations, roles in biochemical processes and occurence in bioactive compounds.[143] Due to smaller orbital overlap between the sulfur atom and the carbonyl group, thioesters are more reactive than oxoesters towards nucleophiles, displaying a reactivity comparable to acid chlorides while being bench stable

[143] a) V. Hirschbeck, P. H. Gehrtz, I. Fleischer, *Chem. Eur. J.* **2018**, *24*, 7092–7107; b) X. Wang, Z.-B. Dong, *Eur. J. Org. Chem.* **2022**, e202200452.

compounds storable for long time under ambient conditions (**Figure 2**). This phenomenon also enhances the acidity of α-protons, facilitating aldol chemistry.

Thioesters can be found ubiquitously in biochemical processes. Acetyl coenzyme A delivers the acetyl group in the Krebs cycle, that establishes respiration, and is involved in several other metabolic pathways such as fatty acid metabolism, steroid synthesis and melatonin synthesis. Thioesters are used as building blocks in the biosynthesis of polyketides via their aldol chemistry.[144] It has also been proposed that they played an important role in the development of life on earth, possibly providing a plausible prebiotic path to protopeptides.[145]

[144] a) F. Pietrocola, L. Galluzzi, J. M. Bravo-San Pedro, F. Madeo, G. Kroemer, *Cell Metab.* **2015**, *21*, 805–821. b) J. Staunton, K. J. Weissman, *Nat. Prod. Rep.* **2001**, *18*, 380–416.

[145] a) G. Wächtershäuser, *Prog. Biophys. Mol. Biol.* **1992**, *58*, 85–201; b) P. J. Bracher, P. W. Snyder, B. R. Bohall, G. M. Whitesides, *Origins Life Evol. Biospheres* **2011**, *41*, 399–412; c) M. Frenkel-Pinter, M. Bouza, F. M. Fernández, L. J. Leman, L. D. Williams, N. V. Hud , A. Guzman-Martinez, *Nat. Commun.* **2022**, *13*, 2569.

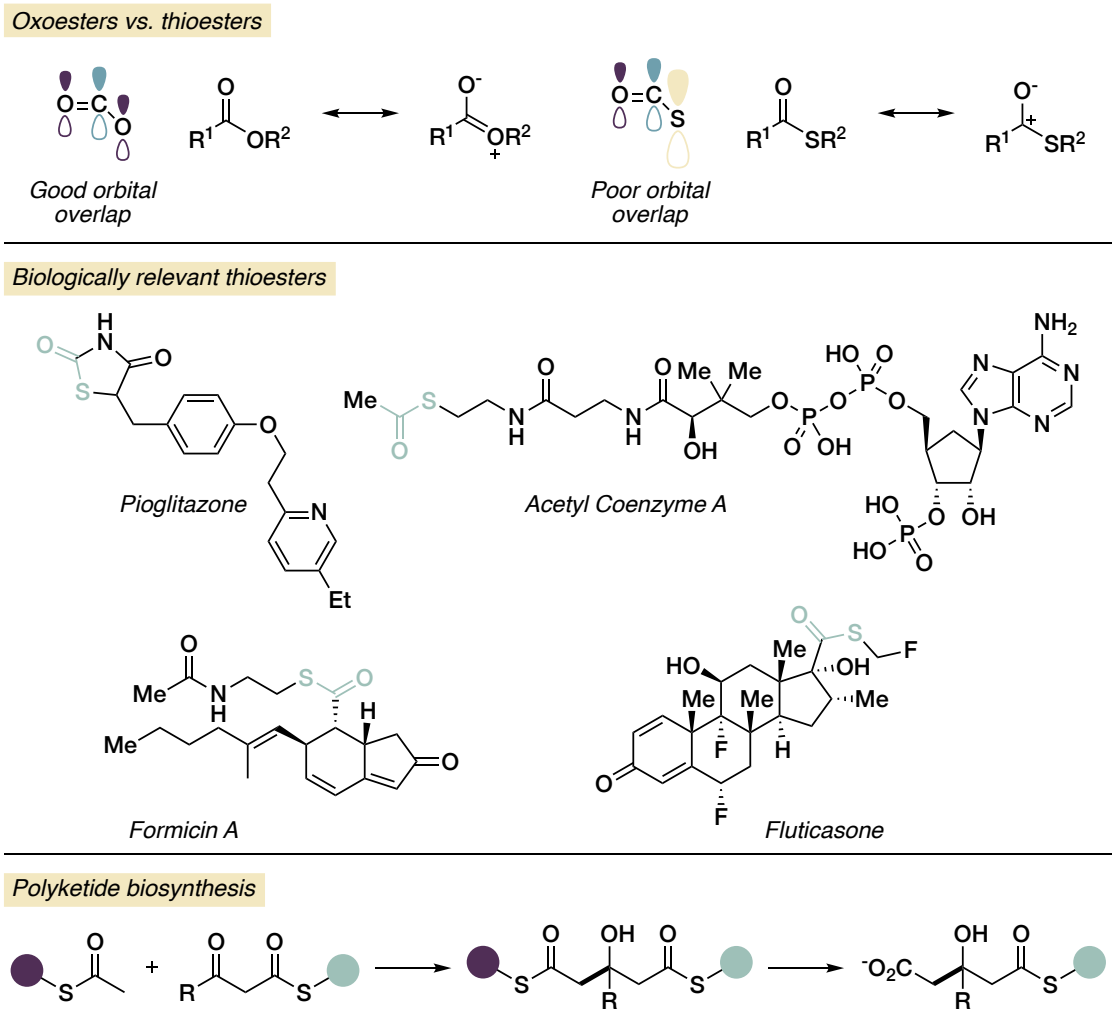

Figure 2. Top: Different electronics of oxoesters and thioesters due to C-S and C-O orbital overlap. Middle: Examples of biologically relevant thioester containing molecules. Bottom: schematic depiction of the biological synthesis of polyketides that exploits thioesters aldol-type chemistry.

The most important synthetic application of the thioester moiety as synthetic handle is in the native chemical ligation method, that reacts a C-terminal peptide fragment derivatized as a thioester with a N-terminal cysteine residue, furnishing another thioester that undergoes acyl transfer to the nitrogen atom to form the amide bond (**Scheme 6**, top). This method featuring high chemoselectivity constitutes the basis of modern chemical protein synthesis allowing access to large peptides otherwise impossible to obtain.[146]

[146] a) P.E Dawson, T. W. Muir, I. Clark-Lewis, S. B. Kent, *Science* **1994**, *266*, 776–779; b) V. Agouridas,O. El Mahdi, V. Diemer, M. Cargoët, J.-C. M. Monbaliu, O. Melnyk, *Chem. Rev.* **2019**, *119*, 7328−7443; c) N. Minh Hien, M. Izumi,

Another notable application is their use as electrophiles in several transition metal catalyzed cross-couplings. The Fukuyama coupling uses a Pd catalyst to couple thioesters and organozinc reagents to access ketones;[147] a related process is the Fukuyama reduction, featuring a silane reductant for highly chemoselective access to aldehydes (**Scheme 6**, middle).[148] The Liebeskind-Srogl coupling is another transition metal catalyzed (originally Pd in combination with stoichiometric Cu was used) protocol that yields ketones from thioesters and a large number of nucleophiles (including boronic acids, stannanes, silanes, organomagnesium and organoindium compounds) (**Scheme 6**, bottom).[149] These classes of reaction have also been developed with Ni and Fe catalysts, including examples of cross electrophile reactivity with halides in the presence of stoichiometric reductants.[150] Organocuprates can react with thioesters in the absence of any catalyst.[151] Decarbonylative methodologies in which thioesters insert their thiol and alkyl(aryl) fragment into unsaturated substrates or act as aryl group synthons have also been engaged.[143a]

H. Sato, R. Okamoto, Y. Kajihara, *Chem. Eur. J.* **2017**, *23*, 6579–6585; d) J.-S. Zheng, S. Tang, Y.-C. Huang, L. Liu, *Acc. Chem. Res.* **2013**, *46*, 2475–2484; e) N. A. McGrath, R. T. Raines, *Acc. Chem. Res.* **2011**, *44*, 752–761.

[147] a) H. Tokuyama, S. Yokoshima, T. Yamashita, T. Fukuyama, *Tetrahedron Lett.* **1998**, *39*, 3189–3192; b) K. Kunchithapatham, C. C. Eichman, J. P. Stambuli, *Chem. Commun.* **2011**, *47*, 12679–12681; c) R. Oost, A. Misale, N. Maulide, Angew. Chem. Int. Ed. 2016, 55, 4587–4590.

[148] a) T. Fukuyama, S.C. Lin, L. Li, *J. Am. Chem. Soc.* **1990**, *112*, 7050–7051; b) H. Tokuyama, S. Yokoshima, S.-C. Lin, L. Li, T. Fukuyama, *Synthesis* **2002**, *2002*, 1121–1123.

[149] a) L. S. Liebeskind, J. Srogl, *J. Am. Chem. Soc.* **2000**, *122*, 11260–11261; b) Y. Yu, L. S. Liebeskind, *J. Org. Chem.* **2004**, *69*, 3554–3557; c) R. Wittenberg, J. Srogl, M. Egi, L. S. Liebeskind, *Org. Lett.* **2003**, *5*, 3033–3035; d) B. W. Fausett, L. S. Liebeskind, *J. Org. Chem.* **2005**, *70*, 4851–4853; e) H. Prokopcová, C. O. Kappe, *Angew. Chem. Int. Ed.* **2009**, *48*, 2276–2286.

[150] a) T. Shimizu, M. Seki, *Tetrahedron Lett.* **2002**, *43*, 1039–1042; b) M. Onaka, Y. Matsuoka, T. Mukaiyama, *Chem. Lett.* **1981**, *10*, 531–534.; c) A. C. Wotal, D. J. Weix, *Org. Lett.* **2012**, *14*, 1476–1479; c) C. Cardellicchio, V. Fiandanese, G. Marchese, L. Ronzini, *Tetrahedron Lett.* **1985**, *26*, 3595–3598; d) W. Oppolzer, C. Darcel, P. Rochet, S. Rosset, J. De Brabander, *Helv. Chim. Acta* **1997**, *80*, 1319–1337.

[151] a) R. J. Anderson, C. A. Henrick, L. D. Rosenblum, *J. Am. Chem. Soc.* **1974**, *96*, 3654–3655; b) N. Yoshikai, R. Iida, E. Nakamura, *Adv. Synth. Catal.* **2008**, *350*, 1063–1072.

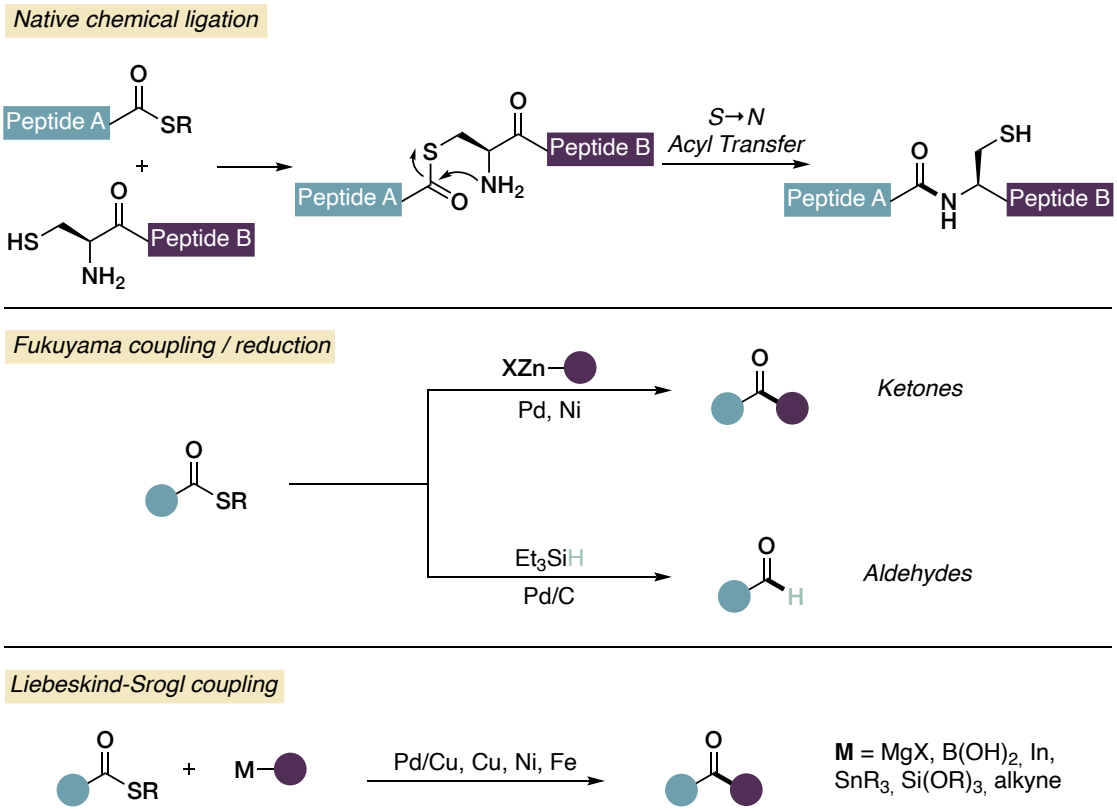

Scheme 6. Top: Native chemical ligation mechanism. Middle: Schematic representation of the Fukuyama coupling and Fukuyama reduction. Bottom: schematic depiction of the Liebeskind-Srogl coupling for thioesters. Thioamides, (hetero)aryl thioethers, thioalkynes, and thiocyanates (not shown) are also competent electrophiles for this type of coupling.

The synthesis of such compounds has been achieved via several strategies. These include: thioesterification of carboxylic acids with coupling reagents or additives, as well a use of acid chlorides, anhydrides, amides and ester as acyl electrophiles; oxidative thioesterification of aldehydes; transition metal catalyzed allylic substitution with thioacids; transition metal catalyzed thiocarbonylation reactions of alkenes, alkynes and iodoarenes with CO and thiols; transition metal catalyzed coupling of thioacids and aryl halides (**Scheme 7**).[143] It is important to note that the identification of an efficient system for TMs catalyzed C-S cross-coupling reactions can present several complications, due to the strong metal-sulfur interactions that can lead to catalyst poisoning,[152] and possible occurrence of unproductive radical pathways.[153]

[152] M. R. DuBois, *Chem. Rev.* **1989**, *89*, 1–9.
[153] F. Dénès, M. Pichowicz, G. Povie, P. Renaud, *Chem. Rev.* **2014**, 114, 2587–2693.

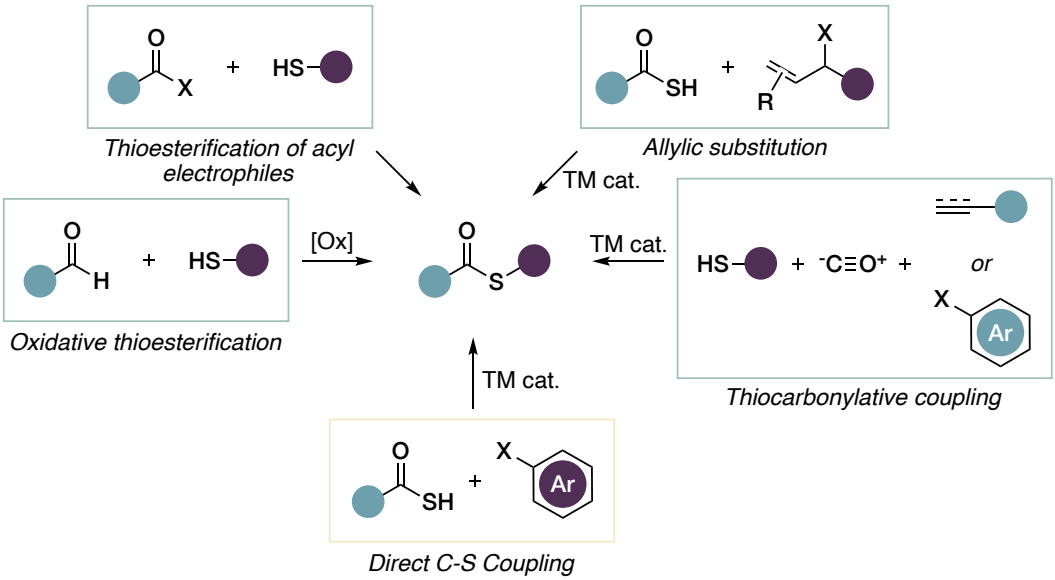

Scheme 7. Prevalent synthetic methodologies for the systhesis of thioesters.

The direct coupling of thioacids and aryl (pseudo)halides constitutes a powerful strategy for expedient access to *S*-aryl thioesters, and a limited number of strategies based on Pd and Cu have been reported.[154] In this context, the utilization of thiocarboxylic acid salts can provide practical advantages, these compounds being easily handled solids with reduced odor with respect to their free acid counterparts, and not requiring any added base. Strategies for this transformation appear underdeveloped, with only three protocols described.

In an early report, Filiberti and coworkers reported the uncatalyzed reaction of tetrafluoroborate aryldiazonium salts with potassium thioacetate (**Scheme 6**, top). The reaction likely involves competitive radical pathways, providing the products in only moderate yields along with symmetrical sulfides and disulfides byproducts (**Scheme 8**, bottom).[155]

[154] a) A. Osuka, N. Ohmasa, Y. Uno, H. Suzuki, *Synthesis* **1983**, *1983*, 68–69; b) D. K. H. Ho, L. Chan, A. Hooper, P. E. Brennan, *Tetrahedron Lett.* **2011**, 52, 820–823; c) B. Li, Z. Chao, C. Li, Z. Gu, *J. Am. Chem. Soc.* **2018**, *140*, 9400–9403; d) N. Sawada, T. Itoh, N. Yasuda, *Tetrahedron Lett.* **2006**, *47*, 6595–6597; e) C. Lai, B. J. Backes, *Tetrahedron Lett.* **2007**, *48*, 3033–3037.

[155] G. Petrillo, M. Novi, G. Garbarino, M. Filiberti, *Tetrahedron Lett.* **1988**, *29*, 4185–4188.

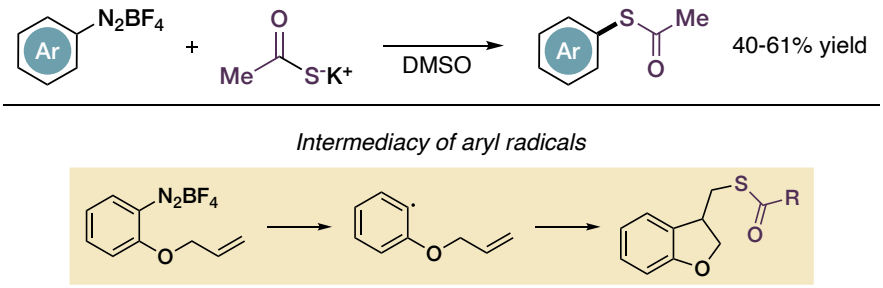

Scheme 8. Top: Direct reaction between potassium thioacetate and aryl diazonium tetrafluoroborates. Bottom: experimental evidence for the involvement of aryl radicals.

In 2013, Peñéñory reported a Cu catalyzed cross-coupling between (hetero)aryl iodides and potassium thioacetate[156] employing a reaction system similar to the one developed by Sawada[154d], featuring CuI as catalyst and 1,10-phenantroline as the ligand in toluene (**Scheme 9**).

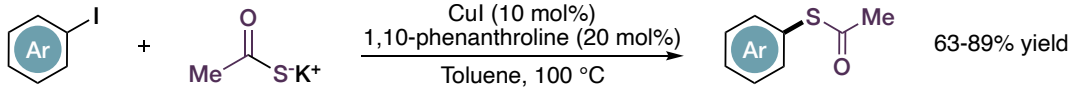

Scheme 9. Copper catalyzed coupling or aryl iodides and potassium thioacetate. Aryl bromides are unreactive.

The reaction requires a slight excess of potassium thioacetate and delivers *S*-aryl thioacetates bearing EWG- and EDG-substituted as well as *ortho*-substituted aryl moieties in high yields. Aryl bromides demonstrated inert in this protocol.

Another report of this transformation *en route* to unsymmetrical aryl sulfides came in 2011 from Lee and coworkers.[157] The combination of $Pd(dba)_2$ and dppf as ligand (dba = dibenzylideneacetone, dppf = 1,1′-Bis(diphenylphosphino)ferrocene) in presence of base afforded *S*-(4-methoxy)phenyl thioacetate from 4-iodoanisole in almost quantitative yield, and only five aryl iodides were engaged in a one-pot protocol for the formation of aryl sulfides from a combination of aryl iodides, bromides and potassium thioacetate (**Scheme 10**).

[156] S. M. Soria-Castro, A. B. Peñéñory, *Beilstein J. Org. Chem.* **2013**, 9, 467–475.
[157] N. Park, K. Park, M. Jang, S. Lee, *J. Org. Chem.* **2011**, *76*, 4371–4378.

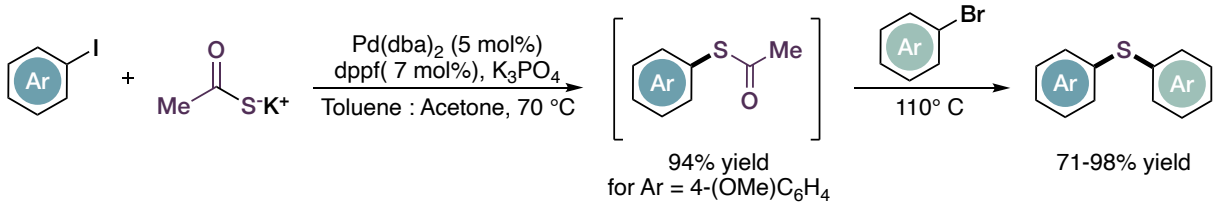

Scheme 10. Lee's palladium catalyzed one-pot protocol for the synthesis of unsymmetrical thioethers from aryl iodides and bromides, via initial formation of a *S*-aryl thioacetate by coupling of potassium thioacetate and aryl iodide.

4.2 Aim of the project

The relevance of *S*-aryl thioesters, together with the fairly limited number of strategies reported for the coupling of thioacids or thiocarboxylate salts with aryl halides spurred our interest towards the development of new catalytic systems for their obtainment. We noted the striking absence of any report involving Ni catalysis in such kind of reactions, reasoning that catalyst poisoning issues in the utilization of thiocarboxylate salts (both preformed or obtained *in situ* in the presence of exogenous base) in a homogenous Ni catalysis setting could be the reason. The promising literature reports regarding the use of NiNPs for cross-coupling reactions, and their highly desirable employment as heterogeneous, sustainable catalysts prompted us to try to develop a NiNPs catalyzed system for the realization of this transformation (**Scheme 11**).
Given our interest in carbon materials chemistry, we decided to focus our attention on the use of NiNPs@rGO nanocomposites as catalysts, and selected aryl iodides and potassium thioacetate as convenient, commercially available precursors.

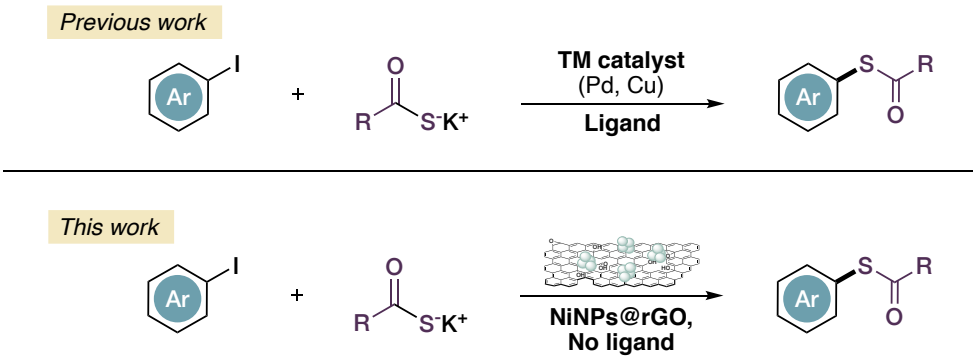

Scheme 11. Top: underdeveloped transition metal-catalyzed access to *S*-aryl thioesters from aryl halides and thiocarboxylate potassium salts; Bottom: schematic representation of the pursued supported NiNPs-catalyzed strategy.

The realization of this endeavor presents several challenges, from the obvious possible catalyst deactivation in the presence of thioacetate salts, to the possible formation of several byproducts such as symmetrical sulfides or disulfides by parallel reaction

pathways, and the careful tuning of reaction conditions to avoid acyl deprotection in the product, that has been observed in such protocols under basic conditions.[156]

4.3 Results and discussion

At the outset of the study, two different synthetic approaches for the realization of rGO deposited NiNPs were attempted with the aim of investigating the role of the NPs size/composition on their catalytic performance. In particular, two different batches of NiNPs@rGO nanocomposites (**NiNPs@rGO Type 1** and **NiNPs@rGO Type 2**) were prepared by employing commercially available GO and $NiCl_2 \cdot 6H_2O$, that upon suspension in deionized water and ethylene glycol as stabilizing agent, were simultaneously reduced in the presence of hydrazine hydrate[158] or $NaBH_4$ (**Scheme 12**).[159]

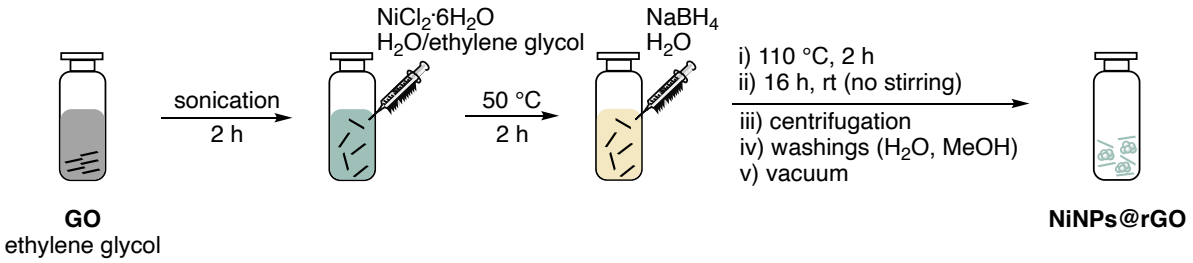

Scheme 12. Schematic representation of the synthetic sequence for the preparation of NiNPs@rGO Type 2 (see SI for details)

The two materials were extensively characterized by means of ICP-OES, P-XRD, HR-TEM, FE-SEM (Field Emission-Scanning Electron Microscopy) and XPS analyses.
ICP-OES analysis revealed a significantly different metal loading for Type 1 and Type 2 metal composites. In particular, while the protocol employing hydrazine as reducing agent delivered a NiNPs@rGO nanocomposite featuring a 69 wt% Ni loading, the use of $NaBH_4$ resulted in a much lower metal content for Type 2 (18 wt%).
Size, morphology, surface area and material polydispersity are crucial parameters that commonly concur to define the overall catalytic properties of NiNPs. **NiNP@rGO NP Type 1** and **Type 2** were subjected to P-XRD investigation to get details on structural differences. The scans are presented in **Figure 3**. Pattern of **NiNP@rGO Type 1**

[158] Z. Ji, X. Shen, G. Zhu, H. Zhou, Z. Yuan, J. *Mater. Chem.* **2012**, *22*, 3471.
[159] X. Zhang, K.-H. Chen, Z.-H. Zhou, L.-H. He, *ChemCatChem* **2020**, *12*, 4825.

features three sharp peaks owing to the cubic phase of crystalline nickel and an asymmetric broad band with maximum at 23.9° (interlayer distance d = 0.372 nm), probably due to the overlap of several peaks deriving from GO portions reduced at different stages. Indeed, the peak of pristine GO appears at 10.5° (d = 0.839 nm) and progressive reduction will shift it towards the position of the main graphite peak at 26.5° (d = 0.335 nm). Scan of **NiNP@rGO Type 2** shows several broad peaks: the major one at 44.5° due to the overlap of (1,1,1) and (2,0,0) reflections of the cubic nickel phase, and the other one at 24.9° (d = 0.357 nm), diagnostic of rGO.

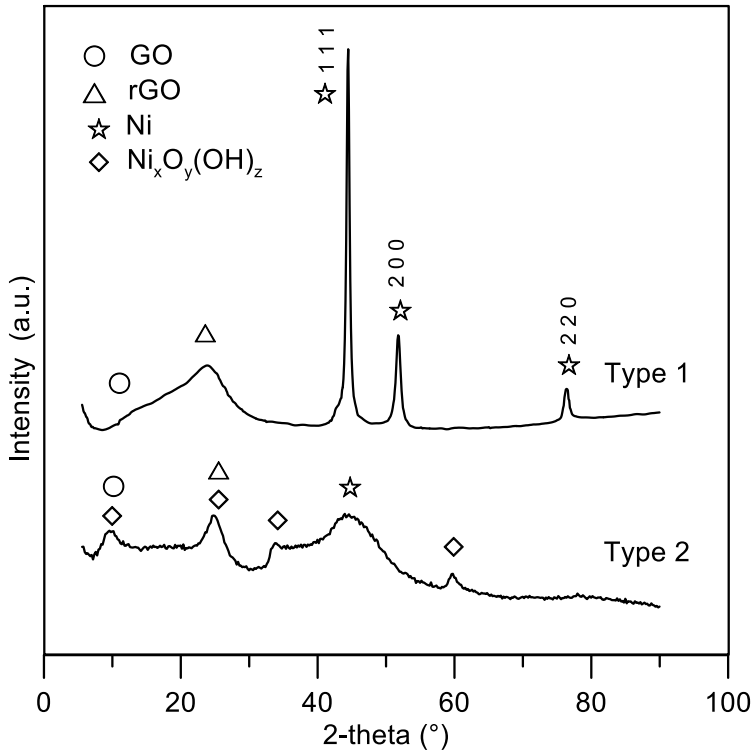

Figure 3. XRD patterns of NiNP@rGO Type 1 and NiNP@rGO Type 2; Miller indexes for cubic nickel phase are reported.

Nickel particles are quite different in size in the two samples. An inverse relationship exists between peak width and size of crystallite domains (crystal size, C.S.), and Type 1 sample presents C.S. of nickel domains equal to 21 ± 2 nm, while they reduce to about 1.2 ± 0.3 nm in Type 2 sample. The peak, or more properly in this case, the band

of reduced GO is narrower, more symmetric and closer to graphite position in Type 2 sample. A small amount of Ni(II) species seems to be also present.

Electron microscopy techniques also highlighted several differences with regard to morphology and composition. **Figure 4a** and **4d** display the FE-SEM micrographs of **NiNP@rGO Types 1** and **2**, showing a deep structural change induced by the different synthetic approach. **NiNP@rGO Type 1** composite is characterized by large spherical nanoparticles with an average size equal to 96 ± 36 nm, whose morphology is often embedded in a material fully covering their surface. On the other hand, **NiNP@rGO Type 2** composite displays much smaller nanoparticles (d = 9 ± 3 nm) decorating a clean substrate. Low magnification HR-TEM micrographs of the same samples also highlight the size difference between nanoparticles, as well as the nanostructured nature of the supporting substrate, displaying the typical wrinkles and folded edges of rGO (**Figure 4b** and **4e**).

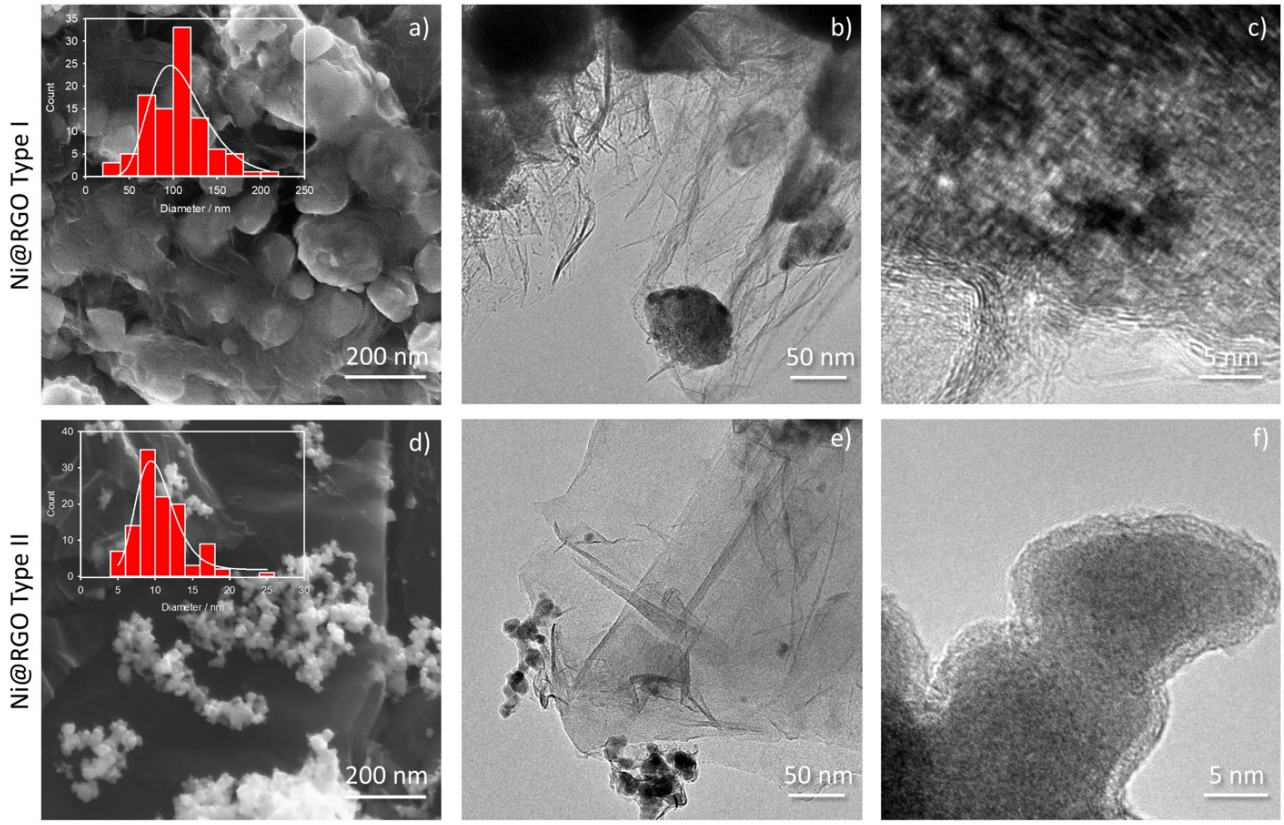

Figure 4. a) FE-SEM, b) Low magnification, and c) High magnification HR-TEM micrographs of **NiNP@rGO Type 1**. In the inset, the size distribution histogram measured from FE-SEM micrograph and fitted with Log-Normal function. Figures d, e, and f display **NiNP@rGO Type 2** counterparts.

Focusing on the rGO substrate (Figure S1), the material displays the typical features of a crystalline graphene-like structure. However, as often observed for rGO and exfoliated graphene,[160] the number of layers is quite inhomogeneous, ranging between 1 and 20, due to the re-stacking of rGO flakes during the reduction process, as also observed in P-XRD where a broad reflection band was detected. **NiNP@rGO Type 1** exhibits crystalline features (**Figure 4c**), with a d-spacing compatible to metallic Ni. In addition, diffraction fringes were observed on the edge of the nanoparticle, with a d-spacing close to 3.4 Å, matching the one of graphite (0,0,2) lattice planes. This suggests that a layer of rGO is fully wrapping the Ni nanoparticles in a tight-close structure. In contrast, **NiNP@rGO Type 2** did not display any crystal structure, probably due to the milder reduction technique employed. The nanoparticles are not wrapped in the rGO matrix, allowing higher accessibility of their surface in the catalytic reaction. However, a thin (< 2 nm) amorphous layer with lower contrast covering the nanoparticles can be noticed on the HR-TEM micrograph (**Figure 4f**). The nature of this shell is hardly understood by HR-TEM due to the lack of crystalline features. However, EDS analysis displays a slight enhancement of the O/Ni ratio on the edge of the nanoparticle (**Figure 5**, bottom), suggesting that a thin, partially oxidized layer is covering the nanoparticles. In contrast, a slight increase in C-related signal is observed on the edge of a single NP in Type 1 sample (**Figure 5**, top). No observed increment of O-related signal confirms the presence of the rGO coating. **NiNP@rGO Type 2** is also characterized by some isolated macro-aggregates of amorphous material exhibiting high nickel and boron content (Supplementary data, Chapter 4.5, Figure S2), resulting from the borohydride oxidation in the reduction process.

[160] R. Mazzaro, A. Boni, G. Valenti, M. Marcaccio, F. Paolucci, L. Ortolani, V. Morandi, P. Ceroni, G. Bergamini, *ChemistryOpen* **2015**, *4*, 268.

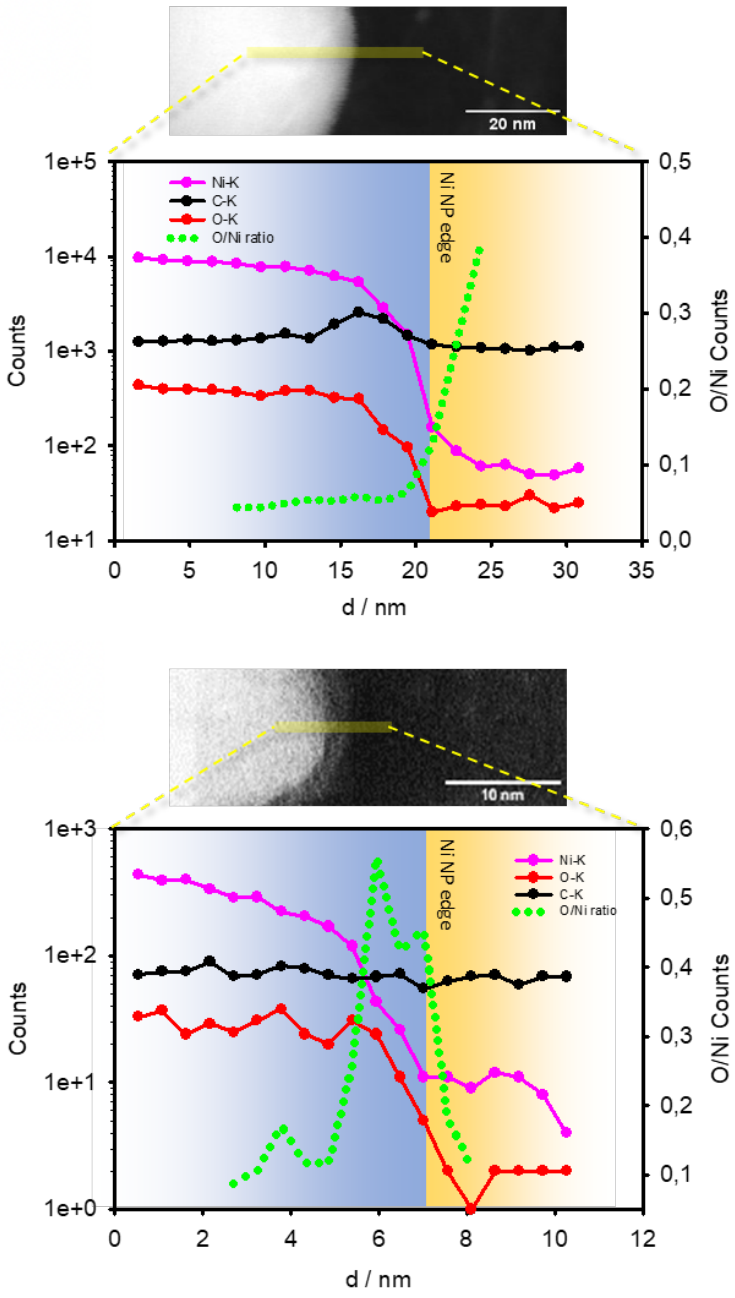

Figure 5. Ni, O, and C K-α signals integrated from EDS spectra, extracted from the highlighted profile on the STEM-HAADF (Scanning Transmission Electron Microscopy- High-Angle Annular Dark-Field imaging) micrographs for Type 1 (top) and Type 2 (bottom) NiNP@rGO composites. The O/Ni signal ratio is also reported (green dotted line). The area relative to the NiNP@rGO is highlighted in light blue, while the supporting rGO area is highlighted in light yellow.

XPS analysis was performed in order to understand the oxidation degree of both Ni nanoparticles and rGO support. Survey spectra of pristine GO and **NiNP@rGO Type**

2 are reported in **Figure 6**, while **NiNP@rGO Type 1** is reported in the Supplementary Data (Chapter 4.5, Figure S3). In particular, the oxidation degree observed for nickel displays significant variations.

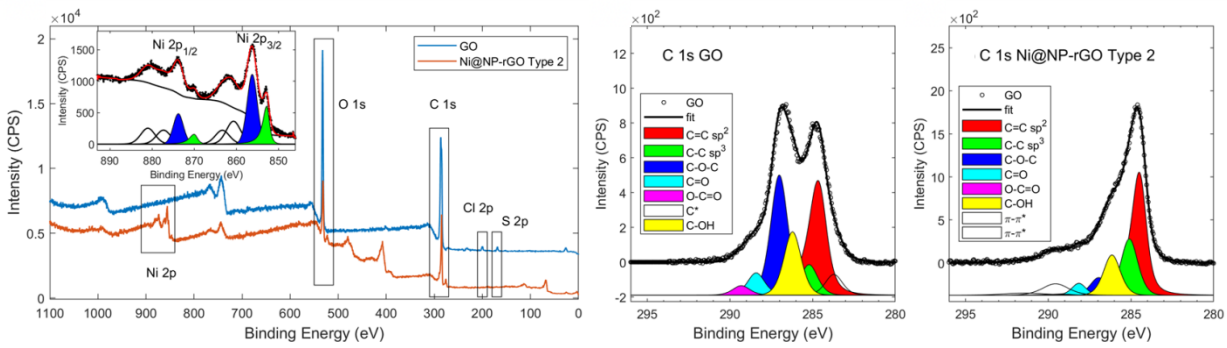

Figure 6. Left: XPS survey spectra of GO and NiNP@rGO Type 2, inset Ni 2p signal fitted with two doublets after Shirley background subtraction: blue for Ni(II) and green for Ni(0), other high energy peaks are shake-up transition; Middle: C 1s signal of pristine GO; Right: NiNP@rGO Type 2.

From the fit of the Ni 2p signal, two chemical states can be discriminated: Ni(II), usually associated with Ni oxides or hydroxides, and metallic Ni(0).[161] The surface amount of Ni in **NiNP@rGO Type 1** was relatively low (**Table 1**) and only Ni(II) was detected. By contrast, both Ni(II) and Ni(0) species were found in higher quantities on the **NiNP@rGO Type 2** surface.

Table 1. Relative amounts of Ni (in metallic and oxidized form) and O/C ratio at the surface of rGO support.[a]

Sample	Ni(II) (%)[b]	Ni(0) (%)[b]	O/C[c]
GO	/	/	0.41 ± 0.01
NiNP@rGO Type 1	0.23 ± 0.05	/	0.13 ± 0.01
NiNP@rGO Type 2	4.7 ± 0.4	2.0 ± 0.3	0.23 ± 0.01

[a] Estimated by XPS data. [b] Atomic concentration, values obtained from Ni 2p fit: Ni(II) 2p3/2 856.3 eV, Ni(0) 2p3/2 852.8 eV. [c] Oxygen to carbon ratio was obtained from the fit of C 1s signal as described in ref. 142.

[161] K. S. Kim, N. Winograd, *Surf. Sci.* **1974**, *43*, 625.

The low amount of Ni present in **NiNP@rGO Type 1** must not mislead: XPS is extremely surface sensitive (few nm) and when the Ni nanoparticles are wrapped in rGO, as assessed in this case by TEM imaging (**Figure 4c**), the XPS signal from Ni is significantly attenuated. Metallic phase was observed exclusively on Type 2 in accordance with previous XPS results by Zhang,[162] where Ni clusters with core-shell structure were observed: the external surface of the NP is composed of NiO and the inner core by metallic Ni. These results match the microscopy analysis. The chemical state of GO after reduction can be estimated by the deconvolution of the C 1s signal. While the signal of oxygen (O 1s) presents overlapping contributions from O atoms on rGO and O atoms on Ni oxides, by using the fit of C 1s it is possible to isolate exclusively the C–O contribution. GO is remarkably reduced in both cases, as showed in **Table 1**. Nevertheless, the two GO materials present some differences: the rGO obtained in Type 2 procedure has a higher oxidation degree compared to Type 1, in agreement with the higher reduction efficiency of hydrazine hydrate with respect to $NaBH_4$. Summarizing, we observed a significant reduction of Ni and GO in Type 2 as well, that was composed mainly by metallic Ni core and oxidized Ni shell nanoparticles supported on the aromatic domains of rGO.

After having obtained structural information on the materials, we decided to test them in a model reaction comprising 4-iodoanisole (**1a**) and potassium thioacetate (**2a**). Interestingly, **NiNP@rGO Type 1** promoted the coupling (**Table 2**, entry 1) in 60% overall conversion (30% yield of **3aa**) and poor chemoselectivity. Indeed, the desired thioacetate **3aa** and the aryl sulfide **3aa′** were obtained in a 2:1 ratio. Differently, the **NiNP@rGO Type 2** displayed better performance, delivering the desired aryl thioacetate **3aa** in 60% yield and with much better chemoselectivity profile (**3aa**/**3aa′** > 25:1, entry 2).

[162] Z. Zhang, Z. Matsubayashi, A. Grisafe, B. Lee, J. R. Lloyd, *Mater. Chem. Phys.* **2016**, *170*, 175.

Table 2. Summary optimization of reaction conditions.

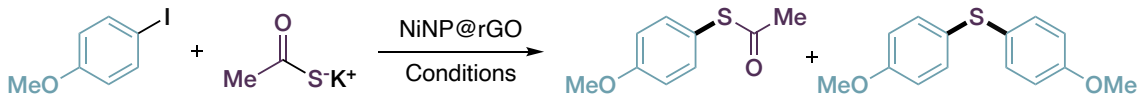

1a **2a** **3aa** **3aa'**

Entry[a]	NiNP@rGO	Conditions	**3aa** Yield (%)[b]	**3aa**:**3aa'**[c]
1	Type 1	Xylenes, 150 °C	30[d]	2:1
2	Type 2	Xylenes, 150 °C	60	> 25:1
3	Type 2	Toluene, 100 °C	trace	/
4	Type 2	DMF, 100 °C	trace	/
5	Type 2	Mesitylene, 150 °C	50	7:1
6	Type 2	PhCl, 150 °C	42	7.3:1
7[e]	Type 2	Xylenes, 150 °C	70	> 25:1
8[f]	Type 2	Xylenes, 150 °C	72	> 25:1
9[g]	Type 2	Xylenes, 150 °C	59	> 25:1
10	/	rGO, Xylenes, 150 °C	0[i]	/
11[h]	/	$(PPh_3)_2NiCl_2$, Zn, Xylenes, 150 °C	0[i]	/

[a] All reactions were set up under N_2 atmosphere using degassed solvents (N_2 bubbling for 2 minutes), for 16 h. **1a** : **2a** = 1:6, [**1a**] = 0.2 M, 8 mg NiNP@rGO (ca. 25 mol%), unless otherwise noted. [b] Determined after flash chromatography. [c] Determined by ^{1}H NMR. [d] NMR yield. [e] **1a** : **2a** = 1:8, 6.5 h. [f] **1a** : **2a** = 1:8, [**1a**] = 0.1M. [g] **1a** : **2a** = 1:8, [**1a**] = 0.05M. [g] 10 mol% Zn, 10 mol% $(PPh_3)_2NiCl_2$. [i] No reaction.

These preliminary outcomes clearly highlight that, the smaller the metal particle size and distribution average, the higher the catalytic performance. This aspect is frequently encountered in nanomaterials-catalyzed organic transformations.[163] Increasing the temperature to 150 °C with xylenes mixture (reagent grade, undried) as reaction medium provided superior results with respect to other reaction conditions screened (i.e. solvents as well as temperatures, entries 3–6), and a slight improvement in the isolated yield (72%) was recorded by increasing the **1a**/**2a** ratio up to 1:8 (**3aa**/**3aa'** >25:1) and lowering the concentration to 0.1 M. An overall Ni loading of 25 mol% (8

[163] H. O. Nasrallah, Y. Min, E. Lerayer, T.-A. Nguyen, D. Poinsot, J. Roger, S. Brandés, O. Heintz, P. Roblin, F. Jolibois, R. Poteau, Y. Coppel, M. L. Kahn, I. C. Gerber, M. R. Axet, P. Serp, J.-C. Hierso, *JACS Au* **2021**, *1*, 187.

mg **NiNPs@rGO Type 2**) demonstrated optimal. Interestingly, an attempt to carry out the titled cross-coupling under homogeneous regime ($(PPh_3)_2NiCl_2$/Zn 10 mol%)[164] failed (entry 11) emphasizing the role of the carbon-based support in modulating the activity of the dispersed NiNPs. A control reaction carried out with rGO proved the genuine metal catalysis of the present C–S bond forming protocol (entry 12). Then, based on the optimal reaction conditions, the generality of the methodology in terms of functional group tolerance was ascertained by subjecting a range of diversely substituted aryl/vinyl-iodides **1b–n** with potassium thioacetate (**2a**) and potassium thiobenzoate (**2b**) and the resulting outcomes are shown in **Figure 7**.

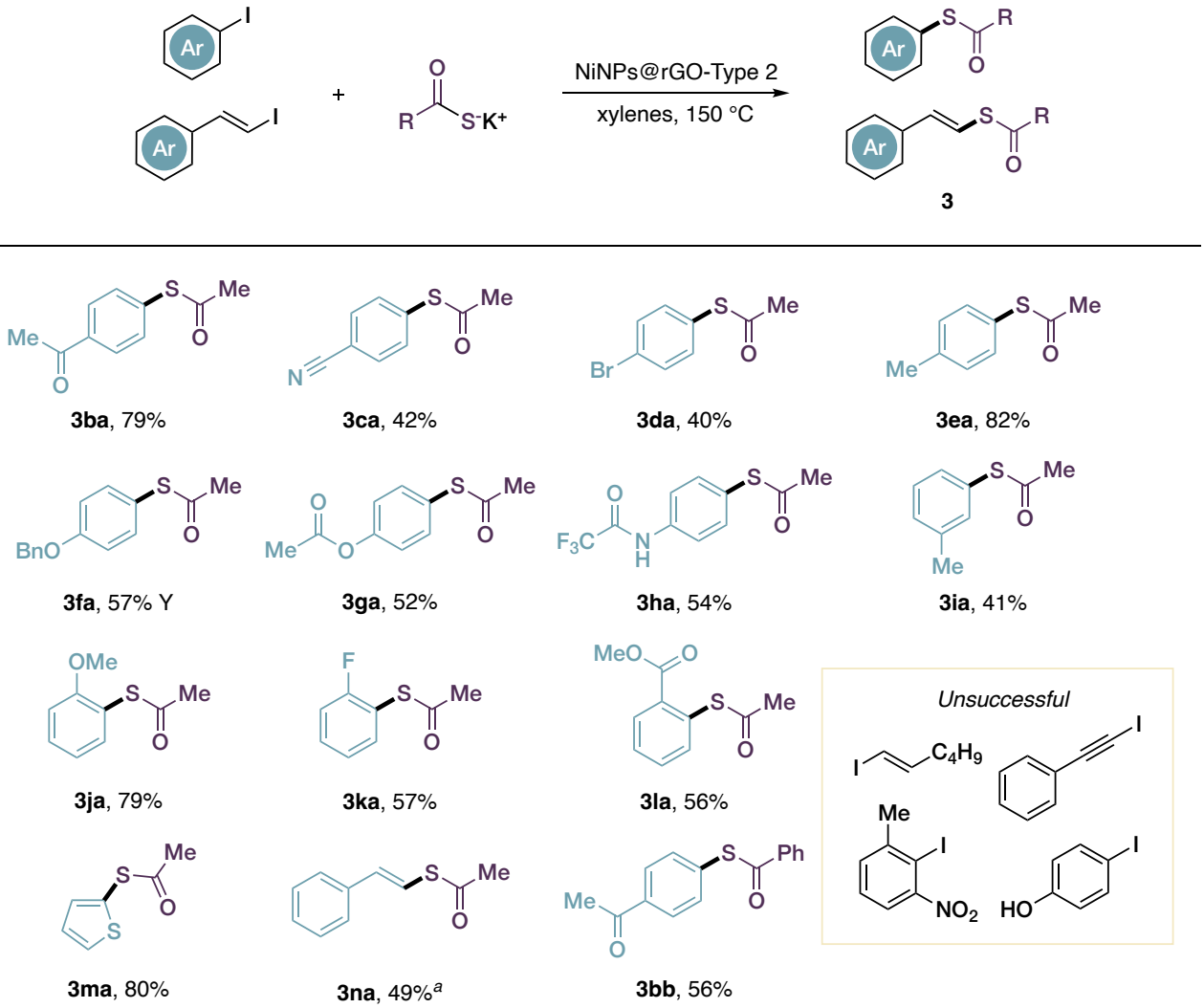

[164] J. B. Sweeney, A. K. Ball, L. J. Smith, *Chem. Eur. J.* **2018**, *24*, 7354.

Figure 7. Scope of the present methodology. All reactions were set up under optimized conditions determined for substrate **1a** (entry 8 in **Table 2**), under N_2 atmosphere using degassed reagent grade xylenes (isomers mixture). All yields are given after flash chromatography. [a]The *E* isomer was obtained exclusively from the *E* styryl iodide.

The protocol demonstrated quite insensitive to electronic perturbation of the aryl ring. Ketone and nitrile functionalities were well tolerated, with substrates **1b,c** delivering the respective thiocarboxylation products **3b,c** in good yields. The striking tolerance towards a bromine substituent (**3d**) highlighted the selectivity of the protocol towards aryl iodides, allowing the possibility of further transition-metal-based functionalization to be carried out sequentially. Interestingly, protected iodophenols or iodoanilines **1g** and **1h**, bearing base- and nucleophile-sensitive moieties such as phenolic acetate and trifluoroacetamide, worked smoothly in the protocol (52 and 54% yield, respectively), demonstrating the mildness of this protocol despite the high temperature employed.
Importantly, *ortho*-substitution of the aromatic ring (**1j–l**) did not hamper the reactivity, showing a general high tolerance towards steric hindrance (yield up to 79%). Moreover, the synthetic versatility of the protocol was not limited to substituted benzene rings, as was assessed by the successful coupling of a heteroaryl iodide, 2-iodothiophene (**1m**), as well as a vinyl iodide **1n** in synthetically good yields and stereoselective manner. Finally, an alternative potassium thioacid salt, potassium thiobenzoate (**2b**), also proved competent in the model reaction (**3bb**) furnishing preliminary evidence of the generality of the methodology. An interesting counterion dependence was observed, with sodium and cesium thioacetates proving completely unsuccessful. Free phenols and nitro group unfortunately proved unsuccessful, as well as alkynyl iodides and aliphatic vinyl ones.
Mechanistically, a tentative pictorial sketch is presented in **Scheme 13**. The Ni(0) nanoparticles could initially undergo oxidative addition on the aryl iodides **1**, providing the corresponding aryl-Ni(II) species **A**. Ligand metathesis with the thiocarboxylate salt **2** would generate the Ni(II)-thiocarboxylate **B** that could evolve into the desired aryl thiocarboxylate **3** via reductive elimination.

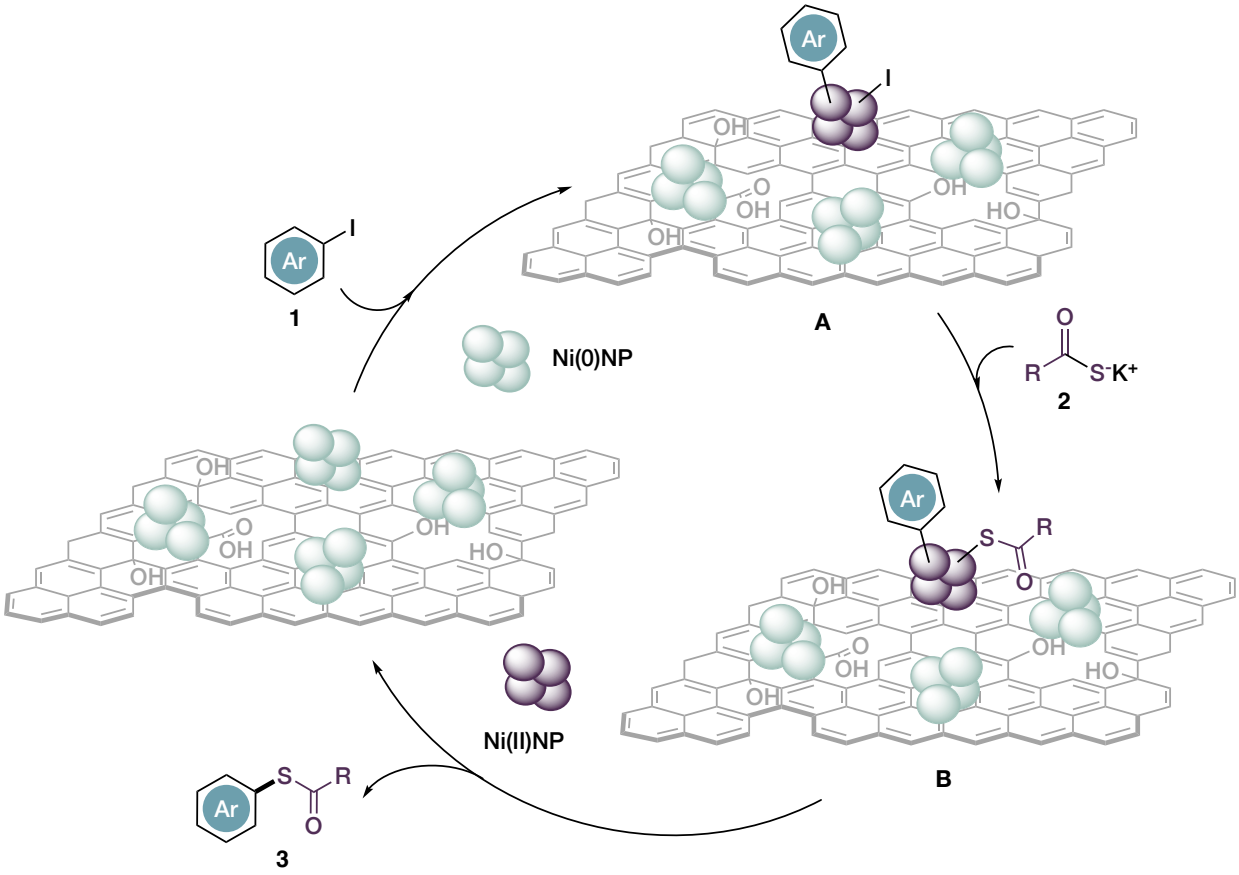

Scheme 13. Sketch of the proposed mechanism.

Although a conclusive answer about possible Ni(0)/Ni(II) or Ni(I)/Ni(III) based mechanisms is still not available, the high temperatures required for the present cross-coupling protocol[239] and the information gained by the XPS analysis, lead us to retain unlikely the involvement of Ni(I) and Ni(III) intermediates. The involvement of radical pathways (formation of aryl radicals) cannot be ruled out at this stage.[155]

In order to get insights regarding the formation of the anticipated byproduct **3′**, a dedicated experimental control was carried out. In particular, when **3aa** was reacted under optimal conditions in the presence of aryl iodide **1a** (i.e. **NiNP@rGO Type 2**, xylene, 150 °C), **3aa′** was formed in 50% yield, proving the competence of aryl thioacetates **3** in providing sulfide **3′**. This could occur via Ni mediated formation of thiophenols (i.e. deacetylation of **3**), followed by C-S cross-coupling with the aryl iodide, although in this aspect as well we cannot completely exclude involvement of

radical pathways arising from SET reduction of the thioacetate product **3**, although less likely given the stability observed for the product in the reaction course.

To assess the genuine heterogeneous catalysis and investigate the possible leaching of NPs, substrate **1b** was subjected to the optimized reaction conditions and a hot filtering experiment was performed when 30% conversion was reached. By re-heating the filtered reaction mixture at 150 °C for 15 h, no further conversion was observed. This suggests that no leaching of any catalytically active species from the material occurs during the reaction course. To support this experimental evidence, a model reaction was carried out and after complete consumption of the starting material, P-XRD analysis was carried out on the dried mother liquors upon removal of the insoluble materials (**Figure 8**, top). Interestingly, no evidence of crystalline Ni-containing species was recorded. As for catalyst recycling, unfortunately any attempt to reuse the filtered **NiNP@rGO Type 2** in subsequent reactions led to unsatisfactory results and only moderate conversion was detected by re-adding fresh reagents upon completion of the first coupling. To assess the fate of the material after the reaction, P-XRD analysis of the recovered solid was performed. This revealed a significant morphological modification of the native **NiNP@rGO Type 2** composite and highlighted the presence of Ni-S materials on the rGO support (**Figure 8**, bottom).

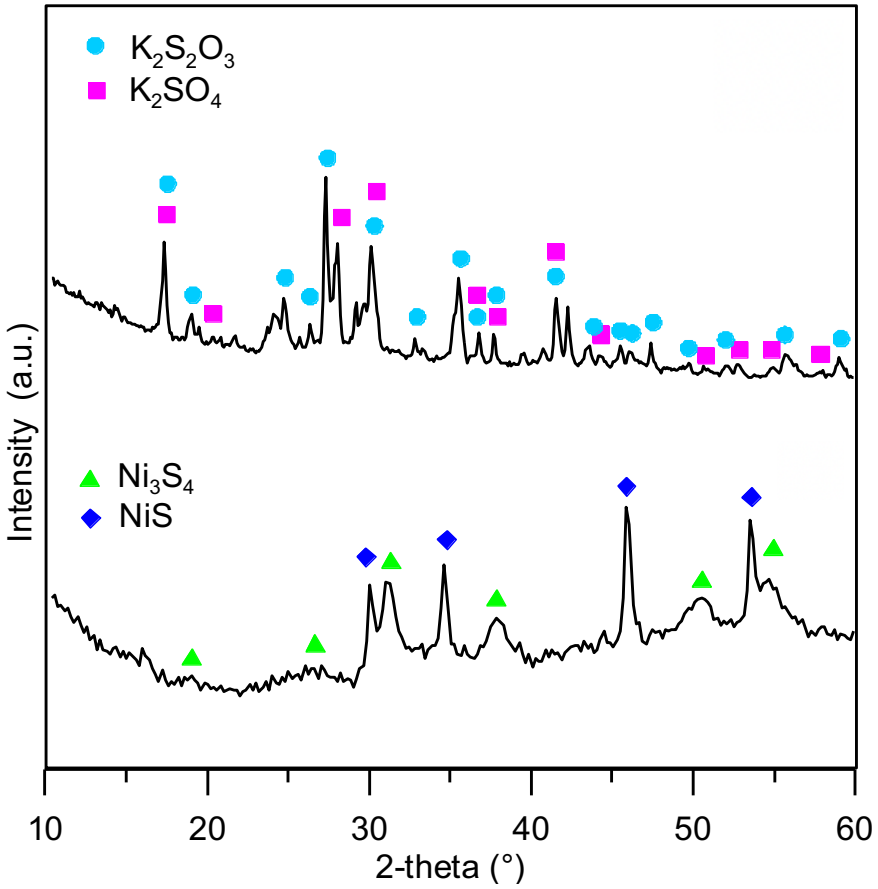

Figure 8. Top: P- XRD analysis of the filtered, dried mixture reaction; Bottom: P- XRD analysis of the recovered NiNP@rGO Type 2 catalyst after reaction. The main peaks are allocated to the reported crystalline phases. Reference files from: $K_2S_2O_3$ ICDD 01-0694, K_2SO_4 ICDD 25-0681, Ni_3S_4 ICSD:60-1828, NiS COD 9009240 (ICDD International Centre for Diffraction).

This evidence is in contrast with a previously reported NiNP@rGO assisted thioarylation of iodoarenes in which reusability up to 6 times was documented.[156] Although a conclusive answer to address this dichotomy is still not available, we could reason that the high amount of thiocarboxylates featuring a softer nature and possible bidentate coordination ability[165] with respect to thiophenols could be responsible for the enhanced poisoning effect on the NiNPs recorded in our protocol.

[165] G. A. Melson, P. T. Greene, R. F. Bryan, *Inorg. Chem.* **1970**, *9*, 1123–1126.

4.4 Conclusions

In conclusion, in this study the preparation and thorough characterization of two types of NiNPs deposited on rGO nanocomposite materials was presented, and a marked dependence of the morphology and chemical nature of the nanostructures on the synthetic methodology was demonstrated. An analogously narrow structure/catalytic activity relationship was observed when the NiNPs were tested in the thiocarboxylative cross-coupling between potassium thiocarboxylates and aryl halides, being this transformation unprecedented under Ni catalysis.

Operationally simple reaction conditions (reagent grade solvent) were identified for the conversion of a wide array of structurally diverse substrates (aryl/vinyl iodides) in good yields, showing no particular constraints with regard to the electronics or sterics of the electrophile. Despite the high temperature, the protocol demonstrated quite mild with a good tolerance towards base sensitive functional groups (including the product itself), and good chemoselectivity was recorded, with minimization of previously observed byproducts.

Although we recognize the somewhat low synthetic relevance of the reported methodology, we consider this study an excellent proof of concept that could hopefully help in expanding the breadth of Ni catalyzed transformations and encourage further investigations in the potentials of NiNPs.

4.5 Supplementary data

General Methods

^{1}H NMR spectra were recorded on Varian 400 (400 MHz) spectrometers. Chemical shifts are reported in ppm from TMS with the solvent resonance as the internal standard (deuterochloroform: 7.26 ppm). Data are reported as follows: chemical shift, multiplicity (s = singlet, d = doublet, dd= doublet doublet, t = triplet, td = triple doublet, dt = double triplet, q = quartet, sext = sextet, sept = septet, p = pseudo, b = broad, m = multiplet), coupling constants (Hz). ^{13}C NMR spectra were recorded on a Varian 400 (100 MHz) spectrometers with complete proton decoupling. Chemical shifts are reported in ppm from TMS with the solvent as the internal standard (deuterochloroform: 77.0 ppm).

GC-MS spectra were taken by EI ionization at 70 eV on a Hewlett-Packard 5971 with GC injection. They are reported as: *m/z* (rel. intense). LC-electrospray ionization mass spectra were obtained with Agilent Technologies MSD1100 single-quadrupole mass spectrometer. Chromatographic purification was done with 240-400 mesh silica gel. Anhydrous solvents were supplied by Sigma Aldrich in Sureseal® bottles and used without any further purification. Commercially available chemicals were purchased from Sigma Aldrich, Fluorochem and TCI and used without any further purification. GO and rGO (partly reduced, 85% atomic C) were purchased from Abalonyx. Agilent Technologies LC/MSD Trap 1100 series (nebulizer: 15.0 PSI, dry Gas: 5.0 L/min, dry Temperature: 325 °C, capillary voltage positive scan: 4000 mA, capillary voltage negative scan: 3500 mA). X-ray diffraction (XRD) patterns were collected in Bragg-Brentano geometry by means of a Malvern Panalytical MRD diffractometer equipped with a copper source (lambda = 0.15418 nm). Each step of 0.1° 2-theta was integrated for 100 s with a multi-channel solid state detector, in the range 5.0° - 90°.

Aryl iodides **1f**,[166a] **1g**,[166b] **1j**[166c] were prepared from the corresponding phenols via known procedures. Aryl iodide **1h**[166d] was prepared from 4-iodoaniline according to a known procedure. Aryl iodide **1l**[166e] was prepared by esterification of the corresponding benzoic acid. Vinyl iodide **1n**[166f] was prepared from cinnamic acid according to a known procedure. All other iodides are commercialy available.

Potassium thiobenzoate **2b** was prepared from benzoyl chloride in two steps: thioacid formation using NaHS[167a] and subsequent salification using KOH in MeOH.[167b]

---

[166] a) M. Uchiyama, T. Furuyama, M. Kobayashi, Y. Matsumoto. K. Tanaka, *J. Am. Chem. Soc.* **2006**, *128*, 8404–8405; b) S. R. Bull, L. C. Palmer, N. J. Fry, M. A. Greenfield, B. W. Messmore, T. J. Meade, S. I. Stupp, *J. Am. Chem. Soc.* **2008**, *130*, 2742–2743; c) K. Lee, H. S. Ban, R. Naik, Y. S. Hong, S. Son, B.-K. Kim, Y. Xia, K. B. Song, H.-S. Lee, M. Won, *Angew. Chem. Int. Ed.* **2013**, *52*, 10286 – 10289; d) A. P. Melissaris, M. H. Litt, *J. Org. Chem.* **1994**, *59*, 5818–5821; e) Y. Soltani, L. C. Wilkins, R. L. Melen, *Angew. Chem. Int. Ed.* **2017**, *56*, 11995–11999; f) R.-S. Xu, L. Yue, Y.-J. Pan, *Tetrahedron* **2012**, *68*, 5046–5052.

[167] a) H. Liu, L. Zhao, Y. Yuan, Z. Xu, K. Chen, S. Qiu, H. Tan, *ACS Catal.* **2016**, *6*, 1732–1736; b) P. Jixian, W. Hui, S. Zhongdong, CN 107840815 A, March 27, 2018. (Add 370 mL of methanol to a 1000 mL four-necked flask. Add 370 mL of ethanol and 51.4 g of thiobenzoic acid. Add 19.0 g of potassium hydroxide. The reaction was vigorously stirred at 50 ° C for 2.5 hours. Concentrate the reaction to a yellow solid. Wash with 200 mL of diethyl ether. 59.4 g of potassium thiobenzoate was filtered, Yield 99%.)

Preparation of NiNP@rGO composites

NiNP@rGO Type 1 was prepared according to a literature procedure.[158]

The composite material was prepared by adapting a reported procedure for the preparation of a silver nanoparticles/rGO composite.[168]

100 mg of GO were added to 60 mL of ethylene glycol in a round bottom flask and the mixture was ultrasonicated for 2h to disperse GO. $NiCl_2 \cdot 6H_2O$ (570 mg) was dissolved in 10 mL H_2O and 30 mL ethylene glycol and the solution thus obtained was added to the GO dispersion in a 250 mL round bottom flask equipped with stirring bar. The mixture was stirred at 50°C for 2h and then transferred to a flame dried 500 mL three-necked round bottom flask equipped with dropping funnel and condenser under nitrogen atmosphere. After degassing the mixture by bubbling nitrogen gas for 3 minutes, a solution of $NaBH_4$ (302 mg) in 80 mL H_2O was slowly added dropwise (hydrogen gas evolution will occur), and the mixture was subsequently heated to 110 °C and stirred for 2h. The mixture was allowed to cool down and was decanted with no stirring overnight to let the obtained composite material deposit.

After decanting, the upper solution was removed by pipette, and the material was washed by centrifugation with water (3 times) and then methanol (2 times), using for each washing roughly 75 mL of fresh solvent. The material was transferred to a glass vial and dried under vacuum to yield **NiNP@rGO Type 2** as a black powder (170 mg).

[168] X. Zhang, K.-H. Chen, Z.-H. Zhou, L.-N. He, *ChemCatChem* **2020**, *12*, 1–7.

SEM/TEM characterization

Nanoscale characterization of the materials was performed by Scanning and Transmission electron microscopy techniques (SEM and TEM). SEM analysis was performed on a Zeiss Leo 1530 FE-SEM operated at 5 kV. TEM analysis was carried out with a FEI Tecnai F20 Shottky-FEG HR-TEM operated at 120kV, equipped with EDAX X-Rays EDS spectrometer and Fischione STEM-HAADF detector. The samples were dispersed in isopropanol and drop casted on Quantifoil Cu R1/2 carbon coated TEM grids.

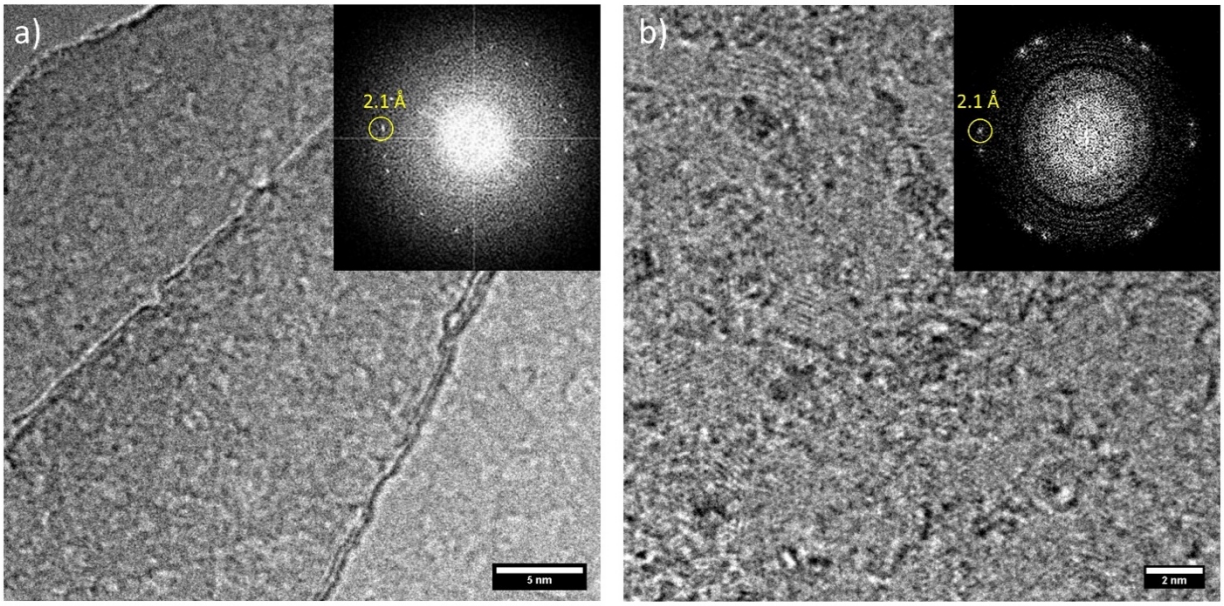

Figure S1. High magnification HR-TEM micrographs of the rGO supporting material in a) **NiNP@rGO Type 1** and b) **NiNP@rGO Type 2**. In the inset, the Fast Fourier Transformate exhibiting 2.1 Å-spaced diffraction fringes, assigned to Graphite (1,1,1) lattice planes.

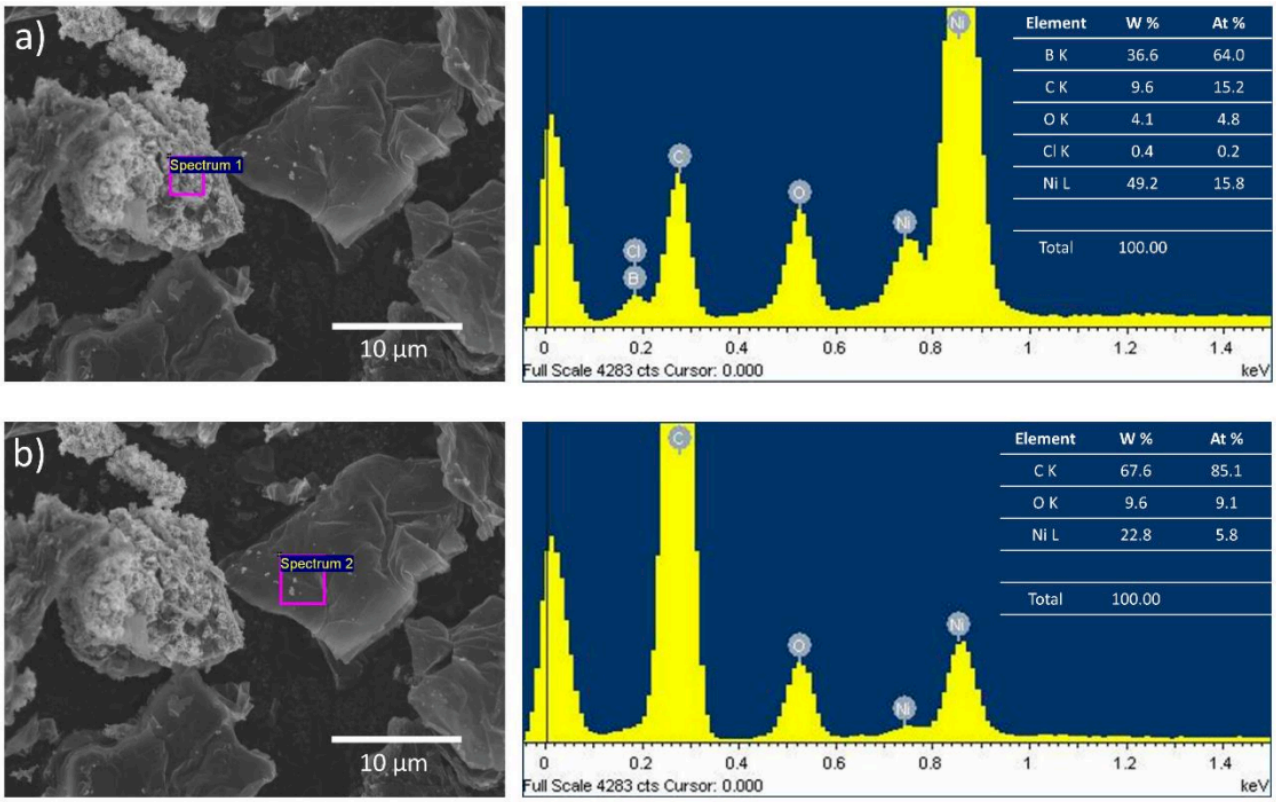

Figure S2. SEM-EDS characterization of different micro-aggregates on sample **NiNP@rGO Type 2**, displaying different composition (table in the inset) rising from the presence of a) Nickel Boride contamination and b) NiNPs decorated rGO flakes.

X-Ray Photoelectron Spectroscopy characterization

XPS spectra were acquired by hemispherical analyser (Phoibos 100, Specs, Germany) by using a Mg Kα excitation. Survey and high resolution spectra were acquired in Fixed Analyser transmission (FAT) mode, with energy resolution 0.9 eV measured on freshly sputtered Silver (Ag 3d). Spectrometer was calibrated to Au $4f_{7/2}$ peak at 84.0 eV. The solid dry powders was deposited on conductive Carbon tape and degassed overnight. Charging effects was corrected by calibrating all spectra to C 1s 284.6 eV. Deconvolutions were performed by using CasaXPS software after Shirley background subtraction. C1 was fitted by using asymmetric line-shape for aromatic Carbon and symmetric line-shapes (pseudo-voigt) for the C-O defects.[169a] The O/C ratio was obtained from C 1s fit according the stoichiometric ratios of C-O groups. Ni 2p was fitted by using asymmetric line-shape (LA(1.1,2.2,10) line-shape in CasaXPS) for metallic Ni(0) and pseudo voigt for Ni(II) and shake-up transitions.[169b] The reference for binding energy for Ni was taken from ref. 169c.

After the chemical reduction the typical contaminants of GO, as S and Cl were removed. The amount of Nitrogen (N 1s) increases in Type 1, due to the hydrazine residuals.

Table S1. Chemical composition (atomic %) of the surface obtained by XPS survey of GO, **NiNP@rGO Type 1** and **NiNP@rGO Type 2**. Binding energy (eV) was reported for each transition. Errors are typically: ±0.8% for values higher that 25%; ±0.3% for values between 25% and 3%.

Sample	C 1s 284.6eV	O 1s 532eV	N 402eV	S 2p 168.4eV	Cl 2p 199.4eV	Ni 2p (II) 856.3eV	Ni 2p(0) 852.8eV
GO	69.0	27.8	0.9	1.2 ± 0.3	0.8 ± 0.2	-	-

[169] a) A. Kovtun, D. Jones, S. Dell'Elce, E. Treossi, A. Liscio, V. Palermo, *Carbon* **2019**, *143*, 268–275; b) M. C. Biesinger, B. P. Payne, A. P. Grosvenor, L. W. M. Lau, A. R. Gerson, R. St. C. Smart, *Appl. Surf. Sci.* **2011**, *257*, 2717–2730; c) K. S. Kim, N. Winograd, *Surf. Sci.* **1974**, *43*, 625–643.

NiNP@rGO Type 1	85.0	12.2	1.5	-	-	0.23 ± 0.05	-
NiNP@rGO Type 2	68.8	24.5	-	-	-	4.7 ± 0.3	2.0± 0.3

Table S2. C 1s deconvolution of GO, **NiNP@rGO Type 1** and **NiNP@rGO Type 2**. Values in % of the total C 1s signal.

Sample	C=C sp^2	C-C sp^3	C-OH	C-O-C	C=O	O-C=O	O/C
GO	39.9	7.3	15.9	29.2	5.4	2.3	0.41 ± 0.01
Ni@NP-rGO Type 1	79.4	7.3	7.9	2.1	3.0	0.3	0.13 ± 0.01
Ni@NP-rGO Type 2	52.7	21.3	15.2	6.7	3.8	0.3	0.23 ± 0.01

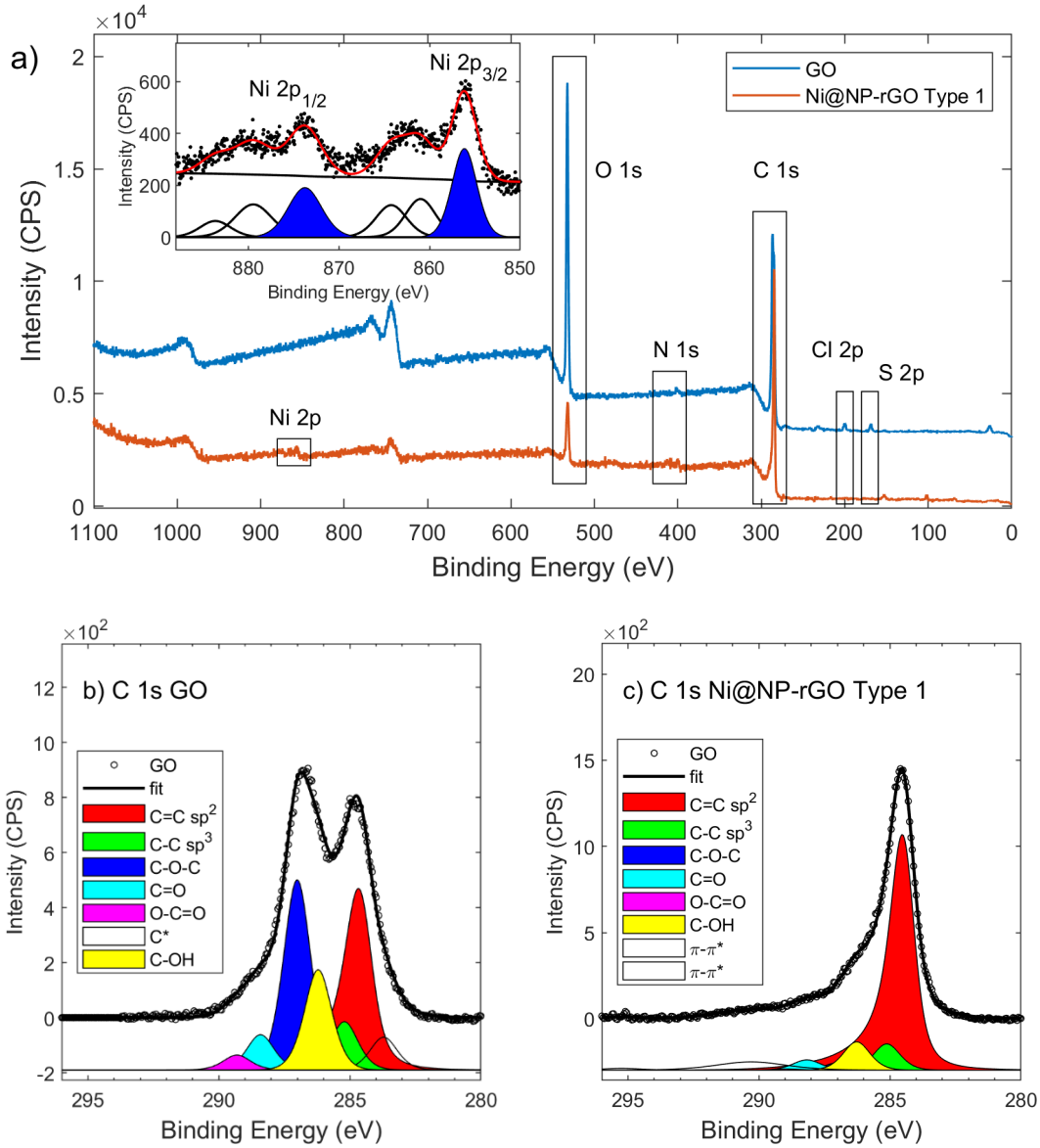

Figure S3. a) XPS survey spectra of GO and **NiNP@rGO Type 1**, inset Ni 2p signal fitted with doublet in blue and shake-up transition. b) C 1s signal of pristine GO. c) C 1s signal of **NiNP@rGO Type 1**.

General procedure for the thiocarboxylation cross coupling

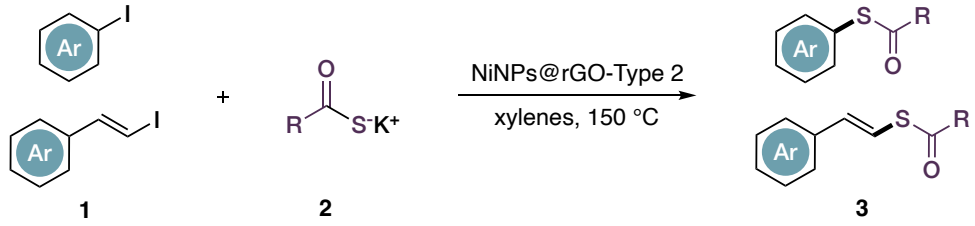

A flame dried Schlenk tube equipped with a stirring bar was charged under nitrogen with reagent grade xylenes (mixture of isomers, 1 mL) and the solvent was degassed by gently bubbling nitrogen gas for 15 seconds. Then potassium thiocarboxylate **2** (0.8 mmol), **NiNP@rGO Type 2** catalyst (8 mg) and aryl iodide **1** (0.1 mmol) were added. The reaction vessel was sealed and the mixture was stirred at 150°C for 18 h or until completion (TLC).

The mixture was filtered on a cotton plug to remove the heterogeneous catalyst and insoluble salts, washing with Et_2O. The filtrate was evaporated under reduced pressure to remove Et_2O and then directly charged as xylene solution into column for flash chromatography purification. When crude mixture ^1H NMR spectra were acquired, xylene was removed under high vacuum.

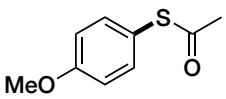

3aa. Colorless oil. *n*Hex:EtOAc: 10:1. Yield = 72%. **^{1}H NMR** (400 MHz, $CDCl_3$) δ 7.35 – 7.29 (m, 2H), 6.97 – 6.91 (m, 2H), 3.83 (s, 3H), 2.39 (s, 3H); **^{13}C NMR** (100 MHz, $CDCl_3$) δ 195.3, 160.8, 136.2, 118.9, 115.0, 55.5, 30.1; **GC-MS**: 182 (15), 140 (100), 125 (41); Anal. Calc. for (C9H10O2S: 182.24): C, 59.32; H, 5.53; found: C, 59.35; H, 5.48.

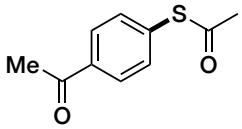

3ba. Off-white solid. *n*Hex:EtOAc: 5:1. Yield = 79%. **^{1}H NMR** (400 MHz, $CDCl_3$) δ 8.01 – 7.95 (m, 2H), 7.56 – 7.48 (m, 2H), 2.61 (s, 3H), 2.46 (s, 3H); **^{13}C NMR** (100 MHz, $CDCl_3$) δ 197.4, 192.8, 137.5, 134.3, 133.9, 128.9, 30.6, 26.8; **GC-MS**: 194 (10), 152 (100), 137 (87), 108

(41); Anal. Calc. for (C10H10O2S: 194.25): C, 61.83; H, 5.19; found: C, 62.01; H, 5.01.

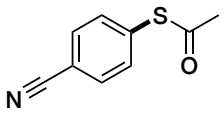

3ca. Yellow solid. *n*Hex:EtOAc: 7:1. Yield = 42%. **^{1}H NMR** (400 MHz, $CDCl_3$) δ 7.68 (d, *J* = 8.4 Hz, 2H), 7.55 – 7.51 (m, 2H), 2.47 (s, 3H); **^{13}C NMR** (100 MHz, $CDCl_3$) δ 192.0, 134.8, 134.5, 132.8, 118.4, 113.3, 30.8; **GC-MS**: 177 (40), 135 (96), 134 (100), 107 (51); Anal. Calc. for (C9H7NOS: 177.22): C, 61.00; H, 3.98; found: C, 61.09; H, 4.07.

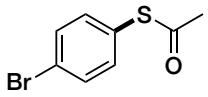

3da. Colorless crystalline plates. *n*Hex:EtOAc: 15:1. Yield = 40%. **^{1}H NMR** (400 MHz, $CDCl_3$) δ 7.56 – 7.52 (m, 2H), 7.29 – 7.26 (m, 2H), 2.43 (s, 3H); **^{13}C NMR** (100 MHz, $CDCl_3$) δ 193.4, 136.0, 132.6, 127.1, 124.3, 30.4; **GC-MS**: 232 (^{81}Br, 21), 230 (^{79}Br, 21), 190 (^{81}Br, 85) 188 (^{79}Br, 85), 108 (100); Anal. Calc. for (C8H7BrOS: 231.11): C, 41.58; H, 3.05; found: C, 41.69; H, 3.03.

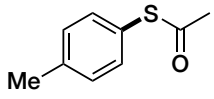

3ea. Colorless oil. *n*Hex:EtOAc: 20:1. Yield = 82%. **^{1}H NMR** (400 MHz, $CDCl_3$) δ 7.32 – 7.28 (m, 2H), 7.24 – 7.20 (m, 2H), 2.41 (s, 3H), 2.38 (s, 3H); **^{13}C NMR** (100 MHz, $CDCl_3$) δ 194.8, 139.9, 134.6, 130.2, 124.6, 30.2, 21.5; **GC-MS**: 166 (15), 124 (100), 91 (77); Anal. Calc. for (C9H10OS: 166.24): C, 65.03; H, 6.06; found: C, 64.99; H, 6.11.

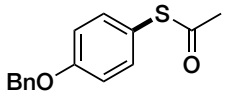

3fa. White powder. *n*Hex:EtOAc: 15:1. Yield = 57%. **^{1}H NMR** (400 MHz, $CDCl_3$) δ 7.47 – 7.37 (m, 4H), 7.37 – 7.30 (m, 3H), 7.05 – 6.99 (m, 2H), 5.08 (s, 2H), 2.40 (s, 3H); **^{13}C NMR** (100 MHz, $CDCl_3$) δ 195.2, 160.0, 136.6, 136.2, 128.8, 128.3, 127.6, 119.2, 115.9, 70.2, 30.1; **GC-MS**: 258 (6), 216 (24), 91 (100); Anal. Calc. for (C15H14O2S: 258.34): C, 69.74; H, 5.46; found: C, 69.81; H, 5.45.

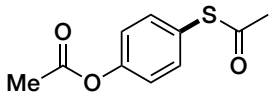

3ga. Off-white solid. *n*Hex:EtOAc: 3:1. Yield = 52%. **^{1}H NMR** (400 MHz, $CDCl_3$) δ 7.45 – 7.37 (m, 2H), 7.19 – 7.11 (m, 2H), 2.42 (s, 3H), 2.31 (s, 3H); **^{13}C NMR** (100 MHz, $CDCl_3$) δ 193.9, 169.2, 151.7, 135.7, 125.3, 122.6, 30.3, 21.3; **GC-MS**: 210 (9), 168 (41), 126 (100); Anal. Calc. for (C10H10O3S: 210.25): C, 57.13; H, 4.79; found: C, 69.81; H, 5.45.

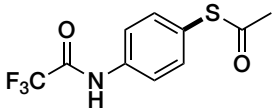

3ha. Off-white solid. *n*Hex:EtOAc: 4:1. Yield = 54%. **^{1}H NMR** (400 MHz, $CDCl_3$) δ 8.18 (bs, 1H), 7.64 – 7.55 (m, 2H), 7.43 – 7.33 (m, 2H), 2.45 (s, 3H); **^{13}C NMR** (100 MHz, $CDCl_3$) δ 194.8, 154.9 (q, J = 37.7 Hz), 136.6, 135.7, 125.3, 121.1, 115.7 (q, J = 288.7 Hz), 30.3; **^{19}F NMR** (376 MHz, $CDCl_3$) δ -75.73 (s, 3F); **GC-MS**: 263 (32), 221 (100), 152 (32); Anal. Calc. for (C10H8F3O2S: 263.33): C, 45.63; H, 3.06; found: C, 45.69; H, 2.97.

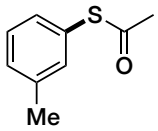

3ia. Colorless oil. *n*Hex:EtOAc: 20:1. Yield = 41%. **^{1}H NMR** (400 MHz, $CDCl_3$) δ 7.33 – 7.28 (m, 1H), 7.25 – 7.20 (m, 3H), 2.41 (s, 3H), 2.37 (s, 3H); **^{13}C NMR** (100 MHz, $CDCl_3$) δ 194.5, 139.2, 135.2, 131.7, 130.5, 129.2, 127.7, 30.3, 21.4; **GC-MS**: 166 (18), 124 (100), 91 (73); Anal. Calc. for (C9H10OS: 166.24): C, 65.03; H, 6.06; found: C, 65.11; H, 5.97.

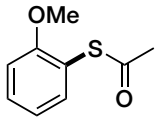

3ja. Viscous oil. *n*Hex:EtOAc: 9:1. Yield = 79%. **^{1}H NMR** (400 MHz, $CDCl_3$) δ 7.45 – 7.37 (m, 2H), 7.05 – 6.93 (m, 2H), 3.86 (s, 3H), 2.41 (s, 3H); **^{13}C NMR** (100 MHz, $CDCl_3$) δ 193.7, 159.3, 136.9, 131.9, 121.3, 116.3, 111.7, 56.1, 30.2 **GC-MS**: 182 (10), 140 (100), 125 (36); Anal. Calc. for (C9H10O2S: 182.24): C, 59.32; H, 5.53; found: C, 59.41; H, 5.55.

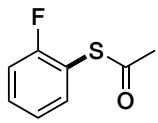

3ka. Colorless oil. *n*Hex:EtOAc: 20:1. Yield = 57%. **^{1}H NMR** (400 MHz, $CDCl_3$) δ 7.50 – 7.37 (m, 2H), 7.25 – 7.13 (m, 2H), 2.45 (s, 3H); **^{13}C NMR** (100 MHz, $CDCl_3$) δ 192.2, 162.2 (d, J = 249.5 Hz), 136.8 (d, J = 0.8 Hz),132.3 (d, J = 8.2 Hz), 124.8 (d, J = 3.9 Hz), 116.4 (d, J = 22.7 Hz), 115.5 (d, J = 18.6 Hz), 30.2;

^{19}F NMR (376 MHz, $CDCl_3$) δ -106.74 (dt, *J* = 8.5, 6.3 Hz, 1F); **GC-MS**: 170 (16), 128 (100); Anal. Calc. for (C8H7FOS: 170.20): C, 56.46; H, 4.15; found: C, 56.38; H, 4.20.

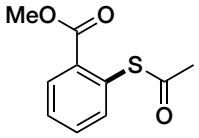

3la. Pale yellow oil. *n*Hex:EtOAc: 6:1. Yield = 56%. **^{1}H NMR** (400 MHz, $CDCl_3$) δ 7.93 (dd, *J* = 7.5, 1.2 Hz, 1H), 7.58 – 7.55 (m, 1H), 7.53 (td, *J* = 7.4, 1.5 Hz, 1H), 7.46 (td, *J* = 7.6, 1.7 Hz, 1H), 3.89 (s, 3H), 2.43 (s, 3H); **^{13}C NMR** (100 MHz, $CDCl_3$) δ 193.2, 166.8, 136.7, 134.0, 132.0, 131.0, 129.4, 128.8, 52.5, 30.4; **GC-MS**: 210 (5), 168 (56), 136 (100); Anal. Calc. for (C10H10O3S: 210.04): C, 57.13; H, 4.79; found: C, 57.02; H, 4.79.

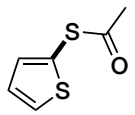

3ma. Colourless oil. *n*Hex:EtOAc: 20:1. Yield = 80%. **^{1}H NMR** (400 MHz, $CDCl_3$) δ 7.56 (dd, *J* = 5.3, 1.2 Hz, 1H), 7.17 (dd, *J* = 3.6, 1.2 Hz, 1H), 7.11 (dd, *J* = 5.3, 3.6 Hz, 1H), 2.41 (s, 3H); **^{13}C NMR** (100 MHz, $CDCl_3$) δ 194.4, 135.9, 132.0, 128.0, 125.2, 29.6; **GC-MS**: 158 (27), 116 (100), 71 (77); Anal. Calc. for (C6H6OS2: 158.23): C, 45.54; H, 3.82; found: C, 45.55; H, 3.69.

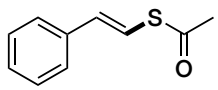

3na. Viscous oil. *n*Hex:EtOAc: 30:1. Yield = 49%. **^{1}H NMR** (400 MHz, $CDCl_3$) δ 7.43 – 7.37 (m, 2H), 7.36 – 7.30 (m, 2H), 7.29 – 7.24 (m, 1H), 7.23 (d, *J* = 16.3 Hz, 1H), 6.72 (d, *J* = 16.3 Hz, 1H), 2.41 (s, 3H); **^{13}C NMR** (100 MHz, $CDCl_3$) δ 192.8, 136.2, 131.8, 128.8, 128.3, 126.5, 117.3, 30.7; GC-MS: 178 (18), 136 (100), 91 (76); Anal. Calc. for (C10H10OS: 178.25): C, 67.38; H, 5.66; found: C, 67.33; H, 5.60.

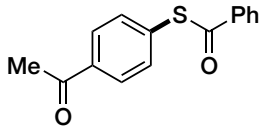

3bb. White solid. *n*Hex:EtOAc: 6:1. Yield = 56%. **^{1}H NMR** (400 MHz, $CDCl_3$) δ 8.06 – 7.99 (m, 4H), 7.67 – 7.59 (m, 3H), 7.55 – 7.46 (m, 2H), 2.64 (s, 3H).**^{13}C NMR** (100 MHz, $CDCl_3$) δ 197.4, 189.0, 137.5, 136.3, 134.9, 134.0, 133.4, 128.9, 128.8, 127.5, 26.7; **GC-MS**: 256 (5),

105 (100), 77 (63); Anal. Calc. for (C15H12O2S: 256.06): C, 70.29; H, 4.72; found: C, 70.33; H, 4.66.

“Hot filtration” leaching experiment

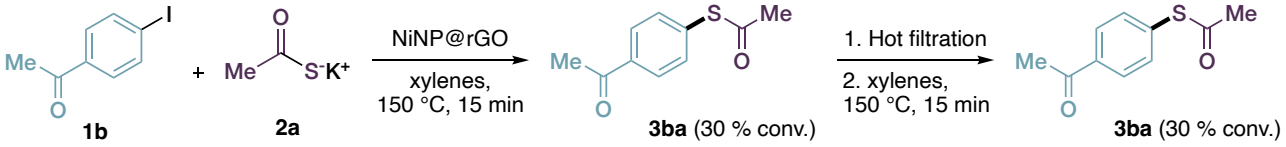

Substrate **1b** was subjected to the optimized reaction conditions according to general procedure. After 15 minutes, the reaction mixture was filtered immediately, while still hot, on a cotton plug and the filtrate was collected in a pre-flame dried Schlenk tube under nitrogen. A small portion of the mixture was withdrawn and analyzed by ^{1}H NMR spectroscopy to assess the initial conversion of the reaction, while the rest of the mixture was sealed again and subjected to heating at 150°C for 18 h. After heating, the solvent was removed and a second portion was again analyzed by ^{1}H NMR spectroscopy to assess the conversion. The second portion crude ^{1}H NMR spectrum was identical to the one of the first portion, suggesting that: the catalyst is genuinely heterogeneous, no leaching of any active form of catalyst from the material occurs during the reaction course, and also that no appreciable reactivity of starting material or product is occurring in the absence of the catalyst.

5. Direct Synthesis of α-Aryl-α-Trifluoromethyl Alcohols via Nickel Catalyzed Cross-Electrophile Coupling

All the procedures and results here described can be found in:

- L. Lombardi, A. Cerveri, R. Giovanelli, M. Castiñeira Reis, C. Silva-Lopez, G. Bertuzzi, M. Bandini, "Direct Synthesis of α-Aryl-α-Trifluoromethyl Alcohols via Nickel Catalyzed Cross-Electrophile Coupling." *Angew. Chem. Int. Ed.* **2022**, e202211732.

ABSTRACT

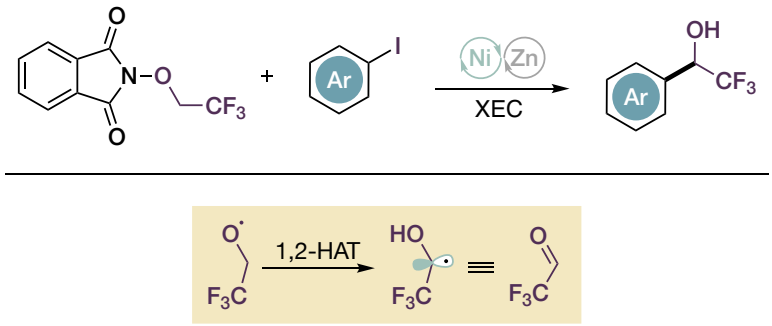

A nickel-catalyzed reductive cross-electrophile coupling between the redox-active *N*-trifluoroethoxyphthalimide and iodoarenes is documented. The protocol reproduces a formal arylation of trifluoroacetaldehyde under mild conditions in high yields (up to 88%) and with large functional group tolerance (30 examples). A combined computational and experimental investigation revealed a pivotal solvent assisted 1,2-Hydrogen Atom Transfer (HAT) process to generate a nucleophilic α-hydroxy-α-trifluoromethyl C-centered radical for the Csp^2-Csp^3 bond forming process.

5.1 Background

Nickel lies just above palladium in the periodic table and as a group 10 metal, it can readily perform many of the same elementary reactions as palladium or platinum. Its price is about 2000 times lower than that of palladium, making its utilization in a sustainability context highly desirable. Apart from this, several features contribute to make nickel more than a mere cheaper and more widely available substitute of his sibling palladium.[123]

Its lower electronegativity with respect to palladium (1.91 *vs* 2.20 in the Pauling scale) makes oxidative addition, which results in loss of electron density around the metal, occur more easily, and conversely, reductive elimination results more difficult.[170] These features allow for the use of electrophiles that would be considerably less reactive or completely unviable under palladium catalysis, such as phenol derivatives, aromatic nitriles or even aryl fluorides.[171]

Being a first row transition metal, nickel has a smaller atomic radius (making it a harder metal), so that Ni-ligand bonds are considerably shorter, resulting in the possible adoption of different ligand classes with respect to Pd.[172] Both this aspect and its high nucleophilicity make binding to olefins very strong, since nickel readily donates electron density from its d-orbitals to π-acceptors.[173]

Importantly, β-hydride elimination tends to be slower with nickel relatively to palladium. Specifically, given the shorter Ni-ligand bonds, the energy barrier to Ni–C bond rotation prior to β-hydride elimination is often significantly higher for nickel than comparable palladium species, due to the more strained geometry in the transition

---

[170] a) T. T. Tsou, J. K. Kochi, *J. Am. Chem. Soc.* **1979**, *101*, 6319–6332; b) E. L. Lanni, A. J. McNeil, *J. Am. Chem. Soc.* **2009**, *131*, 16573–16579; c) R. Giovannini, T. Stüdemann, D. Gaelle, P. Knochel*, Angew. Chem., Int. Ed.* **1998**, *37*, 2387; d) C.-Y. Huang, A. G. Doyle, *J. Am. Chem. Soc.* **2012**, *134*, 9541−9544.

[171] a) B.-J. Li, D.-G. Yu, C.-L. Sun, Z.-J. Shi, *Chemistry* **2011**, *17*, 1728–1759; b) B. M. Rosen, K. W. Quasdorf, D. A. Wilson, N. Zhang, A.-M. Resmerita, N. K. Garg, V. Percec, *Chem. Rev.* **2011**, *111*, 1346–1416; c) T. Mesganaw, N. K. Garg, *Org. Process Res. Dev.* **2013**, *17*, 29–39; d) J. J. Garcia, N. M. Brunkan, W. D. Jones, *J. Am. Chem. Soc.* **2002**, *124*, 9547–9555; e) M. Tobisu, T. Xu, T. Shimasaki, N. Chatani, *J. Am. Chem. Soc.* **2011**, *133*, 19505–19511.

[172] B. Cordero, V. Gómez, A. E. Platero-Prats, M. Revés, J. Echeverría, E. Cremades, F. Barragan, S. Alvarez, *Dalton Trans.* **2008**, 2832-2838.

[173] C. Massera, G. Frenking, *Organometallics* **2003**, *22*, 2758–2765.

state.[174] In addition, β-H elimination occurs via an intermediate with a β-agostic interaction, and the lower electronegativity of Ni results in a weaker agostic interaction relatively to Pd, also contributing to this phenomenon.[175]

This offers Ni a significant edge over palladium in the realization of cross-coupling reactions of Csp^3 fragments, that can be challenging and plagued by unwanted β-hydride elimination reactivity under Pd regime. Csp^3 electrophiles, being more electronrich than their sp^2 counterparts, are also less prone to oxidative insertion, and while primary ones can react via S_N2-like pathways, this is very slow for secondary and tertiary ones.[176] Indeed, secondary electrophiles have been shown viable with Pd in only a handful of reports.[177d] In addition to reducing alkene formation from Csp^3 electrophiles, and providing their easier activation (*vide infra*), the use of Ni has also been shown advantageous in circumventing isomerization of secondary and tertiary Csp^3 nucleophiles, retaining high levels of regiofidelity.[177]

Another crucial aspect in nickel catalysis is its ability to readily access all oxidation states ranging from Ni(0) to Ni(IV), whereas Pd is most often revolving in a Pd(0)/Pd(II) cycle.[178] In particular, the open-shell configurations of Ni(I) and Ni(III) result more stable than for Pd and Pt, likely because of a higher pairing energy of Ni due to a more condensed electron cloud.[179] This results in the fact that nickel can react in single electron processes, making radical mechanistic pathways accessible. This possibility of engaging nickel in catalytic transformations involving radicals has greatly contributed in the blossoming of nickel catalysis in recent years, permitting the development of unprecedented strategies and disconnections.

---

[174] B.-L. Lin, L. Liu, Y. Fu, S.-W. Luo, Q. Chen, Q.-X. Guo, *Organometallics* **2004**, *23*, 2114–2123.

[175] a) H. Xu, P. B. White, C. Hu, T. Diao, *Angew. Chem. Int. Ed.* **2017**, *56*, 1535–1538; b) H. Xu, C. Hu, X. Wang, T. Diao, *Organometallics* **2017**, *36*, 21, 4099–4102.

[176] I. D. Hills, M. R. Netherton, G. C. Fu, *Angew. Chem. Int. Ed.* **2003**, *42*, 5749–5752.

[177] a) R. Jana, T. P. Pathak, M. S. Sigman, *Chem. Rev.* **2011**, *111*, 1417–1492; b) M. O'Neill, J. Cornella, Synthesis 2018, 50, 3974–3996; c) M. R. Netherton, G. C. Fu, *Adv. Synth. Catal.* **2004**, *346*, 1525–1532; d) A. Rudolph, M. Lautens, *Angew. Chem. Int. Ed.* **2009**, *48*, 2656–2670.

[178] a) C.-Y. Lin, P.P. Power, *Chem. Soc. Rev.* **2017**, *46*, 5347–5399; b) B. Zheng, F. Tang, J. Luo, J. W. Schultz, N. P. Rath, L. M. Mirica, *J. Am. Chem. Soc.* **2014**, *136*, 6499–6504; c) N. M. Camasso, M. S. Sanford, *Science* **2015**, *347*, 1218–1220.

[179] R. Poli, I. Cacelli, *Eur. J. Inorg. Chem.* **2005**, 2324–2331; L. E. Roy, E. Jakubikova, M. G. Guthrie, E. R. Batista, *J. Phys. Chem. A* **2009**, *113*, 24, 6745–6750.

Both Ni(0)/Ni(II) and Ni(I)/Ni(III) two-electron manifolds, as well as Ni(II)/Ni(IV), are known. Bielectronic oxidative addition constitutes, similar to Pd chemistry, the main activation pathway for Csp^2 electrophiles as well as benzylic or allylic ones (in the latter two cases, either via direct oxidative insertion or in an S_N2-like manner).[180] Examples of bielectronic oxidative addition to methyl or primary electrophiles are also known.[181] Unactivated Csp^3 electrophiles tend to react via single electron processes, resulting in the formation of organic radicals that are captured by the metal complex leading to the formation of alkyl organonickel species. These reactions, involving single electron oxidation events of the nickel center, often proceed via Ni(I)/Ni(II)/Ni(III) or Ni(0)/Ni(I)/Ni(II)/Ni(III) manifolds.

Generally speaking, reactions proceeding via two-electron manifolds make use of strong field ligands, such as phosphines, N-Heterocyclic carbenes or olefins. On the contrary, in single electron type of chemistry the use of weak-field, bi- or tridentate N ligands such as diamines, bipyridines, terpyridines, phenanthrolines, pyBox (pyridine-bioxazoline), pyOx (pyridine-oxazoline), bis-oxazolines (Box) and bi-oxazoline(biOx) is most frequently encountered (**Figure 1**).[123c] These ligands determine lower ligand field splitting that enhances the stability of paramagnetic species, and some ligands have been shown to be redox active, meaning that the redox events at the metal centers are actually best described by oxidation or reduction of the ligand. For examples, several Ni(I) complexes are best described as Ni(II) species bound to reduced, radical anion ligands, as determined by EPR (electron paramagnetic resonance) studies.[182]

---

[180] a) M. R. Harris, L. E. Hanna, M. A. Greene, C. E. Moore, E. R. Jarvo, *J. Am. Chem. Soc.* **2013**, *135*, 3303–3306; b) S.-Q. Zhang, B. L. H. Taylor, C.-L. Ji, Y. Gao, M. R. Harris, L. E. Hanna, E. R. Jarvo, K. N. Houk, X. Hong, *J. Am. Chem. Soc.* **2017**, *139*, 12994−13005; c) Q. Zhou, K. M. Cobb, T. Tan, M. P. Watson, *J. Am. Chem. Soc.* **2016**, 138, 37, 12057–12060; d) J. Xu, O. P. Bercher, M. P. Watson, *J. Am. Chem. Soc.* **2021**, *143*, 8608–8613.

[181] a) M. I. Lipschutz, X. Yang, R. Chatterjee‖, T. Don Tilley, *J. Am. Chem. Soc.* **2013**, *135*, 15298–15301; J. Terao, H. Watanabe, A. Ikumi, H. Kuniyasu, N. Kambe, J. *Am. Chem. Soc.* **2002**, *124*, 4222–4223.

[182] C. L. Wagner, G. Herrera, Q. Lin, C. T. Hu, T. Diao, *J. Am. Chem. Soc.* **2021**, 143, 5295−5300 and references therein.

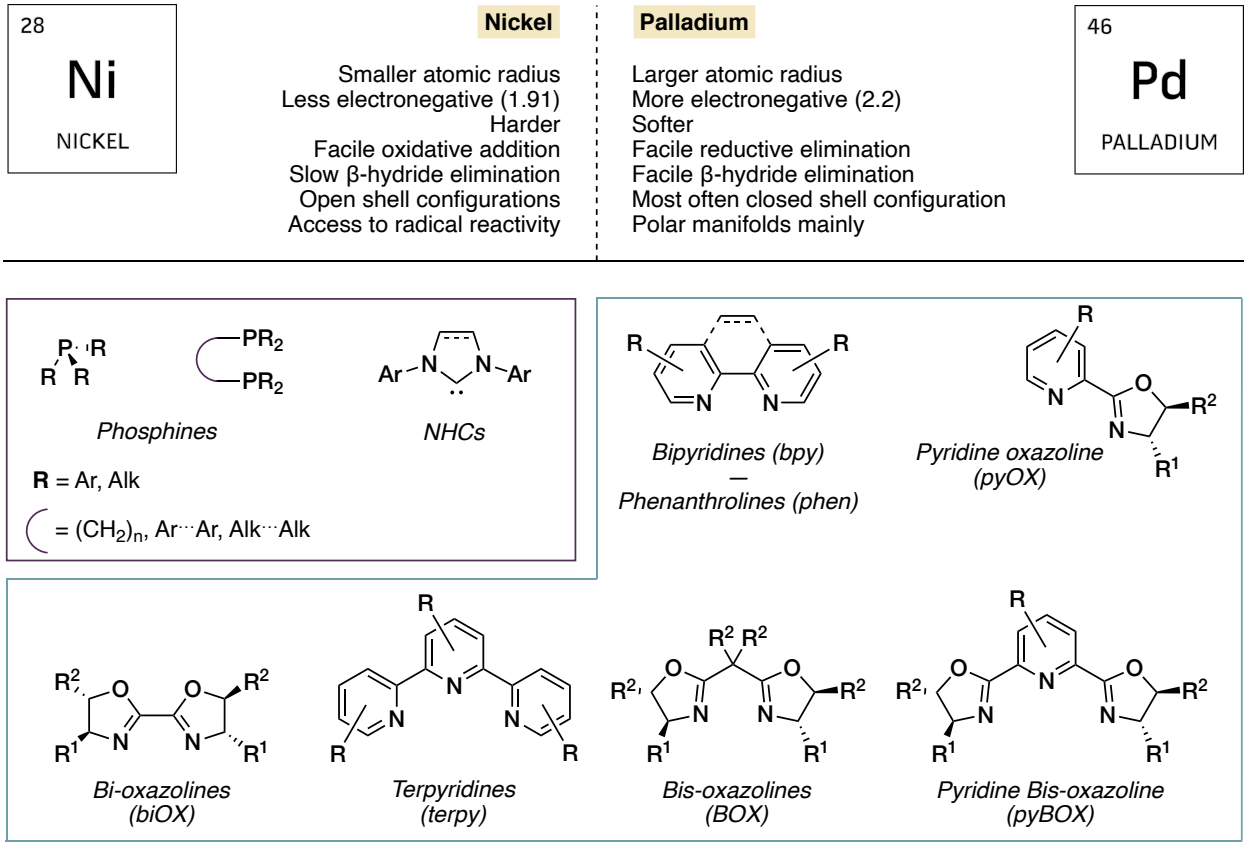

Figure 1. Top: Summary comparison of nickel and palladium properties. Bottom: commonly used ligands in Ni catalysis. In the purple box, strong field ligands commonly encountered in bielectronic-type, Ni(0)/Ni(II) manifolds. In the teal box, weak field ligands routinely used in single electron events-based chemistry, when odd oxidation states are involved. 1,2-diamines (non shown) are also used.

The use of secondary unactivated Csp^3 electrophiles with β-hydrogens was first demonstrated by Fu in 2003. The authors described a Negishi coupling of primary alkylzinc reagents with a range of secondary and primary alkyl bromides and iodides, using $Ni(COD)_2$ as the nickel source and tridentate pyBox ligand, that probably aids suppressing β-hydride elimination by blocking vacant coordination sites (**Scheme 1**).[183]

[183] J. Zhou and G. C. Fu, *J. Am. Chem. Soc.* **2003**, *125*, 14726-14727.

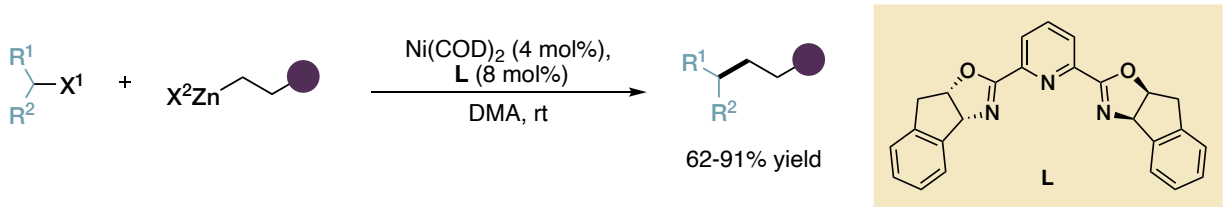

Scheme 1. Fu's Negishi coupling of alkylzinc reagents and secondary/primary alkyl iodides and bromides. When secondary, only achiral electrophiles with $R^1 = R^2$ have been demonstrated in this report.

Csp^2-Csp^3 and Csp^3-Csp^3 Suzuki-type couplings were also later reported by same the group, using secondary alkyl bromides and iodides with aryl boronic acids and 9-BBN alkyl boranes respectively (**Scheme 2**). The first system makes use of a bathophenanthroline ligand, while the second use a *trans*-1,2-cyclohexanediamine ligand.[184] This highlights the difficult quest of identifying general ligands for this kind of nickel catalyzed processes.

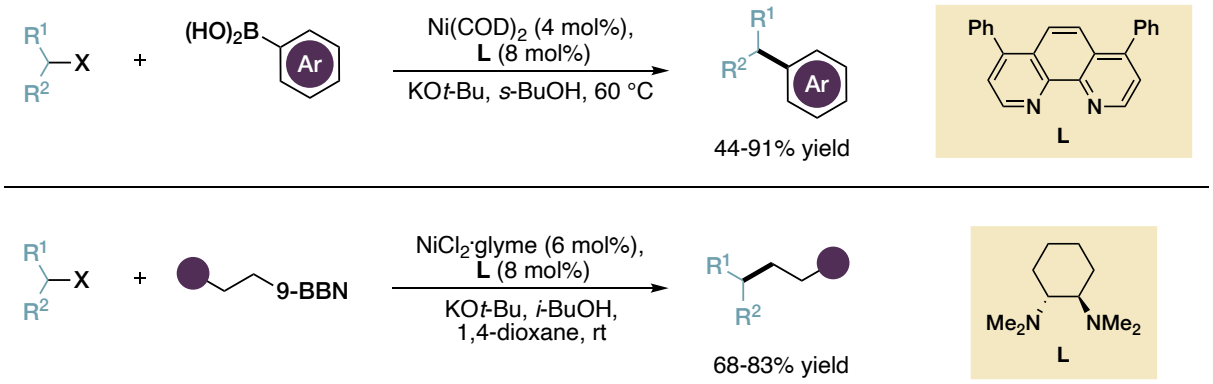

Scheme 2. Suzuki-type alkyl cross couplings reported by Fu. Top: cross coupling of aryl boronic acids with secondary alkyl iodides and bromides. Bottom: cross coupling between 9-BBN alkyl borane reagents and secondary/primary alkyl iodides and bromides.

Xile Hu is also a prominent contributor in the field, and reported a peculiar N-pincer catalyst for the Kumada alkyl-alkyl cross coupling of functionalized primary bromides

[184] a) J. Zhou, G. C. Fu, *J. Am. Chem. Soc.* **2004**, *126*, 1340-1341; b) B. Saito, G. C. Fu, *J. Am. Chem. Soc.* **2007**, *129*, 9602-9603.

and iodides with Grignard reagents (**Scheme 3**, top).[185] A Sonogashira cross coupling reaction with aliphatic alkynes was also documented (**Scheme 3**, bottom).[186]

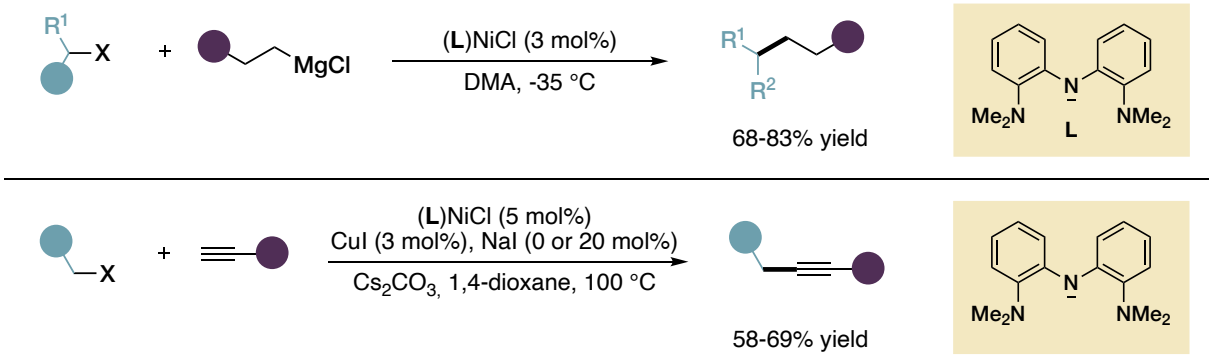

Scheme 3. Top: Xile Hu's Kumada cross coupling of functionalized alkyl halides (X = Br, I). Bottom: use of the same nickel complex in the Sonogashira coupling of functionalized aliphatic alkynes with functionalized primary alkyl halides (X = Cl, Br, I).

From a mechanistic standpoint, the involvement of Ni(I) species has been demonstrated and most commonly two scenarios starting from Ni(I) can be encountered, differing in the order of transmetalation and electrophile activation.[123c] In the so-called "radical rebound cycle", transmetalation of the nucleophile occurs first, leading to a Ni(I)-carbyl complex. This species can interact with the alkyl electrophile producing a Ni(II)-halide complex and an organic radical that stays within the solvent cage and rapidly recombines with the metal center (rebound process) to yield a Ni(III)-biscarbyl complex that undergoes reductive elimination (**Scheme 4**, left cycle). This type of mechanism has been supported by Vicic, who synthetized and investigated the reactivity of a terpyNi(I)Me complex demonstrating its competence in the activation of alkyl halides. A discussion on the redox activity of the ligand was also given.[187] DFT calculations on the same system further verifies this hypothesis.[188] In regard to the activation mode of the alkyl halide, this computational study points towards a halogen

[185] O. Vechorkin, X. Hu, *Angew. Chem. Int. Ed.* **2009**, *48*, 2937–2940.
[186] O. Vechorkin, D. Barmaz, V. Prouse, X. Hu, *J. Am. Chem. Soc.* **2009**, *131*, 12078–12079.
[187] G. D. Jones, J. L. Martin, C. McFarland, O. R. Allen, R. E. Hall, A. D. Haley, R. J. Brandon, T. Konovalova, P. J. Desrochers, P. Pulay, D. A. Vicic, *J. Am. Chem. Soc.* **2006**, *128*, 13175-13183.
[188] X. Lin, D. Lee Phillips, *J. Org. Chem.* **2008**, *73*, 3680–3688.

abstraction mechanism, that is favored over oxidative addition and SET events. A very recent investigation by Diao and coworkers on the activation of benzyl bromide partially supports this result, proposing that a net halogen atom abstraction proceeding via a concerted inner-sphere electron transfer and halogen atom dissociation is operating. The actual abstractor in this study was found to be a $[(bpy)Ni(I)ArBr]^-$ anionic complex that reacts with the electrophile prior to bromide dissociation from the Ni center[189] Similar results were shown by the same group for [(Xantphos)Ni(I)Ar] complexes.[190] This mechanism is thought to be in operation in the coupling reactions by Fu showed earlier, and in many related reports.

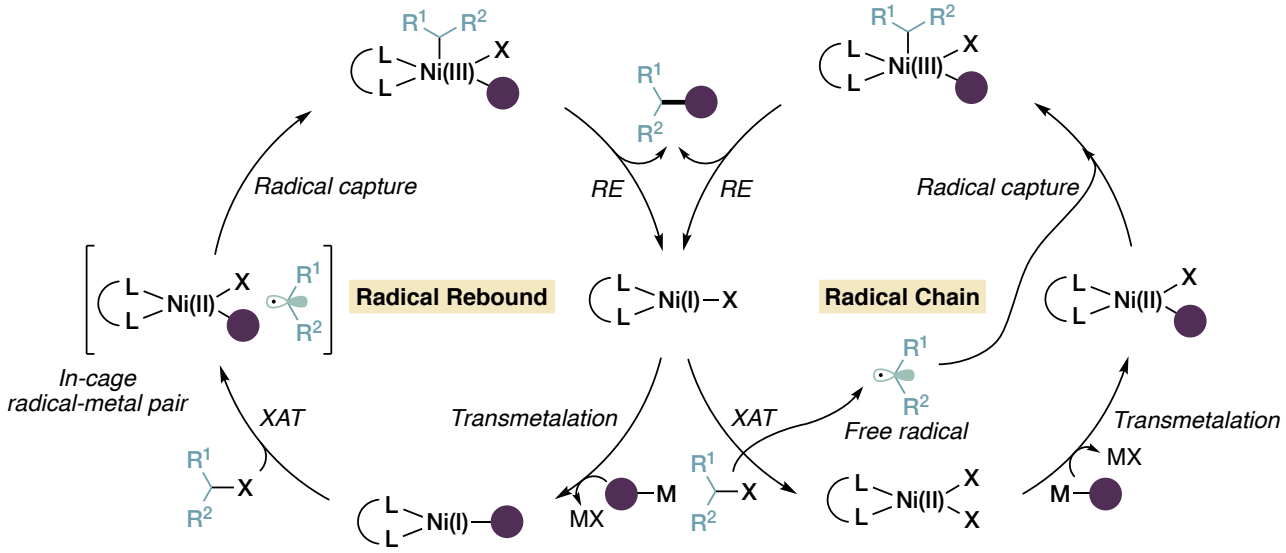

Scheme 4. Left: catalytic cycle for the "radical rebound" mechanism. Right: catalytic cycle for the "radical chain" mechanism. The purple circle denotes a (functionalized) carbyl moiety. XAT = halogen atom transfer; RE = reductive elimination; M = metal or alkyne; X = (pseudo)halide.

In the other mechanistic possibility, dubbed "radical chain", activation of the electrophile occurs first from a Ni(I)-halide complex to generate the radical and a Ni(II) complex (**Scheme 4**, right cycle). The radical escapes the solvent cage, and recombines with a Ni(II)-carbyl compex formed via transmetalation to yield a Ni(III)-biscarbyl

[189] Q. Lin, Y. Fu, P. Liu, T. Diao, *J. Am. Chem. Soc.* **2021**, *143*, 14196–14206.
[190] J. B. Diccianni, J. Katigbak, C. Hu, T. Diao, *J. Am. Chem. Soc.* **2019**, *141*, 1788−1796.

species, that ultimately leads to the product. This mechanism was found to be in operation, by Fu and coworkers, in the enantioconvergent coupling of racemic propargyl bromides (and chlorides) with diaryl zinc or alkyl-aryl zinc reagents (**Scheme 5**).[191]

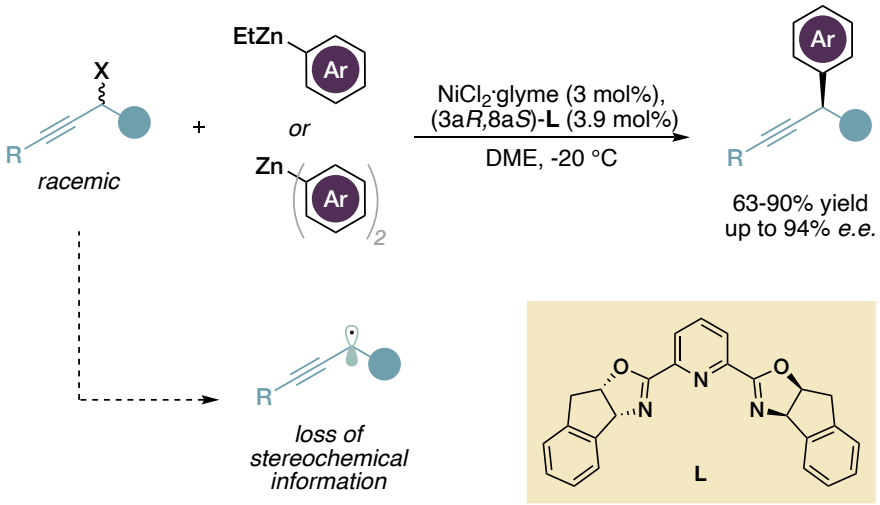

Scheme 5. Enantioconvergent cross coupling of racemic propargylic halides (X = Br, Cl) and diaryl/alkyl-aryl zinc reagents. The reaction proceeds via a radical chain mechanism, in which the stereochemical information of the electrophile is erased upon interaction with Ni(I), leading to the same radical intermediate from both enantiomers. DME = glyme = 1,2-dimethoxyethane.

The formation of the same radical intermediate from the two enantiomers of the electrophile provides the basis for the enantioconvergence of the process, and enantioselectivity is entirely dictated by the chiral ligand, with no kinetic resolution in operation. This reaction has been demonstrated successful for various nucleophiles and activated alkyl (pseudo)halides.[192] The presence of a stabilizing α-substituent on the electrophile seems to be mandatory.

The out-of-cage behavior of the radical can be determined by the ratio of cyclized to uncyclized products at varying concentrations of metal complex, when a radical clock electrophile is employed.[123c] Solvent-cage escape of the radicals would determine a

[191] a) N. D. Schley, G. C. Fu, *J. Am. Chem. Soc.* **2014**, *136*, 16588−16593; b) S. W. Smith, G. C. Fu, *J. Am. Chem. Soc.* **2008**, *130*, 12645–12647.
[192] G. C. Fu, *ACS Cent. Sci.* **2017**, *3*, 692−700.

higher ratio of uncyclized to cyclized product with increasing catalyst concentration, given that the radical is more quickly trapped in the presence of increased amount of metal species. If radicals stay within the solvent cage, then no significant variation is observed. Importantly, this experiment can only give information on the presence of out-of-cage radicals but is not sufficient to distinguish the order of partner activation, as other slightly different mechanistic scenarios can be in operation. The Kumada reaction developed by Hu with the Ni pincer ligand, for example, is thought to proceed via with initial transmetalation of the Grignard reagent and to involve formation of out-of-cage radicals that recombine with a second nickel center.[193] As can be reasonably expected, the most likely mechanism of a given process can vary depending on substrates, ligands and reaction conditions, although the two depicted mechanistic manifolds are the most commonly invoked.

Traditional cross-coupling methodology rely on partner differentiation by employing one electrophilic and one nucleophilic partner in a polarity-matched scenario, with the metal revolving in each cycle around the required oxidation states in a net redox neutral process. Such couplings can proceed in absence of any added oxidant or reductant, and the different activation modes for each partner guarantee high cross-selectivity. However, the use of defined organometallic species as nucleophiles for C-C cross-couplings poses several drawbacks, given that these compounds can display limited functional group tolerance, be rather sensitive and/or need to be prepared, and when commercially available usually more expensive than the corresponding (pseudo)halides. An alternative approach involving two different electrophiles can be envisioned, resulting in a net oxidation of the metal centered, so that a stoichiometric reductant is needed for catalytic turnover (**Figure 2**). This strategy (cross-electrophile coupling, XEC) can offer a significant advantage, as organic electrophiles are much more widely available, thus providing a greater diversity of structures, and are usually highly stable compounds, often commercially available at a low cost.

[193] J. Breitenfeld, J. Ruiz, M. D. Wodrich, X. Hu, *J. Am. Chem. Soc.* **2013**, *135*, 12004−12012.

Indeed, the dimerization of electrophiles has been studied for more the 100 years, and venerable reactions such as the Ullmann and Wurtz couplings are early examples.[194] For it to be of general synthetic use without resorting to an excess of one component, this strategy needs to feature a high cross-selectivity over homocoupling, which poses an obvious challenge given the lack of polarity discrimination between the two coupling partners.

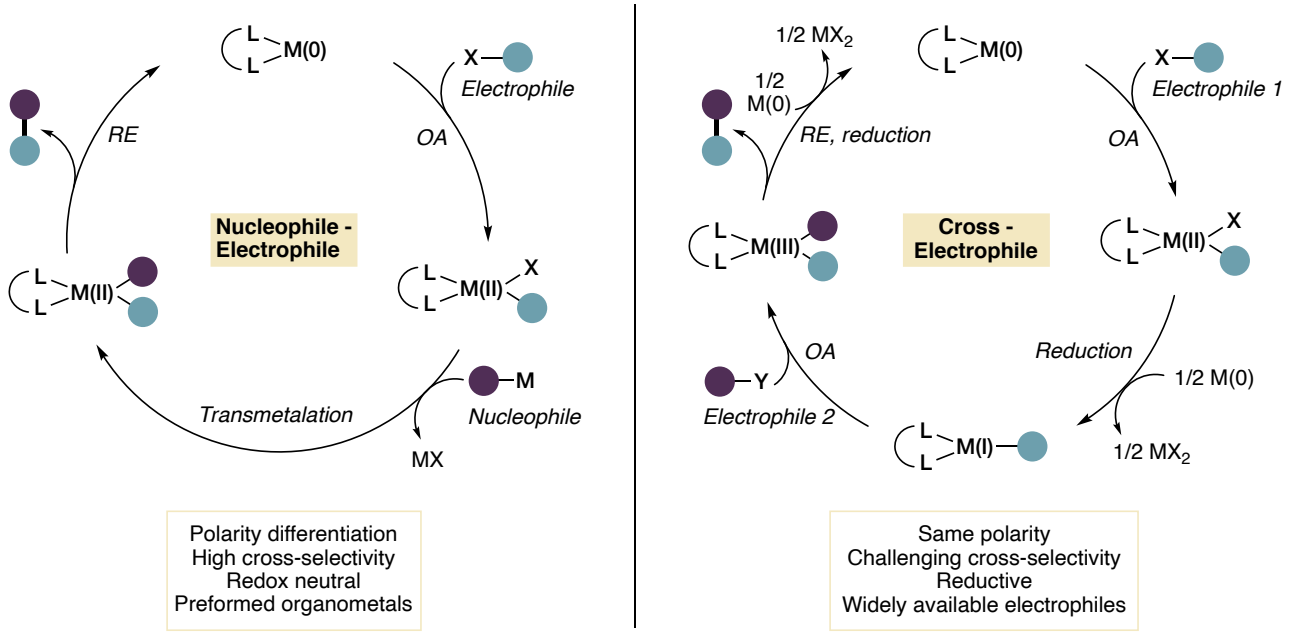

Figure 2. Left: example of a catalytic cycle for a conventional nucleophile-electrophile coupling. A generic metal in a M(0)/M(II) cycle is shown. Right: example of a catalytic cycle for a cross electrophile coupling. A generic metal revolving in a M(0)/M(II)/M(I)/M(III) cycle is shown. A generic divalent metal reductant, like commonly employed Zn or Mn is shown in this case.

Building on previous electrochemical work[195], modern solutions for XEC have started being developed from around 2010 in a number of independent reports.[196]

Weix reported in 2010 a highly selective XEC between aryl and alkyl (mainly primary) iodides and bromides used in equimolar amounts, employing $NiI_2 \cdot H_2O$ as the nickel

[194] a) A. Wurtz, *Ann. Chem. Pharm.* **1855**, *96*, 364−375; b) F. Ullmann, J. Bielecki, *Chem. Ber.* **1901**, *34*, 2174−2185.
[195] A. Jutand, *Chem.Rev.* **2008**, *108*, 2300−2347.
[196] a) D. A.Everson, R. Shrestha, D. J. Weix, *J. Am. Chem. Soc.* **2010**, *132*, 920−921; b) D. A. Everson, B. A. Jones, D. J. Weix, *J. Am. Chem. Soc.* **2012**, *134*, 6146−6159; c) M. Durandetti, J.-Y Nédélec, J. Périchon, *J. Org.Chem.* **1996**, *61*, 1748−1755; d) M. Amatore, C. Gosmini, *Chem. Eur. J.* **2010**, 16, 5848−5852; e) C.-S. Yan, Y. Peng, , X.-B. Xu, Y.-W. Wang, *Chem. Eur. J.* **2012**, *18*, 6039−6048; f) S. Wang, Q. Qian, H. Gong, *Org. Lett.* **2012**, *14*, 3352−3355.

source, 4,4′-di-tert-butyl-2,2′-bipyridine (dtbbpy) and as ligand and Mn as reducing agent (**Scheme 6**, top).[196a] In some cases, addition of 5 mol% of 1,2-Bis(diphenylphosphino)benzene as a co-ligand proved beneficial to achieve high yields. The formation of organomanganese compounds was shown to be unlikely by the competence of the organic reductant 1,1,2,2-tetrakis(dimethylamino)ethylene (TDAE). The protocol was later extended to aryl and alkyl bromides, with the most notable difference being the use of Zn instead of Mn as reductant.[196b]

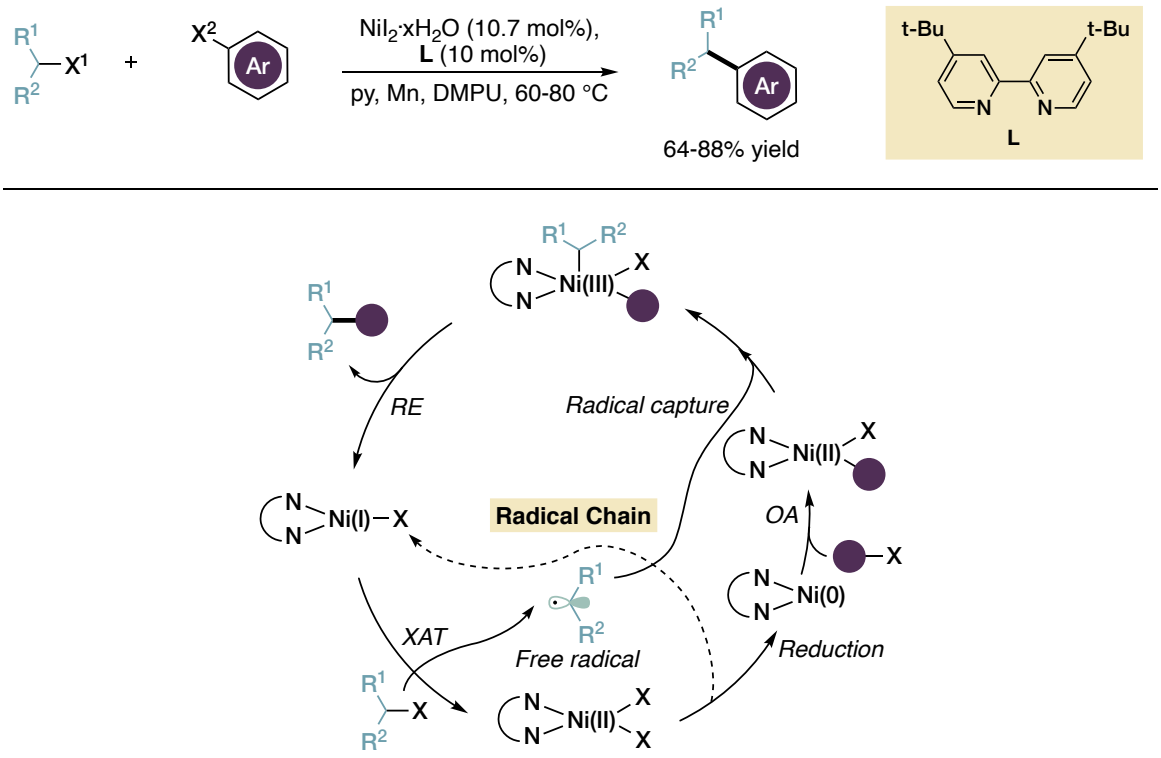

Scheme 6. Top: Weix's original report on the cross electrophile coupling of alkyl and aryl iodides and bromides. Bottom: proposed radical chain mechanism, with alkyl halide activation occurring at a Ni(I)-halide complex.

On the basis of stoichiometric and radical clock experiments and previous results, Weix proposed a "radical chain" mechanism in which alkyl radicals are generated and then trapped at distinct nickel centers, actually preceding the similar proposal by Fu in the context of enantioconvergent cross couplings (**Scheme 6**, bottom).[197] In this scenario,

[197] S. Biswas, D. J. Weix *J. Am. Chem. Soc.* **2013**, *135*, 16192−16197.

a Ni(II)-aryl intermediate is formed fist, by oxidative addition of Ni(0) to the aryl iodide. A Ni(I)-halide complex is responsible for the activation of the alkyl partner, producing a radical that is then trapped at the Ni(II)-aryl species to yield the pivotal Ni(III) intermediate that evolves towards the product, regenerating Ni(I), that can be reduced to Ni(0) by the metal reductant. Selectivity arises from the different activation modes, with faster reaction of the Csp^2 electrophile at Ni(0) and selective formation of alkyl radicals over aryl ones at Ni(I).

Very interestingly, the much less basic conditions than those needed for the transmetalation of preformed nucleophiles allow the coupling in the presence of acidic or electrophilic functionalities (free phenols, amines, alcohols, triflates, acetates), as well as common cross-coupling handles such as C-B, C-Sn and C-Si bonds, permitting great functional group tolerance. Moreover, the presence of a stoichiometric reductant permits the use of easy-to-handle Ni(II) precatalysts and the reactions can be run under air atmosphere.[196b]

Another kind of possible mechanism, more similar to the "radical rebound" one, was proposed by Gong in the XEC of acid chlorides and anhydrides with alkyl iodides and bromides (**Scheme 7**, top and middle).[198]

[198] a) F. Wu, W. Lu, Q. Qian, Q. Ren, H. Gong, *Org. Lett.* **2012**, *14*, 3044−3047. b) H. Yin, C. Zhao, H. You, K. Lin, H. Gong, *Chem. Commun.* **2012**, *48*, 7034−7036.

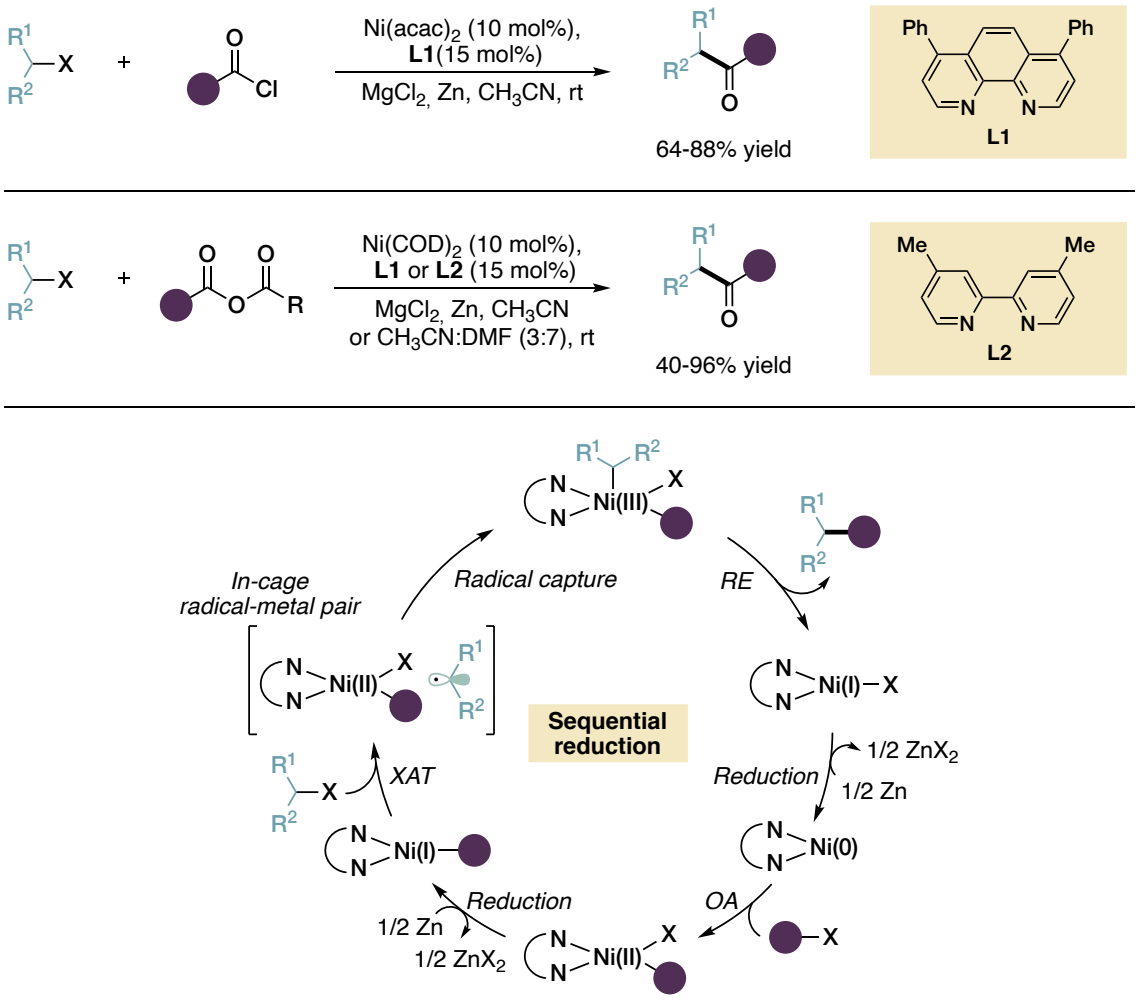

Scheme 7. Top: ketone synthesis by XEC between alkyl halides (X = Cl, Br, I) and acid chlorides. Middle: analogous protocol by using acid anhydrides. In this case, **L1** in pure CH_3CN is used for alkyl iodides, while alkyl bromides require **L2** and a CH_3CN:DMF mixed solvent system. Bottom: "sequential reduction" mechanism proposed by Gong for this coupling. Note that activation of the alkyl halide occurs at a Ni(I) carbyl species, with subsequent in-cage radical recombination.

In this "sequential reduction" mechanism, the Csp^2 electrophile reacts with Ni(0) to form a Ni(II) species that is reduced to Ni(I). This Ni(I)-carbyl complex (in contrast to an halide complex) is responsible for the single-electron activation of the alkyl partner, producing a radical that is trapped at the same Ni(II) center, ultimately leading to product formation[199] (**Scheme 7**, bottom). DFT calculations for both "sequential reduction" and "radical chain" mechanisms were performed by the same group for the

[199] D. A. Everson, D. J. Weix, *J. Org. Chem.* **2014**, *79*, 4793−4798.

XEC between aryl iodides and tertiary bromides, and showed very similar energetics, not allowing a clear differentiation between the two.[200]

Diao and coworkers realized an intramolecular 1,2-difunctionalization of bromide tethered alkenes via XEC with (hetero)aryl and alkyl bromides, iodides and mesylates towards functionalized cyclopentane and cyclohexane scaffolds (**Scheme 8**, top). Zn was used as the reductant in combination with $NiBr_2$·glyme and 1,10-phenantroline in DMA (*N*,*N*-dimethylacetamide) solvent. Almost quantitative yields are obtained for five-membered rings with aromatic electrophiles, while aliphatic halides of six-membered rings (presenting slower cyclization rates) lead to poorer performances. Confirming the pivotal importance of the right ligand and the quite high sensitivity to even minor modifications in this kind of chemistry, subtle differences in the ligand scaffold cause a complete switch in chemoselectivity. In particular, dimerization of the cyclized alkene moiety without trapping of the electrophile is obtained in quantitative yield when 4,4′-di-tert-butyl-2,2′-bipyridine (dtbbpy) is used in place of 1,10-phenantroline.[201]

[200] X. Wang, G. Ma, Y. Peng, C. E. Pitsch, B. J. Moll, T. D. Ly, X. Wang, H. Gong, *J. Am. Chem. Soc.* **2018**, *140*, 14490−14497.

[201] Y. Kuang, X. Wang, D, Anthony, T. Diao, *Chem. Commun.* **2018**, *54*, 2558−2561.

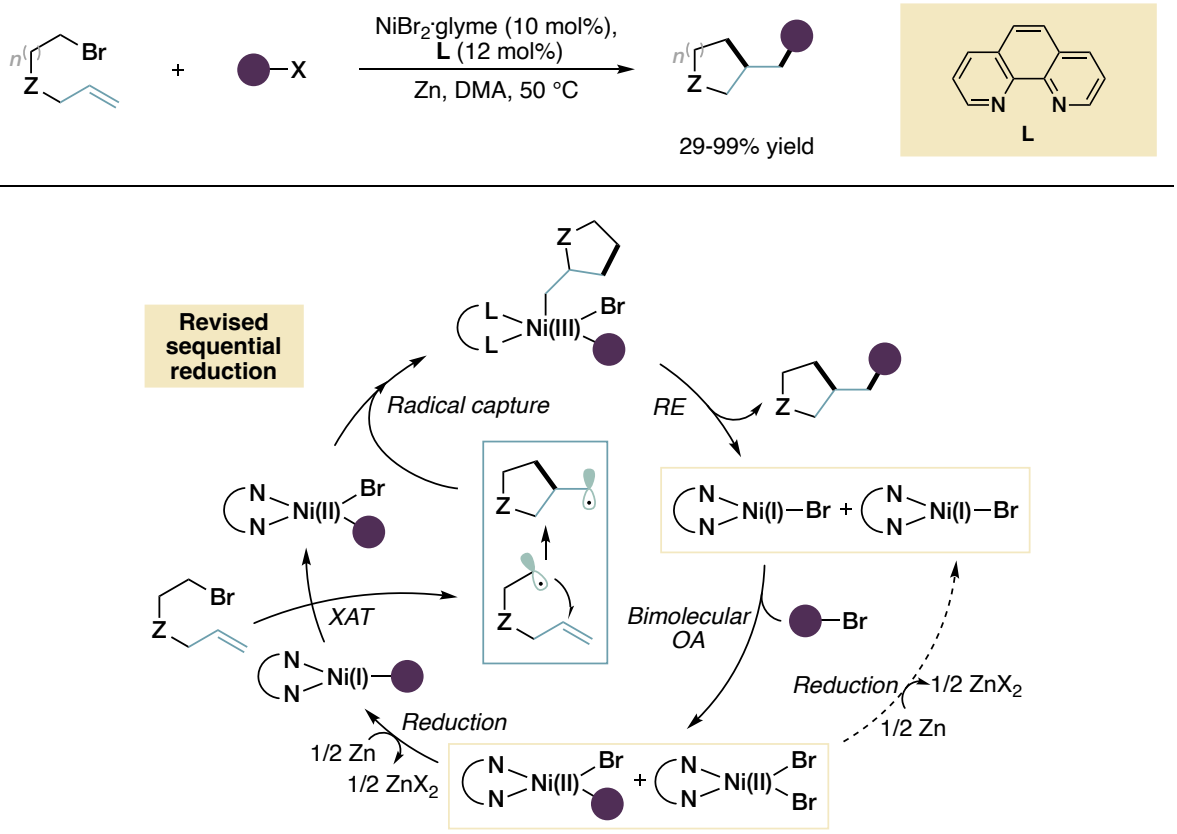

Scheme 8. Top: Diao's intramolecular difunctionalization of alkenes via XEC. Z = O, NTs, $C(CO_2Et)_2$. Bottom: proposed "revised sequential reduction" mechanism. The main features are: Ni(0) is not formed, and oxidative addition involves two distinct Ni(I)-halide centers (via several possible pathways); the fact that radicals produced at a Ni(I)-carbyl center do not undergo in-cage recombination, and instead engage a free-radical 5(6)-*exo*-trig cyclization, followed by the capture of the resulting alkyl radical in a fashion similar to the "radical chain" scenario.

An excellent mechanistic investigation (using model substrates bromobenzene and *N*-allyl-*N*-(2-bromoethyl)-4-methylbenzenesulfonamide) was carried out, with the heterogeneous reduction by Zn found to be rate determining.[202] Interestingly, by spectroscopical, electrochemical, EPR and NMR studies the product of reduction was found to be a [(phen)Ni(I)Br] complex, and Ni(0) does not seem to be involved. This complex reacts with an aryl bromide three times faster than with an alkyl bromide, and stoichiometric reaction with bromobenzene yields a mixture of [(phen)Ni(II)Br_2] and [(phen)Ni(II)PhBr]. This could proceed via a bimolecular oxidative addition involving two nickel centers, or by oxidative addition at Ni(I) followed by comproportionation

[202] Q. Lin, T. Diao, *J. Am. Chem. Soc.* **2019**, *141*, 17937−17948.

of the resulting [(phen)Ni(III)PhBr$_2$] with [(phen)Ni(I)Br]. Very recently, MacMillan and Bird have proved by pulse radiolysis and spectroelectrochemistry that OA from [(dtbbpy)Ni(I)Br] towards aryl iodides is fast, while its dimer [(dtbbpy)Ni(I)Br]$_2$ is unreactive.[203] Interestingly, they found that comproportionation of Ni(0) and Ni(II) under synthetically relevant conditions occurs rapidly, so even that reactions in which Ni(0) is reached could proceed via Ni(I) intermediates, at least when aryl iodides are employed. In a recent mechanistic study, Nocera also demonstrated the relevance of Ni(I)-X complexes as active species for oxidative addition in the Ni-catalyzed etherification of aryl bromides, and found their dimerization with Ni(II)-X$_2$ to yield an inactive dimer. Moreover, the data suggest that a deleterious comproportionation of the active Ni(I) and Ni(III) complexes, favored at high metal concentrations, leads to off-cycle Ni(II) species.[204] In Diao's study, the reactivity of the Ni(II) aryl complex towards alkyl bromide and its reduction were investigated, concluding that a Ni(I)-aryl complex was responsible for generation of the radicals that were determined to escape the solvent cage, so that generation and trapping at different Ni(II) centers should be operating, although this aspect was not fully addressed. Interestingly, while [(phen)Ni(I)Br] is a metal centered radical, [(phen)Ni(I)Mes] is a ligand centered radical species. The overall results are in contrast with the previously proposed preferential activation of alkyl halides at Ni(I)-halide complexes. Altogether, a "revised sequential reduction" mechanism was proposed (**Scheme 8**, bottom). Selectivity arises from the different rates of reaction of Ni(I)-halide and Ni(I)-aryl complexes towards the two electrophiles, the first reacting faster than the second with aryl halides likely due to steric reasons, while halogen abstraction from the second is faster due to its higher electron density.

Anyway, Ni(I)-halide species (or their dimers) do be competent in reaction with Csp^3 electrophiles, as observed in this and previous works and supported by excellent organometallic investigations by Hazari and coworkers.[205] Altogether, the sequential

[203] N. A. Till, S. Oh, D. W. C. MacMillan, M. J. Bird, *J. Am. Chem. Soc.* **2021**, *143*, 9332–9337.
[204] R. Sun, Y. Qin, S. Ruccolo, C. Schnedermann, C. Costentin, D. G. Nocera, *J. Am. Chem. Soc.* **2019**, *141*, 89−93.
[205] M. M. Beromi, G. W. Brudvig, N. Hazari, H. M. C. Lant, B. Q. Mercado, *Angew. Chem. Int. Ed.* **2019**, *58*, 6094–6098.

reduction and radical rebound mechanisms above-depicted (with possible minor variations) appear to be fairly accurate, and recent works regarding reductive nickel catalysis routinely invoke one of the two kinds. Interestingly, stoichiometric studies from different authors show that in some cases preformed Ni(II)-acyl or aryl complexes are reactive towards Csp^3 halides and can give XEC products in the absence of reductant, probably via their *in situ* disproportionation to Ni(I)-halide (and Ni(III)) species. The success of this kind of experiment, or the competence of catalytic Ni(0) in the absence of reductant, can be used to support a radical rebound mechanism, whereas if a sequential reduction mechanism is operating, no product should be observed under these conditions.[206]

Overall, it is evident that the machinery of this reactions can be very complex, reasonably dependent on substrates, ligands, reductants and additives (metal halide salts are frequently employed), and mechanistic studies are complicated by the fleeting nature of low valent Ni species.[203] A great number of XEC methodologies have been successfully realized in the last 10 years, including enantioconvergent and enantioselective ones, employing various kinds of Csp^2 and Csp^3 electrophiles.[123c,207]

A particular class of Csp^3 electrophiles that has found extensive use in nickel cross-coupling is represented by *N*-acyloxyphthalimides (RAEs), with one example of their use shown in chapter 1.3. Introduced by Baran in 2016,[208] these compounds are activated via single electron reduction and fragment releasing a phthalimide anion, CO_2 and an alkyl radical, providing a way to access radicals from carboxylic acids, and have been widely used in C-C bond forming protocols in both catalyzed (metal based and not) and uncatalyzed processes.[209]

---

[206] H. Ji, D. Lin, L. Tai, X. Li, Y. Shi, Q. Han, L.-A. Chen, *J. Am. Chem. Soc.* **2022**, *144*, 23019−23029 and refs therein.
[207] a) M. J. Goldfogel, L. Huang, D. J. Weix, *Cross Electrophile Coupling: Principles and New Reactions* in *Nickel Catalysis in Synthesis: Methods and Reactions*, Ed: S. Ogoshi, Wiley-VCH: Weinheim, **2020**, pp. 183-222; b) K. E. Poremba, S. E. Dibrell, S. E. Reisman, *ACS Catal.* **2020**, *10*, 8237–8246.
[208] J. Cornella, J. T. Edwards, T. Qin, S. Kawamura, J. Wang, C.-M. Pan, R. Gianatassio, M. Schmidt, M. D. Eastgate, P. S. Baran, *J. Am. Chem. Soc.* **2016**, *138*, 7, 2174–2177
[209] a) S. Murarka, *Adv. Synth. Catal.* **2018**, *360*, 1735 –1753; b) S. K. Parida, T. Mandal, S. Das, S. K. Hota, S. D. Sarkar, S. Murarka, *ACS Catal.* **2021**, *11*, 1640−1683; c) P. Niu, J. Li, Y. Zhang, C. Huo, *Eur. J. Org. Chem.* **2020**, 5801–5814.

Weix reported their use in Ni-catalyzed XEC with aryl iodides, using methyl, primary and secondary radicals (**Scheme 9**, top).[210] A successful employment of this system with an acid chloride in place of the aryl halide was also documented. As for the mechanism, the authors propose that a Ni(I)-aryl species is most likely the active species in the reduction of the RAE electrophile, although no conclusive evidence was provided.

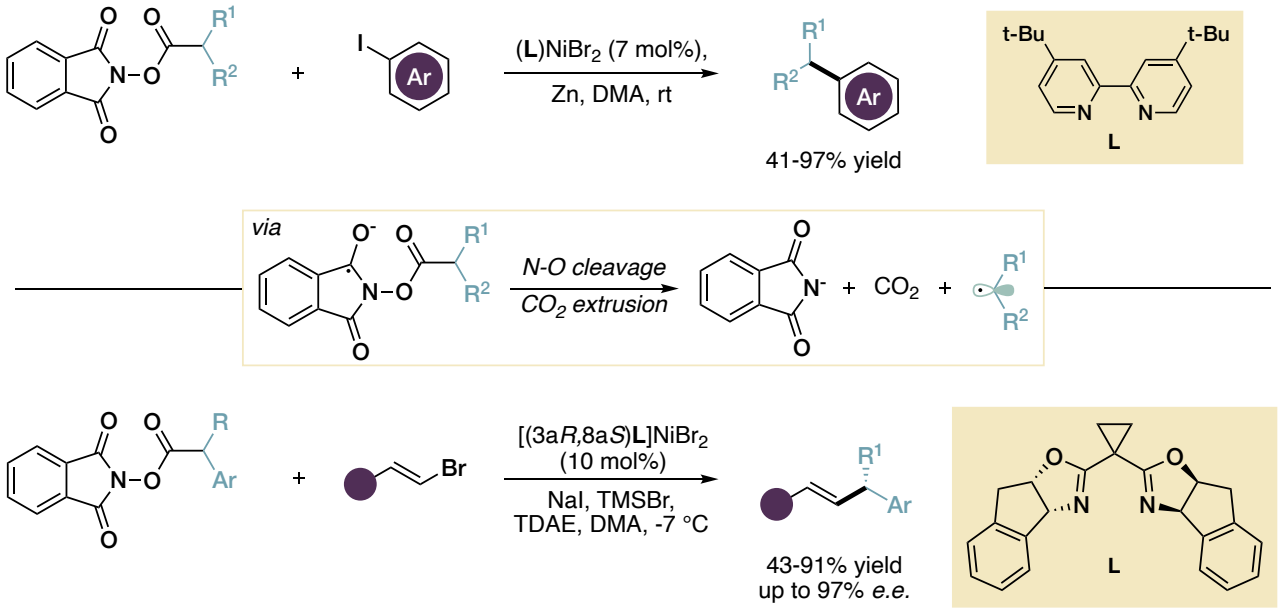

Scheme 9. Top: Weix's protocol for the XEC between aryl iodides and *N*-acyloxyphthalimides. Bottom: Sarah Reisman's enanantioconvergent XEC between vinyl bromides and phenylacetic acids-derived RAEs.

The Reisman group used RAEs in an enantioconvergent XEC with vinyl bromides, employing a BOX (bis-oxazoline) ligand and TDAE as organic reductant.[211] As in Fu's report, the reaction seems to be limited to stabilized radicals, and only benzylic electrophiles were engaged (**Scheme 9**, bottom).

[210] K. M. M. Huihui, J. A. Caputo, Z. Melchor, A. M. Olivares, A. M. Spiewak, K. A. Johnson, T. A. DiBenedetto, S. Kim, L. K. G. Ackerman, D. J. Weix, *J. Am. Chem. Soc.* **2016**, *138*, 5016−5019.
[211] N. Suzuki, J. L. Hofstra, K. E. Poremba, S. E. Reisman, *Org. Lett.* **2017**, *19*, 8, 2150–2153.

Structurally related *N*-alkoxyphthalimides (OPthth), in which the carbonyl moiety is replaced by a CR_2 unit, are similarly reactive towards reduction, but in this case the radical anion fragments by cleavage of the weak N-O bond to yield an alkoxy radical (**Scheme 10**, top).[212]

Alkoxy radicals can evolve via different pathways, namely: addition to electronrich double bonds; β-fragmentation to yield C-centered radicals; intermolecular hydrogen atom transfer (HAT) with hydridic and/or weak C-H bonds, intramolecular 1,*n*-HAT processes yielding C-centered radicals (**Scheme 10**, bottom).[213]

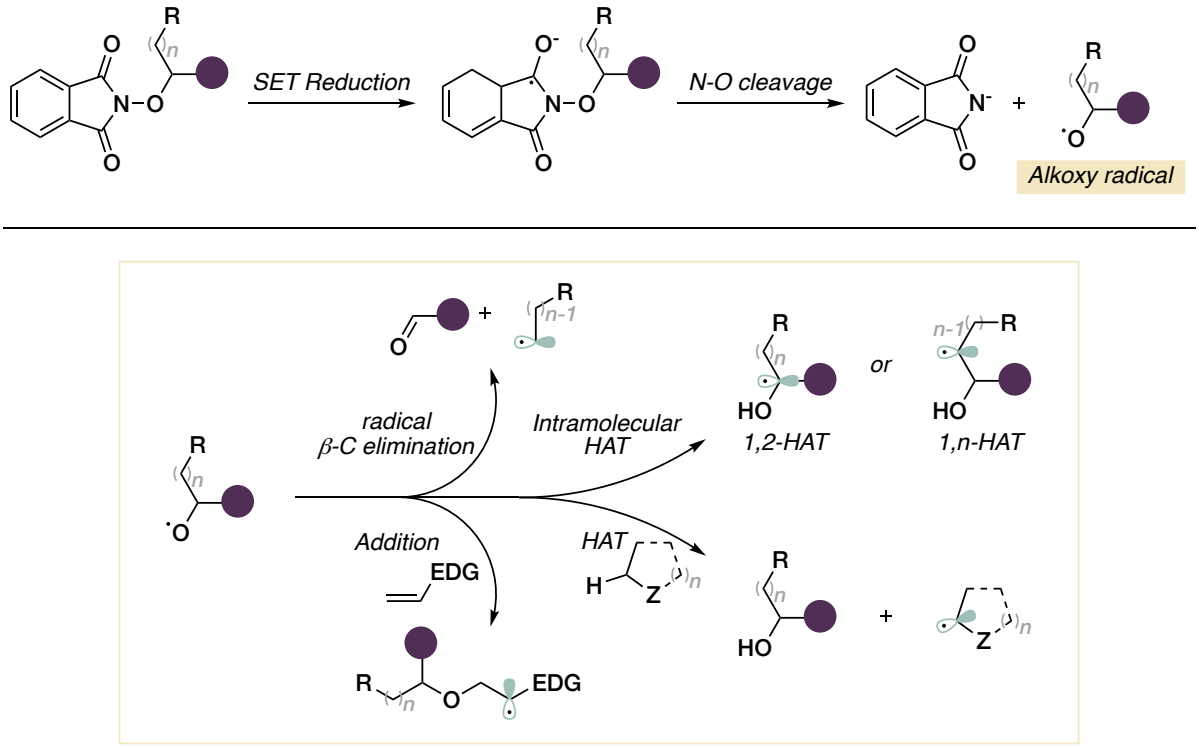

Scheme 10. Top: Reduction of *N*-alkoxyphthalimides to yield alkoxy radicals. Bottom: reactive pathways of alkoxy radicals.

[212] a) S. Kim, T. A. Lee, Y. Song, *Synlett* **1998**, *1998*, 471–472; b) A. S. Budnikov, I. B. Krylov, A. V. Lastovko, B. Yu, A. O. Terent'ev, *Asian J. Org. Chem.* **2022**, *11*, e2022002.

[213] a) L. Chang, Q. An, L. Duan, K. Feng, Z. Zuo, *Chem. Rev.* **2022**, *122*, 2429−2486; b) M. Murakami, N. Ishida, *Chem. Lett.* **2017**, *46*, 1692–1700; c) E. Tsui, H. Wang, R. R. Knowles, *Chem. Sci.* **2020**, *11*, 11124–11141; d) J. M. Mayer, *Acc. Chem. Res.* **2011**, *44*, 36–46; e) F. Liu, S. Ma, Z. Lu, A. Nangia, M. Duan, Y. Yu, G. Xu, Y. Mei, M. Bietti, K. N. Houk, *J. Am. Chem. Soc.* **2022**, *144*, 6802–6812; f) A. Ruffoni, R. C. Mykura, M. Bietti, D. Leonori, *Nat. Synth.* **2022**, *1*, 682–695; g) A. Hu, J.-J. Guo, H. Pan, Z. Zuo, *Science* **2018**, *361*, 668-672; h) C. Banoun, F. Bourdreux, E. Magnier, G. Dagousset, *Org. Lett.* **2021**, *23*, 8926–8930.

Martin made use of the β-fragmentation reactivity to realize a nickel-photoredox catalyzed XEC between OPthth reagents, prepared from the corresponding alcohols, and (hetero)aryl or alkyl bromides using and Hantzsch ester (HE) as a reductant (**Scheme 11**).[214] The reaction works for α-heteroatom, secondary, strained tertiary and stabilized primary radicals and has great functional group compatibility. While dtbbpy was used as ligand for aryl bromides, the use alkyl bromides required a tridentate terpyridine ligand, probably to suppress β-hydride elimination events. Preliminary mechanistic investigations suggest that Ni is not involved in the reduction of OPhth, and instead only traps the radicals generated by reduction of OPhth from the HE, likely proceeding via formation of an EDA (electron donor-acceptor) complex.[215]

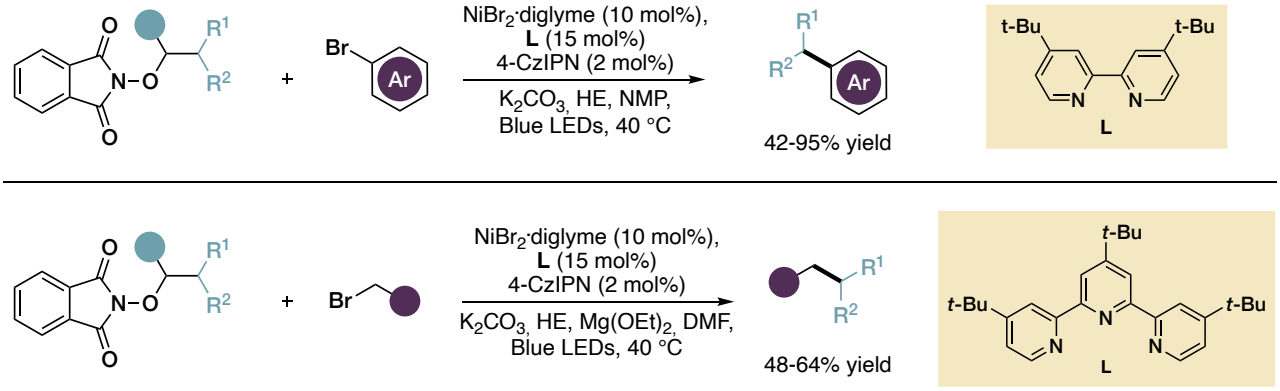

Scheme 11. Martin's photochemical methodology for the Csp^3-Csp^2 and Csp^3-Csp^3 XEC of *N*-alkoxyphthalimides (OPhth) and bromides. Radicals are formed from OPhth reagents via β-carbon elimination. Top: conditions for the reaction of (hetero)aryl bromides. Bottom: conditions for the reaction of alkyl bromides. Note the use of a tridentate ligand in this case. HE = Hantzsch ester. 4-CzIPN = 1,2,3,5-Tetrakis(carbazol-9-yl)-4,6-dicyanobenzene (photocatalyst).

Aggarwal used *N*-trifluoroethoxypthalimide in combination with *B*-chlorocathecolborane (BcatCl) as HAT reagent and B_2cat_2 (Bis(catecholato)diboron) as boron source in a photocatalyzed Csp^3-H borylation of unactivated alkanes. An

[214] F. Cong, X.-Y. Lv, C. S. Day, R. Martin *J. Am. Chem. Soc.* **2020**, *142*, 20594−20599.
[215] J. Zhang, Y. Li, R. Xu, Y. Chen, *Angew. Chem. Int. Ed.* **2017**, *56*, 12619–12623.

adduct between the *O*-trifluoroethoxy radical formed by reduction of *N*-trifluroethoxypthalimide and BcatCl is thought to be the active species (**Scheme 12**).[216]

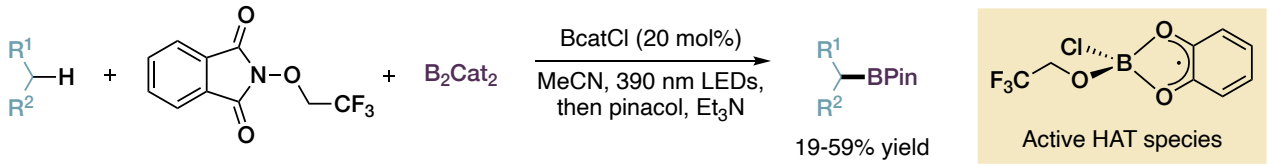

Scheme 12. Csp^3-H borylation of unactivated alkanes using *N*-trifluoroethoxypthalimide as HAT reagent. Yields are generally low, but the methodology provides access to borylated alkanes very difficult to obtain otherwise, and an ample scope including functionalized substrates was demonstrated.

The reaction provides great selectivity for aliphatic over aromatic C-H bonds due the different C-H bond strengths, thus providing a complementary reactivity to the more common aromatic C-H borylation.

Whereas 1,5-HAT processes, proceeding via a six-membered cyclic transition state, are facile and found extensive synthetic use,[217] intramolecular 1,*n*-HAT for *n* different from 5 are more challenging, although several examples exist, mainly for $n = 4$-8.[218] In particular, 1,2-HAT processes are predicted to be much more difficult, requiring a strained three-membered TS with a high energy barrier of above 30 kcal/mol for the methoxy radical.[219,213a.] First EPR studies demonstrated this process to be feasible and rather fast in aqueous medium,[220] and later work demonstrated the same in nucleophilic alcoholic solvents, proposing the involvement of one hydrogen bonding alcohol molecule in the process.[221] Later work by Francisco calculated for the methoxy radical

---

[216] C. Shu, A. Noble, V. K. Aggarwal, *Nature* **2020**, *586*, 714–719.

[217] a) W. Guo, Q. Wang, J. Zhu, *Chem. Soc. Rev.* **2021**, *50*, 7359–7377; b) G. Majetich, K. Wheless, *Tetrahedron* **1995**, *51*, 7095-7129; c) J. Robertson, J. Pillaia, R. K. Lush, *Chem. Soc. Rev.* **2001**, *30*, 94–103.

[218] a) M. Nechab, S. Mondal, M. P. Bertrand, *Chem. Eur. J.* **2014**, *20*, 16034–16059; b) S. Sarkar, K. P. S. Cheung, V. Gevorgyan, *Chem. Sci.* **2020**, *11*, 12974–12993.

[219] a) S. Saebø ,L. Radomand, H. F. Schaefer III, *J. Chem. Phys.* **1983**, *78*, 845;b) L. Batt, J. P. Burrows, G. N. Robinson, *Chem. Phys. Lett.* **1981**, *78*, 467–470; c) X. L. Huang, J. J. Dannenberg, *J. Org. Chem.* **1991**, *56*, 5421–5424; d) H. Tachikawa, S. Lunell, C. Tornkvist, A. Lund, *THEOCHEM* **1994**, *110*, 25; e) M. L. Poutsma, *J. Org. Chem.* **2007**, *72*, 150–161 and references therein.

[220] a) B. C. Gilbert, R. G. G. Holmes, H. A. H. Laue, R. O. C. Norman, *J. Chem. Soc., Perkin Trans. 2* **1976**, 1047−1052; b) A. J. Dobbs, B. C. Gilbert, H. A. H. Laue, R. O. C. Norman, *J. Chem. Soc., Perkin Trans. 2* **1976**, 1044−1047.

[221] a) P. E. Elford, B. P. Roberts, *J. Chem. Soc., Perkin Trans. 2* **1996**, 2247−2256; b) K. G. Konya, T. Paul, S. Lin, J. Lusztyk, J., K. U. Ingold, *J. Am. Chem. Soc.* **2000**, *122*, 7518−7527.

that in gas phase, water, formic acid and sulfuric acid could successfully engage in hydrogen bonded TSs to reduce the barrier to 25.7, 4.2 and 2.3 kcal/mol respectively.[222] Work on 1,2 and 1,3-HAT processes for thiyl radicals also supports the feasibility of the process and the involvement of water.[223]

Very recently, Chen *et al.* reported the successful implementation of 1,2-HAT reactivity of alkoxy radicals resulting from OPthth in a photocatalyzed Giese reaction to accomplish the hydroxyalkylation of allylic sulfones, using methanol as solvent (**Scheme 13**).[224] The process reproduces a formal allylation of aldehydes, and the authors highlight that allylated products deriving from problematic aldehydes, such as gaseous and toxic trifluoroacetaldehyde, can be easily accessed by this method.

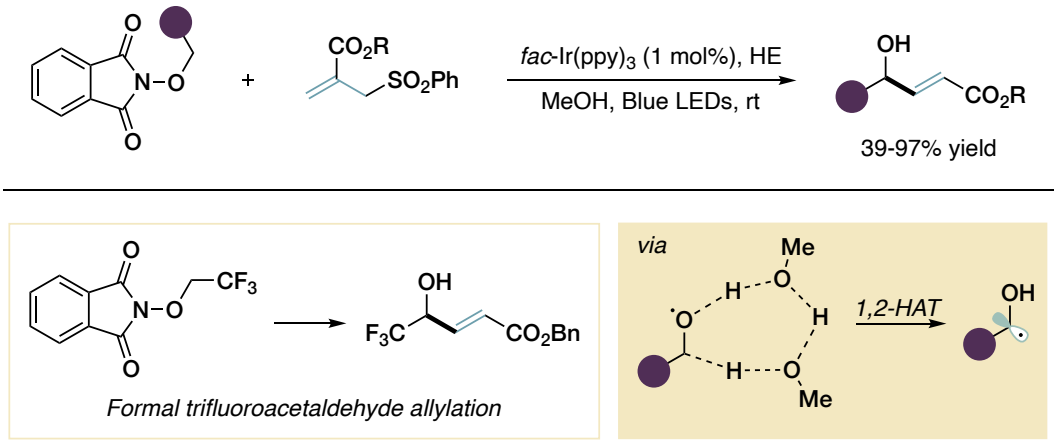

Scheme 13. 1,2-HAT enabled formal allylation of aldehydes using *N*-alkoxyphthalimides as radical precursors in a Giese reaction with allylic sulfones. The computed TS for the methanol promoted 1,2-HAT event is shown. *fac*-Ir(ppy)3 = Tris[2-phenylpyridinato-C^2,*N*]iridium(III).

The 1,2-HAT mechanism was supported by DFT calculations that showed an isomerization barrier of only 6 kcal/mol when two methanol molecules where included in the TS. The authors also provided further argumentations in favor of their proposed mechanism in a separate study.[225]

[222] R. J. Buszek, A. Sinha, J. S. Francisco, *J. Am. Chem. Soc.* **2011**, *133*, 2013−2015.
[223] C. Schçneich, O. Mozziconacci, W. H. Koppenol, T. Nauser, *Isr. J. Chem.* **2014**, *54*, 265–271.
[224] J. Zhang, D. Liu, S. Liu, Y. Ge, Y. Lan, Y. Chen, *iScience* **2020**, *23*, 100755.
[225] D. Liu, J. Zhang, Y. Chen, *Synlett* **2021**, *32*, 356-361.

Despite most literature on the topic has dealt with the use of protic, hydrogen bonding solvents and that this requirement is proposed as stringent for the feasibility of 1,2-HAT events, a handful of methodologies in polar aprotic solvents that seem to proceed via mechanisms that involve this isomerization have also emerged. Gangguo Zhu and coworkers reported a series of photocatalytic protocols in which a pivotal 1,2-HAT shift was proposed, in CH_3CN, DMSO and DMA as solvent.[226] In a recent report, the same group performed DFT calculations showing that a DMA-assisted-1,2-HAT shift was operating, with a free energy barrier of 7.6 kcal/mol for a considered cyclopentenyl alcohol. Assistance by CH_3CN was less favorable, with a barrier of 18.4 kcal/mol.[227] An and coworkers reported the use of 1,2-HAT chemistry in a photocatalyzed XEC reaction between *N*-benzyloxyphthalimides and cyanopyridines to access di(hetero)arylmethanols.[228] The reaction proceeds via isomerization of the benzyloxy radical derived from reduction of OPhth to yield a C-centered α-hydroxy-α-aryl radical that is trapped by the persistent radical anion formed by SET reduction of the cyanoarene from the same Ir(II) species (or by direct ipso-addition to the cyanopyridine) (**Scheme 14**).

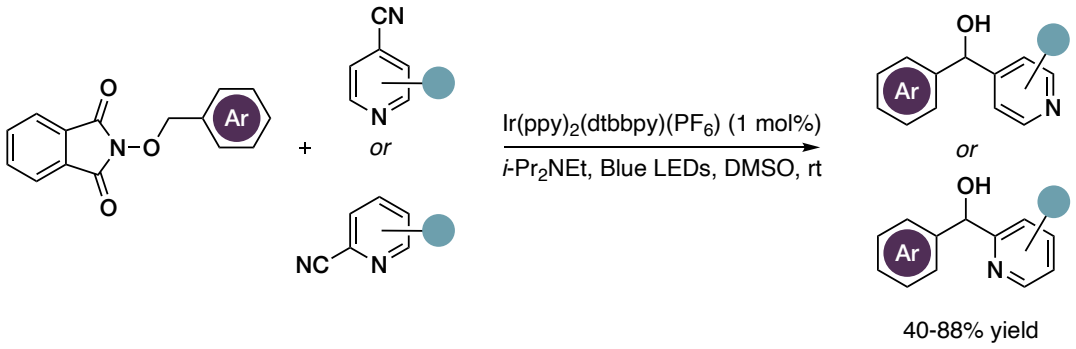

Scheme 14. Di(hetero)arylmethanols synthesis from cyanopyridines by photocatalytic activation of *N*-benzyloxy phthalimides.

[226] a) C. Che, Q. Huang, H. Zheng, G. Zhu, *Chem. Sci.* **2016**, *7*, 4134–4139; b) Y. Chen, C. Shu, F. Luo, X. Xiao, G. Zhu, *Chem.Commun.* **2018**, *54*, 5373–5376; c) Y. Zhou, Z. Xiong, J. Qiu, L. Kong, G. Zhu, *Org. Chem. Front.*, **2019**, *6*, 1022.
[227] H. Zhu, H. Zhen, J. Zhang, J. Feng, L. Kong, F. Zhang, X. Xue, G. Zhu, *Chem. Sci.* **2021**, *12*, 11420–11426.
[228] L.-J. Zhong, H.-Y. Wang, X.-H. Ouyang, J.-H. Li, D.-L. An, *Chem. Commun.* **2020**, *56*, 8671–8674.

Water was proposed to assist the process, given the lower yields obtained in thoroughly dried DMSO.

5.2 Aim of the project

Fascinated and encouraged by the previous reports on 1,2-HAT chemistry with OPhth and given our interest in Ni-catalyzed couplings and their mechanisms, we decided to pursue a formal arylation of trifluoroacetaldehyde with *N*-trifluoroethoxyphthalimide and aryl iodides. The reaction would yield valuable α-aryl-α-trifluoromethyl alcohols, that constitute a volume of biologically and pharmacologically active compounds and useful building blocks in medicinal chemistry (**Figure 3**, top).[229]

The state-of-the-art methodologies for assembling this kind of scaffold rely exclusively on polar chemistry, resulting in two predominant disconnecting approaches. In particular, the dominant one is the direct nucleophilic trifluoromethylation of carbonyl compounds (mainly aldehydes), that has been extensively investigated and accomplished by use of the Ruppert-Prakash reagent ($TMSCF_3$) and other analogous systems (i.e. ICF_3/TDAE, HCF_3/base, B-CF_3 adducts, CF_3CHO hydrate, hemiaminals and S-based transfer reagents (**Figure 3**, middle, pathway a).[230] However, the relatively high cost and limited choice of "F_3C^-" synthons still represent major shortcomings, especially towards large scale applications. In addition, several of these protocols employ strongly basic conditions, incompatible with acidic substrates and may require cryogenic temperatures due to the instability of trifluoromethide anion.

---

[229] Z.-C. Shi, A. Devasagayaraj, K. Gu, H. Jin, B. Marinelli, L. Samala, S. Scott, T. Stouch, A. Tunoori, Y. Wang, Y. Zang, C. Zhang, S. D. Kimball, A. J. Main, W. Sun, Q. Yang, A. Nouraldeen, X.-Q. Yu, E. Buxton, S. Patel, N. Nguyen, J. Swaffield, D. R. Powell, A. Wilson, Q. Liu, *J. Med. Chem.* **2008**, *51*, 3684–3687; b) D. O'Shea, C.-Y. Chen, D. Gauvreau, F. Gosselin, G. Hughes, C. Nadeau, R. P. Volante *J. Org. Chem.* **2009**, *74*, 1605–1610; c) D. R. Goldberg, S. De Lombaert, R. Aiello, P. Bourassa, N. Barucci, Q. Zhang, V. Paralkar, A. J. Stein, M. Holt, J. Valentine, W. Zavadoski, *Bioorg. Med. Chem. Lett.* **2017**, *27*, 413–419.

[230] G. K. S. Prakash, A. K. Yudin, *Chem. Rev.* **1997**, *97*, 757–786; b) G. K. S. Prakash, M. Mandal, *J. Fluorine Chem.* **2001**, *112*,123–131; c) R. P. Singh, J. N. M. Shreeve, *Tetrahedron*, **2000**, *56*, 7613–7632; d) J.-A. Ma, D. Cahard, *J. Fluorine Chem.* **2007**, *128*, 975–996; e) N. Shibata, S. Mizuta, H. Kawai, *Tetrahedron: Asymmetry* **2008**, *19*, 2633–2644; f) A. D. Dilman, V. V. Levin, *Eur. J. Org. Chem.* **2011**, 831–841; g) G. K. S. Prakash, P. V. Jog, P. T. D. Batamack, G. A. Olah, *Science*, **2012**, *338*, 1324–1327; h) G. K. Surya Prakash, Z. Zhang, F. Wang, S. Munoz, G. A. Olah, *J. Org. Chem.* **2013**, *78*, 3300–3305; i) J. B. Geri, M. M. W. Wolfe, N. K. Szymczak, *Angew. Chem. Int. Ed.* **2018**, *57*, 1381–1385; j) H. Jia, A. P. Häring, F. Berger, L. Zhang, T. Ritter, *J. Am. Chem. Soc.* **2021**, *143*, 7623–7628.

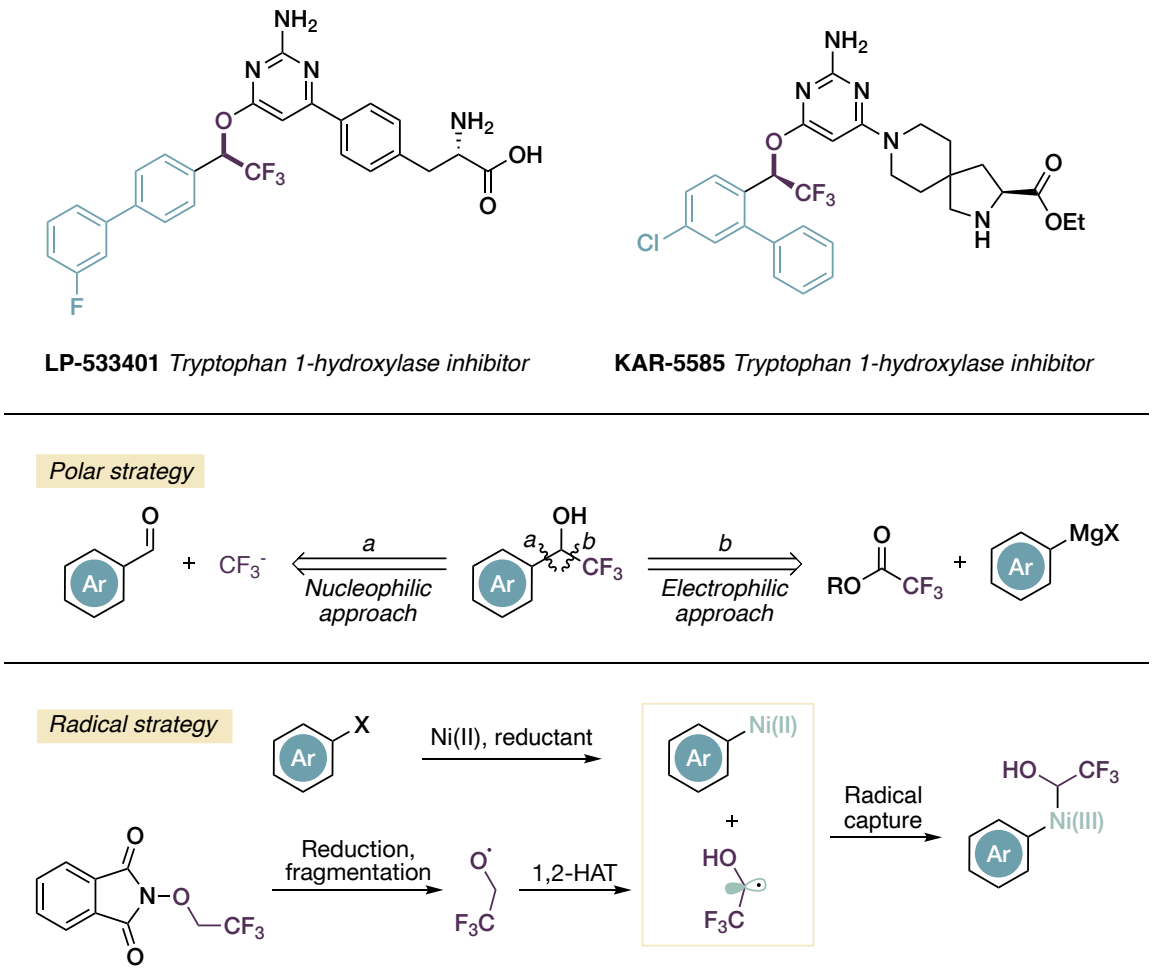

Figure 3. Top: examples of biologically active α-aryl-α-trifluoromethyl alcohol derivatives; Middle: established polar disconnections *en route* to α-aryl-α-trifluoromethyl alcohols; Bottom: present radical-based nickel catalyzed strategy.

A complementary electrophilic approach, involving the addition of organometallic reagents to trifluoroacetates, is also viable (**Figure 3**, middle, pathway b).[231] However, the reaction displays limited scope, stringent substrate-depending conditions and the requirement of highly reactive organometallics in stoichiometric amount do affect the generality and feasibility of this method. Finally, direct Friedel-Crafts-like protocols

[231] a) T. Yamazaki, T. Terajima, T. Kawasaki-Taskasuka, *Tetrahedron* **2008**, *64*, 2419–2424; b) K. Funabiki, A. Hayakawa, R. Kani, T. Inuzuka, Y. Kubota, *Eur. J. Org. Chem.* **2019**, 5978–5984; c) R. Kani, T. Inuzuka, Y. Kubota, K. Funabiki, *Eur. J. Org. Chem.* **2020**, 4487–4493.

involving CF_3CHO derivatives as alkylating agent are limited to electron-rich arenes.[232]

We envisioned a different, radical retrosynthetic strategy in which the *O*-trifluoroethoxy radical formed upon reduction of OPhth under XEC conditions could rearrange, via a 1,2-HAT event, to provide a nucleophilic[233] α-hydroxy-C-centered radical that would react with a Ni(II)-aryl complex formed by oxidative addition of the halide, yielding a Ni(III) that should give the product after RE (**Figure 3**, bottom).

The same kind of radical nucleophilic radical could also be attainable, in principle, via intermolecular HAT on the corresponding alcohol or alkoxide. Indeed, the MacMillan group has shown the utilization of α-hydroxy C-centered radicals formed in this way in a Ni-catalyzed α-arylation of alcohols under photochemical regime.[234] However, trifluoroethanol (TFE) was not engaged in the transformation, perhaps due to the slow kinetics of HAT processes with electrophilic abstractors on fluorinated alcohols/alkoxides.[235]

Therefore, the realization of the titled process would represent the first catalytic strategy to access α-aryl-α-trifluoromethyl alcohols from aryl halides, as well as the first example of utilization of a 1,2-HAT process in the context of Ni catalysis. This unprecedented radical strategy, by turning inexpensive and stable TFE in a formal CF_3CHO equivalent, could offer a significant contribution to the development of sustainable and selective methodologies for the introduction of fluorine-based functional groups in carbon skeletons, a topic that receives ever-growing attention by the entire chemical community[236]

---

[232] a) Y. Gong, K. Kato, H. Kimoto, *Synlett* **1999**, 1403–1404; b) G.-W. Zhang, L. Wang, J. Nie, J.-A. Ma, *Adv. Synth. Catal.* **2008**, *350*, 1457–1463; c) D. A. Borkin, S. M. Landge, A. Török, *Chirality*, **2011**, *23*, 612–616; d) J. Zhang, Y.-J. Chen, L. Zhang, *Synth. Commun.* **2011**, 3045–3052.

[233] a) F. De Vleeschouwer, V. Van Speybroeck, M. Waroquier, P. Geerlings, F. De Proft, *Org. Lett.* **2007**, *9*, 2721–2724; b) F. Parsaee, M. C. Senarathna, P. B. Kannangara, S. N. Alexander, P. D. E. Arche, E. R. Welin, *Nat Rev Chem* **2021**, *5*, 486–499.

[234] J. Twilton, M. Christensen, D. A. DiRocco, R. T. Ruck, I. W. Davies, D. W. C. MacMillan, *Angew. Chem. Int. Ed.* **2018**, *57*, 5369–5373.

[235] a) L. Zhang, J. Cradlebaugh, G. Litwinienko, B. E. Smart, K. U. Ingold, W. R. Dolbier Jr., *Org. Biomol. Chem.* **2004**, *2*, 689–694; b) I. Morozov, S. Gligorovski, P. Barzaghi, D. Hoffmann, Y. G. Lazarou, E. Vasiliev, H. Herrmann, *Int. J. Chem. Kinetic* **2008**, *40*, 174–188.

[236] a) T. Liang, C. N. Neumann, T. Ritter, *Angew. Chem. Int. Ed.* **2013**, *52*, 8214–8264; b) B. Lontaño, A. Postigo, *Org. Biomol. Chem.* **2017**, *15*, 9954–9973; c) R. Szpera, D. F. J. Moseley, L. B. Smith, A. J. Sterling, V. Gouvereur, *Angew. Chem. Int. Ed.* **2019**, *58*, 14824–14848; d) F.-G. Zhang, X.-Q. Wang, Y. Zhou, H.-S. Shi, Z. Feng, J.-A. Ma, I. Marek,

5.3 Results and discussion

At the outset of our investigation, we tested the reaction of *p*-iodotoluene **1a** with **2** (3 eq.) in the presence of various [**L**Ni(II)X_2] complexes as catalysts, either preformed or obtained *in situ* (**Table 1**). To our delight, the use of simple phenanthroline (**L1**) as ligand, DMA solvent and Zn as reductant yielded the desired trifluoromethyl benzyl alcohol **3a** in a modest 36% yield, showing the feasibility of the titled process. Interestingly, while the use of Mn provided the product in much reduced yield (entry 2), organic reductant TDAE resulted in no conversion of both starting materials (entry 3). Both Ni catalyst and reductant (Zn) proved mandatory for product formation. TMSCl was included as an additive (1 eq.) as it consistently provided better reproducibility and faster triggering of the Ni(II) reduction by Zn. In its absence, induction periods and erratic yields could be observed from time to time, so that its role is probably to activate the Zn dust in the heterogeneous process.

Chem. Eur. J. **2020**, *26*, 15378–15396; e) F. Auria-Luna, S. Mohammadi, M. Divari, M. Concepción Gimeno, R. P. Herrera, *Adv. Synth. Catal.* **2020**, *362*, 5275–5300; f) T. T. Bui, W. P. Hong, H.-K. Kim, *J. Fluor. Chem.* **2021**, *247*, 109794; g) X. Wang, J. Lei, Y. Liu, Y. Ye, J. Li, K. Sun, *Org. Chem. Front.* **2021**, *8*, 2079–2109; h) E. A. Meucci, S. N. Nguyen, N. M. Camasso, E. Chong, A. Ariafard, A. J. Canty, M. S. Sanford, *J. Am. Chem. Soc.* **2019**, *141*, 12872–12879; i) Y. Y. See, M. T. Morales-Colón, D. C. Bland, M. S. Sanford, *Acc. Chem. Res.* **2020**, *53*, 10, 2372–2383.

Table 1. Summary optimization of reaction conditions.

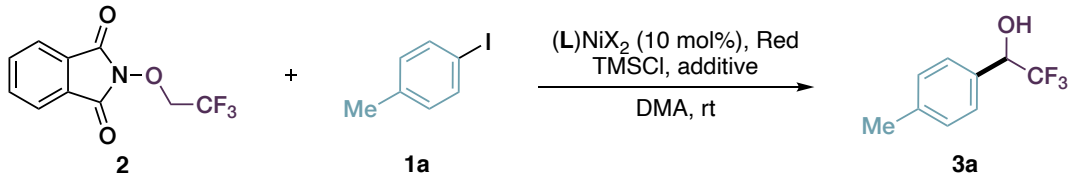

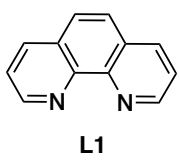
L1

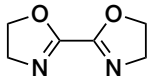
L2

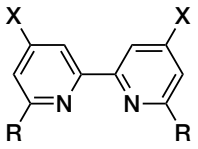

L3: X = OMe, R = H
L4: X = CO_2Me, R = H
L5: X = Ph, R = H
L6: X = tBu, R = H
L7: X = H, R = Me
L10: X = 4-$CF_3(C_6H_4)$

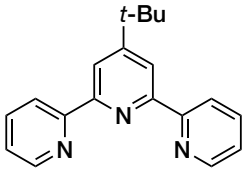

L8

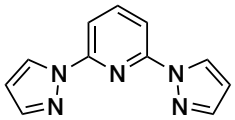

L9

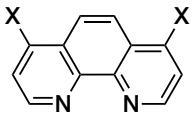

L11: X = Ph
L12: X = OMe

Entry[a]	(**L**)NiX_2	Red / Additive	Time (h)	Yield **3a** (%)[b]
1	(**L1**)$NiCl_2$	Zn / -	16	36
2	(**L1**)$NiCl_2$	Mn / -	16	16
3	(**L1**)$NiCl_2$	TDAE / -	16	0
4[c,d]	(**L2**)$NiCl_2$	Zn / -	16	0
5[c]	(**L3**)$NiCl_2$	Zn / -	16	55
6	(**L3**)$NiBr_2$	Zn / -	16	54
7[c,d]	(**L4**)$NiCl_2$	Zn / -	16	8
8[f]	(**L5**)$NiCl_2$	Zn / -	16	59
9[c]	(**L6**)$NiCl_2$	Zn / -	16	48
10[c,d]	(**L7**)$NiCl_2$	Zn / -	16	0
11[c]	(**L8**)$NiCl_2$	Zn / -	16	5
12	(**L5**)$NiCl_2$	Zn / NaI	2	95 (88)
13	(**L5**)$NiCl_2$	Zn / -	2	30
14[e]	(**L5**)$NiCl_2$	Zn / NaI	2	60

[a] All reactions were set up under N_2 atmosphere in dry DMA ([**1 a**]: 0.2 M, **2**: 3 eq., Red: 2 eq., TMSCl: 1 eq.; additive: 1 eq., cat: 10 mol%, unless otherwise specified). [b] Determined by ^{19}F NMR on the reaction crude with an internal standard ($CF_3C_6H_5$). In brackets, isolated yields after flash chromatography. [c] The catalytic complex was prepared in situ (**L**/$NiCl_2$·glyme: 15/10 mol%). [d] Dehalogenative homocoupling of **1a** was determined as the major product. [e] With reagent grade DMA and under air. Red: reductant.

With DMA as solvent and Zn as reductant, a range of bidentate and tridentate N ligands **L2**–**8** were tested. While bi-oxazoline **L2** and terpyridine ligand **L8** proved ineffective (entries 4, 11), bipyridine ligands displayed variable performance, strongly influenced by electronic as well as steric properties. Specifically, the introduction of methyl groups at the 6,6' positions (**L7**) resulted in the exclusive dehalogenative homocoupling product of **1a**. Bipyridines bearing electron-donating (OMe, **L3** and *t*-Bu, **L6**) or conjugating phenyl groups (**L5**) at the 4,4' positions (i.e. Ph, OMe and *t*Bu) led to increased yields, regardless of the type of counterion on the nickel complex (48–59%, entries 5, 6, 8, 9). Electron-withdrawing substituents such as ester (**L4**) only gave homocoupling of **1a**. Based on these findings, we selected **L5** as the optimal ligand for this XEC.

At this point, we performed an extensive survey of additives, being aware of the profound effects they can have in Ni-catalyzed XEC (see Supplementary data, Chapter 5.5 for an exhaustive list). Pleasingly, the addition of NaI (1 eq.) sped up the reaction enabling **3a** to be obtained in almost quantitative yield in only 2 h when preformed [Ni(**L5**)Cl2] complex was utilized as the catalyst (yield = 88%, entry 12). Finally, the protocol proved very robust, and use of reagent grade DMA under air atmosphere provided **3a** in synthetically useful 60% yield (2 h, entry 14). The beneficial role of halide salts is well documented in reductive Ni-based XEC reactions, and although the origin of this effect is still under debate, several possibilities have been proposed.[237]

[237] a) M. R. Prinsell, D. A. Everson, D. J. Weix, *Chem. Commun.* **2010**, *46*, 5743-5745; b) A. H. Cherney, S. E. Reisman, *J. Am. Chem. Soc.* **2014**, *136*, 14365-14368; c) L. Huang, L. K. G. Ackerman, K. Kang, A. M. Parsons, D. J. Weix, *J. Am. Chem. Soc.* **2019**, *141*, 10978-10983; d) S. Ni, N. M. Padial, C. Kingston, J. C. Vantourout, D. C. Schmitt, J. T. Edwards, M. M. Kruszyk, R. R. Merchant, P. K. Mykhailiuk, B. B. Sanchez, S. Yang, M. A. Perry, G. M. Gallego, J. J. Mousseau, M. R. Collins, R. J. Cherney, P. S. Lebed, J. S. Chen, T. Qin, P. S. Baran, *J. Am. Chem. Soc.* **2019**, *141*, 6726-6739; e) D. Wang, T. XU, *ACS Catal.* **2021**, *11*, 12469-12475. f) D. A. Everson, B. A. Jones, D. J. Weix, *J. Am. Chem. Soc.* **2012**, *134*, 6146-6159.

Halide ions could accelerate the reduction of Ni(II) species by acting as a bridging ligand with the metal reductant,[238a-b] or by removing Zn(II) salts from the metal surface.[238d–e] Promotion of ligand exchange processes with coordinating solvents[238c] and the formation of metal species with enhanced catalytic activity[237e,238b,f] have been suggested as well; based on the results of computational calculations on this system (*vide infra* and see Supplementary Data, Chapter 5.5, page 241), we also advance the hypothesis that halide ions could favor productive mechanistic pathways over possible competitive ones. Interestingly, despite the ease of C-O reductive elimination from Ni(III),[239,204] we never observed etherification products with TFE, that could be formed from reduction of the alkoxy radical. We reason that this might be due to either a fast 1,2-HAT event, or the low basicity of the reaction system that would not allow enough concentration of trifluoroethoxide anions, or the preferential coordination of trifluoroethoxide ions by zinc.

With the optimized reaction conditions in hand we assessed the generality of the protocol by reacting a range of iodoarenes with **2**. The data reported in **Figure 4** unequivocally accounts for the robustness of the catalytic protocol and the wide functional group tolerance. Remarkably, electron-donating groups (i.e. OMe, OBn, OAllyl, OAc, Me, NBn_2, $NHCOCF_3$ and NPhth, **1b**–**j**) could be adequately accommodated both at the *meta* and *para* positions with respect to the iodoarene substitution. In all cases, good yields were achieved (up to 74%). The tolerance towards trifluoroacetamide moiety (**1h**) underlined also the suitability of protic functional groups in the present methodology. Analogously, a wide range of electron-withdrawing groups (i.e. halogens, CF_3, ester, ketone, **3k**–**s**) were effectively handled in *meta* and *para* positions. 4-bromoiodobenzene **1m** was tolerated (60% yield for **3m**) under reductive conditions, showing a notable I/Br selectivity (9:1). Simple iodobenzene **1t**

[238] a) M. Zembayashi; K. Tamao, J.-I. Yoshida, M. Kumada, *Tetrahedron Lett.* **1977**, *18*, 4089−4091; b) I. Colon, D. R. Kelsey, *J. Org. Chem.* **1986**, *51*, 2627-2637; c) A. Klein, A. Kaiser, W. Wielandt, F. Belaj, E. Wendel, H. Bertagnolli, S. Zàlis, *Inorg. Chem.* **2008**, *47*, 11324-11333; d) C. Feng, D. W. Cunningham, Q. T. Easter, S. A. Blum, *J. Am. Chem. Soc.* **2016**, *138*, 11156-11159; e) X. Wang, G. Ma, P. C. Yu, E. Pitsch, B. J. Moll, T. D. Ly, X. Wang, H. Gong, *J. Am. Chem. Soc.* **2018**, *140*, 14490-14497; f) L. Cassar, M. Foà, *J. Organomet. Chem.* **1973**, *51*, 381-393.

[239] a) R. Sun, Y. Qin, D. G. Nocera, *Angew. Chem. Int. Ed.* **2020**, *59*, 9527–9533; b) C. Zhu, H. Yue, J. Jia, M. Rueping, *Angew. Chem. Int. Ed.* **2021**, *60*, 17810.

and benzofused 1-iodonaphthalene **1u** performed analogously well, providing the corresponding α- aryl-α-trifluoromethyl alcohols **3t**,**u** in 70% and 61% yield, respectively.

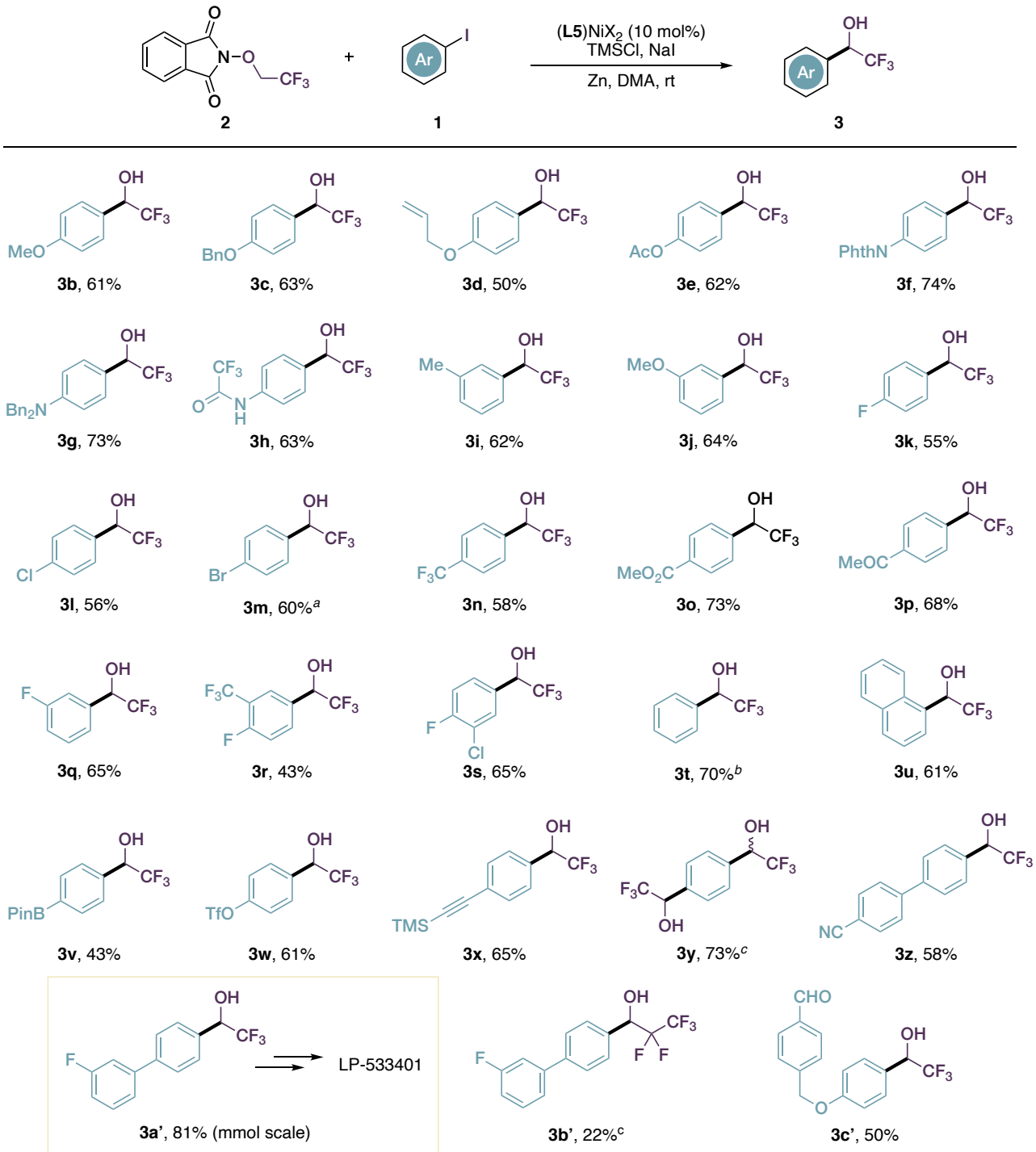

Figure 4. Generality of the present Ni-catalyzed cross-electrophile-coupling. All reactions were set up accordingly to optimized conditions (entry 12 in **Table 1**). Isolated yields after flash chromatography are provided, unless otherwise specified. [a] Isolated as a 9:1 mixture of Br/I

containing alcohols. [b] Given as ^{19}F NMR yield based on internal standard ($CF_3C_6H_5$). Product **3t** resulted too volatile to be isolated. [c] The General Procedure was slightly modified by doubling the amount of [Ni(**L5**)Cl_2], Zn and **2**. [d] From *N*-pentafluoropropoxyphthalimide **2'**. Bpin: boron pinacolate, Nphth: phthalimide, OTf: trifluoromethanesulfonate; TMS: trimethylsilyl.

Then, to properly assess the chemoselectivity and site- specificity of our procedure, we subjected to optimal conditions iodobenzenes carrying cross-coupling active handles such as Bpin (**1v**) and OTf (**1w**). Remarkably, these substituents were nicely tolerated and the corresponding trifluoromethyl benzyl alcohols (**3v,w**) were isolated in satisfactory yields (43–61%), providing room for further cross-coupling functionalization. Moreover, the TMS-protected alkynyl unit (**1x**) was also tolerated delivering the secondary alcohol **3x** in 65% yield. Unfortunately, terminal arylacetylenes only furnished product in low yields. Finally, the possibility to carry out two consecutive formal reductive arylations with **2** was verified with 1,4-diiodobenzene **1y**. The corresponding dialkylated compound **3y** was isolated in synthetically useful 73% yield. We then focused our attention on 1,4-biaryl scaffolds due to their predominance in biologically active α-aryl-α-trifluoromethyl alcohols. In particular, the recorded efficiency on 1,4-biaryl scaffold **1z** (58% yield) led us to extend our methodology to 3-fluoro-4'-iodo-1,1'-biphenyl **1a'**, whose product **3a'** constitutes one of the key building blocks for the preparation of pharmacologically active LP533401. When optimal conditions were applied to readily available **1a'** (1 mmol scale), the resulting benzyl alcohol **3a'** was isolated in 81% yield.

In order to assess the extendibility of the process to other perfluoroalkyl chains, *N*-pentafluoropropoxyphthalimide **2'** was prepared and reacted with substrate **1a'**. Thus, **3b'**, a homologue of the pharmaceutical building block **3a'**, was obtained in a modest 22% yield (unoptimized). Finally, the methodology was tested on a formyl-containing substrate that would result unsuitable in a classic trifluoromethylation protocol under Ruppert-Prakash conditions. Here, the complementarity of our methodology vs $TMSCF_3$-based approaches was verified by subjecting iodoarene **1c'** to optimal conditions effectively delivering **3c'** in 50% isolated yield. It is worth noting that products bearing an amino group (**3g,h**) would also be inconvenient to prepare with a

polar approach, requiring expensive and relatively unstable 4-aminobenzaldehyde as starting material.

In parallel, and encouraged by these results, we decided to carry out molecular modelling studies to gain a deeper understanding of the reaction mechanism operating in this catalytic system (**Scheme 15**, right). For this purpose, we adopted [Ni(**L3**)Br_2] (**I**) as the precatalyst and compounds **1p** and **2** as the model substrates.[240] We have found that, in the presence of Zn, the Ni(II) precatalyst is reduced to Ni(I), yielding the active catalyst (**III**), which is capable of complexing both iodoarene and **2**. While the coordination of the latter is endergonic by 5.9 kcal/mol, the coordination of the former renders a complex that is slightly more stable than III (see **Scheme 2** and Figure S2). Hence, the formation of **IV** will predominate in solution. The possible reduction to Ni(0) was also considered, and despite it might be energetically accessible under the reaction conditions, it involves less exergonic steps and features slightly higher barriers, so that we consider it less likely (see Supplementary Data, Chapter 5.5 for details). This is also supported by the very low reactivity of aryl bromides in the present system. Subsequently, **IV** can further progress via the oxidative addition of iodoarene, rendering **V**, followed by a SET process between Zn and intermediate **V** to yield Ni(II)-aryl intermediate **VI**. Then, trapping of nucleophilic C-centered radical species **VIII** (see below) by **VI** would deliver the Ni(III)-alkyl-aryl adduct **XIII**, that undergoes a very facile reductive elimination (with a barrier of only 5.5 kcal/mol) yielding the observed product and the simultaneous recovery of the active catalyst **III**. In principle, trapping of **VIII** by the Ni(I)-aryl complex **IV** can also be possible, yielding a Ni(II) complex that can evolve via RE to give the product and a Ni(0) complex, but this RE features a five-fold higher barrier than RE from Ni(III). (see Supplementary data, Chapter 5.5 for details).

[240] Experimentally, complex [Ni(**L3**)Br2] provided **3 p** in high yield even in the absence of NaI and TMSCl, as observed in initial optimization studies (See Table S1 in see Supplementary data, Chapter 5.5). We considered this simplified system more appropriate for the computations.

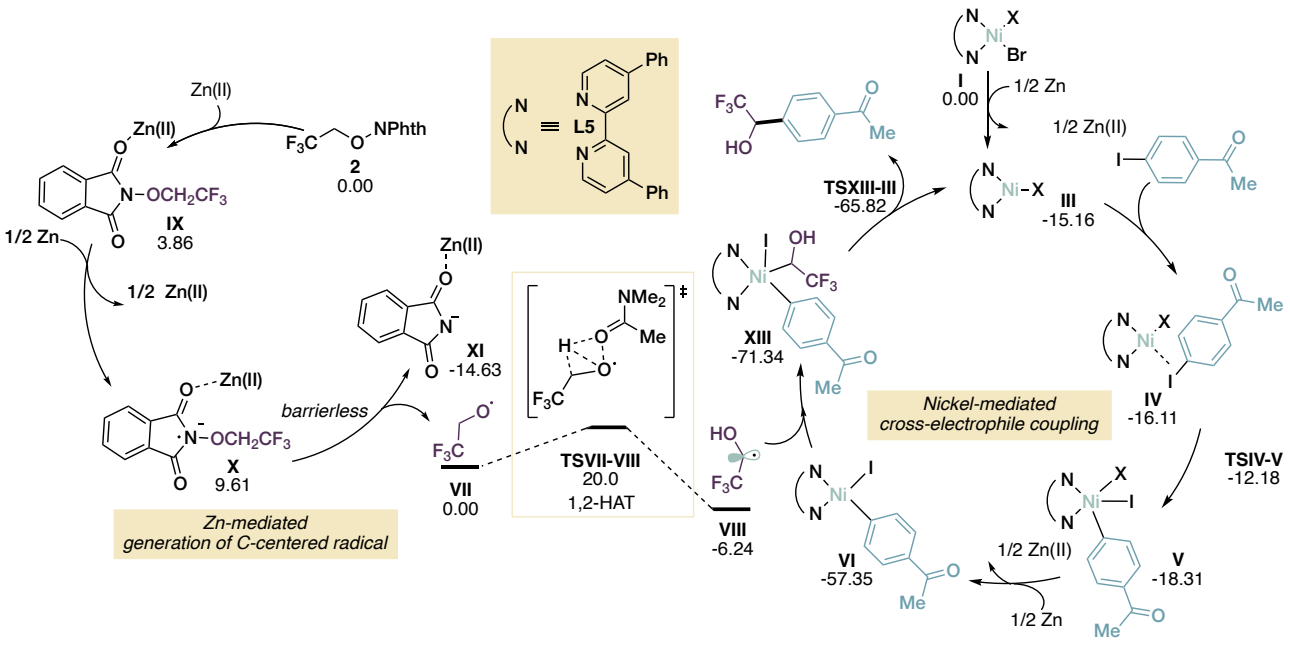

Scheme 15. Proposed mechanistic paths for: cross electrophile coupling (right) and 1,2-HAT process to deliver the postulated C-centered radical **VIII** (left). Computations have been performed at the PCM(*N,N*-dimethylacetamide)[241]-M06/def2svpp[242] computational level. Counterions have been disregarded in this scheme for the sake of clarity but considered in the simulations (see SI for further details).

The generation of key radical **VIII** was also investigated computationally (**Scheme 15**, left). Interestingly, the role of Zn goes beyond mere ligand exchange and reducing tasks, and we have found that, upon coordination of a Zn(II) cation to **2**, Zn(0) can be responsible for reduction and N-O bond cleavage of the phthalimide core, resulting in the facile release of the alkoxy radical **VII**. Zn(II) salts should be readily available from reduction of the Ni complex with Zn, and this finding might explain the incompetence of the organic reductant TDAE, while Mn could afford small quantities of product. This is reminiscent of Martin's photocatalytic methodology presented earlier, in which reduction of the OPthth reagent was thought to be accomplished by the stoichiometric reductant (HE) and Ni was only involved in activation of the aryl partner and radical

[241] J. Tomasi, B. Mennucci, R. Cammi, *Chem. Rev.* **2005**, *105*, 2999–3093.
[242] a) Y. Zhao, D. G. Truhlar, *Theor. Chem. Acc.* **2008**, *120*, 215– 241; b) Y. Zhao, D. G. Truhlar, *Acc. Chem. Res.* **2008**, *41*, 157– 167; c) F. Weigend, *Phys. Chem. Chem. Phys.* **2006**, *8*, 1057– 1065; d) F. Weigend, R. Ahlrichs, *Phys. Chem. Chem. Phys.* **2005**, *7*, 3297–3305.

capture.[214] Attempts to model the reduction of **2** from a Ni(I) species resulted in non-competitive pathways (see Supplementary Data for details).

The O-centered radical **VII** can evolve via a DMA promoted 1,2-HAT, furnishing the pivotal species **VIII**. The barrier for this step was determined to be 20 kcal/mol, significantly higher than the one reported by Zhu for a cyclopentenyl moiety,[227] which is reasonable given the stronger C-H bond of the migrating hydrogen in TFE and the lower stabilization of the resulting radical.

To gain experimental support to the involvement of the radical intermediate **VIII** in the present transformation, the model reaction was carried out in the presence of radical trapping agents such as tert-butyl acrylate (**4a**) and TEMPO (**4b**) (**Scheme 16**). As expected, when **4a** was utilized, a Giese-type trapping of **VIII** occurred at the β-position (35% isolated yield). Importantly, product **5a** was also obtained (12%) in the absence of nickel, providing decisive evidence that both reductive activation of **2** and 1,2-HAT processes are not nickel-mediated. Analogously, the addition of 1 eq. of TEMPO largely suppressed reactivity and generated a small amount of the silylated acetal **5b** that was detected in the reaction crude (see Supplementary data, Chapter 5.5).

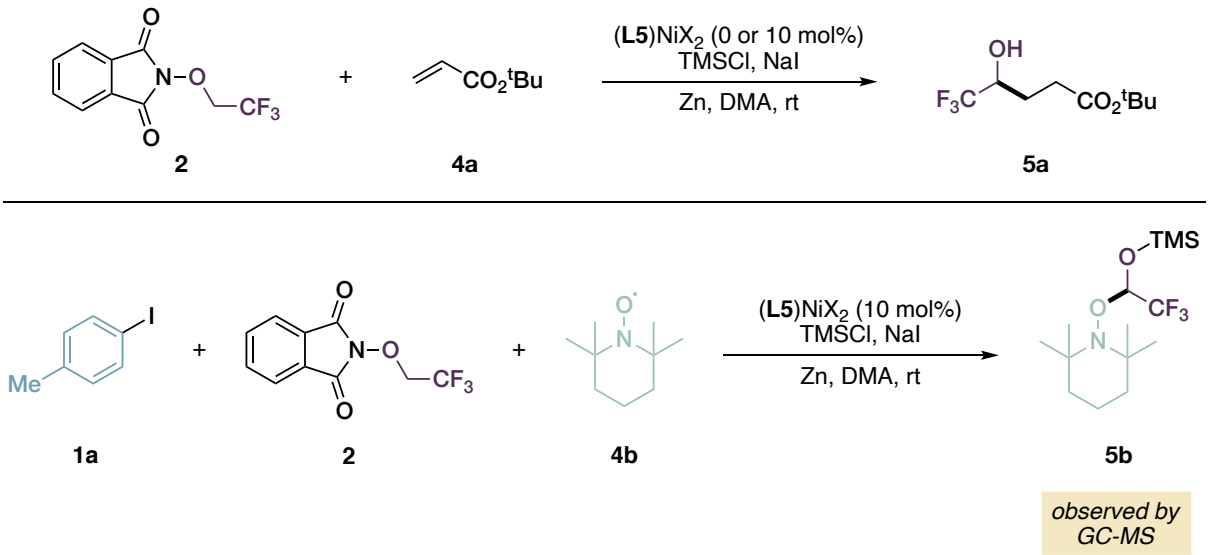

Scheme 3. Control experiments addressing the intermediacy of the C-centered radical **VIII**. Top: Giese reaction with tert-butyl acrylate (**4a**). Bottom: radical trapping with TEMPO (**4b**).

Finally, the synthetic significance of the methodology was tested on the functionalization of derivatized biologically relevant scaffolds **6a–c** (**Figure 5**). Successful XEC was recorded with *N*-(4-iodobenzoyl)phenyl alanine **6a** that delivered the corresponding trifluoromethyl alcohol **7a** in 65% yield. Additionally, highly lipophilic scaffolds such as menthol-ester **6b** and functionalized pregnenolone **6c** proved suitable as well, providing the desired alcohols **7b** and **7c** in 46% and 32% yield, respectively.

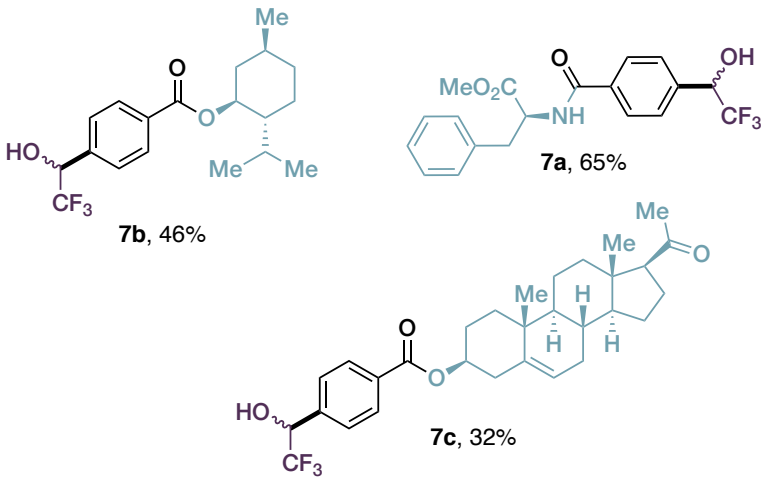

Figure 5. Functionalization of derivatized biologically relevant motifs obtained from 4-iodobenzoyl chloride (**7a–c**). The reactions were set up accordingly to entry 12 in **Table 1**.

5.4 Conclusions

In conclusion, in this work we reported a new radical approach for the synthesis of valuable α-aryl-α-trifluoromethyl alcohols, bypassing the use of toxic and gaseous trifluoroacetaldehyde via nickel catalyzed cross-electrophilic coupling. Our strategy exploits the generation of a key C-centered α-hydroxy radical, difficult to access via intermolecular HAT chemistry, by capitalizing on a DMA promoted 1,2-HAT event that smoothly blends with the nickel redox manifold. Notably, this is the first example of utilization of 1,2-HAT chemistry in the context of nickel catalysis and, to best of our knowledge, metal catalysis in general, as well as the first catalytic access to such compounds from readily available aryl iodides.

The entire mechanistic profile was investigated through a comprehensive computational investigation that was also supported by *ad hoc* control experiments. This revealed interesting features, such as reductive cleavage of OPhth without involvement of Ni and confirmation of an energetically accessible 1,2-HAT pathway. The protocol was found to have great functional group tolerance, allowing preparation of α-aryl-α-trifluoromethyl alcohols that would be challenging or derived from inconvenient starting materials under a polar regime. Finally, suitability for the application to biologically relevant building blocks and functionalization of naturally occurring motifs were shown.

5.5 Supplementary data

General experimental methods

^{1}H NMR, ^{13}C NMR and ^{19}F NMR spectra were recorded on Varian 400-MR (400 MHz) (equipped with autoswitchable PFG probe) and Bruker Avance Neo 600 MHz (equipped with CryoProbe Prodigy Broadband 5mm) spectrometers. Data are reported as follows: chemical shift, multiplicity (s = singlet, d = doublet, dd= double doublet, t = triplet, td = triple doublet, dt = double triplet, q = quartet, sext = sextet, sept = septet, p = pseudo, b = broad, m = multiplet), coupling constants (Hz). Chemical shifts are reported in ppm from TMS with the solvent resonance as the internal standard.

HRMS spectra were obtained with a G2XS QTof mass spectrometer using either ESI or APCI ionization techniques, as specified case by case.

Melting points were determined with a Büchi Melting Point B-540 apparatus and are not corrected.

Chromatographic purification was done with 240-400 mesh silica gel.

Anhydrous solvents, except for DMA, were supplied by Sigma Aldrich in Sureseal® bottles and used without any further purification. Reagent grade DMA was purchased from Fluorochem and dried as follows: DMA was stirred overnight with CaO at r.t., then the mixture was refluxed for 1 h, followed by distillation under reduced pressure (ca. 50 mbar, 50°C). The first 5% head distillate was discarded, the rest collected in a receiving flask with activated 4Å MS and then degassed by sparging N_2 for 15 minutes.

Room temperature (r.t.) refers to the ambient temperature of the laboratory, ranging from 22 °C to 26 °C.

Commercially available chemicals and (non-anhydrous) solvents were purchased from Sigma Aldrich, Fluorochem and TCI Chemicals and used without any further purification.

Zn dust refers to a particle size <10 μm and was purchased from Sigma Aldrich, having ≥98% purity, and was used as received unless otherwise mentioned.

General computational details and considerations

We have used the Density Functional Theory (DFT) in the Kohn-Sham formulation to optimize all the stationary points presented in this manuscript. Geometries of all the stationary points were fully optimized at the M06[243]/def2svpp[244,245] computational level. The effect of solvent (DMA) was modelled using the polarizable continuum model (PCM)[246] with the default parameters implemented in the Gaussian 09 package.[247] Explicit solvation was also included in some instances since the solvent has the potential ability to coordinate the metallic center and even aid in hydrogen transferences.

All geometry optimizations have been performed using tight convergence criteria in the SCF and requesting a pruned (99.590) grid to guarantee the accuracy of the reported results. Moreover, calculations were performed considering 1.0 atm and 298.1 K to properly simulate the reaction conditions.

Frequency analysis was used to establish the nature of all optimized structures as either minima or transition structures. For all stationary points, the stability of the wave function was examined.[248] When different spin-states are possible for a stationary point those states were explored by running single point energy calculations starting from the optimized structure with the expected multiplicity. IRC calculations[249] were

---

[243] a) Y. Zhao, D. G. Truhlar, *Theor. Chem. Acc.* **2008**, *120*, 215–241; b) Y. Zhao, D. G. Truhlar, *Acc. Chem. Res.* **2008**, *41*, 157–167.

[244] F. Weigend, *Phys. Chem. Chem. Phys.* **2006**, *8*, 1057–1065.

[245] F. Weigend, *Phys. Chem. Chem. Phys.* **2005**, *7*, 3297–3305.

[246] J. Tomasi, B. Mennucci, R. Cammi, *Chem. Rev.* **2005**, *105*, 2999–3093.

[247] Gaussian 09, Revision A.02, M. J. Frisch, G. W. Trucks, H. B. Schlegel, G. E. Scuseria, M. A. Robb, J. R. Cheeseman, G. Scalmani, V. Barone, G. A. Petersson, H. Nakatsuji, X. Li, M. Caricato, A. Marenich, J. Bloino, B. G. Janesko, R. Gomperts, B. Mennucci, H. P. Hratchian, J. V. Ortiz, A. F. Izmaylov, J. L. Sonnenberg, D. Williams-Young, F. Ding, F. Lipparini, F. Egidi, J. Goings, B. Peng, A. Petrone, T. Henderson, D. Ranasinghe, V. G. Zakrzewski, J. Gao, N. Rega, G. Zheng, W. Liang, M. Hada, M. Ehara, K. Toyota, R. Fukuda, J. Hasegawa, M. Ishida, T. Nakajima, Y. Honda, O. Kitao, H. Nakai, T. Vreven, K. Throssell, J. A. Montgomery, J. E. Peralta, F. Ogliaro, M. Bearpark, J. J. Heyd, E. Brothers, K. N. Kudin, V. N. Staroverov, T. Keith, R. Kobayashi, J. Normand, K. Raghavachari, A. Rendell, J. C. Burant, S. S. Iyengar, J. Tomasi, M. Cossi, J. M. Millam, M. Klene, C. Adamo, R. Cammi, J. W. Ochterski, R. L. Martin, K. Morokuma, O. Farkas, J. B. Foresman, D. J. Fox, Gaussian, Inc., Wallingford CT.

[248] a) H. B. Schlegel, J. J. W. McDouall, "Do You Have SCF Stability and Convergence Problems?" in *Computational Advances in Organic Chemistry: Molecular Structure and Reactivity*, Dordrecht: Springer Netherlands, 1991, pp. 167–185; b) R. Bauernschmitt, R. Ahlrichs, *J. Chem. Phys.* **1996**, *104*, 9047–9052; c) R. Seeger, J. A. Pople, *J. Chem. Phys.* **1977**, 66, 3045–3050.

[249] a) S. Maeda, Y. Harabuchi, Y. Ono, T. Taketsugu, K. Morokuma, *Inter. J. Quantum Chem.* **2015**, *115*, 258–269; b) K. Fukui, *Acc. Chem. Res.* **1981**, *14*, 363–368.

conducted for important transition states to ensure their connectivity with the expected reactants and products. The nudged elastic band method was used to locate difficult transition states.[250] When the substrates showed conformational freedom, conformational analysis was performed manually, it must be indicated that only the most stable conformer of each stationary point was considered and reported unless otherwise indicated. The visualization of the reported structures was performed using MOLDEN.[251] The representation of the structures here presented were generated using CYLView.[252]

The reduction steps constitute a troublesome point in this research since they involve metallic Zn. We have worked here under the consideration that in the presence of such a coordinating solvent such as DMA part of the metallic Zn will be efficiently solvated and leached in the form of $Zn(DMA)_3$. Different number of solvent molecules coordinated to the metal center has been explored obtaining that three is the enthalpically preferred coordination.

Table S1. Data on the solvation of metallic Zn.[a]

ID	Im Freqs	Stable	SCF	SCF+ZPVE	H[b]	G[c]
DMA	-	Yes	-287.4093664	-287.280614	-287.272025	-287.312298
Zn	-	Yes	-1779.098406	-1779.098406	-1779.096045	-1779.114283
Zn(DMA)	-	Yes	-2066.517272	-2066.387867	-2066.377097	-2066.425476
$Zn(DMA)_2$	-	Yes	-2353.937241	-2353.676407	-2353.657118	-2353.723942
$Zn(DMA)_3$	-	Yes	-2641.356003	-2640.965713	-2640.937012	-2641.026676

[a] SCF energies correspond to the electronic energies expressed in a.u. Imaginary frequencies are expressed in cm^{-1}. [b] H denotes the Sum of electronic and thermal Enthalpies. [c] G denotes the Sum of electronic and thermal Free Energies.

[250] a) D. Sheppard, R. Terrell, G. Henkelman, *J. Chem. Phys.* **2008**, *128*, 134106; b) G. Henkelman, G. Jóhannesson, H. Jónsson, *Methods for Finding Saddle Points and Minimum Energy Paths* in *Progress on Theoretical Chemistry and Physics*, Ed. S. D. Schwartz, 269–300 (Kluwer Academic Publishers, 2000); c) G. Henkelman, B. P. Uberuaga, H. Jónsson, *J. Chem. Phys.* **2000**, *113*, 9901; d) G. Henkelman, H. Jónsson, *J. Chem. Phys.* **2000**, *113*, 9978; e) H. Jónsson, G. Mills, K. W. Jacobsen, *Nudged Elastic Band Method for Finding Minimum Energy Paths of Transitions* in *Classical and Quantum Dynamics in Condensed Phase Simulations*, Ed. B. J. Berne, G. Ciccotti, D. F. Coker, 385 (World Scientific, 1998).

[251] G. Schaftenaar, E. Vlieg, G. Vriend, *J. Comput. Aided. Mol. Des.* **2017**, *31*, 789–800.

[252] CYLview20; C. Y. Legault, Université de Sherbrooke, 2020 (http://www.cylview.org).

Synthesis of starting materials

Synthesis of *N*-trifluoroethoxyphthalimide **2**

Compound **2** was synthesized from *N*-hydroxyphthalimide (NHPI) and 2,2,2-trifluoroethyl trifluoromethanesulfonate according to the literature.[216] The latter was prepared from trifluoroethanol (TFE) and triflic anhydride following a described procedure.[253] Please note that the compound is also commercialy available (CAS No. 6226-25-1, Sigma Aldrich Cat. No. 752924).

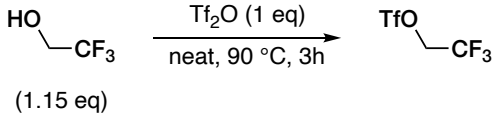

In a heat-gun dried, 25 mL two-necked round bottom flask under N_2 atmosphere equipped with reflux condenser were added TFE (4.17 g, 3.0 mL, 41.7 mmol, 1.15 eq) and triflic anhydride (10.00 g, 6 mL, 35.7 mmol, 1 eq). The mixture was stirred for 15 minutes at rt (**CAUTION! Heat is produced when mixing the two liquids**) and then refluxed for 3 hours at 90 °C.

Under N_2 flow, the reflux condenser was removed, and the flask connected to a previously heat-gun dried distillation apparatus equipped with two receiving flasks also under N_2 flow.

Fractionate distillation under N_2 atmosphere at atmospheric pressure was carried out (oil bath temperature ca. 120 °C), discarding the head distillate (ca. 0.5 mL, containing residual TFE) to obtain pure 2,2,2-trifluoroethyl trifluoromethanesulfonate (7.46 g, 32.1 mmol, 90% yield). Spectral data are in accordance with the literature.[253]

[253] J. C. Son, B. J. Kim, J. H. Kim, I. Y. Lee, C. S. Yun, S. H. Lee, C. K. Lee, Novel Antiviral Pyrrolopyridine Derivatives and Method for Preparing the Same. US 2014/249162 A1, September 4, 2014.

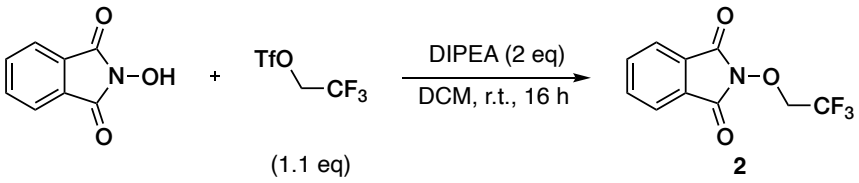

A 250 mL three -necked round bottom flask was evacuated and back-filled with N_2 for three times. NHPI (2.90 g, 17.8 mmol, 1 eq) was added to the flask, followed by DCM (50 mL). DIPEA (4.60 g, 6.2 mL, 35.6 mmol, 2 eq) was added slowly to the suspension, immediately producing a color change to orange/red, indicating formation of NHPI anion. The mixture was stirred until homogeneous (5 to 10 minutes). At this point 2,2,2-trifluoroethyl trifluoromethanesulfonate (4.53 g, 19.5 mmol, 1.1 eq) was added in one portion, and the mixture was stirred overnight under N_2 atmosphere.

The reaction was quenched with H_2O, transferred to a separatory funnel, the aqueous phase extracted with DCM, the combined organic phases dried on anhydrous Na_2SO_4 and the solvent removed under reduced pressure. Flash chromatography on silica gel (5:1 *n*Hex/EtOAc until a 365 nm light absorbing impurity is eluted, then 3.5:1 *n*Hex/EtOAc) furnished *N*-trifluoroethoxyphthalimide as a white, fluffy solid. (3.14 g, 12.8 mmol, 72% yield). Spectral data are in accordance with the literature.[216]

Additional notes:

1. Special care must be taken in properly sealing all the glass joints before the distillation. This is to avoid any leakage of TfOH that would react with grease in the joints, making the system not well sealed, ultimately leading to very slow distillation, loss of product as well as posing safety issues.

2. We noticed that compound **2** is not stable in the reaction crude upon dryness, probably due to sensitivity to strongly basic conditions. Therefore, solvent should be evaporated only right before flash chromatography. Anyway, compound **2** resulted stable in the reaction mixture in the presence of solvent for at least one day.

Synthesis of *N*-pentafluoropropoxyphthalimide **2'**

Compound **2'** was synthesized from *N*-hydroxyphthalimide (NHPI) and 2,2,3,3,3-pentafluoro-1-propanol via an adapted literature procedure described for the synthesis of **2**.[254] The corresponding triflate ester was prepared in situ and reacted with *N*-hydroxyphthalimide in the presence of base.

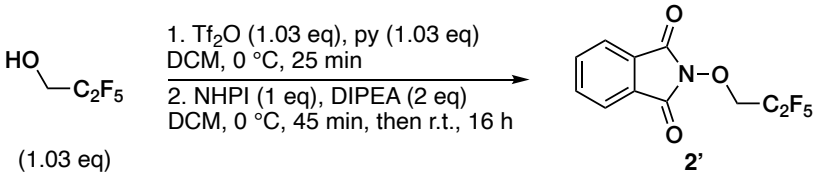

In a heat-gun dried, 25 mL three-necked round bottom flask equipped with a dropping funnel under N_2 atmosphere were added Tf_2O (5.13 mmol, 1.45 g, 0.86 mL) and DCM (8 mL). After cooling to 0 °C, a solution of 2,2,3,3,3-pentafluoro-1-propanol (5.13 mmol, 0.77 g, 0.64 mL) and pyridine (5.13 mmol, 0.41 g, 0.41 mL) in DCM (2 mL) was added dropwise. After stirring at 0 °C for 25 minutes, a solution of NHPI (5 mmol, 0.81 g) and DIPEA (10 mmol, 1.29 g, 1.8 mL) in DCM (5.75 mL) was added dropwise (this solution was prepared in a heat-gun dried two neck round bottom flask and transferred via syringe). The mixture was stirred at 0 °C for 45 minutes and then at r.t. for 16 h. The reaction was quenched with 2 N HCl (*ca.* 15 mL), transferred to a separatory funnel, the aqueous phase extracted with DCM, the combined organic phases washed with H_2O and brine, dried on anhydrous Na_2SO_4 and the solvent removed under reduced pressure. Flash chromatography on silica gel (5:1 *n*Hex/EtOAc) furnished *N*-trifluoropropoxyphthalimide as a white solid. (398 mg, 1.35 mmol, 27% yield).

[254] K. Hayashi, K .Kunitani, S. Uehara, T. Morita, Novel Arylamidine Derivative, Salt Thereof, and Antifungal Containing These. US 2008/319016 A1, December 25, 2008.

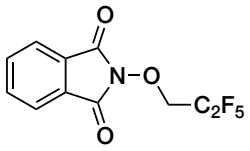

2'. White solid. **MP** = 89 – 91 °C. **^{1}H NMR** (400 MHz, $CDCl_3$) δ = 7.88 – 7.83 (m, 2H), 7.80 – 7.75 (m, 2H), 4.64 (t, *J* = 12.9 Hz, 2H); **^{13}C NMR** (100 MHz, $CDCl_3$) δ = 162.4 (2C), 134.9 (2C), 128.6 (2C), 123.9 (2C), 72.4 (t, *J* = 25.4 Hz), the CF_2 and CF_3 carbons of the pentafluoroethyl group were not detected; **^{19}F NMR** (377 MHz, $CDCl_3$) δ = -83.73 (s, 3F), -124.26 (t, *J* = 12.9 Hz, 2F). **GC-MS**: 295 (13), 276 (4), 176 (3), 147 (12), 105 (100).

Synthesis or aryl iodides

Aryl iodides **1a**, **1b**, **1i-1n**, **1p-1v**, **1y** are commercially available and were used without as received.

Aryl iodides **1c**,[255] **1d**,[256] **1e**,[257] **1w**[258] were prepared from 4-iodophenol according to the literature.

Aryl iodides **1f**,[259] **1g**,[260] **1h**[261] were prepared from 4-iodoaniline according to the literature.

Aryl iodide **1o**[262] was prepared from 4-iodobenzoic acid according to the literature.

Aryl iodide **1x**[263] was prepared from 1,4-diiodobenzene according to the literature.

Aryl iodides **1z**[264] and **1a'**[265] were prepared following a literature procedure by a two-step sequence: Suzuki cross coupling between 4-(trimethylsilyl)phenylboronic acid and 4-iodobenzonitrile (**1z**) or 3-fluoroiodobenzene (**1a'**) followed by *ipso*-iodination with ICl.[264]

---

[255] H. Yuan, K. Bi, W. Chang, R. Yue, B. Li, J. Ye, Q. Sun, H. Jin, L. Shan, W. Zhang, *Tetrahedron* **2014**, *70*, 9084–9092.
[256] R. M. Denton, J. T. Scragg, J. A Saska, *Tetrahedron Lett.* **2011**, *52*, 2554–2556.
[257] C. S. Yeung, V. M. Dong, *J. Am. Chem. Soc.* **2008**, *130*, 7826–7827.
[258] Y. H. Lee, B. Morandi, *Angew. Chem. Int. Ed.* **2019**, *58*, 6444–6448.
[259] P. Boehm, S. Roediger, A. Bismuto, B. Morandi, *Angew. Chem. Int. Ed.* **2020**, *59*, 17887–17896.
[260] S. M. Goldup, D. A. Leigh, P. J. Lusby, R. T. McBurney, A. M. Z. Slawin, *Angew. Chem. Int. Ed.* **2008**, *47*, 3381–3384.
[261] A. P. Melissaris, H. M. Litt, *J. Org. Chem.* **1994**, *59*, 5818–5821.
[262] T. Suzuki, Y. Ota, M. Ri, M. Bando, A. Gotoh, Y. Itoh, H. Tsumoto, P. R. Tatum, T. Mizukami, H. Nakagawa, S. Iida, R. Ueda, K. Shirahige, N. Miyata, *J. Med. Chem.* **2012**, *55*, 9562–9575.
[263] C. Montoro-García, M. J. Mayoral, R. Chamorro, D. González-Rodríguez, *Angew. Chem. Int. Ed.* **2017**, *56*, 15649–15653.
[264] I. Medina-Mercado, S. Porcel, *Synthesis* **2022**, *54*, A–L.
[265] H.-L. Lia, Y. Kuninobu, *Adv. Synth. Catal.* **2020**, *362*, 2637–2641.

Aryl iodide **1c'** was prepared from 4-iodobenzyl bromide and 4-hydroxybenzaldehyde according to the literature.[266]

Aryl iodides **6a**,[267] **6b**[268] and **6c**[269] were prepared from 4-iodobenzoyl chloride and the corresponding alcohol or amine according to the literature.

[266] H. Bölcskeia, A. Német-Hanzelika, I. Greinera, Z. Dubrovaya, V. Hádaa, G. Keglevich, *Lett. Drug Des. Discov.* **2017**, *14*, 233–239.
[267] Q.-W. Zhao, Z.-F. Yang, X.-P. Fu, X. Zhang, *Synlett* **2021**, *32*, 1565–1569.
[268] Y.-Q. Han, X. Yang, K.-X. Kong, Y.-T. Deng, L.-S. Wu, Y. Ding, B.-F. Shi, *Angew. Chem. Int. Ed.* **2020**, *59*, 20455–20458.
[269] V. G. Landge, A. J. Grant, Y. Fu, A. M. Rabon, J. L. Payton, M. C. Young, *J. Am. Chem. Soc.* **2021**, *143*, 10352–10360.

Synthesis of Ligand **L5** and nickel complex [Ni(**L5**)Cl_2].

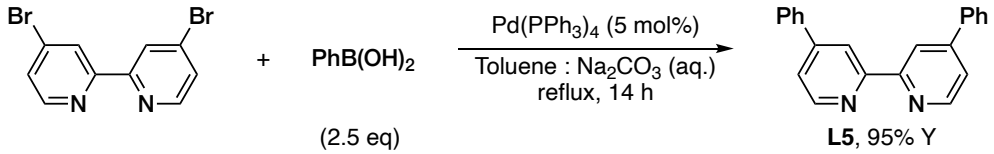

Ligand **L5** was prepared according to the literature from 4,4'-dibromo-2,2'-bipyridine and phenyl boronic acid via Suzuki Cross Coupling.[270]

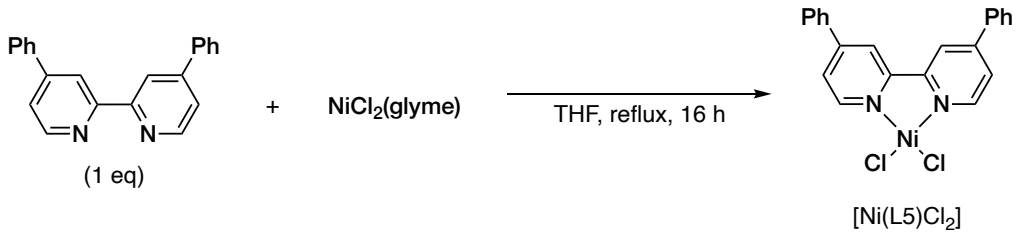

Nickel complex [Ni(**L5**)Cl_2] was prepared via modification of a described procedure for the synthesis of [Ni(dtbbpy)Cl_2],[271] as follows: in a heat-gun dried Schlenk tube were added **L5** (0.3 mmol, 92.4 mg, 1 eq), $NiCl_2$(glyme) (0.3 mmol, 65.9 mg, 1 eq) and dry THF (2 mL). The heterogeneous mixture was refluxed for 18 h, cooled to room temperature and diluted with EtOAc (6 mL). The solid was separated by centrifugation, washed with EtOAc and dried under vacuum to obtain [Ni(**L5**)Cl_2] as a pale green solid (0.285 mmol, 124.8 mg, 95% yield).

[270] W.-S. Han, J.-K. Han, H.-Y. Kim, M. J. Choi, Y.-S. Kang, C. Pac, S. O. Kang, *Inorg. Chem.* **2011**, *50*, 3271–3280.
[271] C.-M. Hsu, S.-C. Lee, H.-E. Tsai, Y.-T. Tsao, C.-L. Chan, S. Miñoza, Z.-N. Tsai, L.-Y. Li, H.-H. Liao, *J. Org. Chem.* **2022**, *87*, 3799–3803.

Additional optimization data

Table S2: Initial screening on substrate **1p**

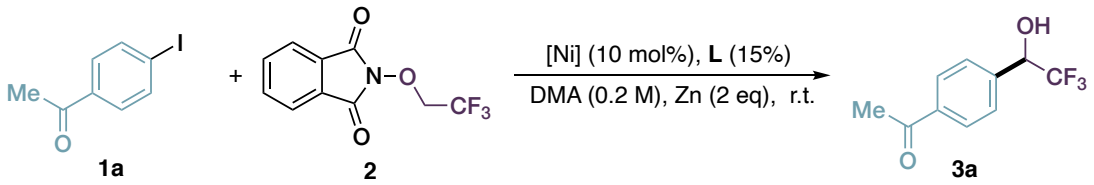

Entry[a]	**1p** : **2**	[Ni]	**L**	Other variations	**3p** Yield (%)[b]
1	1 : 1.5	$NiCl_2$(glyme)	**L6**	/	50
2	1.5 : 1	$NiCl_2$(glyme)	**L6**	/	28
3	1 : 1.5	NiI_2	**L6**	/	36
4	1 : 1.5	$NiCl_2$(glyme)	**L6**	$MgCl_2$ (1.5 eq)	traces
5	1 : 3	$NiCl_2$(glyme)	**L6**	/	72
6	1 : 3	$NiCl_2$(glyme)	**L3**	/	82
7	1 : 3	$NiCl_2$(glyme)	**L3**	DMF as solvent	55
8	1 : 3	$NiCl_2$(glyme)	**L3**	TBAI (50 mol%)	76
9	1 : 3	[Ni(**L3**)Cl_2][c]	/	2 eq of Zn	93

[a] All reactions were conducted on 0.1 mmol scale of the limiting reagent (**1p** or **2a** depending on the ratio chosen) and checked after 16 h. [b] Yields determined on the crude mixture by ^{1}H NMR with 1,3-dimethoxybenzene as internal standard after work up. [c] 10 mol% of preformed metal complex was used.

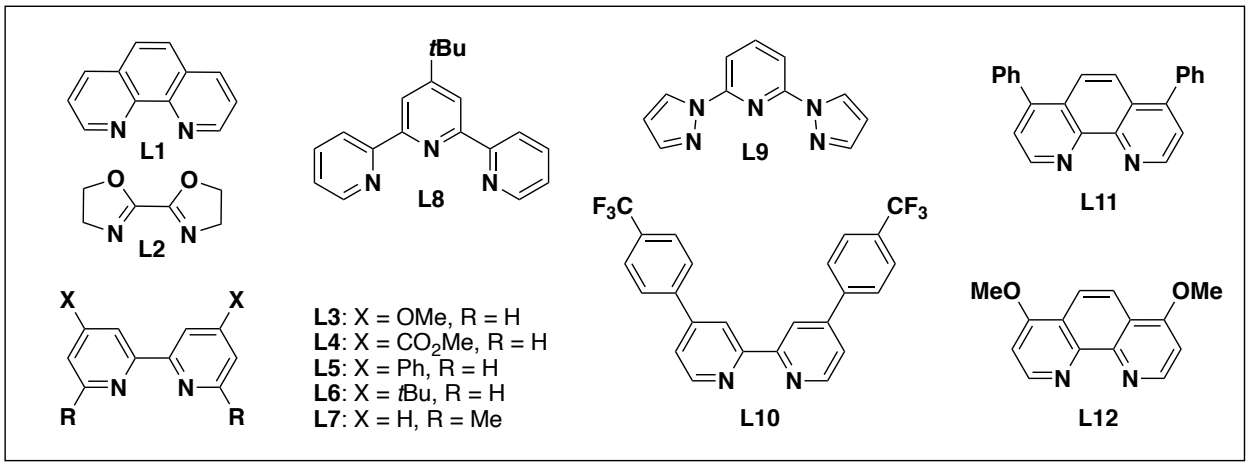

Optimal conditions for substrate **1p** (entry 8) turned out not to be general for other substrates. These conditions appear to be limited to substrates carrying EWGs, and

more electron-rich aryl iodides failed to provide satisfactory conversions. Therefore, we further explored conditions choosing **1u** as model substrate (*i.e.* non-volatile and easily detectable product) and the results are summarized in the **Table S3**.

Table S3: Screening on substrate **1u**

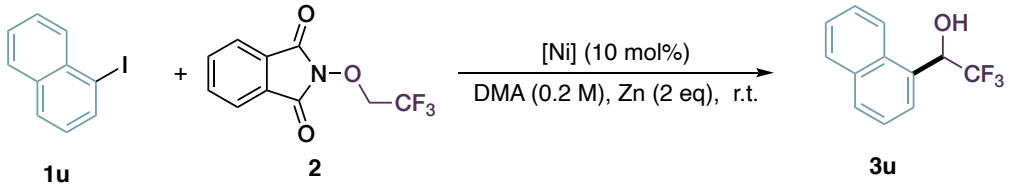

1u **2** **3u**

Entry[a]	[Ni]	Other variations	**3u** Yield (%)[b]
1	[Ni(**L3**)Cl_2]	/	14
2	[Ni(**L3**)Cl_2]	TMSCl (1 eq)	32
3	[Ni(**L1**)Cl_2]	/	18
4	[Ni(**L1**)Cl_2]	DMSO as solvent	14
5	[Ni(**L1**)Cl_2]	DMF as solvent	10
6	[Ni(**L1**)Cl_2]	NMP as the solvent	11
7	[Ni(**L1**)Cl_2]	DMA:dioxane (2:3) as solvent	18
8	[Ni(**L1**)Cl_2]	TMSCl (1 eq)	61
9	[Ni(**L1**)Cl_2]	TMSCl (2 eq)	29
10	[Ni(**L1**)Cl_2]	TMSCl (0.5 eq)	50
11	[Ni(**L1**)Cl_2]	TMSCl (0.75 eq)	56

[a] All reactions were conducted on 0.1 mmol scale of **1u** (**1u**:**2** = 1:3) and checked after 16 h. [b] Yields determined on the crude mixture by ^{19}F NMR with trifluorotoluene as an internal standard, after quenching.

TMSCl was identified as a useful additive to ensure reproducibility, as some reactions showed sluggish initiation periods that resulted in low yields and incomplete conversion. In each case it was used, its addition provided similar or higher yields than the reaction run in its absence.

Again, optimal conditions for substrate **1u** (entry 8) demonstrated to be specific for this substrate and proved low-yielding for several others. For example, electron-rich substrate **1b** bearing a 4-OMe group was unreactive under these optimized conditions, as well as with optimal conditions for substrate **1p**.

Therefore, we chose substrate **1a** as unbiased model iodide for the final optimization, and the most significant results are summarized in the main text (**Table 1**). The following two tables present additional optimization data.

Table S4: Additional screening data on substrate **1a**

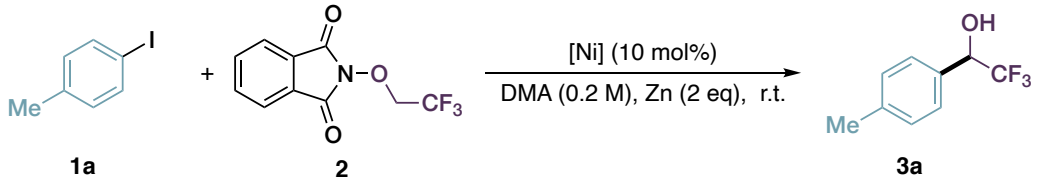

Entry[a]	[Ni]	**L**	Other variations	**3a** Yield (%)[b]
1	[Ni(**L1**)Cl_2][c]	/	/	36
2	[Ni(**L1**)Cl_2][c]	/	40 °C	22
3	[Ni(**L1**)Cl_2][c]	/	50 °C	16
4[d]	[Ni(**L1**)Cl_2][c]	/	TMSCl (1 eq)	36
5	[Ni(**L1**)Cl_2][c]	/	TMSCl (1 eq) and HNPhth (1 eq)	16
6	[Ni(**L1**)Cl_2][c]	/	TMSCl (1 eq) and KNPhth (1 eq)	NR
7	[Ni(**L1**)Cl_2][c]	/	TMSCl (1 eq) and TMG (2 eq)	0
8	[Ni(**L1**)Cl_2][c]	/	TMSCl (1 eq) and 20% of [Ni]	33
9	[Ni(**L1**)Cl_2][c]	/	TMSCl (1 eq) and NaI (1 eq)	40
10	$NiCl_2$(glyme)	**L12**	/	21
11	$NiCl_2$(glyme)	**L9**	TMSCl (1 eq)	3
12	$NiCl_2$(glyme)	**L10**	TMSCl (1 eq) and NaI (1 eq)	9
13	$NiCl_2$(glyme)	**L11**	TMSCl (1 eq)	38
14	$NiCl_2$(glyme)	**L11**	TMSCl (1 eq) and NaI (1 eq)	62
15	$NiCl_2$(glyme)	**L3**	TMSCl (1 eq) and NaI (1 eq)	53
16	[Ni(**L3**)Cl_2][c]	/	TMSCl (1 eq) and NaI (1 eq)	77

[a] All reactions were conducted on 0.1 mmol scale of **1a** (**1a**:**2** = 1:3) and checked after 16 h. [b] Yields determined on the crude mixture by ^{19}F NMR with trifluorotoluene as the internal standard, after quenching. [c] 10 mol% of preformed metal complex was used. [d] Entry 1 in **Table 1** in the main text. NR = no reaction.

Table S5: Additional screening data on substrate **1a** with **L5**

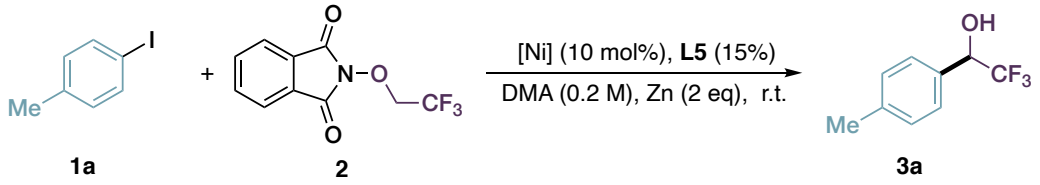

Entry[a]	[Ni]	**L**	Other variations	**3a** Yield (%)[b]
1	$NiCl_2$(glyme)	**L5**	/	22
2	$NiCl_2$(glyme)	**L5**	TMSCl (1 eq)	55
3	$NiCl_2$(glyme)	**L5**	TMSCl (1 eq) and NaI (1 eq)	74
4	$NiCl_2$(glyme)	**L5**	TMSCl (1 eq) and NaI (1.5 eq)	63
5	$NiCl_2$(glyme)	**L5**	activated Zn[c] and NaI (1 eq)	66
6	$NiCl_2$(glyme)	**L5**	TMSCl (1 eq), NaI (1 eq) and 20 mol% **L5**	67
7	$NiCl_2$(glyme)	**L5**	TMSCl (1 eq) and NaI (1 eq), and 0.1 M	71
8	$NiBr_2$(glyme)	**L5**	TMSCl (1 eq) and NaI (1 eq)	54
9	NiI_2	**L5**	TMSCl (1 eq) and NaI (1 eq)	71
10	$NiCl_2$(glyme)	**L5**	TMSCl (1 eq) and KI (1 eq)	54
11	$NiCl_2$(glyme)	**L5**	TMSCl (1 eq) and TBAI (1 eq)	20
12	$NiCl_2$(glyme)	**L5**	TMSCl (1 eq) and NaBr (1 eq)	59
13	$NiCl_2$(glyme)	**L5**	TMSCl (1 eq) and $MgBr_2 \cdot (Et_2O)$ (1 eq)	28
14	$NiCl_2$(glyme)	**L5**	TMSCl (1 eq) and LiCl (1 eq)	traces
15	$NiCl_2$(glyme)	**L5**	TMSCl (1 eq), NaI (1 eq) and pyridine (25 mol%)	72

16	$NiCl_2$(glyme)	**L5**	TMSCl (1 eq), NaI (1 eq) and 1,5-hexadiene (75 mol%)	75
17[d,e]	[Ni(**L5**)Cl_2][f]	/	TMSCl (1 eq) and NaI (1 eq)	95

[a] All reactions were conducted on 0.1 mmol scale **1a** (**1a**:**2** = 1:3) and checked after 16 h. [b] Yields determined on the crude mixture by ^{19}F NMR with trifluorotoluene as internal standard, after quenching. [c] 1.6 g of commercial Zn dust were stirred with 10 mL aqueous 2% HCl for 4 minutes, washed with 20 mL H_2O (x3) by decanting the solution each time, filtered and washed with EtOH (5 mL), Acetone (10 mL), Et_2O (5 mL). The solid was dried under vacuum at 90°C for 10 minutes and stored under N_2. [d] Entry 12 in Table 1 in the main text. [e] Reaction time = 2h. [f] 10 mol% of preformed metal complex was used.

Explorative screening of chiral ligands

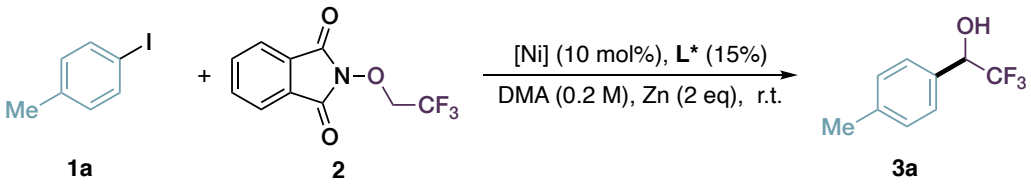

After optimization with ligand **L5**, we tested several chiral ligands to assess the feasibility of an enantioselective version of the protocol. Unfortunately, we did not record any encouraging outcome, as the product was always obtained in low yields and almost racemic form.

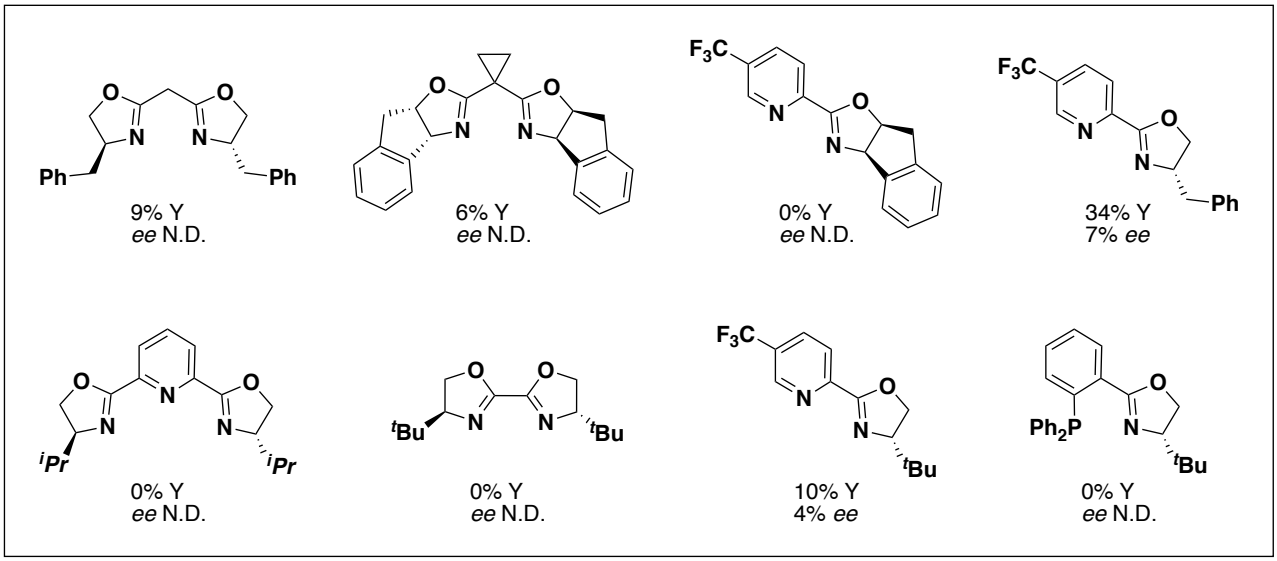

Ni catalyzed cross-coupling

General procedure for the Ni catalyzed cross-coupling reaction

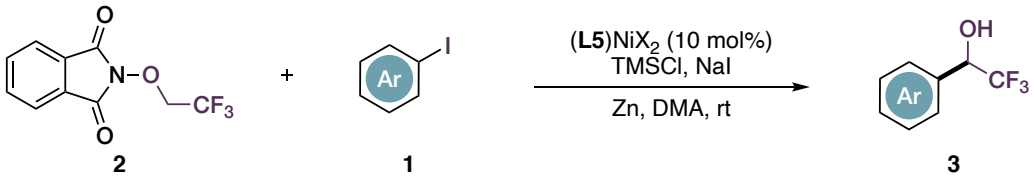

A heat-gun dried pressure Schlenk under N_2 atmosphere was charged with [Ni(**L5**)Cl_2] (4.4 mg, 0.01 mmol, 0.1 eq), and dry/degassed DMA (0.5 mL). The mixture was stirred until complete dissolution of the metal complex to yield an emerald-green solution (few minutes) (**Figure S1**, top left).

N-trifluoroethoxyphthalimide **2** (73.5 mg, 0.3 mmol, 3 eq), Zn dust (13 mg, 0.2 mmol, 2 eq), NaI (15 mg, 0.1 mmol, 1 eq) and, if solid, aryl iodide **1** (0.1 mmol, 1 eq) were added at once (due to its hygroscopic nature, NaI was weighed last). For liquid aryl iodides, they were added with a 50 µL Hamilton syringe after the solids (**Figure S1**, top right). The heterogeneous mixture appears olive green and turbid (**Figure S1**, bottom left). TMSCl (12.5 µL, 0.1 mmol, 1 eq) was added, and within seconds, a sudden change of color to deep red occurs (**Figure S1**, bottom right).

The Schlenk was sealed and the mixture stirred @ 1250 rpm for the indicated time (until **2** disappeared, judged by TLC). *Vide infra* for the time employed for each substrate.

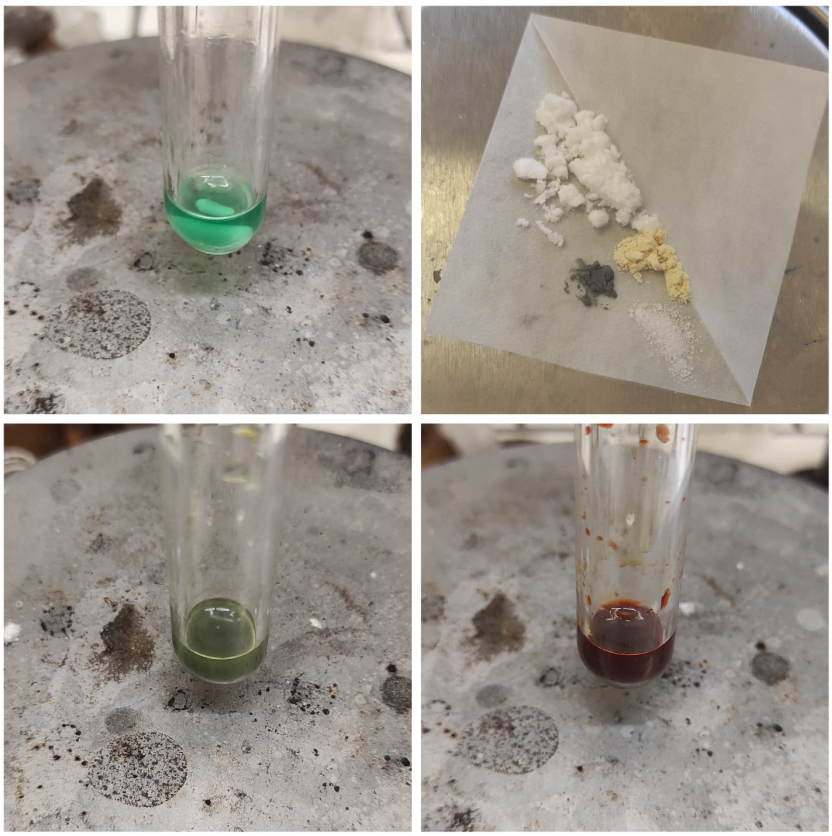

Figure S1. Top Left: [Ni(**L5**)Cl_2] solution in DMA. Top right: Solid reagents (**2**, **1p**, Zn, NaI). Bottom left: Reaction mixture after addition of all solids. Bottom right: Reaction mixture few seconds after the addition of TMSCl.

After the indicated time, the Schlenk was opened to air and EtOAc was added, followed by 2N HCl, and the biphasic mixture was shaken and stirred until all Zn was consumed (roughly 5 minutes). The red color of the organic phase gradually disappears to give a pale-yellow solution. For ^{19}F NMR yield determination, $PhCF_3$ was added to the reaction mixture as an internal standard and an aliquot was taken without solvent evaporation. To isolate the product, the biphasic mixture was directly transferred to a separatory funnel, the aqueous phase extracted with EtOAc (10 mL x 3), and then the combined organic phases were washed twice with diluted HCl (ca 0.1 N, 10 mL x 2). The organic layer was separated, dried on anhydrous Na_2SO_4, and the solvent removed under reduced pressure. Flash chromatography on silica gel with the appropriate eluent yields the product.

Additional notes:

1. In our experience, the observation of the color change towards red does not guarantee high yields, but usually indicates initiation of the reaction and full or almost full conversion of **2** is observed when it occurs. When it does not occur, the reaction provides low yields and low conversion. Addition of TMSCl is not mandatory to observe this change in color, but we noticed that in its presence it always occurs readily, while when it is not added, this phenomenon seems to be more substrate- and conditions dependent.

2. Vigorous stirring (1250 rpm) is beneficial given the heterogeneous nature of the reductant used, and the reaction should not be run at lower stirring speeds.

3. For product **3g**, due to its basic nature, the aqueous phase was brought to pH = 10 by adding saturated Na_2CO_3 solution prior to extraction.

4. For products **3e**, **3f**, **3h**, **3p**, **3y**, **3z**, **3a'**, **3c'**, **7a**, **7c** chromatographic separation from phthalimide coproduct was troublesome, therefore after FC a basic wash (aqueous 1N NH_3 / Et_2O) was carried out to obtain the pure compounds.

5. Products **3a**, **3b**, **3d**, **3i**, **3j**, **3k**, **3l**, **3n**, **3q**, **3r**, **3s** are volatile, therefore special care must be taken when removing the solvent. In particular, products **3k**, **3n**, **3q**, **3r** were prepared on 0.2 mmol scale and Et_2O was used in place of EtOAc for extraction and FC to allow product isolation without significant loss.

6. Product **7c** is scarcely soluble in EtOAc, therefore *i*PrOAc was used for extraction and chromatographic purification.

7. For product **3y** the General Procedure was slightly modified by doubling the amount of [Ni(**L5**)Cl_2], Zn and **2**.

8. For product **3b'**, *N*-pentafluoropropoxyphthalimide **2'** (88.5 mg, 0.3 mmol, 3 eq) was used instead of **2**.

Unsuccessful substrates

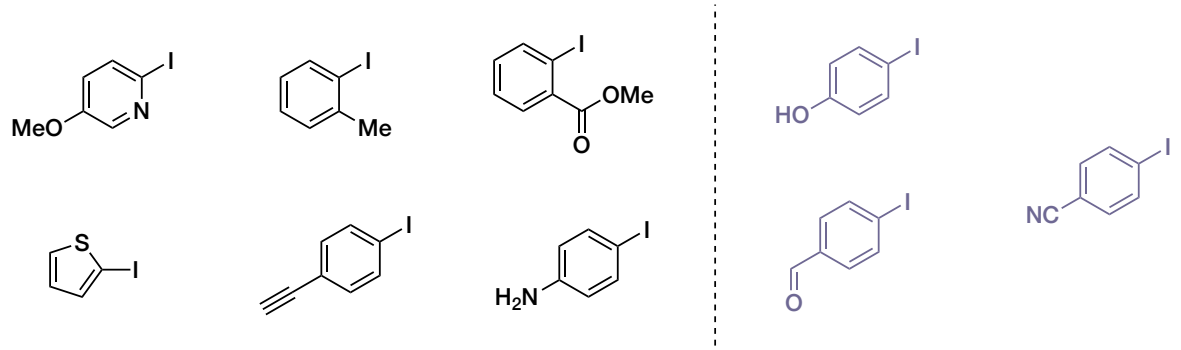

Substrates on the left (in black) gave the corresponding products in less than 15% yield. Substrates on the right (in purple) could give the product in more than 50% yield (based on ^{19}F NMR) but it resulted impossible to separate from phthalimide by flash chromatography and resulted unstable to basic washes. Therefore, they were not included in the scope.

Characterization data of products

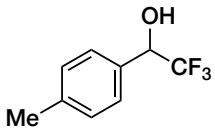

3a. Viscous colorless oil. Reaction time: 2 h. FC eluent: *n*Hex/EtOAc: 7:1. Yield = 88%, (0.088 mmol, 16.7 mg). **^{1}H NMR** (400 MHz, $CDCl_3$) δ = 7.38 – 7.31 (m, 2H), 7.23 – 7.18 (m, 2H), 4.97 (q, *J* = 6.8 Hz, 1H), 2.54 (bs, 1H), 2.36 (s, 3H); **^{13}C NMR** (100 MHz, $CDCl_3$) δ = 139.5, 131.0, 129.3 (2C), 127.3 (q, *J* = 1.0 Hz, 2C), 124.3 (q, *J* = 282.0 Hz), 72.7 (q, *J* = 31.9 Hz), 21.2; **^{19}F NMR** (377 MHz, $CDCl_3$) δ = -78.47 (d, *J* = 6.7 Hz, 3F). This is a known compound and spectral data are in accordance with the literature.[272]

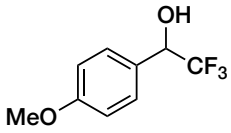

3b. Viscous colorless oil. Reaction time: 3 h. FC eluent: *n*Hex/EtOAc: 6:1. Yield = 61%, (0.061 mmol, 12.6 mg). **^{1}H NMR** (400 MHz, $CDCl_3$) δ = 7.42 – 7.33 (m, 2H), 6.97 – 6.88 (m, 2H), 4.95 (qd, *J* = 6.7, 4.2 Hz, 1H), 3.81 (s, 3H), 2.53 (d, *J* = 4.3 Hz, 1H); **^{13}C NMR** (100 MHz, $CDCl_3$) δ = 160.5, 128.7 (q, *J* = 1.0 Hz, 2C), 126.1 (q, *J* = 1.1 Hz), 124.3 (q, *J* = 281.9 Hz), 114.0 (2C), 72.5 (q, *J* = 32.0 Hz), 55.3; **^{19}F NMR** (377 MHz, $CDCl_3$) δ = -78.60 (d, *J* = 6.8 Hz, 3F). This is a known compound and spectral data are in accordance with the literature.[273]

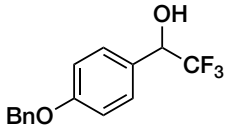

3c. White solid. Reaction time: 5 h FC eluent: *n*Hex/EtOAc: 6:1. Yield = 63%, (0.063 mmol, 17.8 mg). **MP** = 101 – 103 °C. **^{1}H NMR** (400 MHz, $CDCl_3$) δ = 7.45 – 7.29 (m, 7H), 7.03 – 6.96 (m, 2H), 5.07 (s, 2H), 4.97 – 4.91 (m, 1H), 2.56 (d, *J* = 4.1 Hz, 1H); **^{13}C NMR** (100 MHz, $CDCl_3$) δ 159.7, 136.6, 128.8 (2C), 128.6 (2C), 128.1, 127.5 (2C), 126.3, 124.30 (q, *J* = 282.0 Hz), 114.9 (2C), 72.5 (q, *J* = 32.0 Hz), 70.1; **^{19}F NMR** (377 MHz, $CDCl_3$) δ = -78.54 (d, *J* = 6.8 Hz, 3F). This is a known compound and spectral data are in accordance with the literature.[274]

---

[272] G. K. S. Prakash, Z. Zhang, F. Wang, S. Munoz, G. A. Olah, *J. Org. Chem.* **2013**, *78*, 3300−3305.
[273] R. Kani, T. Inuzuka, Y. Kubota, K. Funabiki, *Eur. J. Org. Chem.* **2020**, 4487–4493.
[274] B. Zhang, X. Zhang, J. Hao, C. Yang, *Eur. J. Org. Chem.* **2018**, 5007–5015.

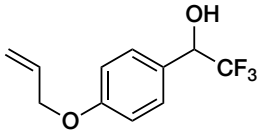

3d. White solid. Reaction time: 5 h. FC eluent: *n*Hex/EtOAc: 6:1. Yield = 50%, (0.050 mmol, 11.8 mg). **MP** = 51 – 53 °C. **^{1}H NMR** (400 MHz, $CDCl_3$) δ = 7.41 – 7.36 (m, 2H), 6.99 – 6.92 (m, 2H), 6.05 (ddt, *J* = 17.3, 10.5, 5.3 Hz, 1H), 5.42 (dq, *J* = 17.3, 1.7 Hz, 1H), 5.30 (dq, *J* = 10.5, 1.4 Hz, 1H), 4.96 (qd, *J* = 6.6, 3.6 Hz, 1H), 4.55 (dt, *J* = 5.3, 1.6 Hz, 2H), 2.47 (d, *J* = 4.3 Hz, 1H); **^{13}C NMR** (100 MHz, $CDCl_3$) δ = 158.5, 131.9, 127.7 (2C), 125.2, 123.3 (q, *J* = 282.2 Hz), 116.9, 113.8 (2C), 71.46 (q, *J* = 32.1 Hz), 67.8; **^{19}F NMR** (377 MHz, $CDCl_3$) δ = -78.53 (d, *J* = 6.8 Hz, 3F). This is a known compound and spectral data are in accordance with the literature.[275]

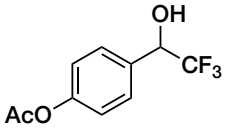

3e. White solid. Reaction time: 5 h. FC eluent: *n*Hex/EtOAc: 4.5:1. Yield = 62%, (0.062 mmol, 14.5 mg). **MP** = 95 – 98 °C. **^{1}H NMR** (400 MHz, $CDCl_3$) δ = 7.52 – 7.45 (m, 2H), 7.17 – 7.08 (m, 2H), 5.01 (q, *J* = 6.7 Hz, 1H), 2.66 (bs, 1H), 2.29 (s, 3H); **^{13}C NMR** (100 MHz, $CDCl_3$) δ = 169.2, 151.5, 131.5, 128.6 (2C), 124.1 (q, *J* = 282.2 Hz), 121.8 (2C), 72.3 (q, *J* = 32.2 Hz), 21.1; **^{19}F NMR** (377 MHz, $CDCl_3$) δ = -78.46 (d, *J* = 6.8 Hz, 3F). This is a known compound and spectral data are in accordance with the literature.[276]

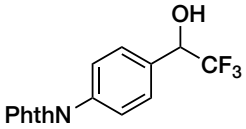

3f. White solid. Reaction time: 16 h. FC eluent: *n*Hex/EtOAc: 2:1. Yield = 74%, (0.074 mmol, 23.8 mg). **MP** = 202 – 204 °C. **^{1}H NMR** (400 MHz, acetone-d_6) δ = 7.97 – 7.93 (m, 2H), 7.93 – 7.90 (m, 2H), 7.74 – 7.68 (m, 2H), 7.61 – 7.54 (m, 2H), 5.97 (d, *J* = 5.4 Hz, 1H), 5.32 (qd, *J* = 7.1, 5.2 Hz, 1H); **^{13}C NMR** (100 MHz, acetone-d_6) δ = 166.8 (2C), 135.3 (q, *J* = 1.6 Hz), 134.5 (2C), 133.0, 132.0 (2C), 128.1 (q, 0.8 Hz, 2C), 126.8 (2C), 125.0 (q, *J* = 281.9 Hz), 123.3 (2C), 71.2 (q, *J* = 31.2 Hz); **^{19}F NMR** (377 MHz, acetone-d_6) δ = -78.64 (d, *J* = 7.0 Hz, 3F); **HRMS (APCI)** m/z: $[M+H]^+$ calcd. for $C_6H_{11}F_3NO_3$ 322.0691; found 322.0682.

---

[275] K. Terashima, T. Kawasaki-Takasuka, I. Minami, T. Yamazaki, *Tetrahedron* **2022**, *104*, 132574.
[276] L. Rushaa, S. C. Miller, *Chem. Commun.* **2011**, *47*, 2038–2040.

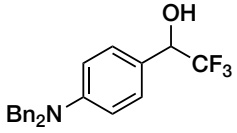

3g. White solid. Reaction time: 3 h. FC eluent: *n*Hex/EtOAc: 4:1. Yield = 73%, (0.073 mmol, 27.1 mg). **MP** = 152 – 154 °C. **^{1}H NMR** (400 MHz, $CDCl_3$) δ = 7.32 – 7.23 (m, 4H), 7.22 – 7.14 (m, 8H), 6.68 – 6.64 (m, 2H), 4.79 (q, *J* = 7.0 Hz, 1H), 4.60 (s, 4H), 2.27 (bs, 1H); **^{13}C NMR** (150 MHz, $CDCl_3$) δ = 149.0, 137.0 (2C), 127.7 (4C), 127.6 (2C), 126.0 (2C), 125.5 (4C), 123.5 (q, *J* = 281.8 Hz), 120.8, 111.1 (2C), 71.70 (q, *J* = 32.0 Hz), 53.1 (2C); **^{19}F NMR** (565 MHz, $CDCl_3$) δ = -78.3 (d, *J* = 6.9 Hz, 3F); **HRMS (ESI)** m/z: $[M+H]^+$ calcd. for $C_{22}H_{20}F_3NO$ 372.1575; found 372.1567.

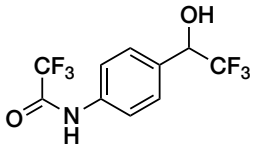

3h. White solid. Reaction time: 16 h. FC eluent: *n*Hex/Acetone: 3:1. Yield = 63%, (0.063 mmol, 18.1 mg). **MP** = 147 – 150 °C. **^{1}H NMR** (400 MHz, acetone-d_6) δ = 10.38 (bs, 1H), 7.80 – 7.74 (m, 2H), 7.61 – 7.54 (m, 2H), 5.97 (d, *J* = 5.5 Hz ,1H), 5.26 – 5.16 (m, 1H), peaks at 10.38 ppm and 5.97 ppm show an integral value lower than unity, probably due to partial H-D exchange with the solvent; **^{13}C NMR** (100 MHz, acetone-d_6) δ = 154.9 and 154.8 (q, *J* = 37.6 Hz, two isotopomeric signals), 137.1 and 137.0 (two isotopomeric signals), 133.1 (two isotopomeric signals), 128.3 (2C), 125.0 (q, *J* = 281.9 Hz), 120.5 and 120.4 (2C, two isotopomeric signals), 116.0 (q, *J* = 287.9 Hz), 71.1 and 70.9 (q, *J* = 31.2 Hz, two isotopomeric signals), some signals appear split due to partial H-D exchange with the solvent giving rise to two isotopomers; **^{19}F NMR** (377 MHz, $CDCl_3$) δ = -76.23 (s, 3F), -78.83 (d, *J* = 7.3 Hz, 3F); **HRMS (ESI)** m/z: $[M-H]^-$ calcd. for $C_{10}H_6F_6NO_2$ 286.0308; found 286.0323.

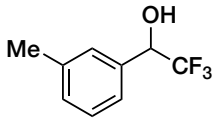

3i. Viscous colorless oil. Reaction time: 3 h. FC eluent: *n*Hex/EtOAc: 7:1. Yield = 62%, (0.062 mmol, 11.8 mg). **^{1}H NMR** (400 MHz, $CDCl_3$) δ = 7.31 – 7.25 (m, 3H), 7.23 – 7.19 (m, 1H), 4.97 (q, *J* = 6.7 Hz, 1H), 2.51 (bs, 1H), 2.37 (s, 3H); **^{13}C NMR** (100 MHz, $CDCl_3$) δ = 138.4, 133.9, 130.3, 128.5, 128.0 (q, *J* = 1.4 Hz), 124.5 (q, *J* = 1.1 Hz), 124.2 (q, *J* = 282.1 Hz), 72.9 (q, *J* = 31.9

Hz), 21.4; **^{19}F NMR** (377 MHz, $CDCl_3$) δ = -78.32 (d, *J* = 6.8 Hz, 3F). This is a known compound and spectral data are in accordance with the literature.[272]

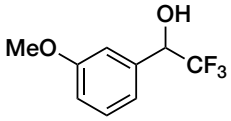

3j. Colorless oil. Reaction time: 6 h. FC eluent: *n*Hex/EtOAc: 6:1. Yield = 64%, (0.064 mmol, 13.2 mg). **^{1}H NMR** (400 MHz, $CDCl_3$) δ = 7.35 – 7.28 (m, 1H), 7.07 – 6.99 (m, 2H), 6.93 (ddd, *J* = 8.4, 2.6, 1.1 Hz, 1H), 4.98 (q, *J* = 6.7 Hz, 1H), 3.81 (s, 3H), 2.63 (bs, 1H); **^{13}C NMR** (100 MHz, $CDCl_3$) δ = 159.7, 135.4 (q, *J* = 1.2 Hz), 129.7, 124.2 (q, *J* = 282.1 Hz), 119.7 (q, *J* = 0.8 Hz), 115.09, 112.9 (q, *J* = 1.0 Hz), 72.7 (q, *J* = 32.0 Hz), 55.3; **^{19}F NMR** (377 MHz, $CDCl_3$) δ = -78.38 (d, *J* = 6.7 Hz, 3F). This is a known compound and spectral data are in accordance with the literature.[277]

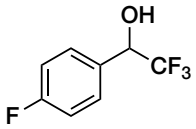

3k. Colorless oil. Reaction time: 16 h. FC eluent: *n*Hex/Et_2O: 4.5:1. Yield = 55%, (0.11 mmol, 21.40 mg, reaction performed on 0.2 mmol scale). **^{1}H NMR** (400 MHz, $CDCl_3$) δ = 7.49 – 7.41 (m, 2H), 7.14 – 7.04 (m, 2H), 5.01 (q, *J* = 6.6 Hz, 1H), the OH signal was not detected; **^{13}C NMR** (100 MHz, $CDCl_3$) δ = 163.4 (d, *J* = 248.5 Hz), 129.7 – 129.6 (m), 129.3 (dq, *J* = 8.6, 0.9 Hz, 2C), 124.1 (qd, *J* = 281.8, 1.1 Hz), 115.6 (d, *J* = 21.8 Hz, 2C), 72.2 (q, *J* = 32.2 Hz); **^{19}F NMR** (377 MHz, $CDCl_3$) δ = -76.93 (d, *J* = 6.6 Hz, 3F), -111.81 – -111.89 (m, 1F). This is a known compound and spectral data are in accordance with the literature.[272]

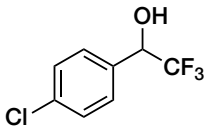

3l. Colorless oil. Reaction time: 16 h. FC eluent: *n*Hex/EtOAc: 10:1. Yield = 56%, (0.056 mmol, 11.8 mg). **^{1}H NMR** (400 MHz, $CDCl_3$) δ = 7.44 – 7.39 (m, 2H), 7.39 – 7.35 (m, 2H), 5.00 (q, *J* = 6.2 Hz, 1H), 2.69 (s, 1H); **^{13}C NMR** (100 MHz, $CDCl_3$) δ = 135.5, 132.3 (q, *J* = 1.0 Hz), 128.8 (2C), 128.8 (q, *J* = 0.9 Hz, 2C) 124.0 (q, *J* = 281.9 Hz), 72.1 (q, *J* = 32.1 Hz); **^{19}F NMR** (377

[277] K. Aikawa, W. Toya, Y. Nakamura, K. Mikami, *Org. Lett.* **2015**, *17*, 4996−4999.

MHz, $CDCl_3$) δ = -78.59 (d, *J* = 6.4 Hz, 3F). This is a known compound and spectral data are in accordance with the literature.[272]

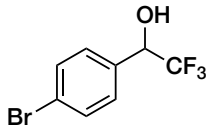

3m. Colorless oil. Reaction time: 16 h. FC eluent: *n*Hex/EtOAc: 10:1. Yield = 60%, (0.060 mmol, 15.2 mg). **^{1}H NMR** (600 MHz, $CDCl_3$) δ = 7.50 – 7.46 (m, 2H), 7.31 – 7.26 (m, 2H), 4.93 (qd, *J* = 6.7, 3.8 Hz, 1H), 2.86 (bs, 1H); **^{13}C NMR** (150 MHz, $CDCl_3$) δ = 136.7, 130.8 (2C), 128.1 (2C), 123.0 (q, *J* = 282.3 Hz), 122.7, 71.2 (q, *J* = 32.2 Hz); **^{19}F NMR** (565 MHz, $CDCl_3$) δ = -78.52 (d, *J* = 6.8 Hz, 3F). This is a known compound and spectral data are in accordance with the literature.[33] This compound was isolated as an inseparable 9:1 mixture with the corresponding *p*-iodo derivative. Relevant signals in the ^{1}H NMR spectrum for this compound are: 7.69 – 7.66 (m, 2H) and 7.16 – 7.14 (m, 2H). The ^{19}F NMR spectrum for this compound shows a doublet at -78.49 ppm. This is a known compound and spectral data are in accordance with the literature.[278]

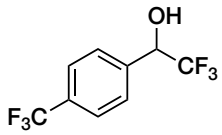

3n. Colorless oil. Reaction time: 16 h. FC eluent: *n*Hex/Et_2O: 4.5:1. Yield = 58%, (0.116 mmol, 28.4 mg, reaction performed on 0.2 mmol scale). **^{1}H NMR** (400 MHz, $CDCl_3$) δ = 7.70 – 7.64 (m, 2H), 7.64 – 7.57 (m, 2H), 5.15 – 5.04 (m, 1H), 2.82 (d, *J* = 3.9 Hz, 1H); **^{13}C NMR** (100 MHz, $CDCl_3$) δ = 137.6 – 137.5 (m), 131.7 (q, *J* = 32.6 Hz), 127.9 (q, *J* = 0.9 Hz, 2C), 125.5 (q, *J* = 3.8 Hz, 2C), 123.9 (q, *J* = 282.4 Hz) partially overlapped with 123.8 (q, *J* = 272.3 Hz), 72.2 (q, *J* = 32.2 Hz); **^{19}F NMR** (377 MHz, $CDCl_3$) δ = -62.90 (s, 3F), -78.59 (d, *J* = 6.4 Hz, 3F). This is a known compound and spectral data are in accordance with the literature.[277]

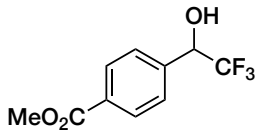

3o. White solid. Reaction time: 16 h. FC eluent: *n*Hex/EtOAc: 5:1. Yield = 73%, (0.073 mmol, 17.1 mg). **MP** = 46 – 49 °C. **^{1}H NMR** (400 MHz, $CDCl_3$) δ = 8.08 – 8.01 (m, 2H), 7.58 – 7.51 (m, 2H),

[278] G. E. Aspnes, R. L. Dow, M. J. Munchhof, 4-Amino-7,8-Dihydropyrido[4,3-d]pyrimidin-5(6H)-one Derivatives. US 2010/197591 A1, August 5, 2010.

5.08 (q, *J* = 6.6 Hz, 1H), 3.91 (s, 3H), 3.02 (bs, 1H); **^{13}C NMR** (100 MHz, $CDCl_3$) δ = 166.6, 138.6 (q, *J* = 1.2 Hz), 131.1, 129.7 (2C), 127.5 (q, *J* = 0.9 Hz, 2C), 124.0 (q, *J* = 282.3 Hz), 72.3 (q, *J* = 32.1 Hz), 52.29; **^{19}F NMR** (377 MHz, $CDCl_3$) δ = -78.24 (d, *J* = 6.7 Hz, 3F). This is a known compound and spectral data are in accordance with the literature.[230j]

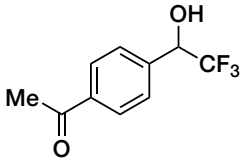

3p. White solid. Reaction time: 16 h. FC eluent: *n*Hex/EtOAc: 5:1. Yield = 68%, (0.068 mmol, 14.8 mg). **MP** = 97 – 99 °C. **^{1}H NMR** (400 MHz, $CDCl_3$) δ = 8.01 – 7.93 (m, 2H), 7.61 – 7.55 (m, 2H), 5.10 (q, *J* = 6.7 Hz, 1H), 2.88 (bs, 1H), 2.60 (s, 3H); **^{13}C NMR** (100 MHz, $CDCl_3$) δ = 197.7, 138.8 (q, *J* = 1.1 Hz), 138.0, 128.6 (2C), 127.8 (q, *J* = 0.9 Hz, 2C), 124.0 (q, *J* = 282.3 Hz), 72.3 (q, *J* = 32.2 Hz), 26.7; **^{19}F NMR** (377 MHz, $CDCl_3$) δ = -78.23 (d, *J* = 6.7 Hz, 3F). This is a known compound and spectral data are in accordance with the literature.[279]

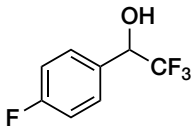

3q. Viscous colorless oil. Reaction time: 16 h. FC eluent: *n*Hex/Et_2O: 4.5:1. Yield = 65%, (0.130 mmol, 25.2 mg, reaction performed on 0.2 mmol scale). **^{1}H NMR** (400 MHz, $CDCl_3$) δ = 7.42 – 7.32 (m, 1H), 7.27 – 7.17 (m, 2H), 7.17 – 7.04 (m, 1H), 5.07 – 4.97 (m, 1H), 2.70 (d, *J* = 4.5 Hz, 1H); **^{13}C NMR** (100 MHz, $CDCl_3$) δ = 162.8 (d, *J* = 246.9 Hz), 136.2 (d, *J* = 8.7 Hz), 130.2 (d, *J* = 8.1 Hz), 124.0 (q, *J* = 282.1 Hz), 123.2 – 123.1 (m), 116.5 (d, *J* = 21.2 Hz), 114.5 (dq, *J* = 22.8, 1.0 Hz), 72.2 (qd, *J* = 32.2, 1.9 Hz); **^{19}F NMR** (377 MHz, $CDCl_3$) δ = -78.45 (d, *J* = 6.5 Hz, 3F), -112.18 (td, *J* = 9.0, 5.6 Hz, 1F). This is a known compound and spectral data are in accordance with the literature.[280]

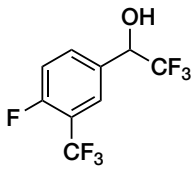

3r. Viscous colorless oil. Reaction time: 16 h. FC eluent: *n*Hex/Et_2O: 4:1. Yield = 43%, (0.086 mmol, 22.6 mg, reaction performed on 0.2 mmol scale). **^{1}H NMR** (400 MHz, $CDCl_3$) δ = 7.75 (d, *J* = 6.7 Hz, 1H),

[279] J. J. Song, Z. Tan, J. T. Reeves, F. Gallou, N. K. Yee, C. H. Senanayake, *Org. Lett.* **2005**, *7*, 2193-2197.
[280] M. Brambilla, M. Tredwell, *Angew. Chem. Int. Ed.* **2017**, *56*, 11981–11985.

7.73 – 7.65 (m, 1H), 7.26 (t, *J* = 9.6 Hz, 1H), 5.09 (q, *J* = 6.5 Hz, 1H), 2.88 (bs, 1H); **^{13}C NMR** (150 MHz, $CDCl_3$) δ = 159.3 (dq, *J* = 259.0, 2.1 Hz), 132.0 (d, *J* = 8.9 Hz), 129.1 (d, *J* = 3.8 Hz), 125.5 (q, *J* = 5.2 Hz), 122.8 (q, *J* = 282.0 Hz) partially overlapped with 121.2 (q, *J* = 272.4 Hz), 117.8 (qd, *J* = 33.4, 12.9 Hz), 116.3 (d, *J* = 20.9 Hz), 70.5 (q, *J* = 32.4 Hz); **^{19}F NMR** (377 MHz, $CDCl_3$) δ = -61.61 (d, *J* = 12.7 Hz, 3F), -78.76 (d, *J* = 6.3 Hz, 3F), -112.95 – -113.14 (m, 1F); **HRMS (ESI)** m/z: $[M+HCOO]^-$ calcd. for $C_{10}H_6F_7O_3$ 307.0211; found 307.0216.

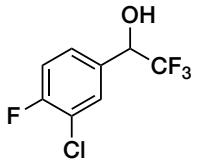

3s. Viscous colorless oil. Reaction time: 16 h. FC eluent: *n*Hex/EtOAc: 10:1. Yield = 65%, (0.065 mmol, 14.8 mg). **^{1}H NMR** (600 MHz, $CDCl_3$) δ = 7.76 (dd, *J* = 6.7, 2.3 Hz, 1H), 7.71 – 7.66 (m, 1H), 7.26 (t, *J* = 9.2 Hz, 1H), 5.09 (q, *J* = 6.5 Hz, 1H), 2.94 (bs, 1H); **^{13}C NMR** (150 MHz, $CDCl_3$) δ = 157.7 (d, *J* = 251.3 Hz), 129.8 (d, *J* = 4.0 Hz), 128.9, 126.3 (d, *J* = 7.6 Hz), 122.9 (q, *J* = 282.1 Hz), 120.5 (d, *J* = 18.1 Hz), 115.8 (d, *J* = 21.6 Hz), 70.6 (q, *J* = 32.4 Hz); **^{19}F NMR** (565 MHz, $CDCl_3$) δ = -78.62 (d, *J* = 6.8 Hz, 3F), -113.87 – -113.93 (m, 1F). This is a known compound and spectral data are in accordance with the literature.[281]

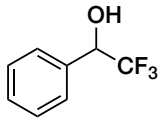

3t. Reaction time: 4 h. Compound **3t** was found to be too volatile to be isolated on 0.1 mmol scale. The yield given (70%) was determined by ^{19}F NMR analysis on the crude reaction mixture. This is a known compound and spectral data observed in the crude is in accordance with the literature.[273]

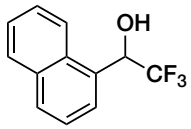

3u. Colorless oil. Reaction time: 16 h. FC eluent: *n*Hex/EtOAc: 9:1. Yield = 61%, (0.061 mmol, 13.8 mg). **^{1}H NMR** (400 MHz, $CDCl_3$) δ = 8.05 (d, *J* = 8.4 Hz, 1H), 7.95 – 7.87 (m, 2H), 7.83 (d, *J* = 7.3 Hz, 1H), 7.60 – 7.42 (m, 3H), 5.89 (q, *J* = 6.5 Hz, 1H), 2.84 (bs, 1H); **^{13}C NMR** (100 MHz, $CDCl_3$) δ = 133.7, 131.1, 130.1, 130.0 (q, *J* = 0.9 Hz), 129.0, 126.8, 125.9, 125.8 (q, *J*

[281] T. Barton, X. Gao, J. Hunter, P. R. Leplae Jr., W. C. Lo, J. Boruwa, R. Tangirala, G. B. Watson, J. Herbert, Molecules Having Pesticida Utility, and Intermediates, Compositions, and Processes, Related thereto. US 2017/208804 A1, July 27, 2017.

= 1.3 Hz), 125.2, 124.7 (q, *J* = 282.6 Hz), 122.8 (q, *J* = 1.4 Hz), 69.0 (q, *J* = 32.3 Hz); **^{19}F NMR** (377 MHz, $CDCl_3$) δ = -76.93 (d, *J* = 6.6 Hz, 3F). This is a known compound and spectral data are in accordance with the literature.[273]

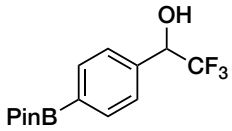

3v. White solid. Reaction time: 16 h. FC eluent: *n*Hex/EtOAc: 5:1. Yield = 43%, (0.043 mmol, 7.5 mg). **MP** = 84 – 87 °C. **^{1}H NMR** (400 MHz, $CDCl_3$) δ = 7.86 – 7.80 (m, 2H), 7.49 – 7.43 (m, 2H), 5.02 (qd, *J* = 6.7, 4.6 Hz, 1H), 2.59 (d, *J* = 4.6 Hz, 1H), 1.33 (s, 12 H); **^{13}C NMR** (100 MHz, $CDCl_3$) δ = 136.7 (q, *J* = 1.0 Hz), 135.0 (2C), 126.7 (2C), 124.1 (q, *J* = 282.3 Hz), 84.0 (2C), 72.8 (q, *J* = 31.9 Hz), 24.8 (4C), the quaternary carbon connected to the B atom is too broad and was not detected; **^{19}F NMR** (377 MHz, $CDCl_3$) δ = -78.27 (d, *J* = 6.7 Hz, 3F); **HRMS (ESI)** m/z: $[M+HCOO]^-$ calcd. for $C_{15}H_{19}BF_3O_5$ 347.1283; found 347.1291.

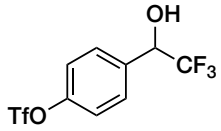

3w. Viscous colorless oil. Reaction time: 7 h. FC eluent: *n*Hex/EtOAc: 7:1. Yield = 61%, (0.061 mmol, 19.8 mg). **^{1}H NMR** (400 MHz, $CDCl_3$) δ = 7.61 – 7.55 (m, 2H), 7.36 – 7.27 (m, 2H), 5.07 (q, *J* = 6.5 Hz, 1H), the OH signal was not detected; **^{13}C NMR** (100 MHz, $CDCl_3$) δ = 150.1, 134.3 (q, *J* = 1.0 Hz), 129.5 (q, *J* = 0.8 Hz, 2C), 123.8 (q, *J* = 282.2 Hz), 121.6 (2C), 118.7 (q, *J* = 320.6 Hz), 71.8 (q, *J* = 32.4 Hz); **^{19}F NMR** (377 MHz, $CDCl_3$) δ = -72.85 (s, 3F), -78.54 (d, *J* = 6.3 Hz, 3F); **HRMS (ESI)** m/z: $[M+HCOO]^-$ calcd. for $C_{10}H_7F_6O_6S$ 368.9873; found 368.9889.

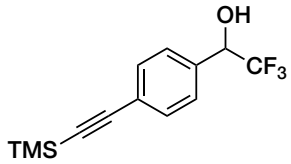

3x. Yellow solid. Reaction time: 16 h. FC eluent: *n*Hex/EtOAc: 8:1. Yield = 65%, (0.065 mmol, 17.7 mg). **MP** = 58 – 60 °C. **^{1}H NMR** (400 MHz, $CDCl_3$) δ = 7.52 – 7.45 (m, 2H), 7.43 – 7.36 (m, 2H), 5.00 (q, *J* = 6.7 Hz, 1H), 2.66 (bs, 1H), 0.24 (s, 9H); **^{13}C NMR** (100 MHz, $CDCl_3$) δ = 133.9 (q, *J* = 1.1 Hz), 132.1 (2C), 127.2 (q, *J* = 0.8 Hz, 2C), 124.5, 124.0 (q, *J* = 282.2 Hz), 104.2, 95.5, 72.5 (q, *J* = 32.1 Hz), -0.14 (3C); **^{19}F NMR** (377 MHz,

$CDCl_3$) δ = -78.38 (d, *J* = 6.7 Hz, 3F);). This is a known compound and spectral data are in accordance with the literature.[282]

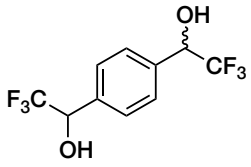

3y. White solid. Reaction time: 16 h. FC eluent: *n*Hex/EtOAc: 8:1. Yield = 73%, (0.073 mmol, 20.0 mg), 1:1 *dr*. **^{1}H NMR** (400 MHz, $CDCl_3$) δ = 7.53 (s, 4H), 5.05 (q, *J* = 6.7 Hz, 2H), 2.65 (bs, 2H), the signals of the two diastereoisomers overlap completely, appearing as a single compound; **^{13}C NMR** (100 MHz, $CDCl_3$) δ = 135.2 (2C), 127.7 (4C), 124.1 (q, *J* = 282.0 Hz, 2C), 72.4 (q, *J* = 32.3 Hz, 2C, two diastereomeric signals), The signals of the two diastereoisomers overlap in some cases, appearing as a single compound, in other cases (as specified in the list) they split; **^{19}F NMR** (377 MHz, $CDCl_3$) δ = -78.38 (d, *J* = 6.5 Hz, 6F), the signals of the two diastereoisomers overlap completely, appearing as a single compound. This is a known compound and spectral data are in accordance with the literature.[283]

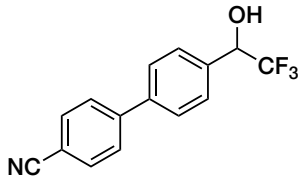

3z. White solid. Reaction time: 16 h. FC eluent: *n*Hex/EtOAc: 5:1. Yield = 58% (0.058 mmol, 16.1 mg). **MP** = 152 – 154 °C. **^{1}H NMR** (400 MHz, $CDCl_3$) δ = 7.75 – 7.70 (m, 2H), 7.69 – 7.65 (m, 2H), 7.64 – 7.56 (m, 4H), 5.09 (q, *J* = 6.7 Hz, 1H), 2.79 (bs, 1H); **^{13}C NMR** (100 MHz, $CDCl_3$) δ = 144.8, 140.3, 134.3, 132.7 (2C), 128.2 (q, *J* = 1.0 Hz, 2C), 127.8 (2C), 127.4 (2C), 124.1 (q, *J* = 282.2 Hz), 118.8, 111.3, 72.4 (q, *J* = 32.1 Hz); **^{19}F NMR** (377 MHz, $CDCl_3$) δ = -78.33 (d, *J* = 6.6 Hz); **HRMS (ESI)** m/z: $[M+HCOO]^-$ calcd. for $C_{16}H_{11}F_3NO_3$ 322.0697; found 322.0700.

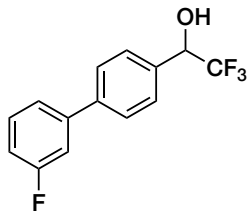

3a'. White solid. Reaction time: 16 h. FC eluent: *n*Hex/EtOAc: 8:1. Yield = 75% (0.075 mmol, 20.3 mg) reaction run on 0.1 mmol scale. Yield = 81% (0.81 mmol, 218.7 mg) reaction run on 1.0 mmol scale (unmodified protocol with the exception of 4.0 mL of DMA

[282] W. J. Hoekstra, C. M. Yates, Metalloenzyme Inhibitor Compounds. WO 2013/090210 A1, June 20, 2013.
[283] A. J. Roche, *Magn. Reson. Chem.* **2004**, *42*, 944–949.

employed as the solvent). **MP** = 67 – 70 °C. **^{1}H NMR** (400 MHz, $CDCl_3$) δ = 7.63 – 7.58 (m, 2H), 7.57 – 7.52 (m, 2H), 7.44 – 7.33 (m, 2H), 7.27 (ddd, *J* = 10.2, 2.5, 1.6 Hz, 1H), 7.09 – 7.02 (m, 1H), 5.07 (q, *J* = 6.7 Hz, 1H), 2.75 (s, 1H); **^{13}C NMR** (100 MHz, $CDCl_3$) δ = 163.2 (d, *J* = 246.0 Hz), 142.6 (d, *J* = 7.6 Hz), 141.2 (d, *J* = 2.3 Hz), 133.4 (q, *J* = 1.1 Hz), 130.3 (d, *J* = 8.5 Hz), 128.0 (q, *J* = 0.9 Hz, 2C), 127.3 (2C), 124.2 (q, *J* = 281.9 Hz), 122.8 (d, *J* = 3.0 Hz), 114.5 (d, *J* = 21.2 Hz), 114.0 (d, *J* = 22.1 Hz), 72.5 (q, *J* = 32.1 Hz); **^{19}F NMR** (377 MHz, $CDCl_3$) δ = -78.32 (d, *J* = 6.7 Hz), -112.89 (ddd, *J* = 10.0, 8.3, 5.5 Hz). This is a known compound and spectral data are in accordance with the literature.[284]

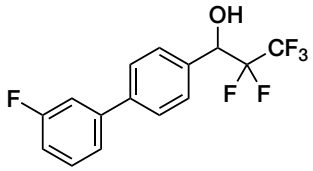

3b'. White solid. Reaction time: 16 h. FC eluent: *n*Hex/EtOAc: 10:1. Yield = 22% (0.022 mmol, 7.0 mg). **MP** = 65 – 68 °C. **^{1}H NMR** (400 MHz, $CDCl_3$) δ = 7.66 – 7.60 (m, 2H), 7.59 – 7.52 (m, 2H), 7.45 – 7.36 (m, 2H), 7.30 (dt, *J* = 10.1, 2.1 Hz, 1H), 7.10 – 7.02 (m, 1H), 5.19 (ddd, *J* = 16.6, 7.2, 4.9 Hz, 1H), 2.56 (d, *J* = 5.0 Hz, 1H); **^{13}C NMR** (100 MHz, $CDCl_3$) δ = 163.2 (d, *J* = 246.0 Hz), 142.5 (d, *J* = 7.6 Hz), 141.3 (d, *J* = 2.1 Hz), 133.4, 130.3 (d, *J* = 8.4 Hz), 128.4 (2C), 127.3 (2C), 122.8 (d, *J* = 3.0 Hz), 114.5 (d, *J* = 21.3 Hz), 114.1 (d, *J* = 22.1 Hz), 71.7 (dd, *J* = 28.1, 22.6 Hz), the CF_2 and CF_3 carbons of the pentafluoroethyl group were not detected; **^{19}F NMR** (377 MHz, $CDCl_3$) δ = -81.20 (s, 3F), -112.87 (td, *J* = 9.3, 5.6 Hz, 1F), -121.66 (dd, *J* = 275.9, 7.3 Hz, 1F), -129.27 (dd, *J* = 276.0, 16.6 Hz, 1F); **HRMS (ESI)** m/z: $[M+HCOO]^-$ calcd. for $C_{16}H_{11}F_6O_3$ 365.0618; found 365.0625.

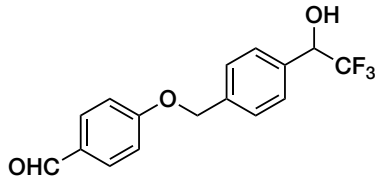

3c'. White solid. Reaction time: 16 h. FC eluent: *n*Hex/EtOAc: 3:1. Yield = 50% (0.050 mmol, 15.5 mg). **MP** = 114 – 117 °C. **^{1}H NMR** (400 MHz, $CDCl_3$) δ = 9.86 (s, 1H), 7.86 – 7.78 (m, 2H), 7.53 – 7.49 (m, 2H), 7.48 – 7.44 (m, 2H), 7.10 – 7.02 (m, 2H), 5.16 (s, 2H), 5.04 (q, *J* = 6.8 Hz, 1H), 2.90 (s, 1H); **^{13}C NMR** (100 MHz, $CDCl_3$)

[284] M. B. Johansen, O. R. Gedde, T. S. Mayer, T. Skrydstrup, *Org. Lett.* **2020**, *22*, 4068−4072.

δ = 190.9, 163.5, 137.4, 134.1, 132.0 (2C), 130.2, 127.8 (2C), 127.5 (2C), 124.2 (q, *J* = 282.3 Hz), 115.1 (2C), 72.5 (q, *J* = 31.9 Hz), 69.7; **^{19}F NMR** (377 MHz, $CDCl_3$) δ = -78.4 (d, *J* = 6.7 Hz); **HRMS (ESI)** m/z: $[M+HCOO]^-$ calcd. for $C_{17}H_{14}F_3O_5$ 355.0799; found 355.0788.

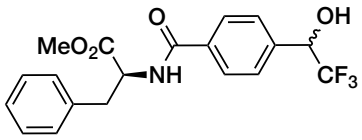

7a. White solid. Reaction time: 16 h. FC eluent: *n*Hex/EtOAc: 3:1. Yield = 65%, (0.065 mmol, 24.8 mg), 1:1 *dr*. **^{1}H NMR** (400 MHz, $CDCl_3$) δ = 7.70 – 7.63 (m, 2H), 7.50 – 7.45 (m, 2H), 7.33 – 7.20 (m, 3H), 7.14 – 7.07 (m, 2H), 6.55 (d, *J* = 7.6 Hz, 1H), 5.09 – 4.98 (m, 2H), 3.76 (s, 3H), 3.32 (bs, 1H) partially overlapped with 3.28 (dd, *J* = 13.9, 5.8 Hz, 1H), 3.20 (dd, *J* = 13.9, 5.6 Hz, 1H), the signals of the two diastereoisomers overlap completely, appearing as a single compound; **^{13}C NMR** (100 MHz, $CDCl_3$) δ = 172.0 (two diastereomeric signals), 166.4 (two diastereomeric signals), 137.8, 135.6, 134.7 (two diastereomeric signals), 129.3 (2C), 128.7 (2C), 127.7 (2C), 127.3, 127.1 (2C, two diastereomeric signals), 124.1 (q, *J* = 282.3 Hz), 72.10 (q, *J* = 31.8 Hz, two diastereomeric signals) 53.6 (two diastereomeric signals), 52.5, 37.8, the signals of the two diastereoisomers overlap in some cases, appearing as a single compound, in other cases (as specified in the list) they split; **^{19}F NMR** (377 MHz, $CDCl_3$) δ = -78.25 (d, *J* = 6.8 Hz, 3F), and -78.26 (d, *J* = 6.8 Hz, 3F), two partially overlapped diastereomeric signals; **HRMS (ESI)** m/z: $[M+Na]^+$ calcd. for $C_{19}H_{18}F_3NNaO_4$ 404.1086; found 404.1079.

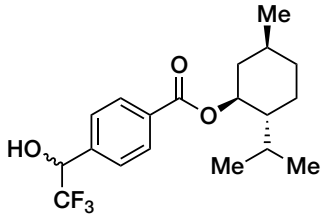

7b. White solid. Reaction time: 16 h. FC eluent: *n*Hex/EtOAc: 5:1. Yield = 46%, (0.046 mmol, 16.5 mg), 1:1 *dr*. **^{1}H NMR** (400 MHz, $CDCl_3$) δ = 8.09 – 8.02 (m, 2H), 7.58 – 7.51 (m, 2H), 5.08 (q, *J* = 6.6 Hz, 1H), 4.92 (td, *J* = 10.9, 4.4 Hz, 1H), 2.84 (bs, 1H), 2.15 – 2.05 (m, 1H), 1.98 – 1.85 (m, 1H), 1.77 – 1.67 (m, 2H), 1.65 – 1.47 (m, 2H), 1.18 – 1.02 (m, 2H), 0.92 (d, *J* = 4.8 Hz, 3H), 0.90 (d, *J* = 5.4 Hz, 3H) overlapped with 0.93 – 0.88 (m, 1H), 0.77 (d, *J* = 6.9 Hz, 3H), the signals of the two

diastereoisomers overlap completely, appearing as a single compound; **^{13}C NMR** (100 MHz, $CDCl_3$) δ = 165.6, 138.3, 131.9, 129.7 (2C), 127.4 (2C), 124.0 (q, *J* = 282.2 Hz), 75.2, 72.4 (q, *J* = 32.3, Hz) and 72.3 (q, *J* = 31.8 Hz, two diastereomeric signals), 47.2, 40.9, 34.3, 31.4, 26.5 (two diastereomeric signals), 23.6 (two diastereomeric signals), 22.0, 20.7 (two diastereomeric signals), 16.5 (two diastereomeric signals). The signals of the two diastereoisomers overlap in some cases, appearing as a single compound, in other cases (as specified in the list) they split; **^{19}F NMR** (377 MHz, $CDCl_3$) δ = -78.25 (d, *J* = 6.5 Hz, 3F) and -78.26 (d, *J* = 6.4 Hz, 3F), two partially overlapped diastereomeric signals; **HRMS (ESI)** m/z: $[M+HCOO]^-$ calcd. for $C_{20}H_{26}F_3O_5$ 403.1738; found 403.1741.

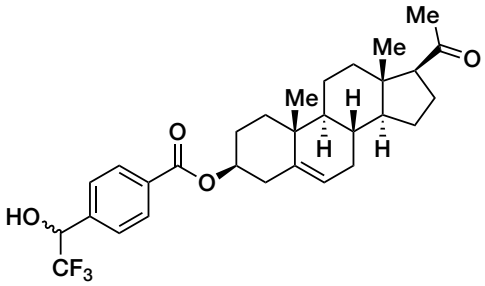

7c. White solid. Reaction time: 16 h. FC eluent: *n*Hex/*i*PrOAc: 2:1. Yield = 32%, (0.032 mmol, 16.6 mg), 1:1 *dr*. **^{1}H NMR** (400 MHz, $CDCl_3$) δ = 8.09 – 8.03 (m, 2H), 7.60 – 7.50 (m, 2H), 5.44 – 5.37 (m, 1H), 5.09 (q, *J* = 6.6 Hz, 1H), 4.85 (dtd, *J* = 16.3, 8.4, 4.5 Hz, 1H), 2.98 (s, 1H), 2.53 (t, *J* = 8.9 Hz, 1H), 2.45 (d, *J* = 7.2 Hz, 2H), 2.21 – 2.13 (m, 1H), 2.11 (s, 3H), 2.07 – 1.96 (m, 3H), 1.91 (dt, *J* = 13.4, 3.5 Hz, 1H), 1.80 – 1.39 (m, 7H), 1.31 – 1.13 (m, 4H), 1.05 (s, 3H) overlapped with 1.07 – 1.01 (m, 1H), 0.62 (s, 3H), the signals of the two diastereoisomers overlap completely, appearing as a single compound; **^{13}C NMR** (100 MHz, $CDCl_3$) δ = 209.8, 165.4, 139.5, 138.4, 131.8, 129.7 (2C), 127.4 (2C), 124.0 (q, *J* = 282.6 Hz), 122.6, 74.7, 72.4 (q, *J* = 32.1 Hz), 63.7, 56.8, 49.9, 44.0, 38.8, 38.1, 37.0, 36.6, 31.8, 31.8, 31.5, 27.8, 24.5, 22.8, 21.0, 19.3, 13.2, the signals of the two diastereoisomers overlap completely, appearing as a single compound; **^{19}F NMR** (377 MHz, $CDCl_3$) δ = -78.25 (d, *J* = 6.3 Hz, 3F), the signals of the two diastereoisomers overlap completely, appearing as a single compound; **HRMS (ESI)** m/z: $[M+HCOO]^-$ calcd. for $C_{31}H_{38}F_3O_6$ 563.2626; found 563.2633.

Computational mechanistic studies

To gain insights into the reaction mechanism behind the presented transformation we resorted to molecular modelling. We envisioned that the first step of this mechanism would involve participation of Zn(0) as a reducing agent ($\xi_{Zn(0)-Zn(II)}$ = 0.76 V). Specifically, we expected that Zn(0) would be responsible for the reduction of the pre-catalyst **I**. In principle, this reduction can render a Ni(0) species **XIV** or a Ni(I) species **III** as a matter of whether a total of two or one electrons are transferred from Zn(0) to the [Ni (II)] complex **I** (**Figure S2**).

Starting with the double reduction of **I** towards **XIV**, we have found that this reduction is endergonic by 3.67 kcal/mol. Once **XIV** is formed it can be stabilized via solvation (**XV**) and/or evolve through the coordination of **II**. Then, the resulting Ni(0) complex (**XVI**) can progress via an oxidative addition involving the insertion of the metal in the Csp^2-I bond resulting in the formation of the Ni(II) complex **VI** (-57.35 kcal/mol). Alternatively, **XIV** can evolve through a SET process in which the Ni(0) complex releases an electron to **II** rendering the pair **XVIII/XIX**. **XIX** can subsequently reorganize towards **VI** in a process that involves two oxidative steps: the first one, consisting of an iodine abstraction at **XVIII** by **XIX,** forming **XXI** and **XXII** (-22.07 kcal/mol). The second oxidative step involves the collapse of the resulting radical **XXII** onto the Ni(I) complex, rendering **XVII**.

*These two paths can, in principle, operate under the reported reaction conditions. They involve an energy span of 5.11 kcal/mol (evolution of **XVI** to **VI**) and 3.67 kcal/mol (evolution of **I** to **XIV**), respectively.*

Alternatively, **I** can evolve via a monoelectronic reduction towards the formation **III** (**Figure S2**, top). We have found that against the direct reduction of Ni(II) to Ni(0), the reduction of Ni(II) to Ni(I) is exergonic by -15.16 kcal/mol. Hence, the formation of species **III** in the reaction process is more likely than the formation of **XIV**. Once **III** is formed it can coordinate **II** and subsequently engage in an intramolecular oxidative

addition towards forming species **V** (-18.31 kcal/mol). **V** can then react with a second molecule of Zn(0) resulting in **XXIII** (-63.90 kcal/mol).

Overall, this latter path involving a Ni(II)-Ni(I)-Ni(III)-Ni(I) triple redox process involves an energy span of 3.58 kcal/mol (*corresponding to the conversion of **IV** to **V***) resulting competitive with the SET path. However, since the formation of **II** is endergonic and not so the formation of **XV**, together with the fact that we are in a large excess of iodine ions* we consider the triple redox path as the one operating.

**** Please note the beneficial effect of adding NaI described in the main text, we hypothesize that the addition of this counterion promotes this path over the radical counterpart hence preventing the initiation of other undesired radical mechanisms that could erode the yield of the reaction.***

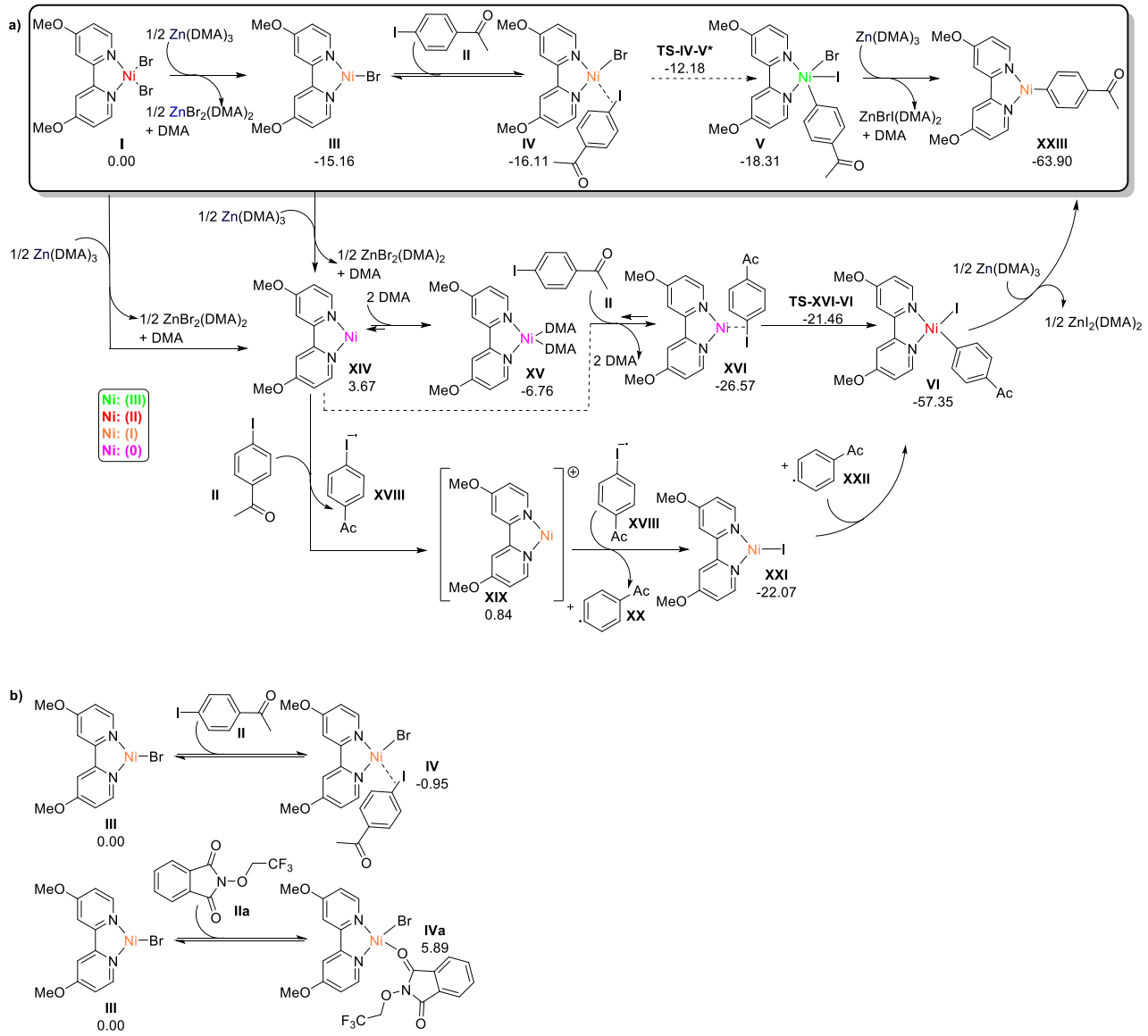

Figure S2. Explored paths for a) the reduction of Ni(II) to Ni(I) mediated by Zn(0) and b) potential equilibrium present in solution. With a star (*) we have marked those barriers estimated via application of the NEB method (see below).

Table S6. Energy data of those stationary points explored in **Figure S2**.[a]

ID	ImFreqs	Stable	SCF	SCF+ZPVE	H[b]	G[c]
I	-	Yes	-7379.142121	-7378.915506	-7378.895061	-7378.967796
Zn(DMA)$_3$	-	Yes	-2641.356003	-2640.965713	-2640.937012	-2641.026676

III	-	Yes	-4805.330318	-4805.105207	-4805.086799	-4805.153919
II	-	Yes	-681.484264	-681.357664	-681.347327	-681.394457
IV	-	Yes	-5486.839878	-5486.487277	-5486.458019	-5486.549899
V	-	Yes	-5486.842713	-5486.489363	-5486.459967	-5486.553394
$ZnBrI(DMA)_3$	-	Yes	-5513.041949	-5512.647318	-5512.615385	-5512.71261
XXIII	-	Yes	-2615.232346	-2614.882141	-2614.856593	-2614.940116
XIV	-	Yes	-2231.461627	-2231.241024	-2231.224297	-2231.285883
DMA	-	Yes	-287.4093664	-287.280614	-287.272025	-287.312298
XV	-	Yes	-2806.342546	-2805.860734	-2805.826508	-2805.9271
XVI	-	Yes	-2913.020057	-2912.66912	-2912.642069	-2912.728527
TS-XVI-VI	-90.87	Yes	-2914.5002434	-2912.662598	-2912.635958	-2912.721789
VI	-	Yes	-2913.070676	-2912.717788	-2912.69069	-2912.77759
XVIII	-	Yes	-756.723557	-756.595153	-756.582620	-756.639416
XIX	-	Yes	-2231.365831	-2231.126133	-2231.125189	-2231.185783
XX	-	Yes	-458.787541	-458.650230	-458.649286	-458.695118
XXI	-	Yes	-2529.341105	-2529.098591	-2529.097647	-2529.166601
IIa	-	Yes	-963.385476	-963.231759	-963.217049	-963.274797

IVa	-	Yes	-5768.73091	-5768.351523	-5768.318054	-5768.419329

[a] SCF energies correspond to the electronic energies expressed in a.u. Imaginary frequencies are expressed in cm^{-1}. [b] H denotes the Sum of electronic and thermal Enthalpies. [c] G denotes the Sum of electronic and thermal Free Energies.

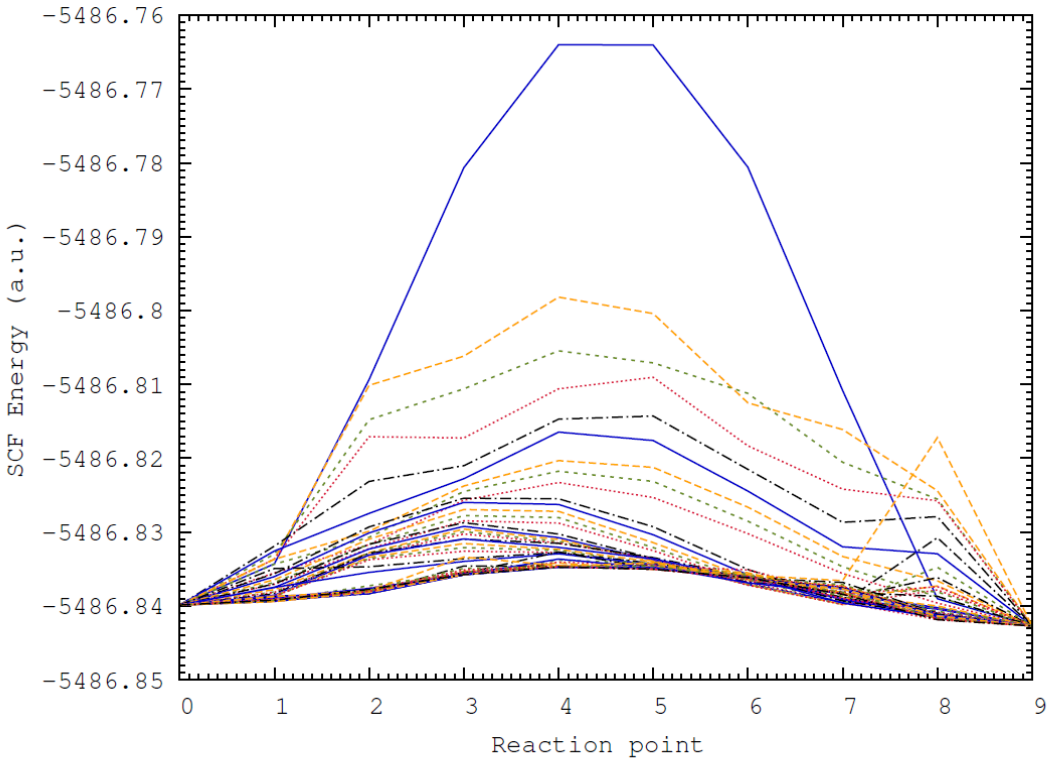

Figure S3. Exploration of the energy profile for the conversion of **IV** to **V** using the NEB. Y-axis represents the SCF energies expressed in a.u. and X-axis represents the reaction points.

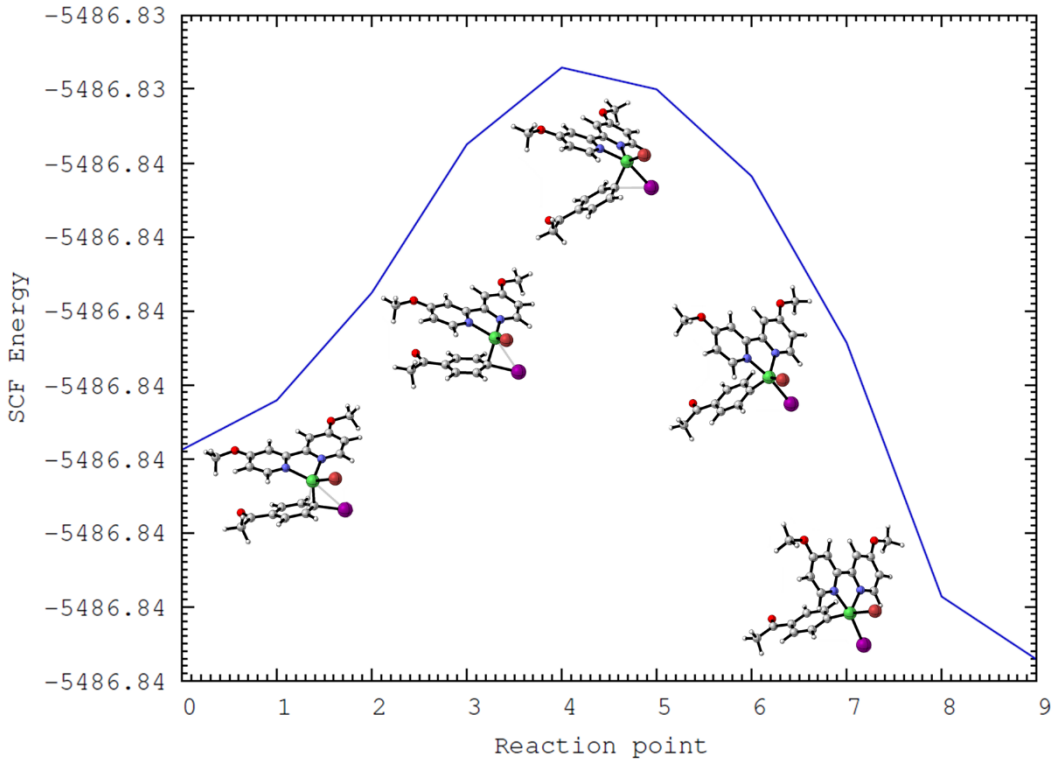

Figure S3a. MEP for the for the conversion of **IV** to **V** obtained using the NEB. Y-axis contains the SCF energies expressed in a.u. and X-axis represents the reaction points.

With this mechanistic picture, we wondered how the second component of the product, *i.e.* the alkoxy-radical, could be formed in solution. We hypothesized that the very Zn(II) released in the previous steps could be responsible for coordinating **2** and activating it to evolve via a SET in the presence of a second unit of Zn(0) and subsequently release the alkoxy-radical **VII**. Alternatively, we also acknowledge that the very Ni(I) complexes formed in previous reaction steps could account for an analogous intramolecular reductive chemistry. Hence, we embarked into exploring all these potential paths.

Starting with the Zn promoted transformation (**Figure S4a**), we have found that the initial coordination of $ZnBr_2$ to **2** is endergonic by 3.86 kcal/mol and its subsequent evolution via SET promoted by Zn(0) is also endergonic by 9.61 kcal/mol. However, the resulting complex **X** can easily reorganize towards **XI** and later evolve towards **XII** (**Figure S4a**). This overall transformation accounts for the release of an alkoxy radical

to the reaction medium. Then, **VII** can easily tautomerize to **VIII** in the presence of DMA (**Figure S4b**). All our attempts to find the direct release of the alkoxy-radical at these steps failed and resulted in its coordination to the metallic center. At this stage, we hypothesized that in the presence of such a coordinating solvent as DMA, perhaps the solvent could impede the coordination of the alkoxy radical and aid in its release. We have found that while solvent does prevent coordination of the alkoxy-radical to the Zn center it also imposes a high energy penalization for the process.

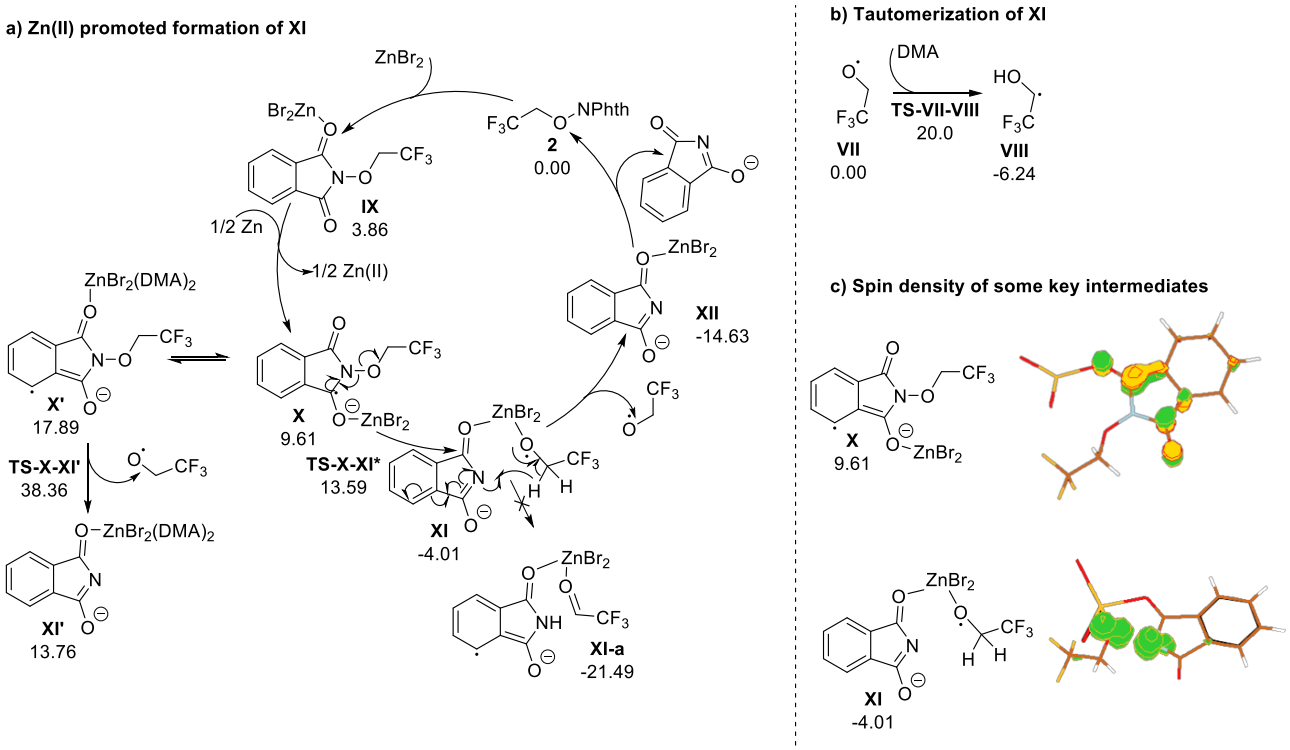

Figure S4. a) Zn promoted formation of an alkoxy-radical from **2**. b) Solvent promoted tautomerization of **VII**. c) Spin density obtained for some key intermediates. *The energy of this transition state was estimated via the use of the NEB method.

Table S7. Energy data of those stationary points explored in **Figure S4**.[a]

ID	ImFreqs	Stable	SCF	SCF+ZPVE	H[b]	G[c]
2	-	Yes	-964.489	-963.232	-963.217	-963.275
IX	-	Yes	-7892.14	-7889.98	-7889.96	-7890.03
X	-	Yes	-8465	-8464.58	-8464.54	-8464.65
XI	-	Yes	-7892.28	-7890.13	-7890.11	-7890.19
XII	-	Yes	-7440.17	-7438.59	-7438.58	-7438.64
X'	-	Yes	-8465.121	-8464.704	-8464.666	-8464.7767
TS-X-XI'	-1292.20	Yes	-8465.088	-8464.6732	-8464.635	-8464.7440
XI'	-	Yes	-8465.123	-8464.708	-8464.669	-8464.7832
VII	-	Yes	-452.115	-451.534	-451.528	-451.564
TS-VII-VIII	-437.56	Yes	-739.866	-738.802	-738.787	-738.845
VIII	-	Yes	-739.902	-738.843	-738.828	-738.887

[a] SCF energies correspond to the electronic energies expressed in a.u.. Imaginary frequencies are expressed in cm^{-1}. [b] H denotes the Sum of electronic and thermal Enthalpies. [c] G denotes the Sum of electronic and thermal Free Energies.

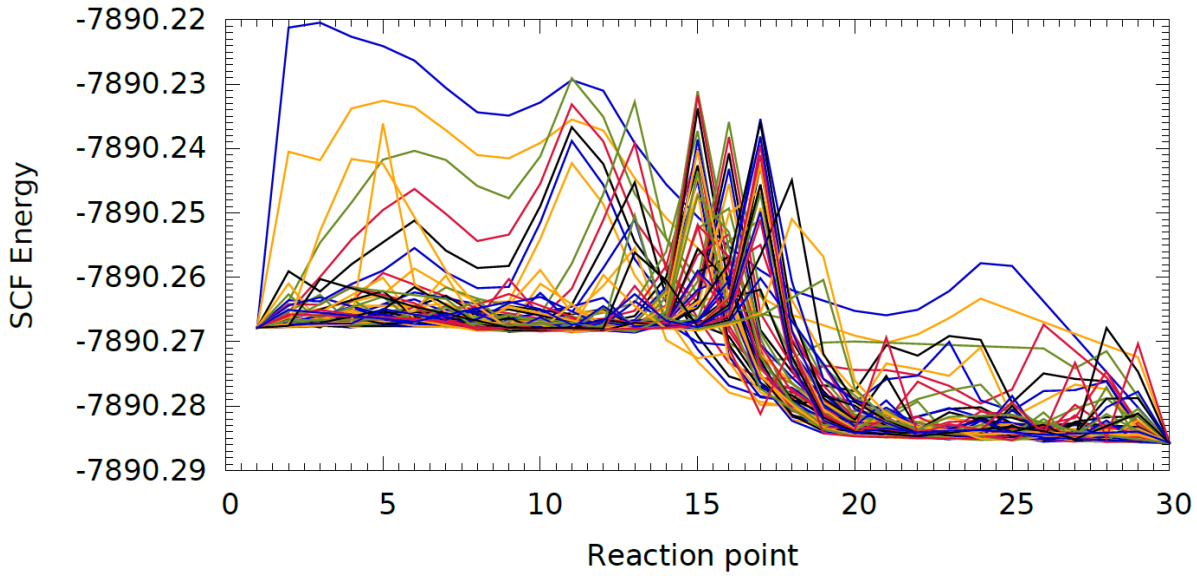

Figure S5. PES evaluation for the transformation of **X** to **XI** using the NEB method.

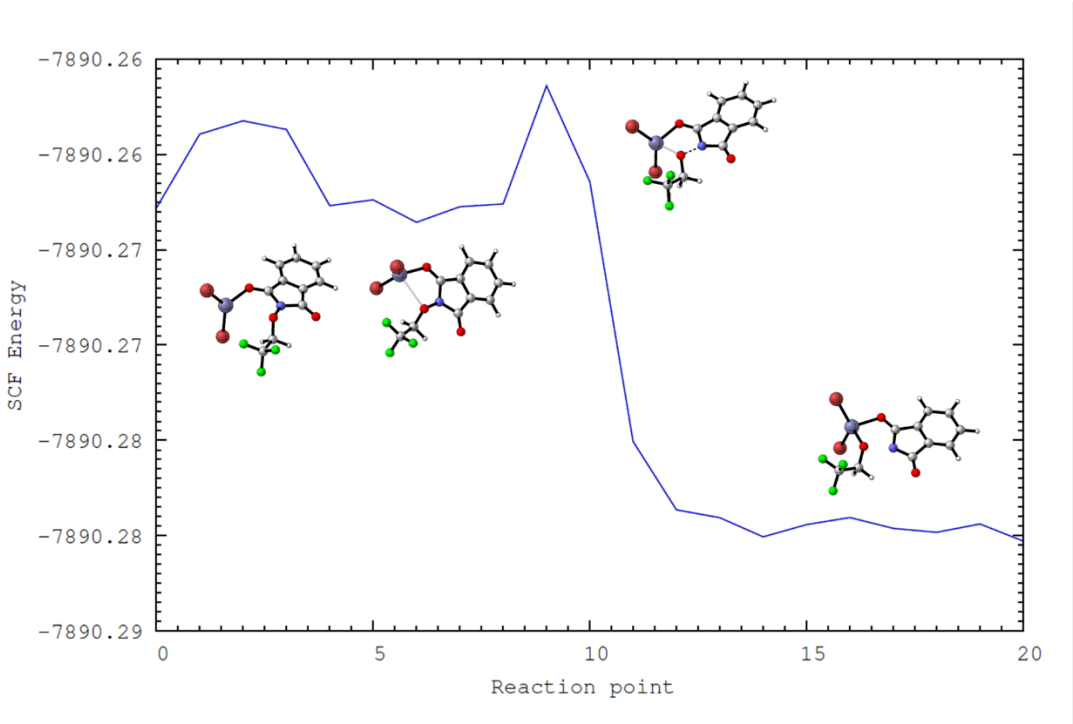

Figure S5a. MEP evaluation for the transformation of **X** to **XI**. This MEP is obtained with the NEB method.

Once **VIII** is formed it can collapse on different complexes already described, namely **XXIII** and **VI**.

Starting with the reactivity of **VIII** with **XXIII**, the interaction between these two fragments renders complex **XXIV** in a step that is exergonic by 36.15 kcal/mol. Then, **XXIV** can evolve via a reductive elimination and render the product **P** and a Ni(0) species (**Figure S6a**). This Ni(0) species can alternatively engage in an oxidative addition with a second **III** molecule forming ultimately **XVII** that after reduction in the presence of Zn allows the recovery of the active catalyst (**Figure S2**).

Following with the collapse of **VIII** on **VI**, we found that the radical collapse on this Ni(II) complex is exergonic by 13.99 kcal/mol, and therefore less favorable than the previously described path. Were complex **XXV** formed it could also evolve towards **3e** via an easy reductive elimination (**Figure S6b**).

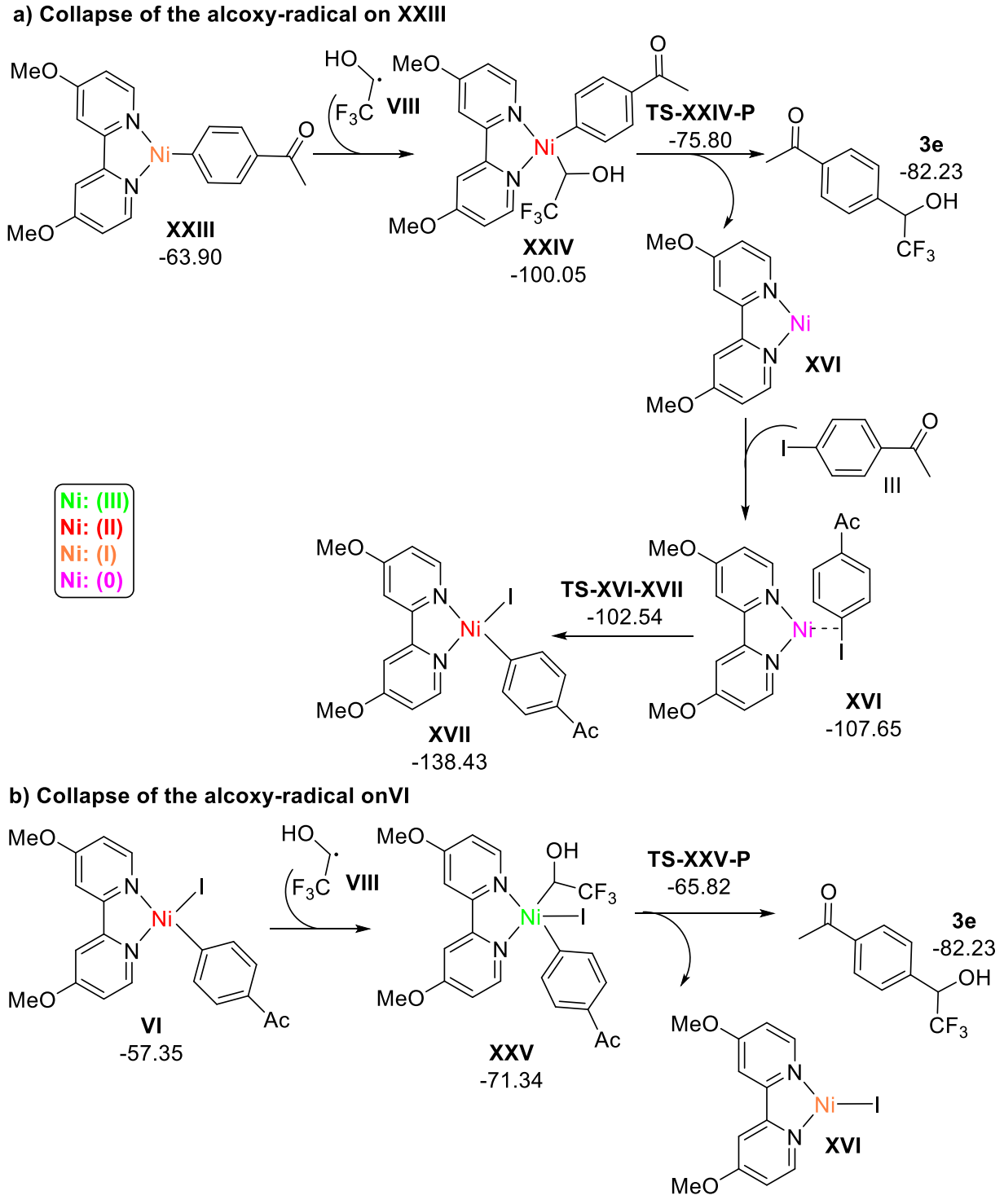

Figure S6. Study of the evolution of the complexes a) **XIII-2D** and b) **XVIII-1S** after collapse of the alkoxy-radical towards **3e**.

Table S8. Energy data of those stationary points explored in **Figure S6**.[a]

ID	ImFreqs	Stable	SCF	SCF+ZPVE	H[b]	G[c]
XXIII	-	Yes	-2615.232346	-2614.882141	-2614.856593	-2614.940116
VIII	-	Yes	-739.017868	-738.843239	-738.827689	-738.886553
XXIV	-	Yes	-3066.907832	-3066.508319	-3066.476921	-3066.571985
TS-XXIV-P	-412.282	Yes	-3066.866966	-3066.470081	-3066.43892	-3066.533343
P(3e)	-	Yes	-835.3916499	-835.216291	-835.201694	-835.257705
XVI	-	Yes	-2231.461627	-2231.241024	-2231.224297	-2231.285883
III	-	Yes	-681.484264	-681.357664	-681.347327	-681.394457
XVI	-	Yes	-2913.020057	-2912.66912	-2912.642069	-2912.728527
TS-XVI-XVII	-90.8689	Yes	-2913.013395	-2912.662598	-2912.635958	-2912.721789
XVII	-	Yes	-2913.070676	-2912.717788	-2912.69069	-2912.77759
XXV	-	Yes	-3364.696455	-3364.296235	-3364.26261	-3364.364129
TS-XXV-P	-256.665	Yes	-3364.695962	-3364.296883	-3364.263407	-3364.365343

[a] SCF energies correspond to the electronic energies expressed in a.u.. Imaginary frequencies are expressed in cm^{-1}. [b] H denotes the Sum of electronic and thermal Enthalpies.[c] G denotes the Sum of electronic and thermal Free Energies.

Alternatively, the formation of the alkoxy radical can be mediated by any of the Ni complexes formed in the reaction media that feature a coordination vacancy, namely **XXIII** and **III**. We have already pointed that the coordination of **2** is endergonic and therefore unlikely to be competitive, but we have found that the coordination of **2** to

XXIII is exergonic and can facilitate the release of this radical (**Figure S7**). This path can continue evolving towards obtaining the product P, however the energy penalization associated with it is too high to be competitive at the working conditions.

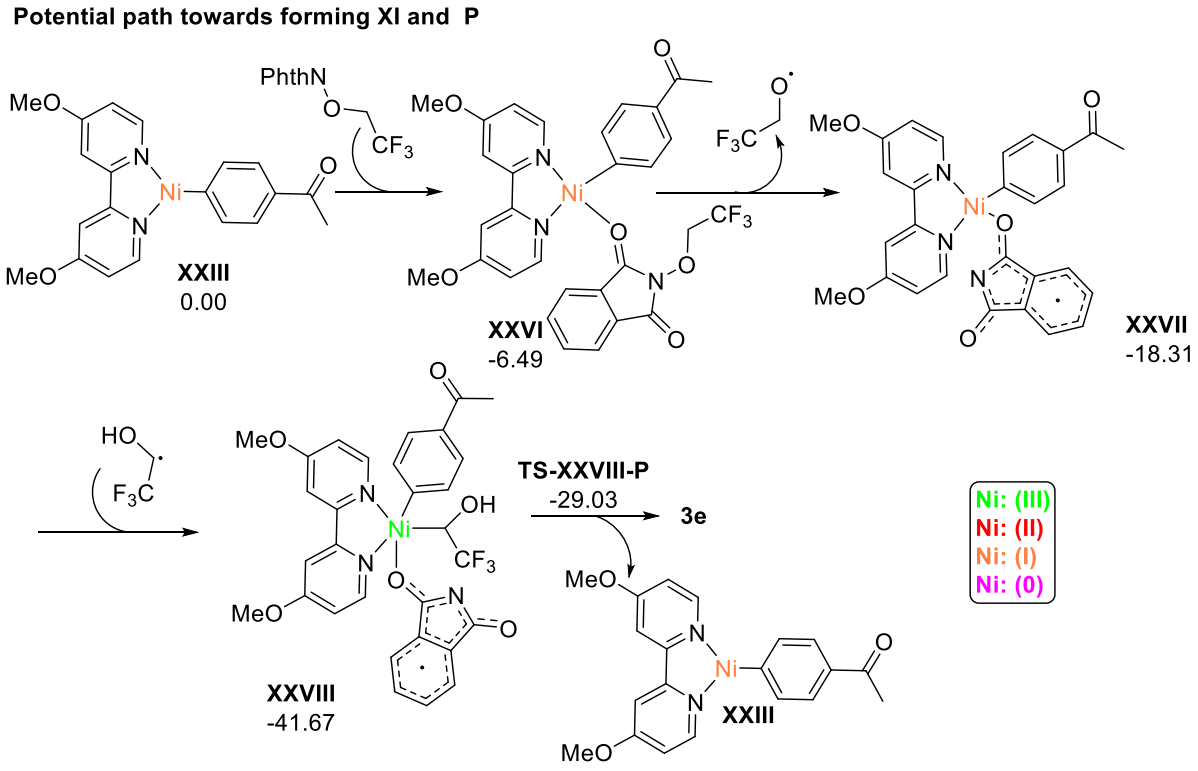

Figure S7. Alternative paths towards the formation of **3e**.

Table S9. Energy data of those stationary points explored in **Figure S7**.[a]

ID	ImFreqs	Stable	SCF	SCF+ZPVE	H[b]	G[c]
XXVI	-	Yes	-3578.66	-3578.15	-3578.11	-3578.23
XXVII	-	Yes	-3127.07	-3126.61	-3126.57	-3126.68
XXVIII	-	Yes	-3578.71	-3578.2	-3578.16	-3578.28
TS-VIII-P	-230.03	Yes	-3578.69	-3578.19	-3578.15	-3578.26

[a] SCF energies correspond to the electronic energies expressed in a.u.. Imaginary frequencies are expressed in cm^{-1}. [b] H denotes the Sum of electronic and thermal Enthalpies. [c] G denotes the Sum of electronic and thermal Free Energies.

At this point, we also evaluated the possibility of **XI** evolving towards **XIa**, we have found that this formal 1,2 migration is energetically quite demanding.

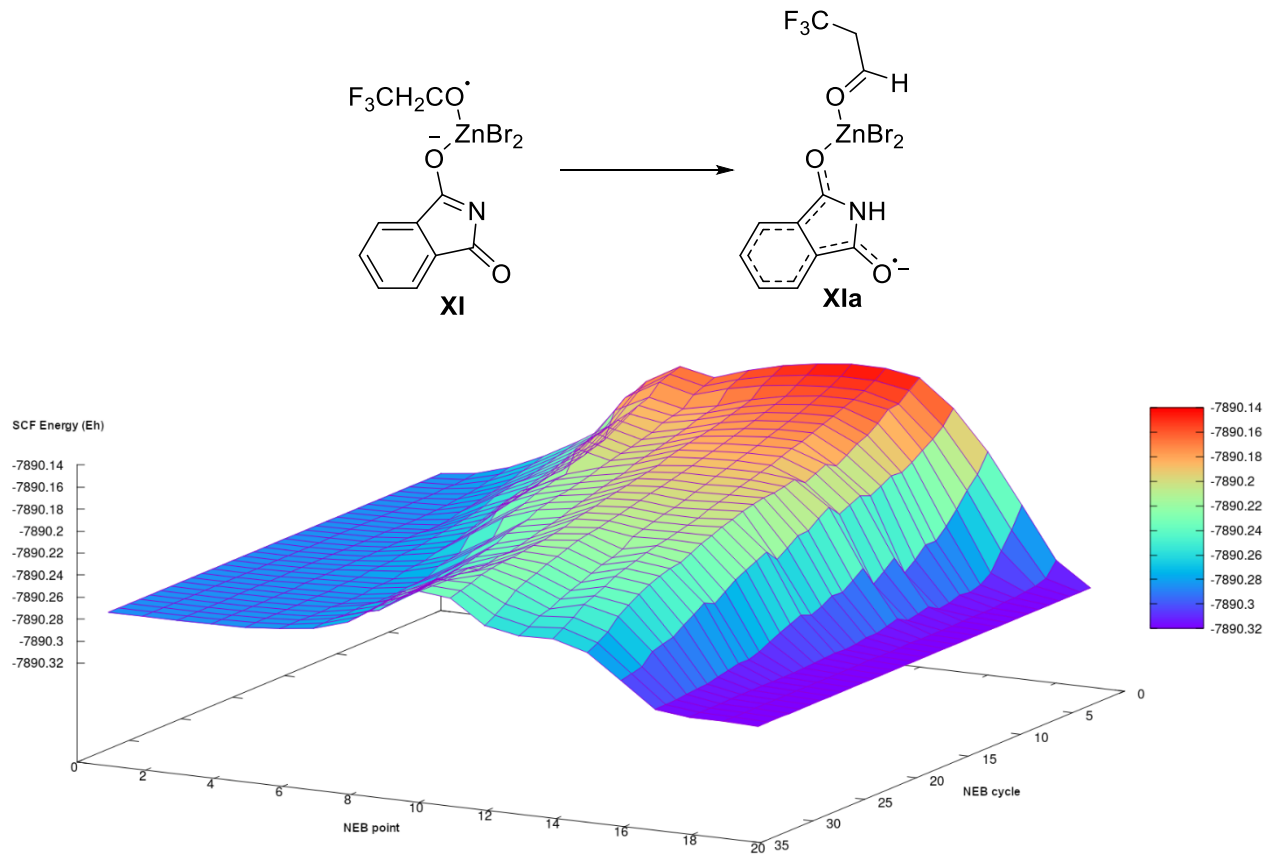

Figure S8. 3D representation of the explored reacting surface related to the H-shift step from **XI** to **Xia** via the NEB method. Arbitrary units used in the configuration space and Hartrees (Eh) used in the energy axis.

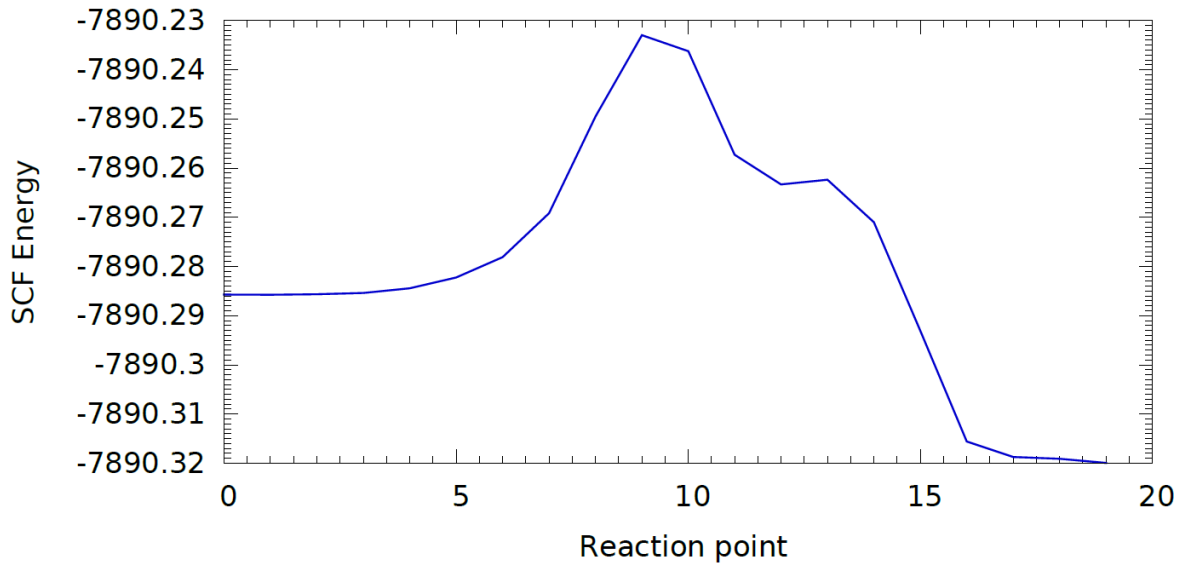

Figure S8a. MEP for the for the conversion of **XI** to **XIa** obtained using the NEB. Y-axis contains the SCF energies expressed in a.u. and X-axis represents the reaction points.

Radical trapping experiments

Trapping with tert-butylacrylate **4a**

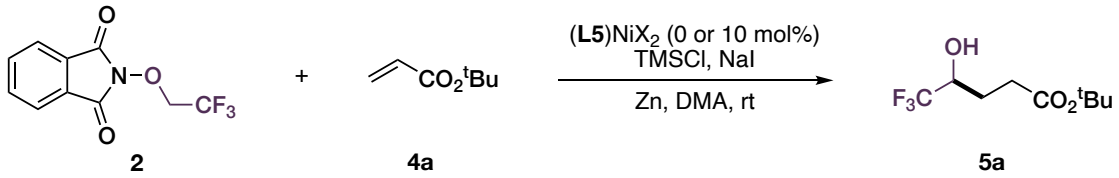

Radical trapping experiment with *tert*-butylacrylate in the presence of Ni catalyst was set up according to General procedure, substituting aryl iodide **1** with *tert*-butylacrylate **4a** (1 eq). Adduct **5a** was isolated in 35% yield after work-up and flash chromatography as a colorless oil.

The same reaction was set up omitting the Ni catalyst and adduct **5a** was isolated in 12% yield. This confirms the presence of the C-centered radical and the fact that Ni is not necessary for the activation of N-trifluoroethoxyphthalimide nor for the isomerization of the O-centered radical.

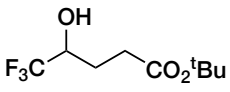

5a. Colourless oil. FC eluent: *n*Hex/EtOAc: 6:1. Yield = 35% (0.035 mmol, 8.0 mg). **^{1}H NMR** (400 MHz, $CDCl_3$) δ = 4.04 – 3.92 (m, 1H), 3.26 (d, *J* = 6.0 Hz, 1H), 2.59 – 2.39 (m, 2H), 2.05 – 1.94 (m, 1H), 1.94 – 1.83 (m, 1H), 1.44 (s, 9H); **^{13}C NMR** (100 MHz, $CDCl_3$) δ = 173.3, 125.0 (q, *J* = 281.9 Hz), 81.5, 70.0 (q, *J* = 31.1 Hz), 31.0, 28.0, 24.6 (q, *J* = 2.0 Hz); **^{19}F NMR** (377 MHz, $CDCl_3$) δ = -80.06 (d, *J* = 6.7 Hz); **HRMS (ESI)** m/z: [M+HCOO]- calcd. for $C_{10}H_{16}F_3O_5$ 273.0955; found 273.0960.

Additional notes:

1. Compound **5a** is fairly volatile, so that thorough drying resulted not possible, and some Et_2O can be observed in the NMR spectrum. Anyway, it is possible to isolate it via flash chromatography and remove the solvent on the rotavap.

Trapping with TEMPO radical **4b**

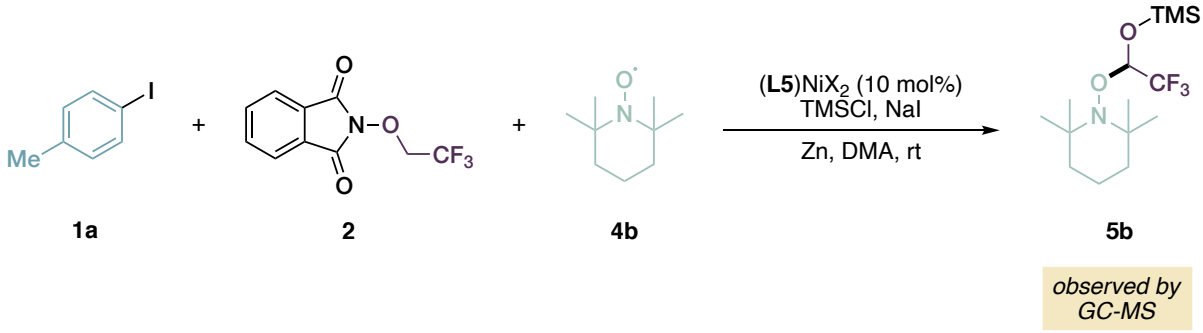

Radical trapping experiment with TEMPO **4b** was set up with substrate **1a** according to General procedure, simply by adding **4b** (2 eq, 0.2 mmol, 31.3 mg) to the reaction mixture right before TMSCl.

After addition of EtOAc the reaction was quenched using sat. aq. NH_4Cl instead of 2N HCl, and an aliquot of the organic phase was directly injected into GC-MS.

GC-MS shows that no product was formed, and the mixture consisted of unreacted **1a**, **2**, phthalimide, small amount of adduct **5b** and some TEMPO-derived byproducts (**Figure S9**).

```
File       :C:\msdchem\1\DATA\Smistamento\LL-1739GR.D
Operator   :
Acquired   : 30 Jun 2022  10:17     using AcqMethod AG.M
Instrument :    GC-MS
Sample Name:
Misc Info  :
Vial Number: 1
```

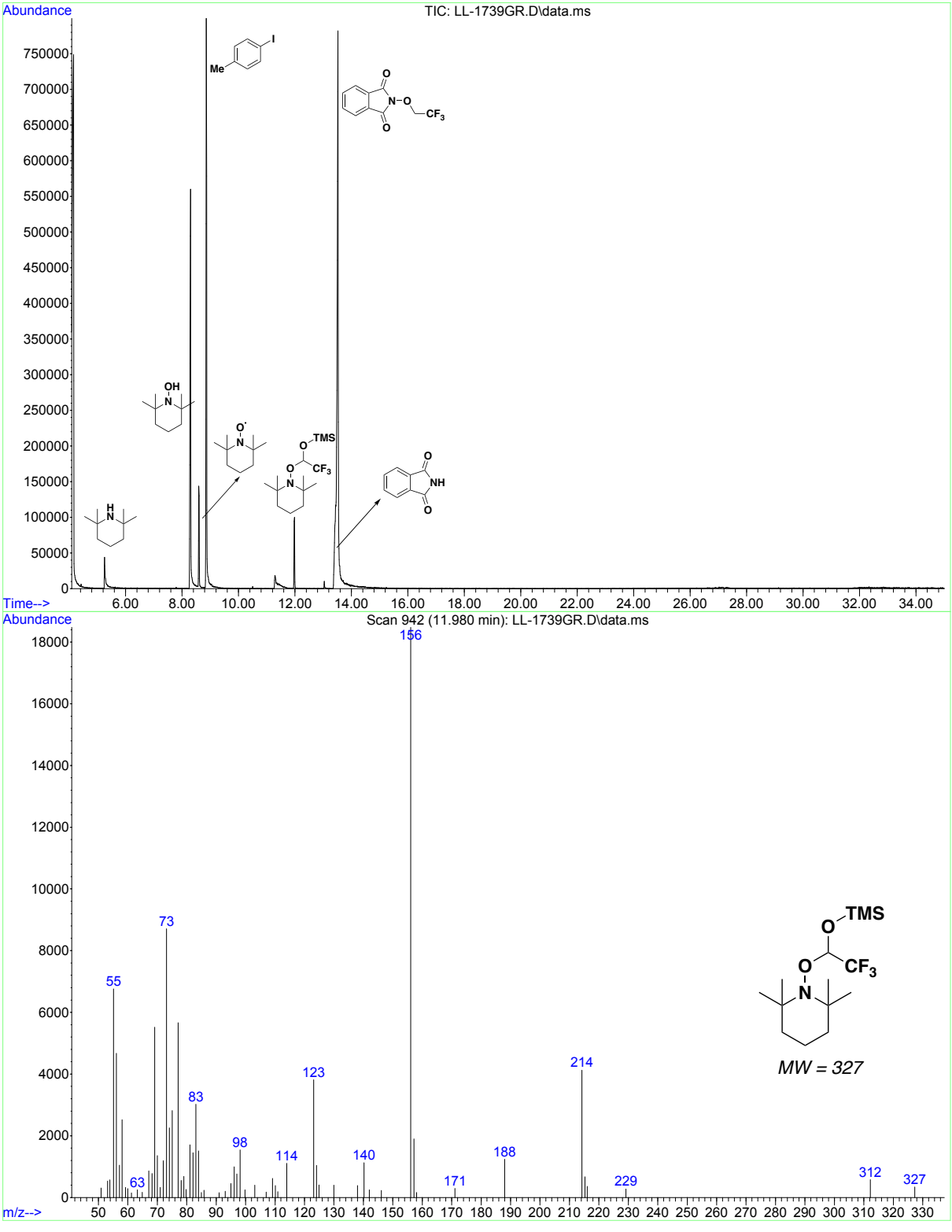

Figure S9: GC-MS analysis of the crude mixture for TEMPO radical trapping experiment. Mass spectrum of the observed adduct **5b** is given.

Control experiments

Experiment without Ni catalyst

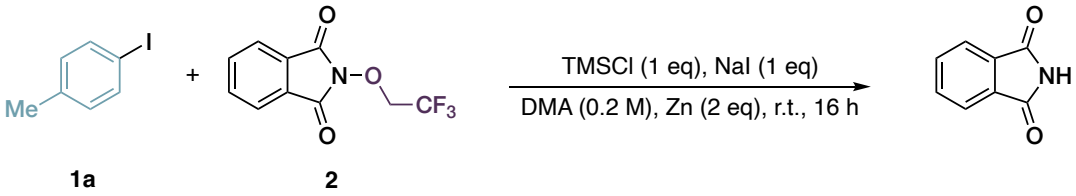

1a 2

The reaction was set up with substrate **1a** according to General Procedure but omitting the catalyst [Ni(**L5**)Cl_2]. GC-MS and ^{19}F-NMR analysis of the mixture after 16 h show unreacted **1a**, complete conversion of **2** to phthalimide, but no product. This further confirms that activation of **2** is mediated by Zn and proves that Ni is essential for the formation of the product.

Experiment without Zn

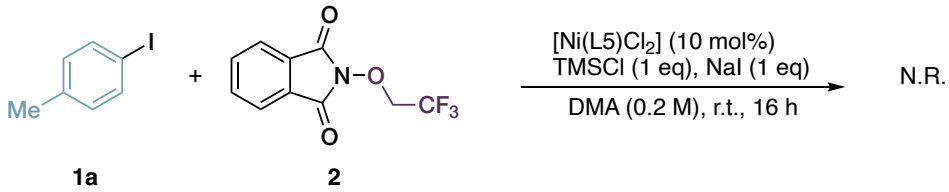

1a **2**

The reaction was set up with substrate **1a** according to General Procedure (see section 5.1) but omitting Zn dust. Both GC-MS and ^{19}F-NMR analysis of the mixture after 16 h only shows both unreacted starting materials.

Experiment for Zn insertion with aryl iodide **1z**

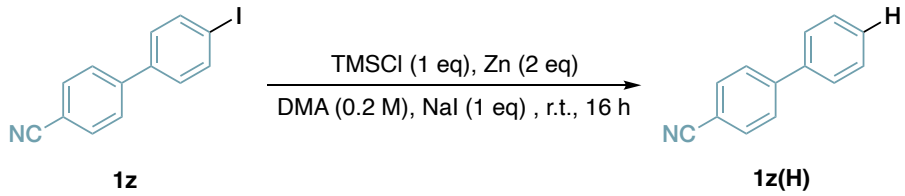

1z **1z(H)**

The reaction was set up with substrate **1z** according to General Procedure (see section 5.1), but omitting both **2** and Ni catalyst, and stopped after 16 h.

Given that homogeneous reductant TDAE proved unsuccessful in promoting any conversion of both starting materials, we considered appropriate to investigate whether Zn insertion into the C-I bond was occurring. This was done by quantifying the amount of dehalogenated starting material **1z(H)**, that would be arising from the protonation of the arylzinc derived from **1z** after work-up.

^{1}H NMR analysis with mesitylene as an internal standard showed that **1z(H)** was formed in 22% yield, the rest being unreacted **1z**. The small extent of protodeiodination observed after 16 h indicates that insertion of Zn into the C-I occurs at a very low rate, leading us to consider unlikely the intermediacy of organozinc species in the present methodology.

Experiment with Trifluoroacetaldehyde ethyl hemiacetal

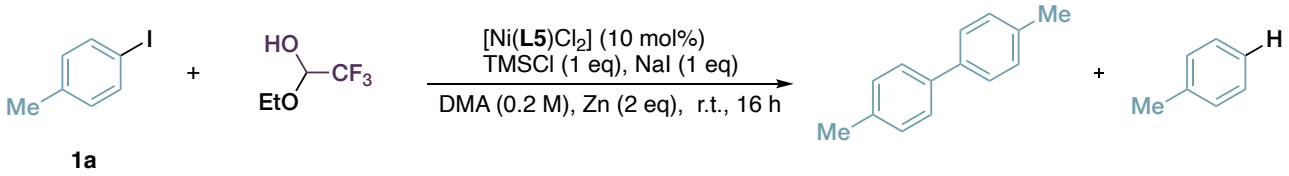

The reaction was set up with substrate **1a** according to General Procedure), substituting **2** with Trifluoroacetaldehyde ethyl hemiacetal (3 eq). GC-MS, ^{1}H NMR and ^{19}F NMR analysis of the mixture after 16 h show complete conversion of **1** to 4,4′-dimethylbiphenyl and toluene (via Ni catalyzed homocoupling and protodehalogenation, respectively), but no product.

6. Merging C–C σ-bond activation of cyclobutanones with CO2 fixation via Ni-catalysis

All the procedures and results here described can be found in:

- L. Lombardi, A. Cerveri, L. Ceccon, R. Pedrazzani, M. Monari, G. Bertuzzi, M. Bandini, "Merging C–C σ-bond activation of cyclobutanones with CO_2 fixation via Ni-catalysis". *Chem. Commun.* **2022**, *58*, 4071-4074.

ABSTRACT

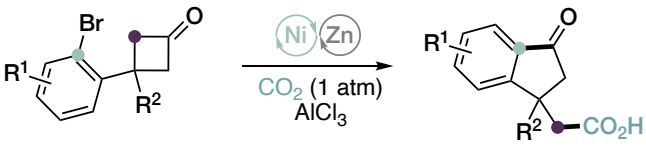

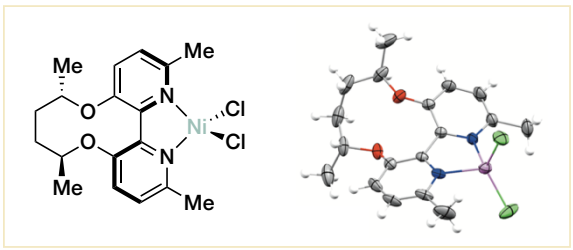

A tandem C-C bond activation-carboxylation of cyclobutanones with CO_2 at atmospheric pressure is presented. Nickel catalysis under reductive conditions is established as a direct route to synthetically valuable, biologically relevant 3-indanone-1- acetic acids. The protocol features $AlCl_3$ as a key additive, that in conjunction with an axially chiral bipyridine ligand provides an adequate functional group tolerance and useful chemical outcomes (yield up to 76%). Manipulations of the target cyclic scaffolds and a mechanistic proposal based on experimental evidence complete the investigation.

6.1 Background

Carbon dioxide (CO_2) is a ubiquitous gaseous molecule that holds a central place in the very existence and sustainment of life on Earth and, in modern times, in the topic of sustainability and environmental preservation. It is the available source of carbon in the carbon cycle, used in photosynthesis for the production of carbohydrates and oxygen and released by aerobic organisms in respiration, and therefore it's naturally present in the atmosphere and its amount regulated by living organisms and geological phenomena.[285] However, CO_2 is also a product of combustion of fossil fuels, which still meet 80% of the world's energy demands, and as a result its amount in the atmosphere has risen from 280 ppm in the pre-industrial era to 417 ppm in the present day.[286] This constitutes a serious environmental concern, given that CO_2 is also a primary greenhouse gas, and its safe upper limit is estimated to be 350 ppm.[287]

On the other hand, CO_2 also stands as an ideal C1 synthon in organic chemistry, given its non-toxicity, non-flammability, inexpensiveness, great (or better excessive) abundance and renewability.[286a] Although synthetic utilization of CO_2 is unlikely to significantly reduce its concentration in the atmosphere, methods that permit utilization of this gas for fine chemicals synthesis holds a great promise in the production of added value, highly relevant compounds (carboxylic acids) that might be able to compensate the potential costs of its capture and recycle.[288]

This endeavor is though complicated by its kinetic and thermodynamic inertness, as CO_2 is a highly stable, symmetric linear molecule that has no dipole moment.[289] As a weak electrophile at carbon, early synthetic efforts involved its capture by strong nucleophiles, such as: Grignard reagents and organolithiums;[290] phenolate anions, as in

---

[285] D. Archer, *The global carbon cycle.* Princeton: Princeton University Press, **2010**.
[286] a) N. von der Assen, P. Voll, M. Peters, A. Bardow, *Chem. Soc. Rev.* **2014**, *43*, 7982–7994; b) https://www.co2.earth.
[287] IPCC, 2014: Climate Change 2014: Synthesis Report. Contribution of Working Groups I II, and III, to the Fifth Assessment Report of the Intergovernmental Panel on Climate Change [Core Writing Team, R. K. Pachauri, L. A. Meyer (eds.)]. IPCC, Geneva, Switzerland, 151 pp.
[288] M. Aresta, A. Dibenedetto, *Dalton Trans.* **2007**, *28*, 2975–2992.
[289] M. Aresta, A. Dibenedetto, E. Quaranta, *Reaction Mechanisms in Carbon Dioxide Conversion.* Springer, Berlin: Heidelberg, **2016**.
[290] A. Correa, R. Martin, *Angew. Chem. Int. Ed.* **2009**, *48*, 6201–6204.

the venerable Kolbe-Schmidt process for the synthesis of salicylic acid;[291] amines, for example in Bosch-Meiser process for producing urea from liquid ammonia and CO_2.[292] Incorporation into epoxide moieties for the production of cyclic carbonates and polycarbonates, or reduction to methanol, formic acid or methane have also been widely explored.[293]

However, strategies for the construction of C-C bonds in functionalized substrates have traditionally lagged behind. To overcome this synthetic void, chemists have successfully elaborated new protocols, relying on transition metals, photo- and electrochemistry as well as organo-based activation.[294]

In the context of transition metal catalysis, it is relevant to discuss the coordination of CO_2 to metal complexes. In its ground state, CO_2 is a linear triatomic molecule with $D_{\infty h}$ symmetry in which the central carbon atom possesses sp hybridization. The C-O bond distance is 1.16 Å. The main molecular orbitals (MOs) that are primarily responsible for the reactivity of CO_2 are the $1_{\pi g}$-occupied MO (HOMO), centered on the oxygen atoms, and $2_{\pi u}$-unoccupied MO (LUMO), which is mainly localized at the carbon atom.[289] This gives CO_2 an ambiphilic character, both exhibiting Lewis basic character at oxygen and Lewis acidic character at carbon. As a result of this electronic configuration, metals in low oxidation states typically bind CO_2 to the carbon atom, whereas highly oxidized metals predominantly interact with the oxygen atoms. In particular, four main coordination modes are known (**Figure 1**).

---

[291] D. Cameron, H. Jeskey, O. Baine, *J. Org. Chem.* **1950**, *15*, 233–236.

[292] X. Xiang, L. Guo, X. Wu, X. Ma, Y. Xia, *Environ. Chem. Lett.* **2012**, *10*, 295–300.

[293] T. Sakakura, J.-C. Choi, H. Yasuda, *Chem. Rev.* **2007**, *107*, 2365–2387; a) W.-H. Wang, Y. Himeda, J. T. Muckerman, G. F. Manbeck, E. Fujita, *Chem. Rev.* **2015**, *115*, 12936−12973; b) J. Chen, L. Falivene, L. Caporaso, L. Cavallo, E. Y. X. Chen, *J. Am. Chem. Soc.* **2016**, *138*, 5321−5333; c) T. Matsuo, H. Kawaguchi, *J. Am. Chem. Soc.* **2006**, *128*, 12362−12363.

[294] a) Q. Liu, L. Wu, R. Jackstell, M. Beller, *Nat. Commun.* **2015**, *6*, 5933; b) Y. Shi, B.-W. Pan, Y. Zhou, J. Zhou, Y.-L. Liu, F. Zhou, *Org. Biomol. Chem.* **2020**, *18*, 8597−8619; c) J. Hou, J.-S. Li, J. Wu, *Asian J. Org. Chem.* **2018**, *7*, 1439−1447; d) J. Song, Q. Liu, H. Liu, X. Jiang, *Eur. J. Org. Chem.* **2018**, 696−713; e) S. Wang, G. Du, G. Xi, *Org. Biomol. Chem.* **2016**, *14*, 3666−3676; f) C. Maeda, Y. Miyazaki, T. Ema*, Catal. Sci. Technol.* **2014**, *4*, 1482−1497; g) A. Tortajada, F. Julià-Hernàndez, M. Börjesson, T. Morgas, R. Martin, *Angew. Chem. Int. Ed.* **2018**, *57*, 15948−15982; h) Y. Cao, N. Wang, H.-R. Li, L. N. He, *Chin. J. Chem.* **2018**, *36*, 644−659; i) J. Luo, I. Larrosa, *ChemSusChem* **2017**, *10*, 3317–3332.

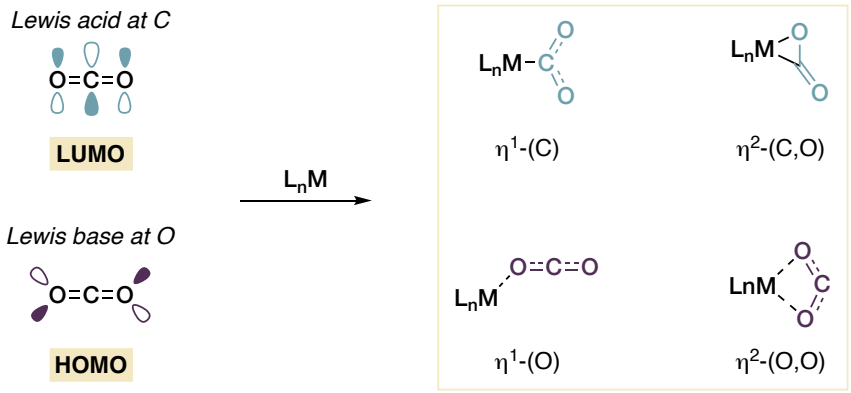

Figure 1. Left: CO_2 HOMO and LUMO schematic depiction. Right: commonly observed coordination modes to transition metals.

The η^1(C) coordination mode is typically observed with rather electron-rich metal complexes possessing a relatively high in energy dσ-type orbital. Binding involves charge transfer between the anti-bonding π* orbital of CO_2 and a d_{z^2} metal orbital. Coordination to the carbon is also possible in a η^2(C,O) side-on coordination mode, that is typically favored by a high-energy dπ-type orbital. In this case, the interaction features two main contributes: a σ bond from the bonding π-orbital of CO_2 to an empty d_{z^2} metal orbital, as well as a π-back bonding from a d_{xy} metal orbital to an empty π* orbital of CO_2, similarly to the binding of an alkene. Conversely, electron-poor metal complexes typically bind the molecule of CO_2 in either a η^1(O) end-on coordination mode or in a η^2(O,O) fashion, the latter being commonly observed for alkali metals. In his pioneering work, Aresta described the first CO_2 transition metal complex that could be structurally characterized, namely $(Cy_3P)_2Ni(CO_2)$, showing a η^2(C,O) coordination mode as could be expected for a highly nucleophilic Ni(0) species.[295] Intriguingly, the IR stretching frequencies of the coordinated CO_2 suggest that this complex may be better described as Ni(I), with lengthening of CO bonds due to transfer of an electron

[295] a) M. Aresta, M., C. F. Nobile, V. G. Albano, E. Forni, M. Manassero, *J. Chem. Soc., Chem. Commun.* **1975**, *15*, 636; b) M. Aresta, M., C. F. Nobile, *J. Chem. Soc., Dalton Trans.* **1977**, 708.

from nickel to the coordinated CO_2.[296] The η^2(C,O) coordination dominates for Ni,[297] although other coordination modes to Ni are also known (**Figure 2**). For example, η^1(O) coordination was described by Liaw for an anionic Ni(II) complex, while Milstein described the rather unusual η^1(C) binding mode for a Ni(0) complex with a P,N,P-pincer ligand.[298] Excluding the typically quasi-linear η^1(O) end-on mode, the coordination of CO_2 to a metal center causes a significant deviation of the O-C-O angle from linearity. This can be an observation of significant relevance, as this distortion significantly reduces the activation energy required for CO_2, rendering it less stable and more polarized.[294g] However, despite the importance of bearing in mind this organometallic results, one must remember that complexes and situations of such kind might not be directly relevant to or involved in catalytic protocols.

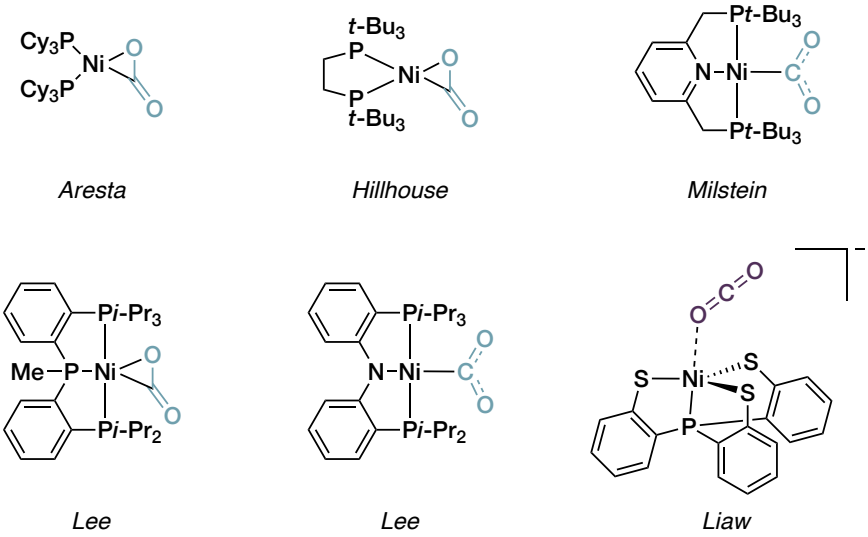

Figure 2. Crystallographically characterized Ni-CO_2 complexes.

[296] M. Aresta, *Coord. Chem. Rev.* **2017**, *334*, 150–183.
[297] a) J. S. Anderson, V. M. Iluc, G. L Hillhouse, *Inorg. Chem.* **2010**, *49*, 10203–10207; b) R. Beck, M, Shoshani, J. Krasinkiewicz, J. A. Hatnean, S. A. Johnson, *Dalton Trans.* **2013**, *42*, 1461–1475; c) S. Yunho, Y. Kim, J. Kim, Y. Lee, Y. *Chem. Commun.* **2014**, *50*, 11458–11461.
[298] a) T-W. Chiou, Y-M. Tseng, T-T. Lu, T-C. Weng, D. Sokaras, W-C. Ho, T-S. Kuo, L-Y. Jang, J-F Lee, W-F. Liaw, *Chem. Sci.* **2016**, *7*, 3640-3644; b) D. Oren, Y. Diskin-Posner, L. Avram, M. Feller, D. Milstein, *Organometallics* **2018**, *37*, 2217–2221.

Among the various modern methodologies, the use of nickel catalysis holds a paramount place. Starting from early results,[299] the field has been greatly advanced, with particular contribution, among others, from the group of Ruben Martin since 2009.[300] These efforts resulted in a great number of protocols for CO_2 fixation into various organic electrophiles for the synthesis of carboxylic acids under reductive Ni catalysis. Substrates engaged include (hetero)aryl, alkyl[301] and alkenyl pseudohalides, allylic alcohols, aziridines, benzylic ammonium salts, aryl sulfonium salts, radical precursors, and unsaturated hydrocarbons (via Ni-hydride chemistry) (**Figure 3**).[294g,302] A remarkable example for the regioconvergent carboxylation of alkyl bromides was given in the introduction.[49]

[299] a) K. Osakada, R. Sato, T. Yamamoto, *Organometallics* **1994**, *13*, 4645–4647; b) C. Amatore, A. Jutand, *J. Am. Chem. Soc.* **1991**, *13*, 2819-2825.

[300] A. Correa, R. Martin, *J. Am. Chem. Soc.* **2009**, *131*, 15974–15975.

[301] Please note that, as of today, no procedures exist for the carboxylation of secondary and tertiary acyclic unactivated alkyl (pseudo)halides. For acyclic alkyl halides, β-hydride elimination and dimerization were reported for secondary alkyl bromides. This is due to the slow carboxylation of unactivated secondary and tertiary alkyl Ni(I) species, so that the few successful examples obtained with cyclic alkyl chlorides require more elevated temperatures (see ref. 243). It can be tentatively assumed that for acyclic alkyl chlorides the necessary temperature increase would also lead to dimerization and β-hydride elimination that could lead either to carboxylation at a primary position or alkenes, or other byproducts. Successful development of such reactions would be of paramount significance, as enantioselective carboxylation processes could be realized.

[302] a) M. Börjesson, T. Moragas, D. Gallego, R. Martin, *ACS Catal.* **2016**, *6*, 6739−6749; b) R. J. Somerville, R. Martin, *Relevance of Ni(I) in Catalytic Carboxylation Reactions* in *Nickel Catalysis in Synthesis: Methods and Reactions*, Ed: S. Ogoshi, Wiley-VCH: Weinheim, **2020**, pp. 285-330; c) J. Davies, D. Janssen-Müller, D. P. Zimin, C. S. Day, T. Yanagi, J. Elfert, R. Martin, *J. Am. Chem. Soc.* **2021**, *143*, 4949–4954; d) A. Tortajada, M. Börjesson, R. Martin, *Acc. Chem. Res.* **2021**, *54*, 3941–3952; e) R. Martin-Montero, V. R. Yatham, H. Yin, J. Davies, R. Martin, *Org. Lett.* **2019**, *21*, 2947−2951; f) T. Yanagi, R. J. Somerville, K. Nogi, R. Martin, H. Yorimitsu, *ACS Catal.* **2020**, *10*, 2117−2123; g) C, Ma, C.-Q. Zhao, X.-T. Xu, Z.-M. Li, X.-Y. Wang, K. Zhang, T.-S. Mei, *Org. Lett.* **2019**, *21*, 2464−2467.

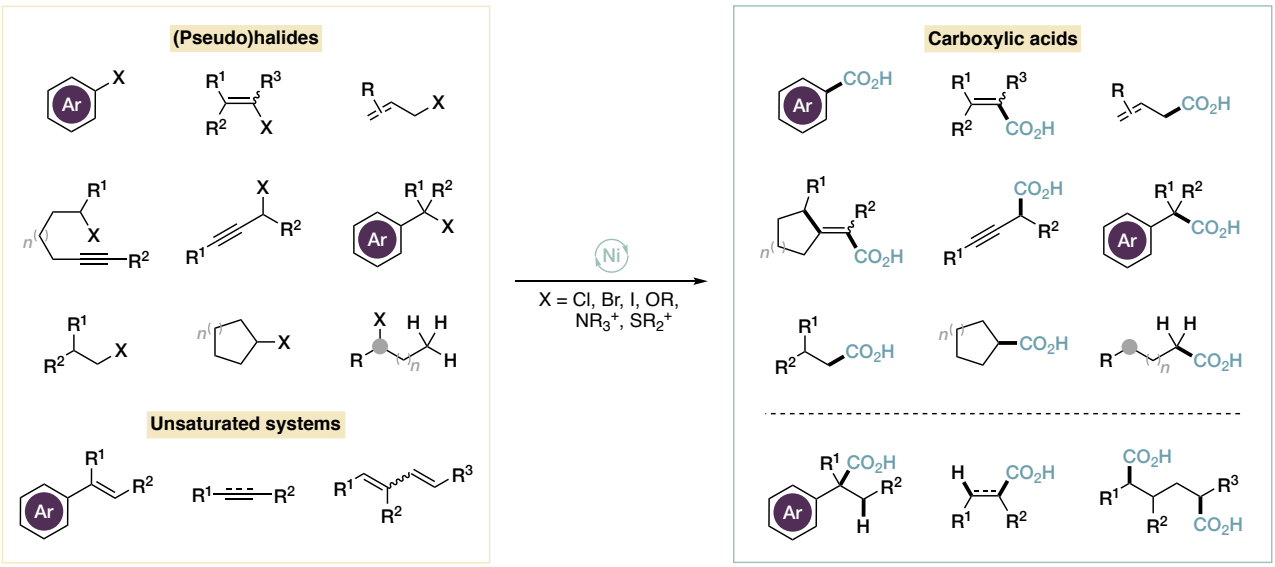

Figure 3. Summary of substrates that have been carboxylated using nickel catalysis.

These are in fact XEC reaction, and conditions are indeed very similar to some of those described in the previous chapter, requiring super-stoiochiometric amounts of metal or organic reductants. Most protocols require polar aprotic amide solvents, mainly DMA and DMF, and they seem to be especially important for the use of metal reductants (mostly Mn and Zn). Similarly, salts additives (especially metal halides) whose role is not yet fully understood, are routinely employed and "a review of the literature indicates that every system for the reductive carboxylation of organic halides and pseudohalides reported to date has both a Lewis acid and halide source present in catalysis, demonstrating the critical nature of these reagents to productive catalysis".[303] Competent ligands are most often phosphines, and bipyridines/phenanthrolines that bear *ortho*-substituents, whose presence seems to be of paramount importance for achieving high yields. In particular, carefully tuned *ortho*-substituted phenanthrolines are the only successful ligands for unactivated Csp^3 electrophiles.

From a mechanistic point of view, Ni(I)-carbyl complexes are thought to be the active species for CO_2 insertion. In 2013, Sakaki and coworkers performed a DFT study on

[303] D. J. Charboneau, G. W. Brudvig, N. Hazari, H. M. C. Lant, A. K. Saydjari, *ACS Catal.* **2019**, *9*, 3228−3241.

the seminal report[304] from Tsuji, who described the carboxylation of aryl chlorides with $(Ph_3P)_2NiCl_2$ as catalyst.[305] In their results, after Ni(0) oxidative addition to the aryl chloride, reduction from manganese affords a Ni(I)-aryl species. This complex can coordinate CO_2 in η^2(C,O) fashion, giving a $(Ph_3P)_2Ni(Ar)(CO_2)$ complex similar to the one reported from Aresta. At this point, the aryl group is easily transferred to the CO_2 ligand in an inner sphere nucleophilic attack, with charge transfer from the significantly negatively charged aryl group. The barrier for aryl group transfer from the Ni(II)-aryl complex was determined to be exceedingly high for such process to occur. They propose that after initial formation of a κ^1-carboxylate, isomerization to a more stable κ^2-carboxylate occurs, and the product is released upon reduction of such Ni(I) carboxylate, enabling turnover. They also determined that the reduction steps of the involved nickel species were all feasible, with the exception of Ni(I)-aryl that indeed should not happen for a productive cycle. In a subsequent study the same authors modelled the carboxylation of benzylic chlorides reported by Martin,[306] with $(Cy_3P)_2NiCl_2$ as catalyst, Zn as a reductant, also focusing on the role of the $MgCl_2$ additive.[307] Similar results were obtained in that transfer of the benzyl group was facile from Ni(I) both in the absence and presence of $MgCl_2$, whereas it resulted in both cases not energetically accessible from Ni(II). Differently from the previous scenario, the Ni(I)-benzyl complex coordinates CO_2 in a η^1(C) fashion prior to attack. When $MgCl_2$ is present, it coordinates the η^1(C) bound CO_2 at one of the oxygen atoms, and transfer of the organic group to CO_2 presents a much lower barrier than in the absence of $MgCl_2$, indicating that its presence significantly accelerates CO_2 insertion, which is very relevant to catalytic conditions.

In a very detailed work, Hazari and coworkers investigated the reactivity of a preformed $(Ph_3P)_2Ni(I)Ar$ species (which is determined to be metal centered radical) and demonstrated in stoichiometric way that this complex yields the carboxylic acid

[304] T. Fujihara, K. Nogi, T. Xu, J. Terao, Y. Tsuji, *J. Am. Chem. Soc.* **2012**, *134*, 9106–9109.
[305] F. B. Sayyed, Y. Tsuji, S. Sakaki, *Chem. Commun.* **2013**, 49, 10715–10717.
[306] T. León, A. Correa, R. Martin, *J. Am. Chem. Soc.* **2013**, *135*, 1221.
[307] F. B. Sayyed, S. Sakaki, *Chem. Commun.* **2014**, *50*, 13026–13029.

product upon exposure to CO_2 in THF followed by acidic work-up, without added additives (except for free PPh_3 that was added to prevent fast decomposition of the unstable metal complex).[303] This confirms that Ni(I)-aryl species are highly nucleophilic. $(Ph_3P)_2Ni(II)ArCl$, instead, did not react with CO_2. They also focused on the role of additives and determined that an added Lewis acid (Li^+) accelerates the insertion, in accordance with the calculations from Sakaki. The putative Ni(I) κ^1-carboxylate could not be observed, and the results suggest that this species is unstable towards disproportionation to Ni(0) and Ni(II) species. Upon addition of excess LiCl, $(Ph_3P)_3Ni(I)Cl$ was isolated in high yield, alongside the carboxylation product. Overall, the authors conclude that a Ni(I) κ^1-carboxylate is an unstable catalytic intermediate, and that its ligand metathesis with metal halide salts is a plausible elementary step in the catalytic cycle, occurring faster than its decomposition. They also suggest that the complexation of the Lewis acid to bound CO_2 found by Sasaki could enhance the stability of the carboxylate. These findings are important also for the final reduction step: on the basis of the results from a reductant screening, they demonstrate that catalytic turnover can operate in the absence of a Lewis acid only if a strong reductant (cobaltocene) is used. They propose that Ni(I)-carboxylates are not easily reduced and that, in the presence of halide salts, the metathesis step to form a Ni(I)-halide complex that undergoes facile reduction is of key importance for catalytic turnover. Finally, they suggest that the role of amide solvents is to guarantee solubility of the Lewis acid. A tentative general catalytic cycle for aryl or benzyl electrophiles is shown in **Scheme 1**.

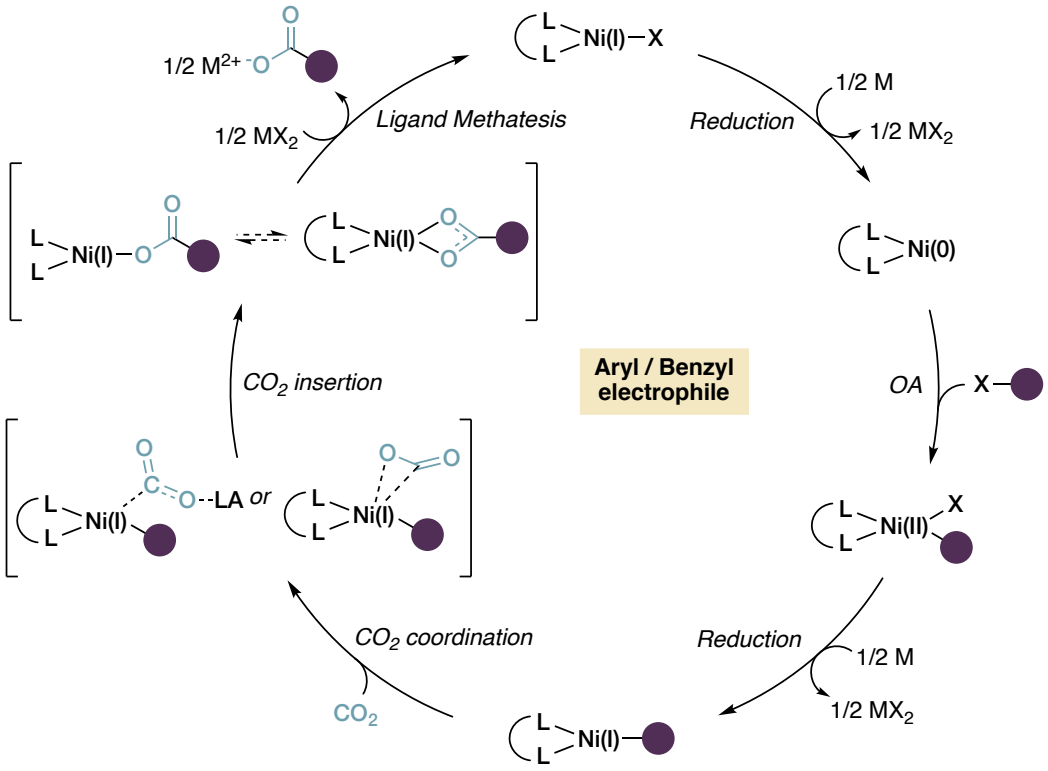

Scheme 1. Proposed general catalytic cycle for aryl or benzyl electrophiles on the basis of the available stoichiometric experiments and computational work.

In a later report, Martin was able to prepare catalytically relevant Ni(I)-halide and Ni(I)-alkyl complexes bearing *ortho*-substituted phenanthroline ligands (phen*), that were also determined to be metal centered radicals, and studied their behavior with IR, EPR and XRD techniques as well as DFT calculations.[308] Ligand metathesis from Ni(I)-halide with a potassium carboxylate afforded a Ni(I) carboxylate which in this case did not prove unstable, and whose IR spectrum suggest κ^2 coordination, as also predicted by computations. EPR measures proved that the same species was obtained upon exposure of the Ni(I)-alkyl complex to CO_2 in THF, and the carboxylic acid was isolated after acidic work-up. This unambiguously proves CO_2 insertion into Ni(I)-alkyl bonds. DFT calculations in this case did not find any precursor complex between Ni and CO_2, but the alkyl group transfer proceeds via an inner sphere pathway, with a TS in which CO_2 interacts with nickel adopting a bent geometry, similarly to η^2(C,O)

[308] R. J. Somerville, C. Odena, M. F. Obst, N. Hazari, K. H. Hopmann, R. Martin, *J. Am. Chem. Soc.* **2020**, 142, 10936−10941.

coordination. Finally, when another (phen*)Ni(I)-alkyl complex was exposed to CO_2 in the presence of $MgBr_2$ (present in the mixture from the complex preparation with a Grignard reagent) the carboxylic acid was obtained after acidic work up, but EPR measurements did not observe any Ni species other than (phen*)Ni(I)Br. Addition of $MgBr_2$ to the above discussed pure (salt-free) Ni(I) carboxylate also afforded an analogous products. This strongly supports the idea that ligand metathesis of the Ni(I)-carboxylate affording a Ni(I)-halide is fast and occurs prior to further reduction. The activation of alkyl halides in their nickel catalyzed carboxylation was demonstrated to proceed via formation of out-of-cage alkyl radicals, most likely from a Ni(0) complex. The active Ni(I)-alkyl species could result from either reduction of a Ni(II) alkyl species or its comproportionation with Ni(0).[309]A general model catalytic cycle for alkyl electrophiles is shown in **Scheme 2**.

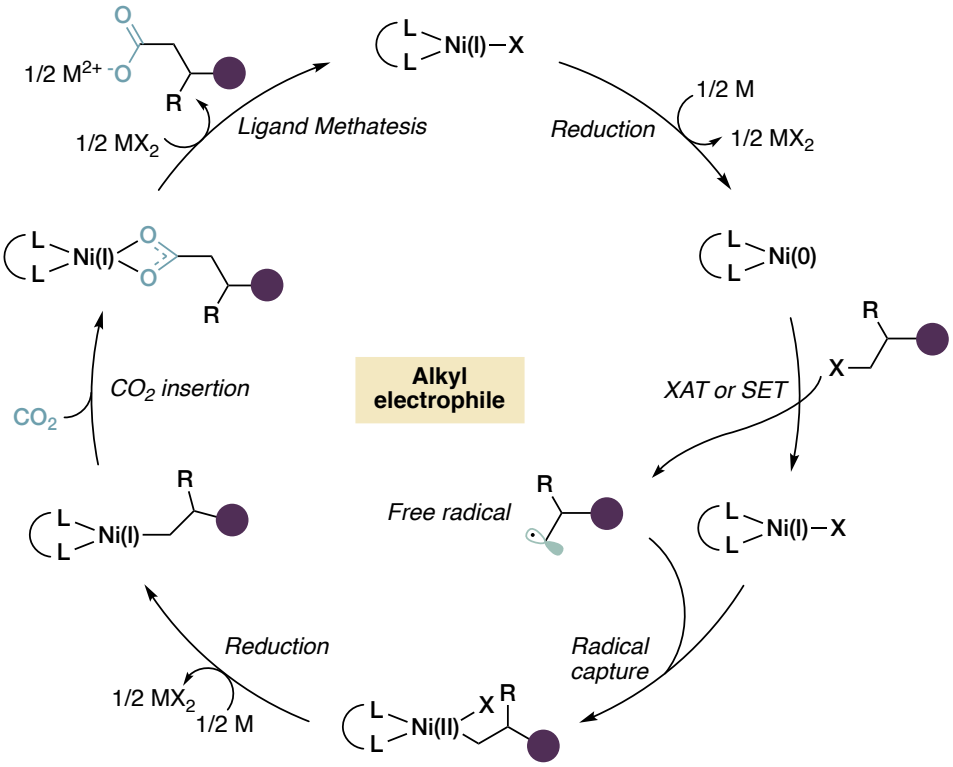

[309] a) Y. Liu, J. Cornella, R. Martin, *J. Am. Chem. Soc.* **2014**, *136*, 11212−11215; b) M. Börjesson, T. Moragas, R. Martin, *J. Am. Chem. Soc.* **2016**, *138*, 7504−7507.

Scheme 2. Proposed general catalytic cycle for alkyl electrophiles on the basis of the available stoichiometric experiments and computational work.

It must be borne in mind that a small number of mechanistic studies are available, and that such results were obtained only for a limited number of ligands, substrates and conditions. Therefore, it might be very well possible that different mechanisms exist under different conditions, and conclusive answers are still not available. For example, CO_2 readily inserts into phosphine or carbene Ni(II)–η^3(allyl)$_2$ complexes in toluene,[310a] (bpy)Ni(II)(alkyl)$_2$ complexes in benzene,[310b] as well as into (bpy)Ni(II)(Ar)(Br) in DMF, as shown by Yamamoto in his seminal work.[299a]

A great opportunity to rapidly and efficiently obtain value-added compounds in the CO_2 fixation context is represented by tandem functionalization-carboxylation processes, in which some kind of transformation leading to enhanced structural complexity is merged with the introduction of CO_2. The advantage of this strategy is to employ a single protocol (that is a complete set of catalysts, additives, and solvents) to achieve both molecular modification and carboxylation of a given scaffold, thus achieving greatly increased step- and waste economy, with significant time and cost saving. Various types of transformations have been productively coupled with CO_2-based carboxylation, ranging from carbofunctionalizations to the introduction of various heteroatoms such as B, F, Si, S, and P.[311] Most work focused on π-systems (as they provide a great platform for concomitant difunctionalization at two different sites) using light-, base- or metal promoted reactivity. Some examples of nickel catalyzed tandem functionalization-carboxylation processes on π-systems will be shown in the next section.

In 2015 Martin, and co-workers developed a stereodivergent intramolecular cyclization-carboxylation protocol to convert alkyne-tethered alkyl bromides into

[310] a) P. W. Jolly, S. Stobbe, G. Wilke, R. Goddard, C. Krüger, J. C. Sakutowski, Y.-H. Tsay, *Angew. Chem. Int. Ed.* **1978**,*17*, 124; b) T. Yamamoto, A. Yamamoto, *Chem. Lett.* **1978**, 615.
[311] G. Bertuzzi, A. Cerveri, L. Lombardi, M. Bandini, *Chin. J. Chem.* **2021**, *39*, 3116−3126.

cyclo-fused acrylic acids. The reaction proceeds under Ni catalysis using an *ortho*-substituted phenanthroline ligands (depending on the substrate, *vide infra*) and manganese as reductant.[312]

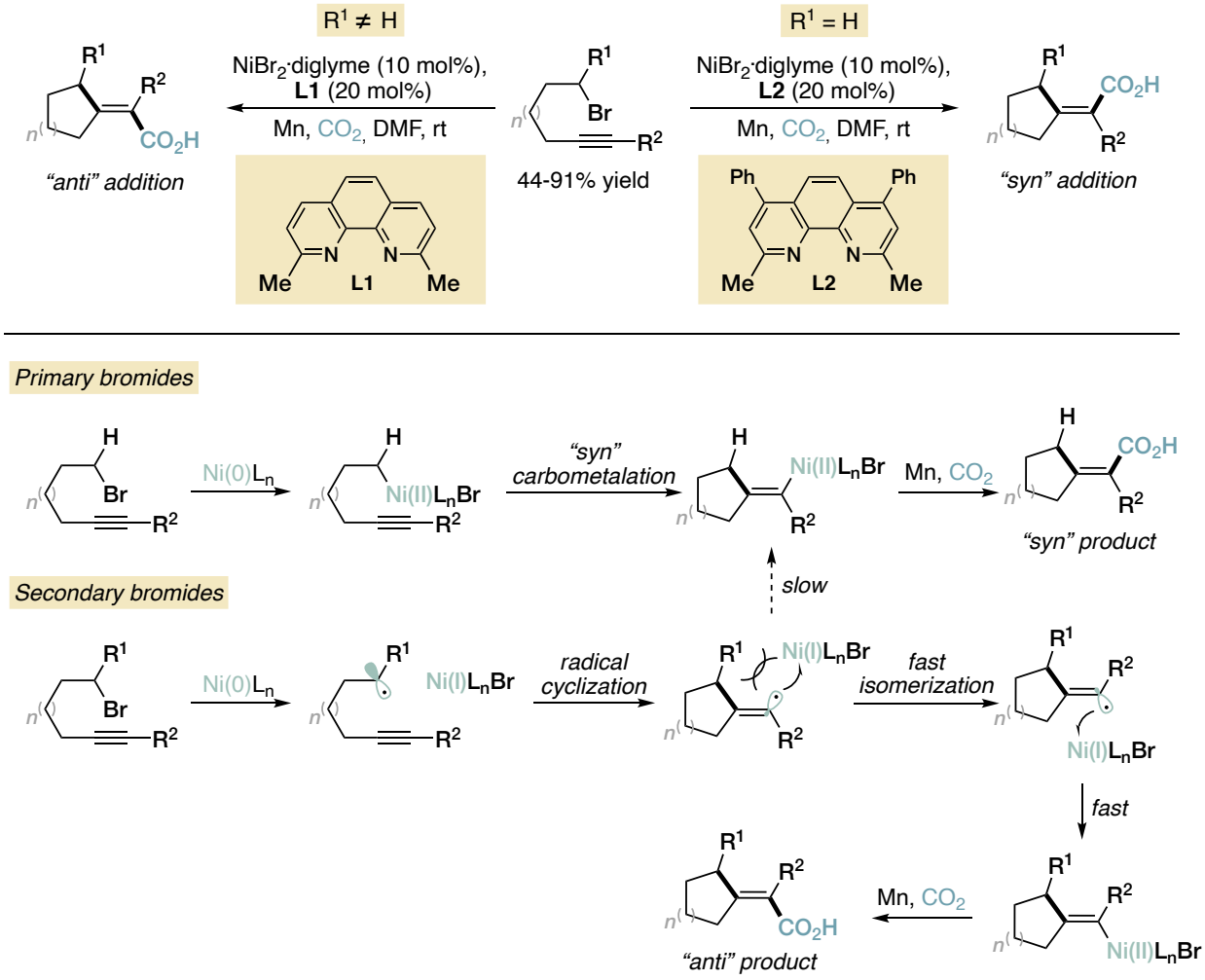

Scheme 3. Top: stereodivergent tandem cyclization-carboxylation of alkyne tethered alkyl bromides. Bottom: proposed mechanistic rationale. For primary substrates, the most likely mechanism involves a "syn" carbometallation followed by CO_2 insertion. For secondary ones the cyclization probably occurs in a radical fashion after XAT from the alkyl bromide. The resulting vinyl radical recombines with Ni after isomerization to yield a formal "*anti*" carbometalated vinyl Ni species that leads to the observed product.

Great chemoselectivity was observed, with commonly synthetic handles for carboxylation such as aryl chlorides, tosylates and pivalates being untouched, and

[312] X. Wang, Y. Liu, R. Martin, *J. Am. Chem. Soc.* **2015**, *137*, 6476−6479.

terminal alkynes are also competent. The stereochemical outcome is substrate-dependent: primary alkyl bromides lead to *syn* addition products, while secondary ones yield *anti* addition products (**Scheme 3**). Since carbometalation normally proceeds in a *syn* fashion, the authors propose that, for secondary alkyl bromides, a radical cyclization of an alkyl radical (formed by low valent Ni) onto the triple bond leads to a vinyl radical that can rapidly isomerize when a group different from H is present *syn* to it, to then recombine with nickel, leading to the *anti* products. Deuterium labeling experiments on a primary alkyl bromide show inversion of configuration at the electrophilic carbon, excluding the formation of free radicals for primary substrates.

In a conceptually related report, the same group reported the Ni catalyzed reductive carboxylation of Csp^2-H bonds at a remote site by employing 1-bromo-3-arylpropanes bearing an *ortho*- alkyne substituent.[313] Particular conditions were employed, with a bipyridine ligand bearing only one *ortho*-substituent, and a manganese-chromium alloy as reductant (**Scheme 4**, top).

[313] M. Börjesson, D. Janssen-Müller, B. Sahoo, Y. Duan, X. Wang, R. Martin, *J. Am. Chem. Soc.* **2020**, *142*, 16234−16239.

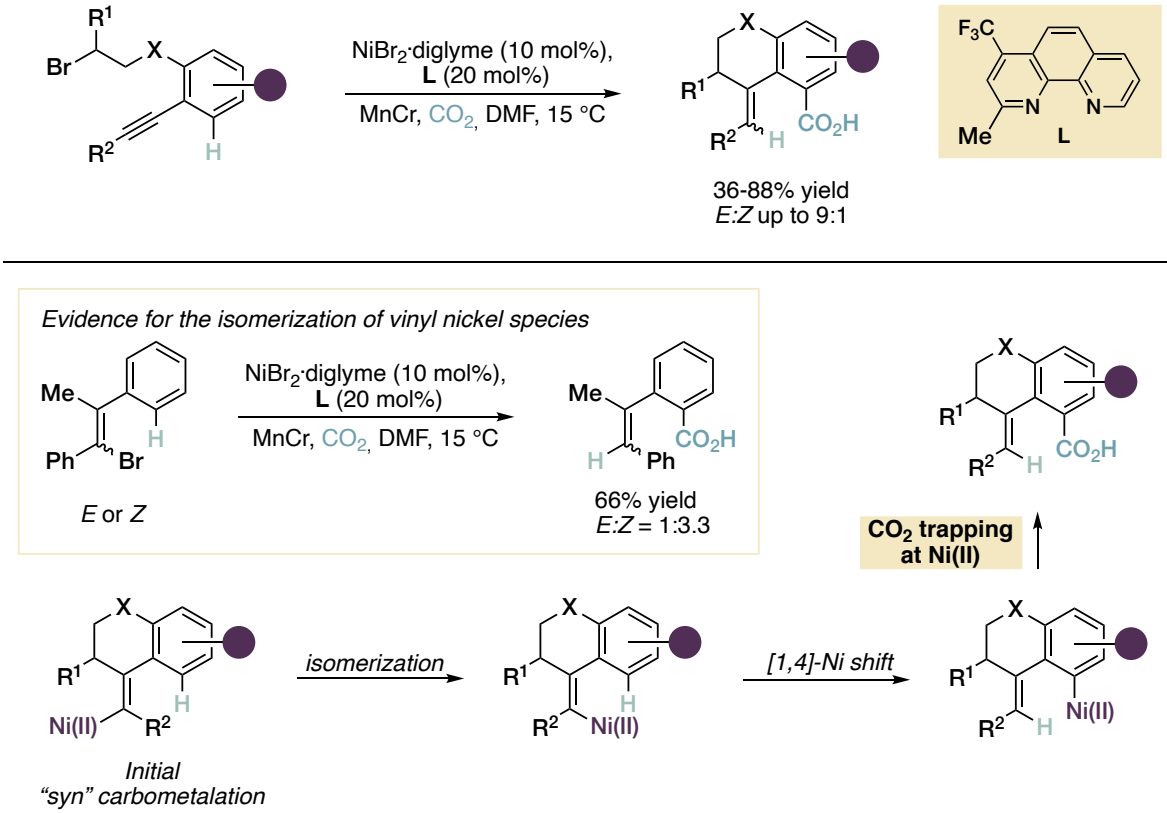

Scheme 4. Top: tandem cyclization-remote carboxylation of Csp^2-H bonds developed by the Martin group. Bottom: proof for the isomerization of vinyl nickel intermediates (yellow box); proposed mechanistic rationale for the formation of the major *E* isomer.

After a carbometalation event to yield a vinyl nickel complex (similarly to the previous example), a [1,4]-nickel migration occurs in some way, so that the final site for carboxylation is the aromatic Csp^2 carbon *ortho* to the alkene moiety. For primary bromides, very good *E*/*Z* selectivity is obtained, and the major product is the one that would arise from the *anti* carbometalation of the triple bond (*E* isomer). Deuterium labeling experiments corroborate that a [1,4]-Ni migration occurs at the *ortho* sp^2 C−H bond prior to CO_2 insertion. When subjecting *Z* and *E* vinyl bromides (that should yield analogous vinyl nickel intermediates to those obtained from carbometalation), identical yields and selectivity for the products were obtained for both isomers. This suggests that *E*/*Z* isomerization of the vinyl nickel species reasonably formed by *syn* carbometalation is in operation. Surprisingly, stoichiometric experiments with preformed Ni(II) vinyl complexes in the absence of reductant suggest that both

migration and carboxylation occur at Ni(II) centers, in contrast with most nickel catalyzed carboxylation protocols (**Scheme 4**, bottom).

Our group recently reported a nickel-catalyzed enantioselective intramolecular interrupted Heck carbo-carboxylation cascade process to access enantioenriched 2,3-dihydrobenzofurans, indolines and indanes bearing a defined quaternary stereogenic center.[314] The starting materials are simple 2-iodoarenes tethered with unactivated pendant alkenes, and cyclized products are obtained with remarkable enantioselectivity (up to 99% e.e.). Optimal conditions feature a preformed nickel complex bearing an electron-rich pyridine-imidazoline chiral ligand, zinc as reductant and DMF as solvent. TMSCl was identified as a key additive, and TBAI (tetrabutylammonium iodide) was also beneficial to the yield (**Scheme 5**, top).

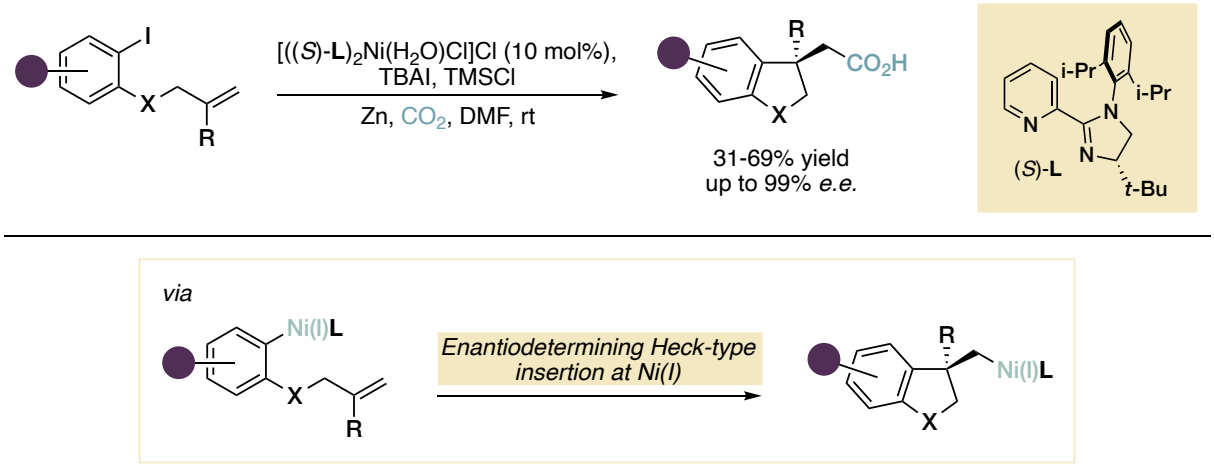

Scheme 5. Top: enantioselective tandem-cyclization carboxylation via interrupted Heck reactivity. Bottom: key enantiodetermining carbometalation event, likely occurring at a Ni(I)-aryl species. X = O, CH_2, N. For X = N, only modest *e.e.* values are obtained, while indenes (X = CH_2) are formed in great enantioselectivity.

DFT investigations were carried out and the following mechanism was proposed. Starting from Ni(0), oxidative addition on the aryl iodide takes place, and the Ni(II) aryl complex is reduced by zinc to Ni(I). Then a regio- and enantioselective Heck-type

[314] A. Cerveri, R. Giovanelli, D. Sella, R. Pedrazzani, M. Monari, O. Nieto Faza, C. Silva López, M. Bandini, *Chem. Eur. J.* **2021**, *27*, 7657-7662.

cyclization occurs, to form an alkyl-Ni(I) intermediate that undergoes carboxylation, followed by ligand metathesis of the Ni(I) κ1-carboxylate and reduction to Ni(0) that closes the cycle. A similar mechanism in which cyclization occurs from a Ni(II) complex prior to reduction is considered less likely given the obtainment of benzoic acids as byproduct, that could only arise from Ni(I) (**Scheme 5**, bottom).

Simultaneously to our group, Kong and Yu reported a conceptually identical nickel-catalyzed enantioselective interrupted Heck carbo-carboxylation of methacrylanilides for the synthesis of oxindole 3-acetic acids bearing a defined C3-quaternary stereogenic center.[315]

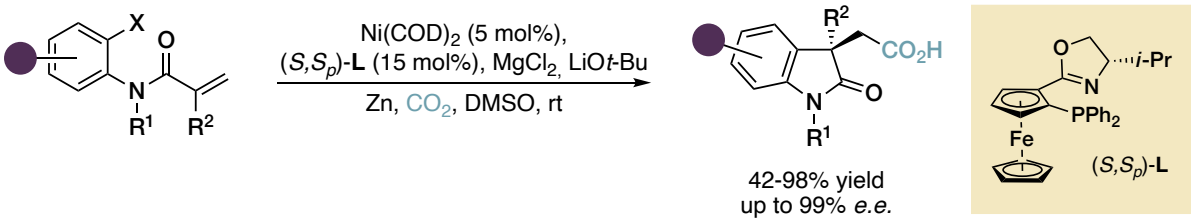

Scheme 6. Kong's enantioselective tandem-cyclization carboxylation.

A completely different set of conditions were identified as optimal: a chiral ferrocenylphosphine-oxazoline ligand and $Ni(COD)_2$ as precatalyst gave the best performances in DMSO as solvent, in the presence of $MgCl_2$ and LiO*t*-Bu as additives (**Scheme 6**). This protocol was applicable not only to aryl bromides: *o*-chloroanilides provided similar results. Aryl triflates were also competent, furnishing the products in comparable enantioselectivity but reduced yields. The authors propose an analogous mechanism to the one found for our protocol, coherently based on the same observation of the presence of the ipso-carboxylation byproduct. This further supports the unusual Ni(I) mediated Heck-type cyclization.

[315] X.-W. Chen, J.-P. Yue, K. Wang, Y.-Y. Gui, Y.-N. Niu, J. Liu, C.-K. Ran, W. Kong, W.-J. Zhou, D.-G. Yu, *Angew. Chem. Int. Ed.* **2021**, *60*, 14068–14075.

Carbon-carbon bonds are ubiquitous moieties, constituting the essence of organic compounds as they compose their very backbone. Therefore, activation of C-C bonds may at first seem a counterintuitive process to pursue, given that most of organic chemistry deals with the formation of such bonds *en route* to target structures. In fact, this kind of transformation holds great synthetic value. As for C-H bonds, the omnipresence of C-C linkages provides an opportunity to avoid prefunctionalization steps by making use of innate handles. Even more, their disconnection and derivatization results in reorganization of the molecular skeleton, so that unique atom-economical and straightforward strategies with great potential in streamlining synthesis can be envisioned.[316] The field of C-C bond activation has been mainly explored with transition metal catalysis, but is considerably underdeveloped with respect to C-H activation, as a number of reasons contribute to make this process more challenging.[317] From a thermodynamic point of view, C-C linkages are relatively strong bonds, although in general weaker than the corresponding C-H bonds.[318] However, metal-carbon bonds (especially for alkyls) are usually much weaker than metal-hydride bonds, so that insertion of a metal into C-C bonds is generally less favorable and endergonic.[319] Indeed, the reverse process, that is reductive elimination, is a fundamental step in transition metal catalysis to forge C-C bonds. From a kinetic perspective, C-C bonds are sterically less exposed than C-H bonds and statistically less abundant. Another difference is the more directional orbitalic nature of carbon with respect to hydrogen atoms: in a metal oxidative addition scenario, the spherical symmetrical s hybridization of hydrogen makes it capable of binding both the carbon and metal atom in the TS, while the sp^3 (and in general sp^n) hybridized carbon orbitals

---

[316] a) B. Wang, M. A. Perea, R. Sarpong, *Angew. Chem. Int. Ed.* **2020**, *59*, 18898; b) P.-h. Chen, B. A. Billett, T. Tsukamoto, G. Dong, *ACS Catal.* **2017**, *7*, 1340−1360.

[317] G. Dong, *C-C bond activation (Topics in Current Chemistry).* Springer-Verlag Berlin: Heidelberg, **2014**; M. Murakami, Y. Ito, *Cleavage of Carbon—Carbon Single Bonds by Transition Metals.* In *Activation of Unreactive Bonds and Organic Synthesis. Topics in Organometallic Chemistry*. Springer, Berlin; Heidelberg, **1999**.

[318] Y.-R, Luo, J.-P. Cheng, *Bond Dissociation Energies* in *CRC Handbook of Chemistry and Physics*, *96th Edition.* CRC Press, **2015**.

[319] a) J. A. M. Simões, J. L. Beauchamp, *Chem. Rev.* **1990**, *90*, 629; b) L. Souillart, N. Cramer, *Chem. Rev.* **2015**, *115*, 9410−9464.

need to deviate from their optimal bonding orientation.[320] So a C-C bond, featuring two C atoms, presents a higher barrier for this process than a C-H bond that only has one, and the agostic interaction that precedes σ-bonds activation is weaker.[321] These aspects concur to the higher kinetic inertness observed for C-C bonds, and this is indirectly supported by the observation that several polyalkyl metal complexes are stable, while alkyl metal hydrides are much rarer (if reductive elimination is in both cases thermodynamically favored, it follows from from the microscopic reversibility principle that C-C bonds feature higher barriers for both OA and RE).[320a]

To overcome these challenges, some driving force that renders the overall process exergonic needs to be provided, by either increasing the energy of the starting materials or reducing that of the products: this has been accomplished by the use of strained compounds, concomitant aromatization processes, chelation stabilization using a directing group (DG), or formation of particularly strong bonds.[322] Such strategies most often also favor the process kinetically: for example thw use of a DG brings the target C-C bond and the metal atom in close proximity decreasing the activation energy.[323] In particular, the use of small tensioned cycles has emerged as a key strategy, as their ring strain lowers their bond strength and provides strain energy release in their activation; being cyclic, C-C bond activation results in a highly atom economical, skeletal reorganizing difunctionalization.[322c] Moreover, these compounds feature peculiar so-called "banana bonds": to permit highly distorted bond angles, their orbital hybridization is different, and presents much more p character than the normal sp^3 carbons in unstrained alkanes.[324] The HOMO and LUMO in cyclopropanes and cyclobutanes are similar in availability and symmetry to those of alkenes, so that they interact strongly with metal orbitals, similarly to olefins, lowering the kinetic barrier

---

[320] a) B. Rybtchinski, D. Milstein, *Angew. Chem. Int. Ed.* **1999**, *38*, 870−883; b) J. J. Low, W. A. Goddard III, *J. Am. Chem. Soc.* **1984**, *106*, 8321; c) P. E. M. Siegbahn, M. R. A. Blomberg, *J. Am. Chem. Soc.* **1992**, *114*, 10548.
[321] M. Etienne, A. S. Weller, *Chem. Soc. Rev.* **2014**, *43*, 242.
[322] a) C.-H. Jun, *Chem. Soc. Rev.* **2004**, *33*, 610–618; b) F. Song, T. Gou, B.-Q. Wanga, Z.-J. Shi, *Chem.Soc.Rev.* **2018**, *47*, 7078–7115; c) G. Fumagalli, S. Stanton, J. F. Bower, *Chem. Rev.* **2017**, *117*, 9404−9432; d) D.-S. Kim, W.-J. Park, and C.-H. Jun, *Chem. Rev.* **2017**, *117*, 13, 8977–9015; Y. Xu, X. Qi, P. Zheng, C. C. Berti, P. Liu, G. Dong, *Nature* **2019**, *567*, 373–378.
[323] Y. Xia, G. Dong, *Nat. Rev. Chem.* **2020**, *4*, 600–614.
[324] K. B. Wiberg, *Acc. Chem. Res.* **1996**, *29*, 229-234.

for their activation.[320a] Two main strategies are employed in metal catalyzed C-C activation, namely direct metal insertion and β-carbon elimination, although metal-free and/or radical pathways are also known (**Scheme 7**).[317,325]

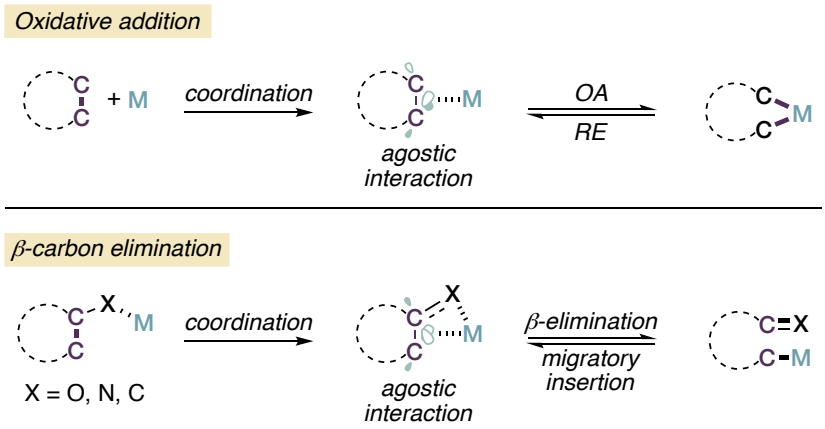

Scheme 7. Two main pathways for metal catalyzed C-C bond activation. Top: direct oxidative addition. Upon coordination of the C-C bond to the metal, an agostic interaction is established. A distorted C-C bond LUMO interacting with an electron rich metal is depicted. Bottom: β-carbon elimination. Upon coordination of the metal to a heteroatom or carbanion (acting like a DG), coordination of the metal and establishment of an agostic complex follows. A distorted C-C HOMO interacting with an electron deficient metal center is in this case depicted. This complex precedes the C-C bond cleave in a process that is the reverse of a migratory insertion into a C-X bond.

β-carbon elimination presents similar kinetic and thermodynamic intrinsic challenges as those discussed above, but since it proceeds in an intramolecular fashion, kinetic barriers are lower. Also, when acyclic substrates are used it results in the elimination of a byproduct molecule, thus generating a favorable entropy increase.

The use of cyclobutanones in particular has been a highly exploited strategy, given that: the C-C(O) bonds in ketones are generally weaker than normal C-C bonds;[326] the ketone moiety offers the possibility of forming, by nucleophilic attack, a metal alkoxide for β-carbon elimination; they are easily handled despite being highly reactive,

[325] a) C. T. To, K. S. Chan, *Eur. J. Org. Chem.* **2019**, 6581–6591; b) Y. Chen, J. Du, Z. Zuo, *Chem* **2020**, *6*, 266–279; c) F. Chen, T. Wang, N. Jiao, *Chem. Rev.* **2014**, *114*, 8613−8661; d) X.-Y. Yu, J.-R. Chen, W.-J. Xiao, *Chem. Rev.* **2021**, *121*, 506−561; e) P. Sivaguru, Z. Wang, G. Zanoni, X. Bi *Chem. Soc. Rev.* **2019**, *48*, 2615−2656; f) F. Ma, X. Xie, Y. Li, Z. Yan, M. Ma, *J. Org. Chem.* **2021**, *86*, 1, 762–769; g) Y. Yuan, H. Tan, L. Kong, Z. Zheng, M. Xu, J. Huang, Y. Li, *Org. Biomol. Chem.* **2019**, *17*, 2725–2733.

[326] a) J. W. Suggs, C.-H. Jun, *J. Am. Chem. Soc.* **1984**, *106*, 3054-3056; b) A. J. Gordon, R. A. Ford, *The Chemist's Companion.* Wiley: New York, **1972**; p 113.

differently from cyclopropanones that are unstable.[327] Also, given their possibility for decarbonylation, these compounds can behave as either a four-carbon or a three-carbon synthon, leading to distinct transformations. Many different transformations of cyclobutanones have been reported, mainly by means of rhodium, palladium or nickel catalysis.[328]

Rh(I) was probably the first metal species known to insert into ketones. Stoichiometric reports are known since 1965.[329] Murakami and co-workers reported a pioneering catalytic example of metal insertion into the C-C(O) bond of a ketone. They found that when treating cyclobutanone with a stoichiometric amount of $RhCl(PPh_3)_3$ (Wilkinson's catalyst) in refluxing toluene at 140 °C for two days, a cyclopropane product was obtained in quantitative yield along with the unreactive complex trans-$[Rh(CO)Cl(PPh_3)_2]$ (**Scheme 8**, top).[330]

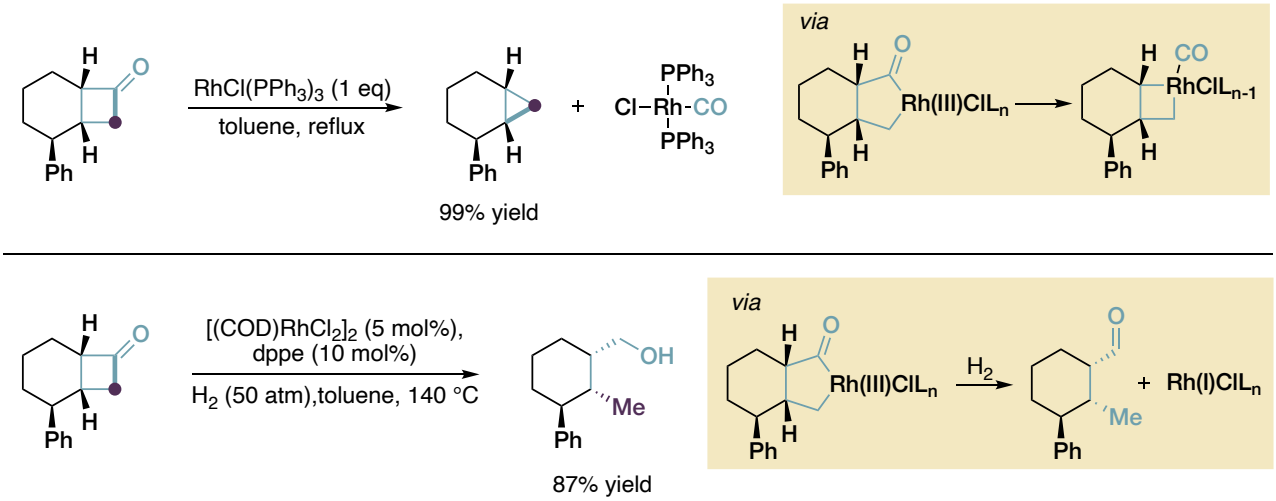

Scheme 8. Pioneering example of C-C activation of cyclobutanones by means of rhodium catalysis. Top: stoiochiometric reaction. Bottom: catalytic C-C activation-hydrogenation methodology.

[327] Y. Xue, G. Dong, *Acc. Chem. Res.* **2022**, *55*, 2341−2354.
[328] a) M. Murakami, N. Ishida, *Chem. Rev.* **2021**, *121*, 264−299; b) L. Deng, G. Dong, *Trends Chem.* **2020**, *2*, 183–198; c) T. Seiser, N. Cramer *Org. Biomol. Chem.* **2009**, *7*, 2835–2840; d) T. Seiser, T. Saget, D. N. Tran, N. Cramer, *Angew. Chem. Int. Ed.* **2011**, *50*, 7740–7752;
[329] A. Dermenci, J. W. Coe, G. Dong, *Org. Chem. Front.* **2014**, *1*, 567–581.
[330] M. Murakami, H. Amii, Y. Ito, *Nature* **1994**, *370*, 540–541.

The authors suggested the formation of a five-membered Rh(III) metallacycle via oxidative addition onto the C-C bond, followed by decarbonylation and reductive elimination. The reaction could be made catalytic when combined with a hydrogenation process. When cyclobutanone was treated with 10 mol% [(COD)Rh(I)Cl] and dppe (1,2-bis(diphenylphosphino)ethane) as ligand in refluxing toluene under 50 atm pressure of hydrogen gas, an alcohol was obtained. This is reasonably formed via hydrogenation of the acyl rhodacycle and indicates that insertion occurs at the less hindered position (**Scheme 8**, bottom).

The same authors later employed the same activation strategy with a cyclobutanone bearing an *ortho*-substituted styryl group at the 3-position.[331] After C-C bond insertion, migratory insertion of the C-Rh unit onto the double bond takes place, and reductive elimination furnished a benzobicyclo[3.2.1]octenone product. An experiment using a ^{13}C-labeled substrate demonstrated that Rh(I) cleaves the bond between the carbonyl carbon and the α-carbon, consistently with the previous observations (**Scheme 9**). In this case a notably reduced reaction time is sufficient, and the authors propose that Rh coordination to the double bond accelerates the insertion step.

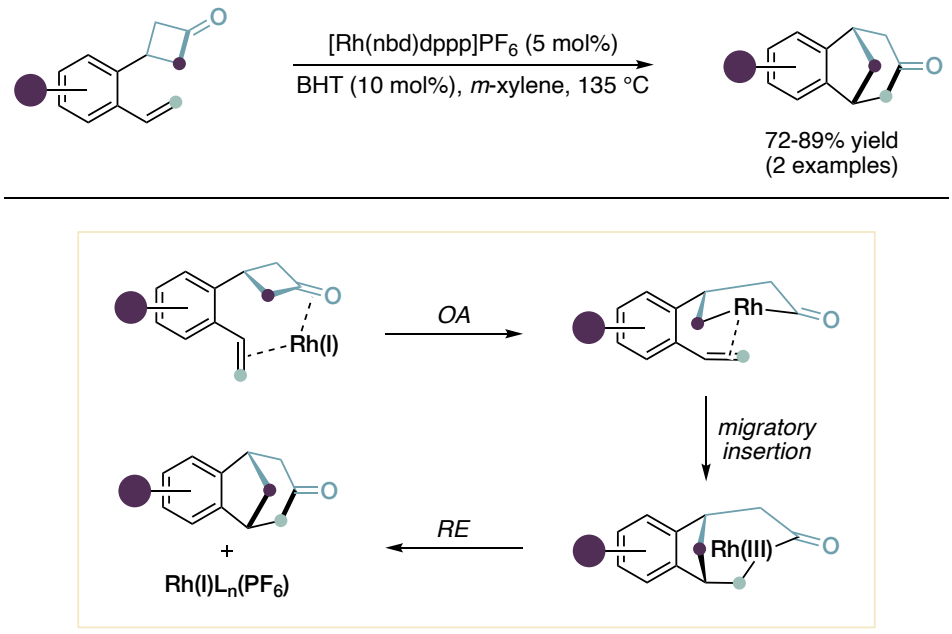

[331] M. Murakami, T. Itahashi, Y. Ito, *J. Am. Chem. Soc.* **2002**, *124*, 13976−13977.

Scheme 9. Top: Rh catalyzed C-C bond activation-cyclization of styryl tethered cyclobutanones en route to benzobicyclo[3.2.1]octenones. A substoichiometric quantity of BHT was used as additive to prevent fast polymerization of the substrate. Bottom: proposed mechanism. The initial insertion onto the C-C(O) double bond was demonstrated. For the sake of clarity, the ligand environment of Rh is not shown, as well as the oxidation state after OA (+3). nbd = 2,5-norbornadiene; dppp = 1,3-bis(diphenylphosphino)propane.

An enantioselective version of the protocol was reported by Cramer in 2014.[332]

Xu and coworkers described a very elegant enantioselective isomerization of cyclobutanones bearing an *o*-iodoarene at the 3-position. Using $Pd_2(dba)_3$ as catalyst and a TADDOL-derived phosphoramidite ligand in refluxing toluene, 1-indanones featuring a stereodefined C3-quaternary center bearing an iodomethyl substituent were obtained in excellent enantiomeric excess (**Scheme 10**, top).[333]

[332] L. Souillart, E. Parker, N. Cramer, *Angew. Chem. Int. Ed.* **2014**, *53*, 3001–3005.
[333] Y.-L. Sun, X.-B. Wang, F.-N. Sun, Q.-Q. Chen, J. Cao, Z. Xu, L.-W. Xu, *Angew. Chem. Int. Ed.* **2019**, *58*, 6747 – 6751.

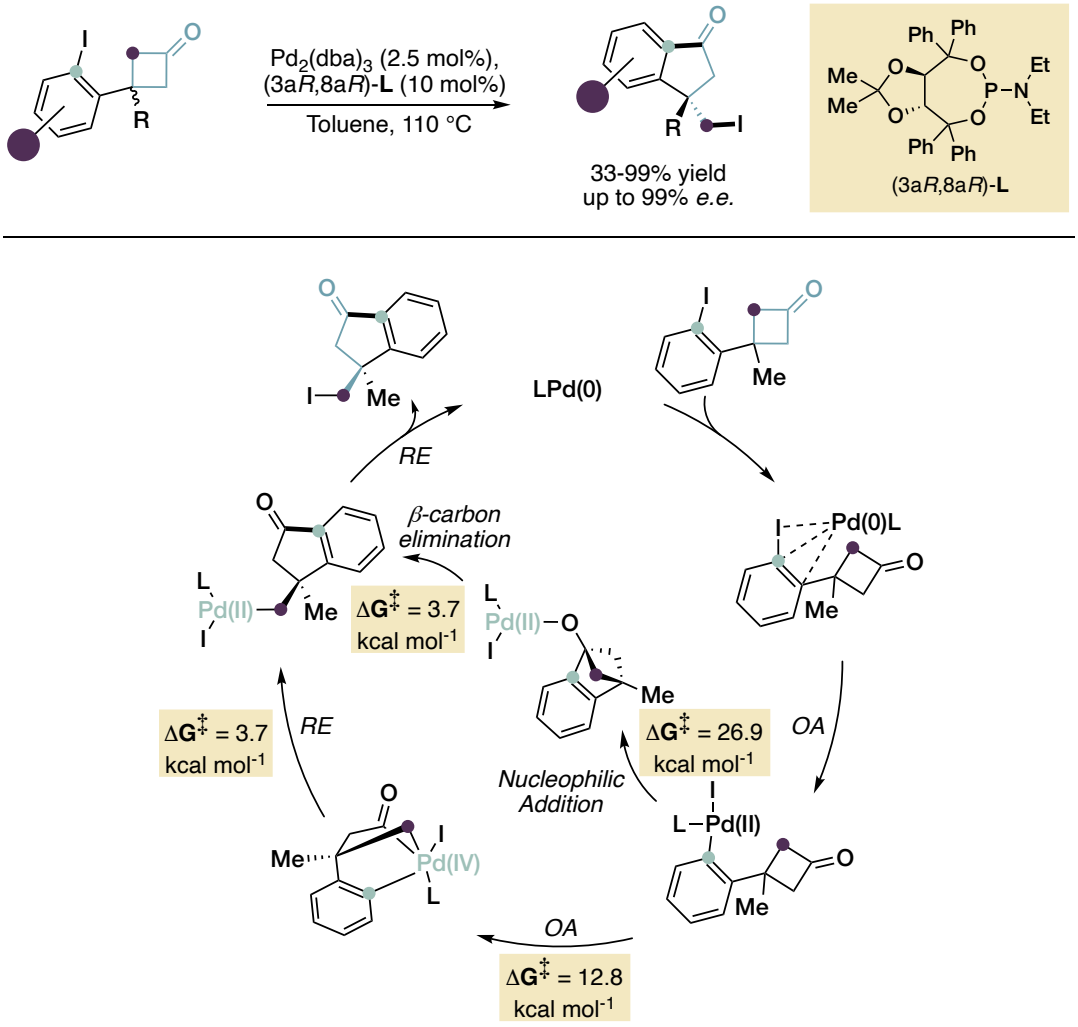

Scheme 10. Top: Enantioselective isomerization of iodoarene bearing a cyclobutanone moiety to obtain indanones. Bottom: proposed mechanisms. DFT calculations suggest a double oxidative addition sequence.

The authors propose two possible mechanisms. One involves nucleophilic attack of the aryl Pd(II) formed after OA to the ketone moiety, followed by β-carbon elimination, to access an alkyl Pd (II) intermediate. The same species can derive from a second OA from Pd(II) to give a Pd(IV) intermediate than reductively eliminates to the Pd(II) alkyl. DFT calculations support the latter mechanism (**Scheme 10**, bottom).

The same group also exploited this activation in a carbonylative protocol to prepare 1-indanones with C3-quaternary centers bearing an ester or amide moiety.[334]

[334] K.-L. Song, B. Wu, W.-E. Gan, W.-C. Yang, X.-B. Chen, J. Cao, L.-W. Xu, *Org. Chem. Front.* **2021**, *8*, 3398–3403.

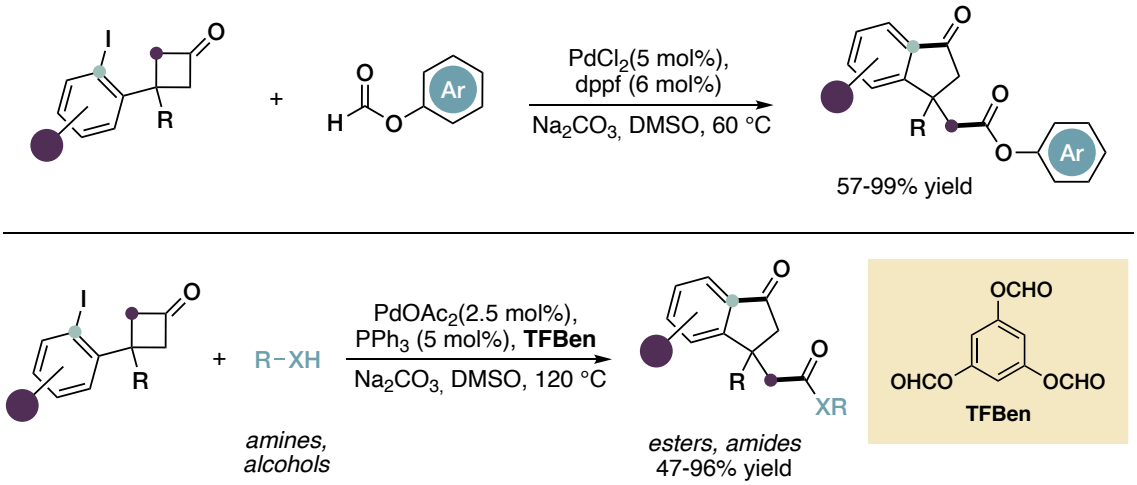

Scheme 11. Top: C-C bond activation-alkoxycarbonylation of iodoarene bearing cyclobutanones with Pd catalysis and aryl formates. Bottom: alkoxycarbonylation with aliphatic alcohols or amines using TFBen (benzene-1,3,5-triyl triformate) as CO surrogate.

Aryl formates were used as CO surrogates in the presence of base (**Scheme 11**, top). Phenol esters can be directly obtained using the corresponding formate, while benzene-1,3,5-triyl triformate (TFBen) was used in combination with an amine or aliphatic alcohol to obtain aliphatic esters or amides, since alkyl formates or formamides do not undergo base-promoted release of CO (**Scheme 11**, bottom).

Nickel catalysis revealed effective for realizing intermolecular insertions of unsaturated moieties into cyclobutanone C-C bonds, whereas rhodium instead fails despite its competence in intramolecular processes. Murakami reported in 2005 a $Ni(COD)_2/PCy_3$ catalyzed insertion of alkynes in 3,3-disubstituted cyclobutanones (**Scheme 12**, top).[335] The authors postulated, in analogy with Ni(0) promoted oxidative cyclizations of aldehydes and alkynes, a cyclization step between the ketone and the alkyne to yield a spyro-fused oxanickelacycle. β-carbon elimination and RE would close the cycle and furnish the product (**Scheme 12**, middle).

[335] M. Murakami, S. Ashida, T. Matsuda, *J. Am. Chem. Soc.* **2005**, *127*, 6932−6933.

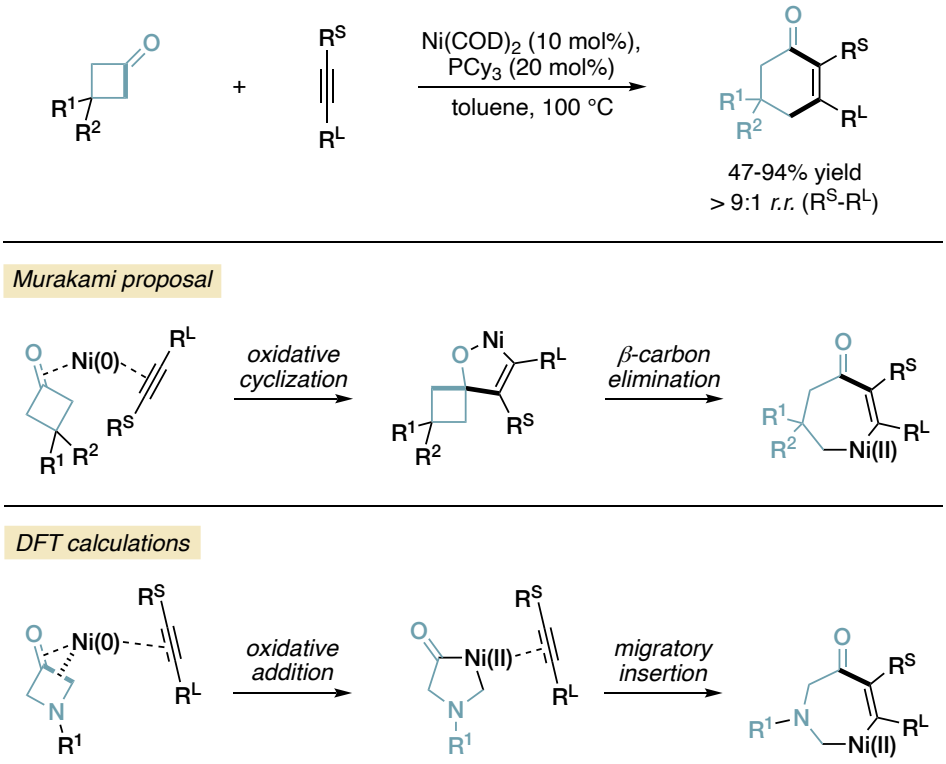

Scheme 12. Top: nickel catalyzed intermolecular alkyne insertion into cyclobutanones. Middle: Murakami's mechanistic proposal involving an initial oxidative cyclization step. Bottom: computed mechanism for the intermolecular nickel catalyzed alkyne insertion into azetidine-3-ones, comprising initial oxidation addition on the C-C(O) bond and subsequent insertion. R^S = smaller substituent; R^L = larger substituent.

However, the same reaction was also later reported with azetidin-3-ones,[336a] and DFT calculations on this system suggested an alternative mechanism in which Ni(0) oxidatively inserts in the C-C bond of the azetidinone, followed by alkyne insertion, casting doubt on the initially proposed pathway from Murakami (**Scheme 12**, bottom).[336b] This pathway is similar to the intramolecular one described for Rh in **Scheme 9**, but in this case the acyl group migrates instead of the alkyl one.

When the same *o*-styryl substituted cyclobutanones that yield benzobicyclo[3.2.1]octenones under Rh catalysis were used with nickel, a different outcome was recorded, and benzobicyclo[2.2.2]octenones were obtained instead.[337] The proposed mechanism involves oxidative cyclization of the ketone and alkene units

[336] a) P. Kumar, J. Louie, *J. Org. Lett.* **2012**, *14*, 2026−2029; b) Y. Li, Z. Lin,, *Organometallics* **2013**, *32*, 3003−3011.
[337] M. Murakami, S. Ashida, *Chem Commun* **2006**, 4599–4601.

to give an oxanickelacycle that undergoes β-carbon elimination to give a bis-alkyl Ni(II) species (**Scheme 13**). No mechanistic experiments were carried out, and similarly to the previous example, the same Ni(II) intermediate could in principle arise from oxidative addition at the C-C(O) bond (like rhodium does) and subsequent migratory insertion of the acyl group (instead of the alkyl one) into the alkene unit (not shown). Regardless, this stands a rare example of an intramolecular carboacylation of alkenes via C-C bond activation.

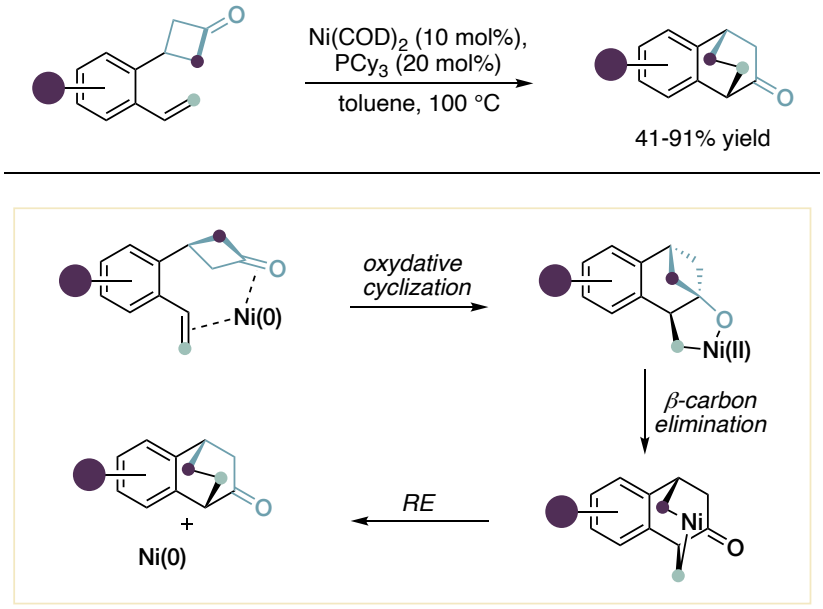

Scheme 13. Top: Ni catalyzed C-C bond activation-cyclization of styryl tethered cyclobutanones en route to benzobicyclo[2.2.2]octenones. Bottom: proposed mechanism. For the sake of clarity, the ligand environment of Ni is not shown, as well as the oxidation state after OA (+2).

In 2020, Wang and coworkers were able to successfully merge C-C bond activation and XEC using nickel catalysis.[338] Their strategy uses the same aryl iodide tethered starting materials shown above for palladium catalysis; in this case though, the alkyl Ni complex undergoes trapping with an electrophile instead of a nucleophile, in this case primary or secondary alkyl bromides. Employing a chiral Trost-type ligand, manganese as reductant and DMI as solvent, a wide range of functionalized indanones

[338] D. Ding, H. Dong and C. Wang, *iScience* **2020**, *23*, 101017.

were prepared in good yield and moderate to good enantiomeric excess (**Scheme 14**, top). Aryl bromides are unreactive in this protocol, and (as for Pd) the monosubstituted cyclobutanones fail to deliver the product (most likely due to β-hydride elimination).

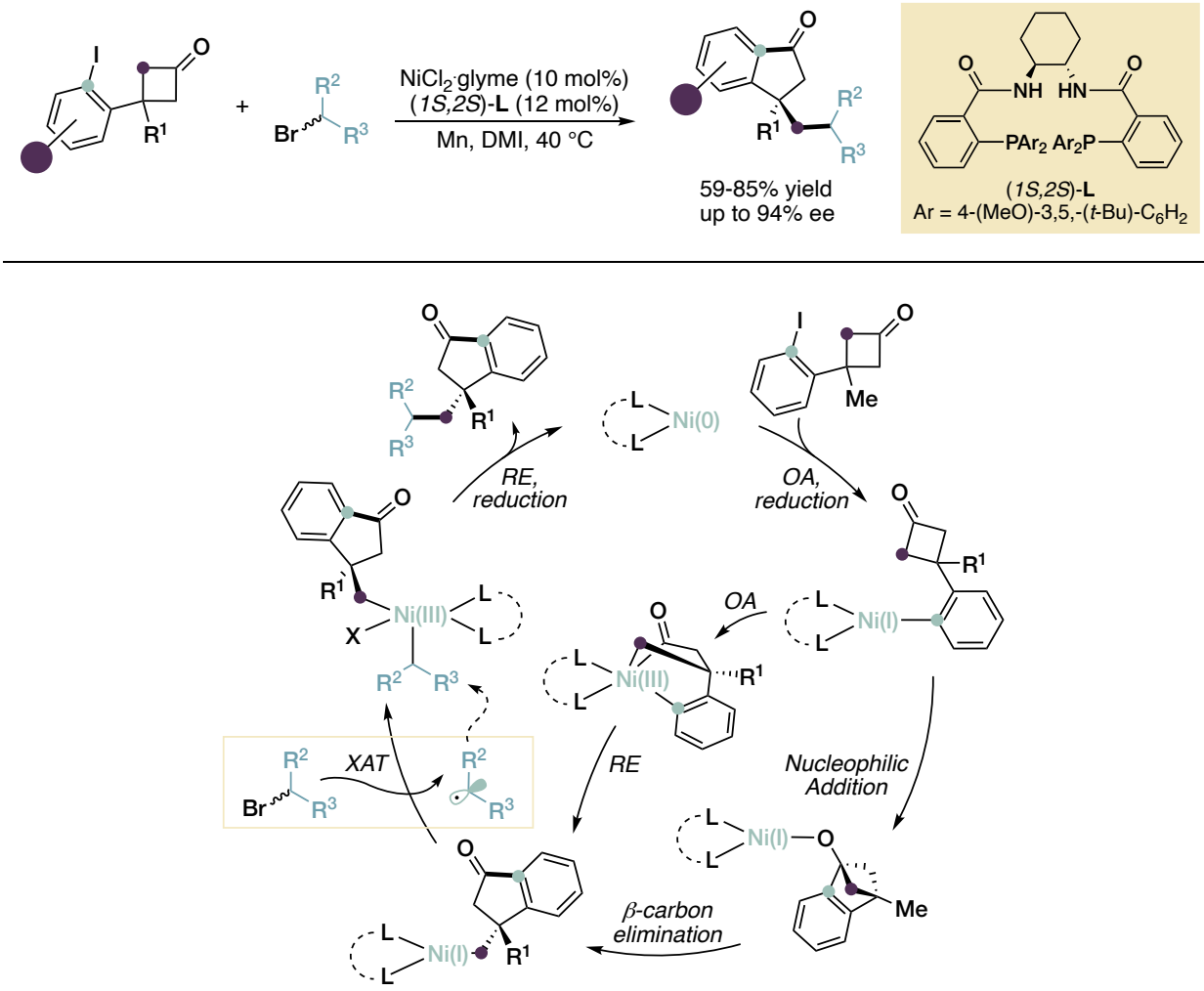

Scheme 14. Top: merging of C-C activation and XEC in an enantioselective Csp^3-Csp^3 bond forming protocol. Bottom: proposed mechanism. The intermediacy of alkyl radicals was demonstrated, although the precise pathway for their generation was not investigated.

Stoichiometric mechanistic experiments with $Ni(COD)_2$ with and without manganese demonstrated the Ni(II) aryl species is not a competent intermediate: reduction to Ni(I) must occur first. At that point, similarly with Pd(II), two pathways can be possible: a redox neutral nucleophilic attack followed by β-carbon elimination or an OA to yield a bicyclic bridged Ni(III) complex that undergoes RE; either the β-carbon elimination

or the OA steps are the enantiodetermining ones. No conclusive answer was given. Use of a radical clock probe indicated, as expected, the formation of alkyl radicals, and the authors propose a “sequential reduction”-like mechanism (**Scheme 14**, bottom).

6.2 Aim of the project

The fascinating results shown in the C-C activation of cyclobutanones clearly highlight the potential of this strategy to concisely access value-added functionalized scaffolds from relatively easily assembled starting materials. Given our interest in direct CO_2-based carboxylation protocols, and especially in Ni-catalyzed tandem functionalization-carboxylations, we considered the possibility of adopting cyclobutanones as a platform for this reactivity. After all, a cycle is an unsaturation, and an endocyclic C-C bond may very well behave as a π-bond in a difunctionalization scenario, if conditions that can cleave it are provided.

In light of Wang's report on C-C cleavage/XEC sequence, we were strongly convinced of the feasibility of using CO_2 as an electrophilic quencher of the Ni(I) complex obtained after the ring cleavage-reconstruction of a 2-haloaryl tethered cyclobutanone (**Figure 4**).

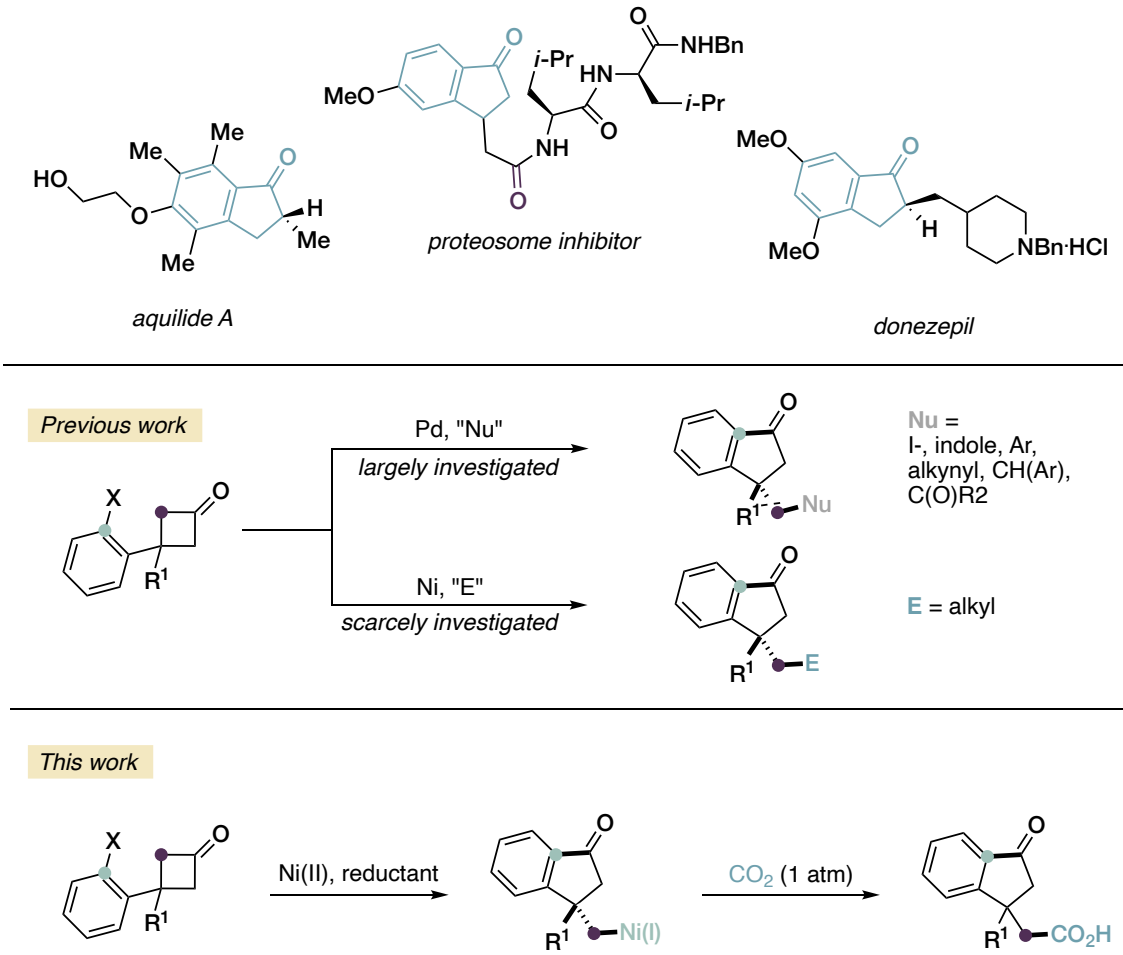

Figure 4. Top: examples of biologically relevant indanones; Middle: established transformations in tandem C-C activation-functionalization of cyclobutanones; Bottom: present carboxylative strategy.

The protocol would furnish expedient access to valuable, biologically relevant 3-indanone-1-acetic acids,[339] making direct use of carbon dioxide, thus avoiding the use of hazardous carbon monoxide or its surrogates. The employment of nickel catalysis in contrast to the most often used precious late transition metals (Rh and Pd) is highly desirable and is likely to require much lower temperatures than those needed with those metals.

Despite the "on-paper" similarity with Wang's work, we anticipated that the realization of this goal could be a significant challenge. Given the complexity of the overall

[339] P. Jimonet, Y. Ribeill, G. A. Bohme, A. Boireau, M. Chevré, D. Damour, A. Doble, A. Genevois-Borella, F. Herman, A. Imperato, S. Le Guern, F. Manfré, J. Prat, J. C. R. Randle, J.-M. Stutzmann, S. Mignani, *J. Med. Chem.* **2000**, *43*, 2371–2381.

sequence, several byproducts can be imagined, namely: hydrodehalogenation and *ipso*-carboxylation of the starting material without C-C cleavage, hydrodemetalation of the Ni(I) intermediate after indanone formation, and finally dimerization of this intermediate. To the best of our knowledge, no report on the use of a Trost-type ligand is available for CO_2 capture by Ni(I), and alkyl Ni(I) intermediates were only shown to be successful with *ortho*-substituted phenanthrolines (although in our case no β-hydrogen elimination is possible). We expected that a very careful choice of ligand and conditions in general was going to be necessary for the success of both the C-C cleavage and carboxylation events, requiring long experimentation as Wang's report is the only one available for the merge of C-C activation and XEC.

6.3 Results and discussion

At the outset of our study, we started optimization by reacting the model substrate bromoarene **1a** with $NiCl_2$·glyme (10 mol%) and 2,2'-bipyridine (bpy, **L1**) (20 mol%) as the ligand, in DMF under a CO_2 atmosphere at room temperature with zinc as a reductant. Under these conditions, no product was formed and a small amount of hydrodehalogenated starting material (**7a**, *vide infra*) was observed, along with substantial recovery of untouched **1a** (entry 1, **Table 1**). Given the key role that additives can have in reductive carboxylation protocols, we tested several metal halide salts, also reasoning that a Lewis acidic cation could favor the overall process via activation of the carbonyl unit (entries 2–5). While no conversion was recorded with monovalent lithium chloride (entry 2), when divalent magnesium chloride was employed (1.5 equiv.) the desired product **2a** was observed in low yield (15%, entry 3). A stronger Lewis acid, namely $AlCl_3$ significantly improvement the yield to a modest 30% (entry 4) and proved to be the best additive (see Supplementary data, Chapter 6.5 for further screening), supporting the idea that activation of the carbonyl unit is of critical importance. In a control experiment, we excluded that any adventitious traces of HCl deriving from $AlCl_3$ could trigger a Brønsted-acid catalysis (entry 5). Very interestingly, $AlCl_3$ is mandatory additive for the desired process to proceed: related $Al(OTf)_3$ was found to be ineffective, even in the presence of an external chloride source (entries 6, 7, complete recovery of **1a**). It is difficult to provide a rational for this behavior, but it can tentatively be proposed that solubility or ion-pairing effects between the cations and anions in DMF could be responsible.[308]

Table 1. Summary optimization of reaction conditions.

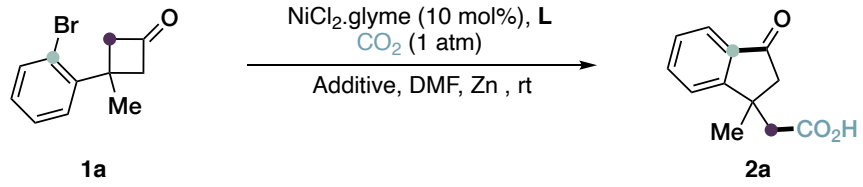

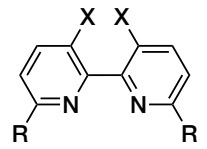

L1: X = R = H
L2: X = OMe, R = Me

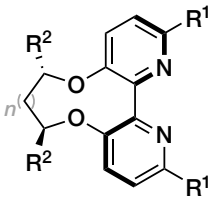

L3: n = 1, R^1 = R^2 = Me
L4: n = 0, R^1 = R^2 = Me
L5: n = 2, R^1 = Me, R^2 = H
L6: n = 2, R^1 = H, R^2 = Me

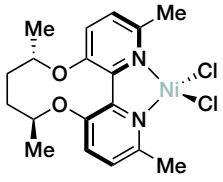

(**L7**)$NiCl_2$

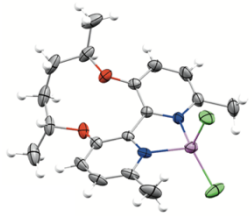

Entry[a]	L	Additive	Yield **2a** (%)[b]
1	**L1**	none	0
2	**L1**	LiCl	0
3	**L1**	$MgCl_2$	15
4	**L1**	$AlCl_3$	30
5	**L1**	HCl[c]	0
6	**L1**	$Al(OTf)_3$	0
7	**L1**	$Al(OTf)_3$ + LiCl[d]	0
8	**L2**	$AlCl_3$	43
9[e]	(**L3**)$NiCl_2$	$AlCl_3$	59
10[e]	(**L4**)$NiCl_2$	$AlCl_3$	traces
11[e]	(**L5**)$NiCl_2$	$AlCl_3$	12
12[e]	(**L6**)$NiCl_2$	$AlCl_3$	18
13[e]	(**L7**)$NiCl_2$	$AlCl_3$	64
14[e,f]	(**L7**)$NiCl_2$	$AlCl_3$	70
15[e,g]	(**L7**)$NiCl_2$	$AlCl_3$	45

[a] All reactions were set up in dry DMF and following conditions. [**1 a**]: 0.1 M, **1a**: 1 eq. Zn: 2 eq., additive: 1.5 eq., $NiCl_2$·glyme: 10 mol%, **L**: 20 mol%, unless otherwise specified). [b] Isolated yields after flash chromatography. [c] 4 mol% HCl 4 M in 1,4-dioxane. [d] LiCl: 4.5 eq. [e] 10 mol% of preformed complex (**L**)NiCl2 was used. [f] 40 °C. [g] 60 °C.

With these findings in hand, we turned our attention to the role of the ligand. An *ortho*-substituted electron-rich bipyridine ligand (**L2**, entry 8) provided **2a** in an improved 43% yield. Prompted by this result, we decided to test C2-symmetric axially chiral bipyridine ligands **L3**-**L7** sharing similar tethering backbones (entries 9–13), employed in the literature for a Pd catalyzed C-H activation process.[340] Pleasingly, our investigation pointed to bipyridine (*R*,*R*)-**L7** as the optimal one, delivering **2a** in 64% yield (entry 13). This ligand displays a 6,6'-Me_2 substitution pattern and a cyclic tethering 3,3'-bis(ether) backbone, and can be readily prepared from (*S*,*S*)-2,5-hexanediol (see Supplementary data, Chapter 6.5 for details). [341]

Aiming at obtaining high reproducibility we isolated the precatalyst (**L7**)$NiCl_2$ in 90% yield as a brown solid by reacting enantiopure (*R*,*R*)-**L7** and $NiCl_2$·glyme in DMF. Interested in obtaining structural information regarding the coordination of this peculiar kind of ligand, we were able to grow single crystals suitable for XRD analysis. The diffraction results showed the expected 1:1 Ni/**L7** ratio, and a distorted tetrahedral geometry of the Ni centered, being coordinated by two chloride ligands and two pyridinic nitrogen atoms with a (N–Ni–N) bite angle of 83.0(1)°. The dihedral angle between the two pyridine rings deviates significantly from planarity (27.6(2)°) as a result of the formation of the ten-membered ring in **L7**: we believe that this feature is crucial for the performance of this ligand. Ligand **L3**, deriving from (*S*,*S*)-2,4-pentanediol and thus featuring a smaller tether, performed only slightly worse than **L7** (59% yield, entry 9). On the contrary, (*S*,*S*)-2,3- butanediol-derived **L4** completely

[340] X. Gao, B. Wu, W.-X. Huang, M.-W. Chen, Y.-G. Zhou, *Angew. Chem. Int. Ed.* **2015**, *54*, 11956–11960.

[341] The enantiomeric excess of **2a** prepared in the presence of enantiopure ligands **L3**-**L7** was in all cases lower than 20% (18% ee with ligand **L7**). Rac-2,5-hexanediol is commercialized only as a 1:1 mixture with the meso isomer. Preparation of the corresponding 2,2'-bipyridine ligand led to an inseparable mixture of *rac*-**L7** and *meso*-**L7**, that proved ineffective in the present transformation. Therefore, enantiopure (*R*,*R*)-**L7** was selected as the optimal ligand, although no asymmetric induction was pursued.

failed to promote the desired reaction (entry 10), highlighting the importance of the size of the cyclic ether scaffold.

Ligand **L5**, lacking methyl groups and therefore stereogenic centers on the tethering moiety (entry 11), provided the product only in low yield. The same was true for **L6**, lacking 6,6'-methyl groups (entry 12), consistently with the importance of *ortho*-substituted ligands for efficient carboxylation of alkyl fragments. Finally, a slight improvement in the catalytic performance was observed by running the reaction at 40 °C (70 % yield, entry 14) while a higher temperature proved detrimental (45 % yield at 60 °C, entry 15). In a comparison with Wang's protocol, the use of aryl bromides is noteworthy, as only aryl iodides were competent in his report and bromides are generally cheaper and more widely available. In our case, the use of an aryl iodide model substrate was found to generate a significant amount of dehalogenation of the aromatic ring and was not further investigated. Interestingly, throughout the whole optimization we never observed the anticipated byproducts **5a** and **6a** (*vide infra*) deriving from protodemetalation or dimerization of the alkylnickel intermediate, respectively.

Having established optimal conditions, (**Table 1**, entry 14), we next moved to assessing the generality of the process by testing a small library of 3-(2-bromoaryl)cyclobutanones **1b–n** (**Figure 5**). Hydrocarbyl (**1b–d**) and electron-donating (**1e–h**) substituents could be effectively accommodated at positions 4-, 5- and 6- of the aromatic ring, smoothly delivering the corresponding 3-indanone-1-acetic acids **2b–h** in good yields (43–76 %). Unfortunately, electron-withdrawing groups (i.e. F and CF_3) at different positions (substrates **1i–k**), led to a decrease in efficiency, and the corresponding product were only obtained in moderate yields (25–45 %). This may reflect a reduced nucleophilicity of the corresponding aryl–Ni intermediates (*vide infra*). Alkyl substituents different than Me at the 3-position of the cyclobutanone where well tolerated (**2l-m**), providing 3-indanone-1-acetic acids with various substitution patterns at the quaternary C1 position. However, if a thienyl moiety was present (substrates **1o,n**), no conversion was observed, most likely due to a poisoning

S-Ni coordination. Instead, when methyl was substituted by hydrogen (**1p**), or a α,α-dichlorocyclobutananone was used (**1r**, intermediate for the synthesis of **1a**) a complex mixture of products was obtained.

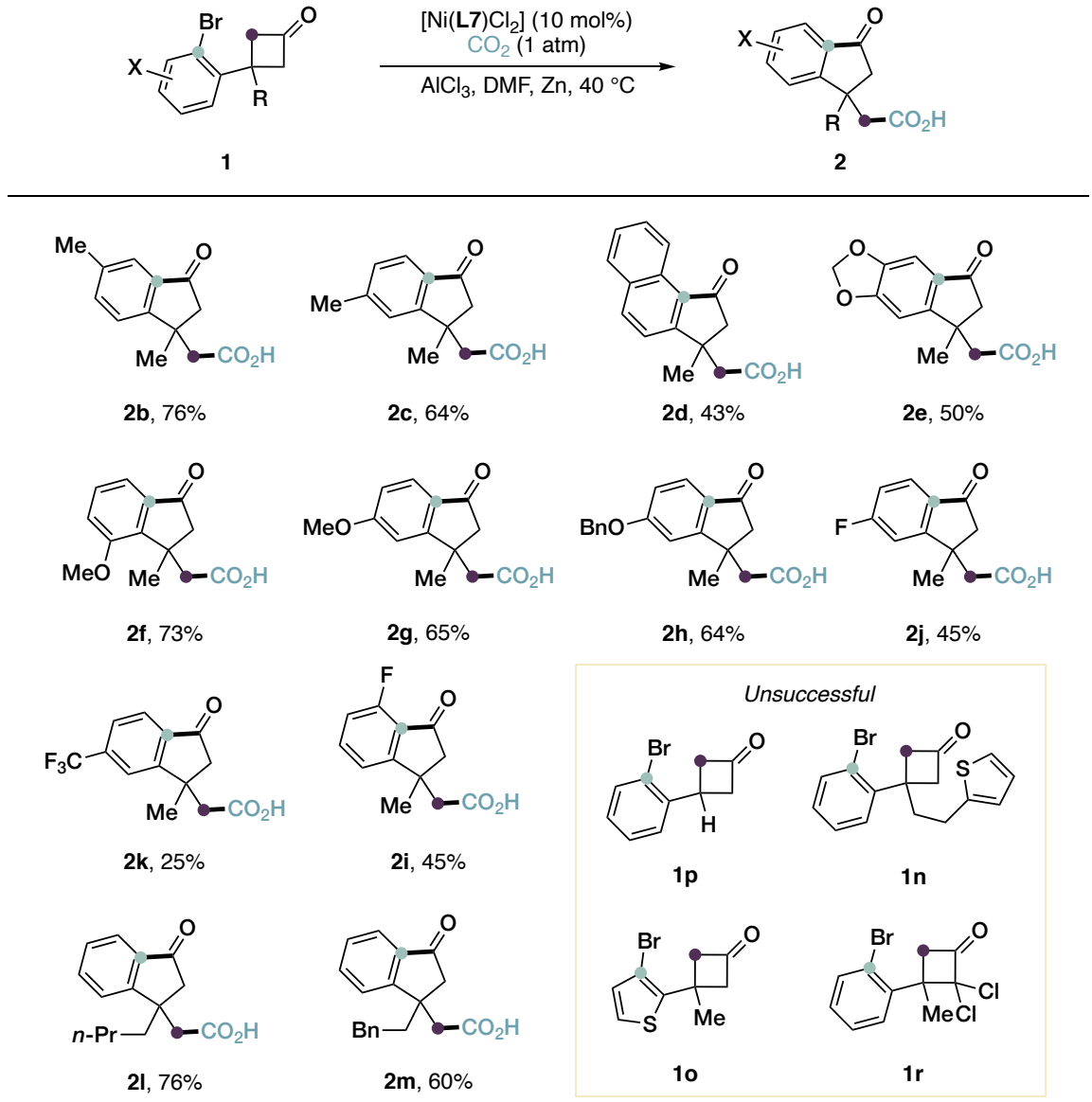

Figure 5. Reaction scope of the present carboxylative methodology. All reactions were set up accordingly to optimized conditions (entry 14 in **Table 1**). Isolated yields after flash chromatography are provided.

To showcase the utility of our methodology in streamlining the synthesis of 3-indanone-1-acetic acids and related structures, we performed a number of simple, routinely used transformations on product **2b** (**Scheme 15**). For example, after

esterification of the carboxylic moiety (***a***), ketone reduction with $NaBH_4$ afforded alcohol **3b** in quantitative yield as an equimolar mixture of diastereoisomers (***b***). In turn, dehydration of diastereomeric alcohols mixture (*p*-TsOH, **c**) yielded the corresponding indene **4b** in 65% yield. Wittig olefination of the ketone moiety was carried out on the methyl ester of **2b**, rendering a 4:1 mixture of methylene–indanes **6b** and **6b'**, bearing an an exocyclic C–C double bond, in good yields. The observed product distribution is due to a partial transesterification with the KO*t*Bu used for ylide formation. No isomerization to the more stable endocyclic indene was observed. Finally, as a proof-of-concept for bioconjugation of **2b**, peptide bond formation (amide coupling reagents, ***d***) with isoleucine methyl ester (H-Ile-OMe) afford amide **5b** in 52% yield and 1.5:1 diastereomeric ratio.

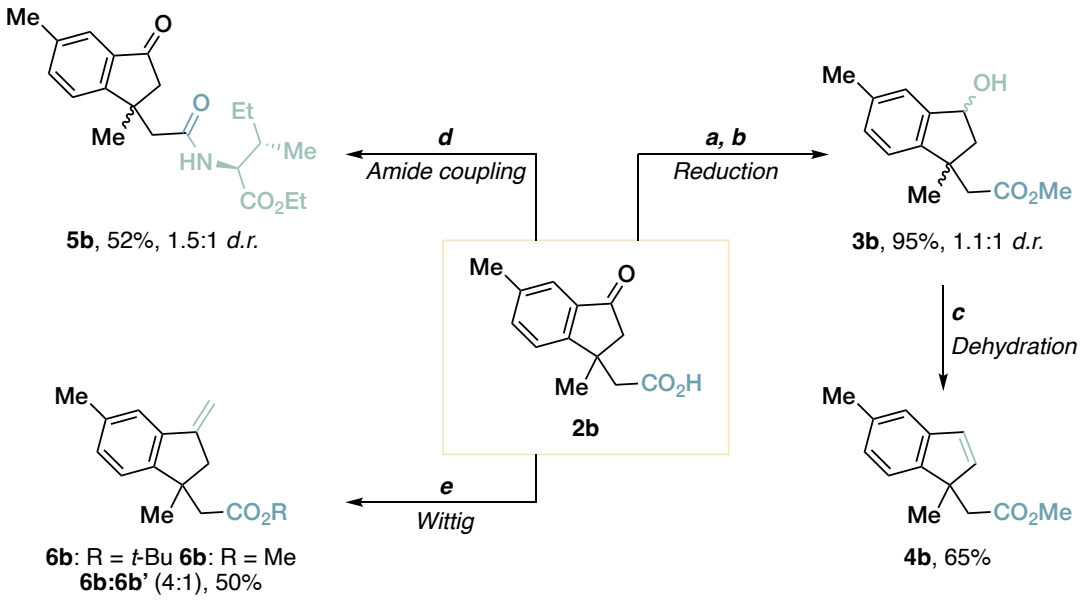

Scheme 15. Transformations of compound **2b**. Conditions: (***a***) H_2SO_4 (1 drop), MeOH, reflux, 18 h; (***b***) $NaBH_4$ (3 equiv.), MeOH, rt, 1 h; (***c***) *p*-TsOH (1 equiv.), PhMe, reflux, 18 h; (***d***) H-Ile-OMe (1 eq.), EDC·HCl (1 eq.), TEA (3 eq.), HOBt (1.2 eq.), DCM/DMF 3:1, 25 °C, 18 h; (***e***) Ph_3PCH_3I (2 eq.), KO*t*Bu (2.5 eq.), THF, 0 °C to reflux, 18 h. *p*-TsOH = p-toluene sulfonic acid; EDC = 1-ethyl-3-(3-dimethylaminopropyl)carbodiimide; TEA = triethylamine; HOBt = hydroxybenzotriazole.

As for the mechanism, we propose the catalytic cycle depicted in **Scheme 16**, based on previous related reports and the experimentally observed product distribution. Starting

from Ni(0), oxidative addition onto the aryl bromide gives an aryl–Ni(II) species **A**.[342] At this point, reminiscent of the Ni(I)/Ni(II) dichotomy discussed earlier for the carbo-carboxylation of alkenes developed by our group (pg. 277), two options can be imagined: the first is an early reduction to Ni(I) prior to the skeletal reorganization, that could occur either via OA to give a bicyclic Ni(III) species (**C**) or direct nucleophilic attack from an aryl-Ni(I) and β-carbon elimination (not shown), just as in Wang's proposal. The second option comprises a C-C bond activation sequence occurring first from Ni(II), with the reduction happening later. In this case, direct nucleophilic attack from an aryl-Ni(II) (intermediate **B**) and β-carbon elimination is one possible pathway, the other one being OA from Ni(II) to a Ni(IV) species (not shown). Overall, the fact that we do not observe any benzoic acid byproduct, the importance of a strong Lewis acid,[343] and the reducing reaction environment, led us to lean towards the cascade occurring from Ni(II) via addition (intermediate **B**) and β-carbon elimination. The resulting alkyl-Ni(II) species (not shown) is reduced to the pivotal alkyl Ni(I) complex (**D**), that undergoes carboxylation (**E**), ligand metathesis and further reduction to close the catalytic cycle. Reduction occurring at the Ni(II) alkoxide (**B**) after nucleophilic attack is also possible (not shown).

[342] An analogous mechanism starting with Ni(I) followed by reduction to Ni(II) after oxidative addition is equally likely, and at present we did not perform mechanistic experiments to distinguish the two scenarios.

[343] At present, we do not a conclusive rationale for the specific role of $AlCl_3$ in promoting the carboxylation reaction. Besides carbonyl activation, facilitation of the final carboxylate metathesis and the possible electrophilic activation of CO_2 cannot be excluded.

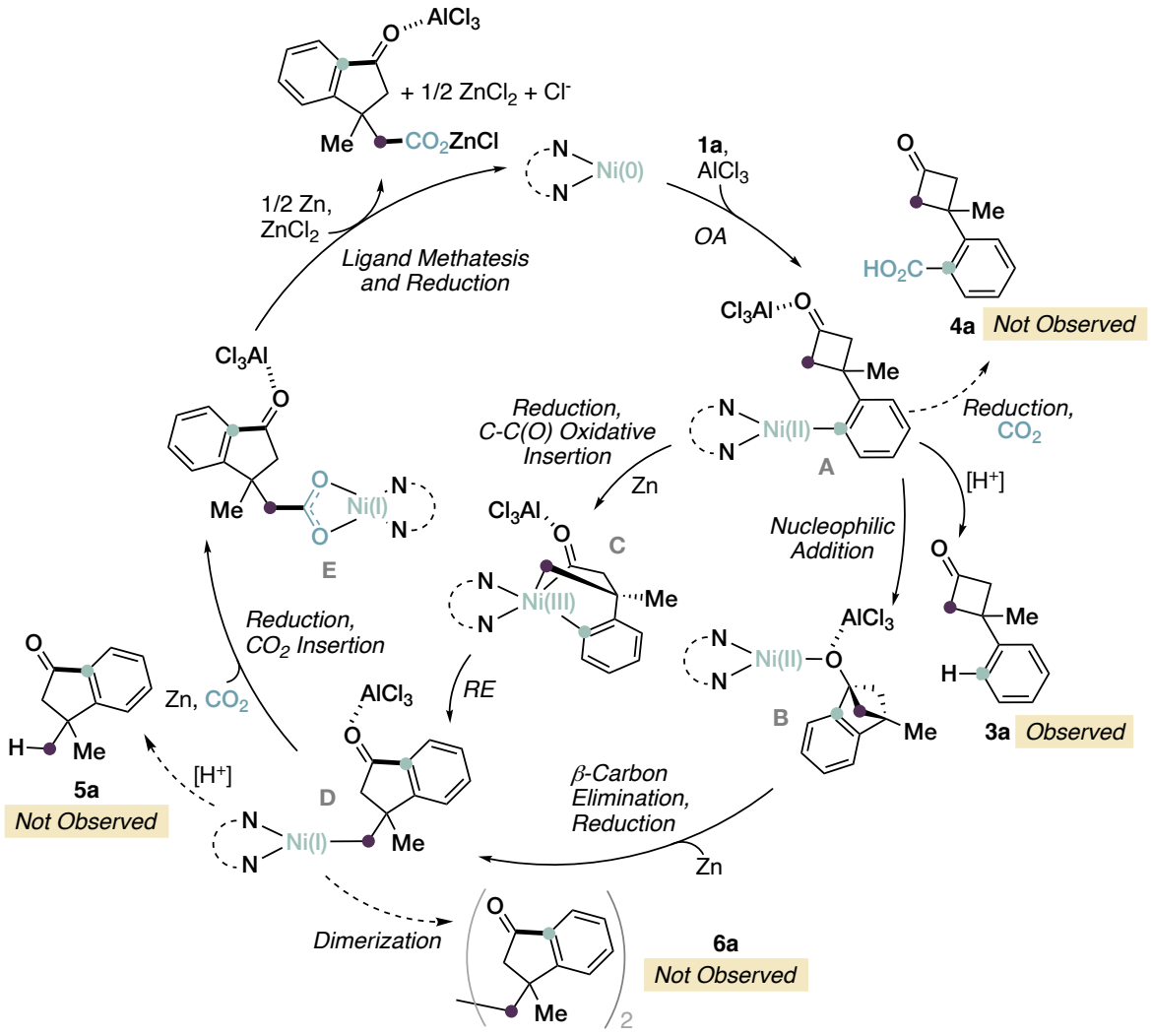

Scheme 16. Proposed mechanism. The most plausible pathway is thought to be **A**-**B**-**D**-**E**. Some alternatives en route to key intermediate **D** are shown.

The fact that dehalogenated starting material was routinely observed, but the conceivable byproducts **5a** and **6a** (often encountered in tandem carboxylation processes) were never formed in detectable amounts may suggest that the C=O addition step is kinetically demanding and the carboxylation of alkyl-Ni(I) intermediate **D** is faster than protodenickelation (**5a**) and dimerization processes (**6a**).

6.4 Conclusions

In conclusion, we have documented an unprecedented nickel catalyzed tandem C-C bond activation-cyclization-carboxylation protocol using CO_2 at atmospheric pressure. A small library of readily accessible 2-bromoaryl tethered cyclobutanones can be converted in good yields to biologically relevant 3-indanone-1-acetic acids, providing a proof of concept for streamlining the synthesis of such compounds by means of early transition metal catalysis and direct carbon dioxide utilization. In this direction, simple and synthetically relevant transformations on the products were documented, demonstrating facile access to structural diverse indane-type scaffolds.

6.5 Supplementary data

General Methods

^{1}H NMR spectra were recorded on Varian 400 (400 MHz) spectrometers. Chemical shifts are reported in ppm from TMS with the solvent resonance as the internal standard (deuterochloroform: 7.24 ppm). Data are reported as follows: chemical shift, multiplicity (s = singlet, d = doublet, dd= doublet doublet, t = triplet, td = triple doublet, dt = double triplet, q = quartet, sext = sextet, sept = septet, p = pseudo, b = broad, m = multiplet), coupling constants (Hz). ^{13}C NMR spectra were recorded on a Varian 400 (100 MHz) spectrometers with complete proton decoupling. Chemical shifts are reported in ppm from TMS with the solvent as the internal standard (deuterochloroform: 77.0 ppm).

GC-MS spectra were taken by EI ionization at 70 eV on a Hewlett-Packard 5971 with GC injection. They are reported as: *m/z* (rel. intense). LC-electrospray ionization mass spectra were obtained with Agilent Technologies MSD1100 single-quadrupole mass spectrometer.

Chromatographic purification was done with 240-400 mesh silica gel. Other anhydrous solvents were supplied by Sigma Aldrich in Sureseal® bottles and used without any further purification. Commercially available chemicals were purchased from Sigma Aldrich, Stream and TCI and used without any further purification. Melting points were determined with Bibby Stuart Scientific Melting Point Apparatus SMP 3 and are not corrected.

$CO_2 \geq 99.5\%$ purity, purchased from SIAD, was used in the Ni-catalyzed tandem C-C σ-bond carboxylation reaction.

Anhydrous DMF, THF and CH_2Cl_2 were purchased from Merck and used as received. Zn dust refers to a particle size <10 μm and was purchased from Merck, having ≥98% purity. All other commercially available starting materials and (non-anhydrous) solvents were purchased from Merck, TCI chemicals, Fluorochem or Alfa Aesar and

were used as such without further purification. Ligands **L1** and **L2** are commercially available and **L6** is a known compound (see ref. 348).

Additional optimization data

Table S1. Optimization of reaction conditions, additional data.

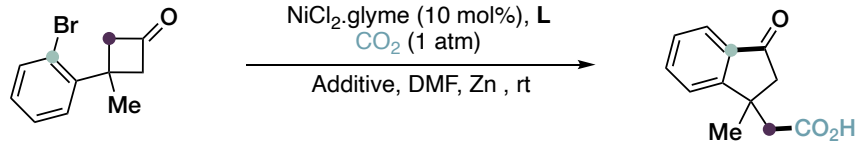

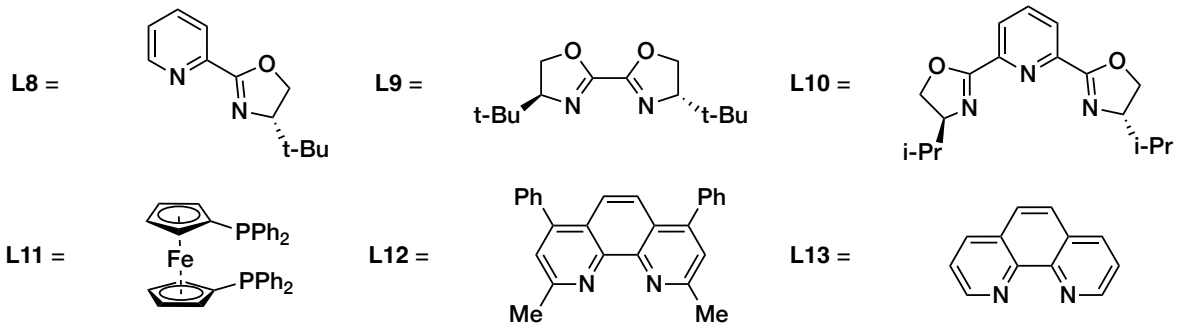

Entry[a]	L	Additive (equiv)	Yield (%)[b]
1	**L8**	None	NR
2	**L8**	TMSCl (1.5)	NR
3	**L8**	$MgCl_2$ (1.5)	25 (27)[c]
4	**L8**	$MgCl_2$[d] (1.5)	22 (29)
5	**L8**	LiCl (1.5)	NR
6	**L8**	$AlCl_3$ (1.5)	43 (19)
7	**L8**	$Al(OTf)_3$ (1.5)	NR
8	**L8**	$Al(OTf)_3$ + LiCl (1.5 + 4.5)	NR
9	**L9**	$AlCl_3$ (1.5)	NR
10	**L10**	$AlCl_3$ (1.5)	NR

11	**L11**	$AlCl_3$ (1.5)	NR
12	**L12**	$AlCl_3$ (1.5)	22
13	**L13**	$AlCl_3$ (1.5)	NR
14	**L7**	$AlCl_3$ (0.5)	38
15	**L7**	$AlCl_3$ (2.0)	56
16	**L7**	$InCl_3$ (1.5)	NR
17	**L7**	$ZnCl_2$ (1.5)	NR

(a) Reaction conditions: **1a** (0.1 mmol, 0.1 M), additive (0.15 mmol), Zn (0.3 mmol), CO_2 (1 atm), Ni(dme)Cl_2 (10 mol%), **L** (20 mol%). (b) Isolated yield after flash chromatography. (c) The number in brackets refers to the yield of dehalogenated starting material **7a**. (d) 20 mol% of TBAI was also added.

Unsuccessful substrates.

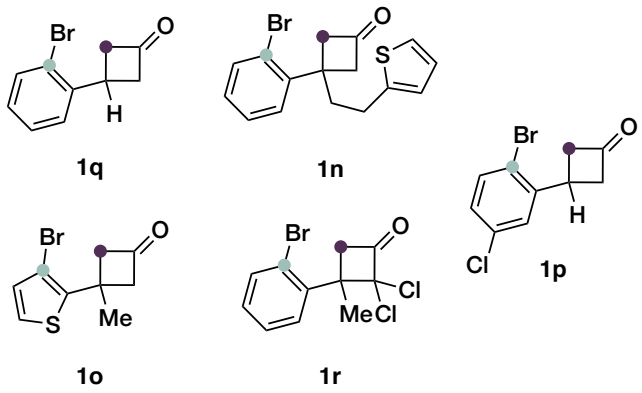

Figure S1. Substrates **1n-1r** were tested under the optimal reaction conditions but failed to give the desired products. Compounds **1n** and **1o** were recovered untouched while in the case of **1p-1r** a complex mixture was observed by ^1H NMR spectroscopy on the reaction crudes.

Synthesis and characterization of starting materials

Preparation of cyclobutanones **1**

Cyclobutanones **1** were synthesized from the corresponding 2-bromobenzaldehydes following literature procedures. A sequence comprising: addition of methylmagnesium bromide, PCC mediated oxidation of the resulting alcohol and then Wittig olefination served for the preparation of α-methylstyrenes. All compounds are known and the characterization, as well as the above-described preparation is reported in the literature.[344]

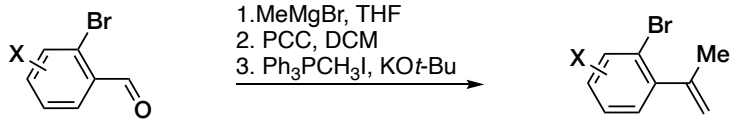

Conversion to cyclobutanones **1** was conducted following a modified literature procedure.[333] In a flame-dried round bottom flask equipped with a reflux condenser and a magnetic stirring bar, anhydrous Et_2O (30 mL), the appropriate α-methylstyrene (5.0 mmol) and Zn dust (1.30 g, 20 mmol) were added in this order under a N_2 atmosphere. Then, trichloroacetyl chloride (15 mmol, 1.7 mL) was added dropwise and the reaction mixture was stirred at room temperature for 18 h.

Caution! A highly exothermic reaction is generally observed within 5-20 min, bringing the solvent to a vigorous boil.

The mixture was then filtered over a Celite pad, concentrated *in vacuo* and filtered over a short silica plug (*c*Hex:EtOAc 10:1), affording crudes α,α-dichlorocyclobutanones that were used in the following step without further purification.

[344] X. Chang, P.-L. Ma, H.-C. Chen, C.-Y. Li, P. Wang, *Angew. Chem. Int. Ed.* **2020**, *59*, 8937.

In a round bottom flask equipped with a magnetic stirring bar, crude α,α-dichlorocyclobutanone (5 mmol) and Zn dust (650 mg, 10 mmol) were vigorously stirred in glacial AcOH (20 mL) at 60 °C for 5 h. Then, additional Zn dust (650 mg, 10 mmol) was added, and the reaction mixture stirred at 60 °C for 18 h. The reaction was monitored *via* GC-MS analysis and additional Zn was be added if completion is not reached. Excess of AcOH was then removed *in vacuo* and the resulting solid was suspended in EtOAc (50 mL), filtered over a Celite pad (washing with EtOAC, 50 mL), concentrated *in vacuo* and purified by flash chromatography (*c*Hex:EtOAc) to afford cyclobutanones **1**. A two-step combined yield is provided. In case of known compounds, the recorded spectroscopic data matched the one reported in literature.[345]

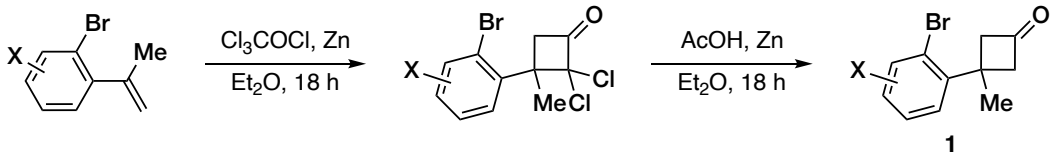

[345]) J. Cao, , L. Chen, F.-N. Sun, Y.-L. Sun, K.-Z. Jiang, K.-F. Yang, Z. Xu, L-W Xu, *Angew. Chem. Int. Ed.* **2019**, *58*, 897.

Characterization of compounds **1a**-**1n**

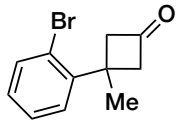

1a. Viscous colorless oil. FC eluent: *n*Hex:EtOAc: 15:1. Yield = 70% (3.5 mmol, 833 mg). **^{1}H NMR** (400 MHz, $CDCl_3$) δ = 7.61 (dt, *J* = 7.6, 3.1 Hz, 1H), 7.38 – 7.30 (m, 2H), 7.14 (ddt, *J* = 11.3, 8.2, 4.0 Hz, 1H), 3.60 – 3.52 (m, 2H), 3.27 – 3.20 (m, 2H), 1.65 (s, 3H); **^{13}C NMR** (100 MHz, $CDCl_3$) δ = 206.5, 145.9, 134.3, 128.3, 128.2, 127.6, 122.2, 59.2 (2C), 36.2, 27.7; **GC-MS**: 238 [^{79}Br] and 240 [^{81}Br] (5), 196 [^{79}Br] and 198 [^{81}Br] (100), 181 [^{79}Br] and 183 [^{81}Br] (20).

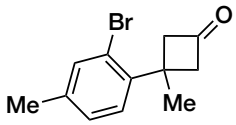

1b. Viscous colorless oil. FC eluent: *n*Hex:EtOAc: 15:1. Yield = 66% (3.3 mmol, 832 mg). **^{1}H NMR** (400 MHz, $CDCl_3$) δ = 7.41 – 7.39 (m, 1H), 7.16 (d, *J* = 7.9 Hz, 1H), 7.10 (ddd, *J* = 7.9, 1.7, 0.7 Hz, 1H), 3.53 – 3.45 (m, 2H), 3.23 – 3.13 (m, 2H), 2.31 (s, 3H), 1.59 (s, 3H); **^{13}C NMR** (100 MHz, $CDCl_3$) δ = 206.8, 142.8, 138.4, 134.7, 128.3, 127.8, 121.9, 59.2 (2C), 35.8, 27.8, 20.4; **GC-MS**: 252 [^{79}Br] and 254 [^{81}Br] (5), 210 [^{79}Br] and 212 [^{81}Br] (100), 195 [^{79}Br] and 197 [^{81}Br] (25).

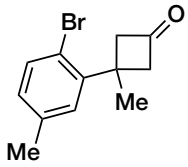

1c. Viscous colorless oil. FC eluent: *n*Hex:EtOAc: 15:1. Yield = 64% (3.2 mmol, 806 mg). **^{1}H NMR** (400 MHz, $CDCl_3$) δ = 7.43 (d, *J* = 8.1 Hz, 1H), 7.08 (d, *J* = 1.9 Hz, 1H), 6.94 – 6.90 (m, 1H), 3.56 – 3.47 (m, 2H), 3.22 – 3.13 (m, 2H), 2.31 (s, 3H), 1.60 (s, 3H); **^{13}C NMR** (100 MHz, $CDCl_3$) δ = 207.0, 145.5, 137.5, 134.0, 129.1, 128.9, 118.8, 59.1 (2C), 36.1, 27.8, 21.0; **GC-MS**: 252 [^{79}Br] and 254 [^{81}Br] (5), 210 [^{79}Br] and 212 [^{81}Br] (100), 131 (85), 115 (90).

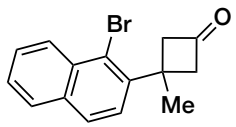

1d. White solid. Mp = 100 -103 °C. FC eluent: *n*Hex:EtOAc: 10:1. Yield = 50% (2.5 mmol, 720 mg). **^{1}H NMR** (400 MHz, $CDCl_3$) δ = 8.38 (d, *J* = 8.6 Hz, 1H), 7.81 (*pseudo*d, *J* = 8.4 Hz, 2H), 7.60 (t, *J* = 7.7 Hz, 1H), 7.51 (t, *J* = 7.5 Hz, 1H), 7.40 (d, *J* = 8.6 Hz, 1H), 3.71 – 3.61 (m, 2H), 3.36 – 3.26 (m, 2H), 1.70 (s, 3H); **^{13}C NMR** (100 MHz, $CDCl_3$) δ = 206.6, 143.7,

133.2, 132.8, 128.1, 128.0, 127.8, 127.1, 126.5, 125.5, 122.2, 59.6 (2C), 37.3, 27.5; **GC-MS**: 288 [^{79}Br] and 290 [^{81}Br] (15), 246 [^{79}Br] and 248 [^{81}Br] (90), 165 (100), 152 (95).

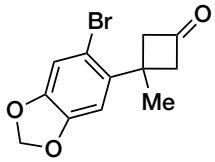

1e. White solid. Mp = 113 - 115 °C. FC eluent: *n*Hex:EtOAc: 10:1 then *n*Hex:EtOAc 5:1. Yield = 35% (1.75 mmol, 492 mg). **^{1}H NMR** (400 MHz, $CDCl_3$) δ = 7.00 (s, 1H), 6.76 (s, 1H), 5.96 (s, 2H), 3.49 – 3.39 (m, 2H), 3.20 – 3.11 (m, 2H), 1.56 (s, 3H); **^{13}C NMR** (100 MHz, $CDCl_3$) δ = 206.4, 147.5, 147.1, 139.2, 113.9, 112.4, 108.0, 101.9, 59.3 (2C), 36.2, 27.7; **GC-MS**: 282 [^{79}Br] and 284 [^{81}Br] (25), 240 [^{79}Br] and 242 [^{81}Br] (100), 225 [^{79}Br] and 227 [^{81}Br] (10).

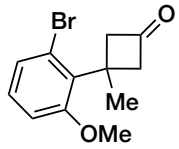

1f. Viscous colorless oil. FC eluent: *n*Hex:EtOAc: 8:1. Yield = 68% (3.4 mmol, 911 mg). **^{1}H NMR** (400 MHz, $CDCl_3$) δ = 7.18 (dd, *J* = 8.0, 1.2 Hz, 1H), 7.05 (t, *J* = 8.1 Hz, 1H), 6.84 (dd, *J* = 8.2, 1.0 Hz, 1H), 3.80 (s, 3H), 3.56 – 3.47 (m, 2H), 3.24 – 3.14 (m, 2H), 1.53 (s, 3H); **^{13}C NMR** (100 MHz, $CDCl_3$) δ = 210.1, 158.7, 134.1, 128.3, 126.5, 123.1, 110.3, 60.5 (2C), 55.6, 34.6, 25.6; **GC-MS**: 268 [^{79}Br] and 270 [^{81}Br] (5), 240 [^{79}Br] and 242 [^{81}Br] (5), 226 [^{79}Br] and 228 [^{81}Br] (20), 211 [^{79}Br] and 213 [^{81}Br] (20), 132 (100).

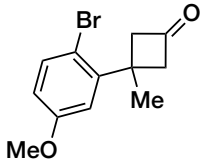

1g. Viscous colorless oil. FC eluent: *n*Hex:EtOAc: 8:1. Yield = 75% (3.75 mmol, 1.0 g). **^{1}H NMR** (400 MHz, $CDCl_3$) δ = 7.46 (d, *J* = 8.7 Hz, 1H), 6.83 (d, *J* = 3.0 Hz, 1H), 6.67 (dd, *J* = 8.7, 3.0 Hz, 1H), 3.80 (s, 3H), 3.57 – 3.47 (m, 2H), 3.24 – 3.10 (m, 2H), 1.61 (s, 3H); **^{13}C NMR** (100 MHz, $CDCl_3$) δ = 201.7, 154.2, 142.2, 130.2, 110.1, 108.2, 107.8, 54.3 (2C), 50.7, 31.5, 22.9; **GC-MS**: 268 [^{79}Br] and 270 [^{81}Br] (15), 226 [^{79}Br] and 228 [^{81}Br] (25), 211 [^{79}Br] and 213 [^{81}Br] (25), 132 (100).

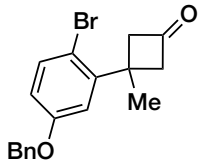

1h. Viscous colorless oil. FC eluent: *n*Hex:EtOAc: 9:1. Yield = 55% (2.75 mmol, 946 mg). **^{1}H NMR** (400 MHz, $CDCl_3$) δ = 7.45 (d, *J* = 8.7 Hz, 1H), 7.42 – 7.30 (m, 5H), 6.90 (d, *J* = 3.0 Hz, 1H), 6.73 (dd, *J* = 8.7, 3.0 Hz, 1H), 5.03 (s, 2H), 3.52 – 3.43 (m, 2H), 3.21 – 3.12 (m, 2H), 1.59 (s, 3H); **^{13}C NMR** (100 MHz, $CDCl_3$) δ = 206.4, 158.1, 147.0, 136.3, 134.9, 128.7 (2C), 128.2 (2C), 127.5, 115.8, 113.9, 112.8, 70.3, 59.1 (2C), 36.2, 27.6; **GC-MS**: 344 [^{79}Br] and 346 [^{81}Br] (5), 302 [^{79}Br] and 304 [^{81}Br] (5), 265 (5), 91 (100).

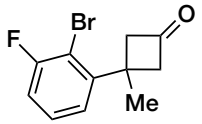

1i. Viscous colorless oil. FC eluent: *n*Hex:EtOAc: 20:1. Yield = 35% (1.75 mmol, 446 mg). **^{1}H NMR** (400 MHz, $CDCl_3$) δ = 7.28 (td, *J* = 8.0, 5.6 Hz, 1H), 7.08 (dt, *J* = 7.9, 1.3 Hz, 1H), 7.03 (td, *J* = 8.2, 1.5 Hz, 1H), 3.59 – 3.49 (m, 2H), 3.30 – 3.17 (m, 2H), 1.65 – 1.61 (m, 3H); **^{13}C NMR** (100 MHz, $CDCl_3$) δ = 205.9, 159.6 (d, *J* = 246.5 Hz), 148.4, 128.6 (d, *J* = 8.4 Hz), 123.3 (d, *J* = 3.2 Hz), 114.6 (d, *J* = 23.5 Hz), 109.6 (d, *J* = 21.0 Hz), 59.3 (2C), 36.4 (d, *J* = 2.1 Hz), 27.6 (2C); **^{19}F NMR** (376 MHz, $CDCl_3$) δ = -103.46 (dd, *J* = 8.1, 5.5 Hz, 1F); **GC-MS**: 256 [^{79}Br] and 258 [^{81}Br] (2), 214 [^{79}Br] and 216 [^{81}Br] (95), 177 (50), 133 (100), 135 (95).

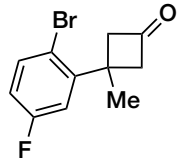

1j. Viscous colorless oil. FC eluent: *n*Hex:EtOAc: 20:1. Yield = 41% (2.1 mmol, 523 mg). **^{1}H NMR** (400 MHz, $CDCl_3$) δ = 7.52 (dd, *J* = 8.7, 5.4 Hz, 1H), 7.01 (dd, *J* = 9.7, 3.0 Hz, 1H), 6.91 – 6.80 (m, 1H), 3.54 – 3.45 (m, 2H), 3.25 – 3.16 (m, 2H), 1.61 (s, 3H); **^{13}C NMR** (100 MHz, $CDCl_3$) δ = 205.6, 162.0 (d, *J* = 247.6 Hz), 148.1 (d, *J* = 6.6 Hz), 135.6 (d, *J* = 8.0 Hz), 116.2 (d, *J* = 3.0 Hz), 115.6 (d, *J* = 2.4 Hz), 115.3 (d, *J* = 3.4 Hz), 59.0 (2C), 36.3 (d, *J* = 1.4 Hz), 27.5; **^{19}F NMR** (376 MHz, $CDCl_3$) δ = -114.21 – -114.32 (m, 1F); **GC-MS**: 256 [^{79}Br] and 258 [^{81}Br] (5), 214 [^{79}Br] and 216 [^{81}Br] (100), 177 (15).

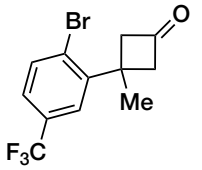

1k. Viscous colorless oil. FC eluent: *n*Hex:EtOAc: 20:1. Yield = 23% (1.2 mmol, 367 mg). **^{1}H NMR** (400 MHz, $CDCl_3$) δ = 7.71 (d, *J* = 8.2 Hz, 1H), 7.51 (d, *J* = 2.2 Hz, 1H), 7.37 (dd, *J* = 8.3, 2.2 Hz, 1H), 3.59 –

3.48 (m, 2H), 3.31 – 3.20 (m, 2H), 1.64 (s, 3H); **^{13}C NMR** (100 MHz, $CDCl_3$) δ = 205.1, 147.0, 135.0, 130.2 (q, *J* = 33.1 Hz), 126.1 (q, *J* = 1.6 Hz), 125.1 (q, *J* = 3.6 Hz), 124.9 (q, *J* = 3.6 Hz), 123.6 (q, *J* = 259.4 Hz) 59.1 (2C), 36.4, 27.5. **^{19}F NMR** (376 MHz, $CDCl_3$) δ = -62.66 (s, 3F); **GC-MS**: 287 [^{79}Br] and 289 [^{81}Br] (10), 264 [^{79}Br] and 266 [^{81}Br] (100), 227 (60), 165 (90).

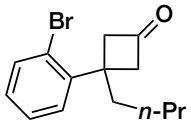

1l. Synthesized according to the general methodology using *n*-BuLi (instead of MeMgBr) in the first step. Viscous colorless oil. FC eluent: *n*Hex:EtOAc: 20:1. Yield = 73% (3.65 mmol, 1.0 g). **^{1}H NMR** (400 MHz, $CDCl_3$) δ = 7.57 (dd, *J* = 7.9, 1.3 Hz, 1H), 7.28 (td, *J* = 7.6, 1.3 Hz, 1H), 7.19 (dd, *J* = 7.8, 1.7 Hz, 1H), 7.10 (td, *J* = 7.6, 1.3 Hz, 1H), 3.50 – 3.40 (m, 2H), 3.28 – 3.17 (m, 2H), 1.94 (bs, 2H), 1.26 – 1.16 (m, 2H), 1.06 - 0.95 (m, 2H), 0.80 (t, *J* = 7.3 Hz, 3H); **^{13}C NMR** (100 MHz, $CDCl_3$) δ = 209.5, 143.8, 134.3, 129.8, 128.3, 127.0, 122.3, 57.8 (b, 2C), 39.8, 38.4, 27.7, 22.7, 13.8; **GC-MS**: 238 [^{79}Br] and 240 [^{81}Br] (5), 196 [^{79}Br] and 198 [^{81}Br] (100), 115 (95).

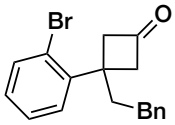

1m. Synthesized according to the general methodology using 2-bromohydrochalcone in the Wittig olefination step.[346] The last two steps of the synthesis were conducted on 1 mmol scale. Viscous colorless oil. FC eluent: *n*Hex:EtOAc: 15:1. Yield = 61% (0.61 mmol, 200 mg). **^{1}H NMR** (400 MHz, $CDCl_3$) δ = 7.62 (dd, *J* = 7.9, 1.3 Hz, 1H), 7.33 (td, *J* = 7.5, 1.3 Hz, 1H), 7.28 (dd, *J* = 7.8, 1.9 Hz, 1H), 7.23 – 7.19 (m, 2H), 7.18 – 7.11 (m, 2H), 7.08 – 7.02 (m, 2H), 3.58 – 3.50 (m, 2H), 3.36 – 3.25 (m, 2H), 2.48 – 2.19 (m, 4H); **^{13}C NMR** (100 MHz, $CDCl_3$) δ = 206.2, 143.1, 141.2, 134.6, 129.9, 128.6, 128.4 (2C), 128.2 (2C), 127.2, 126.0, 122.4, 65.8 (2C), 40.5, 39.9, 32.1; **GC-MS**: 328 [^{79}Br] and 330 [^{81}Br] (2), 286 [^{79}Br] and 288 [^{81}Br] (15), 259 (10), 91 (100).

[346] Known compounds (Nicholson, K.; Langer, T.; Thomas, S. P. Borane-Catalyzed, Chemoselective Reduction and Hydrofunctionalization of Enones Enabled by B–O Transborylation. *Org. Lett.* **2021**, *23*, 2498-2504). Prepared by Rh/Al_2O_3 (5 wt%) hydrogenation of the corresponding chalcones.

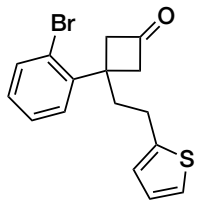

1n. Synthesized according to the general methodology using 1-(2-bromophenyl)-3-(thiophen-2-yl)propan-1-one in the Wittig olefination step.[346] The last two steps of the synthesis were conducted on 1 mmol scale. Viscous colorless oil. FC eluent: *n*Hex:EtOAc: 20:1. Yield = 57% (0.57 mmol, 190 mg). **^{1}H NMR** (400 MHz, $CDCl_3$) δ = 7.61 (dd, *J* = 7.9, 1.3 Hz, 1H), 7.37 – 7.30 (m, 1H), 7.26 (dd, *J* = 7.8, 1.8 Hz, 1H), 7.15 (ddd, *J* = 7.9, 7.2, 1.8 Hz, 1H), 7.06 (dd, *J* = 5.2, 1.2 Hz, 1H), 6.85 (dd, *J* = 5.1, 3.4 Hz, 1H), 6.69 (dd, *J* = 3.4, 1.1 Hz, 1H), 3.62 – 3.48 (m, 2H), 3.38 – 3.25 (m, 2H), 2.56 (t, *J* = 8.2 Hz, 2H), 2.44 (bs, 2H). **^{13}C NMR** (100 MHz, $CDCl_3$) δ = 205.9, 143.9, 142.8, 134.6, 129.8, 128.7, 127.2, 126.8, 124.1, 123.1, 122.5, 57.9 (b, 2C), 40.3, 39.8, 26.2; **GC-MS**: 334 [^{79}Br] and 336 [^{81}Br] (10), 292 [^{79}Br] and 294 [^{81}Br] (100), 223 [^{79}Br] and 225 [^{81}Br] (10).

Synthesis and characterization of ligands and catalyst

Preparation and Characterization of Optimal Ligand **L7** and Ligands **L3-5**

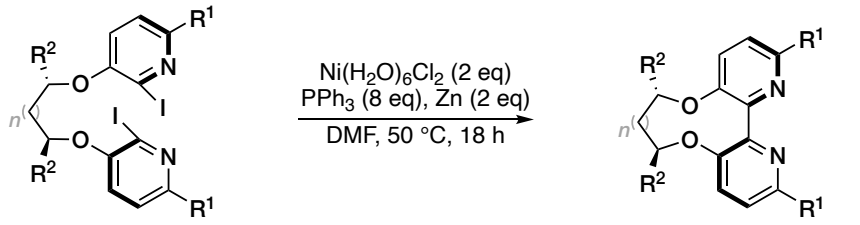

S1: n = 1, R^1 = R^2 = Me
S2: n = 0, R^1 = R^2 = Me
S3: n = 2, R^1 = Me, R^2 = H
S4: n = 2, R^1 = H, R^2 = Me

L3: n = 1, R^1 = R^2 = Me
L4: n = 0, R^1 = R^2 = Me
L5: n = 2, R^1 = Me, R^2 = H
L7: n = 2, R^1 = H, R^2 = Me

L7 was prepared by intramolecular reductive homocoupling of **S4** (prepared form 2-iodo-6-methylpyridin-3-ol[347] and commercially available (2*S*,5*S*)-2,5-hexanediol) following and unmodified literature procedure.[348]

In a flame-dried, nitrogen-filled Schlenk tube equipped with a magnetic stirring bar, $NiCl_2 \cdot 6H_2O$ (855 mg, 3.6 mmol) and PPh_3 (3.78 g, 14.4 mmol) were stirred in DMF (20 mL) at room temperature until a clear dark blue solution was obtained (ca. 10 min). Then, Zn dust (234 mg, 3.6 mmol) was added, and the resulting mixture was stirred at 50 °C for 1 h, leading to the formation of a red-brown slurry. The mixture was then cooled to room temperature and a solution of **S4** (1.0 g, 1.8 mmol) in DMF (3 mL) was added dropwise. The resulting black mixture was then stirred at 50 °C for 18 h and then cooled to room temperature. A concentrated aqueous NH_3 solution (28% wt., 30 mL) and CH_2Cl_2 (50 mL) were added, and the biphasic mixture was moved to a separatory funnel and vigorously shaken (the formation of the violet NH_3-Ni complex in the aqueous phase was observed). The organic layer was separated and washed with the NH_3 solution again (15 mL each time) until the washings became colorless, dried over anhydrous Na_2SO_4, and concentrated under reduced pressure. Once all DMF was

[347] M. A. Massa, W. C. Patt, K. Ahn, A. M. Sineros, S. B. Herman, A. Doherty, *Bioorg. Med. Chem. Lett.* **1998**, *8*, 2117-2122.
[348] X. Gao, B. Wu, W.-X. Huang, M.-W. Chen, Y.-G. Zhou, *Angew. Chem. Int. Ed.* **2015**, *54*, 11956.

removed, the residue was re-dissolved in CH_2Cl_2 (30 mL) placed in a separatory funnel and treated with an aqueous HCl solution (3 M, 2 x 15 mL). The combined aqueous layers (containing **L7***2HCl) were washed with CH_2Cl_2 (2 x 15 mL), moved to a beaker, and cooled to 0 °C. Solid NaOH (pellets) was added until pH = 12-14 and the precipitation of a white solid was observed. CH_2Cl_2 (30 mL) was added, and the biphasic mixture was moved to a separatory funnel. The organic layer was separated, and the aqueous layer was extracted with CH_2Cl_2 (2 x 30 mL). The combined organic layers were dried over anhydrous Na_2SO_4 and concentrated under reduced pressure. The crude residue was purified by FC on silica gel (CH_2Cl_2:Et_2O 2:1) to afford **L7** as a white powder in 55% yield (297 mg, 0.99 mmol). **MP** = 216 - 218 °C. **^{1}H NMR** (400 MHz, $CDCl_3$) δ = 7.18 (d, *J* = 8.4 Hz, 2H), 7.08 (d, *J* = 8.4 Hz, 2H), 4.34 – 4.23 (m, 2H), 2.56 (s, 6H), 1.87 – 1.77 (m, 2H), 1.77 – 1.66 (m, 2H), 1.38 (d, *J* = 6.3 Hz, 6H); **^{13}C NMR** (100 MHz, $CDCl_3$) δ = 152.1, 150.7, 145.7, 123.4, 121.4, 80.4, 35.5, 23.8, 22.3; **GC-MS**: 298 (75), 216 (90), 199 (100); **Anal. Calc.** for ($C_{18}H_{12}N_2O_2$: 298.17): C, 72.46; H, 7.43; found: C, 72.79; H, 7.37. $[\alpha]_D^{25}$ = + 159° (*c* = 0.25, CH_2Cl_2).

L3 was prepared by intramolecular reductive homocoupling of **S1** (prepared form 2-iodo-6-methylpyridin-3-ol and commercially available (2*S*,4*S*)-2,4-pentanediol) following the same procedure employed for **L7**. Yield = 60% (performed on 1.2 mmol scale, 0.72 mmol, 204 mg). FC on silica gel (EtOAc 100%). **^{1}H NMR** (400 MHz, $CDCl_3$) δ = 7.29 (d, *J* = 8.3 Hz, 2H), 7.09 (d, *J* = 8.3 Hz, 2H), 4.58 – 4.47 (m, 2H), 2.57 (s, 6H), 1.89 (t, *J* = 4.2 Hz, 2H), 1.37 (d, *J* = 6.5 Hz, 6H); **GC-MS**: 284 (70), 202 (95), 185 (100).

L4 was prepared by intramolecular reductive homocoupling of **S2** (prepared form 2-iodo-6-methylpyridin-3-ol and commercially available (2*S*,3*S*)-2,3-butanediol) following the same procedure employed for **L7**. Yield = 52% (performed on 0.8 mmol scale, 0.42 mmol, 112 mg). FC on silica gel (EtOAc 100%). **^{1}H NMR** (400 MHz,

$CDCl_3$) δ = 7.32 (d, *J* = 8.3 Hz, 2H), 7.16 (d, *J* = 8.3 Hz, 2H), 3.91 – 3.81 (m, 2H), 2.62 (s, 6H), 1.42 – 1.33 (m, 6H); **GC-MS**: 270 (65), 188 (85), 171 (100).

L5 was prepared by intramolecular reductive homocoupling of **S3** (prepared form 2-iodo-6-methylpyridin-3-ol and commercially available 1,4-butanediol) following the same procedure employed for **L7**. Yield = 31% (performed on 1.0 mmol scale, 0.31 mmol, 88 mg). FC on silica gel (EtOAc 100%). **^{1}H NMR** (400 MHz, $CDCl_3$) δ = 7.28 (d, *J* = 8.4 Hz, 2H), 7.12 (d, *J* = 8.4 Hz, 2H), 4.41 (bs, 2H), 4.11 (bs, 2H), 2.58 (s, 6H); **GC-MS**: 284 (55), 202 (80), 185 (100).

Preparation and Characterization of Precatalyst [Ni(**L7**)Cl_2]

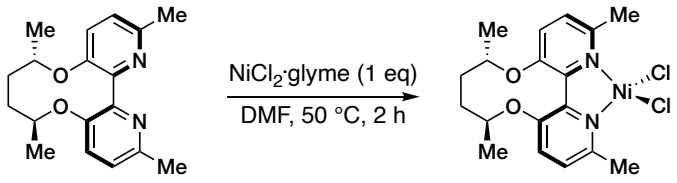

L7 (**L7**)$NiCl_2$

In a flame-dried, nitrogen-filled Schlenk tube equipped with a magnetic stirring bar, Ni(dme)Cl_2 (110 mg, 0.5 mmol) was stirred in anhydrous DMF (1 mL) at room temperature until a clear blue solution was obtained (10 min). Then, ligand **L7** (150 mg, 0.5 mmol) was added in one portion, resulting almost immediately in a dark brown slurry. The mixture was stirred at 50 °C for 2 h to ensure complete complexation, then cooled to room temperature and evaporated *in vacuo* to dryness. The residue was suspended in Et_2O (5 mL) and stirred vigorously for 2 h until a thick brown solid precipitate is obtained. The solid was filtered, washed several times with Et_2O and dried *in vacuo* to yield [Ni(**L7**)Cl_2] as a light brown bench-stable powder in 90% yield (186 mg, 0.45 mmol). Mp > 400 °C (decomposition). $[\alpha]_D^{25}$ = + 246° (*c* = 0.20, DMF). Crystals suitable for X-ray diffraction analysis were obtained by layering a solution of [Ni(**L7**)Cl_2] in THF with *c*Hex.

The X-ray intensity data were measured on a Bruker Apex III CCD diffractometer. Cell dimensions and the orientation matrix were initially determined from a least-squares refinement on reflections measured in four sets of 20 exposures, collected in three different ω regions, and eventually refined against all data. A full sphere of reciprocal space was scanned by 0.5° ω steps. The software SMART[3] was used for collecting frames of data, indexing reflections and determination of lattice parameters. The collected frames were then processed for integration by the SAINT program,[349] and an

[349] *SMART & SAINT Software Reference Manuals*, version 5.051 (Windows NT Version), Bruker Analytical X-ray Instruments Inc.: Madison, Wi, **1998.**

empirical absorption correction was applied using SADABS.[350] The structures were solved by direct methods (SIR 2014)[351] and subsequent Fourier syntheses and refined by full-matrix least-squares on F^2 (SHELXTL)[352] using anisotropic thermal parameters for all non-hydrogen atoms. The aromatic, methyl, methylene and methine hydrogen atoms were placed in calculated positions, refined with isotropic thermal parameters *U(H)* = 1.2 *Ueq*(C) and allowed to ride on their carrier carbons.

Crystal data and details of the data collection for compound [Ni(**L7**)Cl_2] are reported in **Table S2**.[353] Crystallographic data have been deposited with the Cambridge Crystallographic Data Centre (CCDC) as supplementary publication number CCDC 2129543. Copies of the data can be obtained free of charge via ww.ccdc.cam.ac.uk/getstructures.

[350] G. M. Sheldrick, *SADABS-2008/1-Bruker AXS Area Detector Scaling and Absorption Correction*, Bruker AXS: Madison, Wisconsin, USA, **2008**.
[351] M. C. Burla, R. Caliandro, B. Carrozzini, G. L. Cascarano, C. Cuocci, C. Giacovazzo, M. Mallamo, A. Mazzone, G. Polidori, *J. Appl. Cryst.* **2015**, *48*, 306-309.
[352] G. M. Sheldrick, *Acta Cryst C71* **2015**, 3-8.
[353] C. F. Macrae, , I. Sovago, S. J. Cottrell, P. T. A. Galek, P. McCabe, E. Pidcock, M. Platings, G. P. Shields, J. S. Stevens, M. Towler, P. A. Wood, *J. Appl. Cryst.* **2020**, *53*, 226-235.

Table S2. Crystal data and structure refinement for compound [Ni(**L7**)Cl_2]

Compound	**[Ni(L7)Cl_2]**
Formula	$C_{18}H_{22}O_2N_2NiCl_2$
Fw	427.98
T, K	296
λ, Å	0.71073
Crystal symmetry	Orthorhombic
Space group	*P2₁2₁2₁*
a, Å	8.797(3)
b, Å	12.158(4)
c, Å	19.362(7)
α	90.00
β	90.00
γ	90.00
Cell volume, $Å^3$	2070.8(1)
Z	4
Dc, Mg m^{-3}	1.373
μ(Mo-$K_α$), mm^{-1}	1.207
F(000)	888
Crystal size/ mm	0.81 x 0.09 x 0.07
θ limits, °	3.129 to 25.496
Reflections collected	26173
Unique obs. Reflections [F_o >	3843 [R(int) =
Goodness-of-fit-on F^2	1.005
R_1 (F)[a], wR_2 (F^2)[b] [$I > 2σ(I)$]	R1 = 0.0379, wR2 =
Largest diff. peak and hole, e. $Å^{-3}$	0.311 and -0.231

[a] $R_1 = Σ||F_o|-|F_c||/Σ|F_o|$.[b] $wR_2 = [Σw(F_o^2-F_c^2)^2/Σw(F_o^2)^2]^{1/2}$ where $w = 1/[σ^2(F_o^2) + (aP)^2 + bP]$ where $P = (F_o^2 + F_c^2)/3$.

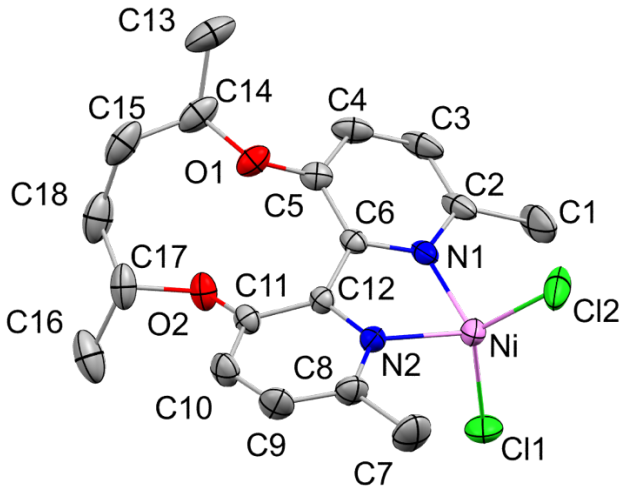

Figure S2. Molecular structure of [Ni(**L7**)Cl_2] with the atom labelling. Hydrogen atoms omitted for clarity. Thermal ellipsoids are drawn at 30% of probability level.

Optimized general procedure for the Ni-Catalyzed Tandem C-C σ-Bond Activation-CO_2 Fixation

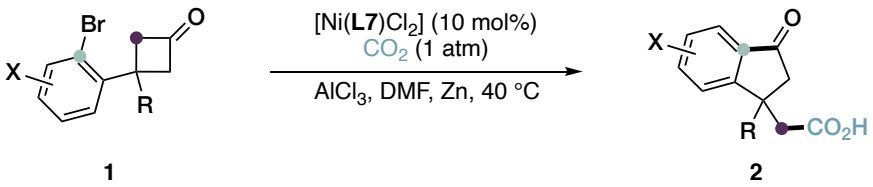

1 2

A flame-dried, nitrogen-filled Schlenk tube equipped with a magnetic stirring bar was charged with Nickel pre-catalyst [Ni(**L7**)Cl_2] (10 mol%, 4.3 mg), zinc dust (0.3 mmol, 19.8 mg) and $AlCl_3$ (0.15 mmol, 20.0 mg). The nitrogen atmosphere was evacuated, and the tube was backfilled with CO_2 (1 bar). This operation was repeated three times. Then DMF (1 mL, 0.1 M) was added under a flow of CO_2, and the reaction mixture was stirred for 5 min. Under a flow of CO_2, substrate **1** (0.1 mmol) was added, CO_2 was bubbled in the solution, the Schlenk flask was closed, and the reaction mixture was stirred (1000 rpm) for 16 h at 40 °C. The reaction was quenched with HCl (5 mL, 2.0 M), and extracted with ethyl acetate (3 x 10 mL). The combined organic layers were washed with HCl (3 x 10 mL, 0.2 M), dried over anhydrous Na_2SO_4, and concentrated under reduced pressure. The residue was purified by flash chromatography (FC) on silica gel [*n*Hex:EtOAc + 1% HCOOH] to afford desired products **2**.

Characterization data of products

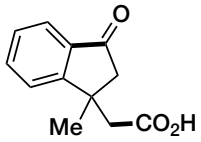

2a. Viscous colorless oil. FC eluent: *n*Hex:EtOAc: 70:30 +1% HCOOH. Yield = 70% (0.070 mmol, 14.3 mg). **^{1}H NMR** (400 MHz, $CDCl_3$) δ = 7.70 (d, *J* = 7.6 Hz, 1H), 7.61 (t, *J* = 7.5 Hz, 1H), 7.47 (d, *J* = 7.8 Hz, 1H), 7.38 (t, *J* = 7.4 Hz, 1H), 3.02 (d, *J* = 19.0 Hz, 1H), 2.80 (d, *J* = 15.4 Hz, 1H), 2.66 (d, *J* = 15.3 Hz, 1H), 2.56 (d, *J* = 19.0 Hz, 1H), 1.47 (s, 3H), the -COOH peak appears as a very broad singlet around 7.8 – 6.9 ppm; **^{13}C NMR** (100 MHz, $CDCl_3$) δ = 200.0, 170.7, 155.6, 130.5, 129.9, 122.8, 118.4, 118.4, 45.0, 40.0, 34.9, 23.4; **LC-MS**: [M-H^+]$^-$ = 203; Anal. Calc. for ($C_{12}H_{12}O_3$: 204.08): C, 70.58; H, 5.92; found: C, 70.76; H, 6.07.

2a is a known compound and the reported spectroscopic data match with the ones reported in the literature.[334]

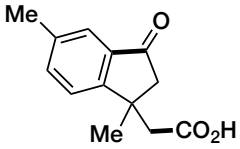

2b. Viscous colorless oil. FC eluent: *n*Hex:EtOAc: 70:30 +1% HCOOH. Yield = 76% (0.076 mmol, 16.6 mg). **^{1}H NMR** (400 MHz, $CDCl_3$) δ = 7.49 (s, 1H), 7.43 (d, *J* = 7.9 Hz, 1H), 7.35 (d, *J* = 7.9 Hz, 1H), 3.02 (d, *J* = 19.0 Hz, 1H), 2.78 (d, *J* = 15.3 Hz, 1H), 2.64 (d, *J* = 15.3 Hz, 1H), 2.55 (d, *J* = 19.0 Hz, 1H), 2.38 (s, 3H), 1.45 (s, 3H), the -COOH peak appears as a very broad singlet around 7.7 – 6.9 ppm; **^{13}C NMR** (100 MHz, $CDCl_3$) δ = 205.2, 176.0, 158.2, 138.1, 136.3, 135.9, 123.5, 123.3, 50.5, 45.2, 39.8, 28.6, 21.0; **LC-MS**: [M-H^+]$^-$ = 217; Anal. Calc. for ($C_{13}H_{14}O_3$: 218.09): C, 71.54; H, 6.47; found: C, 71.36; H, 6.77.

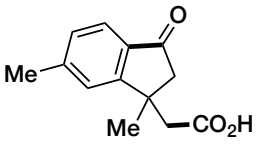

2c. Viscous colorless oil. FC eluent: *n*Hex:EtOAc: 67:33 +1% HCOOH. Yield = 64% (0.064 mmol, 14.1 mg). **^{1}H NMR** (400 MHz, $CDCl_3$) δ = 7.59 (d, *J* = 7.8 Hz, 1H), 7.26 (s, 1H, overlapped with the $CHCl_3$ peak), 7.18 (d, *J* = 7.8 Hz, 1H), 6.26 (bs, 1H), 3.01 (d, *J* = 19.0 Hz, 1H), 2.79 (d, *J* = 15.4 Hz, 1H), 2.64 (d, *J* = 15.4 Hz, 1H), 2.54 (d, *J* = 19.0 Hz, 1H), 2.43 (s, 3H), 1.46 (s, 3H); **^{13}C NMR** (100 MHz, $CDCl_3$) δ = 204.8, 175.9, 161.3, 146.3, 133.4,

129.3, 123.9, 123.4, 50.4, 45.1, 39.9, 28.5, 22.2; **LC-MS**: $[M\text{-}H^+]^-$ = 217; Anal. Calc. for ($C_{13}H_{14}O_3$: 218.09): C, 71.54; H, 6.47; found: C, 71.69; H, 6.30.

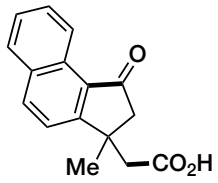

2d. White solid. Mp = 177 - 180 °C. FC eluent: *n*Hex:EtOAc: 75:25 +1% HCOOH. Yield = 43% (0.043 mmol, 10.9 mg). **^{1}H NMR** (400 MHz, $CDCl_3$) δ = 9.13 (d, *J* = 8.3 Hz, 1H), 8.07 (d, *J* = 8.5 Hz, 1H), 7.87 (d, *J* = 8.1 Hz, 1H), 7.66 (ddd, *J* = 8.3, 7.0, 1.1 Hz, 1H), 7.55 (ddd, *J* = 6.9, 6.2, 1.6 Hz, 1H) partially overlapped with 7.52 (d, *J* = 8.5 Hz, 1H), 3.14 (d, *J* = 18.8 Hz, 1H), 2.86 (d, *J* = 15.2 Hz, 1H), 2.71 (d, *J* = 15.2 Hz, 1H) partially overlapped with 2.67 (d, *J* = 18.8 Hz, 1H), 1.52 (s, 3H) the -COOH peak appears as a very broad singlet around 6.7 – 4.4 ppm; **^{13}C NMR** (100 MHz, $CDCl_3$) δ = 205.5, 175.7, 163.2, 136.3, 132.7, 129.5, 129.2, 129.0, 128.1, 126.9, 124.4, 120.5, 50.7, 44.8, 39.8, 28.2; **LC-MS**: $[M\text{-}H^+]^-$ = 253; Anal. Calc. for ($C_{16}H_{14}O_3$: 254.09): C, 75.58; H, 5.55; found: C, 75.32; H, 5.81.

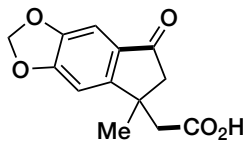

2e. White solid. Mp = 164 - 165 °C. FC eluent: *n*Hex:EtOAc: 70:30 +1% HCOOH, then *n*Hex:EtOAc: 60:40 +1% HCOOH. Yield = 50% (0.050 mmol, 12.3 mg). **^{1}H NMR** (400 MHz, acetone-d_6) δ = 7.25 (s, 1H), 7.02 (s, 1H), 6.24 (s, 2H), 3.09 (d, *J* = 18.6 Hz, 1H), 2.91 (d, *J* = 15.5 Hz, 1H), 2.81 (d, *J* = 15.5 Hz, 1H), 2.55 (d, *J* = 18.6 Hz, 1H), 1.53 (s, 3H) the -COOH peak appears as a very broad singlet around 4.3 – 3.3 ppm; **^{13}C NMR** (100 MHz, acetone-d_6) δ = 204.2, 174.5, 161.4, 156.8, 151.2, 133.3, 106.2, 105.3, 103.6, 52.9, 46.9, 42.4, 30.8; **LC-MS**: $[M\text{-}H^+]^-$ = 247; Anal. Calc. for ($C_{13}H_{12}O_5$: 248.07): C, 62.90; H, 4.87; found: C, 62.72; H, 5.04.

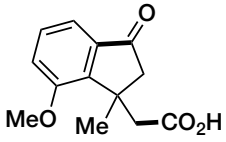

2f. Viscous colorless oil. FC eluent: *n*Hex:EtOAc: 75:25 +1% HCOOH. Yield = 73% (0.073 mmol, 17.0 mg). **^{1}H NMR** (400 MHz, $CDCl_3$) δ = 7.34 (t, *J* = 7.6 Hz, 1H), 7.29 (d, *J* = 6.9 Hz, 1H), 7.04 (d, *J* = 7.3 Hz, 1H), 3.87 (s, 3H), 3.03 (d, *J* = 15.6 Hz, 1H), 2.98 (d, *J* = 19.2 Hz, 1H), 2.90

(d, J = 15.6 Hz, 1H), 2.53 (d, J = 19.2 Hz, 1H), 1.52 (s, 3H), the -COOH peak appears as a very broad singlet around 8.1 – 6.4 ppm; **^{13}C NMR** (100 MHz, $CDCl_3$) δ = 205.5, 176.8, 157.1, 147.4, 138.0, 130.0, 116.3, 115.3, 55.4, 50.8, 42.4, 40.3, 26.3; **LC-MS**: $[M\text{-}H^+]^-$ = 233; Anal. Calc. for ($C_{13}H_{14}O_4$: 234.09): C, 66.66; H, 6.02; found: C, 66.68; H, 5.87.

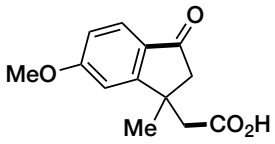

2g. Viscous colorless oil. FC eluent: *n*Hex:EtOAc: 64:36 +1% HCOOH, then *n*Hex:EtOAc 60:40 + 1% HCOOH. Yield = 65% (0.065 mmol, 15.1 mg). **^{1}H NMR** (400 MHz, $CDCl_3$) δ = 7.64 (d, J = 8.5 Hz, 1H), 6.90 (dd, J = 8.5, 2.1 Hz, 1H), 6.87 (d, J = 2.0 Hz, 1H), 3.87 (s, 3H), 3.01 (d, J = 18.9 Hz, 1H), 2.78 (d, J = 15.3 Hz, 1H), 2.65 (d, J = 15.3 Hz, 1H), 2.55 (d, J = 18.9 Hz, 1H), 1.46 (s, 3H), the -COOH peak appears as a very broad singlet around 8.0 – 6.2 ppm; **^{13}C NMR** (100 MHz, $CDCl_3$) δ = 200.9, 173.2, 163.0, 161.2, 126.4, 122.9, 112.8, 104.8, 53.1, 47.9, 42.5, 37.4, 25.9; **LC-MS**: $[M\text{-}H^+]^-$ = 233; Anal. Calc. for ($C_{13}H_{14}O_4$: 234.09): C, 66.66; H, 6.02; found: C, 66.73; H, 6.20.

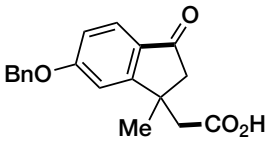

2h. Viscous colorless oil. FC eluent: *n*Hex:EtOAc: 70:30 +1% HCOOH, then *n*Hex:EtOAc 62:38 + 1% HCOOH. Yield = 64% (0.064 mmol, 20.3 mg). **^{1}H NMR** (400 MHz, $CDCl_3$) δ = 7.64 (d, J = 8.7 Hz, 1H), 7.45 – 7.31 (m, 5H), 7.00 – 6.94 (m, 2H), 5.12 (s, 2H), 3.01 (d, J = 18.9 Hz, 1H), 2.75 (d, J = 15.3 Hz, 1H), 2.63 (d, J = 15.3 Hz, 1H), 2.54 (d, J = 18.9 Hz, 1H), 1.45 (s, 3H), the -COOH peak appears as a very broad singlet around 5.3 – 4.3 ppm; **^{13}C NMR** (100 MHz, $CDCl_3$) δ = 203.5, 175.3, 164.7, 163.8, 135.8, 129.2, 128.7 (2C), 128.3, 127.6 (2C), 125.5, 115.9, 108.5, 70.4, 50.5, 45.1, 40.0, 28.4; **LC-MS**: $[M\text{-}H^+]^-$ = 309; Anal. Calc. for ($C_{19}H_{18}O_4$: 310.12): C, 75.53; H, 5.85; found: C, 75.81; H, 5.68.

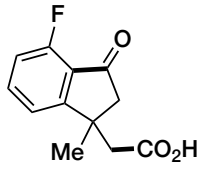

2i. Viscous colorless oil. FC eluent: *n*Hex:EtOAc: 75:25 +1% HCOOH. Yield = 45% (0.045 mmol, 10.0 mg). **^{1}H NMR** (400 MHz, $CDCl_3$) δ = 7.61 (dt, *J* = 12.6, 6.3 Hz, 1H), 7.27 (d, *J* = 7.5 Hz, 1H, overlapped with the $CHCl_3$ peak), 7.03 (t, *J* = 8.6 Hz, 1H), 3.07 (d, *J* = 18.9 Hz, 1H), 2.84 (d, *J* = 15.6 Hz, 1H), 2.74 (d, *J* = 15.6 Hz, 1H), 2.61 (d, *J* = 18.9 Hz, 1H), 1.51 (s, 3H), the -COOH peak appears as a very broad singlet around 4.8 – 3.1 ppm; **^{13}C NMR** (100 MHz, $CDCl_3$) δ = 201.1, 174.7, 162.9 (d, *J* = 2.1 Hz), 158.4 (d, *J* = 264.6 Hz), 137.0 (d, *J* = 8.3 Hz), 123.7 (d, *J* = 12.7 Hz), 119.3 (d, *J* = 4.1 Hz), 114.9 (d, *J* = 19.3 Hz) 50.6, 44.7, 40.1 (d, *J* = 1.5 Hz, 1H), 28.8; **^{19}F NMR** (376 MHz, $CDCl_3$) δ = -114.44 (dd, *J* = 9.1, 4.9 Hz, 1F); **LC-MS**: $[M\text{-}H^+]^-$ = 221; Anal. Calc. for ($C_{12}H_{11}FO_3$: 222.07): C, 64.86; H, 4.99; found: C, 64.89; H, 4.87.

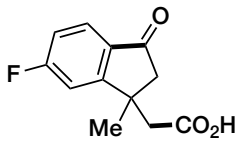

2j. Viscous colorless oil. FC eluent: *n*Hex:EtOAc: 75:25 +1% HCOOH. Yield = 45% (0.045 mmol, 10.0 mg). **^{1}H NMR** (400 MHz, $CDCl_3$) δ = 7.71 (dd, *J* = 8.4, 5.3 Hz, 1H), 7.14 – 7.04 (m, 2H), 3.02 (d, *J* = 19.0 Hz, 1H), 2.79 (d, *J* = 15.6 Hz, 1H), 2.68 (d, *J* = 15.6 Hz, 1H), 2.58 (d, *J* = 19.0 Hz, 1H), 1.47 (s, 3H), the -COOH peak appears as a very broad singlet around 7.7 – 6.0 ppm; **^{13}C NMR** (100 MHz, $CDCl_3$) δ = 203.0, 175.3, 167.3 (d, *J* = 256.9 Hz), 163.6 (d, *J* = 8.9 Hz), 132.2 (d, *J* = 1.9 Hz), 126.1 (d, *J* = 10.4 Hz), 116.3 (d, *J* = 23.8 Hz), 110.5 (d, *J* = 22.5 Hz), 50.4, 44.7, 40.0 (d, *J* = 2.0 Hz), 28.6; **^{19}F NMR** (376 MHz, $CDCl_3$) δ = -101.49 - -101.59 (m, 1F); **LC-MS**: $[M\text{-}H^+]^-$ = 221; Anal. Calc. for ($C_{12}H_{11}FO_3$: 222.07): C, 64.86; H, 4.99; found: C, 64.91; H, 5.11.

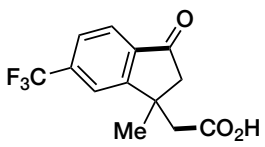

2k. Viscous colorless oil. FC eluent: CH_2Cl_2:MeOH: 30:1. Yield = 25% (0.025 mmol, 6.8 mg). **^{1}H NMR** (400 MHz, $CDCl_3$) δ = 7.84 (d, *J* = 7.9 Hz, 1H), 7.76 (s, 1H), 7.68 (d, *J* = 7.9 Hz, 1H), 3.10 (d, *J* = 19.2 Hz, 1H), 2.88 (d, *J* = 15.8 Hz, 1H), 2.77 (d, *J* = 15.8 Hz, 1H), 2.66 (d, *J* = 19.1 Hz, 1H), 1.55 (s, 3H), the -COOH peak appears as a very broad singlet around 4.3 – 3.5 ppm; **^{13}C NMR** (100 MHz, $CDCl_3$) δ = 203.7, 172.1, 160.6, 138.5 (q, *J* = 1.5 Hz) ,

136.3 (q, J = 32.1 Hz), 125.3 (q, J = 3.6 Hz), 123.5 (q, J = 273.7 Hz), 124.2, 120.8 (q, J = 3.8 Hz), 50.4, 40.2, 29.7, 28.7; **^{19}F NMR** (376 MHz, $CDCl_3$) δ = -62.93 (s, 3F) **LC-MS**: $[M\text{-}H^+]^-$ = 269; Anal. Calc. for ($C_{13}H_{11}F_3O_3$: 272.07): C, 57.36; H, 4.07; found: C, 57.55; H, 3.93.

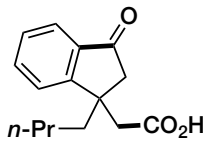

2l. Viscous colorless oil. FC eluent: *n*Hex:EtOAc: 75:25 +1% HCOOH. Yield = 76% (0.076 mmol, 18.7 mg). **^{1}H NMR** (400 MHz, $CDCl_3$) δ = 7.69 (d, J = 7.6 Hz, 1H), 7.63 – 7.57 (m, 1H), 7.42 (d, J = 7.8 Hz, 1H), 7.38 (t, J = 7.4 Hz, 1H), 2.92 (d, J = 19.1 Hz, 1H), 2.83 (d, J = 15.3 Hz, 1H), 2.70 (d, J = 15.3 Hz, 1H), 2.63 (d, J = 19.1 Hz, 1H), 1.88 – 1.78 (m, 1H), 1.74 – 1.63 (m, 1H), 1.30 – 1.04 (m, 4H), 0.78 (t, J = 7.2 Hz, 3H), the -COOH peak appears as a very broad singlet around 6.6 – 4.2 ppm; **^{13}C NMR** (100 MHz, $CDCl_3$) δ = 205.2, 175.7, 159.1, 136.7, 134.9, 128.0, 123.8, 123.5, 47.6, 44.0, 43.6, 40.6, 26.5, 22.9, 13.8; **LC-MS**: $[M\text{-}H^+]^-$ = 259; Anal. Calc. for ($C_{16}H_{20}O_3$: 260.14): C, 73.82; H, 7.74; found: C, 74.00; H, 7.97.

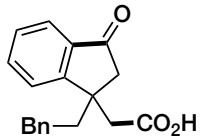

2m. Viscous colorless oil. FC eluent: *n*Hex:EtOAc: 75:25 +1% HCOOH. Yield = 60% (0.060 mmol, 17.7 mg). **^{1}H NMR** (400 MHz, $CDCl_3$) δ = 7.72 (dd, J = 7.5, 1.1 Hz, 1H), 7.62 (td, J = 7.5, 1.2 Hz, 1H), 7.47 (d, J = 7.7 Hz, 1H), 7.39 (t, J = 7.4 Hz, 1H), 7.23 – 7.18 (m, 2H), 7.16 – 7.10 (m, 1H), 7.05 – 7.00 (m, 2H), 2.99 (d, J = 19.1 Hz, 1H), 2.88 (d, J = 15.4 Hz, 1H), 2.78 – 2.65 (m, 2H), 2.48 – 2.40 (m, 1H), 2.16 (td, J = 9.9, 3.4 Hz, 2H), 2.05 – 1.98 (m, 1H), the -COOH peak was not detected; **^{13}C NMR** (100 MHz, $CDCl_3$) δ = 205.0, 175.5, 158.7, 141.1, 136.8, 135.1, 128.5 (2C), 128.2, 128.1 (2C), 126.0, 123.9, 123.6, 47.5, 44.2, 43.7, 42.6, 30.9; **LC-MS**: $[M\text{-}H^+]^-$ = 293; Anal. Calc. for ($C_{19}H_{18}O_3$: 294.13): C, 77.53; H, 6.16; found: C, 77.39; H, 5.94.

Transformations of compound 2b

Esterification of acid **2b**

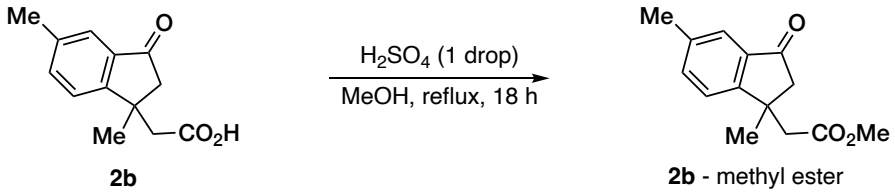

A nitrogen-filled Schlenk tube equipped with a stirring bar was charged with acid **2b** (64.4 mg, 0.3 mmol), MeOH (4 mL) and 1 droplet of concentrated H_2SO_4. The resulting mixture was heated to reflux for 18 h, then cooled to room temperature, diluted with EtOAc (10 mL), saturated aqueous $NaHCO_3$ (15 mL) was added. The organic phase was separated, and the aqueous phase was extracted with EtOAc (2 x 10 mL). The combined organic phases were washed with brine (10 mL), dried over anhydrous Na_2SO_4, and concentrated under reduced pressure. The residue was purified by flash chromatography (FC) on silica gel [*n*Hex:EtOAc 4:1] to afford product **2b-methyl ester** as a colorless oil (46.1 mg, 0.2 mmol, 66% yield). **^{1}H NMR** (400 MHz, $CDCl_3$) δ = 7.52 (s, 1H), 7.44 (d, *J* = 8.0 Hz, 1H), 7.37 (d, *J* = 7.9 Hz, 1H), 3.57 (s, 3H), 3.03 (d, *J* = 18.9 Hz, 1H), 2.78 (d, *J* = 15.0 Hz, 1H), 2.64 (d, *J* = 14.9 Hz, 1H), 2.56 (d, *J* = 18.9 Hz, 1H), 2.40 (s, 3H), 1.58 (s, 3H). **^{13}C NMR** (100 MHz, $CDCl_3$) δ = 205.0, 171.3, 158.2, 138.0, 136.1, 136.0, 123.4, 123.3, 51.5, 50.8, 45.5, 40.0, 28.5, 21.1. **GC-MS**: 232 (40), 159 (100), 115 (35); Anal. Calc. for ($C_{14}H_{16}O_3$: 232.11): C, 72.39; H, 6.94; found: C, 72.44; H, 7.05.

Preparation of Alcohol **3b**

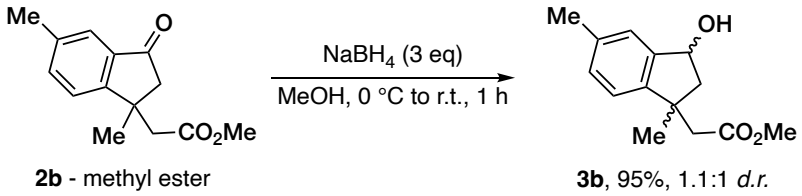

2b - methyl ester

3b, 95%, 1.1:1 *d.r.*

In a screw-capped vial equipped with a magnetic stirring bar **2b-methyl ester** (23.2 mg, 0.1 mmol) was dissolved in MeOH (1 mL). The resulting solution was cooled to 0 °C and $NaBH_4$ (3 equiv., 11.4 mg, 0.3 mmol) was added. The reaction mixture was then stirred at room temperature for 1 h then quenched with saturated aqueous NH_4Cl (5 mL), diluted with EtOAc (5 mL) and moved to a separatory funnel. The organic phase was separated, and the aqueous phase was back-extracted with EtOAc (2 x 5 mL). The combined organic phases were washed with brine (5 mL), dried over anhydrous Na_2SO_4, and concentrated under reduced pressure to afford analytically pure **3b** as a white foam in quantitative yield (*dr* = 1.1:1). **^{1}H NMR** (400 MHz, $CDCl_3$) δ = 7.22 (s, 1H minor), 7.19 (s, 1H major), 7.13 – 7.08 (m, 1H minor + 1H major), 7.07 (d, *J* = 7.8 Hz, 1H major), 7.03 (d, *J* = 7.8 Hz, 1H minor), 5.23 (t, *J* = 6.4 Hz, 1H major), 5.17 (dd, *J* = 7.5, 4.1 Hz, 1H minor), 3.59 (s, 3H major), 3.56 (s, 3H minor), 2.76 (dd, *J* = 13.5, 7.2 Hz, 1H minor) partially overlapped with 2.73 (d, *J* = 15.2 Hz, 1H minor), 2.58 (d, *J* = 15.2 Hz, 1H minor), 2.52 (d, *J* = 14.2 Hz, 1H major), 2.46 – 2.38 (m, 2H major), 2.34 (s, 3H major + 3H minor), 2.22 (dd, *J* = 14.1, 4.1 Hz, 1H minor), 1.82 (dd, *J* = 13.5, 5.8 Hz, 1H major), 1.45 (s, 3H major), 1.29 (s, 3H minor), the -OH peak was not detected; **^{13}C NMR** (100 MHz, $CDCl_3$) δ = 172.7 (minor), 172.0 (major), 146.4 (minor), 146.2 (major), 144.2 (major), 144.1 (minor), 137.4 (minor), 137.3 (major), 129.7 (major), 129.5 (minor), 125.3 (minor), 124.8 (major), 122.6 (minor), 122.2 (major), 74.4 (minor), 74.2 (major), 51.4 (minor), 51.3 (major), 49.6 (major), 49.3 (minor), 46.4 (minor), 45.9 (major), 44.3 (major), 44.0 (minor), 29.0 (minor), 28.2 (major) 21.3 (major), 21.2 (minor); **GC-MS**: 234 (15), 161 (100), 143 (50); Anal. Calc. for ($C_{14}H_{18}O_3$: 234.13): C, 71.77; H, 7.74; found: C, 71.66; H, 7.92.

Preparation of indene **4b**

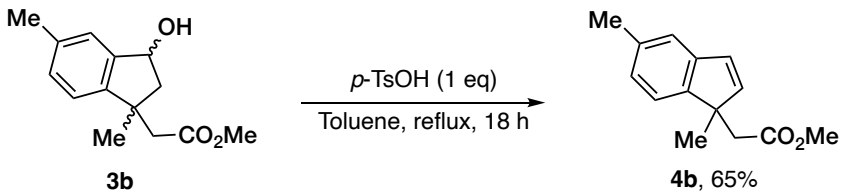

3b **4b**, 65%

In a screw-capped vial equipped with a magnetic stirring bar **3b** (23.4 mg, 0.1 mmol) and *p*-toluenesulfonic acid monohydrate (1 equiv., 19.0 mg, 0.1 mmol) were suspended in toluene (1 mL) and heated to reflux for 18 h. The reaction mixture was then cooled to room temperature, quenched with saturated aqueous $NaHCO_3$ (5 mL), diluted with EtOAc (5 mL) and moved to a separatory funnel. The organic phase was separated, and the aqueous phase was back-extracted with EtOAc (2 x 5 mL). The combined organic phases were washed with brine (5 mL), dried over anhydrous Na_2SO_4, and concentrated under reduced pressure. The residue was purified by flash chromatography (FC) on silica gel [*n*Hex:EtOAc 40:1] to afford product **4b** as a colorless oil (14.0 mg, 0.065 mmol, 65% yield). **^{1}H NMR** (400 MHz, $CDCl_3$) δ = 7.18 (d, *J* = 7.6 Hz, 1H), 7.11 (s, 1H), 7.00 (d, *J* = 7.7 Hz, 1H), 6.63 (d, *J* = 5.5 Hz, 1H), 6.56 (d, *J* = 5.5 Hz, 1H), 3.62 (s, 3H), 2.75 (d, *J* = 14.4 Hz, 1H), 2.37 (d, *J* = 14.3 Hz, 1H) partially overlapped with 2.35 (s, 3H), 1.35 (s, 3H). **^{13}C NMR** (100 MHz, $CDCl_3$) δ = 171.9, 148.3, 144.6, 142.9, 136.6, 129.0, 125.9, 122.2, 121.2, 51.4, 50.5, 42.5, 22.2, 21.4; **GC-MS**: 216 (70), 156 (100), 141 (80), 128 (70), 115 (60); Anal. Calc. for ($C_{14}H_{16}O_2$: 216.12): C, 77.75; H, 7.46; found: C, 77.54; H, 7.66.

Preparation of amide **5b**

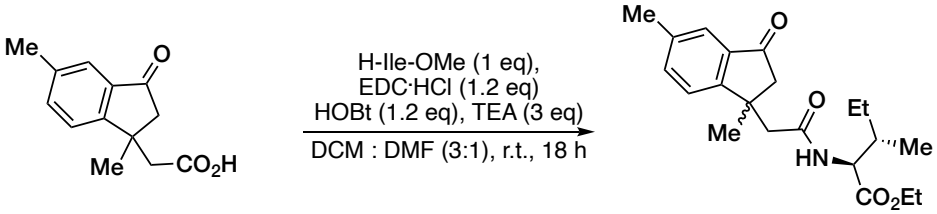

2b **5b**, 52%, 1.5:1 *d.r.*

A nitrogen-filled Schlenk tube equipped with a stirring bar was charged with acid **2b** (21.8 mg, 0.1 mmol), HOBt (1.2 equiv., 18.4 mg, 0.12 mmol), CH_2Cl_2 (1.2 mL) and DMF (0.4 mL). The resulting solution is stirred for 10 min. at room temperature, then EDC hydrochloride (1.2 equiv., 21.0 mg, 0.12 mmol) and isoleucine methyl ester (H-Ile-Ome, 1.0 equiv., 13.2 mg, 0.1 mmol) were added in this order. Finally, TEA (3.0 equiv., 42 μL, 0.3 mmol) was added dropwise and the resulting mixture was stirred at room temperature for 18 h. The reaction was then diluted with EtOAc (10 mL), treated with saturated aqueous NH_4Cl (15 mL) and moved to a separatory funnel. The organic phase was separated, and the aqueous phase was back-extracted with EtOAc (2 x 10 mL). The combined organic phases were washed with brine (10 mL), dried over anhydrous Na_2SO_4, and concentrated under reduced pressure. The residue was purified by flash chromatography (FC) on silica gel [*n*Hex:EtOAc 1.5:1] to afford product **5b** as a colorless oil (dr = 1.5:1, 17.9 mg, 0.052 mmol, 52% yield). Partial separation of the diastereoisomers was possible *via* FC. Two fractions of the column were thus obtained. The first (7.6 mg) containing the pure major diastereoisomer and the second (10.3 mg) containing a 1.3:1 diastereomeric mixture in favor of the minor diastereoisomer. **^{1}H NMR of major diastereoisomer** (400 MHz, $CDCl_3$) δ = 7.51 (s, 1H), 7.43 (dd, *J* = 8.0, 1.7 Hz, 1H), 7.38 (d, *J* = 7.9 Hz, 1H), 5.70 (d, *J* = 8.4 Hz, 1H), 4.44 (dd, *J* = 8.4, 4.8 Hz, 1H), 3.66 (s, 3H), 3.07 (d, *J* = 19.0 Hz, 1H), 2.63 – 2.59 (m, 3H), 2.38 (s, 3H), 1.78 (ddt, *J* = 9.3, 6.9, 4.7 Hz, 1H), 1.47 (s, 3H), 1.34 – 1.20 (m, 1H), 1.02 (ddt, *J* = 13.8, 9.0, 7.1 Hz, 1H), 0.85 (t, *J* = 7.4 Hz, 3H), 0.80 (d, *J* = 6.9 Hz, 3H). **^{1}H NMR of minor diastereoisomer** (400 MHz, $CDCl_3$) δ = 7.52 (s, 1H), 7.46 (dd, *J*

= 7.8, 1.7 Hz, 1H), 7.39 (d, *J* = 7.7 Hz, 1H), 5.64 (d, *J* = 8.6 Hz, 1H), 4.44 (dd, *J* = 8.7, 4.8 Hz, 1H), 3.68 (s, 3H), 3.16 (d, *J* = 19.1 Hz, 1H), 2.64 – 2.58 (m, 2H), 2.54 (d, *J* = 19.0 Hz, 1H), 2.38 (s, 3H), 1.78 (ddt, *J* = 9.5, 7.0, 4.8 Hz, 1H), 1.47 (s, 3H), 1.34 – 1.25 (m, 1H), 1.17 – 1.07 (m, 1H), 0.85 (t, *J* = 7.3 Hz, 3H), 0.60 (d, *J* = 6.9 Hz, 3H). **^{13}C NMR of major diastereoisomer** (100 MHz, $CDCl_3$) δ = 205.1, 172.1, 169.8, 158.5, 138.0, 136.1, 136.0, 123.6, 123.2, 56.3, 52.0, 50.5, 47.8, 40.5, 37.7, 28.9, 25.2, 21.0, 15.4, 11.5; **^{13}C NMR of minor diastereoisomer** (100 MHz, $CDCl_3$) δ = ^{13}C NMR (101 MHz, $cdcl_3$) δ 205.0, 172.4, 169.6, 158.3, 138.0, 136.3, 136.1, 123.7, 123.2, 56.1, 52.1, 50.1, 47.9, 40.7, 37.8, 29.3, 24.8, 21.0, 15.1, 11.4; **LC-MS**: [M+H$^+$] = 346, [M+Na$^+$] = 368.

Wittig olefination for the preparation of **6b** and **6b'**

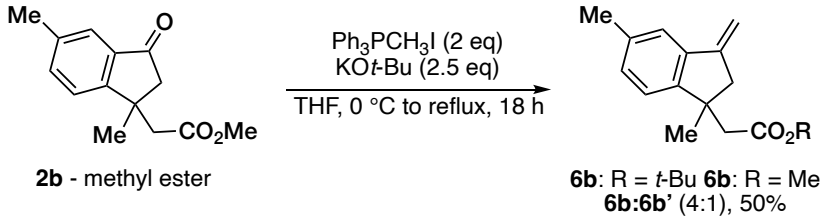

2b - methyl ester

6b: R = *t*-Bu **6b**: R = Me
6b:6b' (4:1), 50%

A nitrogen-filled Schlenk tube equipped with a stirring bar was charged with methyl triphenylphosphonium iodide (2.0 equiv., 80.8 mg, 0.2 mmol), KO*t*Bu (2.5 equiv., 28.0 mg, 0.25 mmol) and THF (0.5 mL) in this order. The resulting bright yellow suspension was stirred at room temperature for 1 h and then cooled to 0 °C. A solution of **2b-methyl ester** (23.2 mg, 0.1 mmol), in THF (0.5 mL) was then added dropwise, the mixture was immediately heated to reflux and stirred at that temperature for 18 h. The reaction was then cooled to room temperature and diluted with EtOAc (5 mL), treated with saturated aqueous NH_4Cl (10 mL) and moved to a separatory funnel. The organic phase was separated, and the aqueous phase was back-extracted with EtOAc (2 x 5 mL). The combined organic phases were washed with brine (5 mL), dried over anhydrous Na_2SO_4, and concentrated under reduced pressure. The residue was purified by flash chromatography (FC) on silica gel [*n*Hex:EtOAc 40:1] to afford product **6b** (colorless oil, 10.9 mg, 0.040 mmol) and **6b'** (colorless oil, 2.3 mg, 0.010 mmol) in 50% combined yield.

6b: **^{1}H NMR** (400 MHz, $CDCl_3$) δ = 7.25 (s, 1H), 7.09 (d, *J* = 7.8 Hz, 1H), 7.05 (d, *J* = 7.9 Hz, 1H), 5.41 (t, *J* = 2.5 Hz, 1H), 5.00 (t, *J* = 2.4 Hz, 1H), 3.08 (dt, *J* = 16.5, 2.3 Hz, 1H), 2.61 (dt, *J* = 16.5, 2.2 Hz, 1H), 2.49 (d, *J* = 13.8 Hz, 1H), 2.42 (d, *J* = 13.8 Hz, 1H), 2.33 (s, 3H), 1.34 (s, 9H), 1.32 (s, 3H); **^{13}C NMR** (100 MHz, $CDCl_3$) δ = 171.0, 150.1, 148.0, 139.8, 136.7, 129.5, 122.9, 120.9, 103.0, 80.2, 47.2, 45.9, 43.8, 28.0, 27.9 (3C), 21.3; **GC-MS**: 272 (35), 157 (25), 57 (100); Anal. Calc. for ($C_{18}H_{24}O_2$: 272.18): C, 79.37; H, 8.88; found: C, 79.56; H, 9.00.

6b': **^{1}H NMR** (400 MHz, $CDCl_3$) δ = 7.27 (s, 1H), 7.10 – 7.04 (m, 2H), 5.42 (t, *J* = 2.1 Hz, 1H), 5.01 (t, *J* = 2.1 Hz, 1H), 3.60 (s, 3H), 3.02 (dt, *J* = 16.3, 2.2 Hz, 1H), 2.64 (dt,

J = 16.4, 2.1 Hz, 1H) partially overlapped with 2.59 (d, *J* = 14.2 Hz, 1H), 2.48 (d, *J* = 14.3 Hz, 1H), 2.34 (s, 3H), 1.34 (s, 3H); **^{13}C NMR** (100 MHz, $CDCl_3$) δ = 172.1, 149.8, 147.7, 139.8, 136.9, 129.6, 122.7, 121.1, 103.2, 51.3, 46.2, 45.7, 43.6, 27.3, 21.3; **GC-MS**: 230 (25), 157 (55), 142 (100); Anal. Calc. for ($C_{15}H_{18}O_2$: 230.13): C, 78.23; H, 7.88; found: C, 78.08; H, 7.65.